INTERDISCIPLINARY APPLIED MATHEMATICS

GEOPHYSICS AND PLANETARY SCIENCES

Mathematics of Multidimensional Seismic Imaging, Migration, and Inversion

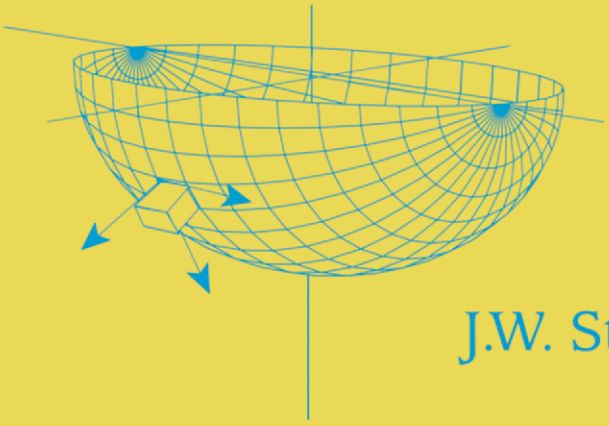

N. Bleistein
J.K. Cohen
J.W. Stockwell, Jr.

Springer

Interdisciplinary Applied Mathematics

Volume 13

Problems in engineering, computational science, and the physical and biological sciences are using increasingly sophisticated mathematical techniques. Thus, the bridge between the mathematical sciences and other disciplines is heavily traveled. The correspondingly increased dialog between the disciplines has led to the establishment of the series: *Interdisciplinary Applied Mathematics.*

The purpose of this series is to meet the current and future needs for the interaction between various science and technology areas on the one hand and mathematics on the other. This is done, firstly, by encouraging the ways that mathematics may be applied in traditional areas, as well as point towards new and innovative areas of applications; and, secondly, by encouraging other scientific disciplines to engage in a dialog with mathematicians outlining their problems to both access new methods and suggest innovative developments within mathematics itself.

The series will consist of monographs and high-level texts from researchers working on the interplay between mathematics and other fields of science and technology.

Interdisciplinary Applied Mathematics

Springer Science+Business Media, LLC

N. Bleistein J.K. Cohen
J.W. Stockwell, Jr.

Mathematics of Multidimensional Seismic Imaging, Migration, and Inversion

With 71 Illustrations

Springer

N. Bleistein
Center for Wave Phenomena
Colorado School of Mines
Golden, CO 80401-1887, USA
norm@dix.mines.edu

J.W. Stockwell, Jr.
Center for Wave Phenomena
Colorado School of Mines
Golden, CO 80401-1887, USA
john@dix.mines.edu

J.K. Cohen (deceased)

Mathematics Subject Classification (2000): 86-01, 86A15, 73Dxx, 35-01

Library of Congress Cataloging-in-Publication Data
Bleistein, Norman.
Mathematics of multidimensional seismic imaging, migration, and inversion / N. Bleistein, J.K. Cohen, J.W. Stockwell, Jr.
p. cm. — (Interdisciplinary applied mathematics ; 13)
Includes bibliographical references and indexes.

1. Seismic reflection method. 2. Inverse scattering transform. I. Cohen, Jack K. II. Stockwell, J.W. (John W.) III. Title. IV. Interdisciplinary applied mathematics ; v. 13.
TN269 .B485 2000
550'.28—dc21 00-041971

Printed on acid-free paper.

Originally published by Springer-Verlag New York, Inc. in 2001
Softcover reprint of the hardcover 1st edition in 2001

Production managed by Allan Abrams; manufacturing supervised by Jacqui Ashri.
Photocomposed copy prepared from the authors' LaTeX files.

9 8 7 6 5 4 3 2 1

SPIN 10770623

ISBN 978-1-4612-6514-6 ISBN 978-1-4613-0001-4 (eBook)
DOI 10.1007/978-1-4613-0001-4

To the late Sandy Bleistein, to Abby and Rich, Steve and Kayu, and to Judy, Clare, and Kevin for their patience and encouragement.

—Norman Bleistein

To Diane, Daniel, and Mara and Alan Marks, and to Irv Cohen.

—Jack K. Cohen

To my Mom and Dad, and to all of my friends and colleagues for their support over the years.

—John W. Stockwell, Jr.

Preface

The disciplines of applied science and engineering have become increasingly mathematical in content during the past twenty-five years. The various branches of geophysics are no exception to this trend.

Since 1921, when J. Clarence Karcher [Karcher, 1993] first used the reflection seismic method for petroleum exploration, geophysicists have sought better ways of employing seismic data to gain information about the Earth's subsurface. While the reflection seismic method is still used primarily by the oil and gas industry for the detection of hydrocarbons (petroleum and natural gas) the technique has been applied successfully to image structures located in environments ranging from the Earth's near surface (for engineering geophysics applications), to the deeper crust and upper mantle (for solid-Earth geophysics applications). Essentially the same technique, though based on different physics, has been applied in the diverse fields of ground penetrating radar, and acoustic and ultrasonic imaging, as practiced in the fields of materials science and medicine. Generically, all of these techniques are special cases of "inverse-scattering" imaging. While our text deals only with the seismic applications of inverse scattering, the mathematical results we present here have applicability in these other fields as well.

In its raw form, the data collected in seismic surveys offers only a crude and distorted view of the subsurface. Techniques, generically called *migration* methods, were developed to correct the raw data, to produce actual images of geologic structures. From a humble beginning as a graphical method for analog data interpretation, migration has evolved into a sophisticated exercise in applied mathematical physics.

The push to an increasingly mathematical description of seismic migration began with the pioneering work of Claerbout, Stolt, Schneider, and others in the early 1970s. The results obtained by these investigators were based largely on the classical principles of geometrical optics, as well as results from signal processing theory. Though intuitively satisfying to the geophysicist, many of the early mathematical constructions of migration formulas lacked mathematical rigor. The result of these investigations was a hodgepodge of formulas that were obviously related but, as a group, lacked a firm mathematical foundation. Furthermore, the heuristic nature of these formulas made them difficult to generalize, hampering their extension to new problems.

In this text, we present a collection of research results created at the Center for Wave Phenomena (CWP), which is currently located the Colorado School of Mines, but was founded at the University of Denver. These materials represent investigations conducted by the faculty and students of CWP from 1977 through 1999. Our goal is to provide a unified approach to seismic imaging, formulated as an inverse scattering problem in a small-perturbation, high-frequency asymptotic regime. Our approach will permit the reader to understand the classical results of seismic migration in a way that reveals the inherent assumptions that were not explicitly stated by the creators of these early results.

This understanding will carry the reader through the hierarchy of increasingly complicated recording geometries and geologic models. Along the way, many of the classical results of seismic migration will appear as special cases of the general theory we present. In addition, the reader will see that other topics, such as dip-moveout (DMO) processing, wave-equation datuming, and offset continuation, also fit naturally in the theoretical framework we present. Our intent is that the reader will develop an appreciation for the open-endedness of this subject, so that he or she may use the general theory we present here as a springboard to many new results.

This text began as a set of notes created by one of the authors (John Stockwell) during the fall semester of 1987, the spring semester of 1988, and the fall semester of 1989 for the courses "Mathematical Methods for Wave Phenomena," and "Multi-dimensional Seismic Inversion," taught by Norm Bleistein of the Center for Wave Phenomena, Department of Mathematical and Computer Sciences, Colorado School of Mines. Portions of the text have been based on Bleistein's book, *Mathematical Methods for Wave Phenomena* and the CWP Report #CWP-043, entitled *Multi-dimensional Seismic Inversion* by Jack Cohen and Norm Bleistein. The latter set of notes was prepared as part of a short course presented by Cohen and Bleistein at the Norwegian Institute of Technology in Trondheim, Norway in 1986. Our text is also based on material from the theses of graduate students of CWP, and the many technical papers by the professors and students of the group.

Our primary goal in writing this book is to create a "hard copy" of a course successfully taught to hundreds of students over a span of eighteen

years, in both full-semester and short-course form. The diverse collection of backgrounds of our students has shaped our approach in teaching this material. Because the intended audience of this text is composed of people with varied mathematical and geotechnical backgrounds, we present a mixture of basic and advanced materials, more basic material than would be in a purely mathematical treatment of the subject, but more advanced material than geophysicists typically see. Thus, we intend that our text bridge the gap between the theoretically minded applied-math community and the applications-minded geotechnical community.

This is a mathematical-geophysics textbook, however. It is not a partial differential equations book, nor is it a book on the mathematical theory of inverse methods. We use the word *Mathematical* in the title as a geophysicist, engineer, or implementation-oriented applied mathematician might use it. Consequently, some mathematical precision is sacrificed to avoid losing the thread of the story we are telling. On the other hand, we provide comments and citations to the literature to direct the interested reader to more rigorous sources. Also, appendices are supplied to familiarize the reader with the topics of distribution theory, causal Fourier transforms, ray theory, and dimensionless versus dimensional variables—topics that are used in the main part of the text, but not discussed at length.

Chapter 1 begins with a heuristic and semihistorical overview, emphasizing the hierarchical structure of the subject of seismic migration, as seen from the mathematical perspective of inverse problems. This hierarchy is extended to delineate a plan for the investigation of more complex aspects of the problem. We also describe the fundamental seismic experiments that provide the data available for inversion, as well as an outline of the fundamental geometrical construction that leads to an image of the Earth's interior from a simple seismic experiment conducted in a correspondingly simple Earth model.

In Chapter 2 we outline our basic approach to the creation of seismic imaging formulas as Fourier-like integral equations, derived in the simplified setting of 1D wave propagation. To do this, we employ the classical methods of perturbation theory (the Born approximation) and Green's theorem to generate 1D modeling and inversion formulas. We rely on the simplicity of 1D to introduce many of the concepts that we employ in later chapters. We do not, however, present any results that depend on characteristics that are exclusive to the problem of one-dimensional wave propagation.

Chapter 3 deals with the derivation of Fourier-like inversion formulas in higher dimensions for the migration of zero-offset, constant-background seismic data. This is really just the 3D application of the ideas introduced in Chapter 2. Both 3D and 2.5D inversion formulas for homogeneous media are derived, with several of the classic migration formulas (such as those of Stolt and Schneider) appearing as special cases of the more general theory. (The terminology *2.5D* will be explained in context in that chapter.) We test the general theory analytically by applying the inversion

formulas to Kirchhoff-approximate data, with the resulting integrals being approximated asymptotically, under a high-frequency or large-wavenumber assumption. Our primary tool for such analyses is the method of stationary phase. Because these results are approximate, being based on asymptotic methods, we introduce techniques to evaluate the robustness of numerical implementations of our formulas.

In Chapters 2 and 3, we find that our zero-offset migration/inversion formulas are Fourier-like integrals, which yield output consisting of a reflectivity function that peaks on the surfaces of reflectors (the singular function of the surface), yielding information about the reflection coefficient, but which give no information about the smoother wavespeed variability of the medium. This is in accordance with practical experience.

Chapter 4 shows that such results are based on fundamental properties of Fourier-like integrals, when evaluated in the large-wavenumber regime. In particular, the cascading of forward and inverse Fourier transforms on data is found to yield, as the leading-order term, the most singular part of the input data, under the large-wavenumber assumption. The most singular part of reflection seismic data is the reflectivity function of the reflectors—exactly the reflection coefficient times singular function results of the previous chapters. Chapter 4 also shows that the effectiveness of the inversion formulas we have created is due primarily to their Fourier-like nature combined with the assumption of high frequencies. This frees us from having to worry about many of the particulars—such as a specific wavespeed profile or a specific type of seismic experiment.

We exploit this freedom to create inversion formulas for heterogeneous media with general source-receiver geometries. Chapters 5 and 6 deal, respectively, with 3D and 2.5D formulations of the problem. In Chapter 5, we also eliminate, to the extent possible, the small-perturbation assumption that was made as a point of departure in Chapters 2 and 3.

Chapter 7 brings us to the present (2000) by extending the concepts and techniques developed in the previous chapters to the more general problem of remapping seismic data from one source-receiver geometry to another. This general subject contains the specific subtopic of dip-moveout (DMO), under the heading of transformation to zero-offset (TZO), but contains sufficient generality to be a potential springboard to other data mapping techniques, including *datuming*, *offset continuation*, and *data regularization*.

A text such as ours is characterized as much by materials omitted, as it is by materials included. We view our text as being introductory, or perhaps "classical" in nature, and therefore we do not include material about elastic wave propagation, anisotropy, multiple elimination, deconvolutional techniques, and many other topics that are important to seismic data processing and are topics of current research.

Furthermore, there are new mathematical approaches to the subject of seismic migration/inversion, which show that the "general" results we

present are imbedded in an even more general theory based on pseudodifferential operators and generalized Radon transforms. This direction of research began with the pioneering work of Doug Miller, Mike Oristaglio, and Gregory Beylkin at Schlumberger c. 1983 and has currently been extended by Maarten de Hoop, of CWP. Similarly, where the development here relies on classical ray theory, on geometrical optics, and (slightly) on geometrical theory of diffraction, the newer methodology exploits Maslov's method to work around some of the difficulties of ray families in the physical domain when the Earth structure is complex enough to produce caustics in the ray fields from point sources. All of these (and more) are topics of ongoing research at the time of this writing.

One of the coauthors, Jack Cohen, passed away while this book project was in progress. Nevertheless, his point of view about exposition, style, and content, as conveyed to the other two authors through many years of friendship and collaboration, is very much a part of the material that was revised and expanded after his death.

If the book has three parents, it also has many "aunts and uncles." These include students who suffered through the underlying course of the same title—before there were lecture notes, and while the lecture notes were in evolving form. The first students took this course in 1983 with Jack Cohen, while the material was in its embryonic form; lectures presented one day might be revised a few days later with new insights and new research results. Students in the last two classes before submission of this manuscript, one at the Colorado School of Mines, the other at the University of Campinas in Brazil, provided many constructive suggestions that were directly integrated into the more fully developed set of lecture notes. Further, we received constructive suggestions from the publisher-reviews. These, too, we incorporated. The foremost of our reviewers, most worthy of special mention, is Ken Larner, famous for his red pen, sharp eye, and incisive remarks. While the red marks do not show in the final text, Ken's hand (and red pen) has touched every chapter. We believe that they are all better than they might otherwise have been, thanks to Ken's persistence and fortitude in working through the book.

We have also been fortunate to have adequate funding for the students and faculty, so that the ideas presented here could be developed. The major source of our funding has been the Consortium Project on Seismic Inverse Methods at the Colorado School of Mines. We have enjoyed this support from the oil industry and its service companies since 1984. We also acknowledge support from the Office of Naval Research, through the Mathematics and Ocean Acoustics Programs, and from the Department of Energy. During the fall semester (spring semester in Brazil), 1999, Bleistein taught a course using the current draft of this text, then under intense near-final revisions, at the University of Campinas in Brazil, under support of FAPESP, the research and educational funding agency of São Paolo State, Brazil.

We have also had support from the Gas Research Institute and the SEG Foundation, specifically for the development of the CWP/SU Seismic Unix package. Seismic Unix is a free seismic processing and research software environment, created at CWP by Jack Cohen, and currently managed by John Stockwell [Stockwell, 1997,1999]. The package may be downloaded at no charge, as full source code, from our web site at **http://www.cwp.mines.edu/cwpcodes**.

With all of the help that we received, to the extent that we have not fulfilled our expositional goals, the responsibility can only reside with us, the authors. If the reader has questions or comments, please send email to the authors at **mmsimi@dix.mines.edu**. For additional information, please see our web site at: **http://www.cwp.mines.edu/mmsimi**.

Golden
Colorado
February, 2000

Norman Bleistein
Jack K. Cohen
John W. Stockwell, Jr.

Memorial: Jack K. Cohen [1]

On 24 October 1996, the Colorado School of Mines community lost a great friend with the death of Jack K. Cohen. He was 56 years old. Jack received his Ph.D. from Courant Institute of Mathematical Sciences, then spent 16 years at the University of Denver before joining the faculty at Mines in 1983. A founding member of the Center for Wave Phenomena at CSM, Jack left his immensely human and caring mark on students and colleagues within CWP, as well as on mathematicians and geophysicists around the world.

In the late 1970s, Jack co-authored two seminal papers characterizing the seismic inverse problem. These works established a mathematical basis for some of the algorithms used in seismic imaging. Thereafter, many more applied mathematicians and theoretical physicists became involved in research on this problem. Within five years of that work, the SEG Annual International Meeting hosted multiple sessions and workshops on the topics generated by these papers.

Jack's skill as an innovator was not limited to the theoretical aspects of his work. Jack saw a need for a line of seismic processing software that would be freely available to everyone. Starting with a handful of codes written by members of the Stanford Exploration Project, with the help of Shuki Ronen, Jack created the Seismic Un*x, or SU package. This was long before the words e-mail, Internet, or free software entered the public lexicon. Today, the CWP/SU Seismic Un*x package is freely distributed on the Internet. The package now includes more than 380 individual modules which

permit the user to perform many of the common seismic data manipulation tasks, as well as provide an environment for the development of new seismic software applications. Currently, there are more than 900 known installations of SU.[2] The package is used by petroleum exploration companies, government research facilities, and education institutions in more than 37 countries. Many users are well beyond the seismic exploration community.

Jack developed an expertise in symbolic mathematical languages, particularly *Mathematica*[3] With a colleague, Frank Hagin, Jack co-authored five versions of a textbook integrating symbolic math software into an undergraduate calculus program. This interest led Jack to become editor of the Classroom Notes column in *The Mathematica Journal.*

Jack mastered the subject of wavelet transforms and provided the world community with free wavelet software packages written in the Mathematica language.

Jack also became interested in seismic anisotropy and contributed several important papers on this complicated subject. His work has provided a solid mathematical basis for some existing inversion methods for anisotropic media and stimulated new research in anisotropic moveout modeling and parameter estimation.

Jack's broad spectrum of interests spanned the subjects of classical literature, impressionist art, folk music, jazz, and Brazilian music. He was always ready to try new things, both scientific and nonscientific. He learned to ride a bicycle at age 37. He was an avid hiker and cross-country skier in his early years in Denver. Somewhat later, he started body-building, an activity that he maintained up to the time of his death.

Jack was a compassionate humanist, with a great love of mankind. He was popular in the classroom and known for having an off-beat sense of humor. At one of the first workshops on inversion at SEG's 1982 convention, a colleague asked him for a simple explanation of inversion compared to the more accepted "migration" of the geophysics community. Jack promptly proceeded to rattle off a list of the then-proponents of inversion and said, "Don't you see? Inversion is Jewish migration!"

He is survived by his wife Diane and daughter Mara. In his memory, Colorado School of Mines has established the Jack K. Cohen Memorial Fund for undergraduate scholarships. Donations may be sent to the Colorado School of Mines Foundation, 931 16th Street, Golden, CO, 80401.

Norman Bleistein
John W. Stockwell, Jr.

---

[2] As of August 2000, there are more than 2000 verified installs, in 54 countries.

[3] Mathematica^{TM} is a trademark of Wolfram Research.

Contents

List of Figures

1

Multidimensional Seismic Inversion

Our goal is to present a theory for determining the characteristics of the interior of a body based only on observations made on some *boundary surface*. In particular, we are interested in finding ways of *imaging* structures inside a body. In addition to imaging, we have the more ambitious goal of actually determining values of certain *material parameters* characteristic to these structures. This problem is encountered in many branches of applied science. These include such diverse disciplines as Earth science, medicine, materials science, archaeology, and the ocean sciences—just to name a few. These disciplines all face the same problem of mapping structures in environments where it is either impossible or impractical to make direct observations.

A complete treatment of this broad subject would require a discussion of a wide variety of techniques and physical settings. We can limit the scope of the discussion, however, by identifying one common physical characteristic that may limit the effectiveness of the many possible techniques—the *length scale* of the targets being studied. Different applications have different characteristic length scales. For example, three important geophysical applications that have widely differing characteristic length scales are *solid-Earth geophysics*, *exploration geophysics* (in particular, *seismic prospecting* surveys), and *engineering geophysics* applications. Solid-Earth geophysicists are interested in mapping the entire volume of the Earth, whose scale is several thousand kilometers, with the goal of imaging structures on the order of a few tens of kilometers to a few hundreds of kilometers in size. Exploration geophysicists are interested in mapping structures that are localized to a few kilometers in extent, with the desire of locating hydro-

carbon deposits measuring a few hundreds of meters to a few tens of meters. The scale of engineering geophysics surveys covers only a few hundreds to a few tens of meters, with the size of the common targets being on the order of a few meters.

The characteristic length scales encountered in medicine and in the nondestructive testing applications of materials science are considerably smaller, with targets of interest ranging from a few centimeters to microscopic size. The distinguishing feature of the methods of this text that makes them applicable to all of these problems is that the wavelengths of the signals in our data are small, in an appropriate sense, compared to the length scale of the physical model.

1.1 Inverse Problems and Imaging

The approaches to solving the imaging problem are as diverse as the physical settings mentioned above. Both active and passive measurements of either static or time-varying quantities may be used for solving this problem. This text, however, is confined to *active* methods that involve the introduction of signals that propagate as waves inside the body. These waves, in turn, scatter from irregularities present inside the body and are subsequently recorded on its surface.

The waves may be acoustic, elastic, or electromagnetic as long as the governing equation is some form of a *wave equation.* Mathematically, this specific type of imaging problem has been successfully treated as an *inverse problem.*

Imagine that we have an equation or a system of equations, written in terms of unknown material parameters, describing the origin and propagation of scattered waves in a medium. We can pose two types of problems with such an equation or system of equations, depending on the type of auxiliary data that we have available. In the classical *direct* problem, the material parameters, boundary conditions, and source mechanism are known, and the wavefield is the unknown quantity to be solved for. This problem is at the heart of any text or course dealing with ordinary or partial differential equations. In mathematical physics, the term *modeling* is usually applied to this subject, with common applications being the subjects of acoustics, fluid dynamics, electrodynamics, or elastodynamics.

In contrast, this text will deal with the *inverse* problem. The available data are the observations of the *scattered wavefield,* that is, the wavefield after it has interacted with the medium.[1] In addition, we may have some sketchy information about the wavespeeds in the interior of the body being

[1]The issues of scattering theory are broad. See Melrose [1995] and Colton and Kress [1983] for different perspectives.

imaged, but this information will always be incomplete. The unknowns to be solved for are the material parameters and their discontinuity surfaces, known as "reflectors."

Fortunately, many of the tools used in solving the direct problem are equally useful in solving the inverse problem. The common techniques associated with solving differential equations and integral equations, including Fourier theory and asymptotic expansions, will play a significant role in our exposition. Thus, we expect the reader to have some familiarity with these topics.

There are many side issues in the inverse-scattering imaging problem that may be lumped under the name "signal processing." These issues arise because the practical problems of data acquisition often involve noise suppression. These techniques, which involve a variety of filtering and deconvolutional processes, are not closely related to the issues that we discuss in this book. Therefore, to concentrate on the fundamentals of the seismic inverse problem, we assume that any corrections in the shapes of the waveforms made through signal processing do not adversely influence the inversion of the data. As a result, our discussions will carry the implied assumption that the waveforms have the shape of bandlimited impulses.

More problematic are the issues of missing data and incomplete angular coverage of the target being imaged. Both of these are important problems in inverse-scattering imaging. If data are not sufficiently finely sampled, then *spatial aliasing* will be introduced. Though a number of techniques for data interpolation have been invented to deal with this problem, no general solution exists.[2] The problem of incomplete coverage is the issue of *aperture limiting* that is discussed in Chapter 4. In each case, we will assume—as a first approximation—that the data are sufficiently well sampled to prevent spatial aliasing, and that targets have sufficient coverage that the large-wavenumber (high-frequency) assumption is not violated.

Fortunately, the techniques described in this book are sufficiently robust that the results "degrade gracefully" when the ideal conditions stated above are not exactly met—as they never can be in the real world. For example, if a surface would be imaged exactly for perfect data, then we seek inverse methods that give only a *slightly* deformed image for *slightly* noisy data, with the error in the image being in proportion to the error in the data.

This concept is well known in applied mathematics. Mathematicians characterize problems as "well-posed" or "ill-posed" according to three important criteria. If a problem (1) has a solution, (2) that is unique, and (3)

---

[2]Though addressing such issues as those involving the approximation of missing data is beyond the scope of this text, the related topics of *offset continuation* and *data regularization* are discussed in Chapter 7 as examples of our general approach to *data mapping*.

depends "continuously" on the data,[3] then it is said to be "well-posed." If the problem does not meet all three of these criteria, then it is said to be "ill-posed." (The term "ill-conditioned" is synonymous with "ill-posed.") The criterion of continuous dependence on data is usually the crucial one and is closely related to the notion of "graceful degradation" mentioned above. While rigorous study of the issue of ill- versus well-posedness is beyond the scope of this text, we must admit immediately that some inverse problems are ill-posed. This includes the seismic inverse problem. See Appendix D for further discussion of this important issue. A general guiding rule for solving such a problem is "Ask only for what you deserve from the data!" Ill-posedness may be built into the mathematics of the problem. If this is the case, the course of action is to make reasonable simplifying assumptions (if possible) to suppress, or remove entirely, the ill-posedness. If the ill-conditioning is related to the characteristics of the recorded data, through the presence of noise, for example, then we know that it is not reasonable to expect to recover all information under these conditions. With knowledge of the characteristics of seismic data, and knowledge of the appropriate mathematics, the goal of creating a seismic inverse theory that "degrades gracefully" can be achieved.

It is important to distinguish between inverse-scattering methods and "generalized linear inversion" methods. Some of these methods are represented by the broadly used term "tomography." As mentioned above, the inverse-scattering method is based on the governing equation (here the wave equation) that produces the recorded data, and is therefore a *full-waveform* inversion method. The simpler tomographic methods rely only on a single attribute of the recorded data such as traveltime or amplitude. By assuming that this attribute can be related to the physical parameter of interest, it is possible to deduce, via a statistical process such as least-squares optimization, the "best" model that would produce the observed data attributes. Unfortunately, there is the potential for confusion because there is a method given the name "diffraction tomography" that is really an inverse scattering method [Devaney and Oristaglio, 1984].

1.2 The Nonlinearity of the Seismic Inverse Problem

If the direct scattering problem is formulated so that the unknown material parameter is represented as a *perturbation* from a known "background" pa-

[3] In the language of mathematicians, the term "data" does not refer exclusively to physical measurements, but may refer to any known quantity that pertains to a given problem. This is often a source of confusion, because many geophysicists use the term exclusively to refer to data collected in the field.

rameter profile, then a wavefield representation is obtained that is the sum of a term that depends linearly on the perturbation in the medium parameters plus a term that depends nonlinearly on those parameters. The linear part of the field may be loosely interpreted as that part of the scattered field largely composed of once-reflected waves, while the nonlinear part may be thought of as being largely composed of the combined effects of multiple reflection. This second term is the product of the unknown perturbation and the unknown scattered field at depth—in this case, this product is the mathematical representation of the nonlinearity in the physical problem. If this second term can be assumed to be small, then it may be ignored in favor of the linear term. The linearized inversion formula that is obtained from the linearized solution to the direct scattering problem may be thought of as a *back-propagator*, in that it approximates a reversal of the process that propagated the signal from the scatterers to the receivers. Here, we are assuming that the signal consists only of single-scattered arrivals. The effect of the inversion formula is to take a collection of time-varying data recorded at positions on the surface of the Earth and convert it into a map of estimated parameter values in the Earth's interior.

This process provides an approximate *image* of the interior structures of the subsurface. Because the back-propagation process is performed using a formula based on the wave equation, the amplitudes of the waveforms on this image can be related to the variation of the Earth parameters from their assumed background values. An important result of this theory is that a relationship can be established between these amplitudes and the *reflection coefficients* of reflector surfaces in the Earth.

Finally, we should note that there are full waveform inversion methods that address the nonlinearity of the inverse problem through optimization. See, for example Mora [1987], Symes [1990], Tarantola [1987], and Sabatier [1987] .

1.3 High Frequency

The mental picture of the solution of the inverse-scattering problem, represented as an *imaging* problem, is based on a "geometrical optics" approach to wave theory. For example, the data recorded in a seismic survey can be interpreted as being largely composed of primary reflections from sharply defined discontinuity surfaces (reflectors) buried in the Earth. It is these reflectors that are to be imaged.

Much has been accomplished by assuming that the rules governing the scattering of waves from boundaries in the real Earth are, as a first approximation, the same as the rules governing the scattering of plane waves from plane boundaries between constant-velocity acoustic media. These simple ideas of the reflection and refraction of plane waves may be applied

to heterogeneous media with curved reflectors only when the waves are of sufficiently "high frequency."

The term "high frequency" does not refer to absolute values of the frequency content of the waves. What must be considered is the relationship between the *wavelengths* (or correspondingly the *wavenumbers*) associated with the frequencies available in the data, and the natural *length scales* of the medium. This relationship is naturally stated in terms of *reciprocal wavenumber*, a quantity proportional to the wavelength of some relevant reference wave. In order for the data to be called "high-frequency data," the length scales of interest in a medium must be "many" (in practice, at least three or π) times as large as the predominant reciprocal wavenumber propagating in the medium (length-scale $\geq \pi$/wavenumber $\leftrightarrow$ length-scale times wavenumber $\geq \pi$). When considering the resolution of closely spaced reflectors (delineating the top and bottom of a rock unit), for example, the high-frequency condition translates roughly into the familiar Rayleigh criterion for resolution (bed thickness $\geq$ wavelength/4).

As stated earlier, the theory does not fail catastrophically if the high-frequency condition is not exactly met. Failure of the theory takes the form of incorrectly predicted amplitudes and a growing error in the location of reflectors. The minimum sizes that can be imaged is often expressed as a fraction of the characteristic wavelength that is available for imaging. A typical criterion for the resolution of narrowly separated beds is $L = \lambda/4$, where L is a physical length parameter and λ is the wavelength of the characteristic signal; however, because of the graceful failure of the theory, it may be possible to detect (without actually being able to resolve) narrow separations of perhaps as little as $L \approx \lambda/12$.[4]

Under the high-frequency approximation, the propagation of wave energy may be modeled approximately as the propagation of "wave packets" along definite paths called "rays." The wave packets, in turn, define definite surfaces called "wavefronts." Simple scattering mechanisms such as reflection, refraction, and transmission as governed by Snell's law may be used to describe the interaction of waves with smooth portions of the reflector. In addition, the geometrical theory of diffraction can be used to successfully model wave interaction with the edges of reflector surfaces, or a variety of other situations in which the simple approximations derived from modeling wave propagation as the interaction of plane waves with planar interfaces is too simplistic.

Mathematically, the high-frequency approximation implies use of *asymptotic* methods to create high-frequency formulations of the forward and inverse problems. At our disposal are a collection of well-established re-

[4]The value of $\lambda/12$ was obtained empirically by one of the authors using the *Ames Package* to model pinchouts and likely represents an extreme that is unattainable in the real world.

sults that we use frequently. These include a small-perturbation assumption called the *Born approximation*, a high-frequency asymptotic result called the WKBJ-approximate Green's function, and an assumption relating high-frequency incident and scattered fields called the *Kirchhoff approximation.* An important method for finding approximate analytic solutions of Fourier-like integrals, called the *method of stationary phase*, will prove to be an invaluable tool for testing inversion formulas, as well as for extending those formulas to specific applications.

1.4 Migration Versus Inversion

Our primary interest is the formulation of inversion theory with application to the problem of seismic exploration.[5] The petroleum industry relies heavily on seismic imaging techniques for the location of hydrocarbons. It has been the fashion in the industry to distinguish between two classes of techniques called, respectively, *migration* and *inversion.*

Migration began as a graphical method [Hagedoorn, 1954] for interpreting analog seismic data,[6] based on applying the simple rules of geometrical optics, which is equivalent to making a *high-frequency* assumption. The problem was further simplified by considering the Earth to be a multilayered fluid, rather than a fully elastic medium. We may illustrate the basic idea by considering a simple example of seismic data recorded over a single interface between two media having different constant wavespeeds. The multilayer fluid assumption means that the wave propagation is governed by scalar wave theory. Thus, the waves are compressional, or P-waves, as these waves are called in seismology. A further simplifying assumption is that the P-wave source and the seismic receiver are located at the same place on the Earth's surface. Common names for this recording geometry in geophysics are *zero-offset* or *backscatter*, with the terms "monostatic" or "pulse-echo" being commonly used in other disciplines. This simple recording geometry is not the only possible one, by any means.

We can deduce the approximate appearance of the recorded data by applying the rules of geometrical optics, which describe waves through the geometrical constructions of raypaths and wavefront surfaces—all high-frequency concepts. Under these rules, the reflections from smooth portions of reflector surface differ markedly from those from "corners" or discontinuities of the slope of the reflector surface. The requirement that incident and reflected ray angles must be equal means that only rays normally (per-

[5] See Dobrin [1976] or Telford et. al [1976] for an introduction to the exploration seismic method.

[6] See Hagedoorn [1954] and Musgrave [1961], or Slotnick [1959] for further information regarding classic analog interpretation methods.

pendicularly) incident on the smooth portions of the reflector will return a signal to the receivers. If the scatterer is an isolated point, an edge, or a corner, however, energy will be backscattered along any ray that impinges on it. The more a reflector deviates from being a planar surface, the more complicated the pattern of the scattered waves. Repeating such an experiment many times along a straight line on the surface of the model produces a line profile of data that can be used to create an image of the "vertical slice" through the Earth that the model represents. The result of making such a line profile may be seen in Figure 1.1. The transverse coordinate is the location of each coincident source-receiver pair; the vertical axis is time. The response to an impulsive source (represented by a "wiggle trace") is drawn vertically at the source-receiver coordinate. Deviations to the right of vertical represent the positive amplitudes of the returned signal; deviations to the left are the negative responses.[7]

There is coherence visible in the ensemble of responses from all source-receiver pairs. In fact, the data display represents a crude image of the subsurface. However, this data-image of the subsurface is markedly different in appearance from the model in many respects. Because we want the image to look as much like the model as possible, the need for processing the data is apparent. The complexity of the data occurs because few of the reflected arrivals come from points on the reflector surface directly below the points where the data were recorded. While it is true for a constant-wavespeed medium that equal traveltime implies equal distance of travel, the *direction* from which each ray has come is not specified. Thus, traveltime on the seismic section cannot be *directly* translated into depth in the model. The question is this: What process can put the arrivals in their proper x, z positions of origin on the reflector surface as to correctly map the reflector?

The vertical axis on the seismic section, such as Figure 1.1a, represents two-way traveltime. This is the time that it takes for the signal to travel from the source at the top of the model down to a reflecting position in the Earth model and return to the receiver, which, for this example, is located at the same place as the source. We have to translate these times into distances by assuming a wavespeed for the upper medium. If we scale the time on the time section by half the wavespeed, then the vertical "length" on that section will be exactly the same as the depth of the original model. Note, for example, that the location of the nonzero part of the leftmost data trace of the time section in Figure 1.1a is almost exactly the same as the depth to the nearly horizontal left end of the reflector in Figure 1.1b. This is a consequence of the particular scaling that we have used in these two plots and allows us to view scaled time and vertical distance interchangeably for

[7]The exploration seismic community also uses the *variable area* display, in which the area between each wiggle trace and its respective zero line is shaded black for one polarity of response.

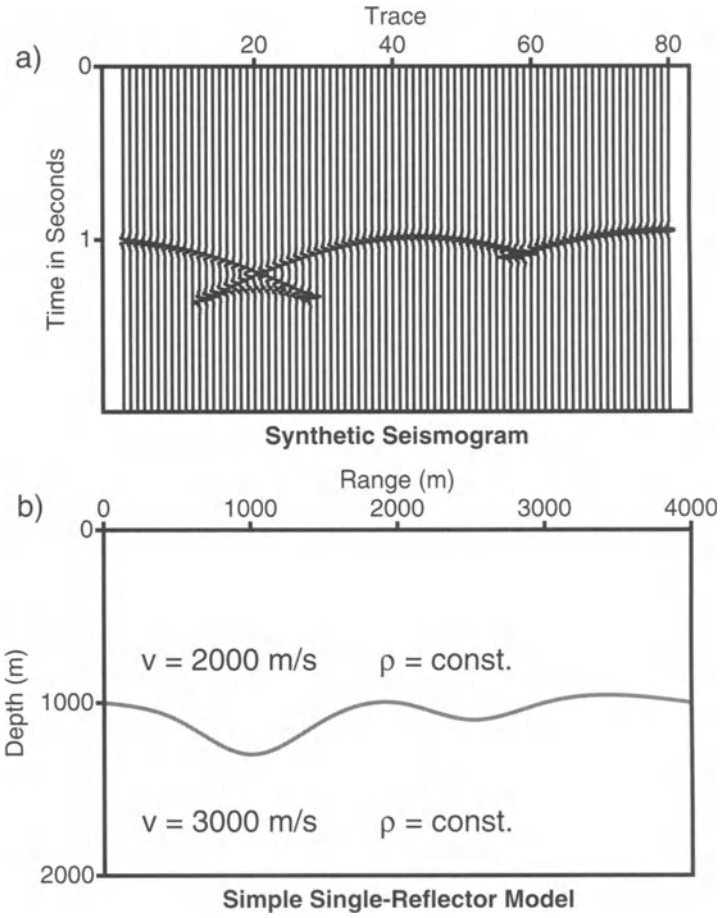

FIGURE 1.1. a) A synthetic *zero-offset* seismic section and b) the Earth model. The synthetic was made with the program CSHOT.

graphical purposes. (Of course, this assumes that we know that wavespeed!) Indeed, if all of the reflections propagated vertically up to the surface, then the scaled time plot would be a graphic display of the (horizontal) reflector that produced the time section. However, the propagation is not vertical, so we have to do better.

Each pulselike signal on a seismic trace is called an "arrival" or an "event." Unfortunately, there is no information about the *direction* from which the signals traveled to get to the receiver, so we cannot specify the reflection point based solely on data from a single seismic trace. Only if the reflector is horizontal will the seismic arrival on this scaled time plot

correspond to the reflector location. In our constant wavespeed example, if we don't know the actual location of the reflector, the best we can say is the following: (i) the reflection point lies on a semicircle centered on the source-receiver position; (ii) the radius of that semicircle is equal to the distance computed by multiplying the traveltime of the event by half the wavespeed of the medium; (iii) the reflector must be tangent to that semicircle at the reflection point so that the ray trajectory is normal to the reflector, as noted earlier.

In Figure 1.5, we show such an ensemble of circles for the time section in Figure 1.1a. A complication to note is that the arrivals are not single spikes—they are wave packets consisting of wiggles that oscillate for a few cycles. If we do not know the exact time history of the source, then there is an uncertainty as to which peak or trough of the wiggle will give us the correct radius for the semicircle of possible reflector locations. In this particular example, we will assume that the largest peak of a given wave packet represents the correct arrival time.

As in the specific example of Figure 1.5, a pattern emerges from the graphic display of the ensemble of semicircles. It is a small leap to realize that the actual reflector is the *envelope* of the ensemble of semicircles. That curve shares a normal direction and "correct" two-way traveltime with each of the semicircles and, hence, matches the observed data at every observation point. (See Exercise 1.1, Figure 1.5 and Bleistein [1999].) Thus, the reflector will be "reconstructed" by exploiting the simple ideas of the geometry of normal reflections. Admittedly, this example contains many oversimplifications, but it represents the fundamental ideas behind migration.

By constructing a *wavefront chart* fitting a particular subsurface velocity model, arrivals can be moved graphically or *migrated* to their correct position on the seismic section. Though the days of analog data and graphical solutions are over, the same ideas have been implemented through both time-domain and frequency-domain methods for processing digital seismic data. Modern migration addresses the traveltime issue by a direct consideration of the wave equation.[8]

Thus traditional migration solves the first part of the inverse problem by considering traveltime to be the only important parameter. The reflector is imaged, in the sense that its position and shape are more correctly represented, but there is no attempt to recover information about the material parameters of the subsurface. This difference in approach represents the major distinction between "migration" and "inversion."

---

[8]Historically important migration papers may be found in Gardner [1985]. Another perspective on seismic migration can be found in Claerbout [1985]. See also Stolt [1978] and Schneider [1978].

To the early migrator, discussions of true amplitudes were moot because of the difficulties of controlling the source and in calibrating the seismometers. Therefore, in the mind of the early migrator, the output of a migration procedure was a *processed seismic section*, as opposed to a *subsurface parameter image*. Consequently, early digital migration schemes were not consciously designed to deal with the issue of true amplitude recovery. All that changed in the early 1970s when the technique of identifying gas-bearing strata by apparent high-amplitude *bright spots* on seismic sections was established. Current interest in amplitude-versus-offset (AVO) measurements for the determination of specific reservoir characteristics has provided further incentive for true amplitude recovery.

The distinction between migration and inversion has blurred in recent years as the more modern approaches to migration *do* attempt to address the amplitude issue. This change was not as difficult as might be thought, thanks to the serendipitous discovery that relative amplitudes are handled correctly, in an inversion sense, by some migration algorithms. This happened because using the wave equation to directly handle the traveltimes has the by-product of handling the amplitudes more correctly as well.

It should be noted with caution that the effects of linearization and the high-frequency assumption are present in migration, just as they are in the inversion techniques we develop in this text. For example, if we were to apply Hagedoorn's graphical migration method to the data in Figure 1.1a, we would draw semicircles that are based on some assumed (constant) background wavespeed profile. Even when this background is taken to be heterogeneous and the semicircles are replaced by more general arcs, the data will be "back-projected" over reasonably accurate curves only if the assumed background wavespeed is approximately the same as the true wavespeed. Thus, a "small perturbation" assumption is hidden within the migration process. Furthermore, migration is based on the ideas of wavefronts, reflectors, and raypaths—all concepts of high-frequency wave theory. These same assumptions appear in the derivations of the inversion formulas in this text. Therefore, it will be a further goal of our text to show how the geophysical "common sense" that is the basis of migration translates into the mathematical assumptions that must be made to derive modern inversion formulas.

As currently implemented, both migration and inversion only partially "invert" the data, because producing images is still stressed over parameter estimation. Accurate background or first-guess wavespeed models are needed if accurate images of the subsurface are to be generated. In response to this need, the seismic exploration community has devised a collection of statistical techniques to do *velocity analysis*. As we will show in this text, velocity information *can* be extracted from the amplitudes of the inverted data under ideal conditions. Owing to the inherent limitations in seismic recording geometries, deficiencies in theory, and the general incompleteness and noisiness of seismic data sets, this information has not been widely ex-

ploited as yet. The quality of the data is simply not yet good enough (but is steadily improving!) to make the amplitude of the output reliable for parameter estimation in most applications in seismic exploration. At best, we can hope to handle relative amplitudes more correctly for such applications as AVO. Inverse-scattering imaging as applied in other disciplines—for example, in nondestructive testing or medical imaging—does not suffer to the same degree from the data limitations we have mentioned. The data in those applications of inverse methods are of higher quality because of the greater control that the experimenter has over the data acquisition process, meaning that greater information about the body being imaged should be recoverable—to the extent that data quality limits the inversion process.

The migration/inversion techniques developed in this text lead, in a natural way, to the process of *migration velocity analysis.* While we do not discuss migration velocity analysis in depth, we will see that a partial inversion can be achieved by studying a limited subset of the data from a seismic survey. Because there can be considerable redundancy between different subsets of such data, it is possible to build multiple images of the same target reflectors. By analyzing the degree to which the different images agree and disagree, we can judge the accuracy of the assumed background velocity that was used for to do the migrations.

The extent of disagreement between such redundant images provides a basis for a technique for correcting the back-propagation velocity which, in turn, will improve the image. Thus, we can generate a background wavespeed that best focuses the images of reflectors. We expect that this "imaging velocity" will be a better representation of the actual wavespeed in the Earth.

1.5 Source-Receiver Configurations

The simple model of a seismic survey discussed in Section 1.4 described an ensemble of data acquired using a *zero-offset* recording scheme, in which the source and receiver are located at the same point on the Earth's surface. Unfortunately, in real seismic experiments it is not possible to use this simple shooting geometry because of persistent high amplitude reverberations associated with the typical explosion, airgun, or vibrator sources used in seismic exploration. Previously, we spoke of the hierarchy of complexity of propagation speeds. Now we consider another hierarchy of complexity, that of recording and data sorting geometries. Seismic surveys are limited to ensembles of experiments with a nonzero offset between sources and their respective receivers. Each of the experiments composing the ensemble usually consists of an arrangement involving one source and many receivers, all in a line, or in a surface array, called a *shot profile.* While all data are

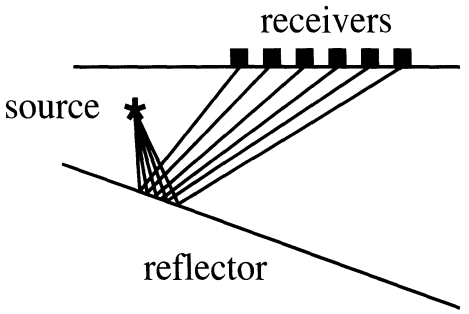

FIGURE 1.2. Schematic for a *common-source* (-shot) seismic profile.

recorded in some form of this geometry, different ways of sorting the data imply different geometries for analysis.

Therefore, a discussion of the different sorting geometries is warranted. The various sorting techniques are usually referred to as *gathers*. We list some common ones below.

Common-source gathers, also called Common-shot gathers, consist of seismograms recorded at many recording positions with increasing range (offset) from a single source.

Common-offset gathers consist of collections of seismograms whose respective source-receiver separation is a constant value.

Common-midpoint gathers, abbreviated as CMP gathers, refer to collections of data, recorded with different source-receiver spacings, but with the same position on the Earth's surface being the midpoint of the source-receiver pair. These are often referred to as common depth point (CDP) gathers in the literature, although, but for rare exception, the reflection depth point in such data is the same only if the reflectors are horizontal and the propagation speed is laterally invariant.

Common-receiver gathers are data sets representing a geometry similar to the common-source gathers, but with many sources and a single receiver.

Each of these implied geometries or gathers has its unique advantages and disadvantages. For example, common-source data have the advantage that a

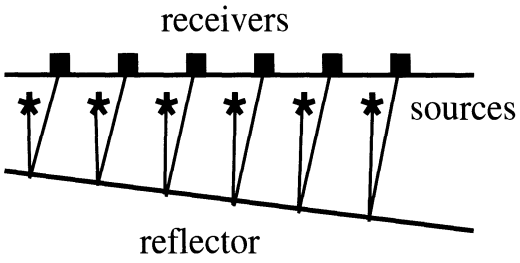

FIGURE 1.3. Schematic for a *common-offset* seismic profile.

single wave equation represents the experiment. Indeed, this is how seismic data are usually collected in a survey, as a collection of common-source gathers, obtained by moving the source and array of receivers along a line, or over an area on the surface of the Earth. The positions of the source and receivers are changed in a systematic way so that overlapping coverage of the subsurface is obtained by the ensemble of the gathers.

For the alternative gathers listed above, each source-receiver pair comes from a different experiment. This is because traces from different common-source gathers in a survey are sorted to produce these other data sets. Thus migration or inversion of these other gathers consists of processing data generated by a collection of different "problems for the wave equation," where the sources and receivers are *different.* Though pains are taken to make the source and receiver responses consistent from shot to shot, there is nothing that says that everything is exactly reproduced from one seismic experiment to another. Thus, there may be effectively a different wave equation operating for each source-receiver gather. Therefore, there is an implied assumption that the solutions to these different wave equations are mutually consistent in a way that will allow data from different experiments to be combined to synthesize a solution of a *single* problem for a single wave equation.

It should be recognized that vertical seismic profiling (VSP), as well as cross-hole (crosswell) seismic experiments, may also be viewed as consisting of ensembles of common-source experiments. The latter geometries are used primarily for *tomographic* imaging, rather than for the inverse scattering that will be discussed in this text. The exception again is diffraction tomography, which *is* a special case of inverse-scattering imaging.

The CMP geometry is important because it provides a collection of data sets that can be used to construct an approximate zero-offset profile. This is possible because all traces of a CMP gather sample approximately the same zone of reflectors in the subsurface. The primary differences among traces within a CMP gather are in reflection traveltimes because the seismic waves have traveled over different distances for different source-receiver offsets in the gather. The systematic traveltime increase caused by a systematic increase in source-receiver offset is called *moveout*, with that seen in the special case of constant wavespeed being called *normal moveout* (NMO). To make an approximate correction for NMO, an estimate of the true wavespeed profile is needed.

By using well log data or by performing *velocity analysis*, which is to say using successive NMO processings or migrations of a CMP gather (or migrations of a range of CMP gathers) with different assumed wavespeed profiles, it is possible to create such a wavespeed estimate. After the NMO correction is performed, the data are summed or "stacked" for each CMP gather. The resulting *stacked section* has the appearance of a zero-offset seismic section with each equivalent source-receiver position located at the midpoint coordinate of the corresponding CMP gather.

The great benefit of stacking is that noise is suppressed and signal is enhanced. However, some information is lost due to stacking because the NMO correction only partially transforms the CMP traces into zero-offset traces. In particular, the higher frequencies of the data may be suppressed by stacking. This is because the arrivals may not be exactly aligned before stacking, causing the stacking process to sum higher frequency components out of phase.

As might be guessed, this misalignment comes, in part, from the traditional NMO correction procedure, which is built on the assumption that the moveout paths are hyperbolic in shape. This is only true for a single horizontal reflector overlain by a constant-wavespeed medium. As we know, the real Earth is better modeled as an anisotropic elastic medium containing dipping layers, curved reflectors, and lateral velocity variations. These are not handled correctly by traditional NMO processing. Modern attempts to deal with this problem include moveout corrections for nonhyperbolic moveouts.

Simply stacking NMO corrected data has the effect of enhancing information about events with near-horizontal dips at the expense of information pertaining to steep dips. This is caused because the offset of source and receiver imposes a wavenumber filter on the data. To preserve information at steep dips, *dip moveout* (DMO) correction algorithms were created. However, the DMO correction is also not perfect, as it does not preserve the amplitudes in the data and will also typically suffer where the medium is laterally varying.

In reality, when we correct a CMP gather for moveout, what we really are trying to do is to find an algorithm that will perform a *transformation to zero-offset* or TZO correction. Such an operation is an area of current research and is discussed as a special case of the *data mapping* theory presented in Chapter 7 of this text. In any case, an important by-product of the NMO-DMO correction process is an improved velocity analysis technique that is useful in choosing background-wavespeed profiles for the migration/inversion process.

If CMP data are satisfactorily preprocessed via NMO followed by DMO corrections, then the data may be stacked with a minimum of information loss, though there may be amplitude distortion where amplitude varies with offset. The resulting seismic section, composed of stacked CMP gathers, may be migrated as though it were true zero-offset data. Despite any disadvantages discussed above, the migration of DMO corrected data provides substantial noise reduction and often provides a sufficiently accurate image of subsurface structure. Furthermore, because the volume of data is substantially reduced by the process of stacking, the migration of DMO-corrected data provides an economical alternative to processing unstacked data.

The above outline of seismic processing steps describes a process called *poststack migration* or *poststack inversion.* A summary of the basic steps involved in poststack migration/inversion may be stated as follows:

1. Seismic data are sorted into CMP gathers.
2. A deconvolutional process is applied to remove the bandlimiting and phase distortion in the waveforms.
3. The data are corrected for the different reflection times associated with differing source/receiver offsets by applying an NMO correction. The data may be corrected for the reflection-time distortions associated with both offset and reflector dip by applying a DMO correction.
4. The results are summed to produce an approximate zero-offset stacked section.
5. The zero-offset migration/inversion algorithm is applied to the stacked section.

Unless these processes are carried out in an amplitude-preserving manner, the amplitudes of zero-offset inversion of these data no longer will be accurate, possibly improving the quality of the image at the expense of the parameter information. Such inversions may still provide useful qualitative information about reflection intensity and parameter changes across reflectors, however.

The issue of moveout correction may be avoided if a *prestack* migration or inversion process is used instead of the poststack process. The prestack process preserves more of the high-frequency information of the seismic data, but is more expensive because each data gather must be migrated or inverted separately. Neither prestack nor poststack migration/inversion will produce a "true" reflector map of the Earth's interior unless the background velocity used is the correct velocity of the Earth. Of course, if the true subsurface wavespeed profile were known, then the inverse problem would essentially be solved, and we would have no further work to do!

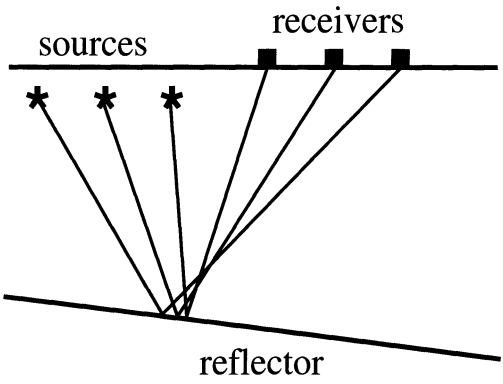

FIGURE 1.4. Schematic for a *common-midpoint* seismic geometry.

Because we can never know the true velocities, the best we can hope for is to create procedures that provide *improved estimates* of the wavespeed profile. Seldom does a first effort of an inversion or migration produce a total success. Nevertheless, the output of a particular inversion often yields clues on how the assumed background model can be changed to improve the results. Thus, migration/inversion is often a recursive or iterative process, beginning with an approximate background velocity profile and working towards the "true" wavespeeds along with estimation of other parameters, through recursive applications of the algorithm on the data.

The first three chapters of this text address the zero-offset source-receiver configuration. Using these inversion methods, it is possible to invert approximate zero-offset data in homogeneous media to obtain an image of the subsurface with the reflectors being mapped as impedance discontinuities. If constant density is assumed, these impedance jumps may be interpreted as jumps in propagation speed.

The following chapters will ascend the hierarchy of increasingly complex recording geometries and background wavespeed structures. Here is included the development of methods for inverting common-offset and common-shot data. This is one branch of the hierarchy of complexity. Introducing heterogeneous media takes us onto another branch of the hierarchy of complexity. If the data are sorted into sets of different common-offset profiles, then the inversion of these different data sets can provide enough data to evaluate changes in both soundspeed and density or even more parameters in an elastic medium. Assembling several common-offset data sets is possible because the conventional shooting geometry contains this redundancy of offsets.

More recent work has also included the development of methods for inverting common-offset and common-shot data. This is another branch of the hierarchy of complexity. If the data are sorted into sets of different common-offset profiles, then the inversion of these different data sets can provide enough data to evaluate changes in both sound speed and density or even more parameters in an elastic medium. Assembling several common-offset data sets is possible because the conventional shooting geometry contains a redundancy of offsets.

From the mathematician's perspective, inversion of common-shot gathers is attractive because data coming from a single experiment are governed by a single wave equation. This is not true for data sets that are created by sorting data from a number of experiments. The extent of reflection events observed in a common-shot gather is limited by the range of coverage of the receivers in that experiment. Typically, that range is less than the coverage achieved by the ensemble of experimnets in a complete seismic survey. While a common-offset gather receives information from reflection events over the full range of the ensemble of experiments, it again is an ensemble of single trace responses from a suite of experiments or, mathematically speaking, an ensemble of solutions of the wave equation. The general issue of

combining data from multiple experiments is unresolved, that is, there is no known exact wave equation describing the generation of such an ensemble.

Nonetheless, there are conventional techniques often labeled under the vague name "wave-equation migration," that are applied to such ensembles. One particular method is reverse-time, finite-difference migration made under the assumption that the data recorded on the surface originated from "exploding reflectors." In Chapter 3, we will show that such wave-equation migrations applied to constant-background zero-offset data satisfy the wave equation, but only to two orders in frequency in the high-frequency limit; they are not *exact* solutions to the wave equation. In short, these turn out to be *asymptotic*, rather than *exact* techniques, contrary to the widely held but erroneous opinion of many of members of the geophysical community!

1.6 Band and Aperture Limiting of Data

As the reader may have gathered from the preceding sections, certain assumptions regarding the frequency content of data must be made so that high-frequency inversion formulas based on inverse scattering theory can be created. Because of the limitations imposed by the high-frequency assumption, our ability to resolve structures of a particular length scale is limited by the frequency band that is available.

Many factors contribute to the bandlimited nature of the inverse-scattering problem; some of the more important ones are listed below:

1. The frequency content of the seismic source is related to the finite nonzero *process time*,[9] and physical geometry of the source mechanism. Equally important is the degree of coupling between the source and the propagating medium.
2. The so-called "Earth filter" is, in part, the effect of anelastic attenuation, behaving as an exponential decay with propagation distance as measured in wavelengths. Because high-frequency implies short wavelength (and hence a greater propagation range as measured in wavelengths), the Earth filter, combined with the omnipresence of noise, has the effect of limiting the upper range of the available frequency band. The other limiting factor is the presence of small heterogeneities randomly distributed throughout the interior of the Earth. The heterogeneities scatter the high-frequency energy in an incoherent fashion, preventing an image of gross structure from being constructed with waves of too high a fre-

[9]From the theory of seismic sources, which deals with explosions, airguns, or earthquakes, the frequency content of the source is directly connected to the natural time constant of the source process; this is the "process time." See Aki and Richards [1980] for further discussion.

quency. Thus, *higher*-frequency signals do not always guarantee *better* resolution.

3. The frequency range of the receiver response is limited by the coupling of the detector to the medium. In land-based surveys, the receivers are geophones mechanically attached to the surface of the Earth, usually by means of a spike pushed into the soil. Because the geophone is not rigidly attached to the Earth, bandlimiting associated with natural resonances of the soil-geophone system exists. Detector coupling is less of an issue in ocean seismic surveys using standard hydrophone streamer[10] arrays.
4. The design of the frequency response of seismic detectors is influenced by the desire to limit ambient noise levels present in imaging surveys of any type.
5. To prevent temporal aliasing of the data, analog frequency filtering is used as part of the recording process before the data are digitized.
6. Seismic preprocessing involving deconvolution or other "wavelet shaping" operations used to remove noise (such as water reverberations) may further limit the bandwidth of the data.
7. The stacking of redundant data (such as traces in an NMO-corrected CMP gather, or traces after migration) bandlimits data whenever the background wavespeed assumed for NMO or for migration is incorrect.

While the causes of bandlimiting are complicated, it is satisfactory to treat these processes as the action of a single filter, $F(\omega)$, which will be assumed to have the necessary properties—symmetric real part, antisymmetric imaginary part—to produce a real-valued output. We will see that the area under the curve that describes the real part of this filter is an important piece of information to have, in order to extract parameter information (such as the reflection coefficient) from seismic data.

Bandlimiting in the frequency domain, however, is not the only limitation that must be considered. The recording geometry introduces a filter of its own in the wavenumber domain, which also degrades the resolution of the image created by inversion. We discuss this for a collection of survey geometries in the first part of Chapter 4. This wavenumber filtering, called *aperture limiting*, worsens as the *opening angle*, the angle between the incident ray and the reflected ray, increases. The reflector image becomes fuzzier with an increase of opening angle.

A correction for aperture limiting will arise naturally in the derivation of the seismic inversion formulas that we will discuss. Remarkably, we will

[10]The detector arrays used both on land and at sea have been designed to suppress internal resonances, or to shift the frequency of internal resonances away from desired seismic frequencies. These efforts have worked so well that investigators experimenting with new instrumentation in different environments, such as mines or boreholes, may be unaware of the potential for problems due to such internal resonances.

see that this correction does not destroy important amplitude-versus-offset information, such as the angularly dependent reflection coefficients of reflectors. We will see that it is possible to extract the value of the opening angle, and thus have an estimate of the angularly dependent reflection coefficient, by computing at least two inversions, while simultaneously seeing an economical way of computing these inversions. This capability depends on an underlying assumption that the events we are observing in the output are the result of isolated reflectors in the Earth. In a subtle way, this is part of the *high-frequency assumption.*

1.7 Dimensions: 2D Versus 2.5D Versus 3D

Traditionally, seismic data have been collected along lines that are straight, whenever possible. In such situations, the data sets are effectively two-dimensional. An inversion formulation using a 2D assumption will not recover amplitudes correctly because the assumed amplitude decay will be cylindrical, approximately varying with the square root of propagation distance. In fact, real seismic data are governed by the rules of 3D wave propagation, meaning that the amplitudes will decay with the first power of propagation distance—which is spherical spreading in a constant-wavespeed medium. A 3D inversion of a single seismic line is also inappropriate as there is insufficient data in the direction transverse to the line for such an inversion to work properly. The appropriate formulation should contain the assumptions of spherical spreading, but with only 2D variability of the medium (no variability transverse to the seismic line).

By applying the methods of high-frequency asymptotics to the formulas that we create for three-dimensional inversion, we will be able to reduce these 3D formulas to formulas that are appropriate for 2D data sets, but handle the 3D amplitude variation of the wavefield correctly. Such "2.5D" formulations will be thoroughly discussed in Chapters 3 through 7.

1.8 Acoustic Versus Elastic Inversion

The final, and perhaps most challenging, step in the seismic inversion hierarchy is that from modeling the Earth as a fluid medium with variable parameters, to viewing the Earth in the more physically correct light, as being a variable-parameter *elastic* medium. We have assumed in all of the discussions above that the propagation of P-waves in an elastic Earth may be approximated by an acoustic wave model. The real Earth, however, supports the propagation of both compressional and shear waves. This inversion issue has only been recently addressed by seismic explorationists.

An inversion formulation that makes use of both the P-wave and the S-wave data provides valuable information about subsurface structure and material parameters that is not available from a fluid model. Better estimates of the elastic moduli representing the compressibility and the rigidity of the medium, as well as other information regarding the microstructure of the rock at depth should be obtainable. Even if we work only with P-wave data, anisotropy can introduce errors in the apparent location of seismic reflectors in the subsurface.

If we work with shear waves, then there are additional phenomena encountered. Considerable evidence suggests that the apparent splitting of shear waves (birefringence) observed on seismic sections is an effect of elastic anisotropy, that is to say, the directional dependence of the elastic material parameters of a medium. It is believed that such observations may be used to determine the orientations of systems of fractures in the subsurface, the knowledge of which would greatly aid petroleum engineers in the evaluation of reservoir permeability. The price for this increase in information will be high, as there are difficult mathematical obstacles that must be surmounted in the pursuit of useful elastic formulations. Inversion techniques, formulated from the theory of elastic wave propagation, though currently in their infancy, promise to provide a more complete view of the subsurface.

While the advanced issues of elastic wave propagation are beyond the scope of this textbook, we expect that material we present—though grounded in scalar wave theory—will provide the reader with an important foundation in the mathematical methods necessary to understand seismic inversion, as it is currently practiced, while providing important tools that will carry over into the anisotropic elastic inversion problem.

Exercises

1.1 Using the graphical migration method discussed in Section 1.4, migrate the seismic section, Figure 1.1a. You will need a compass and

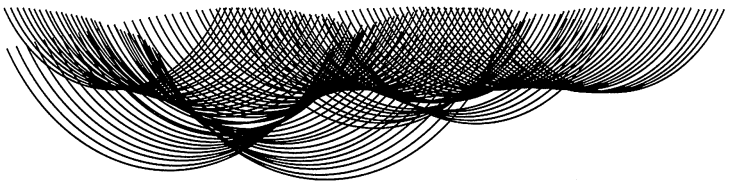

FIGURE 1.5. An example of graphical migration, see Exercise 1.1.

you may wish to enlarge this figure via photocopier. Your result should look something like Figure 1.5.

1.2 Graphically construct a synthetic seismogram using the Earth model in Figure 1.1b. This synthetic should agree with Figure 1.1a.

1.3 Discuss possible strategies for creating a computer program that would perform an operation equivalent to the graphical migration technique discussed in Exercise 1.1.

1.9 A Mathematical Perspective on the Geometry of Migration

At the risk of destroying the nonmathematical festivity of this chapter, let us examine the process of Exercise 1.1 with an eye toward the underlying mathematics, so we may see how that mathematics will recur later in the text. Denote by $(\xi, 0)$ the coordinates along the horizontal upper surface in Figures 1.1a and 1.5, and denote by (x, z) the coordinates in the subsurface in Figure 1.5.

The peak values on the traces in Figure 1.1a denote a two-way traveltime for the normal-incidence reflection from the model reflector in Figure 1.1b. We can denote this input traveltime by $t_I(\xi)$. In terms of the reflection point, that two-way traveltime is given by

$$\tau(x, z, \xi) = \sqrt{(x - \xi)^2 + z^2}/c, \tag{1.9.1}$$

with (x, z) being a point on the reflector and c being the propagation speed. Unfortunately, we do not know that point on the reflector, so we draw a family of semicircles in Figure 1.5 as a representation of all candidates for possible reflection points. That is, for each ξ, we plotted the function,

$$\Phi(x, z, \xi) = t_I(\xi) - \tau(x, z, \xi) = 0. \tag{1.9.2}$$

We then proposed that points on the *envelope* of this family of curves with respect to ξ form a surface for which each point is a normal-incidence point with exactly the correct traveltime to satisfy (1.9.2). Mathematically, given a family of curves $\Phi(x, z, \xi) = 0$, the way we find the envelope is to set the first derivative of Φ with respect to ξ equal to zero, solve for ξ as a function of x and z, and then substitute it back into the equation of the family of curves given by

$$\Phi(x, z, \xi(x, z)) = 0. \tag{1.9.3}$$

The graph of this function is the envelope.

In Chapters 3 and 5, we will develop a general inversion technique for a variety of source-receiver configurations and for variable back-propagation speed. We will then test the inversion formula by applying it to asymptotic data for a single reflector. Both the inversion operator and the model data

will have as part of their structure a complex exponential of the form $\exp\{i\omega\phi(\cdot,\xi)\}$. Integration will have to be carried out over both ξ and ω in order to produce an inversion or migration output.

The inversion operator will have a phase function that will be a generalization of the function, τ. That is, for each ξ, it will propagate the data back to a curve (or surface in 3D), τ = constant, that is the generalization of the semicircles of Figure 1.5. The modeling phase function will be a generalization of the function, t_I, indicating an arrival time of the reflection response for that particular ξ. Thus, the combined phase will be just the function Φ in (1.9.2).

Setting the first derivative of Φ equal to zero is the first step in the *method of stationary phase*, applied to the integral in ξ. Thus, we will approximate that integral by finding the envelopes with respect to ξ of the functions, Φ = constant. The question arises as to how the particular choice, $\Phi = 0$, might be distinguished in that mathematical process. That has to do with the structure of the remaining integral in ω. Stripped of details, that integral is of the form,

$$\gamma(x,z) = \int_{-\infty}^{\infty} F(\omega)e^{i\omega\Phi}d\omega, \tag{1.9.4}$$

with the real part of F being an even function of ω and the imaginary part of F being an odd function of ω. This makes $\gamma(x,z)$ real. Furthermore, the level curves of $\gamma(x,z)$ are the curves, Φ = constant. In particular, the level curve, $\Phi = 0$, is where the peak value of $\gamma(x,z)$ resides.

Thus we could now plot wiggle traces of the output of our operator applied to data, similar to the wiggle traces representing the input in Figure 1.1a. Whereas the peak values of the latter represent arrival times of data at the upper surface, the peak values of the former locate the reflector. Consequently, the plot of the function $\gamma(x,z)$ constitutes *mathematical imaging* of the reflector, an alternative to the geometrical construction here. In Figure 6.5, we have used an intensity plot rather than a wiggle plot for the inversion of model data from a physical model that is similar to that of Figure 1.1a.

This alternative will work in far broader contexts, provided we appropriately define the necessary traveltimes for those applications. Indeed, this *reduction to geometry*, which is the core of the geophysicists' "common sense" approach to migration, is the primary reason that seismic migration methods based on scalar wave theory have worked so well, in spite of the fact that anisotropic elastic effects have traditionally been ignored.

2

The One-Dimensional Inverse Problem

While presenting solutions to the migration/inversion/imaging problem we also intend to familiarize the reader with the philosophy of research that has proven to be effective in leading to these solutions. We hope that the student will benefit from this text both by gaining insights into the specific mathematical issues associated with the seismic inversion problem and by acquiring a "feeling" for how to decide what issues take precedence in the stages of a research project.

In Chapter 1, the hierarchy of geometrical complexity of the seismic inversion problem was outlined. Identifying the natural levels of technical difficulty of a problem is the first important step to finding a systematic approach to its solution. *Clearly, the simplest problems that can be formulated must be solvable for there to be hope of solving the more difficult problems.* This chapter will begin with the problem of inverting plane-wave data in an Earth model with one dimension of parameter variability to produce an image of a single plane reflector. After reading the discussion in Chapter 1, the reader may be surprised that we have chosen such a simple starting point—even the graphical migration technique discussed there is a *two-dimensional* imaging method.

Indeed, while our starting model will have little direct geophysical applicability, it will permit us to introduce some important ideas in a simple context. Those ideas will, in turn, provide motivation for our discussions of the higher-dimensional problems that represent seismic imaging and inversion in the real world. Furthermore, the asymptotic techniques that are presented near the end of this chapter will lead us to similar methods for imaging in *heterogeneous* 2D and 3D media.

Owing to the simplicity of 1D models, more powerful mathematical methods are available to us here than will be available in the multidimensional inverse problem. We will have the power to create an *analytical* solution to our 1D test model. Rarely, beyond the 1D problem, will we have that luxury! In contrast, the complexities introduced by higher dimensions will force us to rely on asymptotic methods to create *approximate* solutions to the problems that we treat in later chapters. In any case, the mathematical concepts that we introduce here will be refined in later chapters to permit us to solve the inversion problem in higher dimensions.

2.1 Problem Formulation in One Spatial Dimension

One-dimensional modeling and inversion theories are of practical interest in situations where data or material parameters have only one dimension of variability. These data may be measurements of a time-independent quantity made in one spatial dimension, or may consist of measurements of a temporally variable quantity that is spatially independent.

Historically, 1D models have played an important role in mathematical physics by providing a starting point for solving higher-dimensional problems; this is how we will employ them here.

2.1.1 The 1D Model in a Geophysical Context

Geophysics has two ready examples of such 1D data sets. A *well log* is an example of a 1D spatially variable, but time-independent data set. An example of a spatially independent but time-dependent data set is a single *seismic trace.*[1]

In the absence of other information, a model with one dimension of parameter variability can be implied by each of these data sets. The problem in the first case is to construct a "synthetic seismogram" from the well log, which is a *forward modeling* problem. In the second case, the problem is to construct the "synthetic well log" that represents the wavespeed profile, using the seismic trace as the input data. This is the corresponding *inverse problem.*

Indeed, comparison of such synthetic traces and synthetic well logs with their real-data counterparts has been an important interpretative tool in seismic prospecting for years. To create a synthetic seismogram from a well log, the geophysicist assumes that a seismic trace on a migrated section can be represented as the convolution of a *wavelet* with a series of spikes,

[1]We will assume that all 3D geometric spreading effects that exist in real seismic data have been eliminated for this example.

each representing an arrival, scaled with the appropriate amplitude composed of the normal-incidence reflection coefficient, and any transmission loss that would be present. The spikes may be primary reflections only, or may include a sufficient number of multiple reflections as are necessary for the specific application. This is called the *convolutional model* of seismic wave propagation and the resulting collection of spikes is called the "reflectivity series." All other attributes of the synthetic trace are delegated to the waveform that is convolved with the reflectivity series to make the synthetic seismogram. The term "reflectivity series," used in the traditional geophysical context must not be confused with the term *reflectivity function* that we use in this text. When we use the term "reflectivity function," we will be talking about, ideally, a spike train with spikes of height equal to the reflection coefficients of the reflectors in the seismic model, placed at positions corresponding to the positions of the reflectors. For the example we are discussing here, these spike heights would be the normally incident reflection coefficients, which is what we would like to see as the output from a "perfect" migration or inversion of the seismic data. See Figure 2.1.

If the seismic data have been migrated correctly, then the synthetic trace created from the well log should agree with the corresponding trace on the migrated section. While a similar comparison can be made with synthetic well logs, creating such synthetic logs is more difficult. This is because the synthetic reflectivity series must be extracted from the seismic data via a deconvolutional process, multiples must be extinguished, and the heights of the remaining spikes of the reflectivity series must be corrected for transmission loss. The result is the "reflectivity function" discussed above. To complete the process of constructing the synthetic well log, the spike train must be integrated to produce the expected steplike profile. In either case, "stretch" problems may exist owing to incorrect velocity models or logging-tool calibration errors.

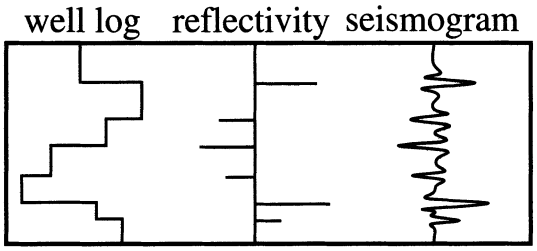

FIGURE 2.1. Cartoon showing a well log, and corresponding reflectivity function represented alternatively as a spike train, and as a seismogram. The reflectivity function differs from the geophysicists' *reflectivity series* in that there are no multiple reflections represented, and the locations of the spikes are the same as the locations of the reflectors. The seismogram form on the right is what we would like a perfect migration to give us.

2.1.2 The 1D Model as a Mathematical Testground

Our interest in 1D models is in using them as a testground for developing a mathematically consistent approach to solving the seismic inverse problem. As we saw in Chapter 1, the early treatment of the seismic imaging problem was based on what might be called "geophysical common sense." It is not our intent to attack the geophysicists' common sense approach, but to support it by providing a solid mathematical structure on which we can build more advanced theories.

Much of geophysical common sense is based on two important assumptions. The first of these is that the process governing wave propagation may be represented in the first approximation as a "linear system." It is this linear-systems approach that is behind the idea of representing a seismic trace as the convolution of a wavelet with a reflectivity series. In contrast, real seismic experiments are subject to complicated behaviors, the most noticeable being *anelastic attenuation*, which degrades the amplitudes of seismic waves exponentially as they propagate.[2]

Another drawback of reflectivity series approach is that while it may be used to represent specific multiply reflected arrivals (if we included more than just primaries, and took into account transmission effects), it cannot be used to represent the general effect caused by the many multiple reflections between layers that are present in real data sets. Again, the reader must keep in mind that the theories we present in this text will assume that data are largely composed of once-scattered waves, called *primary reflections*, and that multiply scattered arrivals compose a less significant portion of a seismic record.

The second assumption is that wave propagation may be represented by the principles of "geometrical optics"—a consequence of the high-frequency assumption discussed in the previous chapter. It is through geometrical-optics ray tracing that the reflection coefficients and the arrival times of the spikes in the reflectivity series are computed.

In the 1D problem, the ray tracing is trivial. In higher dimensions, however, difficulties are introduced by the complexity of the wavespeed profile. An example of such a difficulty is the presence of multiple propagation

---

[2]There are linearized models of attenuation, the simplest being the assumption that material parameters, such as the wavespeed, have complex values, thus yielding an exponential decay that has the appearance of the decay seen in seismic wave propagation. Such models, called "near-elastic models" are justified from laboratory stress-strain measurements, which exhibit a phase delay between stress and strain, when stress is varied in time on rock samples. Near-elastic models cannot be the whole story, because attenuation observed in seismic wave propagation is frequency dependent. In response to this, numerous relaxation models have been proposed, which are also linear models. See Ben-Menahem and Singh [1981], for a discussion of a number of these. For strain values of the order of magnitude of 10^{-5}, stress-strain curves show nonlinear effects; see White [1983] .

paths between source and receiver (multi-pathing) or, conversely, the absence of ray coverage in shadow-zones. Such difficulties can be overcome (at the expense of accuracy) by making simplifying assumptions regarding the smoothness of the model.

2.2 Mathematical Tools for Forward Modeling

The ultimate goal of this investigation is to derive a formula that represents the solution to the *inverse scattering problem.* However, our analysis will begin with a mathematical statement of the *forward scattering problem.* Our specific goal in this section is to create an integral equation that describes the wavefield seen at a specific receiver location due to a source located at a different specified position. It is this integral equation that we will seek to invert.

Formulation of the forward scattering problem requires knowledge of the physics of wave propagation, expressed mathematically as a *governing equation.* The solutions of the governing equation will be constrained by a specific set of boundary (or, for unbounded media, radiation) conditions. The final result will be obtained via application of *Green's theorem.*

For background information in the subject of ordinary differential equations (ODEs), we refer the reader to Coddington and Levinson [1984].

2.2.1 The Governing Equation and Radiation Condition

The formulation of the forward scattering problem will be conducted in the frequency domain for some observable parameter, $u(x, x_s, \omega)$, called the "field." Here, x represents the general field or observation position, while x_s represents the location of the source, and ω represents frequency. The field may represent plane acoustic pressure waves (propagating parallel to the x-axis) in a two- or three-dimensional medium, the transverse displacement of a string in one dimension, or some other equally appropriate parameter that may be represented as a one-dimensional wave. The specific physical meaning of the variable $u(x, x_s, \omega)$ is not important for this exposition. The only important condition is that the propagation of $u(x, x_s, \omega)$ be governed by the scalar Helmholtz equation

$$\mathcal{L}u = \left[\frac{d^2}{dx^2} + \frac{\omega^2}{v^2(x)}\right] u = -\delta(x - x_s), \tag{2.2.1}$$

where we have used the symbol $\mathcal{L}$ on the left as shorthand for the expression in brackets in the middle. The wavespeed of the medium is given by $v(x)$. The forcing function on the right-hand side represents an impulse located at the position $x = x_s$.

The Helmholtz equation is just the temporal Fourier transform of the familiar scalar wave equation,

$$\left[\frac{d^2}{dx^2} - \frac{1}{v^2(x)}\frac{d^2}{dt^2}\right] U(x, x_s, t) = -\delta(t)\delta(x - x_s).$$

In place of frequency dependence, we have time dependence, and for the forcing function, we have a temporal impulse located acting at the position $x = x_s$.

We will assume that u is bounded for all x, and satisfies the conditions

$$\frac{du}{dx} \mp \frac{i\omega}{v(x)}u \to 0 \ , \quad \text{as} \quad x \to \pm\infty. \tag{2.2.2}$$

This expression is called a *radiation condition.* Physically, the radiation condition insures that the primary energy from the source is outward propagating. Mathematically, this condition insures that the solutions to the Helmholtz equation are unique.

2.2.2 Fourier Transform Conventions

An important tool in wave theory for both forward and inverse problems is the Fourier transform. In fact, our inversion formulas will be Fourier transform–like integrals. A discussion of the Fourier transform conventions that we will be using is therefore important.

For example, the choice of signs in the statement of the radiation condition in equation (2.2.2) must be consistent with the signs of the exponents of the exponentials in the respective forward and inverse Fourier transform definitions.

We will use the following forward and inverse temporal Fourier transform conventions,

$$\begin{aligned} f(\omega) &= \int_0^\infty F(t)e^{i\omega t}dt, \qquad \text{forward,} \\ F(t) &= \frac{1}{2\pi}\int_\Gamma f(\omega)e^{-i\omega t}d\omega, \qquad \text{inverse.} \end{aligned} \tag{2.2.3}$$

The reader should note that the limits of integration of the forward transform imply that no data exist for $t < 0$. This is a statement of the physical condition of *causality*; that is, the source is initiated at some finite time that we can take to be $t = 0$. Therefore, we will refer to the forward Fourier transform definition above as the *causal* Fourier transform.

In problems that can be solved exactly, it is common that complex variables methods will be used to analytically evaluate inverse Fourier transforms.[3] The choice of the integration path in such an evaluation is

[3]We refer the reader to such classic texts as Levinson and Redheffer [1970], or Spiegel [1953] for an introduction to complex variables methods.

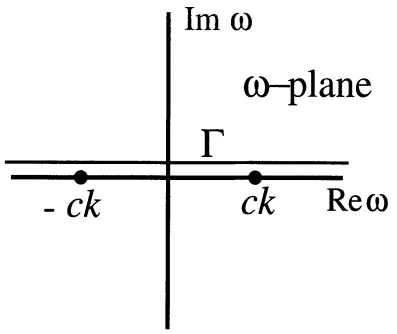

FIGURE 2.2. Sketch of the integration contour Γ, for the case of simple poles at $\omega = \pm ck$.

influenced by the requirement that the result be causal in the t-domain. Therefore, the integral expression for the inverse Fourier transform is represented here as a contour integral, with Γ being the path of integration in the complex-ω plane.

The condition of causality translates into a condition of analyticity in the complex-ω plane, restricting the possible choices for this integration contour. The general rule that we will follow when dealing with causal inverse Fourier transforms may be simply stated. *In causal problems, given the exponent sign convention above,* **Re** ω *ranges from* $-\infty$ *to* ∞ *on the contour of integration,* Γ. *The contour of integration passes above all singularities of the integrand.* (This rule is explained in Appendix B.)

Causal Fourier and Fourier-like integrals appear in many places in this text. Often, we will simply write the integrals as having integration limits of $\pm\infty$, however, the reader should be aware that the rules stated above apply to each of these integrals. See Figure 2.2.

For the transforms of spatially varying functions that are defined on $-\infty < x < \infty$, we will use the opposite exponent sign conventions, represented in the definitions of the forward and inverse spatial transforms

$$f(k) = \int_{-\infty}^{\infty} F(x) e^{-ikx} dx, \qquad \text{forward},$$

$$F(x) = \frac{1}{2\pi} \int_{\Gamma} f(k) e^{ikx} dk, \qquad \text{inverse}.$$

Again, it will be common for us to use complex variables methods to evaluate inverse Fourier transform integrals in problems that have analytical solutions. The result of such an evaluation will be a function that will be defined over the full range of $-\infty < x < \infty$. The integrands commonly seen in wave theoretic problems will generally have more than one simple pole on the real axis. Commonly poles will be the pair of values $\pm k_0$, where $k_0 \equiv \omega/c$, with c being the wavespeed. While the preferred method of solution of such problems is a simple residue evaluation, the fact that there are

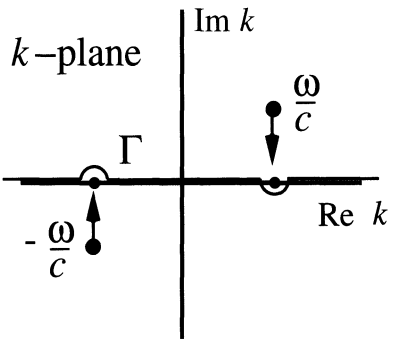

FIGURE 2.3. Sketch of the integration contour Γ, for the case of simple poles at $k = \pm\omega/c$.

multiple poles (or other singularities, for that matter) is a potential source of confusion as it increases the number of possible choices for the path of integration.

Actually, the confusion occurs because the implications of causality are discarded too soon. It is necessary to consider all integrals in k and ω under the condition that **Im** ω is positive. In this case, the poles that would otherwise appear on the **Re** k axis will no longer be there, but will reside above and below that axis. In this case, it is easy to see which poles are avoided by passing below them—those with **Im** k positive—and and which are avoided by passing above them—those with **Im** k negative. Now, when **Im** ω approaches zero, the path in k passes above and below the various poles properly and the solution for **Im** $\omega = 0$ is obtained as an *analytic continuation* of the solution for **Im** $\omega > 0$. See Figure 2.3.

The integration contour Γ is then chosen to pass along the real k-axis, on the interval $-\infty <$ **Re** $k < \infty$, passing above or below singularities as dictated by the analysis just described. When the only singularities are poles, for example, the integral is evaluated by the residue method for the two cases of the closure of Γ in the upper and lower half planes, respectively. The choice is determined by exponential decay of the integrand, which in turn is usually different for x sufficiently positive or sufficiently negative. The two choices will cover the entire range of x values and will combine to form $f(x)$ on the full range, $-\infty < x < \infty$.

Such a result will typically contain a factor of $\exp\{ik_0|x - x_0|\}$ from the residue evaluation of the exponential in the integrand, with the choices of $x - x_0$ positive or negative tying directly to choice of closure of the contour of integration in the upper or lower half k-plane. We have said that k_0 has a small imaginary part, η, such that $k_0 \equiv \mu + i\eta$. This means that the exponential factor will be of the form $\exp\{i\mu|x|\}\exp\{-\eta|x|\}$, ensuring that the solution is either purely oscillatory, or is oscillatory with exponential *decay* (rather than growth), as $|x| \to \infty$. This will occur only if $\eta \geq 0$, which is equivalent to the pole-shifting convention chosen above.

The reader may have some question as to the justification of assuming a complex-valued k_0. In wave problems, $k_0 \equiv \omega/c$, where ω is frequency and c is wavespeed. Some authors (for example Aki and Richards [1980]) make the argument that the possibility of attenuation, expressed through a complex wavespeed, c, is a potential source of this complex-valuedness. It is our preference, however, to consider ω to be complex-valued. Such an assumption is entirely consistent with the discussion of causal Fourier transforms given in Appendix B and does not introduce any new physics into the problem.

2.2.3 Green's Functions

If the problem consisted of the Helmholtz equation, with the wavespeed v = const., then the forward modeling problem could be solved with the information given in the previous three subsections. Given the Helmholtz equation, a set of boundary conditions or a set of radiation conditions (boundary conditions at infinity) for unbounded problems, and the principle of causality, we could find a unique solution for the field u.

When the forcing function (source function) of the Helmholtz equation is an impulse, as in equation (2.2.1), then the solution is a special result called the *Green's function*. In linear systems usage, the terms *transfer function* in the frequency domain or *impulse response* in the time domain are alternate names for the Green's function. For problems with constant coefficients, as in the case of a constant-wavespeed problem, the Green's function can be found analytically for unbounded-media problems by using Fourier transform methods. (A few cases of bounded-media problems can be solved this way, but this is beyond the scope of our discussion.)

Because the wavespeed is not a constant in most geophysical problems, we usually do not have analytical expressions for the Green's function. At best, we can imagine starting with an approximate representation of the wavespeed profile that is arrived at by some other method, for example from velocity measurements made from well logs or from seismic velocity analysis. Our best hope is to use this approximate representation as a first guess, and then solve for a better estimate of the wavespeed profile using our (yet to be derived) inversion formula.

We will, therefore, use approximate Green's functions created by a modeling scheme that uses the first-guess wavespeed profile. If the guessed wavespeed profile is constant, then the exact Green's function for that profile may be used as an approximate Green's function. If the guess wavespeed profile is something other than constant wavespeed, then other methods may be needed to construct the approximate Green's function. For example, the wave equation can be solved by the finite-difference method or, as emphasized in this text, an asymptotic method such as *ray theory* may be used to construct the approximate Green's function.

2.2.4 Green's Theorem

Though we are interested in solving the 1D problem for the specific example in this chapter, it will be beneficial for subsequent chapters to discuss the more general problem for an arbitrary number of dimensions.

From the discussions so far, we have a governing equation that describes a particular wave propagation problem, with a given source function. The field in this equation is unknown. As auxiliary information, we have boundary (or radiation) conditions and the Green's function for the medium.

The forward modeling problem may be stated mathematically as two equations

$$\begin{aligned} \mathcal{L}u(\boldsymbol{x}) &= -f(\boldsymbol{x}) \\ \mathcal{L}g(\boldsymbol{x}, \boldsymbol{x}_0) &= -\delta(\boldsymbol{x} - \boldsymbol{x}_0). \end{aligned} \tag{2.2.4}$$

Here, the boldface of $\boldsymbol{x}$ and $\boldsymbol{x}_0$ indicates that these are vector quantities. The first equation describes the unknown field $u(\boldsymbol{x})$ in terms of a known source $-f(\boldsymbol{x})$. The second equation describes the Green's function $g(\boldsymbol{x}, \boldsymbol{x}_0)$ for the problem, which is assumed to be a known quantity. The $\mathcal{L}$ for our problem is the Helmholtz[4] operator.

Our plan is to create an integral-equation representation for the field $u(\boldsymbol{x}_0)$, using the information from the source $-f(\boldsymbol{x})$ and the Green's function $g(\boldsymbol{x}, \boldsymbol{x}_0)$, while taking into account any boundary conditions that may be present. Here, the location $\boldsymbol{x}_0$ is a distinguished location in the medium, which for our purposes will be identified with the position of a recording instrument.

If the $\mathcal{L}$ is the Laplacian, ∇^2, we can combine the left-hand sides of equations (2.2.4), and integrate the result to form Green's theorem,

$$\begin{aligned} &\int_D [g(\boldsymbol{x}, \boldsymbol{x}_0)\nabla^2 u(\boldsymbol{x}) - u(\boldsymbol{x})\nabla^2 g(\boldsymbol{x}, \boldsymbol{x}_0)]dV \\ &\qquad = \int_D \nabla \cdot [g\nabla u - u\nabla g]dV \\ &\qquad = \int_{\partial D} [g(\hat{\boldsymbol{n}} \cdot \nabla)u - u(\hat{\boldsymbol{n}} \cdot \nabla)g]dS. \end{aligned} \tag{2.2.5}$$

Here, D is the domain or volume of the problem and ∂D is the bounding surface. The surface integral has been created using the divergence[5] theo-

---

[4]The Green's theorem method that we outline here is generally applicable to many problems in mathematical physics. Examples of other equations that might appear in such a formalism include the *Laplace*, *Poisson*, *Schroedinger*, and *heat* equations. See Morse and Feshbach [1953], Butkov [1968], or other mathematical physics texts for additional information about the Green's-function method.

[5]The reader should note that in 1D the divergence theorem reduces to simple integration by parts, with the "boundary" term being the part that is evaluated

rem. The expression $(\hat{\boldsymbol{n}} \cdot \nabla)$ is the derivative normal to the boundary ∂D and will often be written as $\partial/\partial n$. Here, $\hat{\boldsymbol{n}}$ points in the outward direction from ∂D.

By applying equation (2.2.4), we solve for $u(\boldsymbol{x}_0)$:

$$u(\boldsymbol{x}_0) = \int_D g(\boldsymbol{x}, \boldsymbol{x}_0) f(\boldsymbol{x}) dV + \int_{\partial D} \left[g(\boldsymbol{x}, \boldsymbol{x}_0) \frac{\partial}{\partial n} u(\boldsymbol{x}) - u(\boldsymbol{x}) \frac{\partial}{\partial n} g(\boldsymbol{x}, \boldsymbol{x}_0) \right] dS. \tag{2.2.6}$$

Boundary conditions on ∂D consist of specified values for u (a *Dirichlet condition*) or $\partial u/\partial n$ (a *Neumann condition*). If ∂D is at infinity, we call the problem "unbounded" and define a *radiation condition*, as in equation (2.2.2).

Many operators can be substituted for ∇^2 in equation (2.2.6) leaving the form of equation (2.2.6) unchanged (see Exercise 2.2); however, this is not *always* the case. In general, we have to write the problem as

$$\begin{aligned} \mathcal{L} u(\boldsymbol{x}) &= -f(\boldsymbol{x}) \\ \mathcal{L}^\star g^\star(\boldsymbol{x}, \boldsymbol{x}_0) &= -\delta(\boldsymbol{x} - \boldsymbol{x}_0), \end{aligned} \tag{2.2.7}$$

where the $\star$ indicates that a different operator and respective Green's function compose the second equation. The operator $\mathcal{L}^\star$, called the *adjoint* of $\mathcal{L}$, is simply the appropriate operator that will make the integrand in the volume integral portion of Green's theorem an *exact* divergence.

If $\mathcal{L}^\star = \mathcal{L}$ then the operator is called *self adjoint*. We will see that problems governed by the Helmholtz equation are self adjoint, but that problems governed by the *variable-density acoustic* wave equation are not. In any case, the volume integral in Green's theorem takes the form

$$\int_D [g^\star(\boldsymbol{x}, \boldsymbol{x}_0) \mathcal{L} u(\boldsymbol{x}) - u(\boldsymbol{x}) \mathcal{L}^\star g^\star(\boldsymbol{x}, \boldsymbol{x}_0)] dV = \int_{\partial D} \hat{\boldsymbol{n}} \cdot \boldsymbol{Q} dS. \tag{2.2.8}$$

That is to say, we choose or construct $\mathcal{L}^\star$ in such a way as to make the integrand of the integral over D an exact divergence, implying that

$$g^\star \mathcal{L} u - u \mathcal{L}^\star g^\star \equiv \nabla \cdot \boldsymbol{Q}.$$

The $\hat{\boldsymbol{n}} \cdot \boldsymbol{Q}$ term will be a function of $g^\star$ and u, and will contain derivatives of one order lower than the original $\mathcal{L}$ and $\mathcal{L}^\star$. For example, in (2.2.6), $\boldsymbol{Q} = g \nabla u - u \nabla g$. However, it is not always possible to write a neat expression like equation (2.2.6), because there may be parts of $\mathcal{L}$ and/or $\mathcal{L}^\star$ that carry over into the $\boldsymbol{Q}$. While boundary and radiation conditions in such problems will still be written as conditions on u and $\partial u/\partial n$, the surface integral expression may be complicated with derivatives on additional parameters

---

on the endpoints of integration. Conversely, we say that the divergence theorem is integration by parts in higher dimensions.

(such as the wavespeed or density). See Exercise 2.5 for a non-self adjoint problem that is of interest to us—the variable-density acoustic problem.

Exercises

2.1 Prove Green's Theorem, equation (2.2.6).

2.2 Show that Green's Theorem (2.2.6). is also true when $\mathcal{L}$ is the Helmholtz operator,

$$\left[\nabla^2 + \frac{\omega^2}{c^2(\boldsymbol{x})}\right].$$

2.3 Verify equation (2.2.6).

2.4 Specialize the problem to 1D. Assume constant coefficients and an unbounded medium. Show that equation (2.2.6) reduces to the convolution theorem

$$u(x_0) = \int_{-\infty}^{\infty} f(x)g(x - x_0)dx,$$

implying that equation (2.2.6) may be thought of as a generalization of the familiar principle of superposition.

2.5 Let $\mathcal{L}u = \rho d/dx[1/\rho du/dx] + [\omega^2/c^2]u$. This is the 1D form of the *variable-density* wave equation. Show that Green's theorem for this equation is

$$\int_a^b \left[g^\star \mathcal{L}u - u\mathcal{L}^\star g^\star\right] dx = \left[g^\star \frac{du}{dx} - \frac{u}{\rho}\frac{d(\rho g^\star)}{dx}\right]\Bigg|_a^b,$$

where $\mathcal{L}^\star g^\star = d/dx[1/\rho d(\rho g^\star)/dx] + [\omega^2/c^2]g^\star$. (Hint: Integrate

$$\int_a^b g^\star \mathcal{L}u \; dx$$

by parts, twice, to construct the other three terms that appear in Green's theorem.)

2.6 Construct a set of radiation conditions for the variable-density acoustic problem for an unbounded medium. (Hint: Consider what happens to the integrated terms, as $x \to \pm\infty$.)

2.3 The Forward Scattering Problem

The mathematical tools of the previous section provide the general recipe for finding analytical solutions to forward modeling or *boundary value* problems. We seldom know the exact Green's function for a problem. However, we often have *approximations* of the Green's function obtained

through techniques such as ray tracing, through finite-difference modeling, or through other approximate techniques. Whether or not we have the exact Green's function, we are probably using an *approximate* wavespeed profile as input for the modeling, anyway.

This means that we cannot write a set of *exact* representations such as those in (2.2.4). What we can write is an equation in terms of the approximate Green's function, with the operator $\mathcal{L}$ depending on the approximate wavespeed profile. To relate this approximate wavespeed profile and Green's function to their true counterparts, we will employ a method known as *perturbation theory.* In our application, perturbation theory amounts to representing an unknown quantity as the sum of a known reference quantity, called the *background,* plus a small deviation from the background called the *perturbation.*

If the approximate wavespeed profile is almost the same as the true wavespeed profile, then we may represent the true wavespeed as being the sum of a background wavespeed profile plus a perturbation, also called the *scatterer.* Following this logic, we may consider the true wavefield u seen in the first equation of (2.2.4) as being the sum of a background wavefield plus a perturbation, also called the *scattered field.*

Because we know the respective background wavespeed and wavefield, our approximate modeling formula will represent the scattered wavefield as a function of the value of the perturbation in wavespeed.

2.3.1 The Forward Scattering Problem in 1D

Keeping all of these ideas in mind, we will formulate the 1D forward scattering problem by considering the propagation of waves in a model with variability in only one spatial dimension. To keep things simple, we will consider a constant-density problem for which the soundspeed is unknown only in part of the wavespeed profile. An impulsive point source will act at time $t = 0$ at the position $x = x_s$ and will be represented by the distributional quantity $-\delta(x - x_s)\delta(t)$. (See Appendix A for an overview of the theory of distributions.) A recording instrument is located at the position x_g, the receiver position, which for geophysical applications, is assumed to be a *geophone* or a hydrophone.

The wavespeed profile will be assumed to be known in the range of distances from $-\infty < x \leq x_g^+$ and unknown in the range $x_g^+ < x < \infty$ (see Figure 2.4). The position x_g^+ is located to the right of x_g. We further assume that the soundspeed is bounded as $x \to \infty$, becoming a constant for large range. If the "source" and "geophone" are located at the same place, $x_s = x_g = \xi$, then this is the simplest example of a *zero-offset* experiment.

The governing equation for the problem is the Helmholtz equation (2.2.1), with the radiation condition specified by equation (2.2.2). Our method of formulating this problem is to use two Helmholtz equations, as in (2.2.4), and apply Green's theorem to create an integral-equation

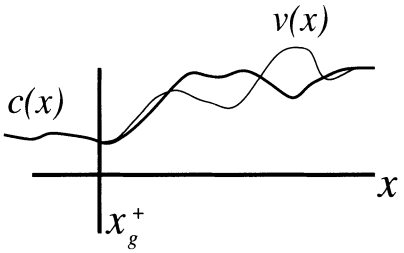

FIGURE 2.4. Cartoon showing a background wavespeed profile $c(x)$ and the actual wavespeed profile $v(x)$.

representation of the scattered field, as in Exercise 2.2. We now show how perturbation theory can be used to create the two Helmholtz equations.

Suppose that the wavespeed profile, $v(x)$, can be represented as a perturbation from a background profile $c(x)$. While there are many ways to represent such a small deviation, our choice will be constrained by a desire to preserve the form of the Helmholtz equation. To do this, we use an expression of the form

$$\frac{1}{v^2(x)} = \frac{1}{c^2(x)}\left[1 + \alpha(x)\right]. \tag{2.3.1}$$

For the present discussion, $\alpha(x)$ will be assumed to always be "small" when compared to other relevant quantities in the problem. We assume that the Green's function (the *impulse response* in linear-systems language) of the Helmholtz equation posed in terms of $c(x)$ is known or can be approximated. Rewriting (2.2.1) using the perturbation representation (2.3.1) yields an equivalent Helmholtz equation

$$\begin{aligned}\mathcal{L}_0 u(x, x_s, \omega) &\equiv \left[\frac{d^2}{dx^2} + \frac{\omega^2}{c^2(x)}\right] u(x, x_s, \omega) \\ &= -\delta(x - x_s) - \frac{\omega^2}{c^2(x)}\alpha(x) u(x, x_s, \omega).\end{aligned} \tag{2.3.2}$$

Here, the term involving $\alpha(x)$ has moved to the right side of the equation.

Equation (2.3.2) is posed in terms of the "total field" $u(x, x_s, \omega)$ generated by the impulsive source $-\delta(x - x_s)$ plus the more complicated "scattering source" represented by the term on the far right in (2.3.2). The scattered waves generated by this new "source" have interacted with regions at greater depth than x_s and x_g and thus contain information about the wavespeed profile at these greater depths.

It is this part of the wavefield that is of greatest interest. It is reasonable to assume that there is a distinction between the direct-wave energy propagating away from the source position and the scattered energy that propagates back to the receiver. Because the wavespeed structure of the medium has been represented as a reference profile plus a perturbation, a

similar representation of the wavefield $u(x, x_s, \omega)$ is also appropriate. It is proper, therefore, to think of $u(x, x_s, \omega)$ as being made up of a reference field, $u_I(x, x_s, \omega)$ (u-**I**ncident), which would be present in the absence of the perturbation, plus $u_S(x, x_s, \omega)$ (u-**S**cattered), which represents the departure from $u_I(x, x_s, \omega)$ due to the presence of the perturbation, $\alpha(x)$. The expression for this decomposition of the total field,

$$u(x, x_s, \omega) \equiv u_I(x, x_s, \omega) + u_S(x, x_s, \omega), \tag{2.3.3}$$

is analogous to the wavespeed perturbation expression (2.3.1).

An advantage of using this formal decomposition of the field is apparent, because we see that the Helmholtz equation (2.3.2) may be written as the sum of two Helmholtz equations. We require that incident field $u_I(x, x_s, \omega)$ be a solution of the problem,

$$\mathcal{L}_0 u_I \equiv \frac{d^2 u_I}{dx^2} + \frac{\omega^2}{c^2(x)} u_I = -\delta(x - x_s), \tag{2.3.4}$$

with u_I bounded for all x and satisfying the radiation conditions,[6]

$$\frac{du_I}{dx} \mp i\frac{\omega}{c(x)} u_I \to 0, \quad \text{as} \quad x \to \pm\infty. \tag{2.3.5}$$

We then substitute the formal field decomposition (2.3.3) and the equation describing the incident field (2.3.4) into (2.3.2), to obtain the Helmholtz equation

$$\mathcal{L}_0 u_S(x, x_s, \omega) = -\frac{\omega^2}{c^2(x)} \alpha(x) \left[u_I(x, x_s, \omega) + u_S(x, x_s, \omega) \right], \tag{2.3.6}$$

written in terms of the background wavespeed $c(x)$, and having the "scattering source" as its forcing function. The Helmholtz equation describing the total field (2.3.2) is equal to the sum of the equation describing the incident field (2.3.4) plus the equation describing the scattered field (2.3.6).

The scattered field representation (2.3.6) has important consequences. Notice that, while there is no explicit representation of the delta function source in (2.3.6), the primary source is contained *implicitly* in u_I, although we also have a term involving the unknown wavefield. The price for creating such a representation is that a more complicated "equivalent source" is needed to generate the correct u_S. This new source is no longer a simple distribution acting at one point (x_s). It is now a source that depends on the general coordinate x, through $\alpha(x)$, and depends also on the values of the field u_S—itself a function of both the general coordinates x and the perturbation $\alpha(x)$.

---

[6] We must require "reasonable" behavior from $c(x)$ as $x \to \pm\infty$. This means that $c(x)$ must "eventually" become constant, or that $c \to$ const. while being "sufficiently" differentiable for large $|x|$.

As noted above, our intent is to create an integral equation that will represent the field at x_g due to a source at x_s. To achieve this, we introduce a Green's function with excitation point $x = x_g$ that satisfies our second Helmholtz equation

$$\mathcal{L}_0 g(x, x_g, \omega) \equiv \left[\frac{d^2}{dx^2} + \frac{\omega^2}{c^2(x)}\right] g(x, x_g, \omega) = -\delta(x - x_g). \tag{2.3.7}$$

We impose the same boundedness and radiation conditions on $g(x, x_g, \omega)$ as were imposed on $u_I(x, x_s, \omega)$ in (2.3.4). Note that, from equation (2.3.4), we know $u_I(x, x_s, \omega) = g(x, x_s, \omega)$, and, since we also know x_g, it follows that, $g(x, x_g, \omega)$ is also a known quantity.

The reader should note that while the equations for the total, incident, and scattered fields ((2.3.2), (2.3.4), and (2.3.6), respectively) depend on each other, this new equation (2.3.7) is independent of all of these. Equations (2.3.6) and (2.3.7) may therefore be solved using Green's theorem to create the desired integral equation for $u_S(x_g, x_s, \omega)$. It is left as an exercise for the reader to show that the integral equation relating the observations of the scattered field at x_g, $u_S(x_g, x_s, \omega)$, to the interior values of that unknown field and the unknown perturbation, $\alpha(x)$, is

$$u_S(x_g, x_s, \omega) = \omega^2 \int_0^\infty \frac{\alpha(x)}{c^2(x)} \left[u_I(x, x_s, \omega) + u_S(x, x_s, \omega)\right] g(x, x_g, \omega) dx. \tag{2.3.8}$$

Exercises

2.7 Prove Green's Theorem in one dimension; that is, show that

$$\int_{-\infty}^{\infty} \{\phi(x)\mathcal{L}_0\psi(x) - \psi(x)\mathcal{L}_0\phi(x)\}\, dx = (\phi(x)\psi'(x) - \psi(x)\phi'(x))\Big|_{-\infty}^{\infty},$$

where $\mathcal{L}_0$ is the Helmholtz operator

$$\mathcal{L}_0 \equiv \frac{d^2}{dx^2} + \frac{\omega^2}{c^2(x)}.$$

2.8 Use Green's Theorem and equations (2.3.6) and (2.3.7) to show that

$$\begin{aligned} u_S(x_g, x_s, \omega) = \omega^2 \int_0^\infty \frac{\alpha(x)}{c^2(x)} u(x, x_s, \omega) g(x, x_g, \omega) dx \\ + g(x, x_g, \omega) u_S'(x, x_s, \omega)\Big|_{-\infty}^{\infty} \\ - g'(x, x_g, \omega) u_S(x, x_s, \omega)\Big|_{-\infty}^{\infty}. \end{aligned}$$

a. Apply the radiation condition (equation (2.3.5)) to the terms evaluated at $\pm\infty$, and use the fact that $\alpha(x) \equiv 0$ for $x < 0$ to obtain the integral equation for the scattered field (2.3.8).

b. Explain why the condition of $c(x) \to$ const. as $x \to \infty$ is necessary for the formulation of this problem.

2.9 Solve the general unbounded-media problem

$$\mathcal{L}g(x, x_s) = -\delta(x - x_s)$$
$$\mathcal{L}^\star g^\star(x, x_g) = -\delta(x - x_g),$$

with $\mathcal{L}$, $\mathcal{L}^\star$, being defined as in equation (2.2.8), to prove the *theorem of reciprocity*

$$g^\star(x_s, x_g) = g(x_g, x_s).$$

2.3.2 The Born Approximation and Its Consequences

We say that the integral equation (2.3.8) is *nonlinear* because it has a term that contains the product of the unknown field u_S and the perturbation $\alpha(x)$. This introduces a difficulty because, in the inverse problem, $\alpha(x)$ is the unknown that we seek. An important approach to solving such nonlinear problems is to find a "nearby" linear problem that we can solve. This solution is then viewed as a first approximation—subject to correction—of a solution to the nonlinear problem. The common method for finding such a nearby linear solution is to linearize the problem.

Here "linearization" means removing the product $u_S(x, x_s, \omega)\alpha(x)$ from the right side of equation (2.3.8). If a justification for ignoring this product can be found, then the linearization can be accomplished. In the worst possible scenario, $u_S(x, x_s, \omega)$ is of comparable size to $u_I(x, x_s, \omega)$, meaning that there is no justification for making the approximation mentioned above.

First observe that the Green's function $g(x, x_g, \omega)$ is of comparable size to $u_I(x, x_s, \omega)$, because our "incident field" is also the response to an impulsive source, located at a different point $x = x_s$. From the scattered-field Helmholtz equation (2.3.6), it is easy to conclude that $u_S(x, x_s, \omega)$ vanishes when $\alpha(x) \equiv 0$. It is reasonable to assume that if $\alpha(x)$ were "small" then $u_S(x, x_s, \omega)$ would also be "small." Hence the product, $\alpha(x)u_S(x, x_s, \omega)$ appearing under the integral in (2.3.8) should be significantly smaller than the product $\alpha(x)u_I(x, x_s, \omega)$. The former is (in some sense) quadratic in $\alpha(x)$, while the latter is only linear in $\alpha(x)$. It is natural to conclude that for small $\alpha(x)$, the former term may be neglected in favor of the latter. Thus, it should be possible to obtain an approximation to $u_S(x, x_s, \omega)$ that

is accurate to linear order in $\alpha(x)$, yielding

$$u_S(x_g, x_s, \omega) = \omega^2 \int_0^\infty \frac{\alpha(x)}{c^2(x)} u_I(x, x_s, \omega) g(x, x_g, \omega) dx. \tag{2.3.9}$$

The linearization performed here is often called the *Born approximation* by physicists.[7] The resulting integral equation is therefore often called the *Born modeling formula.*

2.3.3 The Inverse Scattering Integral Equation

In the problem, the wavefield $u(x_g, x_s, \omega)$ is observed and the wavefield $u_I(x_g, x_s, \omega)$ is assumed to be known, implying that we can deduce the values of the scattered field at x_g, represented by $u_S(x_g, x_s, \omega)$. Thus, the objective of our inverse problem will now be to determine $\alpha(x)$ from the "observed data," $u_S(x_g, x_s, \omega)$.

As noted above, $u_I(x, x_s, \omega) = g(x, x_s, \omega)$, permitting (2.3.9) to be rewritten as

$$u_S(x_g, x_s, \omega) = \omega^2 \int_0^\infty \frac{\alpha(x)}{c^2(x)} g(x, x_g, \omega) g(x, x_s, \omega) dx. \tag{2.3.10}$$

We have formally reduced the inverse problem to the problem of solving this integral equation for $\alpha(x)$ using the observed data $u_S(x_g, x_s, \omega)$.

In the formal theory of integral equations, equation (2.3.10) is called a *Fredholm integral equation of the first kind.* That part of the integrand excluding $\alpha(x)$ is called the *kernel* of this integral equation (or integral operator). An important issue that arises when trying to solve such an equation is whether or not small changes in the data u_S lead to small changes in the solution α. When this is not the case, then the integral equation is said to be "ill-conditioned," or to have an "unstable inverse."

In general, there is no guarantee that a "Fredholm I" integral equation will have a stable inverse. There is, however, a class of such integral equations that *does* have stable inverses. These are the Fourier transforms and their extensions, the *pseudodifferential operators*, and *Fourier integral operators*, with the inverses being respectively, the inverse Fourier transform and the *inverse pseudodifferential operator*, and the pseudo-inverse Fourier integral operator. In addition to being stable analytically, these inverse operators are also stable numerically.

As we will see in the body of this text, the choices of approximate Green's functions will contain factors of complex exponentials, meaning that our Born modeling formula may be treated as a Fourier transform or a Fourier transform–like integral. Though Fourier transforms have stable inverses,

---

[7] Actually, this approximation was first applied to the Schrödinger equation by Kirchhoff, but the origin has been blurred, as to both the originator and the implementation.

finite bandwidth and finite spatial range may degrade the solution if the inverse transform is not handled correctly. We will see below how we *regularize* the solution to avoid problems associated with finite bandwidth and finite spatial range.

The reader should keep in mind that this is the *linearized* problem and that infinite-bandwidth information in ω has been assumed. No rational claim can be made about the "exact" solution to the finite-bandwidth, fully nonlinear problem, from the information provided here.

2.4 Constant-Background, Zero-Offset Inversion

The Born approximate integral equation for the scattered field (2.3.9) may be understood more clearly if applied to a simple problem. Consider, therefore, the case where the source and receiver are located at the same place (for simplicity we choose $x_s = x_g \equiv 0$ and $c(x) \equiv c_0$). This is the simplest "zero-offset problem." The Green's function may then be written explicitly as

$$g(x,0,\omega) = -\frac{c_0 e^{i\omega|x|/c_0}}{2i\omega}, \tag{2.4.1}$$

(see Exercise 2.10), making (2.3.10) take the form[8]

$$u_S(0,\omega) = -\int_0^\infty \frac{\alpha(x)}{4} e^{2i\omega x/c_0} dx. \tag{2.4.2}$$

Note that x values are assumed to be positive, so $|x|$ has been replaced with x.

Consistent with the assumptions made in formulating the inverse problem, $\alpha(x) = 0$ for $x < x_s$ ($x < 0$, here) meaning that $\alpha(x)$ behaves as a causal function of the time variable, $2x/c_0$ (the *two-way traveltime* of a reflected arrival is the minimum time at which a once-scattered signal can exist). It is permissible, therefore, to treat this equation as a causal Fourier transform, (see Appendix B and equation (2.2.3)), and proceed to invert using the definition of the inverse Fourier transform, with the caveat that if there are any singularities on or above the real ω axis the integral must be interpreted as a contour integral that passes above those singularities. Except for this caution, this is an equation for the Fourier transform of $\alpha(x)$ evaluated at the "wave number" $k \equiv 2\omega/c_0$ representing the data $u_S(0, c_0 k/2)$. Thus, $\alpha(x)$ is represented in the inverse Fourier transform form as

$$\alpha(x) = -\frac{4}{\pi c_0} \int_{-\infty}^{\infty} u_S(0,\omega) e^{-2i\omega x/c_0} d\omega. \tag{2.4.3}$$

---

[8] Here and below, whenever the source and receiver are coincident, and located at the origin, we will write the argument, 0, only once.

The constant multiplier is a simplified form of

$$\frac{1}{2\pi} \cdot 4 \cdot \frac{dk}{d\omega},$$

with the first factor coming from the definition of the inverse Fourier transform, the second coming from the divisor of 4 in (2.4.2), and the third coming from the relationship between ω and the "true" Fourier variable $k = 2\omega/c_0$, noted above. The reader should note that through this transformation, temporal/frequency information has been equated to spatial/wavenumber information. A form of this transformation will be common to all of the inversion formulas that will be derived in this text. That is to say, we will always "trade" the time dimension for one spatial dimension.

Exercises

2.10 Given the heterogeneous scalar wave equation

$$\left[\frac{d^2}{dx^2} - \frac{1}{c_0^2}\frac{d^2}{dt^2}\right] G(x, x_s, t) = -\delta(x - x_s)\delta(t),$$

use the definitions of the causal Fourier transform in Section 2.1 and Appendix B to show that

$$g(x, x_s, \omega) = -\frac{c_0 e^{i\omega|x-x_s|/c_0}}{2i\omega}.$$

2.4.1 Constant-Background, Single-Layer

The zero-offset, constant-background inversion formula (2.4.3) derived above is the first example of the kind of formula that is the goal of our investigations. We rely on the fact that the properties of the integral represented here (an inverse Fourier transform) are well established in the world of applied mathematics, from both theoretical and computational standpoints, at least for arguments that are, in some sense, "well behaved." It is easy to test this preliminary result to see if further investigations in this direction may be profitable.

An advantage in the 1D problem is that exact scattered-field data can be generated analytically for a variety of wavespeed profiles. The simplest of these profiles is a perturbation of size ε. This steplike wavespeed change, located at the position $x = h$, defines the boundary between two constant-wavespeed media and is represented mathematically as:

$$\alpha(x) = \varepsilon H(x-h), \tag{2.4.4}$$

$$v(x) = \begin{cases} c_0, & x < h, \\ \\ c_1 \equiv c_0/\sqrt{1+\varepsilon}, & x > h. \end{cases}$$

Here, $H(x-h)$ is the Heaviside step function, equal to 0 for $x < h$ and equal to 1 for $x > h$. The second line follows from the definition of $\alpha(x)$ in (2.3.1).

The exact solution to the problem (2.2.1) for this wavespeed profile is

$$u(x,\omega) = \begin{cases} u_I(x,\omega) + u_R(x,\omega), & x < h, \\ \\ u_T(x,\omega), & x > h, \end{cases} \tag{2.4.5}$$

with

$$u_I(x,\omega) = -\frac{c_0 e^{i\omega x/c_0}}{2i\omega}, \quad u_R(x,\omega) = -\frac{c_0 R e^{-i\omega(x-2h)/c_0}}{2i\omega}, \tag{2.4.6}$$

$$u_T(x,\omega) = -\frac{c_0 T e^{i\omega[(x-h)/c_1 + h/c_0]}}{2i\omega},$$

where the "reflection coefficient" R and the "transmission coefficient" T have the usual definitions

$$R = \frac{c_1 - c_0}{c_1 + c_0} = \frac{1-\sqrt{1+\varepsilon}}{1+\sqrt{1+\varepsilon}} \quad \text{and} \quad T = \frac{2c_1}{c_1 + c_0} = \frac{2\sqrt{1+\varepsilon}}{1+\sqrt{1+\varepsilon}}. \tag{2.4.7}$$

Remark 2.1. We have used the notation u_I to represent a part of the solution in the region, $x < h$. Previously, we defined u_I as the wavefield in the absence of the perturbation, α. In fact, with c_0 taken to be the reference speed c in our formalism, the function u_I introduced here is *exactly* the incident wave of our derivation.

The scattered wave $u_S(0,\omega)$ needed for (2.4.3) is then just the expression for the reflected wave $u_R(x,\omega)$ in (2.4.6), evaluated at $x \equiv 0$. Thus, the integral representation of the wavespeed perturbation is

$$\alpha(x) = \frac{4R}{\pi} \int_{-\infty}^{\infty} \frac{e^{2i\omega(h-x)/c_0}}{2i\omega}\, d\omega. \tag{2.4.8}$$

For this analytic representation of the data, the caveat about passing above singularities on the real ω-axis becomes important. It is left as an exercise for the reader to verify that

$$\alpha(x) = -4RH(x-h), \tag{2.4.9}$$

under the assumption that equation (2.4.8) represents a causal Fourier transform.

If we compare the result in equation (2.4.9) with equation (2.4.4), we see that the discontinuity is in the right location but that the magnitude of the jump is not exact. However, for small ε,[9]

$$R = -\varepsilon/4 + O(\varepsilon^2). \tag{2.4.10}$$

This result follows by using the binomial theorem to expand the square roots in the numerator and denominator of the expression for R in (2.4.7) and by expanding the resulting factor of $1/(1+\varepsilon/4)$ into its geometric-series representation. The theory was presumed to be valid only to leading-order in α, meaning that this result is a verification of the method when applied to this simple problem.

Two important questions can be raised:

1. How would numerical integration deal with the singular integral in (2.4.8)?
2. How would the bandlimiting present in any real-world experiment change the result?

The answer to the first question is fairly straightforward, but has some implications regarding the implementation of the theory. First, no real-world experiment will provide observations at $\omega = 0$. If the value for $\omega = 0$ is simply taken to be zero, the result would be akin to the *principal value* integral, which is the *odd* function

$$\alpha(x) = -4R\,[H(x-h) - 1/2] = -2R\,\mathrm{sgn}\,(x-h).$$

Therefore, the error caused by the lack of zero-frequency information is an additive constant, converting the step into something more like a signum function.

The result may be signum-like, but it need not be placed symmetrically about the x-axis, as is seen by the following simple argument. The zero-frequency portion of $\alpha(x)$ is just the integral of this function over its domain in x, meaning that the absence of zero-frequency data implies that the integral of $\alpha(x)$ over its entire domain of support is zero. If the $x = h$ position (where $\alpha(x)$ begins to act) is located in the exact center of the range of integration, or if the range of integration is infinite, then the result will be an exactly symmetric signum function (see Figure 2.5). If, however, the point $x = h$ is located off-center, with the range of integration in x being finite (as will be the case in numerical representations), then the signum-like function will be asymmetric. (The result will be two rectangles of equal area, one above and one below the x-axis.) The practical meaning of this

[9]The expression $f(\varepsilon) = O(\varepsilon)$ means that $f(\varepsilon)/\varepsilon$ is bounded as $\varepsilon \to 0$. Similarly, in this equation, $-(R+\varepsilon/4)/\varepsilon^2$ is bounded as $\varepsilon \to 0$. This convention is a means of measuring the "order of vanishing" of a small quantity with respect to some scale, in this case, ε. At times, we will measure the order of vanishing as a parameter approaches infinity, using a corresponding definition in that case.

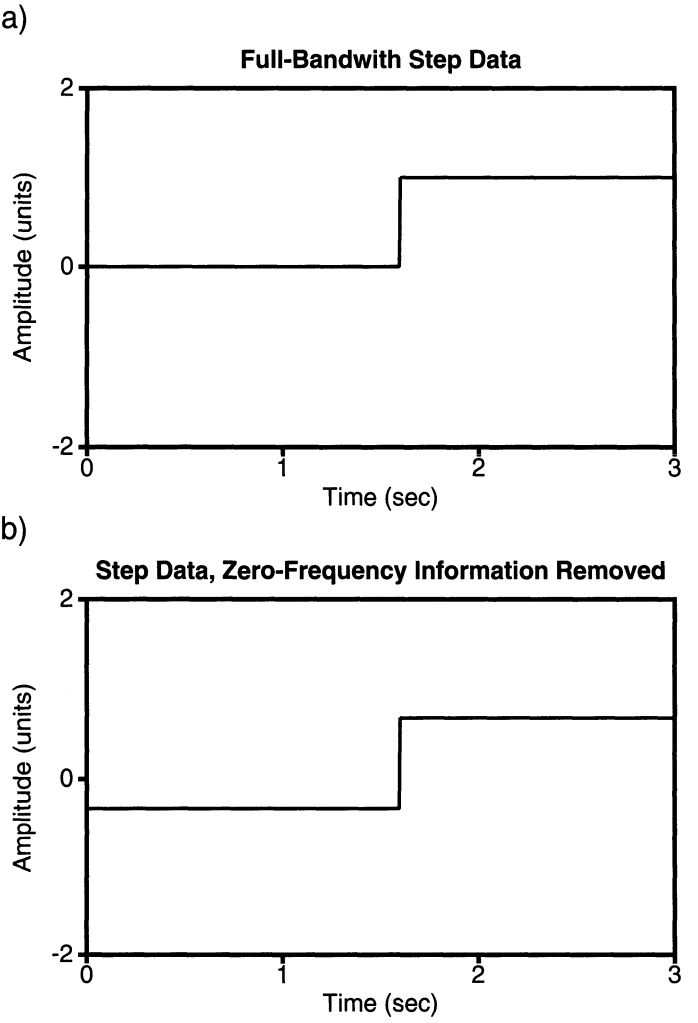

FIGURE 2.5. a) A full-bandwidth representation of a step function. b) A step function lacking only zero-frequency information.

error is that in the absence of zero frequency data, we can reconstruct $\alpha(x)$ only up to an additive constant. If the background wavespeed is known to be the *exact* wavespeed for $x = 0$, then $\alpha(0) \equiv 0$, which defines the constant needed to make the result of the inversion formula agree with reality. In practice, it should be possible for the experimentalist to know the value of $v(0)$ by direct measurement.

In summary, for a step in wavespeed like the one in Figure 2.5a, numerical inversion in the absence of zero-frequency information produces the output

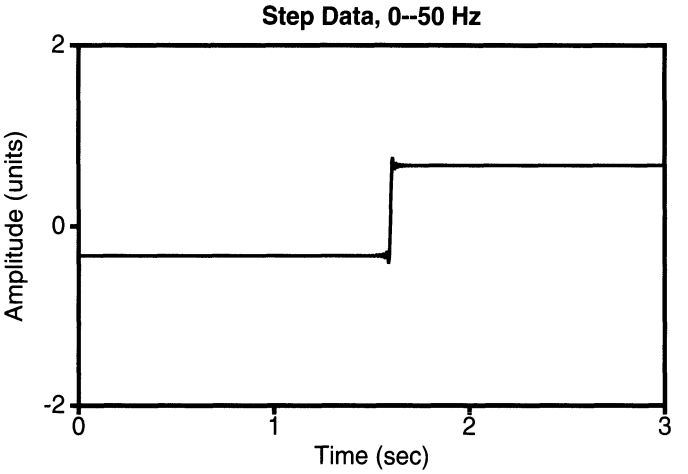

FIGURE 2.6. A 0–50 Hz bandwidth (sampling interval, 4 ms) representation of a step function.

in Figure 2.5b. The positive and negative lobes have equal area above and below the horizontal axis, exactly canceling each other.

Let us now consider the second important question raised above, that of *limited bandwidth.* Bandlimiting of observed data has a variety of causes, some of the more important of which have been listed in Section 1.6.

Although the causes of bandlimiting are clearly complicated, the combined action of these processes on the inversion problem may be treated satisfactorily by assuming that a real-valued filter $F(\omega)$ has been applied to data. The question that must be answered is: How much of the information regarding the jump in parameters is retained in bandlimited data? Assume that the observed field is similar to the expression in (2.4.6), but with a multiplicative factor $F(\omega)$. Because data must be real-valued in the space/time domain, the filter, $F(\omega)$, must be symmetric and nonnegative in the ω-domain. The scattered field in (2.4.6) is then replaced by

$$u_S(x,\omega) = -F(\omega)\frac{c_0 R e^{-i\omega(x-2h)/c_0}}{2i\omega}. \tag{2.4.11}$$

When this function is substituted into (2.4.3), the output will be some *bandlimited* version of $\alpha(x)$, represented here as $\alpha_B(x)$, given by

$$\alpha_B(x) = \frac{4R}{\pi}\int_{-\infty}^{\infty} F(\omega)\frac{e^{2i\omega(h-x)/c_0}}{2i\omega}\,d\omega. \tag{2.4.12}$$

Where (2.4.8) yielded the step function of (2.4.9) as a solution, this integral yields a bandlimited version of the same step function.

Remark 2.2. Note that we have not tried to solve the bandlimited inverse problem directly. Instead, we have introduced bandlimited data into our solution of the *full-bandwidth* inversion problem. We will proceed to analyze the influence of bandlimiting on this "solution." This approach to the problem of bandlimited data will be a theme that will be repeated throughout the text. In contrast, some approaches attempt to directly solve the ill-posed problem of finding a full-bandwidth solution from bandlimited data. Such an approach is equivalent to numerical analytic continuation of a (complex-valued) function of a complex variable (ω) away from its original domain of definition. That problem is known to be ill-conditioned and admits exponentially growing solutions.

Numerical comparisons

What, then, is the result of bandlimiting on the step function example of Figure 2.5a? If we think of the 4 ms (.004 s) sampling interval commonly used in geophysical exploration, this is a "full-bandwidth," 0-to-125 Hz (zero to Nyquist) step. Figure 2.6 shows the result of limiting the bandwidth to 0–50 Hz. The result is not seriously degraded. From the discussion of the causes of bandlimiting in Chapter 1, we see that it is necessary to study the result of the truncation of the spectrum at the lower limit if we are to obtain an accurate picture of the bandlimiting experienced by real data.

We already know what to expect if the sample at 0 Hz is the only low-frequency information that is missing—the step is shifted to make the mean value of α equal to zero. In Figures 2.7a and 2.7b, we show this, with 4–50 Hz and 10–50 Hz outputs, respectively. From the former we conclude that even a moderate loss of low frequency energy already makes the step unrecognizable and *indistinguishable* from an $\alpha(x)$ that is slowly varying—except in the neighborhood of $x = h$, where it exhibits a rapid, doublet-like behavior. From Figure 2.7b, an even further degradation of the output is apparent, although the region of the discontinuity of the propagation speed is certainly still recognizable. It should be noted that the frequency range, 4–50 Hz, corresponds here almost exactly to data points 4–50 in the (dimensionless) frequency domain. In accordance with the Rayleigh criterion for resolution (discussed in Chapter 3), any dimensionless frequency larger than 3 (or π) is a *high frequency.* Thus, the qualitative features that we are observing here are features of *high-frequency bandlimited* Fourier inversion.

From this example, the reader should conclude that slow variations in propagation speed cannot be recovered from high-frequency data by this method. However, it is apparent that the *discontinuity* of the original function still produces a recognizable artifact in this bandlimited inversion. This suggests that for inversion of high-frequency data, we should first concern ourselves with finding the *discontinuities* of the propagation speed (and/or other appropriate Earth parameters). That is, we should seek the *reflectors* in the unknown medium. Of course, this is the geophysicists' traditional

goal, motivated by geometrical optics "common sense." [10]

If the discontinuities are our primary interest, there is a better way to process the data than to simply take the inverse transform. *Bandlimited delta functions* are easier to identify than are bandlimited step functions. It is not difficult to obtain Fourier data for a bandlimited delta function from Fourier data for a bandlimited step function. All that is required is to introduce a multiplicative factor of $\pm i\omega$ or $\pm ik$, depending on the type of forward and inverse transform under consideration. Such a factor corresponding to the derivative operation in the respective frequency or wavenumber domain. For the numerical example of the previous figures, the correct multiplier is $-i\omega$ because the inverse Fourier transform (from frequency to time) is defined to have a kernel $\exp\{-i\omega t\}$ The result of applying this multiplier to the 10-50 Hz step function Fourier data is shown in Figure 2.8. The location and polarity of the discontinuity are clearly revealed by the peak of the spike that represents the bandlimited delta function. Furthermore, we will show below that the height of the spike equals the magnitude of the step scaled by the area under the filter applied to the data. This is, of course, only within the numerical accuracy of the discretization process used in carrying out the Fourier inversion, and the picking process for obtaining the peak amplitude.

As a check that this result is not peculiar to a single step, we show in Figure 2.9b the bandlimited delta function output for the series of steps in Figure 2.9a. Each delta function is properly centered on the discontinuity and has peak amplitude proportional to the jump in the input function multiplied by the area under the filter. Because the amplitudes in the figure have been divided by the area under the filter, the heights of the spikes in Figure 2.9b are the *same* as the heights of the steps in Figure 2.9a.[11]

---

[10] We have chosen here to extend the bandwidth of the inversion by interpreting the telltale signature of Figure 2.7 as the infinite bandwidth Fourier transform of a step function. It is tempting to believe that we are extending, or perhaps analytically continuing, the data back to zero frequency, and thus overcoming the ill-posedness imposed by bandlimiting, effectively recovering data that we did not have in the first place. This is not the case. We have simply chosen a particular method of "regularizing" the solution, which means that we have made assumptions that lead to a result that is *stable*, but which is not necessarily *correct*, in general.

[11] It is important note that these diagrams represent only the properties of Fourier transforms as applied to step functions that have been converted to bandlimited delta functions. These are not actual *reconstructions* of jumps in wavespeed made from seismic data. Real data may have amplitude and travel-time distortions arising from the transmission of seismic waves through overlying layers, as well as possibly large multiply reflected arrivals. We have not yet addressed these issues. However, if we can successfully correct for these sources of error, then the discussion here shows that the bandlimited Fourier transform will give us the desired result.

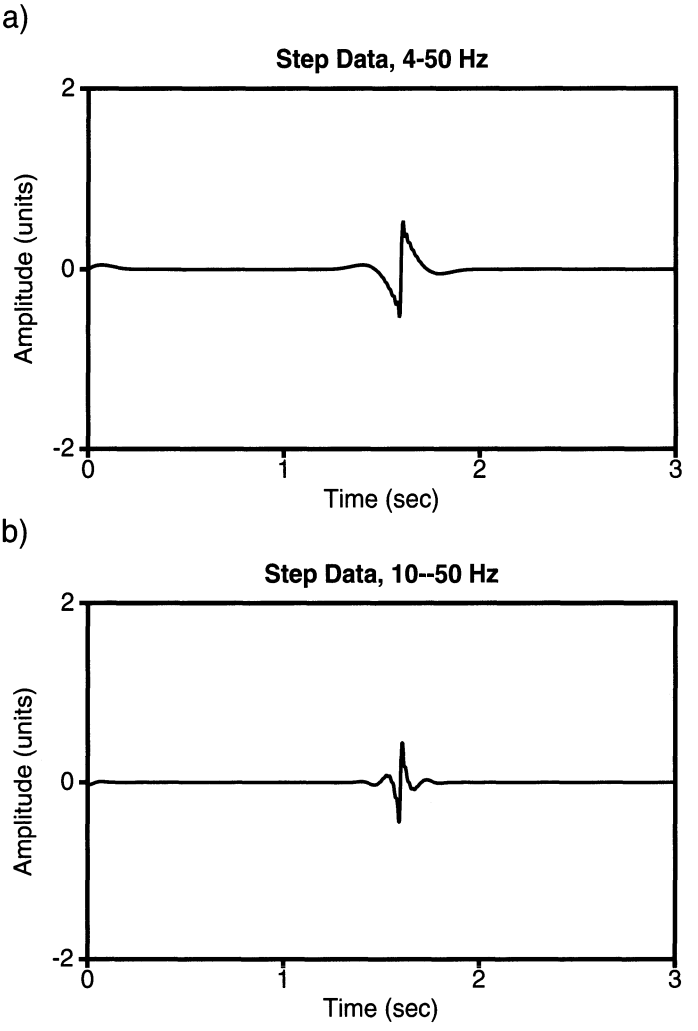

FIGURE 2.7. a) A 4–50 Hz bandwidth (4-ms sampling interval) representation of a step function. b) A 10–50 Hz bandwidth (4-ms sampling interval) representation of a step function.

We return now to consideration of the bandlimited solution in (2.4.12). Following the line of the discussion above, we will take the x-derivative of α_B by multiplying the integrand in (2.4.12) by the factor, $-2i\omega/c_0$. The result is a new function $\beta_B(x)$ defined by the expression

$$\beta_B(x) = \frac{-4R}{\pi c_0} \int_{-\infty}^{\infty} F(\omega) e^{2i\omega(h-x)/c_0} \, d\omega. \tag{2.4.13}$$

If $F(\omega)$ were replaced by unity here, the integral would be proportional to the Dirac delta function:

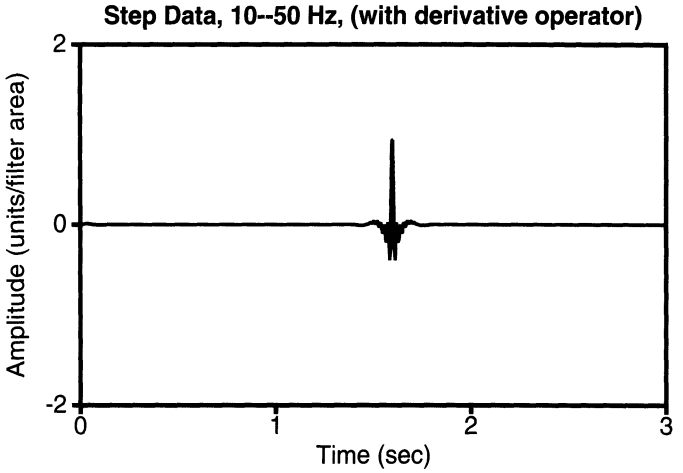

FIGURE 2.8. A 10-50 Hz (4 ms sampling interval) representation of a step function with the $-i\omega$ (derivative) operator applied, and the resulting amplitude scaled by the area under the filter.

$$\frac{1}{\pi c_0}\int_{-\infty}^{\infty} e^{2i\omega(h-x)/c_0}\, d\omega = \frac{1}{c_0}\delta\left((h-x)/c_0\right) = \delta(x-h). \tag{2.4.14}$$

To obtain the last equality we have used the evenness of the delta function and the scaling property, $a\delta(ax) = \delta(x)$.

This result may seem to be a bit puzzling at first, because the value of a delta function $\delta(0)$ is not defined. In real life, however, we never have infinite bandwidth, so the expression that we really have is a bandlimited representation of a delta function, rather than being an actual distribution. If we define the *bandlimited delta function*, $\delta_B(x-h)$, as

$$\delta_B(x-h) \equiv \frac{1}{\pi c_0}\int_{-\infty}^{\infty} F(\omega)e^{2i\omega(h-x)/c_0}\, d\omega, \tag{2.4.15}$$

then our expression for the bandlimited reflectivity function, $\beta_B(x)$ will become

$$\beta_B(x) = -\frac{4R}{c_0}\delta_B\left((h-x)/c_0\right) = -4R\delta_B(x-h). \tag{2.4.16}$$

This a promising result! By multiplying by $-2i\omega/c_0$ before taking the inverse transform of the data, we have produced a bandlimited delta function that peaks at the location of the reflector. Furthermore, the peak amplitude of the output is $-4R\delta_B(0)$. Thus, division of the peak amplitude by the *known factor*, $-4\delta_B(0)$, yields an estimate of the *reflection coefficient* as well!

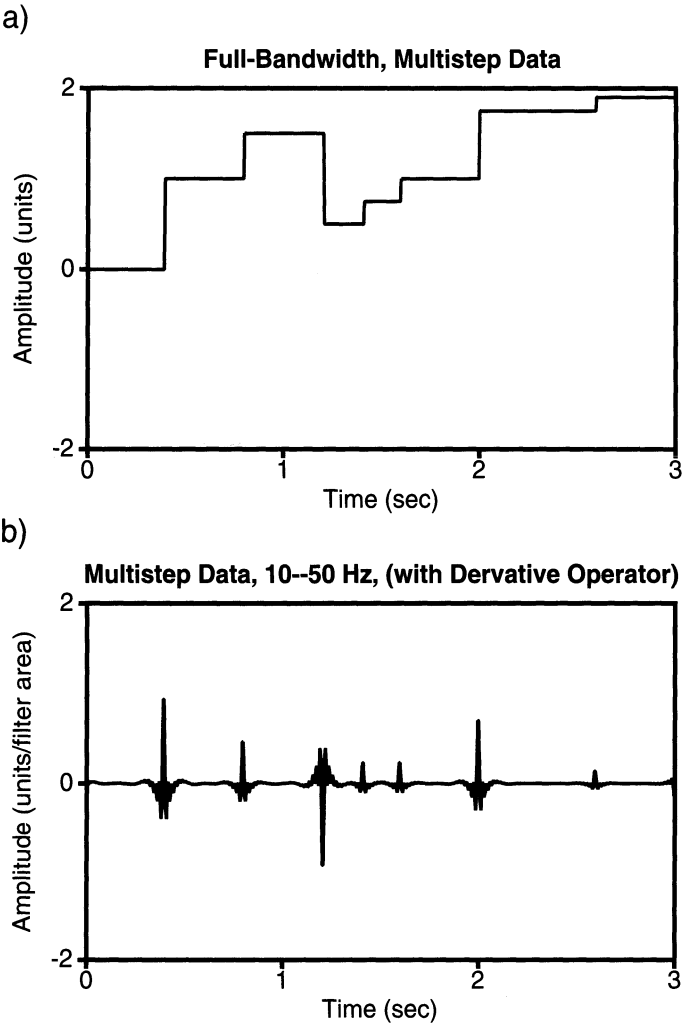

FIGURE 2.9. a) A full-bandwidth representation of a series of steps. b) A 10-50 Hz (4-ms sampling interval) representation of the above series of step functions, with the $-i\omega$ (derivative) operator applied.

Redefining Our Goals for Inversion

This result suggests that our goal needs to be redefined. To correct for bandlimiting, we will purposely design our inversion formulas to correctly identify the location of reflectors as bandlimited delta functions. This requires the introduction of the appropriate derivative operator (here, a factor of $-2i\omega/c_0$). Also, the appropriate scaling factors (here, $-1/4$) will be incorporated into our inversion formulas so that the peak amplitudes of these bandlimited delta functions will yield the reflection coefficient scaled only

by the area under the filter $F(\omega)$. This means that we will introduce an overall multiplier of $i\omega/2c_0$ into the inversion formula, (2.4.3), to obtain an inversion that produces a "properly scaled" delta function; the result will be referred to as the *reflectivity function*,

$$\beta_B(x) = -\frac{2}{\pi c_0^2}\int_{-\infty}^{\infty} i\omega u_S(0,\omega)e^{-2i\omega x/c_0}\,d\omega. \tag{2.4.17}$$

This operator, when applied to the specific example under consideration here would yield the result

$$\beta_B(x) = R\delta_B(x-h), \tag{2.4.18}$$

with a peak value at $x = h$ given by

$$\beta_B(h) = R\delta_B(0) = \frac{R}{\pi c_0}\int_{-\infty}^{\infty} F(\omega)\,d\omega. \tag{2.4.19}$$

(The reader should remember that $F(\omega)$ has support over a finite range, so that the infinite limits of integration written here are really just formal.)

It remains to be seen what the output of the inversion formula (2.4.17) will yield for more general problems. We will check its validity and utility with both analytical and numerical examples below. It must be mentioned that, in computer implementations, β may be defined so that the peak amplitude is just the reflection coefficient, R. This would be done here by multiplying by πc_0 and dividing by the area under the filter. However, the scaling of $-i\omega/2c_0$ used to obtain equation (2.4.17) yields a result that is more aesthetically pleasing for analytic investigations.

Exercises

2.11 Let $u(x,\omega)$ be a solution of the problem

$$\frac{d^2u}{dx^2} + \frac{\omega^2}{v^2(x)}u = -\delta(x)$$

with radiation condition

$$\frac{du}{dx} \mp i\frac{\omega}{v(x)}u \to 0, \quad \text{as} \quad x \to \pm\infty.$$

Here,

$$v(x) \equiv \begin{cases} c_0, & x < h_1, \\ c_1, & h_1 < x < h_2, \\ c_2, & h_2 < x. \end{cases}$$

The objective here is solve this problem by writing down fairly general solutions in each of the three regions, with constants to be determined

by interface and radiation conditions. However, we can take advantage of some advanced knowledge to simplify the most general of representations. For example, we know that for $x < 0$ there should only be a left-propagating scattered wave, the left-propagating incident wave that was initiated by the source and the left-propagating scattered wave that has already passed by the receiver. Similarly, for $x > h_2$, there is only a right-propagating wave. We also know the form of the Green's function in the absence of any variation in the propagation speed—the *free-space* Green's function.
Part of this exercise is to demonstrate that the choice of a smart general solution form can simplify the computations for the coefficients.

a. Such a smart choice for this problem is

$$u = -\frac{c_0}{2i\omega}\left[e^{i\omega|x|/c_0} + A_1 e^{i\omega(2h_1 - x)/c_0}\right], \qquad \text{for} \quad x < h_1,$$

$$u = -\frac{c_0}{2i\omega}\left[A_2 e^{i\omega(h_1/c_0 + (x-h_1)/c_1)} + A_3 e^{i\omega(h_1/c_0 + (h_1-x)/c_1)}\right], \qquad \text{for} \quad h_1 < x < h_2,$$

$$u = -\frac{c_0}{2i\omega} A_4 e^{i\omega[h_1/c_0 + (h_2-h_1)/c_1 + (x-h_2)/c_2]}, \qquad \text{for} \quad h_2 < x.$$

Explain the choices of the phases in the exponentials. Also, verify that this solution is continuous at $x = 0$ and that its first derivative is discontinuous there, with "jump" -1.

b. Require that u and its first derivative be continuous at $x = h_1$ and $x = h_2$. Show that this leads to the system of equations,

$$A_1 - A_2 - A_3 = -1$$

$$-\frac{A_1}{c_0} - \frac{A_2}{c_1} + \frac{A_3}{c_1} = -\frac{1}{c_0}$$

$$A_2 e^{i\omega\tau/2} + A_3 e^{-i\omega\tau/2} - A_4 e^{i\omega\tau/2} = 0$$

$$\frac{A_2}{c_1} e^{i\omega\tau/2} - \frac{A_3}{c_1} e^{-i\omega\tau/2} - \frac{A_4}{c_2} e^{i\omega\tau/2} = 0.$$

Here

$$\tau \equiv 2[h_2 - h_1]/c_1.$$

c. Solve for A_1 and thereby show that

$$u(0,\omega) = -\frac{c_0}{2i\omega}\left[1 + \frac{R_1 + R_2 e^{i\omega\tau}}{1 + R_1 R_2 e^{i\omega\tau}} e^{2i\omega h_1/c_0}\right].$$

Here,

$$R_1 \equiv \frac{c_1 - c_0}{c_1 + c_0}, \qquad \text{and} \qquad R_2 \equiv \frac{c_2 - c_1}{c_2 + c_1}.$$

d. Show that

$$u(0,\omega) = -\frac{c_0}{2i\omega}\Big[1 + R_1 e^{2i\omega h_1/c_0} + R_2[1 - R_1^2]e^{i\omega\tau + 2i\omega h_1/c_0} + \dots\Big],$$

where ... denotes higher order terms in R_1 and R_2. Explain each term in the above sum in terms of primary radiation, reflection, and transmission and explain the relationship between the phases and traveltime.

2.12 The purpose of this exercise is to provide the reader with some insight into the nature of bandlimited delta functions. We define

$$I(t) = \frac{1}{2\pi}\int_\Omega e^{-i\omega t}dt. \tag{2.4.20}$$

Here, Ω is the symmetric domain, $\omega_- \le |\omega| \le \omega_+$. This is equivalent to introducing a filter,

$$F(\omega) = \begin{cases} 1, & \omega_- \le |\omega| \le \omega_+ \\ 0 & \text{otherwise,} \end{cases}$$

and setting

$$I(t) = \frac{1}{2\pi}\int_{-\infty}^{\infty} F(\omega)e^{-i\omega t}dt.$$

Note that for $F(\omega)$ replaced by 1, $I(t) = \delta(t)$.

a. Show that

$$\begin{aligned} I(t) &= \frac{1}{\pi t}[\sin\omega_+ t - \sin\omega_- t] \\ &= \frac{2}{\pi t}\sin\left[\left(\frac{\omega_+ - \omega_-}{2}\right)t\right]\cos\left[\left(\frac{\omega_+ + \omega_-}{2}\right)t\right]. \end{aligned} \tag{2.4.21}$$

b. Define the *sinc function* $\operatorname{sinc}(\eta)$ by

$$\operatorname{sinc}(\eta) = \begin{cases} \dfrac{\sin\pi\eta}{\pi\eta}, & \eta \neq 0, \\ 1, & \eta = 0. \end{cases} \tag{2.4.22}$$

Show that

$$I(t) = 2f_+ \operatorname{sinc}(2f_+ t) - 2f_- \operatorname{sinc}(2f_- t), \quad \omega_\pm = 2\pi f_\pm. \tag{2.4.23}$$

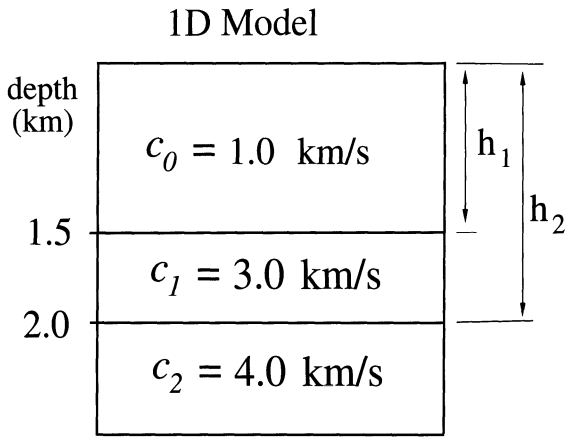

FIGURE 2.10. The 1D wavespeed profile for the numerical example shown in Figure 2.11.

c. The percentage bandwidth of the $I(t)$ is defined by

$$\text{percentage bandwidth} = 100 \cdot \frac{\omega_+ - \omega_-}{\omega_+ + \omega_-}.$$

Generate plots of $I(t)$ for 40%, 50%, and 60% bandwidths. Note that Figure 2.7 is the plot of a sinc function of 66.66% bandwidth.

2.4.2 More Layers, Accumulated Error

The next logical question is: What is the result of applying the inversion formula to data gathered in a multilayer model? To address this question, we will apply our constant-background inversion formula (2.4.17) to data gathered in the two-layer model of Exercise 2.11. The wavespeed profile, $v(x)$, is assumed to consist of three constant values,

$$v(x) = \begin{cases} c_0, & x < h_1, \\ c_1, & h_1 < x < h_2, \\ c_2, & h_2 < x \end{cases} \tag{2.4.24}$$

as in Figure 2.10. We will assume that the total bandlimiting may be represented satisfactorily by simply introducing the filter $F(\omega)$.

It follows from Exercise 2.11 that the analytic expression for the scattered field is

$$u_S(0,\omega) = -F(\omega)\frac{c_0}{2i\omega}\frac{R_1 + R_2 e^{i\omega\tau}}{1 + R_1 R_2 e^{i\omega\tau}} e^{2i\omega h_1/c_0}, \tag{2.4.25}$$

where

$$R_1 = \frac{c_1 - c_0}{c_1 + c_0}, \qquad R_2 = \frac{c_2 - c_1}{c_2 + c_1}, \qquad \text{and} \qquad \tau = 2[h_2 - h_1]/c_1. \tag{2.4.26}$$

Expanding the denominator in (2.4.25) in a geometric series yields

$$u_S(0,\omega) = -F(\omega)\frac{c_0}{2i\omega}\Bigg[R_1 e^{2i\omega h_1/c_0} + R_2\left[1-R_1^2\right]\sum_{n=1}^{\infty}\left[-R_1R_2\right]^{n-1} e^{in\omega\tau+2ih_1\omega/c_0}\Bigg]. \tag{2.4.27}$$

First consider the case $F(\omega) = 1$. The Fourier inversion of each term in this series is exactly like the inversion carried out above for the case of a single layer. The only difference will be that the step at $x = h$ in (2.4.9) will have to be replaced by a step at the appropriate position determined by the phase of the particular term in the series. We find that

$$\alpha(x) = -4\Bigg[R_1 H(x-h_1) + R_2[1-R_1^2]H\left((h_2-h_1)c_0/c_1 + h_1 - x\right) + R_2[1-R_1^2]\sum_{n=2}^{\infty}\left[-R_1R_2\right]^{n-1} H\left(n(h_2-h_1)c_0/c_1 + h_1 - x\right)\Bigg]. \tag{2.4.28}$$

The first term in this expression is just what was obtained for the single layer, $-4R_1$, where R_1 is the reflection coefficient of the first boundary. For small perturbations $\alpha = O(\varepsilon)$, this term reproduces the step at $x = h_1$ to all orders in ε. The second term produces a step at $x = h_1 + (h_2 - h_1)c_0/c_1$, instead of a step at $x = h_2$. This timing error is caused by the failure of the assumed background wavespeed model to agree with the true wavespeed in the region $h_1 < x < h_2$. For small perturbations, the error here in the location of the second step is $O(\varepsilon)$ times the length of the interval between the steps. Furthermore, the amplitude, $R_2(1 - R_1^2)$ is correct to order ε.

The remaining terms in the series produce steps at multiples of the erroneous interval between steps, $x = h_1 + n(h_2 - h_1)c_0/c_1$, with amplitudes decreasing as $\varepsilon^{2(n-1)}$. These subsequent terms arise from the multiple reflections that are disregarded in the Born approximate integral equation (2.3.9), from which the inversion formula was derived. These terms produce spurious reflector images, but with amplitudes that rapidly decrease. Unfortunately, it is possible that one or more of these false images will appear in the output with amplitude greater than the noise threshold of the data. A theory that does not account for multiple reflections cannot accommodate these terms!

Let us now return to the bandlimited data, which is to say $F(\omega)$ is no longer identically equal to 1. Here, as above, we compute the reflectivity function $\beta(x)$, defined by (2.4.17), to the solution representation (2.4.27). The computations are exactly as they were for the example of a single layer. Analogous to the result in (2.4.18), we obtain

$$\beta(x) = R_1\delta_B(x - h_1) + R_2[1 - R_1^2]\delta_B\left((h_2 - h_1)c_0/c_1 + h_1 - x\right) + R_2[1 - R_1^2]\sum_{n=2}^{\infty}[-R_1R_2]^{n-1}\delta_B\left(n(h_2 - h_1)c_0/c_1 + h_1 - x\right) \tag{2.4.29}$$

as the output from the inversion formula.

The result is a series of delta functions. The first spike is at the correct location with amplitude equal to the reflection coefficient of the first reflector. The second delta function peaks at a point that is slightly misplaced from the true location, of the second reflector and has amplitude that is $1 - R_1^2$ times the desired value of R_2. Again, the errors are caused because the background wavespeed profile deviates from the true profile in the $h_2 < x < h_1$ region. We might anticipate that an inversion that accounted for the change in propagation speed from c_0 to c_1 at h_1 would place this second reflector properly. It would also be desirable if that theory could produce the reflection coefficient R_2 at that location, as well. This is the topic of Section 2.5.

2.4.3 A Numerical Example

In Figure 2.11a we show a synthetic seismic trace generated over the wavespeed profile shown in Figure 2.10. In Figure 2.11b we show the inversion of these data, assuming a constant wavespeed of 1.0 km/s, which is the wavespeed in the top layer. As expected, the location of the first reflector is correct, whereas the location of the second is at approximately 1.67 km, instead of the correct value of 2.0 km. This is in accordance with our expectations, as the theory above predicts the location of the second reflector image to be at $h_1 + (h_2 - h_1)c_0/c_1 = 1.5 + (2.0 - 1.5)(1.0/3.0) = 1.667$ km. As expected there are additional multiples present, but only two have sufficient size to be seen.

Similarly, the estimates of the reflection coefficients also follow our predictions. The exact reflection coefficient for the first reflector is $R_{1exact} = 0.5$. The value extracted from the peak amplitude of the inversion is $R_{1est.} = 0.50055$, which represents an overestimate of 0.11% caused by numerical and picking errors. The exact reflection coefficient of the second reflector is $R_{2exact} = 1/7 \approx 0.14286$. The value extracted from the height of the second peak is $R_{2est.} = 0.1072795$. This is a 25.1% underestimate of the correct value. Our theory above predicts that the estimate of $R_{2est.} = (1 - R_1^2)R_{2exact}$, which for our case is $0.75R_{2exact}$—a 25.0% underestimate of R_{2exact}. Thus, our numerical results differ by only about 0.1% from the theoretical predictions.

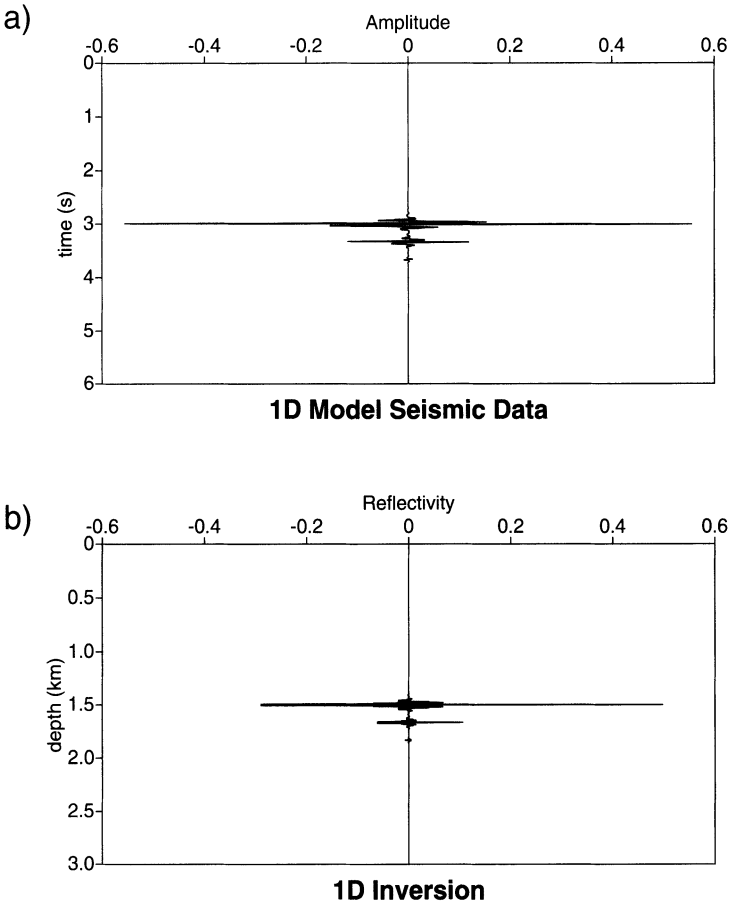

FIGURE 2.11. a) A single synthetic seismic trace recorded over the model in Figure 2.10. The bandwidth of the data is a trapezoid with corner frequencies of 10, 20, 50, and 60 Hz, respectively. Though five multiple reflections were generated, only three arrivals are easily seen. b) Inversion of the synthetic data set performed according to the theory presented in Section 2.4.2. The exact reflection coefficients for the first and second reflectors are $R_{1exact} = 1/2$ and $R_{2exact} = 1/7$, respectively. The estimates from the inversion differ from those predicted by the theory by only about 0.1% due to numerical and picking errors.

2.4.4 Summary

Before proceeding, let us review what has been learned from these simple examples.

1. The theory was applied to data that would be obtained from piecewise-constant wavespeed models consisting of a single reflector, as well as that for a model with two reflectors. A constant-background wavespeed

equal to the first wavespeed that waves would encounter was assumed for the inversion. The inversion formula reproduced $\alpha(x)$ to leading order, assuming that $\alpha(x)$ represents a small change from the background wavespeed.

2. When the data are bandlimited to a range of frequencies that might be typical of a seismic experiment, the inversion output suggests that recovery of information about discontinuities of $\alpha(x)$ from the data should be expected. (This is not peculiar to this application; it is a property of high-frequency bandlimited Fourier data.)
3. By multiplying the data by a scale factor proportional to $i\omega$ before inverting, a series of Dirac delta functions peaking at the discontinuities of the previous output is obtained. Because these discontinuities are just the reflectors in the medium (plus possibly some small spurious artifacts), the output obtained in this way is called the *reflectivity function* or *reflectivity map* of the medium. The scaling is chosen so that the output is approximately the reflection coefficient at each reflector multiplied by the peak value of the bandlimited delta function, with the argument of the delta function being the (signed) distance from the reflector. This is the reflectivity function first discussed in Section 2.1.1.
4. It is important to note that the appropriate scaling factor for producing the reflectivity function form of the inversion formula depends on the formulation of the problem. In particular, the factors scaling the argument of the delta function, as in (2.4.16), will contribute to the final form of the scaling factor.

2.5 Inversion in a Variable-Background Medium

Based on the insights gained in the previous section, we will seek only a "high-frequency" solution to the inverse scattering integral equation (2.3.10). This means that we are free to use a high-frequency approximation of the Green's function. To this end, we replace the Green's function by a high-frequency approximation. Furthermore, because the Born approximation implies that multiply scattered energy is ignored, only the downward propagating component of the Green's function will be used. Therefore, we define the approximate Green's function to be the so-called "WKBJ[12] Green's function"

$$g(x,0,\omega) \equiv g_{\text{WKBJ}}(x,0,\omega) = -\frac{A(x)}{2i\omega} e^{i\omega\tau(x,0)}, \tag{2.5.1}$$

[12]The letters stand for names Wentzel, Kramers, Brillouin, and Jeffreys, several of the many physicists who independently employed this and similar representations.

$$\text{where} \quad \tau(x,0) \equiv \int_0^x \frac{dx'}{c(x')} \qquad \text{for} \quad x > 0.$$

The phase factor $\tau(x,y)$ here represents the total traveltime for the earliest possible transmitted wave that departs from a position x and arrives at the position y in a variable-wavespeed medium. (See Exercise 2.13.) The WKBJ amplitude, $A(x)$, is somewhat harder to define. In the simplest case, when $c(x)$ is a continuous function,

$$A(x) = \sqrt{c(0)c(x)}. \tag{2.5.2}$$

The WKBJ Green's function may be thought of as the leading-order term in a series of inverse powers of ω, the sum of which represents the total field in the variable-wavespeed medium. A formal derivation of this important result has been included as an exercise. (The result is "formal" because we do not prove that the derived expression has any particular relationship to the exact solution of the differential equation. In fact, it does; it is possible to show that it is the leading term of the asymptotic expansion in powers of $(i\omega)^{-1}$ of an exact solution to the differential equation. See Bleistein [1984].)

The same formula, (2.5.1), can be used when $c(x)$ is discontinuous, except, in that case, the amplitude must include scaling factors to account for transmission losses at each interface across which the propagation speed jumps, which is to say, at each reflector. An example of the type of factor needed is demonstrated in the last part of Exercise 2.14. In that example, the factor $\sqrt{c_0(0)c_0(h)/c_1(h)}$ exactly matches the amplitude of the transmitted wave to the amplitude of the incident wave at the discontinuity and the factor T is the same transmission coefficient that arises in piecewise homogeneous medium (which is to say that the wavespeed is described by a piecewise-constant function $c(x)$).

Because this discussion deals with high-frequency solutions, $u_I = F(\omega)g(0,x,\omega)$ will be taken to be the representation of the incident field. Using the WKBJ Green's function (2.5.1) for $g(0,x,\omega)$ in the inverse scattering integral equation (2.3.10), with the bandlimited incident field $u_I(0,x,\omega)$, the integral equation for the scattered field becomes

$$u_S(0,\omega) = -\int_0^\infty F(\omega)\frac{\alpha(x)A^2(x)}{4c^2(x)}e^{2i\omega\tau(x,0)}dx. \tag{2.5.3}$$

This Fourier-type integral (so called because of the oscillatory exponential multiplier) bears strong resemblance to the constant coefficient integral equation, (2.4.2). That equation was solved by Fourier inversion. The essential feature of the inverse operator was the multiplication by another complex exponential whose phase was just the negative of the phase in the integral equation, (2.4.2). Though the phase of the exponential in (2.5.3) is more complicated than in the previous case, the same logic will be used here; however, the form of the amplitude factor in this more general Fourier

inversion remains to be deduced, and will be left as an unknown for the time being. The general form of the inversion operator will be written as

$$\alpha(y) = \int_{-\infty}^{\infty} b(y,\omega) u_S(0,\omega) e^{-2i\omega\tau(y,0)}\, d\omega, \tag{2.5.4}$$

with the amplitude factor $b(y,\omega)$ remaining to be determined.

Now, we will see why making a careful distinction between the *input variable* x, and the *output variable* y was a good idea. This is because our next step is to substitute (2.5.3) for $u_S(0,\omega)$ into this equation:

$$\alpha(y) = -\int_0^{\infty} dx \frac{\alpha(x)A^2(x)}{4c^2(x)} \int_{-\infty}^{\infty} d\omega F(\omega) b(y,\omega) e^{2i\omega\tau(x,y)}. \tag{2.5.5}$$

The result is an equation of the form,

$$\alpha(y) = \int_0^{\infty} \alpha(x) f(x,y) dx, \tag{2.5.6}$$

with

$$f(x,y) = -\frac{A^2(x)}{4c^2(x)} \int_{-\infty}^{\infty} F(\omega) b(y,\omega) e^{2i\omega\tau(x,y)}\, d\omega. \tag{2.5.7}$$

For x and y greater than zero, the equation (2.5.6) will be satisfied asymptotically if we set

$$f(x,y) = \delta_B(x-y). \tag{2.5.8}$$

(This choice is motivated by the fact that $f(x,y)$ exhibits a delta function–like *sifting property*, but is bandlimited by the $F(\omega)$ present in the original definition of the problem.) In (2.5.7), it is possible to construct that result with a b that is independent of ω; that is, $b(y,\omega) \equiv b(y)$. Then,

$$f(x,y) = -\frac{A^2(x)}{4c^2(x)b(y)} \int_{-\infty}^{\infty} F(\omega) e^{2i\omega\tau(x,y)}\, d\omega = -\frac{\pi A^2(x)b(y)}{4c^2(x)} \delta_B(\tau(x,y)), \tag{2.5.9}$$

where we have applied the definition of the bandlimited delta function from equations (2.4.14) and (2.4.15), and have recognized that the $(h-x)/c_0$ that appears in (2.4.14) is replaced with $\tau(x,y)$ in (2.5.9). Applying the property $|f'(x_0)|\delta(f(x)) = \delta(x-x_0)$ to the bandlimited delta function, recognizing that $\tau'(x) = 1/c(x)$, and noting that the action of the delta function is at $x = y$ yields,

$$f(x,y) = -\frac{\pi A^2(x)b(y)}{4c(x)} \delta_B(x-y) = -\frac{\pi A^2(y)b(y)}{4c(y)} \delta_B(x-y). \tag{2.5.10}$$

The reader should remember that these are "asymptotic" equalities that depend on the high-frequency assumption. At best, the construction above is an heuristic sketch which avoids dealing with deeper mathematical issues.

If the bandlimited delta function is visualized as being a sinc-like waveform, then sufficient content of high frequencies will sharpen the main lobe

of the function, while sufficiently broad bandwidth will make the side lobes small compared with the main lobe. If both of these conditions exist, then the equalities stated above will be true, asymptotically.

The choice of $b(y)$ needed to make (2.5.8) true is apparent from (2.5.10), because

$$b(y) = -\frac{4c(y)}{\pi A^2(y)}, \tag{2.5.11}$$

and the inversion operator, (2.5.4) becomes

$$\alpha(y) = -\frac{4c(y)}{\pi A^2(y)} \int_{-\infty}^{\infty} u_S(0,\omega) e^{-2i\omega\tau(y,0)}\, d\omega. \tag{2.5.12}$$

As a simple check on this result, note that when $c(y) = c_0 =$ constant, this result reduces to the constant-background inversion formula (2.4.3) derived earlier in this chapter. It must be remembered that high-frequency approximations were freely used to arrive at this inversion formula. Therefore, good results should not be expected a priori if full-bandwidth data are processed for $\alpha(y)$ using this formula.

In the constant-background example it was possible to extract meaningful information about the discontinuities in α, that is, the location of *reflectors* in the unknown medium, and an estimate of their reflection coefficients. This required that the processing formula be altered to produce the formula for the *reflectivity function* $\beta(y)$, equation (2.4.16). That change was achieved by differentiating the expression for $\alpha(y)$ with respect to y and multiplying by $-1/4$.

The same idea will be used here. We are now committed to using the leading-order asymptotic results of a high-frequency assumption, and do not need to include terms of lower order in ω. Therefore, when performing the differentiation of $\alpha(y)$ it is permissible to keep only the leading-order term. This is the term resulting from the differentiation of the exponent in (2.5.12), which introduces a factor of $i\omega$ in the integrand. Differentiation of the amplitude multiplier outside the integral sign produces no such factor and therefore the result must be lower order in ω.

In summary, paralleling the procedure that was used to obtain equation (2.4.16), the reflectivity function for the variable-background wavespeed case is obtained by multiplying the solution, (2.5.12), by $(-2i\omega/c(y)) \cdot (-1/4) = i\omega/2c(y)$ yielding,

$$\beta(y) = -\frac{2}{\pi A^2(y)} \int_{-\infty}^{\infty} i\omega u_S(0,\omega) e^{-2i\omega\tau(y,0)}\, d\omega. \tag{2.5.13}$$

Again, note that, for constant background, this result reduces to the constant-background inversion formula (2.4.17).

But is there justification for these assumptions? Considered as the result of truncating an asymptotic expansion, equation (2.5.10) is equivalent to the statement that $x = y$ is the dominant "critical point" (see Bleistein and

Handelsman [1986]) of the double integral (2.5.5) and that (2.5.12) is really a leading-order asymptotic approximation of $\alpha(y)$ for high-frequency data. (This can be proven rigorously—see Bleistein [1989]—and will be discussed at greater length in Chapter 4.) With this in mind, it is possible to simplify the integrand of equation (2.5.5). If the phase $\tau(x, y)$ is replaced by the first term of its Taylor series expansion in x about the point, y,

$$2\omega\tau(x, y) = k(x - y), \quad \text{with} \quad k = \frac{2\omega}{c(y)}, \tag{2.5.14}$$

and then (2.5.5), with b independent of ω, takes the form

$$\alpha(y) = -\frac{b(y)c(y)}{2} \int_0^\infty dx \, \frac{\alpha(x)A^2(x)}{4c^2(x)} \int_{-\infty}^\infty dk \, F(c(y)k/2)e^{ik(x-y)}. \tag{2.5.15}$$

Here, ω has been replaced by k in the last integral and an extra factor, $c(y)/2 = d\omega/dk$ has been introduced outside the integral.

For $F(c(y)k) \equiv 1$, this double integral is just the cascade of a forward and an inverse spatial Fourier transform. For the bandlimited integration here, we denote the result by $\alpha_B(y)$. Then, to the same order of approximation made above,

$$\alpha_B(y) = -\frac{\pi A^2(y)b(y)}{4c(y)} \int_0^\infty \alpha(x)\delta_B(x - y)dx. \tag{2.5.16}$$

This result leads to the same choice of $b(y)$ as does (2.5.10). That is, the double integral (2.5.5) behaves asymptotically like the cascade of a forward and an inverse Fourier transform with respect to x and $k = 2\omega/c(y)$. This insight will prove useful in the higher-dimensional problems seen later in the text. Furthermore, it lends further credence to approximating the derivative of $\alpha(y)$ by multiplying by $-ik = -2i\omega/c(y)$ to obtain the reflectivity function.

2.5.1 Modern Mathematical Issues

In fact, there is even stronger mathematical justification for these ideas in the theory of pseudodifferential and Fourier integral operators, as first discussed in the context of inverse-scattering imaging by Beylkin [1985]. In particular, the loss of low frequencies in our solution means that we can recover $\alpha(x)$ only up to an "entire function," one that has a power series with infinite radius of convergence. That is, we are giving up knowledge of the smoother part of the solution and determining, at best, only the "singular part" of the solution. Indeed, we have interpreted our output as arising from a step and have used further Fourier filtering—multiplication by $-2i\omega/c(y)$—to enhance our identification of steps, converting them into their derivatives, which are bandlimited delta functions. We are further regularizing away problems arising from bandlimiting when we choose to

interpret all "spikelike" images in our output as being bandlimited delta functions, seeking nothing more exotic in our output.

The representation of $\alpha(y)$ in equation (2.5.4) has the general form of an operator, represented in the frequency domain by its "symbol," which for the general class of problems we are considering is of the form of some function $\sigma(\omega, y)$. Think of this as a kind of "dynamic filter." If $\sigma(\omega, y)$ is the symbol of a special class of operators, called a "pseudodifferential" operator, then it has the property that it will not add singularities (which is to say, spurious artifacts that look like reflectors) to the output. In our problems, the symbol will be of the form of $\sigma(\omega, y) = \omega^{\beta} b(y)$, where β is an integer. For the specific case of the 1D problem, $\beta = 0$, making $\sigma = b(y)$.

If $\sigma(\omega, y)$ has the property of being invertible, and preserves the singularities of the data, then the operator corresponding to this symbol (the result of applying the "filter" in the frequency domain) is called an "elliptic" pseudodifferential operator. In mathematical language, elliptic pseudodifferential operators are said to preserve the *singular support* (discontinuity information) of the data. If, however, the operator has the property of destroying reflector information contained in the data u_S, then this would be called a "smoothing operator."

Fortunately, for us, the symbols of the pseudodifferential operators that we encounter in the construction of our inversion formulas all meet the criterion of ellipticity stated above. All of these symbols are invertible (or, at worst, approximately invertible) by algebraic manipulations, such as those that precede equation (2.5.13), implying that the corresponding pseudodifferential operators are invertible or at worst, approximately invertible.

By the same argument, we can see that any process that we may apply to the data as a filtering process is required to *also* have the property of ellipticity, if the singular support of the data is to be preserved. Indeed, the factor $-2i\omega/c$ that we introduced into equation (2.4.12) to obtain the inversion formula for the reflectivity, β_B, given by equation (2.4.13), may be viewed as being the "symbol" of an elliptic pseudodifferential operator, and thus will preserve the singular support of the original data. Thus, by the arguments above, this filter will not destroy the reflector information, or add spurious reflector–like artifacts.

We must recognize that our good fortune in obtaining invertible pseudodifferential operators is a result of the asymptotic formulation we chose. While the approximate problem is elliptic, and thus possesses the desirable properties mentioned above, we cannot say the same about the *exact* inverse problem. The reader should note that we set the stage for generating this type of formulation by choosing a Fourier–like integral representation, through linearization by the Born approximation, for the process by which the data were generated. Indeed, allowing an increasing amount of "reality" into the inverse problem requires mathematical objects that are more general than pseudodifferential operators.

Even if we still use the Born approximation, the choice of more realistic approximations for the Green's function will cause our formulas to be more general than pseudodifferential operators. The simplest of these will consist of Fourier-like integrals having more complicated phase functions than those obtained by simply cascading forward and inverse Fourier transforms. In turn, the simplest of these operators are the *Fourier integral operators*. The discussion of these more general operators is beyond the scope of this text. There is, however, an issue that we discuss at length in Chapter 4. This issue is the influence of restricted recording geometry, as well as bandlimiting on Fourier-like integrals of the type we derive in this text.

It is the desire of the mathematician to be able to tell a priori the type of operator that he or she possesses. For the kinds of operators encountered in imaging theory, these issues are still a topic of current research, especially as investigators try to extract more information from their data. In contrast, seismic data processor approaches this problem experimentally by performing inversions on test suites of known data. This is, of course, not acceptable as a mathematical proof, but works well in practice. Though their methods differ, the seismic processor and the operator theorist have the same goal—preserving the reflector information (the singular support) of the data.

See Saint Raymond [1994], Taylor [1984], and the first volume of Treves [1980] for an introduction to the theory of pseudodifferential operators. The second volume of Treves [1980] contains an introduction to the theory of Fourier integral operators.

2.5.2 Summary

We have derived a formal asymptotic solution to the 1D inverse problem in a variable-background medium. In that solution, we interpret our output as a series of bandlimited delta functions located at the position of the steps in α as approximated by the background propagation speed $c(x)$ through the relationship between space and time defined by the second equation in (2.5.1). This formal solution suffers from the same problem with multiples as does the earlier constant-background solution. The introduction of a variable-background propagation speed here, however, opens the possibility of properly locating reflectors beyond the first one, which we could not do correctly with the constant-background wavespeed solution.

Exercises

2.13 The objective of this exercise is to derive the leading-order term of the WKBJ solutions to the homogeneous form of equation (2.3.4) with

radiation condition (2.3.5). This will be an asymptotic solution for "large" values of ω and, hence, will be determined as series in inverse powers of $i\omega$.

a. Assume a solution of the form

$$u(x,\omega) = (i\omega)^{\beta} e^{i\omega\tau(x)} \sum_{n=0}^{\infty} \frac{A_n(x)}{(i\omega)^n}.$$

(The equality here is an "asymptotic equality" only; in general, such series do not converge.) Substitute this form into (2.3.4) and collect terms in like powers of $i\omega$ to obtain the following equation.

$$\mathcal{L}_0 u(x,\omega) = (i\omega)^{\beta} \exp\{i\omega\tau(x)\} \sum_{n=0}^{\infty} \{(i\omega)^{2-n} A_n \left[(\tau')^2 - 1/c^2\right] + (i\omega)^{1-n} \left[2A_n'\tau' + A_n\tau''\right] + (i\omega)^{-n} A_n''\}.$$

Here, $(')$ means d/dx.

b. To determine τ and the values of A_n for $n = 0, 1, 2, \ldots$, set the coefficient of each power of $i\omega$ equal to zero, starting with $(i\omega)^{\beta+2}$ and proceeding to lower powers. Show that setting the coefficient of this highest power equal zero leads to the equation

$$(\tau')^2 = 1/c^2,$$

(the 1D *eikonal equation*) with two solutions,

$$\tau' = \pm 1/c \quad \text{and} \quad \tau(x) = \pm \int^x \frac{dx'}{c(x')}.$$

Here, we use x' as a dummy variable of integration to distinguish it from the endpoint x. That is, the lower limit is arbitrary in the integral—τ is determined up to a constant—and there are two possible solutions, which we denote by $u_{\pm}$, below.
Note that the entire first series in $\mathcal{L}_0 u(x,\omega)$ is now zero.

c. Show that we can eliminate the next order in $i\omega$ by requiring that

$$2\tau' A_0' + \tau'' A_0 = 0,$$

(the 1D *transport equation*) with solution

$$A_0^2 = c(x) \quad \rightarrow \quad A_0 = K\sqrt{c(x)}.$$

Of course, each of the two solutions $u_{\pm}$ will have its own constant.

d. Conclude that the two leading-order solutions are of the form

$$u_{\pm}(x,\omega) = (i\omega)^{\beta} K_{\pm} \sqrt{c(x)} \exp\left\{\pm i\omega \int^x \frac{dy}{c(y)}\right\},$$

with the constants, $K_\pm$, the lower limits of integration, and the choice of β undetermined without further information about the solutions we seek.

e. Define the *Wronskian*, W, by

$$W = \det \begin{bmatrix} u_+(x,\omega) & u_-(x,\omega) \\ u'_+(x,\omega) & u'_-(x,\omega) \end{bmatrix}.$$

Show that, to leading order,

$$W = -2K_+K_-(i\omega)^{2\beta+1}.$$

That is, the Wronskian is equal to zero only if we take one of the constants $K_\pm$ equal to zero. This insures that the two solutions are *linearly independent* and that we can build solutions to heterogeneous equations in terms of them. We remark also that the theory underlying this method assures us that the two formal series solutions we generate are asymptotic to two *exact* solutions to the given homogeneous equation. (For further information about Wronskian theory, see any standard text on ordinary differential equations, such as Coddington and Levinson [1984].)

f. Show that we can now determine all of the amplitudes A_n recursively by solving the system of equations

$$2\tau' A'_n + \tau'' A_n = -A''_{n-1}, \quad n \geq 1$$

(the 1D form of the *higher-order transport equations*).

Remark 2.3. Each solution, $u_\pm$, should have only one free constant. By leaving the lower limit of integration in the phase free, as well as having two constants, $K_\pm$, we effectively have *two* free constants in each solution. In practice, however, as in the next example, we pick the lower limit of integration of the phase conveniently and put all of the burden of satisfying radiation and continuity conditions on the K's.

2.14 The purpose of this exercise is to derive the leading-order WKBJ approximation of the Green's function, $g(x,\xi,\omega)$, that is a solution of the heterogeneous Helmholtz equation (2.3.4) with radiation condition (2.3.5) (see Bleistein [1984], pp.136–140.)

a. We begin by assuming that for $x > \xi$ and for $x < \xi$, $g(x,\xi,\omega)$ is a (different for each range) linear combination of the two solutions, $u_\pm$, derived in the previous exercise. For convenience, we take all the lower limits of integration in the integrals that appear in the phase to be ξ. (Note the remark at the end of the previous exercise.)

b. Use the radiation condition (2.3.5), saving only terms of leading order in $i\omega$, to eliminate one term on each side, $x > \xi$ and $x < \xi$, and conclude that[13]

$$g(x,\xi,\omega) = \begin{cases} C_+(i\omega)^\beta \dfrac{\sqrt{c(x)}}{2i\omega} \exp\left\{ i\omega \displaystyle\int_\xi^x dx'/c(x') \right\}, & x > \xi, \\ \\ C_-(i\omega)^\beta \dfrac{\sqrt{c(x)}}{2i\omega} \exp\left\{ i\omega \displaystyle\int_x^\xi dx'/c(x') \right\} & x < \xi. \end{cases}$$

c. Now, to determine $C_\pm$ and β, we must apply the correct conditions at $x = \xi$. First, we must require that g itself be continuous at ξ. (If not, the first derivative would be a delta function and the second derivative would be an even more singular distribution.) Show that continuity at $x = \xi$ leads to the requirement that $C_+ = C_-$.

d. The first derivative will be discontinuous at $x = \xi$. We want to pick that jump so that the second derivative exactly matches the delta function on the right hand side of (2.3.4). Choosing that jump to be equal to -1 will do the trick! Show that this condition determines the power β as well as the common constant $C_\pm$, and that the WKBJ approximate Green's function is

$$g(x,\xi,\omega) = \begin{cases} -\dfrac{\sqrt{c(\xi)c(x)}}{2i\omega} \exp\left\{ i\omega \displaystyle\int_\xi^x dx'/c(x') \right\}, & x > \xi, \\ \\ -\dfrac{\sqrt{c(\xi)c(x)}}{2i\omega} \exp\left\{ i\omega \displaystyle\int_x^\xi dx'/c(x') \right\}, & x < \xi. \end{cases}$$

2.15 A neutralizer is an infinitely smooth function that is equal to 1 on an interval I and vanishes outside a larger interval J, where I is a subset of J. Neutralizers are convenient mathematical tools for restricting the support of a function without introducing new singularities into the function or its derivatives. Consider the x-integral in (2.5.5), except that $b \equiv b(y)$, independent of ω. Introduce a neutralizer, $\nu(x)$, such that, on the support interval of this function, each of the functions of x are infinitely differentiable. Multiply the integrand by this factor. Call the resulting integral $\alpha_\nu(y)$:

---

[13] Note that one negative power of $i\omega$ has been introduced here, as compared to the general discussion of the previous exercise. The reason for doing this is that we "know" this is right from the constant-coefficients Green's function, which has already been calculated. However, it has the effect of shifting β by 1, compared to the discussion of the previous exercise.

$$\alpha_\nu(y) = -b(y) \int_0^\infty dx\, \nu(x) \frac{\alpha(x)A^2(x)}{4c^2(x)} \int_{-\infty}^\infty d\omega\, F(\omega) e^{2i\omega\tau(x,y)}.$$

Assume also that $c(x)$ is bounded away from zero. Now carry out the x-integration symbolically via repetitive integration by parts, integrating the exponential and differentiating the amplitude. Introduce multipliers (and divisors) of the derivative of $\tau(x,y)$ as necessary. Conclude that

$$\alpha_\nu(y) = \int_0^\infty dx \frac{d}{dx}\left[-c(x)\frac{d}{dx}\right]^{n-1}\left[\nu(x)\frac{\alpha(x)A^2(x)}{4c(x)}\right] \cdot \int_{-\infty}^\infty d\omega\, (2i\omega)^{-n} F(\omega) b(y) e^{2i\omega\tau(x,y)}, \qquad n = 1,2,3,\cdots.$$

Conversely, suppose that on the support of $\nu(x)$ the perturbation $\alpha(x)$ has a discontinuity at x_0, an interior point of the interval where $\nu(x) \equiv 1$, but that the integrand is otherwise as described above. Now show that

$$\alpha_\nu(y) = [\alpha(x_0+) - \alpha(x_0-)] \frac{A^2(x_0)b(y)}{4c(x_0)} \int_{-\infty}^\infty d\omega (2i\omega)^{-1} F(\omega) e^{2i\omega\tau(x_0,y)} + \left\{\int_0^{x_0-} + \int_{x_0+}^\infty\right\} dx \frac{d}{dx}\left[\nu(x)\frac{\alpha(x)A^2(x)}{4c(x)}\right] \cdot \int_{-\infty}^\infty d\omega\, (2i\omega)^{-1} F(\omega) b(y) e^{2i\omega\tau(x,y)}.$$

That is, x-intervals where the integrand is infinitely differentiable lead to Fourier integrals in which the integrand decays faster than any algebraic power of ω. On the other hand, x-intervals where $\alpha(x)$ (or $A(x)$ or $c(x)$) are discontinuous lead to Fourier integrals with an integrand that is of order $1/i\omega$. Thus, the latter double integrals are "asymptotically dominant" over the former integrals over smooth functions for the condition of high frequency. Similarly, a discontinuity in some derivative of the integrand leads to contributions of one higher negative order in ω. Because the x-integral can be decomposed into such "neutralized" integrals, we can conclude that contributions of algebraic order in ω arise from these discontinuities of the integrand, while intervals where the integrand is infinitely differentiable contribute more negligibly to the Fourier integral.

2.5.3 *Implementation of the Variable-Wavespeed Theory*

Consider again the scattered field $u_S(0,\omega)$, from the two-reflector model of Exercise 2.14 and equation (2.4.27), given as

$$u_S(0,\omega) = -F(\omega)\frac{c_0}{2i\omega}\frac{R_1 + R_2 e^{2i\omega[h_2-h_1]}}{1 + R_1 R_2 e^{2i\omega[h_2-h_1]}} e^{2i\omega h_1/c_0}. \tag{2.5.17}$$

We will now perform a more sophisticated inversion of this u_S than was done in Section 2.4.2. Our plan will be to use the variable-wavespeed inversion formula for the reflectivity $\beta(y)$, derived in the previous section.

In the first medium, for $0 \leq y < h_1$, the wavespeed is c_0 and the WKBJ Green's function has exactly the same form as the exact Green's function that we have seen before. This means that for this case, the WKBJ Green's function in (2.5.1) is the same as the exact right-traveling wave (where positive y lies in the direction to the right of the source), represented by equation (2.4.1). Consequently, the first pass at inverting these data for the reflectivity function is just the result (2.4.29). As before, the first reflector is found to be located at $y = h_1$, with reflection coefficient R_1. (Remember, the output is now measured in terms of the output coordinate y instead of the input coordinate x.) From this output it is possible to solve for the propagation speed, c_1 for $y > h_1$.

Updating the Incident Field with Approximate Green's Functions

We now go beyond the constant-background theory of Section 2.4. For $y > h_1$, we use the WKBJ Green's function that takes account of the jump in propagation speed at $y = h_1$. In fact, the WKBJ Green's function in this range is just the function, $u_T(y, \omega)$ defined in (2.4.6), with h replaced by h_1. Therefore, in the range $y > h_1$, the amplitude, phase, and Green's function are now

$$\begin{aligned} A &= -c_0 T_1 = -\frac{2c_0 c_1}{c_0 + c_1}, \\ \tau(y, 0) &= \frac{y - h_1}{c_1} + \frac{h_1}{c_0}, \\ g_{\text{WKBJ}}(y, \omega) &= \frac{A}{2i\omega} e^{i\omega\tau(y,0)}. \end{aligned} \tag{2.5.18}$$

Note, this is not the exact right-traveling field in the range $h_1 \leq y < h_2$. It is only the representation of the first right-traveling arrival and, as such, does not contain any of the contributions of the multiple scattering in the $h_1 \leq y < h_2$ layer.

Changing both the factor of A and the phase in the inversion formula effectively "updates" the incident field $u_I(0, \omega)$ to account for transmission through the first interface. If $u_I(0, \omega)$ is modified in this manner, the single reflection from the interface back towards $x = 0$ becomes part of the *incident field.* That is, if the second line of (2.4.5) represents u_I for $x > h_1$, the first line of (2.4.5) represents u_I for $x < h_1$. In this case, equation (2.4.25) no longer represents u_S for this new u_I. Just as one term was subtracted from the total field of Exercise 2.11 to obtain the scattered field in (2.4.25), a second term should now be subtracted.

In higher-dimensional problems, however, such an updating would be computationally expensive and numerically impractical. Owing to the lack

of accuracy in the identification of layers and the determination of propagation speeds in the real world, it is not reasonable to expect to see the *perfect* cancellations in field data like those seen in this analytical example. For the present we will continue the processing *without* modifying u_S, and reserve that correction for the next subsection.

Under this assumption, the formula for $\beta(y)$ is given by

$$\beta(y) = \frac{-2}{\pi c_0^2 T_1^2} \int_{-\infty}^{\infty} i\omega \, u_S(0,\omega) e^{-2i\omega[(y-h_1)/c_1 + h_1/c_0]} d\omega. \tag{2.5.19}$$

Substituting the u_S from equation (2.4.27) into this formula for $\beta(y)$ (with the denominator of u_S expanded into its geometrical series representation), yields

$$\begin{aligned}\beta(y) = \frac{2}{\pi c_0^2 T_1^2} \int_{-\infty}^{\infty} F(\omega) c_0 \Big[& R_1 e^{2i\omega h_1/c_0} + R_2[1 - R_1^2] e^{2i\omega[h_2 - h_1]/c_1 + 2i\omega h_1/c_0} \\ & + R_2[1 - R_1^2] \sum_{n=2}^{\infty} [-R_1 R_2]^{n-1} e^{2in\omega[h_2 - h_1]/c_1 + 2i\omega h_1/c_0} \Big] \\ & \cdot e^{-2i\omega[(y-h_1)/c_1 + h_1/c_0]} \, d\omega, \quad y > h_1.\end{aligned} \tag{2.5.20}$$

Here, the first term of the sum in (2.4.27) has been placed on the first line and the lower limit of the sum has been taken to start from $n = 2$.

The integration is to be carried out term-by-term. The result is a series of bandlimited delta functions, as in (2.4.29). The locations of the support of some of the delta functions have changed, however. The first integrand had phase $-2i\omega[y - h_1]/c_1$. Therefore, this output (the first integrated term in (2.5.20) is proportional to $\delta(y - h_1)$. This representation is valid only for $y > h_1$, however. We reject this term, therefore, because we are concerned only with $y \leq h_1$, at this point in our discussion. (Note that if this term were retained, the reflection coefficient would be R_1/T_1^2, representing an error from the correct value.)

The second integral in (2.5.20) has phase $-2i\omega[h_2 - y]/c_1$, producing a delta function with support at h_2. Note that the modified phase of this inversion integral, as compared with the phase of the constant-background inversion integral, places the second reflector at its proper location. Denote this contribution to $\beta(y)$ by $\beta_2(y)$. The complete value is

$$\begin{aligned}\beta_2(y) &= \frac{1}{\pi c_0^2 T_1^2} \cdot c_0 R_2 \left[1 - R_1^2\right] \int_{-\infty}^{\infty} F(\omega) e^{-2i\omega[y - h_2]/c_1} \, d\omega \\ &= \frac{R_2}{\pi c_1} \int_{-\infty}^{\infty} F(\omega) e^{-2i\omega[y-h_2]/c_1} \, d\omega \\ &= R_2 \delta_B(y - h_2).\end{aligned} \tag{2.5.21}$$

The first line here is just a direct substitution, as stated above the equation; the second line is obtained by using the definitions of R_1 in (2.4.26) and T_1 in (2.5.12); the third line uses the result (2.4.14).

This result properly locates the second reflector and identifies its correct reflection coefficient. From the reflection coefficient and the known value of c_1 it is possible, in this analytic example, to determine the speed c_2. This is an improvement over the constant-background inversion.

The remaining integrals in (2.5.20) yield spurious "reflectors" beyond h_2, now at multiples of $h_2 - h_1$ rather than multiples of $[h_2 - h_1]c_0/c_1$, the positions of the constant-background inversion in (2.4.29). Given the now-known change in propagation speed at $y = h_2$, however, we know those outputs are inaccurately placed. Of course, we also know that these multiples are spurious artifacts.

To proceed further, it is necessary to determine the WKBJ Green's function for $y > h_2$. As in the previous case, it is not the exact Green's function, but only the first arrival of the right-traveling wave. As in the inversion in the region $h_1 \leq y \leq h_2$, the WKBJ Green's function does not take into account the portion of the right-traveling field that results from the multiple bounces in the layer. Using this Green's function is consistent with the fact that our inversion theory is based, in part, on the Born approximation, which ignores multiply scattered events.

The solution needed for the theory developed above is deduced by treating the Green's function defined in (2.5.18) as an incident wave. We then determine the transmitted wave through the interface at h_2, while disregarding the presence of multiple reflections. This function is given by

$$\begin{aligned} g(y,\omega) &= \frac{A}{2i\omega} e^{i\omega\tau(y,0)}, \\ \tau(y,0) &= \frac{y-h_2}{c_2} + \frac{h_2-h_1}{c_1} + \frac{h_1}{c_0}, \\ A &= -c_0 T_1 T_2, \qquad T_2 = \frac{2c_2}{c_1+c_2}. \end{aligned} \tag{2.5.22}$$

The corresponding formula for the reflectivity in the region $y > h_2$ is given by

$$\beta(y) = \frac{-2}{c_0^2 T_1^2 T_2^2} \int_{-\infty}^{\infty} i\omega\, u_S(0,\omega) e^{2i\omega[(y-h_2)/c_2 + (h_2-h_1)/c_1 + h_1/c_0]} d\omega. \tag{2.5.23}$$

When the data are substituted into equation (2.5.23) we have

$$\begin{aligned} \beta(y) = \frac{2}{\pi c_0^2 T_1^2 T_2^2} \int_{-\infty}^{\infty} F(\omega) c_0 \Bigg[\left(R_1 + R_2[1-R_1^2] e^{2i\omega[h_2-h_1]/c_1} \right) e^{2i\omega h_1/c_0} \\ + R_2[1-R_1^2] \sum_{n=2}^{\infty} [-R_1 R_2]^{n-1} e^{2in\omega\Psi + 2i\omega h_1/c_0} \Bigg] \\ \cdot e^{-2i\omega[(y-h_2)/c_2 + h_1/c_0]}\, d\omega, \quad \text{for} \quad y > h_2. \end{aligned} \tag{2.5.24}$$

Here $\Psi \equiv [(y-h_2)/c_2 + (h_2-h_1)/c_1]$.

The first two integrated terms in (2.5.24) will now produce delta functions with support outside the domain of validity of this inversion formula. The remaining terms produce delta functions with support at $y = h_2 + (n-1)(h_2 - h_1)c_2/c_1$. Therefore, the spurious reflectors that arise from multiple reflections in the interval (h_1, h_2) survive this inversion using a "primaries-only" Green's function. On the other hand, a third reflector beyond h_2 may be hypothesized. It should be clear that the phase of this primaries-only Green's function is ideally suited for the identification of this next hypothetical reflector.

Updating the Field with the Exact Green's Function

We now consider using the exact Green's function for $y > h_2$. This function is derived in Exercise 2.16. The new Green's function is the same as the result (2.5.22), except for the value of A:

$$A = -\frac{c_0 T_1 T_2}{1 + R_1 R_2 e^{2i\omega(h_2 - h_1)/c_1}} \tag{2.5.25}$$

This amplitude is a function of ω. Our inversion theory was developed for an amplitude that is independent of ω. If we are to use this amplitude in the inversion formula (2.5.13), at the very least the amplitude must appear under the integral sign instead of outside of it. Though an inversion theory has not been created to justify this extension, we substitute this amplitude in (2.5.13), the phase $\tau(y, 0)$ defined in (2.5.22), and the representation (2.4.25) for $u_S(0, \omega)$.

The resulting integral is

$$\beta(y) = \frac{1}{\pi c_0 T_1^2 T_2^2} \int_{-\infty}^{\infty} \left[R_1 + R_2 e^{2i\omega[h_2 - h_1]/c_1}\right] \left[1 + R_1 R_2 e^{i\omega[h_2 - h_1]/c_1}\right] \cdot F(\omega) e^{-2i\omega[(y-h_2)/c_2 + (h_2 - h_1)/c_1]}\, d\omega. \tag{2.5.26}$$

Note that one result of using this amplitude has been to remove the denominator of the response. This was the factor that led to the geometric series and the set of spurious reflectors from the multiple reflections. The integral is now a finite sum; it is a linear combination of four delta functions. The supports of these delta functions are at the points, $h_2 - (h_2 - h_1)c_2/c_1 < h_2$, h_2, (two of them), and $h_2 + (h_2 - h_1)c_2/c_1$. All but the last of these points are in $y > h_2$, which is outside the region of validity of this inversion. For bandlimited data, the support of the middle delta function does extend into the domain of validity. Because the location and reflection strength of the reflector at $y = h_2$ will have been determined before this computation, this output would not be used to identify the reflector at $y = h_2$. The last delta function has support in the domain of interest, but an amplitude that is $O(R^3)$, generally significantly smaller than the output from primary reflections and no worse than the first term of the infinite series obtained with the cruder inversion. This operator, though of questionable theoretical

validity, has successfully annihilated all but one of the spurious reflectors arising from multiple reflection responses in the input data.

It is obvious that the two spurious delta functions here result from the extra factor of $(1 + R_1 R_2 e^{2i\omega[h_2 - h_1]})$ in the numerator which comes from the square of the Green's function present in the inversion formula. It may occur to the reader that simply introducing a single factor of this variety in any of the WKBJ Green's function–based inversion formulas would remove the spurious multiples. We might justify this by considering that we should use the WKBJ Green's function for the right-traveling Green's function, but use the exact Green's function for the left-traveling Green's function. Our use of the Born approximation makes it difficult to justify this choice, because our theory explicitly rejected the importance of multiple scattering.

Multiple-Suppression by Deconvolution

An alternate way of looking at this is to consider applying a factor of $(1 + R_1 R_2 e^{2i\omega[h_2 - h_1]})$ to u_S as a frequency-domain *preprocessing* step before performing the inversion. In other words, we might consider applying a step to "deconvolve" the signal to suppress the multiples. Indeed, a classical technique for suppressing water-bottom multiples is to convolve a seismic trace with all or some part of itself [Backus, 1959]. Because of our exact knowledge of the wavespeed and water-layer thickness in the example above, we are able to construct an exact, amplitude-preserving deconvolution operator from wave-theoretic considerations. (For classic papers in the use of deconvolution, see Webster [1978], and for more recent papers on related topics, see Robinson and Osman [1996].)

Unfortunately, the computation of the Green's function amplitude in a way that accounts for multiple reflections is far more difficult in higher-dimensional problems owing to curved reflecting surfaces, and an imprecise knowledge of the wavespeeds and layer thicknesses in the media. In earlier times, the techniques that were used involved identifying attributes of the spectra of the data that are characteristic of such multiples, and suppressing them via techniques such as *Wiener filtering*. More recently, operator-based theories have been developed. While they seem promising at this time, they are also highly computer intensive. The discussion of such techniques is beyond the scope of this text, although we include some references to the approaches that are more closely related to our inversion procedures. Here, we will assume only that, if such techniques have been applied as a preprocessing step, they do not degrade the amplitudes of the data.

The demonstration of an exact wave-theoretic, amplitude-preserving deconvolution operator presented here is encouraging, but it will certainly be difficult to realize in higher-dimensional problems. Even in one dimension, it is not likely that estimates of the reflector locations and their respective reflection coefficients can be determined with sufficient accuracy to yield the perfect annihilation of spurious reflectors seen in this analytical exam-

ple. Such approaches should lead to an amplitude at the spurious reflectors that is smaller than predicted by the multiple powers of reflection coefficients appearing in the previous inversion result. Finally, note that even for small reflection strengths, ultimately the error has to accumulate, and both the location of reflectors and estimates of reflection strength must degrade. Thus, to be practical, such methods most likely must exploit the primary reflections in the data itself, as a way of constructing the necessary estimates of the secondary, tertiary, and so forth, reflections that constitute the multiples. The estimate of the multiples could then be used to annihilate the multiples in the data.

Approximate methods of multiple suppression, related to the method we describe above, have been studied. One such method is the inverse-scattering series method of multiple suppression of Weglein, et al. [1997], Weglein and Matson, [1998] and Weglein, [1999], which is a higher-dimensional version of the simple example we present, but which exploits the primary reflections in the data in the manner we have discussed at the end of the previous paragraph.[14]

2.5.4 Summary

We have seen from our 1D example some features of the implementation of the WKBJ inversion operator.

1. First, an inversion using a "free-space" Green's function is carried out, with the output variable allowed to range far enough to identify the bandlimited delta function corresponding to the first reflector.
2. The peak amplitude of that output is used to estimate the change in propagation speed.
3. The Green's function is revised beyond the first reflector to account for the change in propagation speed. Although this effectively revises what is meant by the incident field and scattered field observations, in practice the scattered field is not adjusted. If the revised amplitude and phase of the Green's function were "perfect," the next reflector and reflection strength would be accurately determined and the WKBJ Green's function could be accurately updated.
4. Beyond the position of the primary reflector, the inversion with the WKBJ Green's function produces false reflectors from the multiple reflection response of the reflectors already determined. An oddity of the one-dimensional problem is that inversion using the exact transmitted Green's function annihilates all but one of these false reflectors arising from multiple reflections. In practice, owing to the practical limitations

[14]See Berkhout and Verschuur [1997] and Berkhout [1999] for a discussion of iterative methods of multiple removal. See also Filpo and Tygel, [1999] and Sen et al. [1998].

stated earlier in the section, there will be no attempt to make such a detailed updating of the Green's function

In the computer implementation of this theory, the primaries-only Green's function for a particular layer is used to process data far enough into the next layer to completely form at least the main lobe of the bandlimited delta function associated with the reflector between the layers. The updated Green's function is then used starting at a distance from the reflector. Clearly, for this process to be successful, the layers must be separated enough for the bandlimited delta functions to be distinct. This is consistent with an asymptotic theory. The length scales of the problem, such as the separation between successive reflectors, have to be "many" units of reciprocal wave number in length; in practice, "many" translates into "at least three." (See the discussion of reciprocal wavenumber in Chapter 1, page 6.) Again, in practice, π is more convenient to use as a scale than three because of the factor of π in the relationship between wavenumber and wavelength.

Exercises

2.16 In Exercise 2.11, show that for $x > h_2$,

$$u(x,\omega) = -\frac{c_0}{2i\omega}\frac{[1+R_1][1+R_2]}{1+R_1R_2e^{2i\omega[h_2-h_1]/c_1}} \cdot \exp\{i\omega[(x-h_2)/c_2 + (h_2-h_1)/c_1 + h_1/c_0]\}.$$

2.6 Reevaluation of the Small-Perturbation Assumption

In the previous sections, we created 1D inversion operators that have the form of Fourier transform–like integrals. Our method of derivation contained an explicit *small-perturbation* assumption that was expressed through our use of the Born approximation. The results of the analytic investigation of the 1D inversion operators, however, showed that, even in multilayer problems with arbitrarily large wavespeed jumps (conditions that clearly violate the small perturbation assumption), it was still possible to extract useful estimates of reflection strength and of reflector locations. The primary error caused by a large wavespeed jump in multilayer media was the introduction of a series of reverberations into the data. Though the size of these reverberations *does* depend on the size of the respective wavespeed jumps, we saw that the arrivals of interest, representing the true reflectors, were not greatly distorted.

While our inversion formulas could not eliminate the reverberations, the formulas did accurately represent the size and location of the reflectors, exhibiting only a systematic error that depends continuously on the size of the perturbation. Where we were able to eliminate reverberations from the data via a preprocessing step, our inversion formulas yielded acceptable results, *even for large jumps in wavespeed.* This degree of success suggests that the small-perturbation assumption, while necessary for the derivation, was really too stringent a requirement of the inversion formulas themselves.

In other words, the formulas work *better* than we expected, given the small-perturbation assumption, because we were able to separate the inversion problem into a preprocessing step to extinguish multiples before actually applying the inversion formula. Again, our experiences parallel those of the geophysical community, reflecting the mathematical support for geophysical common sense. In the real world, multiple suppression has traditionally been treated as a separate subject from migration.

2.7 Computer Implementation

We can see other parallels between our theoretical approach and the experiences of geophysicists when we try to implement equations (2.5.12) and (2.5.13) in a computational setting. These two equations represent a simple *data transformation* operation. In particular, note that (2.5.12) is just the inverse Fourier transform of the data, $u_S(0,\omega)$, evaluated at the "time" $2\tau(0,y)$, making

$$\alpha(y) = -\frac{8c(y)}{A^2(y)} U_S(0, 2\tau(0,y)). \tag{2.7.1}$$

Here, U_S denotes the signal in the time domain. This result shows that it is not necessary to transform the data to the frequency domain to obtain $\alpha(y)$. In practice, however, there are good reasons to do so. The data may contain high-frequency noise, beyond the range where coherent information can propagate. Thus, a filter could be applied in the frequency domain to truncate the bandwidth of the data and taper it smoothly to zero. Again, this is an example of separating the inversion or imaging problem into a preprocessing step followed by a migration.

To continue the discussion, let U_S denote the time-domain data, which may or may not have been filtered. Seismic data are usually acquired with a constant time sampling interval. Any processing (Fourier transform, followed by filtering, followed by an inverse transform) produces output with the same constant time interval. For uniform values of the output spatial variable y, however, the associated traveltime values, $\tau(0,y)$, which are required for the migration process, are not guaranteed produce values that fall exactly on the time sample values of the original data. Thus, given a value of y, with a corresponding value of $\tau(0,y)$, it usually is necessary to

interpolate between adjacent values of t to convert the computed $\tau(0, y)$ values into the y values necessary for the computation of $\alpha(y)$ or $\beta(y)$. The best interpolation scheme is to resample the data by fitting a sinc-function to the datapoints. This is computationally expensive, so linear interpolation is often used. It has been the experience of the authors that linear interpolation gives somewhat ragged results, even for numerically generated synthetic data. A compromise is to use quadratic interpolation, which gives satisfactory results in most cases.

Computation of $\beta(y)$ using (2.5.13) requires one additional step. The data either have to be differentiated in the time domain or have to be multiplied by $i\omega$ in the frequency domain, along with whatever other filtering is done. In practice the latter approach is used because finite-difference differentiation on noisy data may not yield satisfactory results. It is useful, therefore, to define the *preprocessed data* as

$$D(t) = \frac{1}{2\pi} \int_{-\infty}^{\infty} i\omega \, u_S(0, \omega) e^{-i\omega t} \, d\omega, \tag{2.7.2}$$

and write the inversion formula as

$$\beta(y) = -\frac{4}{A^2(y)} D(2\tau(0, y)). \tag{2.7.3}$$

Again, we must interpolate the data from the uniform grid in t to the uniform grid in y.

Note that, in the course of creating these computational algorithms, we have reduced the 1D inversion problem to, at most, a frequency-domain filtering operation followed by a shift of the data—both linear processes. The higher-dimensional results that we derive in Chapters 3 and 5 are also reducible to a "data transformation" operation, which involves summing over equal traveltimes in the data.

This simplification is no surprise to the geophysicist, because this result fits the traditional *linear systems* model of data processing. The advantage of our more mathematically rigorous approach is that it allows us to see why our results work and, more importantly, to analyze potential problems that may arise. Our approach will allow us to extend our formulas to more general inversion problems. Our mathematical insights will also prove invaluable in dealing with additional computer implementation issues.

2.7.1 Sampling

We return to the issue of spatial and temporal sampling of data. The sampling interval in y should be determined by the bandwidth of the data. Recall that the theory predicts that $\beta(y)$ has the form of a series of bandlimited delta functions. Suppose, for example, that the useful bandwidth of the data ranges from $2\pi f_{min} = \omega_{min}$ to $2\pi f_{max} = \omega_{max}$ and the filter

is a simple box function in the frequency domain. Then, using $c(h)$[15] as an approximation of $c(y)$ near $y = h$, the bandlimited delta function observed on output has the form

$$\begin{aligned}\delta_B(y-h) &= \frac{1}{\pi c(h)} \int_{\omega_{min} \le |\omega| \le \omega_{max}} e^{-2i\omega(y-h)/c(h)}\, d\omega \\ &= \frac{1}{\pi(y-h)} \left[\sin 2\omega_{max}(y-h)/c(h) - \sin 2\omega_{min}(y-h)/c(h)\right] \\ &= \frac{2}{\pi(y-h)} \sin\left[(\omega_{max} - \omega_{min})(y-h)/c(h)\right] \\ &\qquad \cdot \cos\left[(\omega_{max} + \omega_{min})(y-h)/c(h)\right] \qquad (2.7.4) \\ &= \frac{2}{\pi(y-h)} \sin\left[2\pi(f_{max} - f_{min})(y-h)/c(h)\right] \\ &\qquad \cdot \cos\left[2\pi(f_{max} + f_{min})(y-h)/c(h)\right].\end{aligned}$$

The first zeros of this function away from $y = h$ occur when the argument of the cosine is equal to $\pi/2$; that is, when $|y-h| = c(h)/4[f_{max} + f_{min}]$. Thus the width, w, of the main lobe of $\delta_B(y-h)$ is just twice this value,

$$w = \frac{c(h)}{2[f_{max} + f_{min}]}. \qquad (2.7.5)$$

The sampling interval in y should be sufficient to delineate this main lobe. A suitable sampling interval is one that will provide four points per wavelength:

$$\Delta y = \frac{c(h)}{8[f_{max} + f_{min}]}. \qquad (2.7.6)$$

It is normal practice to select a constant sampling interval for the entire output. In this case, instead of $c(h)$, we choose the minimum background propagation speed for the entire section.

This interval should be compared with the alternative based on the sample interval in time, Δt; the sampling interval $c\Delta t/2$ is often used. The extra factor of 2 occurs here as in the definition of the wave number k, because of the effective speed $c/2$ in the two-way traveltime between the source/receiver position and the scatterer. Using values reasonable for a seismic experiment, suppose that

$$f_{max} = 40 \text{ Hz}, \quad f_{min} = 10 \text{ Hz}, \quad c = 1500 \text{ m/s}, \quad \Delta t = .004 \text{ s}. \qquad (2.7.7)$$

In this case,

$$\frac{c}{8[f_{max} + f_{min}]} = 3.75\text{m}, \quad \frac{c\Delta t}{2} = 3\text{m}. \qquad (2.7.8)$$

---

[15] For the discontinuous example of the previous section, we would use the limit from the right, $c(h-)$.

The latter choice samples 25% more densely than the former. Such oversampling, while not a computational burden in one-dimensional inverse problems, may prove too expensive in higher-dimensional problems.

This discussion is a bit of a red herring, because, in field-recording practice, Δt is *purposely* chosen to oversample the data. Instead of using $c\Delta t/2$, one could certainly choose $c\Delta/k$, where k is a tunable parameter, if $c\Delta t/2$ was seen to be too much of an oversampling.

2.8 Variable Density

The one-dimensional problem for both variable density and variable wavespeed will be considered here. The main result will be that inversion will now yield an estimate of the *impedance* of the medium, involving the product ρv, with ρ and v being the density and the propagation speed, respectively. We will see that, from the type of experiment discussed so far, it is not possible to obtain changes in medium parameters; something more has to be done. It is not our intent to present the best solution to the one-dimensional inverse problem here. (Recall that this chapter is really just a "warm-up" for the more difficult higher-dimensional inversion problems of later chapters.) For inversion in higher dimensions, the same methods we employ here will provide a means of separating out parameters. The problem considered in this chapter will correspond to the simplest configuration of coincident source and receiver (zero-offset, backscatter, pulse-echo, monostatic) in higher dimensions. Thus, this final section is presented because of its more general problem formulation and because it presents a more realistic inversion output than does the simpler problem of variable soundspeed alone, treated above.

We begin by considering the acoustic equation for pressure in a variable-soundspeed, variable-density medium with source at a point x_s:

$$\begin{aligned}\mathcal{L}u(x,x_s,\omega) &\equiv \rho(x)\frac{d}{dx}\left[\frac{1}{\rho(x)}\frac{du(x,x_s,\omega)}{dx}\right]+\frac{\omega^2}{v^2(x)}u(x,x_s,\omega)\\ &= -\delta(x-x_s). \end{aligned} \tag{2.8.1}$$

The radiation condition

$$\frac{du}{dx}\mp i\frac{\omega}{v(x)}\to 0, \quad \text{as} \quad x\to\pm\infty$$

is the same as in previous problems.

The density and wavespeed functions, $\rho(x)$ and $v(x)$, are assumed to be known in the vicinity of the source and to be bounded at some large value of $x > 0$, finally becoming constant at large range. The impulse response will be observed at a point x_g, located in the range of x where the density and velocity functions are known.

As before, perturbation theory will be used to describe the problem. It is desirable here to introduce a notation that allows variations in density and soundspeed to have parallel form. Therefore, set

$$\rho(x) = \rho_0(x) + \delta\rho(x), \qquad \frac{1}{\rho(x)} = \frac{1}{\rho_0(x)}\left[1 - \frac{\delta\rho(x)}{\rho_0(x)}\right],$$
$$v(x) = v_0(x) + \delta v(x), \qquad \frac{1}{v^2(x)} = \frac{1}{v_0^2(x)}\left[1 - \frac{2\delta v(x)}{v_0(x)}\right]. \tag{2.8.2}$$

These representations are substituted into (2.8.1), and only linear terms in $\delta\rho$ and δv are retained. After some algebra, the resulting equation is

$$\begin{aligned}\mathcal{L}_0 u &= \rho_0 \frac{d}{dx}\left[\frac{1}{\rho_0}\frac{du}{dx}\right] + \frac{\omega^2}{v_0^2}u \\ &= -\delta(x - x_s) + \frac{\omega^2}{v_0^2}\frac{2\delta v}{v_0}u + \frac{d}{dx}\left[\frac{\delta\rho}{\rho_0}\right]\frac{du}{dx}.\end{aligned} \tag{2.8.3}$$

As in the previous derivation, we introduce $u_I(x, x_s, \omega)$ as the response to the delta function in the unperturbed medium and $u_S(x, x_s, \omega)$ as everything else:

$$u(x, x_s, \omega) = u_I(x, x_s, \omega) + u_S(x, x_s, \omega), \tag{2.8.4}$$

with

$$\mathcal{L}_0 u_I(x, x_s, \omega) = -\delta(x - x_s). \tag{2.8.5}$$

We now use equations (2.8.4) and (2.8.5) in (2.8.3). As in the earlier derivation, we neglect terms in products of the perturbations and u_S on the left side of the equation and obtain

$$\mathcal{L}_0 u_S(x, x_s, \omega) = \frac{\omega^2}{v_0^2(x)}\frac{2\delta v(x)}{v_0(x)}u_I(x, x_S, \omega) + \frac{d}{dx}\left[\frac{\delta\rho(x)}{\rho_0(x)}\right]\frac{du_I(x, x_S, \omega)}{dx}. \tag{2.8.6}$$

We now propose to write down a Green's function representation of the solution to this equation, observed at the point x_g (geophone location). It should be noted here that the differential operator $\mathcal{L}_0$ is not self-adjoint. Therefore, we use the Green's function $g^\star(x, x_g, \omega)$ which is the impulse response for the "adjoint equation,"

$$\begin{aligned}\mathcal{L}_0^\star g^\star(x, x_g, \omega) &\equiv \frac{d}{dx}\left[\frac{1}{\rho_0(x)}\frac{d}{dx}[\rho_0(x)g^\star(x, x_g, \omega)]\right] + \frac{\omega^2}{v_0^2(x)}g^\star(x, x_g, \omega) \\ &= -\delta(x - x_g).\end{aligned} \tag{2.8.7}$$

We use the symmetry of the Green's function, or theorem of reciprocity, (see 2.3.1, and Exercise 2.9) to set

$$g^\star(x, x_g, \omega) = g(x_g, x, \omega). \tag{2.8.8}$$

Here, $g(x_g, x, \omega)$ is the Green's function for the operator, $\mathcal{L}_0$. Note that this Green's function differs from u_I, defined by (2.8.5). First, the source point is different: x_g instead of x_s. Second, the arguments have been interchanged, with the source point as first argument and the running variable x as second variable.

The solution of (2.8.6), written in terms of this Green's function, is

$$u_S(x_g, x_s, \omega) = -\int_0^\infty \left[\frac{\omega^2}{v_0^2(x)} \frac{2\delta v(x)}{v_0(x)} u_I(x, x_s, \omega) g(x_g, x, \omega) + \frac{d}{dx}\left[\frac{\delta\rho(x)}{\rho_0(x)}\right] \frac{du_I(x, x_s, \omega)}{dx} g(x_g, x, \omega) \right] dx \tag{2.8.9}$$

$$= -\int_0^\infty \left[\frac{\omega^2}{v_0^2(x)} \frac{2\delta v(x)}{v_0(x)} u_I(x, x_s, \omega) g(x_g, x, \omega) - \frac{\delta\rho(x)}{\rho_0(x)} \frac{d}{dx}\left[g(x_g, x, \omega) \frac{du_I(x, x_s, \omega)}{dx} \right] \right] dx.$$

In the second form of the result, we have integrated by parts to eliminate the differentiation of $\delta\rho$. The reason is that we ultimately expect to apply this result when $\delta\rho$ is discontinuous, thus this derivative is a distribution. In this form, the differentiation is carried out on the continuous functions instead.

We are concerned only with high-frequency inversion of this equation. To that end, we will use WKBJ approximations for u_I and g,

$$\begin{aligned} u_I(x, x_s, \omega) &= -\frac{1}{2i\omega} F(\omega) A(x, x_s) e^{i\omega\tau(x, x_s)}, \\ g(x_g, x, \omega) &= -\frac{1}{2i\omega} A(x_g, x) e^{i\omega\tau(x_g, x)}, \\ \tau(x, \xi) &= \int_{x_<}^{x_>} dx'/v_0(x') \\ x_< &= \min(x, \xi), \quad x_> = \max(x, \xi). \end{aligned} \tag{2.8.10}$$

It is important to note that, for the case of continuous v_0 and ρ_0,

$$A(x, x_s) = \sqrt{c(x)c(x_s)\rho(x)/\rho(x_s)}, \quad A(x_g, x) = \sqrt{c(x)c(x_g)\rho(x_g)/\rho(x)}. \tag{2.8.11}$$

We then substitute these WKBJ approximations into (2.8.10) and retain only the leading-order terms in ω $[O(\omega^2)]$, to yield the result,

$$u_S(x_g, x_s, \omega) = \int_0^\infty F(\omega) \frac{1}{2} \left[\frac{\delta v(x)}{v_0(x)} + \frac{\delta\rho(x)}{\rho_0(x)} \right] \frac{A(x, x_s) A(x_g, x)}{v_0^2(x)} \cdot e^{i\omega\{\tau(x, x_s) + \tau(x_g, x)\}} dx. \tag{2.8.12}$$

This equation should be compared with (2.5.3). Here, the source and receiver points are separated along the line; there, they were coincident. As a consequence, the observed field is $u_S(x_g, x_s, \omega)$ as opposed to $u_S(0, \omega)$, and we have two different amplitudes arising from u_I and g, whereas in (2.5.3) the square of a single amplitude appeared. Here, phase involves a sum of traveltimes from the source and receiver points to the scattering point at depth; there, the phases were the same and a two-way traveltime appeared in the exponent. The unknown $-\alpha/4$ of the previous expression is replaced by $[\delta\rho/\rho_0 + \delta v/v_0]/2$. We leave it as an exercise to show that these unknowns are "identical" when $\delta\rho = 0$.

The derivation of the inversion formula carried out below (2.5.3) can be repeated here step-by-step with these modifications in place. With some thought, it becomes apparent that the result of inversion for this equation can be deduced from (2.5.12) by making the same changes in the inversion formula as were observed in the comparison of (2.5.3) and (2.8.12). That is, we

1. rewrite (2.5.12) as an equation for $-\alpha(y)/4$;
2. replace $c(y)/A^2(y)$ by $v_0(x)/A(x, x_s)A(x_g, x)$;
3. replace $2\tau(y, 0)$ by $\tau(y, x_s) + \tau(y, x_g)$.

The result of these replacements is

$$\frac{1}{2}\left[\frac{\delta v(y)}{v_0(y)} + \frac{\delta\rho(y)}{\rho_0(y)}\right] = \frac{v_0(y)}{\pi A(y, x_s)A(x_g, y)} \int_{-\infty}^{\infty} u_S(x_g, x_s, \omega) e^{-i\omega\{\tau(y,x_s)+\tau(x_g,y)\}}\, d\omega. \tag{2.8.13}$$

Similarly, for the reflectivity, $\beta(y)$, we obtain the result,

$$\beta(y) = \frac{-2}{\pi A(y, x_s)A(x_g, y)} \int_{-\infty}^{\infty} i\omega\, u_S(x_g, x_s, \omega) e^{-i\omega\{\tau(y,x_s)+\tau(x_g,y)\}} d\omega. \tag{2.8.14}$$

Previously, $\beta(y)$ produced bandlimited delta functions, scaled by the jump in $-\alpha(y)/4$, which turned out to be just the linearized reflection coefficient. With the above replacement, this quantity is replaced by

$$\frac{1}{2}\left[\frac{\delta v(y)}{v_0(y)} + \frac{\delta\rho(y)}{\rho_0(y)}\right] = \frac{\delta(\rho v)}{2\rho v} = \frac{1}{2}\delta[\ln(\rho v)]. \tag{2.8.15}$$

That is, the bandlimited delta functions in the output $\beta(y)$ will now be scaled by the linearized approximation of the *impedance* of the medium. At a discontinuity,

$$\frac{\delta(\rho v)}{2\rho v} \approx \frac{\rho_+ v_+ - \rho_- v_-}{2\rho_- v_-} \approx \frac{\rho_+ v_+ - \rho_- v_-}{\rho_+ v_+ + \rho_- v_-} = Z. \tag{2.8.16}$$

The right side here is the exact impedance (reflection) coefficient in a variable-density medium.

In Section 2.4 it was shown that an inversion theory based on a Born approximation for the forward scattering problem yields the "exact" reflection coefficient as the scaling factor of the bandlimited delta functions in the output $\beta(y)$. The same result follows here. That is, if $u_S(x_g, x_s, \omega)$ for a discontinuous medium were replaced by its WKBJ approximation, then the exact impedance coefficient would scale the bandlimited delta functions of $\beta(y)$; that is,

$$\beta(y) \sim \sum_j \delta_B(y - h_j) Z_j. \tag{2.8.17}$$

Verification of this result will be carried out in the exercises. Unfortunately, we cannot separate the jumps in soundspeed from the jumps in density in this result. Some other kind of experiment is needed to do this. In higher dimensions, we can use source-receiver offset to provide additional information. Here, this method can go no further.

Exercises

2.17 Repeat the derivation of the 1D inversion formula in Sections 2.3.3–2.4.1 under the assumption that the data are observed at $x_g \neq 0$, still in the negative x-direction of the support of $\alpha(x)$. The source for the experiment is still at $x_s = 0$. Specialize the problem to constant-background wavespeed c_0, as in Section 2.4.1. Use the data for a single step in $\alpha(x)$ to obtain the same inversion formula (2.4.8).

2.18 Consider the propagation of a 1D acoustic wave that begins at position $x = 0$ and propagates in the positive x-direction through a medium composed of many layers. The boundaries of these layers are taken to be at the positions x_j, with $j = 1, k$. The thickness of each layer is $\Delta x_j \equiv x_j - x_{j-1}$, with $x_{-1} \equiv 0$. The wavespeed in the negative x-direction from x_0 is c_0, with the speed in each subsequent interval in the positive x-direction being c_j.

a. If the incident field in the layer Δx_0 is the free-space Green's function for a medium with wavespeed c_0, verify that the transmitted field seen at position x_k is

$$u_T(x_k, \omega) = -\frac{c_0}{2i\omega} \prod_{j=1}^{k} \left[\frac{2c_j}{c_j + c_{j-1}} \right] \exp\left\{ i\omega \sum_{i=0}^{k} \frac{\Delta x_i}{c_i} \right\}.$$

b. Show that, in the limit as the wavespeed profile becomes continuously and smoothly varying, the transmitted field is described by the WKBJ Green's function

$$g_{WKBJ}(x,0,\omega) = -\frac{\sqrt{c(0)c(x)}}{2i\omega} \exp\left\{ i\omega \int_0^x \frac{d\sigma}{c(\sigma)} \right\}.$$

Hint: Rewrite the factor in square brackets [ ] in part (a) as

$$\exp\{-\ln(1-\Delta_j/2c_j)\} = \exp\{\Delta_j/2c_j + O(\Delta_j^2)\}, \quad \text{for} \quad \Delta_j = c_j - c_{j-1}.$$

Now carry out the product over j by summing in the exponent to obtain the result

$$\sum_{j=1}^{k} = \frac{1}{2}\ln[c(x_{max})/c(x_{min})] + O(\Delta), \quad \Delta = \max_j(\Delta_j).$$

In fact, using this method, an exact series solution (called the Bremmer Series [Bremmer, 1950]) can be constructed for the 1D problem for selected wavespeed profiles. The WKBJ Green's function is the first term of this exact series.

2.19 Derive the WKBJ Green's function for the variable-density problem using the same method.

2.20 In Section 2.8, a variable-density/variable-wavespeed inversion operator was derived. Verify the derivation in the text. Assume that the perturbation is now represented as small variations in density ρ and bulk modulus κ, such that

$$\rho(x) \equiv \rho_0(x) + \delta\rho(x), \qquad \kappa(x) \equiv \kappa_0(x) + \delta\kappa(x).$$

Show that the relationship $v(x) \equiv \sqrt{\kappa(x)/\rho(x)}$ and the above definitions imply

$$\frac{1}{\rho(x)} = \frac{1}{\rho_0(x)}\left[1 - \frac{\delta\rho(x)}{\rho_0(x)}\right]$$
$$\frac{1}{v^2(x)} = \frac{1}{v_0^2(x)}\left[1 + \frac{\delta\rho(x)}{\rho_0(x)} - \frac{\delta\kappa(x)}{\kappa_0(x)}\right]$$

for small perturbations in density and bulk modulus and define $\alpha(x)$ in terms of the density and bulk modulus.

2.21 Following the method of Section 2.8, derive the inversion formula assuming variable density and variable bulk modulus.

2.22 Let $u(x,\omega)$ be a solution of (2.8.1) subject to the radiation conditions stated below that equation. Furthermore, assume that

$$v(x) \equiv v_0 = \text{constant}$$

and

$$\rho(x) = \begin{cases} \rho_0, & x < h_1, \\ \rho_1, & h_1 < x < h_2, \\ \rho_2, & h_2 < x, \end{cases}$$

with ρ_0, ρ_1, and ρ_2, constants. Furthermore, assume that at each of the interfaces,

$$u(x,\omega) \text{ continuous}, \qquad \frac{1}{\rho}\frac{du(x,\omega)}{dx} \text{ continuous}.$$

a. Show that these continuity conditions lead to exactly the same system of equations as in Exercise 2.11b, except that in the phase, all propagation speeds are replaced by v_0 and the coefficients c_0, c_1, and c_2, in the resulting continuity equations are replaced by ρ_0, ρ_1, and ρ_2. Thus, conclude that

$$u(0,\omega) = -\frac{v_0}{2i\omega}\left[1 + \frac{R_1 + R_2 e^{i\omega\tau}}{1 + R_1 R_2 e^{i\omega\tau}} e^{2i\omega h_1/v_0}\right],$$

except that now

$$R_1 \equiv \frac{\rho_1 - \rho_0}{\rho_1 + \rho_0}, \quad R_2 \equiv \frac{\rho_2 - \rho_1}{\rho_2 + \rho_1}, \quad \text{and} \quad \tau \equiv 2[h_2 - h_1]/v_0.$$

b. Conclude that the inversion (2.4.17) now yields the result

$$\beta_B(x) = R_1\delta_B(x - h_1) + R_2[1 - R_1^2]\delta_B(x - h_2) + \ldots,$$

where $(\ldots)$ represents bandlimited delta functions with support beyond h_2. That is, the locations of the first two reflectors are now *correct* because the background propagation speed is the exact speed throughout the medium and only the density changes.

3

Inversion in Higher Dimensions

In Chapter 2, formulas were created to determine the wavespeed profile of a medium with one dimension of parameter variability only, via high-frequency inversion of plane-wave data. The original plan of Chapter 2 was to invert the data for the actual wavespeed profile or, rather, the perturbation $\alpha(y)$ from a known background wavespeed profile. However, results influenced by the bandlimited nature of the data, represented by a symmetric filter $F(\omega)$, motivated a change to the new goal of imaging the *discontinuities* of the wavespeed profile—the reflectors. This yields a new output, the "reflectivity function" $\beta(y)$, which was found to consist of bandlimited delta functions having peak amplitudes occurring at reflector locations, with size scaled by the normal-incidence, plane-wave reflection coefficient. The reflectivity function is analogous to a similar reflection coefficient series that may be obtained in the process of creating a synthetic well log from seismic data. Equivalent results in higher dimensions will be the goal of all subsequent inversion formulations found in this text.

In this chapter, we will extend the one-dimensional high-frequency inversion method to the three-dimensional problem. Paralleling the derivation in Chapter 2, the starting point is a statement of a forward modeling formula, which will be an integral equation created by applying perturbation theory to the Helmholtz equation to create two Helmholtz equations. We will then create the desired integral equation by solving for the scattered field via Green's theorem. As before, the resulting integral equation will be

linearized using the Born approximation. It is this linearized formula that we will invert.[1]

Owing to the greater number of degrees of freedom afforded by the greater number of dimensions, the 3D problem has added richness. A greater number of possible recording geometries and phenomena exist (first discussed in Chapter 1), owing to the higher-dimensional variation of the background propagation speed.

A recapitulation of the method that was used to derive the high-frequency inversion formulas in Chapter 2 is outlined here as an aid to the reader. This outline is also a statement of the general program that we follow in this chapter.

Deriving a High-Frequency Inversion Formula

1. Derive a linearized forward modeling formula, written in terms of the unknown material parameters, describing the processes that generate the seismic data.
2. Find a way to invert the modeling formula to solve for the unknown material parameters.
3. Test the inversion formula, analytically if possible, on a set of known model data to see if the form of the output is satisfactory for the desired application. (If the test data are created numerically, it should be done using a *different* modeling formula than the one in step (1) to avoid a circular result.)
4. If the form of the output is not what is desired, adjust the formula accordingly. ("Adjustment" can include searching for errors in the derivation, redefining the desired goals to take into account aspects of the physics of the model and characteristics of real data, or choosing a new mathematical approach to the problem.)

As in the one-dimensional inversion problem, much insight will be gained by first deriving an inversion formula assuming a constant-background wavespeed. To simplify the problem, we introduce the added restriction that the source and receiver be located at the same place. (This source-receiver geometry is given various names, including zero-offset, normal-incidence, pulse-echo, monostatic, or backscatter experiments. See discussion on page 81.)

Solutions to this special case will be the topic of this chapter. In later chapters, we will remove this restriction, permitting the derivation of inversion formulas for a variety of source-receiver geometries.

In addition to the issue of limited bandwidth addressed in Chapter 2, the problem of limited spatial aperture—the angular coverage of the target be-

[1]Papers relevant to this discussion are Bleistein and Cohen [1979a, 1979b] and Bleistein, Cohen, and Hagin [1985].

ing imaged—must be addressed before the reader will be prepared to handle the more general problem of variable-background inversion with nonzero offset between source and receiver. This topic is addressed in Chapter 4.

3.1 The Scattering Problem in Unbounded Media

As stated above, the first step in the derivation of a high-frequency inversion formula is the creation of a forward model describing the "scattered waves." We begin the derivation by introducing the familiar right-handed Cartesian coordinate system such that $(x, y, z) = (x_1, x_2, x_3)$, with $z = x_3$ positive in the *downward* direction. The propagation speed is assumed to be known for $z < 0$ and unknown in some portion of the region $z > 0$. For now we will assume that the medium has constant density.

The waves originate from a bandlimited impulsive point source acting at the position $\boldsymbol{x}_s$ and at the time $t = 0$. The response generated by this source is observed at one or more receivers located at the receiver position(s) $\boldsymbol{x}_g$. The objective is to obtain information about the propagation speed $v(\boldsymbol{x})$ from observations of the wavefield. We assume that the signal propagation is governed by the three-dimensional Helmholtz equation,

$$\mathcal{L}u(\boldsymbol{x}, \boldsymbol{x}_s, \omega) = \left[\nabla^2 + \frac{\omega^2}{v^2(\boldsymbol{x})}\right] u(\boldsymbol{x}, \boldsymbol{x}_s, \omega) = -F(\omega)\delta(\boldsymbol{x} - \boldsymbol{x}_s). \tag{3.1.1}$$

The function $u(\boldsymbol{x}, \boldsymbol{x}_s, \omega)$ and all wavefields introduced below are assumed to satisfy the *Sommerfeld radiation conditions*,

$$ru \quad \text{bounded}, \quad r\left[\frac{\partial u}{\partial r} - \frac{i\omega}{v}u\right] \to 0 \quad \text{as} \quad r \to \infty, \quad r = |\boldsymbol{x}|. \tag{3.1.2}$$

(Compare these radiation conditions with the much simpler radiation condition in the 1D problem, stated in equation (2.2.1).) These conditions ensure the uniqueness of solutions to the Helmholtz equation in unbounded media. These conditions prevent waves from propagating inward to the source from infinity (part of the physical constraint of causality), while guaranteeing that their amplitudes decay with range at least as quickly as do those of the Green's function. By "Green's function," here we mean the impulse response obtained under the condition of causality. The added condition insures that the decay in amplitude due to geometrical spreading is represented correctly.

As in the one-dimensional problem, the wavespeed is represented as a perturbation with respect to a known reference speed, $c(\boldsymbol{x})$, expressed mathematically as

$$\frac{1}{v^2(\boldsymbol{x})} = \frac{1}{c^2(\boldsymbol{x})}\left(1 + \alpha(\boldsymbol{x})\right). \tag{3.1.3}$$

Substitution of the perturbation representation (3.1.3) into the original equation (3.1.1) produces the equivalent Helmholtz equation,

$$\mathcal{L}_0 u(\boldsymbol{x}, \boldsymbol{x}_s, \omega) = -F(\omega)\delta(\boldsymbol{x} - \boldsymbol{x}_s) - \frac{\omega^2}{c^2(\boldsymbol{x})}\alpha(\boldsymbol{x})u(\boldsymbol{x}, \boldsymbol{x}_s, \omega). \tag{3.1.4}$$

Here

$$\mathcal{L}_0 \equiv \left[\nabla^2 + \frac{\omega^2}{c^2(\boldsymbol{x})}\right]$$

is the Helmholtz operator with the known background wavespeed $c(\boldsymbol{x})$.

Again following the one-dimensional derivation, we decompose the wavefield into a reference or incident field, $u_I(\boldsymbol{x}, \boldsymbol{x}_s, \omega)$, which is the impulse response in the absence of the perturbation $\alpha(\boldsymbol{x})$, plus a scattered field, $u_S(\boldsymbol{x}, \boldsymbol{x}_s, \omega)$, which is the modification of $u_I(\boldsymbol{x}, \boldsymbol{x}_s, \omega)$ in response to $\alpha(\boldsymbol{x})$. Thus, the formal decomposition of the field is represented by

$$u(\boldsymbol{x}, \boldsymbol{x}_s, \omega) = u_I(\boldsymbol{x}, \boldsymbol{x}_s, \omega) + u_S(\boldsymbol{x}, \boldsymbol{x}_s, \omega), \tag{3.1.5}$$

with the requirement that $u_I(\boldsymbol{x}, \boldsymbol{x}_s, \omega)$ be a solution of the unperturbed equation,

$$\mathcal{L}_0 u_I(\boldsymbol{x}, \boldsymbol{x}_s, \omega) = -F(\omega)\delta(\boldsymbol{x} - \boldsymbol{x}_s), \tag{3.1.6}$$

subject to the Sommerfeld radiation conditions, (3.1.2). The factor of $F(\omega)$ contains the combined losses owing to bandlimiting discussed in Chapter 2 and will appear throughout the derivation.

An additional constraint is required for the Sommerfeld radiation conditions to hold. The size of perturbation $\alpha(\boldsymbol{x})$, must be restricted to some small subset of the total volume of the problem. Without such a restriction, the spatial extent of the scattering region could conceivably be the entire volume of the body being imaged—the total volume of the Earth, in the seismic problem.

In practice, seismic recording for a given source is done over an area of the Earth's surface limited to few kilometers, at most. In addition, the recording time of seismic data sets is restricted to no more than several seconds. If the data (possibly after a stage of preprocessing) are assumed to be high-frequency bandlimited impulses, then these spatial and temporal restrictions translate into a restriction on the volume of the Earth that is being sampled. Consequently, $\alpha(\boldsymbol{x})$ can be treated as if it is of finite extent, permitting us to assume that $v(\boldsymbol{x}) \rightarrow c(\boldsymbol{x})$ for great distances from the source. We can equate "great distance" with the distance r that appears in the statement of the Sommerfeld radiation conditions (3.1.2), greatly simplifying the derivation of the forward and inverse integral equations.[2]

[2]Owing to the petroleum industry's long experience with seismic prospecting, geophysicists select sources and recording equipment that generate data compatible with these assumptions. In other problems, for example seismology involving

We may continue the derivation, as in Chapter 2, by subtracting (3.1.6) from (3.1.4) to obtain the Helmholtz equation describing the scattered field,

$$\mathcal{L}_0 u_S(\boldsymbol{x}, \boldsymbol{x}_s, \omega) = -\frac{\omega^2}{c^2(\boldsymbol{x})}\alpha(\boldsymbol{x})\left[u_I(\boldsymbol{x}, \boldsymbol{x}_s, \omega) + u_S(\boldsymbol{x}, \boldsymbol{x}_s, \omega)\right]. \tag{3.1.7}$$

An integral equation for $u_S(\boldsymbol{x}_g, \boldsymbol{x}_s, \omega)$ can be written in terms of the Green's function, $g^\star(\boldsymbol{x}, \boldsymbol{x}_g, \omega)$, that is a solution of

$$\mathcal{L}_0^\star g^\star(\boldsymbol{x}, \boldsymbol{x}_g, \omega) = -\delta(\boldsymbol{x} - \boldsymbol{x}_g). \tag{3.1.8}$$

The superscript "$\star$" is used to distinguish the *adjoint operator* and the *adjoint Green's function*, from the *direct operator* and the direct *Green's function*, respectively. While the constant-density problem *is* self-adjoint, we will still retain the $\star$ notation for generality.

The general form of the integral equation for the scattered field u_S is created by solving equations (3.1.7) and (3.1.8) using Green's theorem, expressed here for a general operator as,

$$\int_D \{g^\star \mathcal{L}_0 u - u\mathcal{L}_0^\star g^\star\}\, dV = \int_{\partial D} \hat{\boldsymbol{n}} \cdot \boldsymbol{Q}\, dS, \tag{3.1.9}$$

where $\hat{\boldsymbol{n}}$ is the outward-directed normal to the boundary surface ∂D and $\{g^\star \mathcal{L}_0 u - u\mathcal{L}_0^\star g^\star\} \equiv \nabla \cdot \boldsymbol{Q}$. The reader should note that $\mathcal{L}_0^\star$ and $g^\star$ are simply the respective operator and Green's function needed to make the integrand of the integral on the left an exact divergence. The fact that the integrand of the left-hand side of equation (3.1.9) is an exact divergence permits us to apply the divergence theorem to create the right-hand side.

For the constant-density problem, we can explicitly write Green's theorem as

$$\int_D \{g^\star \mathcal{L}_0 u - u\mathcal{L}_0^\star g^\star\}\, dV = \int_{\partial D} \left\{ g^\star \frac{\partial u}{\partial n} - u\frac{\partial g^\star}{\partial n} \right\} dS, \tag{3.1.10}$$

where $\partial/\partial n$ is the outward normal derivative to ∂D, often written as $\hat{\boldsymbol{n}} \cdot \nabla$. For an unbounded problem (boundary ∂D at infinity), the surface integral term is zero, by the application of the Sommerfeld radiation conditions (3.1.2).[3]

Under these conditions, we may further simplify the notation by applying the reciprocity theorem,

$$g^\star(\boldsymbol{x}, \boldsymbol{x}_g, \omega) = g(\boldsymbol{x}_g, \boldsymbol{x}, \omega). \tag{3.1.11}$$

See Exercise 3.1c.

---

the whole Earth, or acoustic imaging of flaws in manufactured items, considerable effort may be required to create data sets for which all of these assumptions hold.

[3]For further details, see Courant and Hilbert [1962], Sommerfeld [1964], Garabedian [1964], or Bleistein [1984].

For the special case of the constant-density Helmholtz equation, the adjoint operator is the same as the direct operator; the constant-density Helmholtz equation is *self-adjoint*, meaning that the identity $g(\boldsymbol{x}_g, \boldsymbol{x}, \omega) = g(\boldsymbol{x}, \boldsymbol{x}_g, \omega)$ holds. In anticipation of extending the method to the more general problem, the arguments of the Green's function have been written in the proper order here.

The solution for the scattered field is the integral equation

$$u_S(\boldsymbol{x}_g, \boldsymbol{x}_s, \omega) = \omega^2 \int_D \frac{\alpha(\boldsymbol{x})}{c^2(\boldsymbol{x})} \left[u_I(\boldsymbol{x}, \boldsymbol{x}_s, \omega) + u_S(\boldsymbol{x}, \boldsymbol{x}_s, \omega)\right] g(\boldsymbol{x}_g, \boldsymbol{x}, \omega) d^3x. \tag{3.1.12}$$

Here, the domain D of integration must contain the support of $\alpha(\boldsymbol{x})$—assumed to be some finite subdomain of $z > 0$. We are free, therefore, to take D to be the semi-infinite domain $z > 0$.

Exercises

3.1 Consider the general problem

$$\mathcal{L}u(\boldsymbol{x}) = -f(\boldsymbol{x})$$
$$\mathcal{L}^\star g^\star(\boldsymbol{x}, \boldsymbol{x}_g) = -\delta(\boldsymbol{x} - \boldsymbol{x}_g).$$

a. Show that the integral equation of the field is

$$u(\boldsymbol{x}_g) = \int_D f(x) g^\star(\boldsymbol{x}, \boldsymbol{x}_g)\, dV + \int_{\partial D} \left\{ g^\star(\boldsymbol{x}, \boldsymbol{x}_g) \frac{\partial u(\boldsymbol{x})}{\partial n} - u(\boldsymbol{x}) \frac{\partial g^\star(\boldsymbol{x}, \boldsymbol{x}_g)}{\partial n} \right\} dS.$$

b. Derive the Sommerfeld radiation conditions (3.1.2) (see Bleistein [1984], pp.180-191) in the 3D problem. That is, show that the surface integral term in the integral equation for the field above vanishes as the radius of the surface becomes infinitely large, thus showing that an unbounded medium is equivalent to a medium with "boundary at infinity."

c. For a general operator $\mathcal{L}$ and its adjoint $\mathcal{L}^\star$, but for an unbounded medium, set $f = -\delta(\boldsymbol{x} - \boldsymbol{x}_s)$ in the problem above to prove the reciprocity theorem:

$$g(\boldsymbol{x}_g, \boldsymbol{x}_s) = g^\star(\boldsymbol{x}_s, \boldsymbol{x}_g).$$

3.2 Let the operator $\mathcal{L}$ be the Helmholtz form of the variable-density, acoustic-wave operator defined by the expression

$$\mathcal{L}u = \rho \nabla \cdot \left[\frac{1}{\rho} \nabla u\right] + \frac{\omega^2}{c^2} u.$$

Begin with the expression

$$I = \int_D g^\star \mathcal{L} u \, dV.$$

a. Through successive applications of the divergence theorem, show that Green's theorem for the variable-density acoustic wave equation problem is

$$\int_D [g^\star \mathcal{L} u - u \mathcal{L}^\star g^\star] \, dV = \int_{\partial D} \left[g^\star \frac{\partial}{\partial n} - \frac{u}{\rho} \frac{\partial}{\partial n} (\rho g^\star) \right] dS.$$

b. As part of this derivation, show that the adjoint operator $\mathcal{L}^\star$ is

$$\mathcal{L}^\star g^\star \equiv \nabla \cdot \left[\frac{1}{\rho} \nabla (\rho g^\star) \right] + \frac{\omega^2}{c^2} g^\star.$$

c. Show that the Sommerfeld conditions work as long as $\nabla \rho / \rho$ remains bounded at infinity.

3.2 The Born Approximation

The same difficulty seen in the 1D problem is encountered here. Equation (3.1.12) is an integral equation for the scattered field containing the product $\alpha(\boldsymbol{x}) u_S(\boldsymbol{x}, \boldsymbol{x}_s, \omega)$, meaning that it is a nonlinear equation in these two unknowns. For small $\alpha(\boldsymbol{x})$, linearization of the equation is possible if it could be argued that $u_S(\boldsymbol{x}, \boldsymbol{x}_s, \omega)$ is also small (that is, $O(\alpha)$) for α small. As in the one-dimensional problem, this quadratic term in α could then be ignored when compared to the product $\alpha(\boldsymbol{x}) u_I(\boldsymbol{x}, \boldsymbol{x}_s, \omega)$ that appears as the first term under the integral sign. Unfortunately, this is not always true in three dimensions. In particular, think of the reflected field beyond the critical angle of reflection. The reflection coefficient has unit magnitude, meaning that the amplitude of the scattered field is of comparable magnitude to that of the incident field, at least in that subdomain of D. Thus, caution must be exercised in the three-dimensional problem, because it is not always possible to neglect $\alpha(\boldsymbol{x}) u_S(\boldsymbol{x}, \boldsymbol{x}_s, \omega)$ in favor of $\alpha(\boldsymbol{x}) u_I(\boldsymbol{x}, \boldsymbol{x}_s, \omega)$.

For near-zero-offset or backscattered observations, however, it *is* true that small α implies small u_S because the major contributions to the scattered field will be the near-normally incident, specularly reflected arrivals. For near-zero-offset source-receiver geometries it is safe to make the Born approximation. The result is an integral equation relating $\alpha(\boldsymbol{x})$ to the observations $u_S(\boldsymbol{x}, \boldsymbol{x}_s, \omega)$ at the source/geophone positions $\boldsymbol{x}_g$. The Born-approximate integral equation for the scattered field is written as

$$u_S(\boldsymbol{x}_g, \boldsymbol{x}_s, \omega) = \omega^2 \int_D \frac{\alpha(\boldsymbol{x})}{c^2(\boldsymbol{x})} u_I(\boldsymbol{x}, \boldsymbol{x}_s, \omega) g(\boldsymbol{x}_g, \boldsymbol{x}, \omega) d^3 x. \tag{3.2.1}$$

This is the modeling equation that we will use as a starting point for generating the inversion formulas of this chapter. Sufficient generality has been retained to make the equation remain valid even for the variable-density problem (non-self-adjoint operator) provided that $u_I(\boldsymbol{x}, \boldsymbol{x}_s, \omega)$ and $g(\boldsymbol{x}_g, \boldsymbol{x}, \omega)$ are properly interpreted, with $\alpha(\boldsymbol{x})$ being replaced by the appropriate linear combination of perturbations of density and propagation speed (or density and bulk modulus as in Exercise 2.20). Furthermore, equation (3.2.1) also extends to scalar decomposition of vector wavefields with mode conversion, again, as long as $u_I(\boldsymbol{x}, \boldsymbol{x}_s, \omega)$ and $g(\boldsymbol{x}_g, \boldsymbol{x}, \omega)$ are properly interpreted and $\alpha(\boldsymbol{x})$ is replaced by the perturbed quantities appropriate to the problem. See the exercises for examples.

So far nothing has been said about the range of values of $\boldsymbol{x}_s$ and $\boldsymbol{x}_g$. A count of the *degrees of freedom* in the Born-approximate integral equation will help us make a decision about what is required. Implicit in the notation $\alpha(\boldsymbol{x})$ is the assumption that this quantity is a function of three variables, meaning that the perturbation has three degrees of freedom in its variation. Of necessity, then, observed data must have at least three degrees of freedom. The first of these degrees of freedom comes from the range of ω (or of time, t). The other two can come only from the range of $\boldsymbol{x}_s$ and $\boldsymbol{x}_g$. Therefore, when $\alpha(\boldsymbol{x})$ depends on all three variables, the source-receiver configuration must range over a *surface* to provide the necessary information to reconstruct the behavior of $\alpha(\boldsymbol{x})$ in the full three dimensions. Given less than surface coverage, it is unreasonable to expect to determine three-dimensional dependence of α on $\boldsymbol{x}$.

With this in mind, let us consider some of the standard configurations of inversion experiments.

Zero-Offset Surface Experiment

For this experiment, the source and receiver occupy the same position on the boundary surface of the domain containing the unknown perturbation α. The data will consist of an ensemble of such experiments.

There are good reasons to study the zero-offset problem. First, it is the easiest multidimensional inverse problem to formulate, meaning that an approach to inversion that fails on zero-offset data is not likely to succeed on more difficult problems. Second, experiments exist for which it is possible to obtain true zero-offset data. Third, though virtually all seismic data are collected using geometries involving a nonzero source-receiver offset, the advantages of processing zero-offset data have encouraged the geophysical community to create a number of preprocessing techniques to transform data to an approximate zero-offset geometry. Because the methods of seismic preprocessing are not be completely successful, amplitude information in such pseudo-zero-offset data often suffers considerable degradation. See Chapter 7 for a discussion of the proper handling of amplitudes in such *data mapping* processes.

Zero-offset geometry is practical for imaging flaws in solids and in medical ultrasound imaging, however, because the same transducer that is used as the source can also be used as the receiver. Also, with sufficient time delay between the initiation of the acoustic source pulse and the first recorded arrival, reverberations originating in the vicinity of the source-receiver array have time to dissipate.

Zero-Offset Linear Experiment

Data gathered along a single straight line with source and receiver coincident are true zero-offset data sets. Seismic data sets collected in CMP gathers, with traces moveout-corrected (by both NMO and DMO) and stacked, yield seismic sections that approximate the zero-offset geometry. In either case, there is only one spatial degree of freedom in addition to that from frequency (or time). It is not a reasonable expectation to reconstruct a three-dimensional $\alpha(\boldsymbol{x})$ from such a dimensionally constrained data set. Instead, we must be content seeking a two-dimensional inversion, with the first spatial variable on the output consisting of the horizontal spatial coordinate running parallel to the seismic line, and the second being depth into the subsurface. When the unknown medium has minimal (or no) variation in the out-of-plane direction, this is a reasonable experiment. Achieving this geometry in practice is often a matter of picking a direction along which to gather data, but the Earth and conditions on its surface may not be so accommodating. Historically, in oil exploration, gathering a single line of data was the method of choice for purely economic reasons. Processing a single line of data might also be the method of choice (as it was in earlier times) because of limited computer capacity.

Single Zero-Offset Experiment

Here, the only independent variable in (3.2.1) is ω and the reasonable expectation is to obtain α as a function of only one variable, usually depth. If it were known a priori that α is a function of one variable making some angle with the vertical, however, inversion would still be possible by a simple coordinate rotation. Such a geometry might be practical in a geologic setting consisting only of planar layers, such as in the shallow sediments of the abyssal plane in deep ocean environments; but, for petroleum exploration, this is too constrained a geological model for practical consideration.

Common-Shot Experiment

In the common- or single-shot experiment, an array of receivers is deployed, and the response to one source is recorded. When the receivers are set out in a surface array, there are again two degrees of freedom in the spatial coordinates, but all in the locations of $\boldsymbol{x}_g$, with no variation in $\boldsymbol{x}_s$. Nonetheless, at least the "count" is right, and it is reasonable to expect to invert data

from such an experiment for $\alpha(\boldsymbol{x})$, at least within some limited volume. If the receivers are set out along a line, again the degrees of freedom are reduced by one in the data, implying the same of the solution. There are two ways to use this kind of experiment. We are either solving for one unknown that is a function of two spatial variables (propagation speed variations, for example) or solving for two unknowns (propagation speed variations and density variations, for example) that are each functions of one independent variable.

In both of these problems, the forward model should still describe propagation in a three-dimensional medium; only the spatial dependence of the medium is lower dimensional. For the case of one unknown, say $v(x, z)$, the spatial dependence is two-dimensional while the propagation is three-dimensional. We call such a problem—3D propagation, 2D medium—*two-and-one-half dimensional.* The model problem should be designed in such a manner that the dependence of the medium parameters on only two spatial variables can be exploited. This cannot always be done in practice.

Synthetic Aperture

In either the three-dimensional or two-and-one-half-dimensional case, one experiment does not provide enough information to obtain an inversion of an adequate region of the unknown medium. Instead, many common-shot experiments are used to broaden the aperture of observations and thereby to increase the region of the subsurface from which upward-scattered waves are observed. These many experiments also offer some redundancy in these data. This redundancy can be used to diminish the noise-induced errors, while also permitting more sophisticated options in the choice of inversion results, such as solving for more than one material parameter. Because of the increase in aperture achieved by employing many experiments, inversion of this type has been called the *synthetic-aperture focusing technique* (SAFT) in nondestructive testing of solids.

Vertical Seismic Profiling (VSP) and Crosswell Surveys

Two special cases of common-shot experiments are worthy of special note. They are *single-offset vertical seismic profiling* and *well-to-well* experiments. In the former, a source is placed on the surface of the Earth and receivers are placed in a borehole (or vice versa). Data that reach receivers after reflection or diffraction from the scattering region are well suited to this theory. Transmitted data are not. A suite of such experiments in which the source is moved progressively further away from the borehole provides a synthetic aperture that increases the region over which an inversion can be achieved. Depending on the range of source positions, this can be a three-dimensional or two-and-one-half dimensional inverse problem.

In well-to-well experiments, sources are placed in one well or borehole, receivers in another. This is strictly a two-and-one-half-dimensional problem.

Reflection experiments of this type are referred to as *diffraction tomography* (here we mean this term in its original usage of Devaney and Oristaglio, [1984]) to distinguish them from true tomographic experiments, which invert transmitted data. Thus, diffraction tomography is neither a tomographic experiment nor a diffraction experiment, but merely another form of common-source *reflection* experiment.

Common-Offset Gathers

In seismic exploration, constructing a common-offset gather is more a matter of rearranging or sorting the data from a suite of common-shot experiments, than it is a method of gathering data in the field. In other applications, such as radar or acoustic nondestructive testing, it may be more practical to actually gather the data using this source-receiver geometry. In either case, a suite of different experiments is represented by each seismic trace, as each is the response from a single (different) source. The offset between each source and each respective receiver is fixed, with the lines between sources and receivers chosen to all be parallel. If the source-receiver pairs all lie on a single straight line, only one spatial degree of freedom exists in the observed data; thus only two-and-one-half-dimensional inversion is possible. If, however, the source-receiver pairs are not confined to a single line, but range over a surface, then, on the basis of degrees of freedom alone, we can conclude that three-dimensional inversion is possible.

Common-Receiver Gathers

This geometry consists of data set representing many sources and a single common receiver. Again, such a data set would be obtained by rearranging or sorting data from a collection of common-source gathers. The principle of reciprocity allows for the derivation of an inversion formula for common-receiver data given an inversion formula for common-shot data. The count of degrees of freedom, then, is the same as in the cases of common-shot inversion, above.

Other Choices

So far we have no other method to evaluate or eliminate from consideration any particular source-receiver configuration other than by counting the degrees of freedom. For the examples cited above, migration and inversion techniques have been demonstrated and techniques for parameter estimation have been established. Some configurations can be eliminated in a fairly straightforward manner. Others are less clear. For example, suppose that sources are all configured on one line and receivers on an orthogonal line. Such arrays always yield some partial success, but the results do not yield complete information about the subsurface. Eventually, we will develop a criterion that at least warns us when to be cautious, if it does not

provide a definitive answer to the question of what we can expect different source-receiver arrays to deliver.

Compatibility with High Frequency

Earlier, we observed that wide offset and the Born approximation might be inconsistent, owing to the large reflectivity of wide-angle reflections. In the current discussion, we have not concerned ourselves with the issue of failure of the Born approximation, but have concentrated only on the count of degrees of freedom. Consequently, we address this issue below. Ultimately, we show that the output of the inversion derived on the basis of the Born approximation has an interpretation in terms of high-frequency "Kirchhoff data," which is to say, model data created using the *Kirchhoff modeling formula.* (See Exercise 3.12.) Because there is no small-perturbation assumption in the Kirchhoff modeling formula regarding reflection coefficients (or, consequently, in any inversion formula derived from it), we will be able to allow for wide offset between source and receiver. Thus, we ask the reader's forbearance while we continue to develop inversion operators based on the Born approximation. We assure the reader that we will ultimately arrive at a result that frees us from the restriction of considering only small changes in parameters across a reflector, so long as the background parameters above that reflector are near to their true values.

Summary

In summary, for techniques in current use, the count of degrees of freedom is consistent with the kind of inversion results that are obtained. While the target is always a three-dimensional Earth model, the *implied geometry* of the experiment is controlled by the number of degrees of freedom available. It is one of these theories, high-frequency inversion for reflector mapping and parameter estimation, that will be developed here.

In practice, data are gathered from "many" experiments, with the shot and receiver locations varied. This produces redundant data from the point of view of the counts we were making in the above discussion. Such data redundancy is important as it may be used to reduce noise and to permit the extraction of more parameters than a simple $\alpha(\boldsymbol{x})$. In addition, data redundancy permits background wavespeed profiles to be generated by a variety of *velocity analysis* techniques that are independent of the actual inversion process. Because our goal is to formulate inversion techniques, we will not discuss these other side issues.

3.2.1 The Born Approximation and High Frequency

The ultimate objective of our derivations is to develop formulas for high-frequency inversion. Because the source term in (3.1.7) involves the product $\omega^2\alpha(\boldsymbol{x})$, it might appear that assuming high frequency is incompatible with

the Born approximation, because "large ω" and "small $\alpha(\boldsymbol{x})$" are competing to determine the ultimate size of this source term. We will show here that this is exactly the "right" combination of powers to create a balance that allows for both high frequency and small perturbations, independently.

Suppose that the true velocity, $v(\boldsymbol{x})$, is known, but that we still want to consider the decomposition of (3.1.3). We will examine the interplay of high frequency and small α on the WKBJ formalism for high-frequency wave propagation. To this end, we represent solutions to the Helmholtz equation in the form of a series in inverse powers of $i\omega$:

$$u(\boldsymbol{x},\omega) \sim e^{i\omega\tau(\boldsymbol{x})} \sum_{n=0}^{\infty} \frac{A_n(\boldsymbol{x})}{(i\omega)^n},$$

where $\tau(\boldsymbol{x})$ is traveltime. (This is the WKBJ series trial solution.) It is assumed that the total solution is made up of one or more series of this type with linearity permitting us to examine each constituent series individually, except at places where they might interact, such as at reflectors. Away from the source point $\boldsymbol{x}_s$, equation (3.1.4) takes the form

$$\mathcal{L}_0(u) = -\frac{\alpha(\boldsymbol{x})\omega^2}{c^2} u(\boldsymbol{x},\boldsymbol{x}_s,\omega). \tag{3.2.2}$$

We then substitute the WKBJ series trial solution into equation (3.2.2) to obtain the series representation that provides a basis for ray theory in a perturbed medium (see Appendix E),

$$\begin{aligned}\mathcal{L}_0 u &= e^{i\omega\tau} \sum_{n=0}^{\infty} \frac{1}{(i\omega)^n} \left[\omega^2 \left\{ \frac{1}{c^2} - (\nabla\tau)^2 \right\} A_n \right. \\ &\qquad \left. + i\omega \left\{ 2\nabla\tau \cdot \nabla A_n + A_n \nabla^2 \tau \right\} + \nabla^2 A_n \right] \\ &= -\omega^2 \frac{\alpha}{c^2} e^{i\omega\tau} \sum_{n=0}^{\infty} \frac{A_n}{(i\omega)^n}. \end{aligned} \tag{3.2.3}$$

In the formal process of solving this equation, we equate the coefficients of like powers of ω appearing on each side of (3.2.3). Note that the leading-order terms on each side are of order ω^2, with each successive order term being in smaller powers of ω. After canceling a common factor of A_0, the leading-order equality is

$$\left[(\nabla\tau(\boldsymbol{x}))^2 - \frac{1}{c^2(\boldsymbol{x})} \right] = \frac{\alpha(\boldsymbol{x})}{c^2(\boldsymbol{x})}.$$

Because

$$\frac{1}{v^2(\boldsymbol{x})} = \frac{1}{c^2(\boldsymbol{x})} \left[1 + \alpha(\boldsymbol{x}) \right], \tag{3.2.4}$$

this equation for τ becomes

$$(\nabla\tau(\boldsymbol{x}))^2 - \frac{1}{v^2(\boldsymbol{x})} = 0, \tag{3.2.5}$$

which is the *eikonal equation* in a medium with velocity v. That is, the product $\omega^2\alpha$, provided the precise balance needed to guarantee that the eikonal equation in the perturbed medium became the correct eikonal equation for the full wavespeed $v(\boldsymbol{x})$.

The eikonal equation describes the traveltime behavior of the waves under the condition of high frequency. To examine the amplitude behavior under this condition, it is necessary to consider terms of lower order in ω. If we equate the coefficients of the terms of the next order in ω of equation (3.2.3), we obtain

$$A_1\left[\frac{1}{c^2} - \frac{1}{v^2}\right] + \left[2\nabla\tau\cdot\nabla A_0 + A_0\nabla^2\tau\right] = -A_1\frac{\alpha}{c^2},$$

where the first term on the left side is obtained by using the eikonal equation (3.2.5). Again, using the relation (3.2.4), this becomes the *transport* equation for a medium with wavespeed v:

$$2\nabla\tau\cdot\nabla A_0 + A_0\nabla^2\tau = 0.$$

We see here, again, that there is no conflict between the small perturbation formalism in α that leads to the Born approximation and the standard high-frequency formalism of ray theory. That is, the factor $\omega^2\alpha$ on the right side of equation (3.1.7) is exactly the correct combination of powers to avoid a conflict between these two limits. Clearly, this balance will occur in all of the higher-order transport equations for $A_2, A_3, \ldots$, leading to the standard equations for each of those coefficients. (We refer the reader to the text of Kravtsov and Orlov [1990] for a comprehensive overview of ray theory. See also Bleistein [1984] and Appendix E of this text.)

Because the solutions of the eikonal and transport equation(s) form the basis of asymptotic ray theory, we will take the position that the assumptions of high frequency and small perturbations are compatible.

There are regions where this analysis does not prevail, which is to say locations where the amplitude of the scattered field $u_S(\boldsymbol{x}, \boldsymbol{x}_s, \omega)$ is large. These regions include the vicinity of the source, areas near caustics, and regions of supercritical reflections. Yet, these are also the places where we generally expect high-frequency theories, including ray theory, to break down.

Another example of a region where this analysis does not apply is the forward-scattering or downward-propagating direction. In that direction, the wave denoted by $u_I(\boldsymbol{x}, \boldsymbol{x}_s, \omega)$ and defined by (3.1.6) accumulates a phase error relative to the "true" downward propagating wave. That error is approximately $i\omega\int\alpha(\boldsymbol{x})/c(\boldsymbol{x})ds$, where s denotes arclength along the geometrical-optics rays or paths of propagation. This is a region in which the product $\omega\alpha$ comes into play. With increasing propagation range through the region of nonzero $\alpha(\boldsymbol{x})$, this integral will increase in magni-

tude, eventually attaining a value of π. At such places, $u_I(\boldsymbol{x}, \boldsymbol{x}_s, \omega)$ and the true downward field are of opposite sign. The field we call $u_S(\boldsymbol{x}, \boldsymbol{x}_s, \omega)$ will have to undo this error, which is of order unity in $\alpha(\boldsymbol{x})$. Consequently, the *downward propagating part* of $u_S(\boldsymbol{x}, \boldsymbol{x}_s, \omega)$ cannot be only $O(\alpha)$. This suggests that inversion as developed here is not the method of choice for tomographic imaging, which depends largely on transmitted, rather than scattered, energy. We will not use our methods on such problems. Indeed, we will see this breakdown in the forward scattering direction more explicitly later, when we see that the "true" large parameter depends also on the cosine of the half-angle between the geometrical-optics rays from source and receiver at the scattering point: for transmitted rays, that half angle is $\pi/2$, and the parameter that we would like to be large is actually equal to zero!

Under the high-frequency assumption, the upward propagating part of $u_S(\boldsymbol{x}, \boldsymbol{x}_s, \omega)$ arises from reflections at jumps in $\alpha(\boldsymbol{x})$. At normal incidence, such waves are scaled by a reflection coefficient proportional to the jump in $\alpha(\boldsymbol{x})$, hence they are of order $O(\alpha)$. For small-offset angles between incidence and reflection, this remains the case. As the offset angle increases towards critical, however, the magnitude of the reflection coefficient approaches unity. For small α, that critical angle will be large; as α increases, that critical angle decreases, restricting the viable range of angles of incidence.

Now we have some idea where we can expect the upward-scattered field to be small when $\alpha(\boldsymbol{x})$ is small. This will be when the offset angle between the direction of incidence and reflection is small compared to the critical angle. For the present, this is the type of experiment to be considered; specifically, we treat the special case of zero-offset in this chapter. Eventually we will show that this inversion has a range of validity that is broader than its basis in the Born approximation would suggest. We will show this by analytically studying the output of this inversion formalism when applied to Kirchhoff-approximate data for a single reflector.

The Kirchhoff approximation is not constrained to small increments in medium parameters across reflectors, nor to angles that are small compared to the critical angle. Furthermore, we will show that the output of the inversion operator can be interpreted in terms of the fully nonlinear geometrical-optics reflection coefficient. This means that estimates of parameter changes can be made without linearization. (We still have a linearized problem, but it is linearized in terms of the reflectivity, instead of in terms of perturbations of material parameters.) Again, this echoes the results already derived for the one-dimensional problem.

Thus, to a degree, the small-perturbation constraint of the Born approximation can be removed (or ignored). To properly locate the "test reflector," it will still be necessary to have a background or reference speed above the reflector that is "close" in some sense to the true propagation speed. It will also be necessary that multiples from reflectors above the test reflector

be small enough that they can be disregarded. This means that the violation of the constraint of small $\alpha(\boldsymbol{x})$ can still be a source of error, if the background-wavespeed profile differs significantly from the true profile.

This suggests that a recursive application of the inversion operator could be used to gain information that progressively improves the estimate of the background wavespeed. If such a procedure were applied in a "layer-stripping" fashion, then each successive reflector could be more precisely located, with its reflection strength yielding information about the wavespeed jump into the next deeper region being imaged.

Therefore, the Born approximation is merely a vehicle for getting the derivation started, rather than being an end in itself. The real power of our methods comes from the robustness of high-frequency asymptotic wave theory. Extensions of the validity of our inversion schemes, through a consideration of the properties of Fourier-like integrals, will provide the means of overcoming many of the constraints of the original derivation.

3.2.2 The Constant-Background Zero-Offset Equation

Some specializations of (3.2.1) will provide insights into solution of the general problem. The simplest problem to deal with is one in which the source and receiver are coincident, $\boldsymbol{x}_s = \boldsymbol{x}_g$ on a flat horizontal surface, $z = x_3 = 0$, and the background speed $c(\boldsymbol{x}) = c_0 =$ constant. In this case, it is convenient to introduce

$$\boldsymbol{\xi} = (\xi_1, \xi_2, 0) = \boldsymbol{x}_s = \boldsymbol{x}_g, \tag{3.2.6}$$

and the exact solutions,

$$g(\boldsymbol{\xi}, \boldsymbol{x}, \omega) = \frac{e^{i\omega r/c_0}}{4\pi r}, \quad u_I(\boldsymbol{x}, \boldsymbol{\xi}, \omega) = F(\omega)\frac{e^{i\omega r/c_0}}{4\pi r}, \quad r = |\boldsymbol{x} - \boldsymbol{\xi}|, \tag{3.2.7}$$

and rewrite (3.2.1) as

$$u_S(\boldsymbol{\xi}, \omega) = F(\omega)\left[\frac{\omega}{4\pi c_0}\right]^2 \int_{z>0} \alpha(\boldsymbol{x})\frac{e^{2i\omega r/c_0}}{r^2} d^3x. \tag{3.2.8}$$

Here, $r = \sqrt{(x_1 - \xi_1)^2 + (x_2 - \xi_2)^2 + x_3^2}$.

3.2.3 One Experiment, One Degree of Freedom in α

Suppose that data are collected for a single zero-offset experiment and that the medium has variability from the background wavespeed in the vertical direction only. For our inversion formula, this means that we let the wavespeed vary from constant velocity as a function of the depth z, only. This is a useful case to study from a geologic perspective, because as a crude estimate, wavespeed can be assumed to generally increase with depth in the Earth. At the very least, if we have only limited well log data,

the variation of wavespeed with depth will be known with greater precision than will the lateral variations.

Whatever the justification for considering such a problem, we will seek an inversion only for $\alpha(\boldsymbol{x}) \equiv \alpha(z)$. Furthermore, the coordinates of the source in that single experiment might as well be taken to be (0,0,0), so that (3.2.8) becomes

$$u_S(0,0,0,\omega) = F(\omega)\left[\frac{\omega}{4\pi c_0}\right]^2 \int_{x_3>0} \alpha(x_3)\frac{e^{2i\omega r/c_0}}{r^2} d^3x,$$
$$\text{where} \qquad r = \sqrt{x^2+y^2+z^2}. \tag{3.2.9}$$

In this case, the integrand depends on x and y only through r, permitting us to perform the integration in (x,y) by exploiting the high-frequency assumption. When we introduce polar coordinates (ρ,θ)[4] in place of (x,y), equation (3.2.9) may be rewritten as

$$u_S(0,0,0,\omega) = F(\omega)\left[\frac{\omega}{4\pi c_0}\right]^2 \int_{z>0} dx_3\, \alpha(x_3) \int_0^{2\pi} d\theta \int_0^{\infty} d\rho\, \rho \frac{e^{2i\omega r/c_0}}{r^2},$$
$$\text{where} \qquad r = \sqrt{\rho^2+x_3^2}. \tag{3.2.10}$$

Integrating with respect to θ yields a multiplier of 2π, and reduces the integral to

$$u_S(0,0,0,\omega) = F(\omega)\frac{\omega^2}{8\pi c_0^2} \int_{x_3>0} dx_3\, \alpha(x_3) \int_0^{\infty} d\rho\, \rho \frac{e^{2i\omega r/c_0}}{r^2}. \tag{3.2.11}$$

While it is not possible to evaluate the integral over ρ exactly, it is possible to find an approximation to this integral that is consistent with the high-frequency assumption. To do this, we require that $\mathbf{Im}\ \omega > 0$ (consistent with $r/c_0 > 0$) and integrate by parts in ρ, retaining only the leading term at high frequency to approximate the ρ-integral. The term being integrated is $\exp\{2i\omega r/c_0\}\cdot\rho/r$, noting that ρ/r is just the ρ-derivative of r. The result of this integration, to leading order in ω, is

$$u_S(0,0,0,\omega) \sim F(\omega)\frac{i\omega}{16\pi c_0} \int_{x_3>0} \frac{\alpha(x_3)}{x_3} e^{2i\omega x_3/c_0} dx_3, \tag{3.2.12}$$

where $\sim$ indicates that this is a high-frequency asymptotic approximation, rather than an exact equality.

For $F(\omega) = 1$, equation (3.2.12) defines the observed data as a multiple of the Fourier transform of $\alpha(x_3)/x_3$. The solution is obtained by Fourier inversion. We seek the bandlimited approximation $\alpha_B(z)$ of the true perturbation. (Note that z is the output variable that corresponds to the x_3 input variable.) As in one dimension, the actual transform variable

[4]The polar coordinate $\rho \equiv \sqrt{x_1^2+x_2^2}$ and the density ρ will not be introduced in the same context.

is $k = 2\omega/c_0$ and the Fourier inversion formula must be with respect to k, with $dk = (2/c_0)d\omega$. Consequently, solving for $\alpha(z)$, we have

$$\alpha_B(z) = 16z \int_{-\infty}^{\infty} \frac{u_S(0,0,\omega)}{i\omega} e^{-2i\omega z/c_0}\, d\omega. \tag{3.2.13}$$

It is important to recognize that $u_S(0,0,\omega)$ contains the bandlimiting represented by the filter $F(\omega)$ in equation (3.2.12).

This result should be compared to the one-dimensional inversion formula, (2.4.3). While these results show certain similarities, they also exhibit important differences. Although $\alpha(z)$ here has only one-dimensional variation, the observed field is still three-dimensional. It is reasonable to expect a difference in the processing formula to account for the differences in propagation in one versus three dimensions. In particular we should expect the 3D formula to account for geometrical spreading, which is not present in 1D wave propagation.

As in the 1D problem, we will test the formula on known data. Suppose we have a horizontal plane reflector in the subsurface at a depth h, but no other perturbations from the background wavespeed c_0. Such a medium is consistent with the assumption that α is a function of z alone. For this problem, the leading-order asymptotic representation of the field scattered from such a reflector is

$$u_S(0,0,\omega) = RF(\omega)\frac{e^{2i\omega h/c_0}}{8\pi h}. \tag{3.2.14}$$

Here, R is the normal-incidence reflection coefficient, exactly the same as in 1D; $2h/c_0$ is the two-way traveltime from the source to the reflector and back to the receiver; $8\pi h = 4\pi \cdot 2h$ is the geometrical-spreading factor for propagation down to the reflector and back to the source-receiver point. When this result is substituted into inversion formula (3.2.13), the result is

$$\begin{aligned} \alpha_B(z) &= \frac{2zR}{\pi h} \int_{-\infty}^{\infty} F(\omega) \frac{e^{2i\omega[h-z]/c_0}}{i\omega} d\omega \\ &= -4R\frac{z}{h} H_B(z-h). \end{aligned} \tag{3.2.15}$$

Comparing this result with the 1D results of Chapter 1, we see that the factor of $-4R$ can be recognized to be equal to $\alpha(z)$ to leading order. The bandlimited step is located at the right place, $z = h$; however, it is scaled by another factor, z/h, which is equal to 1 on the reflector surface. This last factor represents a further degradation of the bandlimited result in three dimensions, as compared with that in the one-dimensional formalism.

Alternately, suppose we were to define a reflectivity function, $\beta(z)$ for this problem, exactly as we did in the 1D problem, by multiplying the data in (3.2.13) by $i\omega/2c_0$ before inverting, just as we did to obtain the formula (2.4.17). Then, the formula for a *reflectivity function* for this point-source problem, replacing (3.2.13), is

$$\beta_B(z) = \frac{8z}{c_0} \int_{-\infty}^{\infty} u_S(0,0,0,\omega) e^{-2i\omega z/c_0} d\omega. \tag{3.2.16}$$

The result (3.2.15) would then be replaced by

$$\beta_B(z) = R\frac{z}{h}\delta_B(z-h),$$

just as in the one-dimensional problem. We might feel more comfortable replacing z/h by 1 because this is also a high-frequency approximation. The reader must remember to visualize $\delta_B(z-h)$ as a sinc-like waveform with peak located at $z = h$. So, while the peak amplitude of $\beta_B(z)$ has the desired value of R, bandlimiting introduces an error that grows for $z > h$. If our reflector location is off, then the error introduced by the factor of z/h will be correspondingly larger.

Also, it is not clear at this point that multiplication by $i\omega/2c_0$ is correct in the general 3D problem. Here, "correct" means a proper general formula for $\beta(\boldsymbol{x})$, whatever that means. This is a subject for further discussion. At the very least, the inversion has the correct appearance for this simple problem.

3.3 Zero-Offset Constant-Background Inversion in 3D

In the previous section we found that making a simplifying assumption on the background-wavespeed profile simplified the problem, permitting us to write an asymptotic approximation of the forward modeling formula. We recognized that the forward modeling formula was a forward Fourier transform, permitting the corresponding inverse Fourier transform-like inversion formula to be written by inspection.

This simplifying assumption of full 3D wave propagation with only 1D variability of the wavespeed profile is often called a "1.5D" or one-and-one-half-dimensional model. The next logical step would be to assume that the perturbation $\alpha(\boldsymbol{x})$ is a 2D-varying quantity. It is as difficult to perform the computation for a 2D result, even as a high-frequency asymptotic approximation, as it is for the full 3D problem, however. So it is really easier to do the full 3D problem first. The so-called "2.5D" (2D media with 3D geometrical spreading) will be postponed to a later section, after we have gained experience and insight from the 3D computation.

We return now to (3.2.8) and assume that the vector $\boldsymbol{\xi}$ ranges over the entire upper surface of the domain of the problem, providing coverage over the full spatial aperture of the medium. When $F(\omega) = 1$, this equation admits an *exact* solution. That solution will be derived here. Ultimately, we will show that limiting the range of these variables limits the domain of val-

ues of the Fourier transform variable, $\boldsymbol{k}$, over which the three-dimensional transform of $\alpha(\boldsymbol{x})$ is defined.

To begin, consider the integral equation (3.2.8) with $F(\omega)$ replaced by unity:

$$u_S(\boldsymbol{\xi},\omega) = \left[\frac{\omega}{4\pi c_0}\right]^2 \int_{z>0} \alpha(\boldsymbol{x}) \frac{e^{2i\omega r/c_0}}{r^2} d^3x, \tag{3.3.1}$$

where $\boldsymbol{\xi} = \boldsymbol{x}_s = \boldsymbol{x}_g$, (3.2.6), and $r = |\boldsymbol{x} - \boldsymbol{\xi}|$, (3.2.7). Here we have also modified the notation used for the observed field. There is no point in noting both the source and receiver position when they are coincident and equal to $\boldsymbol{\xi}$. Thus, we have set $u_S(\boldsymbol{x}_g, \boldsymbol{x}_s, \omega) \equiv u_S(\boldsymbol{\xi}, \omega)$.

The key to solving this integral equation is to realize that it is in *convolution form* in the transverse spatial variables, the function $\alpha(\boldsymbol{x})$ being convolved with the function $r^{-2}\exp\{2i\omega r/c_0\}$. Thus, a Fourier transform in these two variables will replace the integration in x_1 and x_2 by *multiplication* of the two transformed functions. Unfortunately, the Fourier transform of this function of r is unknown to us. If there were only *one* power of r in the denominator, that is, if the kernel of the integral equation were $r^{-1}\exp\{2i\omega r/c_0\}$ instead, then the kernel would take the form of the free-space Green's function, a function which has a known Fourier transform. We can achieve this change in the integrand by differentiating the integral in (3.3.1) with respect to ω, but only after the multipliers in ω are moved to the left side. Multiplying each side of (3.3.1) by c_0^2/ω^2 and taking the ω derivative of the resulting equation yields

$$\frac{\partial}{\partial\omega}\int_D \frac{e^{2i\omega r/c_0}}{(4\pi r)^2}\alpha(\boldsymbol{x})\, d^3x = \frac{\partial}{\partial\omega}\left(\frac{c_0^2}{\omega^2}u_S(\boldsymbol{\xi},\omega)\right),$$

or

$$\int_D d^3x\, \alpha(\boldsymbol{x}) g_1(\boldsymbol{\xi}-\boldsymbol{x},\omega) = -2\pi i c_0^3 \frac{\partial}{\partial\omega}\left(\frac{u_S(\boldsymbol{\xi},\omega)}{\omega^2}\right), \tag{3.3.2}$$

where

$$g_1(\boldsymbol{\xi}-\boldsymbol{x},\omega) \equiv \frac{e^{2i\omega r/c_0}}{4\pi r}, \quad r \equiv |\boldsymbol{x}-\boldsymbol{\xi}|. \tag{3.3.3}$$

The function g_1 is the free-space Green's function for a medium with a constant wavespeed of $c_0/2$ (a "half-speed" free-space Green's function). The two-dimensional "transverse" Fourier transform of this function will be derived below.

It will prove useful to define the spatial Fourier transform for this problem with a factor of two in the exponent. This corresponds to the apparent "wavenumber" $2\omega/c_0$ appearing in the integral equation. The forward spatial transform

$$\tilde{f}(\boldsymbol{\kappa}) = \int_{-\infty}^{\infty}\int_{-\infty}^{\infty} d^2\rho\, e^{-2i\boldsymbol{\kappa}\cdot\boldsymbol{\rho}} f(\boldsymbol{\rho}) \tag{3.3.4}$$

and the inverse transform

$$f(\boldsymbol{\rho}) = \frac{1}{\pi^2}\int_{-\infty}^{\infty}\int_{-\infty}^{\infty} d^2\kappa\, e^{2i\boldsymbol{\kappa}\cdot\boldsymbol{\rho}}\tilde{f}(\boldsymbol{\kappa}) \tag{3.3.5}$$

are defined with the conventions $\boldsymbol{\rho} \equiv (x_1, x_2)$ and, similarly, the *wavevector* $\boldsymbol{\kappa}$, is defined in terms of the two *wavenumbers*, k_1 and k_2, by $\boldsymbol{\kappa} \equiv (k_1, k_2)$. The fact that the components of the wavevector $\boldsymbol{\kappa}$ are really *half* of the normal definition of the wavevector accounts for the absence of the factor of $1/4$ normally found in the 2D inverse Fourier transform definition. Application of the spatial Fourier transform equation (3.3.4) to (3.3.2), as noted above, converts the convolution to a multiplication in the $\boldsymbol{\kappa}$-domain,

$$\int_0^{\infty} dx_3\, \tilde{\alpha}(\boldsymbol{\kappa}, x_3)\tilde{g}_1(\boldsymbol{\kappa}, x_3, \omega) = -2\pi i c_0^3 \frac{\partial}{\partial\omega}\left(\frac{\tilde{u}_S(\boldsymbol{\kappa}, \omega)}{\omega^2}\right), \tag{3.3.6}$$

with the transverse Fourier transform of $g_1(\boldsymbol{x}, \omega)$ being given by

$$\tilde{g}_1(\boldsymbol{\kappa}, x_3, \omega) \equiv \int_{-\infty}^{\infty}\int_{-\infty}^{\infty} d^2\rho \frac{\exp\left(-2i\boldsymbol{\kappa}\cdot\boldsymbol{\rho} + (2i\omega/c_0)\left[\rho^2 + x_3^2\right]^{1/2}\right)}{4\pi\left[\rho^2 + x_3^2\right]^{1/2}}.$$

There are several ways of obtaining $\tilde{g}_1(\boldsymbol{\kappa}, x_3, \omega)$ by explicitly performing the above integration. The simplest and most physically enlightening way of finding the expression is by recognizing that (3.3.3) is the Green's function for the Helmholtz equation with wavespeed $c_0/2$:

$$\left[\nabla^2 + \frac{4\omega^2}{c_0^2}\right] g_1(x_1, x_2, x_3, \omega) = -\delta(x_1)\delta(x_2)\delta(x_3).$$

The transverse Fourier transform defined in (3.3.4) may be applied to this equation to yield

$$\left[\frac{\partial^2}{\partial x_3^2} - 4\kappa^2 + \frac{4\omega^2}{c_0^2}\right]\tilde{g}_1(\boldsymbol{\kappa}, x_3, \omega) = -\delta(x_3).$$

(Note that the factor of 4 multiplying κ^2 is a result of having a factor of 2 in the exponent of the transform kernel.) We may rewrite this equation using the following definition for the vertical wavenumber k_3 (again, this is really a *half-wavenumber* in the traditional sense) if we recall that $k^2 = \omega^2/c_0^2 = k_1^2 + k_2^2 + k_3^2$. Thus,

$$k_3^2 \equiv \left(\frac{\omega^2}{c_0^2} - \kappa^2\right), \tag{3.3.7}$$

permitting us to write

$$\left[\frac{\partial^2}{\partial x_3^2} + (2k_3)^2\right]\tilde{g}_1(\boldsymbol{\kappa}, x_3, \omega) = -\delta(x_3).$$

It is now apparent that $\tilde{g}_1(\boldsymbol{\kappa}, x_3, \omega)$ is just the Green's function for a *one*-dimensional wave equation. As this problem has already been solved in

Chapter 2 (with wavenumber ω/c_0 rather than $2k_3$), we may write the result,

$$\tilde{g}_1(\boldsymbol{\kappa}, x_3, \omega) = -\frac{1}{4ik_3} e^{2ik_3|x_3|},$$

directly, taking care that an additional factor of 2 appears in both the exponent and the denominator of the expression.

Upon substitution of the expression for $\tilde{g}_1(\boldsymbol{\kappa}, x_3, \omega)$, we obtain

$$\int_0^\infty dx_3 \, \tilde{\alpha}(\boldsymbol{\kappa}, x_3) e^{2ik_3|x_3|} = -8\pi k_3 c_0^3 \frac{\partial}{\partial \omega} \left(\frac{\tilde{u}_S(\boldsymbol{\kappa}, \omega)}{\omega^2} \right), \tag{3.3.8}$$

which is an integral that is nearly a Fourier transform in x_3. To complete this identification, first note that $|x_3| = x_3$ on the domain of integration, so we can extend the lower limit of integration to $-\infty$. Recall that $\alpha(\boldsymbol{x})$ was defined to be zero for $x_3 \leq 0$, meaning that $\tilde{\alpha}(\boldsymbol{\kappa}, x_3) = 0$ for this range of x_3, as well. Note that we assume that the range of k_3 is restricted to real values only. We will present a discussion of the rationale for this choice at the end of this section.

We may thus rewrite (3.3.8) as

$$\int_0^\infty dx_3 \, \tilde{\alpha}(\boldsymbol{\kappa}, x_3) e^{2ik_3 x_3} = -8\pi k_3 c_0^3 \frac{\partial}{\partial \omega} \left(\frac{\tilde{u}_S(\boldsymbol{\kappa}, \omega)}{\omega^2} \right) \Bigg|_{\omega=\omega_0}, \tag{3.3.9}$$

where ω_0 represents the specific range of ω where k_3 is real-valued. While we clearly have the relation that

$$\omega_0^2(\boldsymbol{\kappa}, k_3) = c_0^2 \left[k_1^2 + k_2^2 + k_3^2 \right],$$

we will define $\omega_0(\boldsymbol{\kappa}, k_3)$ more carefully in equation (3.3.14) in the next section. The left side of this equation has the form of a causal Fourier transform, but to a variable, k_3, which is itself only partially defined by (3.3.7) as a function of $\boldsymbol{\kappa}$ and ω. Below, we will complete that definition. For the present, assume that this has been accomplished and that we can invert this Fourier transform to write

$$\tilde{\alpha}(\boldsymbol{\kappa}, x_3) = -8c_0^3 \int_{-\infty}^\infty dk_3 \, k_3 \frac{\partial}{\partial \omega} \left(\frac{\tilde{u}_S(\boldsymbol{\kappa}, \omega)}{\omega^2} \right) \Bigg|_{\omega=\omega_0} e^{-2ik_3 x_3}.$$

Hence, inverting the Fourier transform in $\boldsymbol{\kappa}$, we find that

$$\alpha(\boldsymbol{x}) = \frac{-8c_0^3}{\pi^2} \int_{-\infty}^\infty d^3k \, k_3 \frac{\partial}{\partial \omega} \left(\frac{\tilde{u}_S(\boldsymbol{\kappa}, \omega)}{\omega^2} \right) \Bigg|_{\omega=\omega_0} e^{2i(\boldsymbol{\kappa}\cdot\boldsymbol{\rho} - k_3 x_3)}. \tag{3.3.10}$$

The result is still not in the most desirable form, because the $\boldsymbol{\xi}$ dependence that existed in the original problem is not present here. Recall that the first step in the derivation was to transform out this dependence with the transverse Fourier transform defined in equation (3.3.4). Therefore, the relationship

$$\tilde{u}_S(\boldsymbol{\kappa},\omega) = \int_{-\infty}^{\infty}\int_{-\infty}^{\infty} d^2\xi\; e^{-2i\boldsymbol{\kappa}\cdot\boldsymbol{\xi}} u_S(\boldsymbol{\xi},\omega)$$

can be substituted back into equation (3.3.10) to yield

$$\alpha(\boldsymbol{x}) = \frac{-8c_0^3}{\pi^2}\int_{-\infty}^{\infty} d^3k\; k_3 \int_{-\infty}^{\infty} d^2\xi\; \frac{\partial}{\partial\omega}\left(\frac{u_S(\boldsymbol{\xi},\omega)}{\omega^2}\right)\Bigg|_{\omega=\omega_0} e^{2i[\boldsymbol{\kappa}\cdot(\boldsymbol{\rho}-\boldsymbol{\xi})-k_3x_3]}. \tag{3.3.11}$$

Similarly, the data are recorded in the time domain, meaning that the inversion formula should be written as a function of time, not frequency. Writing $u_S(\boldsymbol{\xi},\omega)$ in its causal temporal Fourier representation further modifies the inversion formula to be

$$\alpha(\boldsymbol{x}) = \frac{-8c_0^3}{\pi^2}\int_{-\infty}^{\infty} d^3k\; k_3 \int_{-\infty}^{\infty} d^2\xi\; e^{2i[\boldsymbol{\kappa}\cdot(\boldsymbol{\rho}-\boldsymbol{\xi})-k_3x_3]} \cdot \int_0^{\infty} dt\; U_S(\boldsymbol{\xi},t)\frac{\partial}{\partial\omega}\left(\frac{1}{\omega^2}e^{i\omega t}\right)\Bigg|_{\omega=\omega_0}.$$

Now, note that the differentiation of the term in parentheses produces

$$\frac{\partial}{\partial\omega}\left(\frac{1}{\omega^2}e^{i\omega t}\right) = \frac{it}{\omega^2}\left[1-\frac{2}{i\omega t}\right]e^{i\omega t},$$

permitting the inversion formula for $\alpha(\boldsymbol{x})$ to be written as

$$\alpha(\boldsymbol{x}) = \frac{8c_0^3}{i\pi^2}\int_{-\infty}^{\infty} d^2\xi \int_{-\infty}^{\infty} d^3k\; \frac{k_3}{\omega_0^2} e^{2i[\boldsymbol{\kappa}\cdot(\boldsymbol{\rho}-\boldsymbol{\xi})-k_3x_3]} \cdot \int_0^{\infty} dt\; tU_S(\boldsymbol{\xi},t)e^{i\omega_0 t}\left[1+\frac{2i}{\omega_0 t}\right], \tag{3.3.12}$$

with ω_0 defined below as a function of $\boldsymbol{\kappa}$ and k_3 by (3.3.14).

This is an exact solution to the integral equation, (3.3.1). More precisely, (3.3.1) is an equation in the space-frequency domain, meaning that (3.3.11) is a solution of (3.3.1) and this equation is the result of reexpressing the observed data in space-time.

As noted earlier, (3.3.1) was an *idealization* of the "true" integral equation, in which both the spatial and frequency domains are of finite extent. There are two ways to approach the solution of the "aperture-limited" inverse problem. First, one could attempt to solve this limited-aperture problem directly. Second, the above solution formula could be applied to the aperture-limited data, in particular *high-frequency data* of limited spatial extent, to ascertain the effects of the high-frequency assumptions present in this formula. For such a solution, the limits of integration should reflect this limited aperture. We will take this latter approach. We will see that it is useful to introduce a *reflectivity function* as we did in the one-dimensional problem. It is possible, therefore, to relate the output of the inversion formula to the normal-incidence reflection coefficient. These ideas

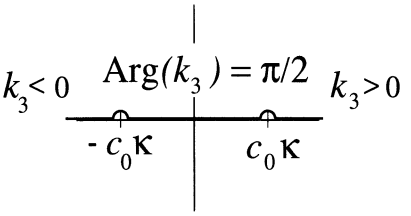

FIGURE 3.1. The restriction of the complex k_3-plane implied by equation (3.3.13).

will be applied in the next section. Later, in the extension to finite-offset data, the inversion output will be related to the fully angularly dependent, geometrical-optics reflection coefficient.

3.3.1 Restrictions on the Choice of k_3

Equation (3.3.12) contains a restriction on the frequencies, which arises from the restriction that k_3 be real-valued. A justification and discussion of this restriction is given in this subsection.

The value of the vertical component of the wavenumber, k_3, is defined by the expression

$$\boldsymbol{k} \equiv (\boldsymbol{\kappa}, k_3) = \frac{\omega}{c_0}\hat{\boldsymbol{k}}.$$

The fact that $\hat{\boldsymbol{k}}$ is a unit vector follows from (3.3.7). We will carefully define k_3 by

$$k_3 \equiv \begin{cases} \operatorname{sgn}(\omega)\left[\dfrac{\omega^2}{c_0^2} - \kappa^2\right]^{1/2} & \text{for } |\omega| \geq c_0\kappa \\ i\left[\kappa^2 - \dfrac{\omega^2}{c_0^2}\right]^{1/2} & \text{for } |\omega| < c_0\kappa \end{cases}. \quad (3.3.13)$$

with the square roots here always real-valued and positive. This permits us to easily see that k_3 will be real-valued only for $|\omega| \geq c_0\kappa$ and that the upper equality in (3.3.13) describes k_3 in this case. The factor of $\operatorname{sgn}(\omega)$ makes sense when we recall that g_1 is an "outgoing" Green's function. That is to say, it must satisfy a radiation condition guaranteeing that each Fourier component, when multiplied by $\exp\{-i\omega t\}$, represents a wave that is directed towards $+\infty$ in x_3 as time increases. This choice of sign guarantees that behavior. In particular, note that for $\boldsymbol{\kappa} = (0,0)$, $k_3 = \omega/c$ and their signs agree.

Purely imaginary values of k_3 represent the contributions of the *evanescent* regime of the data, being arrivals associated with leaky modes, boundary waves, and the transmitted fields of supercritically reflected arrivals. If present in the data, evanescent contributions decay as $\exp\{-|k_3|L\}$, with L the upward propagation distance of these modes, and may be assumed to be vanishingly small owing to the relatively large size

of the product $|k_3|L$ for the separation of the support of $\alpha(\boldsymbol{x})$ from the upper surface. It is, therefore, safe to assume that the condition of $|\omega| \geq c_0\kappa$ exists for our data, that is to say, k_3 is real. If evanescent data do survive, amplitude-consistent inversion of such arrivals will require exponential enhancement, and we would have to change the sign of $\mathbf{Im}\ (k_3)$ to process the data in this range. This would lead to the undesirable result that any noise present in the data will be enhanced exponentially along with the data, reducing the overall signal-to-noise ratio in the output. (See Appendix D for a discussion of the ill-conditioning arising from the attempt to invert waves in the evanescent regime.) Fortunately, $\alpha(\boldsymbol{x})$ can be constructed from purely real values of $\boldsymbol{k}$, hence from purely real k_3 data. Thus, discarding evanescent contributions to the data *regularizes* the solution for $\alpha(\boldsymbol{x})$.

An important consequence of the above definition of k_3 is that ω will be represented by

$$\omega \equiv \omega_0(\boldsymbol{\kappa}, k_3) = c_0 \operatorname{sgn}(k_3)\sqrt{\kappa^2 + k_3^2} = c_0 \operatorname{sgn}(k_3)\sqrt{k_1^2 + k_2^2 + k_3^2} \tag{3.3.14}$$

in the range $|\omega| \geq c_0\kappa$. As ω varies from $-\infty$ to $-c_0\kappa$ and from $c_0\kappa$ to ∞, k_3 varies from $-\infty$ to ∞, meaning that k_3 has the appropriate behavior to be the conjugate Fourier variable to x_3.

As long as we can believe the above justifications, the forward Fourier transform

$$\tilde{f}(k_3) = \int_{-\infty}^{\infty} f(x_3)e^{2ik_3x_3}dx_3 \tag{3.3.15}$$

and the inverse Fourier transform

$$f(x_3) = \frac{1}{\pi}\int_{-\infty}^{\infty} \tilde{f}(k_3)e^{-2ik_3x_3}dk_3 \tag{3.3.16}$$

are both defined for our problem; provided ω is evaluated at ω_0, the value of ω implied by the assumption that k_3 is always real-valued.

Exercises

3.3 This exercise is a repeat in three dimensions of the derivation of the inverse-scattering integral equation for acoustic waves in a variable-propagation-speed, variable-density medium from Section 2.8. Follow that derivation. Note that the divergence theorem is the generalization of integration by parts to three dimensions. Let $u(\boldsymbol{x}, \boldsymbol{x}_s, \omega)$ be a solution of the equation

$$\mathcal{L}u(\boldsymbol{x}, \boldsymbol{x}_s, \omega) = \rho\nabla \cdot \left[\frac{1}{\rho}\nabla u\right] + \frac{\omega^2}{v^2(\boldsymbol{x})}u = -\delta(\boldsymbol{x} - \boldsymbol{x}_s).$$

a. Introduce

$$\rho = \rho_0 + \delta\rho, \qquad v = v_0 + \delta v$$

and derive the following equation linear in $\delta\rho$ and δv:

$$\mathcal{L}_0 u(\boldsymbol{x}, \boldsymbol{x}_s, \omega) = -\delta(\boldsymbol{x} - \boldsymbol{x}_s) + \frac{\omega^2}{v_0^2}\frac{2\delta v}{v_0}u + \nabla\left[\frac{\delta\rho}{\rho_0}\right]\cdot\nabla u.$$

b. Introduce, $u = u_I + u_S$ and linearize in the above equation to obtain

$$\mathcal{L}_0 u_S = +\frac{\omega^2}{v_0^2}\frac{2\delta v}{v_0}u_I + \nabla\left[\frac{\delta\rho}{\rho_0}\right]\cdot\nabla u_I.$$

3.4 Derive the integral equation,

$$u_S(\boldsymbol{x}, \boldsymbol{x}_s, \omega) = -\int_{z>0}\left[\frac{\omega^2}{v_0^2}\frac{2\delta v}{v_0}u_I + \nabla\left(\frac{\delta\rho}{\rho_0}\right)\cdot\nabla u_I\right]g^\star d^3x.$$

In this equation, $g^\star = g^\star(\boldsymbol{x}, \boldsymbol{x}_g, \omega)$ is the Green's function for the adjoint equation,

$$\mathcal{L}_0^\star g^\star = \nabla\cdot\left[\frac{1}{\rho_0}\nabla(\rho_0 g^\star)\right] + \frac{\omega^2}{v_0^2}g^\star = -\delta(\boldsymbol{x} - \boldsymbol{x}_g).$$

Be sure to show where the Sommerfeld radiation condition is needed in this derivation.

a. Now use the divergence theorem on the first integrand in the integral equation above to rewrite that equation as

$$u_S(\boldsymbol{x}_g, \boldsymbol{x}_s, \omega) = -\int_{z>0}\left[\frac{\omega^2}{v_0^2}\frac{2\delta v}{v_0}u_I g^\star - \frac{\delta\rho}{\rho_0}\nabla\cdot(\nabla u_I g^\star)\right]d^3x.$$

b. Finally, assume the following forms:

$$u_I = A_I e^{i\omega\tau_I}, \qquad g^\star = A_g e^{i\omega\tau_g},$$

and obtain

$$u_S(\boldsymbol{x}_g, \boldsymbol{x}_s, \omega) = -\omega^2\int_{z>0}A_I A_g\left[\frac{2}{v_0^2}\frac{\delta v}{v_0} + \left((\nabla\tau_I)^2 + \nabla\tau_I\cdot\nabla\tau_g\right)\frac{\delta\rho}{\rho_0}\right]e^{i\omega[\tau_I+\tau_g]}d^3x.$$

3.4 High Frequency, Again

When considering the one-dimensional problem in the previous chapter, we introduced the idea that in most experimental problems the recorded data are *high-frequency* data. One consequence of this bandlimiting was that it was no longer feasible to attempt to reconstruct $\alpha(x)$ itself, but instead we

found that it was more desirable to reconstruct a scaled derivative of $\alpha(x)$—the reflectivity function, $\beta(x)$. The same will prove to be true in higher dimensions. Developing these ideas in higher dimensions and exploiting them constitute the major purpose of the remainder of this text. Our goal will be to create formulas for imaging discontinuities—reflectors—using aperture-limited, large-wavenumber, or high-frequency data. In addition to imaging the reflectors, we are also interested in estimating parameter changes across reflectors using these data. High-frequency inversion is then reduced to the problem of relating the observed wavefield data to the Fourier data describing the interior medium.

As discussed in Chapter 2, deciding what constitutes high and low frequency in imaging problems depends on the relative size of the scattering object compared to the dominant wavelengths or reciprocal wavenumbers that interact with it. Thus, frequencies that are considered "low" when imaging small objects may be easily considered "high" when imaging larger scatterers.

The Rayleigh Criterion

But how small is *small*? We will answer this question by considering the minimum permissible length scale L as a fraction of the dominant wavelength Λ to be the deciding value. One such measure used in optics is the *Rayleigh criterion*[5] for resolution for a single-frequency wave, which we interpret to mean that length L is considered "large" if

$$L \geq \frac{\Lambda}{4}.$$

This quasi-empirical criterion has been used in optics to characterize smoothness of optical reflector surfaces and in geophysics to characterize the resolution of closely spaced beds. Here both L and Λ have units of length. As we show in Appendix C, it is mathematically desirable to express the large parameters appearing in asymptotic analyses in a *dimensionless* form. Assuming that the waves travel at the background wavespeed c_0, we may write several equivalent forms

$$1 \leq \frac{4L}{\Lambda} = \frac{4Lf}{c_0} = \frac{2\omega L}{\pi c_0} = kL/\pi, \tag{3.4.1}$$

where the two equalities on the right follow by recalling that $\omega = 2\pi f$ and noting that the wavenumber of interest for our problem is the two-way wavenumber, $k = 2\omega/c_0$. If we introduce a dimensionless parameter, λ, defined by

---

[5]The Rayleigh criterion states that two components of equal intensity are "just resolved" when the maximum (the peak) of one component coincides with the principal intensity minimum (first zero crossing) of the other of the other. See Born and Wolf [1980] for details. The original reference is Rayleigh [1879].

$$\lambda = \frac{4\pi f L}{c_0}, \tag{3.4.2}$$

then the condition

$$\lambda \geq \pi \tag{3.4.3}$$

is equivalent to the Rayleigh criterion (3.4.1). We will, therefore, use this as the criterion for deciding if data are *high-frequency.*

A few examples are in order. A plausible range of frequencies that might be used in seismic investigations (including high-resolution surveys) is from about 5 Hz to about 500 Hz. (This frequency range, while not realistic for any individual seismic data set, is useful for illustrating the overall limitations of the seismic method.) If $c_0 = 2000$ m/s, and $f = 5$ Hz, then L must be 100 m (328 ft) or greater for 5 Hz to be considered high-frequency; that is, for $\lambda \geq \pi$. On the other extreme, if the same wavespeed is used, $f = 500$ Hz may be considered high-frequency for any $L \geq 1$ m because, again, this lower limit on L guarantees that $\lambda \geq \pi$ for this frequency and wavespeed.

The L may represent the depth to a reflector, the distance between reflectors, or a measure of the lateral variability of reflectivity. In seismic experiments, while there is little danger of the reflector depth being a length that might violate our high-frequency criterion, the spacing between reflectors may easily be a problem. Indeed, the detection and resolution of thin bedding is an ongoing issue in reflection seismic investigations.

There is one additional modification of this criterion that becomes important when the sources and receivers are separated. In this case, equation (3.4.2) should be replaced by

$$\lambda = \frac{4\pi f L \cos\theta}{c_0}. \tag{3.4.4}$$

Here, θ is half the opening angle between converging rays from a source and receiver. In inversion, the effect of separating the source and receiver is to scale the "aperture" in the wave-vector domain by this factor of $\cos\theta$, and this, in turn, leads to a loss of resolution in the spatial domain wherein the main lobe of bandlimited delta functions delineating reflectors is broadened by $\sec\theta$. The reason for this modified large parameter will become apparent in Chapter 5.

Current research into amplitude-versus-offset (AVO) behavior has been motivated by the desire to characterize the spatial variability of reflectivity as an aid in evaluating the properties of prospective hydrocarbon reservoirs. While the horizontal extent of a producing reservoir may be measured in hundreds to thousands of meters, variations in rock properties on the scale of tens of meters can be important in the analysis of a reservoir. Thus, the validity of the high-frequency assumption may be an issue here, too.

Failure of the High-Frequency Assumption

What does the failure of the high-frequency assumption mean to our theory of reflector imaging? Simply this. The ability of an imaging/inversion process to represent the geometry of a scatterer deteriorates as the wavelengths of the problem fall below the limit required by (3.4.3), using either (3.4.2) or (3.4.4) for λ. So, instead of the sharp reflector surfaces envisioned above, lower-frequency data produce an image with thick fuzzy zones delineating the reflectors. Where the lateral variability is expressed as a substantial curvature of the reflecting surface, local focusing may further violate the high-frequency assumption. It is easy to imagine that, for a sufficiently long wavelength, all of the reflector images will run together, causing the output of the inversion to fail to produce a meaningful image of the subsurface. Mathematically, as $\omega \to 0$,

$$\left[\nabla^2 + \frac{\omega^2}{c_0^2}\right] \to \left[\nabla^2\right];$$

that is, the Helmholtz operator becomes the Laplace operator, and the wave problem becomes a quasi-static potential problem in the extreme case. Thus the validity of the high-frequency assumption appears to be a necessary condition for successful imaging.

High-Frequency, Aperture-Limited Inversion

Owing to the high-frequency assumption, any result that can be expressed as a series of quantities multiplied by inverse powers of ω may be accurately approximated by the leading-order term(s) of the series. Equation (3.3.12) is a result with just this form, and the $2i/\omega_0 t$ term is dropped in practice. That is, we neglect a term of magnitude $2/\omega_0 t$ compared to unity. Note that neglecting this term is justified by considering the consequences of the Rayleigh criterion, (3.4.1), in the temporal-frequency domain instead of the spatial-wavenumber domain. That is, for L the distance to the first scatterer of interest, $T = 2L/c_0$ is the minimum traveltime for a nonzero response to be recorded as part of U_S. Now, with $2\pi f = \omega$, (3.4.2) is seen to take the form

$$\lambda = \omega T. \tag{3.4.5}$$

Thus, if a condition like the Rayleigh criterion is taken as the basis for neglecting terms of lower order, neglecting this term in (3.3.12) is justified. This assumes that the data U_S are bandlimited and that the temporal Fourier transform in (3.3.12) yields a function that does not cover the full frequency domain with nonzero data. Further, it is necessary to acknowledge that the spatial integral in (3.3.12) will be carried out over only a finite domain. This is an added feature of the multidimensional solution over the one-dimensional solution of the previous chapter. In analogy with the early discussion, the result of processing this bandlimited and spatially

aperture-limited data will be called $\alpha_B(\boldsymbol{x})$, defined by

$$\alpha_B(\boldsymbol{x}) = \frac{8c_0^3}{i\pi^2}\int_\Sigma d^2\xi \int_\Omega d^3k\, \frac{k_3}{\omega_0^2} e^{2i[\boldsymbol{\kappa}\cdot(\boldsymbol{\rho}-\boldsymbol{\xi})-k_3 x_3]} \int_0^\infty dt\, tU_S(\boldsymbol{\xi},t)e^{i\omega_0 t}, \tag{3.4.6}$$

where, again, $\boldsymbol{\rho} \equiv (x_1, x_2)$. Here Σ represents the total domain of recording positions $\boldsymbol{\xi}$ on the surface of the Earth; Ω represents the $\boldsymbol{k}$-domain corresponding to the bandlimited range of ω and the requirement that k_3 be real.

At this point, all we have is a formal integral whose relationship to the true unknown $\alpha(\boldsymbol{x})$ is unclear. It is an aperture-limited and bandlimited version of the operator that produces an exact solution to the integral equation (3.3.1), applicable when the data are not band- or aperture limited. Our task in later sections will be to clarify the meaning of this equation.

3.4.1 Reflection from a Single Tilted Plane

Following the development of the previous chapter, we will test equation (3.4.6) using the high-frequency representation of the waves that would be scattered from a single plane reflector. Because the reflector need not be horizontal, we will consider the general case of the response of an inclined reflector (see Figure 3.2). The angle of inclination will be θ (the dip) with respect to a horizontal axis, which itself makes an azimuthal angle ϕ (the direction of maximum dip) with the ξ_1 axis. The plane is assumed to be at depth h at $\boldsymbol{\xi} = 0$. The source-receiver point is located at surface coordinates (ξ_1, ξ_2), and the normal distance from this point to the reflector is l. For such a reflector, the high-frequency temporal data will be

$$U_S(\boldsymbol{\xi},t) = R\frac{\delta_B(t-2l/c_0)}{8\pi l}, \tag{3.4.7}$$
$$\text{where} \qquad l = h\cos\theta - (\xi_1\cos\phi + \xi_2\sin\phi)\sin\theta.$$

Here, R is the normal-incidence reflection coefficient, which is the same as the one-dimensional, or plane-wave reflection coefficient,

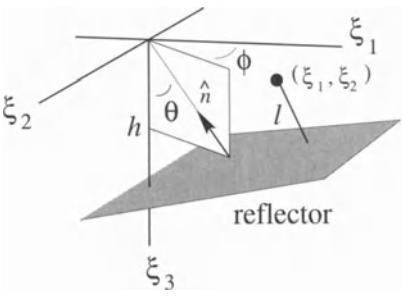

FIGURE 3.2. A single tilted plane.

$$R = \frac{c_1 - c_0}{c_1 + c_0}.$$

By δ_B we mean a bandlimited delta function whose temporal Fourier transform is $F(\omega)$ instead of unity. Clearly, this plane will intersect the upper surface for some finite choice of $\boldsymbol{\xi}$ whenever $\theta \neq 0$. The domain Σ in (3.4.6) is assumed to not include such an intersection. Because our immediate interest is in the leading-order contribution only, the effects of finite integration limits will be ignored here. Later, we will address this important issue in the context of a more general problem.

We begin the computation in (3.4.6) by carrying out the integral with respect to t for the data in (3.4.7). The result is

$$\int_0^\infty t\, U_S(\boldsymbol{\xi}, t) e^{i\omega_0 t} dt = \frac{R}{4\pi c_0} F(\omega) e^{2i\omega_0 l/c_0}, \tag{3.4.8}$$

with $\omega_0(\boldsymbol{k}) \equiv c_0 \operatorname{sgn}(k_3)\sqrt{k_1^2 + k_2^2 + k_3^2}$, as defined by (3.3.14). The integrations in ξ_1 and ξ_2 will now be carried out. Note that these variables appear only linearly in the phase. If the domain of integration were of infinite extent, the integrals would each be just delta functions with arguments equal to the respective multipliers of ξ_1 and ξ_2. This result is correct to leading order for high-frequency data. To this order of accuracy, we continue to use an equal sign for the result of this computation, though we really mean "asymptotic equality." The result is

$$\alpha_B(\boldsymbol{x}) = \frac{8c_0^2 R}{i\pi} \int_{-\infty}^{\infty} d^3k \frac{k_3}{\omega_0^2} F(\omega) \delta[f_1(\boldsymbol{k})] \delta[f_2(\boldsymbol{k})] e^{2i\{\boldsymbol{\kappa}\cdot\boldsymbol{\rho} - k_3 x_3 + \omega_0 h \cos\theta/c_0\}}, \tag{3.4.9}$$

where

$$f_1(\boldsymbol{k}) = 2\left[\frac{\omega_0(\boldsymbol{k})}{c_0}\cos\phi\sin\theta + k_1\right], \quad f_2(\boldsymbol{k}) = 2\left[\frac{\omega_0(\boldsymbol{k})}{c_0}\sin\phi\sin\theta + k_2\right].$$

The Dirac delta functions can now be exploited to carry out two more integrations. (See Appendix A for information about properties of delta functions.) We choose to compute the integrals in k_1 and k_2. There are two ways to proceed. First, one could compute the integrals iteratively, say, solving for k_1 as a function of (k_2, k_3) by setting $f_1 = 0$, and then computing the integral in k_2, taking account of this new function of k_2. The second method is to simultaneously compute the double integral in the two variables and use the result that

$$\delta[f_1(\boldsymbol{k})]\delta[f_2(\boldsymbol{k})] = \frac{\delta(k_1 - k_{10})\delta(k_2 - k_{20})}{|J|}, \quad J = \left.\frac{\partial(f_1, f_2)}{\partial(k_1, k_2)}\right|_{k_1 = k_{10}, k_2 = k_{20}}.$$

Here k_{10}, k_{20} is the simultaneous solution of the pair of equations $f_1 = 0$ and $f_2 = 0$. We leave it to the reader to verify that

$$\begin{aligned} &k_{10} = -k_3\cos\phi\tan\theta, \quad k_{20} = -k_3\sin\phi\tan\theta, \\ &\omega_0 = c_0 k_3 \sec\theta, \quad J = 4\cos^2\theta. \end{aligned} \tag{3.4.10}$$

When these results are used in (3.4.9), that representation reduces to

$$\alpha_B(\boldsymbol{x}) = \frac{2R}{\pi}\int_{-\infty}^{\infty}\frac{dk_3}{ik_3}F(c_0k_3\sec\theta)e^{-2ik_3\{(x_1\cos\phi+x_2\sin\phi)\tan\theta+(x_3-h)\}}. \tag{3.4.11}$$

It will simplify our discussion below if we recast this result as an integral in $\omega = c_0k_3\sec\theta$. The result is

$$\alpha_B(\boldsymbol{x}) = \frac{2R}{\pi}\int_{-\infty}^{\infty}\frac{d\omega}{i\omega}F(\omega)e^{-2i\omega\{(x_1\cos\phi+x_2\sin\phi)\sin\theta+(x_3-h)\cos\theta\}/c_0}. \tag{3.4.12}$$

This result should be compared with (2.4.12), which was shown to represent a bandlimited step function with height $-4R$ located at the position representing the zero of the phase function. The same result obtained here places the step at the right location, because the zero of the phase is the location of the reflector of the model data, (3.4.7). Furthermore, $-4R$ is the "right" height of the step at that location, confirming the validity of our inversion formula for this simple example.

3.4.2 The Reflectivity Function

The structure of the result (3.4.11) suggests that we can proceed, at least for this simple example, to introduce a *reflectivity function*, exactly as in one dimension, by multiplying the data by $i\omega/2c_0$. (Again, remember that ω is restricted to ω_0, which are the frequencies for which k_3 is real-valued.) That is, starting from (3.4.6), introduce this factor to define $\beta(\boldsymbol{x})$ by

$$\beta(\boldsymbol{x}) = \frac{4c_0^2}{\pi^2}\int_\Sigma d^2\xi\int_\Omega d^3k\frac{k_3}{\omega_0}e^{2i[\boldsymbol{\kappa}\cdot(\boldsymbol{\rho}-\boldsymbol{\xi})-k_3x_3]}\int_0^\infty dt\, tU_S(\boldsymbol{\xi},t)e^{i\omega_0t}. \tag{3.4.13}$$

This equation is similar to Stolt's [1978] Fourier-based migration formula, although our method of derivation is quite different from that used by Stolt.[6] Our approach relates the output to reflection coefficients, whereas the stated goal of the migration approach is to propagate the ensemble of zero-offset observations back to their locations at some initiation time, under the assumption that the ensemble is, itself, a solution of the wave equation with propagation speed $c_0/2$. A detailed comparison of the Stolt migration formula with equation (3.4.13) is left as an exercise.

For the specific example of a single reflector, the result of applying this operator to the model data (3.4.7) is obtained by introducing the same multiplier, $i\omega/2c_0$, in (3.4.12). That is, for the single reflector,

[6] See also Gardner [1985].

$$\beta(\boldsymbol{x}) = \frac{R}{\pi c_0} \int_{-\infty}^{\infty} d\omega F(\omega) e^{-2i\omega\{(x_1 \cos\phi + x_2 \sin\phi)\sin\theta + (x_3 - h)\cos\theta\}/c_0}. \tag{3.4.14}$$

From the analysis of Chapter 2, it follows that

$$\beta(\boldsymbol{x}) = R\delta_B \left\{(x_1 \cos\phi + x_2 \sin\phi)\sin\theta + (x_3 - h)\cos\theta\right\}. \tag{3.4.15}$$

The argument of the delta function measures distance normal to the planar reflector. It should be noted that this is true *independent of the inclination of the reflector.* (This bandlimited delta function of normal distance to a surface will arise in a more general context later. It is sufficiently important to have its own name. It is called the *singular function of the surface.* In the next chapter, it will be more rigorously defined. See also Appendix A for a discussion of the properties of singular functions.)

Usually, one would expect to obtain a normal derivative by multiplying the Fourier data by $i\boldsymbol{k} \cdot \hat{\boldsymbol{n}}$ where $\hat{\boldsymbol{n}}$ is a vector normal to the reflector. Here, we obtained a normal derivative by multiplying by $i\omega/c_0$ for *any choice of normal direction.* The question arises: Why should this work? The answer lies in the results (3.4.10). First, note that in our definition of the Fourier transform, $\boldsymbol{k} = (k_1, k_2, -k_3)$, because the sign of the last Fourier variable was opposite to the signs of the first two. From (3.4.10), note that the action of the delta functions was to evaluate $\boldsymbol{k}$ at

$$\begin{aligned} \boldsymbol{k} &= -k_3(\cos\phi\tan\theta, \sin\phi\tan\theta, 1) \\ &= \pm k_3 \sec\theta \hat{\boldsymbol{n}} \\ &= \pm k\hat{\boldsymbol{n}}, \end{aligned} \tag{3.4.16}$$

with the choice of $\pm$ being opposite to the sign of k_3. That is, $\boldsymbol{k} \cdot \hat{\boldsymbol{n}} = \pm k$, so that multiplication by $\omega/c_0 = -\operatorname{sgn}(\omega)k$ is asymptotically equivalent to multiplication by $\pm\boldsymbol{k} \cdot \hat{\boldsymbol{n}}$. The specific choice and the extra scaling introduced in our definition of $\beta(\boldsymbol{x})$ has resolved the ambiguity in sign here to produce the desired result, that is, a bandlimited Dirac delta function multiplied by the reflection coefficient, R. We will verify this result for a more general reflector below. In the next chapter we will show this result as a property of Fourier transforms. We will then be prepared to apply its generalization in later chapters to inversion in heterogeneous media, where the relationship between k and ω is more complicated than it is for the homogeneous background case considered here.

Exercises

3.5 In this exercise we will explore the properties of the singular function of a dipping plane reflector in a somewhat simplified setting, by considering the 2D singular function of a line through the origin at an arbitrary angle. Define the singular function of the line as

$$f(x, y) = \delta(x \cos\phi + y \sin\phi).$$

a. Draw the support of this delta function in two dimensions and find its Fourier transform, $\tilde{f}(\boldsymbol{k})$. Verify that the support of the Fourier transform is line whose direction is the normal to the support of $f(x, y)$.

b. Suppose that we limit the bandwidth of the Fourier data by setting the data values to zero in a strip, $|k_1 \sin\phi - k_2 \cos\phi| < l$, for any finite l. Find the bandlimited inversion.

c. Define the dipping step function

$$g(x, y) = H(x \cos\phi + y \sin\phi).$$

Find its Fourier transform, $\tilde{g}(\boldsymbol{k})$.

d. Show that

$$-i(\boldsymbol{k} \cdot \hat{\boldsymbol{n}})\tilde{g}(\boldsymbol{k}) = \tilde{f}(\boldsymbol{k}).$$

In this equation, $\hat{\boldsymbol{n}} = (\cos\phi, \sin\phi)$ is the normal to the support of $f(x, y)$.

e. Exploit the constraints imposed by the delta functions in $\tilde{g}$ to show that

$$-ik \ \text{sgn}\,(k_2)\ \tilde{g}(\boldsymbol{k}) = \tilde{f}(\boldsymbol{k}),$$

as long as $\phi > 0$. The point of this last result is that we need not know the normal direction in advance to process data for $\tilde{g}$ to produce the singular function of its line of discontinuity. (The multiplier $-ik\,\text{sgn}\,(k_2)$ is independent of $\hat{\boldsymbol{n}}$ or, equivalently, independent of ϕ).

3.4.3 Alternative Representations of the Reflectivity Function

There are two alternative representations of the solution (3.4.13), arising from requiring $\omega = \omega_0(\boldsymbol{k})$, as defined by (3.3.14), as one of the variables of integration instead of k_3. Note, from that equation that

$$d\omega = c_0\,\text{sgn}\,(k_3)\frac{k_3}{\sqrt{k_1^2 + k_2^2 + k_3^2}}dk_3 = c_0^2\frac{k_3}{\omega}dk_3, \tag{3.4.17}$$

implying that

$$dk_3 = \frac{\omega}{c_0^2 k_3}\, d\omega. \tag{3.4.18}$$

Using equation (3.4.17) in (3.4.13) yields

$$\beta(\boldsymbol{x}) = \frac{4}{\pi^2}\int_\Sigma d^2\xi \int_\Omega d^2\kappa \int d\omega\ e^{2i[\boldsymbol{\kappa}\cdot(\boldsymbol{\rho}-\boldsymbol{\xi}) - k_3 x_3]} \int_0^\infty dt\ tU_S(\boldsymbol{\xi}, t)e^{i\omega t}, \tag{3.4.19}$$

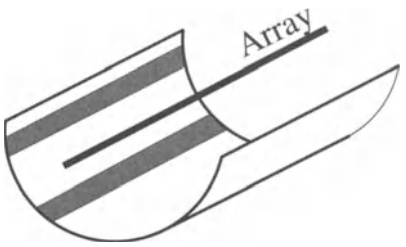

FIGURE 3.3. The black line depicts a source-receiver array located on the axis of a buried half-cylinder. The shaded strips are only two of the many possible zones on the half-cylinder that could be represented by the data collected by the array.

where $\boldsymbol{\rho} \equiv (x_1, x_2)$, $\boldsymbol{\kappa} \equiv (k_1, k_2)$, and $d^2\kappa \equiv dk_1\, dk_2$. Now, k_3 is defined by (3.3.13); Ω is still the domain of real values of $\boldsymbol{k}$ within the bandwidth of the data. This result allows an integration by parts in ω to eliminate the power of t appearing in the Fourier transform. That is, we integrate the term $\exp\{i\omega t\}$ and differentiate the term $\exp\{-2ik_3x_3\}$. There are no contributions from the endpoints of integration because the data have finite bandwidth and are assumed to vanish smoothly. The result is

$$\beta(\boldsymbol{x}) = \frac{8x_3}{\pi^2 c_0^2} \int_\Sigma d^2\xi \int_\Omega d^2\kappa \int d\omega\, \frac{\omega}{k_3} e^{2i[\boldsymbol{\kappa}\cdot(\boldsymbol{\rho}-\boldsymbol{\xi})-k_3x_3]} \int_0^\infty dt\, U_S(\boldsymbol{\xi}, t) e^{i\omega t}. \tag{3.4.20}$$

Applying equation (3.4.18) to this equation yields an inversion formula,

$$\beta(\boldsymbol{x}) = \frac{8x_3}{\pi^2} \int_\Sigma d^2\xi \int_\Omega d^2\kappa \int dk_3 e^{2i[\boldsymbol{\kappa}\cdot(\boldsymbol{\rho}-\boldsymbol{\xi})-k_3x_3]} \int_0^\infty dt\, U_S(\boldsymbol{\xi}, t) e^{i\omega t}, \tag{3.4.21}$$

that is free of explicit dependence on ω.

On one hand, the explicit factor of t seen in equation (3.4.19) is familiar to the geophysicist, being a common *gaining* factor that is applied as a preprocessing step, prior to migration, to correct for geometrical spreading. On the other hand, there is an advantage of using equations of the form of (3.4.20) or (3.4.21), which do not have the explicit factor of t. While we expect seismic signals to have amplitude decay proportional to t^{-1}, consistent with the multiplicative factor of t seen in (3.4.19), the noise seen in real data need not decay at that rate. Consequently, inversion formulas with the explicit factor of t could possibly enhance noise at large observation times. Equations (3.4.20) and (3.4.21) will not suffer from that problem. Such considerations follow because the inversion of data consisting of signal plus noise need not be a linear process.

3.5 Two-and-One-Half Dimensions

Though computer technology has advanced to permit the processing of areal surveys as single data sets, line-by-line processing of seismic data is still widely used because of the cost benefits. Equation (3.4.13) cannot be used to process a single line of data. In fact, a single line of data cannot be used to reconstruct a 3D medium. Here is a simple example of why this is the case. Consider a single line of sources and receivers lying at the axis of a buried half-cylinder. If the "reflector" consisted of a single strip lying on the surface of the cylinder, parallel to the data line, then the observed data would be the same, *no matter where the strip is located*. It takes observations from other data lines to distinguish one strip of the cylinder from another. See Figure 3.3.

There are situations, however, where the gathering and/or processing of a single line of data will suffice to produce an adequate inversion for the interior medium. Suppose, for example, that in a given region, the parameter variations were (nearly) two-dimensional such that the primary variations in the subsurface parameters were in one lateral direction.

Let us designate that direction as the direction of *maximum dip*, and the orthogonal direction as the direction of *strike*, echoing the geologists' terms characterizing the orientation of a rock layer. It is reasonable to expect that data gathered along the maximum dip direction of such a model will provide enough information to invert for the profile.

Mathematically, we idealize the problem as follows. Assume that the medium parameters vary only in one lateral direction, say x, and in depth z. Let the survey be conducted along a line in the x-direction, at a particular y value, say at $y = 0$. Our first objective, therefore, is to invert this one line of data to produce an image of the subsurface. See Figure 3.4.

The reader should realize that this is *not* a two-dimensional inversion problem. The medium is still three-dimensional; our sources are point sources in three dimensions with all their three-dimensional propagation characteristics. The 3D Helmholtz equation is still the governing equation for the problem. Only the nature of the medium parameters and our fortuitous choice of the direction of the experimental line suggest a two-dimensional problem. A fully two-dimensional problem would be equivalent to using *line sources* in this three-dimensional world, with quite different propagation characteristics. (In 2D, the incident wave has nonzero energy propagating throughout the $y = 0$ plane for *all time* greater than zero, and all spatial positions. This is in contrast to the 3D incident wave, which passes through a given range from the source at a given time and is gone after a time governed only by the duration of the source.)

We will refer to problems involving three-dimensional wave propagation in media having only two-dimensional parameter variability as *two-and-one-half-dimensional* problems. The key to solving the two-and-one-half-dimensional inverse problem is to realize that there really is enough

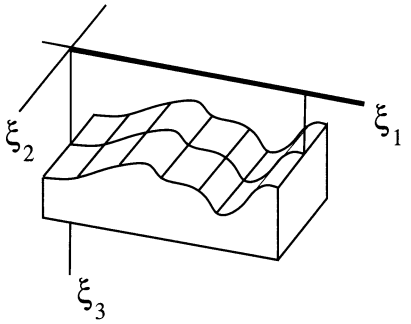

FIGURE 3.4. The black line depicts a source-receiver array located over a 2.5D model. All raypaths are confined to the $\xi_2 = 0$ plane.

information from a single line of data to solve the three-dimensional inverse problem, as long as the medium parameters really depend on only two variables.

Given such a line of data, say at $\xi_2 = 0$, we propose the following

Thought experiment: Consider the data for which the entire source-receiver array for each experiment in the ensemble of experiments is moved to any line ξ_2, different from zero, and

Claim: The data for the ensemble of experiments on the new line are exactly the same as the data for the ensemble of experiments on the line at $\xi_2 = 0$.

Note that the presentation here is not tied to the particular ensemble of zero-offset experiments of interest in this chapter, but to *any* suite of experiments carried out on a single line, as long as the assumptions about the medium parameters and the direction of the experimental line are as described above.

Application of our thought experiment implies that, from a single line of data, we really have an areal survey of data for the two-and-one-half-dimensional inverse problem. Furthermore, *those data are independent of* ξ_2, the surface coordinate in the strike direction. Now, in (3.4.13), for example, the only dependence on ξ_2 in the inversion formula is in the known kernel of the inversion operator. This is prototypical. Whenever a three-dimensional inversion formula is derived, specialization to two-and-one-half dimensions leads to an integral in which the ξ_2 dependence is in the inversion operator, and not in the data. Therefore, the ξ_2 integral in the inversion formula can be computed analytically, at least to leading order, by asymptotic means.

Exercises

3.6 In this exercise, we will explore the concept of the 2.5D geometry.

a. Suppose that a seismic survey is to be carried out in a region in which the subsurface is essentially cylindrical, that is, it varies only with one lateral variable and with depth. Define a coordinate system and design a suite of zero-offset experiments over the entire surface, so that the observed data are represented by a function of only one surface variable, and time.

b. Repeat for a suite of common-offset experiments. Call the half-offset h; introduce surface coordinates, ξ_1 and ξ_2, and write down the coordinates of x_s and x_g in terms of ξ_1, ξ_2, and h. The experimental design should be such that the data are a function of ξ_1, independent of ξ_2.

c. Repeat (b) for a suite of common-shot experiments in which the receivers are restricted to lie along a line.

3.5.1 Zero-Offset, Two-and-One-Half Dimensional Inversion

Let us apply the idea of the previous section to (3.4.13). We will assume that the zero-offset survey was gathered along a dip line at $\xi_2 = 0$ and we fill out the data needed in (3.4.13) by using the same data for every ξ_2. We can do this because the data are independent of ξ_2. Now consider the ξ_2 integral in (3.4.13). The result is a Dirac delta function with support at $k_2 = 0$. More explicitly,

$$\int_\Sigma d\xi_2 e^{-2ik_2\xi_2} = 2\pi\delta(2k_2) = \pi\delta(k_2). \tag{3.5.1}$$

With this result, we can now proceed to carry out the k_2 integration by simply evaluating the integrand in (3.4.13) at $k_2 = 0$. In addition to the explicit k_2 dependence, we must take care to evaluate ω_0, defined in (3.3.14), at $k_2 = 0$. Note that a subsidiary result of this evaluation is that the resulting inversion formula is independent of x_2. Therefore, we might as well disregard the second coordinate entirely in all further discussion, setting

$$\begin{gathered} \boldsymbol{k} = (k_1, k_3), \quad \boldsymbol{x} = (x_1, x_3), \\ \omega_0 = c_0 \operatorname{sgn}(k_3)\sqrt{k_1^2 + k_3^2}. \end{gathered} \tag{3.5.2}$$

Using (3.5.1) in (3.4.13) yields the two-and-one-half-dimensional inversion formula

$$\beta(\boldsymbol{x}) = \frac{4c_0^2}{\pi}\int_\Sigma d\xi \int_\Omega d^2k \frac{k_3}{\omega_0} e^{2i[k_1(x_1-\xi)-k_3x_3]} \int_0^\infty dt\, tU_S(\xi, t)e^{i\omega_0 t}. \tag{3.5.3}$$

In this equation, we have set $\xi_1 = \xi$ and denoted the data as a function of this scalar spatial variable.

We could try verifying this formula on data reflected from an inclined plane; however, that calculation has already been carried out in the previous

section. In particular, consider the data in (3.4.7) with $\phi = 0$. For such data, $\xi_2 = 0$ defines the plane of maximal dip. Furthermore, the fourfold integral in $\boldsymbol{\xi}$ and $\boldsymbol{k}$, carried out in that discussion, includes exactly the integral in ξ_2 and k_2 carried out here. Thus, it follows that the result of applying the inversion formula above to the data (3.4.7) with $\phi = 0$ is the result (3.4.15) with $\phi = 0$, which is the desired output.

The same computations as those that led to the results (3.4.19) and (3.4.20) can be carried out for this two-and-one-half dimensional inversion result. We state, with no further discussion, the alternative representations,

$$\beta(\boldsymbol{x}) = \frac{4}{\pi} \int_\Sigma d\xi \int_\Omega dk_1 \int d\omega e^{2i[k_1(x_1-\xi)-k_3 x_3]} \int_0^\infty dt\, tU_S(\xi,t)e^{i\omega t}, \quad (3.5.4)$$

and

$$\beta(\boldsymbol{x}) = \frac{8x_3}{\pi c_0^2} \int_\Sigma d\xi \int_\Omega dk_1 \int d\omega \frac{\omega}{k_3} e^{2i[k_1(x_1-\xi)-k_3 x_3]} \int_0^\infty dt\, U_S(\xi,t)e^{i\omega t}. \quad (3.5.5)$$

Finally, applying equation (3.4.18) we can arrive at a result that does not explicitly depend on ω,

$$\beta(\boldsymbol{x}) = \frac{8x_3}{\pi} \int_\Sigma d\xi \int_\Omega dk_1 \int dk_3 e^{2i[k_1(x_1-\xi)-k_3 x_3]} \int_0^\infty dt\, U_S(\xi,t)e^{i\omega t}. \quad (3.5.6)$$

Exercises

3.7 The purpose of this exercise is to compare Stolt's [1978] 3D migration formula and the 3D inversion formula for $\beta(\boldsymbol{x})$, (3.4.19). The relevant equations in Stolt's paper are as follows. The data are written as $\psi(X,Y,0,t)$, with Fourier transform

$$A(P,Q,\omega,0) = \frac{1}{[2\pi]^{3/2}} \int dX \int dY \cdot \int dt\, \psi(X,Y,0,t) \exp\{-i[PX+QY-\omega t]\}.$$

The output of Stolt's method is defined by

$$\psi(\tilde{X},\tilde{Y},\tilde{Z},0) = \frac{1}{[2\pi]^{3/2}} \int dP \int dQ \cdot \int d\tilde{\omega}\, B(P,Q,\tilde{\omega}) \exp\left\{i[P\tilde{X}+Q\tilde{Y}-2\tilde{\omega}\tilde{Z}/c]\right\}.$$

In this equation,

$$B(P,Q,\tilde{\omega}) = \frac{1}{\sqrt{1+[P^2+Q^2]c^2/4\tilde{\omega}^2}} \cdot A\left[P,Q,\tilde{\omega}\sqrt{1+[P^2+Q^2]c^2/4\tilde{\omega}^2},0\right].$$

Earlier, Stolt defines

$$A(P,Q,\omega,\tilde{Z}) = A(P,Q,\omega,0)\exp\left[-i\tilde{Z}\sqrt{4\omega^2/c^2-P^2-Q^2}\right].$$

Stolt does not distinguish between input and output variables. Here, tildes have been introduced over the output variables. (In particular, note that there is now an $\tilde{\omega}$, as well as an ω. Make a table identifying Stolt's variables with the variables of the inversion formula (3.4.19) for $\beta(\boldsymbol{x})$.

3.6 Kirchhoff Inversion

The inversion formulas of the previous section, obtained by Fourier transform methods, were seen to be almost identical (within a scale factor) to Stolt's zero-offset migration formulas (see Stolt [1978]). In this section, we apply the method of stationary phase to the $\boldsymbol{\kappa}$ integrals to obtain formulas in which the processing of the data will consist of a temporal transform, (followed possibly by the application of filter), followed by an inverse (frequency to time) transform, and followed finally by an integration over source-receiver points.

This result will be seen to agree with Schneider's Kirchhoff zero-offset migration formula to within a scale factor (see [Schneider 1978]).[7] The names—Kirchhoff migration, Kirchhoff inversion—are a consequence of the resemblance of these processes to the Kirchhoff integral representation of solutions to the forward problem. Indeed, Schneider started from that representation to obtain his result. The derivation here establishes the analytical equivalence of the Fourier and Kirchhoff methods of migration/inversion to leading order, asymptotically, for high-frequency data. Of course, in practice, each has its own numerical artifacts. These are discussed extensively in the literature.

3.6.1 Stationary Phase Computations

The high-frequency criterion—(3.4.2) and (3.4.3)—allows us to make asymptotic approximations in the integral inversion formulas (3.4.13), (3.4.19), (3.4.20) and (3.5.3), (3.5.4), (3.5.5) to recast them in other useful forms. This is by no means apparent, because the criterion is expressed in

[7] See also Gardner [1985].

terms of a dimensionless parameter, and the integrals in the above set of equations are written in dimensional variables, with that parameter not in evidence.

In Appendix C, we show how to convert formulas of the type listed above into formulas with dimensionless variables. In this way we can see that the method of stationary phase can be applied to any of these integrals. The formal calculations of the method of stationary phase can actually be carried out either in the dimension*al* or the dimension*less* variables, however, when doing the former, one must remember that the justification is based on the fact that an appropriate representation in dimension*less* variables can be achieved.

The Multi-dimensional Stationary Phase Formula

The method of stationary phase provides a means of approximating integrals of the form

$$I(\lambda) = \int f(\boldsymbol{\eta}) e^{i\lambda\Phi(\boldsymbol{\eta})} d^n\eta. \tag{3.6.1}$$

It is assumed here that the parameter λ is "large." In fact, although the mathematical formalism is a statement of the leading-order approximation of the integral as $|\lambda| \to \infty$; in practice, we apply the method for finite values of λ that large enough, in a sense to be described more fully below, for the leading term provided by the method of stationary phase to give adequate numerical accuracy.

!defined The method predicts that the value of the integral is dominated by the value of the integrand in the neighborhood of certain critical points called *stationary points*, provided such points exist. At a stationary point, say $\boldsymbol{\eta}_0$, all of the first derivatives of the phase function Φ must be zero (hence the name, *stationary phase*):

$$\nabla\Phi(\boldsymbol{\eta}) = 0 \qquad \text{at} \qquad \boldsymbol{\eta} = \boldsymbol{\eta}_0. \tag{3.6.2}$$

If there is one such point in the domain of integration, then the method predicts that the integral (3.6.1) is well approximated as follows:

$$I(\lambda) = \int f(\boldsymbol{\eta}) e^{i\lambda\Phi(\boldsymbol{\eta})} d^n\eta \sim \left[\frac{2\pi}{|\lambda|}\right]^{n/2} \frac{f(\boldsymbol{\eta}_0) e^{i\lambda\Phi(\eta_0) + i\pi/4\,\mathrm{sgn}\,(\lambda)\,\mathrm{sig}\,(\Phi_{ij})}}{\sqrt{|\det \Phi_{ij}|}},$$

$$\text{where} \qquad \Phi_{ij} \equiv \left[\frac{\partial^2\Phi(\boldsymbol{\eta}_0)}{\partial\eta_i \partial\eta_j}\right]. \tag{3.6.3}$$

The matrix Φ_{ij}, is the matrix of second derivatives or *Hessian* matrix of the phase Φ. The term, $\mathrm{sig}\,(\Phi_{ij})$ denotes the *signature* of the matrix Φ_{ij}, which is the number of positive eigenvalues minus the number of negative eigenvalues of the matrix. The symbol $\sim$ should be read as "is asymptotically equal to." The reader should understand that there is a precise mathematical definition to this type of approximation. It states that the difference

between $I(\lambda)$ and the given approximation vanishes "faster than" $1/|\lambda|^{n/2}$ as $|\lambda| \to \infty$; that is,

$$|\lambda|^{n/2} \left| I(\lambda) - \left[\frac{2\pi}{|\lambda|}\right]^{n/2} \frac{f(\boldsymbol{\eta}_0) e^{i\lambda\Phi(\eta_0) + i\pi/4 \operatorname{sgn}(\lambda) \operatorname{sig}(\Phi_{ij})}}{\sqrt{|\det \Phi_{ij}|}} \right| \to 0,$$
$$\text{as} \quad |\lambda| \to \infty.$$

See Bleistein [1984] or Bleistein and Handelsman [1986] for further discussion. If there are more stationary points, then the leading-order approximation is a sum of such contributions over all of the stationary points. If there are no stationary points, then the integral approximation involves a higher negative power of λ and the value of the integral is smaller, at least for λ large enough (more precisely, in the limit as $|\lambda| \to \infty$). The result also assumes that the matrix Φ_{ij} is nonsingular, that is, that all of its eigenvalues are nonzero. When the matrix Φ_{ij} is singular, one or more of the eigenvalues is zero and the above formula is no longer valid, the power of $1/\lambda$ is smaller and the value of the integral is larger. Both the case of integrals with no interior stationary points and the case of vanishing eigenvalues can be dealt with by the theory that produces the result stated here; see Bleistein [1984] or Bleistein and Handelsman [1986] for further details.

The One-Dimensional Stationary Phase Formula

The case of one-dimensional integrals arises often enough that it is worthwhile to list its formula separately. That result is

$$I(\lambda) = \int f(\eta) e^{i\lambda\Phi(\eta)} d\eta \tag{3.6.4}$$
$$\sim \sqrt{\frac{2\pi}{|\lambda||\Phi''(\eta_0)|}} f(\eta_0) e^{i\lambda\Phi(\eta_0) + i\pi/4 \operatorname{sgn}(\lambda) \operatorname{sgn}(\Phi''(\eta_0))}.$$

In these formulas, the integrands can depend on other parameters that are allowed to vary over some range for which the matrix Φ_{ij} or the second derivative $\Phi''(\eta_0)$ is bounded away from zero. Such a situation arises most naturally in a multifold integral in which the method of stationary phase is applied only to some of the integrals and not to others. Also, it is natural for the integral $I(\lambda)$ to be a function of position, a function of time, or a function of position and time. The former case will arise in our inversion integrals as well as in forward modeling problems, while the latter case arises in forward modeling problems.

While the theoretical convergence as $|\lambda| \to \infty$, mentioned above, is reassuring, we are concerned about the practical application of these approximations for some finite value of λ. Then, the question of how large is "large enough" becomes an issue.

Accuracy of 1D Stationary Phase

Let us begin this discussion by considering the one-dimensional integral (3.6.4). There are two relevant issues here. First, further analysis of this approximation reveals that subsequent terms contain increasing integer powers of $|\lambda||\Phi''(\eta_0)|$ in the denominator, so that this is the "true" large parameter in this asymptotic expansion. Second, these subsequent terms involve higher derivatives of both $\Phi(\eta)$ (beyond the second) and $f(\eta)$ (from the first derivative onward). Thus, for any fixed finite choice of λ, we would want that the correction terms—at the very least, the *first* correction term—really be smaller than the term that is retained.[8] For this to be true, we would want that the derivatives of f and Φ not grow significantly with increasing order and that $|\lambda||\Phi''(\eta_0)|$ be "large" enough. Assuming the former, what we have earlier proposed on empirical grounds for the latter is

$$|\lambda||\Phi''(\eta_0)| \geq \pi. \tag{3.6.5}$$

In our applications, λ is proportional to frequency, ω or f, for which there is a whole range of values involved—the bandwidth of the signal that arrives at the receivers. If this asymptotic criterion fails only for some frequencies, then, to a degree, the failure of the asymptotic expansion is "mild." As progressively more frequencies fall below the threshold indicated here, the amplitude will tend to degrade before the phase does. In our applications, phase is related to position, while amplitude is related to parameter estimation. Thus, with such partial failure of our asymptotic criterion, a reasonably accurate image will be produced, but parameter estimation should be viewed as suspect.

If the criterion in (3.6.5) fails, we can think of $|\Phi''(\eta_0)|$ as being "small" at the stationary point. In this case, $\Phi''(\eta_0)$ might be equal to zero for some nearby value of η and the integrand is likely to have another stationary point too near η_0 for asymptotic expansions based on isolated stationary points to be valid. There are other ways that the asymptotic expansion (3.6.4) might fail that are not indicated by the size of the second derivative, however. The method depends on all types of critical points being isolated. In particular, these include endpoints of integration or points where f or Φ or one of its derivatives is discontinuous, or singular in some manner. As an example, let us consider the case of an isolated endpoint, say, η_1, where the integrand is "well behaved" and f is nonzero. Then, the leading order asymptotic expansion of the contribution from this point, treated in isolation, begins with the power $1/i\lambda\Phi'(\eta_1)$. If η_0 is "near" η_1, then the denominator here will fail to satisfy a criterion similar to (3.6.5), say

---

[8] See the last part of Appendix C for further discussion of this issue. The issue is how we scale the dimensional variables to obtain this dimensionless form of the phase and its derivatives.

$$|\lambda\Phi'(\eta_1)| \geq \pi.$$

The situation is actually a little more severe than that, however. If the asymptotic expansion of the *entire integral* is to be given by this one stationary phase contribution, (3.6.4), then we would want this endpoint term to be small compared to the stationary point contribution. Thus, for interaction between a stationary point and a "regular" endpoint, we need to impose the requirement

$$\left|\frac{1}{\lambda\Phi'(\eta_1)}\right| \leq \frac{1}{\pi}\frac{1}{\sqrt{|\lambda\Phi''(\eta_0)|}} \quad \longrightarrow \quad \frac{\sqrt{|\lambda|}|\Phi'(\eta_1)|}{\sqrt{|\Phi''(\eta_0)|}} \geq \pi. \tag{3.6.6}$$

We will not bother to test this ratio in applications. The reader should be aware that the leading-order asymptotic expansion obtained by the method of stationary phase will break down when the stationary point is too near the endpoint of integration, however. In our analysis, we will apply the method of stationary phase to the source-receiver coordinates, in particular, for given values of the output point, $\boldsymbol{y}$. For some range of output points, the stationary point may well be near an endpoint of integration. While the traveltime at stationarity will be correct, the amplitude will not. That is, our processing will recover an image, perhaps obscured somewhat by the endpoint contribution, but the amplitude will be unreliable for parameter estimation.

Accuracy of Multidimensional Stationary Phase

For the multidimensional case, the criterion for numerical accuracy of an asymptotic expansion derived by the method of stationary phase becomes a little more complicated. A result similar to this last one arises for each of the iterated integrals in this case, but only after the independent variables are transformed to the principal directions defined by the eigenvectors of the matrix Φ_{ij}. Then, the eigenvalues play the same role as the second derivative of the one-dimensional case. That is, if we define λ_j, $j = 1, ..., n$, to be the eigenvalues of Φ_{ij}, then we find that there are really n correction terms at the next level of accuracy and each of those has to be appropriately small. Equivalent to (3.6.5), in this case, we must require that

$$\min_j(|\lambda||\lambda_j|) \geq \pi. \tag{3.6.7}$$

When we deal with problems in dimensional variables, the parameter λ will not appear explicitly. In these cases, we apply the above formulas with $\lambda = 1$—or some other constant multiplier that naturally arises in the phase of an integral—and the symbolic variables, $\boldsymbol{\eta}$, being one or more of the dimensional variables of the problem. Always, one will find in the result that the neglected terms will involve a dimensionless large parameter, such as the product $\omega_0 t/2$ in equation (3.3.12), that justified neglecting this term compared to unity in deriving equation (3.4.6).

Applying Multidimensional Stationary Phase to Equations (3.4.19) and (3.4.20)

Indeed, this is exactly the case for the integrals appearing in the inversion formulas (3.4.13), (3.4.19), (3.4.20) and (3.5.3), (3.5.4), (3.5.5). With this point of view, we consider the phase function in (3.4.19) and (3.4.20), and introduce the phase function

$$\Phi = \boldsymbol{\kappa} \cdot (\boldsymbol{\rho} - \boldsymbol{\xi}) - k_3 x_3, \tag{3.6.8}$$

where $\boldsymbol{\rho} \equiv (x_1, x_2)$, $\boldsymbol{\kappa} \equiv (k_1, k_2)$, $\boldsymbol{\xi} = (\xi_1, \xi_2)$, and $k_3^2 \equiv \omega^2/c_0^2 - \kappa^2$. We evaluate the integrals in $\boldsymbol{\kappa}$ by the method the stationary phase . For future reference, note that with this definition, the formal large parameter in (3.4.19) and (3.4.20) is just 2. In this application all variables other than k_1 and k_2, are treated as parameters. Thus we will apply formula (3.6.3) with $n = 2$, and η_1 and η_2 replaced by k_1 and k_2.

To apply the method of stationary phase, we need the first and second derivatives of the phase function (3.6.8):

$$\begin{aligned} \frac{\partial \Phi}{\partial k_i} &= x_i - \xi_i + \frac{k_i}{k_3} x_3, \quad i = 1, 2, \\ \frac{\partial^2 \Phi}{\partial k_i \partial k_j} &= \left[\frac{\delta_{ij}}{k_3} + \frac{k_i k_j}{k_3^3} \right] x_3, \quad i, j = 1, 2. \end{aligned} \tag{3.6.9}$$

$$\text{where} \quad \delta_{ij} = \begin{cases} 1, & i = j, \\ 0, & i \neq j. \end{cases}$$

The stationary points are the solutions of the equations

$$\frac{\partial \Phi}{\partial k_i} = x_i - \xi_i + \frac{k_i}{k_3} x_3 = 0. \tag{3.6.10}$$

Recognizing that

$$k_3 = |k| \hat{\boldsymbol{x}}_3 = \frac{\omega}{c_0} \frac{x_3}{r}, \qquad \text{where} \qquad r = \sqrt{\rho^2 + x_3^2},$$

we may solve for k_i in equation (3.6.10):

$$k_i = -\frac{\omega}{c_0} \frac{x_i - \xi_i}{r} \qquad \text{implying that} \qquad \Phi = -\frac{\omega r}{c_0}. \tag{3.6.11}$$

The last equation is the result of evaluating Φ as defined in (3.6.8), using the derived solution for $\boldsymbol{\kappa}$ at the stationary point.

The method of stationary phase also requires the value of the determinant and signature of the matrix of second derivatives at the stationary point. The determinant is fairly straightforward to compute from (3.6.9). The result is

$$\det \left[\frac{\partial^2 \Phi}{\partial k_i \partial k_j} \right] = \frac{x_3^2}{k_3^4} \frac{\omega^2}{c_0^2} = \frac{r^4}{x_3^2} \frac{c_0^2}{\omega^2}, \tag{3.6.12}$$

with the last result obtained by using the stationary value of k_3 determined by (3.6.11). This determinant is positive. Therefore, the eigenvalues of the matrix are of the same sign. This is true for any choice of $\boldsymbol{k}$. Therefore, to check the sign of the eigenvalues (to determine the signature of the matrix), we might as well check when $\boldsymbol{\kappa} = 0$. In this case,

$$\left[\frac{\partial^2 \Phi}{\partial k_i \partial k_j}\right] = \begin{vmatrix} 1/k_3 & 0 \\ 0 & 1/k_3 \end{vmatrix}.$$

For this diagonal matrix, the eigenvalues are each $1/k_3$ and hence have the same sign as ω. Therefore, we may write

$$\operatorname{sig}\left[\frac{\partial^2 \Phi}{\partial k_i \partial k_j}\right] = 2\operatorname{sgn}(\omega). \tag{3.6.13}$$

It is possible in this simple two-by-two case, to determine the explicit eigenvalues and simply read off their signs. The indirect method presented here has wider application and will prove useful later in determining signatures of larger matrices, however.

We now have the necessary components to compute the leading-order asymptotic expansion in (3.4.19) and (3.4.20) by the method of stationary phase. By applying the formula (3.6.3) to the present example, with $n = 2$, $\lambda = 2$, and using (3.6.9) in (3.6.3) to evaluate (3.4.19), we obtain the result

$$\beta(\boldsymbol{x}) = \frac{4x_3}{\pi c_0} \int_\Sigma \frac{d^2\xi}{r^2} \int_\Omega i\omega \, d\omega \, e^{-2i\omega r/c_0} \int_0^\infty dt \, t U_S(\boldsymbol{\xi}, t) e^{i\omega t}. \tag{3.6.14}$$

In a similar fashion, we obtain the following result for (3.4.20):

$$\beta(\boldsymbol{x}) = \frac{8x_3}{\pi c_0^2} \int_\Sigma \frac{d^2\xi}{r} \int_\Omega i\omega \, d\omega \, e^{-2i\omega r/c_0} \int_0^\infty dt \, U_S(\boldsymbol{\xi}, t) e^{i\omega t}. \tag{3.6.15}$$

In this last result, the temporal integral is just the Fourier transform of the data. Therefore, we can also write

$$\beta(\boldsymbol{x}) = \frac{8x_3}{\pi c_0^2} \int_\Sigma \frac{d^2\xi}{r} \int_\Omega i\omega \, d\omega \, u_S(\boldsymbol{\xi}, \omega) e^{-2i\omega r/c_0}. \tag{3.6.16}$$

In each of the results here, the output is obtained as an integral (a sum) over all source-receiver locations. The integrand (summand) is frequency-filtered data evaluated at the two-way traveltime $2r/c_0$, and then spatially filtered or weighted, as well. It is left as an exercise to show that the last result is the same as Schneider's [1978] Kirchhoff migration formula, to within a constant scaling factor.

Applying Multidimensional Stationary Phase to Equation (3.4.13)

To complete the discussion of modifying the three-dimensional inversion formulas, we should compute the asymptotic expansion in (3.4.13). In that

formula, k plays the role of ω in the above analysis, and the asymptotic expansion should be carried out with respect to the polar angles of $\boldsymbol{k}$. When this is done, the results obtained are exactly (3.6.9) and (3.6.14). Some extra care is necessary in this calculation because ω_0, as defined by (3.3.14), is a function of the polar angle in the $\boldsymbol{k}$-domain, in the fairly trivial way that the sign changes in the upper and lower half k-spaces.

Accuracy

Let us now consider the implications of the criterion (3.6.7) in terms of these dimensional variables. To do so, we introduce dimensionless variables $\boldsymbol{\eta}$ through the equation

$$\boldsymbol{\kappa} = \frac{\omega}{c}\boldsymbol{\eta}$$

and rewrite the phase in (3.4.19) as

$$\phi(\boldsymbol{\kappa}) = -2\frac{\omega r}{c}\left[\boldsymbol{\eta}\cdot\frac{(\boldsymbol{\rho}-\boldsymbol{\xi})}{r} - \eta_3\frac{x_3}{r}\right].$$

Here, we cannot neglect the factor of -2 in the original phase; hence, we use a new variable name, ϕ, for the phase function. In addition,

$$r = \sqrt{(\boldsymbol{\rho}-\boldsymbol{\xi})\cdot(\boldsymbol{\rho}-\boldsymbol{\xi}) + x_3^2} \quad \text{and} \quad \eta_3 = \sqrt{1-\eta_1^2-\eta_2^2}.$$

The dimensional phase has now been rewritten in dimensionless variables as

$$\phi(\boldsymbol{\kappa}) = \phi(\boldsymbol{\eta}/L) = \lambda\Phi(\boldsymbol{\eta}), \tag{3.6.17}$$

with

$$\lambda = -\frac{2\omega r}{c} \quad \text{and} \quad L = \frac{c}{\omega}.$$

and Φ now used as the "generic" phase in (3.6.1).

Now, differentiate in (3.6.17) to obtain

$$\lambda\frac{\partial^2\Phi(\boldsymbol{\eta}_0)}{\partial\eta_i\partial\eta_j} = \frac{1}{L^2}\frac{\partial^2\phi(\boldsymbol{\kappa}_0)}{\partial k_i\partial k_j}.$$

From this last equation, we conclude that if λ_j is an eigenvalue of the matrix Φ_{ij} (in dimensionless variables) and ν_j is an eigenvalue of the matrix ϕ_{ij} (in dimensional variables), then

$$\lambda\lambda_j = L^{-2}\nu_j, \quad j = 1, 2.$$

Therefore, we can rewrite (3.6.7) as

$$\min_j(L^{-2}|\nu_j|) \geq \pi. \tag{3.6.18}$$

We leave it as an exercise to show that, for ϕ_{ij}, the eigenvalues are given by

$$\nu_1 = -\frac{2rc}{\omega}, \quad \nu_2 = -\frac{2rc}{\omega}\frac{r^2}{x_3^2},$$

with the first one having the smaller absolute value. Thus, after multiplying by L^{-2}, we conclude that the asymptotic expansion will provide a sufficiently accurate result when

$$\frac{2|\omega|r}{c} = \frac{4\pi|f|r}{c} \geq \pi.$$

We see here that the criterion for validity is exactly the condition, (3.4.3), with the length scale of that equation just being the distance between a source-receiver point on the upper surface and the output point of the inversion formalism at depth. Of course, we would want this criterion to hold as the source-receiver point ranges over the entire upper surface, hence for minimum of r. Thus, we revise the criterion to be

$$\frac{2|\omega|x_3}{c} = \frac{4\pi|f|x_3}{c} \geq \pi.$$

The implication of this result is that this transformation from a Stolt-like inversion to a Kirchhoff-like inversion is only valid when the data acquisition surface is as far away from the output points as defined by our high frequency asymptotics criterion or, equivalently, by the Rayleigh criterion. In deleting a term of order $1/\omega_0 t$, earlier, we have already restricted our results to such a domain. This adds no new constraint to our analysis; the Kirchhoff inversions here are valid under the same high-frequency constraint as the earlier Stolt inversion.

Exercises

3.8 The purpose of this exercise is to compare equation (3.6.16) with Schneider's [1978] Kirchhoff migration formula,

$$U(x,y,z,0) = -\frac{1}{2\pi}\frac{\partial}{\partial \tilde{z}}\int\int d\tilde{x}d\tilde{y}\,\frac{U(\tilde{x},\tilde{y},0,R/C)}{R}.$$

This is the 3D migration formula presented in Schneider [1978], p. 53, Figure 4. Here, the notation has been changed to distinguish the input variables $(\tilde{x},\tilde{y},\tilde{z})$ from the output variables (x,y,z). Also

$$R = \sqrt{(x-\tilde{x})^2 + (y-\tilde{y})^2 + z^2}.$$

a. Show that multiplying by the factor $-2i\omega x_3/rc_0$ on the right side of equation (3.6.16) is asymptotically equivalent to taking the derivative with respect to x_3. Rewrite equation (3.6.16) in Schneider's form by using this fact.

b. Recognize that this new form of equation (3.6.16) contains an implicit correction for geometric spreading that may be represented

by a multiplication by $2r/c_0$. Remove this correction factor to permit a direct comparison with Schneider's formula. The formulas should differ by a factor of 8.

c. Verify (3.6.1).

3.6.2 Two-and-One-Half-Dimensional Kirchhoff Inversion

The objective here is to obtain analogous asymptotic expansions for the two-and-one-half-dimensional inversion formulas (3.5.4) and (3.5.5). There are two ways to proceed. First, we could carry out the one-dimensional stationary phase computation for the k_1 integrals in those equations. Second, we could apply the method of stationary phase to the ξ_2 integrals in (3.6.14), (3.6.15), (3.6.16), above, under the assumption that the data are independent of ξ_2. The latter method presents another example of the application of stationary phase; the former method is exactly like the results carried out above and we leave it to the exercises.

For any of the integrals (3.6.14), (3.6.15), (3.6.16), the phase to be considered is

$$\Phi = r, \tag{3.6.19}$$

with formal large parameter $-2\omega/c_0$. The first derivative of this phase function with respect to ξ_2 is

$$\frac{\partial \Phi}{\partial \xi_2} = \frac{\xi_2 - x_2}{r}, \tag{3.6.20}$$

which is stationary when $\xi_2 = x_2$. That is, in the two-and-one-half-dimensional survey, the dominant contribution occurs in the vertical plane passing through the survey line. The stationary phase calculation, then, will effectively carry out the delta function computation that led to the exact result when we passed from three dimensions to two-and-one-half dimensions in Section 3.5.

At the one and only stationary point,

$$\frac{\partial^2 \Phi}{\partial \xi_2^2} = \frac{1}{r}, \quad \xi_2 = x_2. \tag{3.6.21}$$

We apply (3.6.3) to (3.4.19), now with $n = 1$, using the results calculated above, to obtain

$$\beta(\boldsymbol{x}) = \frac{4x_3}{\sqrt{\pi c_0}} \int_\Sigma \frac{d\xi}{r^{3/2}} \int_\Omega d\omega \sqrt{|\omega|} e^{-2i\omega r/c_0 + i\pi/4 \operatorname{sgn}(\omega)} \int_0^\infty dt\, t U_S(\xi, t) e^{i\omega t}, \tag{3.6.22}$$

$$\text{where} \qquad r = \sqrt{(x_1 - \xi)^2 + x_3^2}.$$

In this equation and the results immediately below, $\boldsymbol{x} = (x_1, x_3) = (x, z)$. Also, we have combined factors of $\operatorname{sgn}(\omega)$ as follows:

$$i\,\mathrm{sgn}\,(\omega) = e^{i\pi/2\,\mathrm{sgn}\,(\omega)}, \quad i\,\mathrm{sgn}\,(\omega)e^{-i\pi/4\,\mathrm{sgn}\,(\omega)} = e^{i\pi/4\,\mathrm{sgn}\,(\omega)}$$

Note here that multiplication by $\sqrt{|\omega|}\exp\{-i\pi/4\,\mathrm{sgn}\,(\omega)\}$ is equivalent to taking the *half-derivative* in the time domain, while multiplication by $i\,\mathrm{sgn}\,(\omega)$ is equivalent to taking the *Hilbert transform* in the time domain. (See Appendix A for a discussion of the Hilbert transform.) Thus, the filter that we are applying in (3.6.22) and below is equivalent to applying the Hilbert transform to the half-derivative in the time domain.

The same analysis applied to (3.6.15) yields the result

$$\beta(\boldsymbol{x}) = \frac{8x_3}{c_0\sqrt{\pi c_0}} \int_\Sigma \frac{d\xi}{r^{1/2}} \int_\Omega d\omega \sqrt{|\omega|} e^{-2i\omega r/c_0 + i\pi/4\,\mathrm{sgn}\,(\omega)} \cdot \int_0^\infty dt\; U_S(\xi, t) e^{i\omega t}. \tag{3.6.23}$$

As in the previous subsection, this last result can be rewritten in terms of $u_S(\xi, \omega)$ as follows.

$$\beta(\boldsymbol{x}) = \frac{8x_3}{c_0\sqrt{\pi c_0}} \int_\Sigma \frac{d\xi}{r^{1/2}} \int_\Omega d\omega \sqrt{|\omega|} u_S(\xi, \omega) e^{-2i\omega r/c_0 + i\pi/4\,\mathrm{sgn}\,(\omega)}. \tag{3.6.24}$$

In each of these formulas, the reflectivity is computed as an integral (sum) over source-receiver points of spatially weighted and frequency-filtered data. In each case, the frequency-domain processing is computed only once, for any choice of background propagation speed. For each term in the integral (sum) the processed data are retrieved at a traveltime, $2r/c_0$, so that only the spatial integral(s) need be recomputed when c_0 is modified.

Exercises

3.9 Apply one-dimensional stationary phase in k_1 to the integrals (3.5.4) and (3.5.5), to obtain the two-and-one-half-dimensional inverse scattering formulas (3.6.22) and (3.6.23).

3.10 Introduce polar coordinates in (3.5.3), for both the two-dimensional wavevector and the position vector. Apply the method of stationary phase to the integral in the polar angle of $\boldsymbol{k}$. Confirm that the asymptotic expansion agrees with the results (3.6.22) or (3.6.23).

3.11 Introduce polar coordinates for the wavevector and the spatial vector in (3.4.13) and carry out stationary phase in the polar angles of $\boldsymbol{k}$ to obtain a result equivalent to (3.4.19) or (3.4.20).

3.12 In (3.3.1), apply the transverse Fourier transform, defined in (3.3.4), directly to this equation. Determine the transverse transform of the function $\exp\{2i\omega r/c_0\}/[4\pi r^2]$ by multidimensional stationary phase, and obtain the result

$$\frac{16\pi i c_0}{\omega} u_S(\boldsymbol{\kappa}, \omega) = \int \frac{\tilde{\alpha}(\boldsymbol{\kappa}, x_3)}{x_3} e^{2ik_3 x_3} dx_3,$$

with k_3 defined by (3.3.13). Introduce k_3 in place of ω as a transform variable, invert the transform, integrate by parts in k_3, and replace $\partial/\partial k_3$ by $\partial\omega/\partial k_3 \cdot \partial/\partial\omega$ to obtain result (3.4.6).

3.13 The purpose of this exercise is to provide insight into the determination of the large dimensionless parameter in integrals where we carry out the method of stationary phase in *dimensional* variables. Let us suppose that we are given a phase function in dimensional variables $\phi(x)$, and that we introduce the dimensionless variable η in a linear manner,[9]

$$x = L\eta.$$

Let us suppose further that this results in a phase as in (3.6.4); that is,

$$\lambda\Phi(\eta) = \phi(x).$$

a. Use the chain rule to show that

$$\lambda\frac{d^2\Phi(\eta)}{d\eta^2} = L^2\frac{d^2\phi(x)}{dx^2}. \tag{3.6.25}$$

b. Use this result to identify the dimensionless large parameter of the stationary phase formula when the integral is calculated in a dimensional spatial variable.

c. Repeat for integrals in time.

d. Make a conjecture about the multidimensional case with a possible temporal integral as well as spatial integrals. Exploit the comment about correction terms below the stationary phase formulas.

3.6.3 2D Modeling and Inversion

The purpose of the series of exercises that concludes this short subsection is the derivation of zero-offset inversion formulas for data collected in a 2D Earth model, with wave propagation governed by the 2D wave equation. In the 3D world that we discuss in this chapter, this would be equivalent to considering the energy to be propagating from a *line source*, rather than a point source. This line source would be oriented in the direction x_2 or y, in which the material parameters of the medium do not vary. This means that the variability of the medium would be in the (x_1, x_3), or (x, z), directions. Parallel lines of receivers in the x_1 direction would record identical 2D data. In that case, the wavefield would be a solution of the 2D wave equation.

The reader may question the need for such a result, considering that we have argued that a single line of seismic data with a point source corresponds to what we have called 2.5D models. Nevertheless, we have a need

[9]See Appendix C for discussion of the choice of L.

for such modeling and inversion formulas for testing purposes. Because of the difficulty of modeling 2.5D or 3D data with finite-difference techniques, for example, 2D models are often used to generate test data sets. We will see in the following exercises that 2D data have special characteristics that are reflected in the structure of the corresponding 2D inversion formulas.

Exercises

3.14 This first set of exercises outlines the formulation of the 2D inverse problem, following the general perturbation method that we have used so far in the text.

a. Explain why the perturbation process of this chapter used for forward modeling, but specialized to zero offset and two dimensions, leads to the following form of equation (3.2.1):

$$u_S(\xi,\omega) = \omega^2 \int_D \frac{\alpha(\boldsymbol{x})}{c^2(\boldsymbol{x})} u_I(\boldsymbol{x},\xi,\omega) g(\boldsymbol{x},\xi,\omega) d^2x. \tag{3.6.26}$$

Here, $\boldsymbol{x} = (x_1, x_3)$ and there is only one spatial coordinate describing the common source-receiver point at $(\xi, 0)$, on the line at $z = 0$. The function u_I is the response to an impulsive source at $(\xi, 0)$ and g is the Green's function, evaluated at this same point, as it is also the observation point.

b. Neglect the issue of source signature for the moment and explain why, when $c = c_0 = \text{constant}$, we should use the function

$$u_I(\boldsymbol{x},\xi,\omega) = g(\boldsymbol{x},\xi,\omega) = \frac{i \operatorname{sgn}(\omega)}{4} H_1^{(0)}(\omega\rho/c_0), \qquad \rho = \sqrt{(x-\xi)^2 + z^2} \tag{3.6.27}$$

for both u_I and g. Here, $H_1^{(0)}$, is the Hankel function of the first kind and zero order, or, equivalently, the Bessel function of the *third* kind and zero order. For $\omega < 0$, the correct solution is the complex conjugate of the solution for $\omega > 0$; hence the multiplier of $i \operatorname{sgn}(\omega)$, rather than i, usually given in references.

c. With experience from the discussion of this chapter, explain why we need not use these exact solutions, but can use instead their asymptotic expansions. Find the asymptotic expansion of the Hankel function in an appropriate reference (such as Abramowitz and Stegun [1972]) and show that

$$u_I(\boldsymbol{x},\xi,\omega) = g(\boldsymbol{x},\xi,\omega) \sim \frac{e^{i\omega\rho/c_0 + i\pi/4 \operatorname{sgn}(\omega)}}{2\sqrt{2\pi|\omega|\rho/c_0}}. \tag{3.6.28}$$

d. Show that, when these asymptotic expansions are substituted into (3.6.26), the following asymptotic integral equation is obtained:

$$u_S(\xi,\omega) = \frac{i\omega}{8\pi c_0}\int_{z>0} \alpha(\boldsymbol{x})\frac{e^{2i\omega\rho/c_0}}{\rho}d^2x. \tag{3.6.29}$$

Hint:

In deriving this result, use the fact that

$$\omega^2\left[\frac{e^{i\pi/4\,\mathrm{sgn}\,(\omega)}}{\sqrt{|\omega|}}\right]^2 = \omega^2\frac{e^{i\pi/2\,\mathrm{sgn}\,(\omega)}}{|\omega|}$$
$$= \frac{i\,\mathrm{sgn}\,(\omega)|\omega|^2}{|\omega|} = i\,\mathrm{sgn}\,(\omega)|\omega| = i\omega.$$

3.15 Equation (3.6.29) is the basic 2D integral equation to be inverted by Fourier transform techniques. This is what we proceed to do in the next exercise.

a. Introduce the Fourier transform in ξ:

$$\hat{u}_S(k_1,\omega) = \int_{-\infty}^{\infty} u_S(\xi,\omega)e^{-2ik_1\xi}d\xi. \tag{3.6.30}$$

This spatial Fourier transform is to be applied to (3.6.29). Observe that this equation has the form of a convolution in the transverse variable of integration; hence, its transform is the product of the transforms of the two functions being convolved. For one of those, derive the result

$$\int_{-\infty}^{\infty}\frac{e^{2i\omega r/c_0-2ik_1x}}{4\pi r}\,dx = \frac{i\,\mathrm{sgn}\,(\omega)}{4}H_1^{(0)}(2k_3|z|)$$
$$\sim \frac{e^{2ik_3|z|+i\pi/4\,\mathrm{sgn}\,(k_3)}}{4\sqrt{\pi|k_3z|}}. \tag{3.6.31}$$

In this equation,

$$r = \sqrt{x^2+z^2}$$

and

$$k_3 = \begin{cases} \mathrm{sgn}\,(\omega)\sqrt{\omega^2/c_0^2-k_1^2}, & \dfrac{\omega^2}{c_0^2} > k_1^2, \\ i\sqrt{k_1^2-\omega^2/c_0^2}, & \dfrac{\omega^2}{c_0^2} < k_1^2. \end{cases} \tag{3.6.32}$$

Hint:

To derive the result in the first line in (3.6.31), note that this is just the Fourier transform of the 3D Green's function, but with a second spatial argument, z^2, rather than $y^2 + z^2$. No matterr; the result is still the 2D Green's function, but of this modified argument. Take some care in recognizing that the transform variable is $2k_1$, rather than simply, k_1. This accounts for the extra factor of 2 in the argument of the Hankel function. The second line is just the asymptotic expansion (3.6.28), modified to take account of the new variables here.

b. Show that the transform of (3.6.29) now becomes

$$\hat{u}_S(k_1,\omega) = \frac{i\omega e^{\pi/4\,\mathrm{sgn}\,(\omega)}}{8c_0\sqrt{\pi|k_3|}}\int_{-\infty}^{\infty}\frac{\hat{\alpha}(k_1,z)}{\sqrt{|z|}}e^{2ik_3|z|}dz. \tag{3.6.33}$$

c. Compare this equation with (3.3.8). Show that the solution is

$$\frac{\hat{\alpha}(k_1,z)}{\sqrt{|z|}} = \frac{8c_0}{\sqrt{\pi}}\int_{-\infty}^{\infty}dk_3\frac{\hat{u}_S(k_1,\omega)\sqrt{|k_3|}}{i\omega(\boldsymbol{k})}e^{-2ik_3z-i\pi/4\,\mathrm{sgn}\,(k_3)}. \tag{3.6.34}$$

In this equation,

$$\omega(\boldsymbol{k}) = \mathrm{sgn}\,(k_3)c_0\sqrt{k_1^2+k_3^2}. \tag{3.6.35}$$

d. Invert back to a function of $\boldsymbol{x}$ to obtain

$$\begin{aligned}\alpha(\boldsymbol{x}) &= \frac{8c_0}{\pi}\sqrt{\frac{z}{\pi}}\int_{-\infty}^{\infty}dk_3\int_{-\infty}^{\infty}dk_1\frac{\hat{u}_S(k_1,\omega)\sqrt{|k_3|}}{i\omega(\boldsymbol{k})}e^{2\,[ik_1x-ik_3z]-i\pi/4\,\mathrm{sgn}\,(k_3)}\\ &= \frac{8c_0}{\pi}\sqrt{\frac{z}{\pi}}\int_{-\infty}^{\infty}dk_3\int_{-\infty}^{\infty}dk_1 \qquad (3.6.36)\\ &\quad\cdot\int_{-\infty}^{\infty}d\xi\frac{u_S(\xi,\omega)\sqrt{|k_3|}}{i\omega(\boldsymbol{k})}e^{2\,[ik_1(x-\xi)-ik_3z]-i\pi/4\,\mathrm{sgn}\,(k_3)}.\end{aligned}$$

Remark 3.1. At this point, we have a 2D solution, $\alpha(\boldsymbol{x})$. This result should be compared with our earlier solution in 3D, (3.3.11).

e. Use (3.6.32) to replace the integration in k_3 with an integral with respect to ω. In doing so, use

$$dk_3 = \frac{dk_3}{d\omega}d\omega = \frac{\omega}{c_0^2k_3}d\omega.$$

Show that

$$\alpha(\boldsymbol{x}) = \frac{8}{\pi c_0}\sqrt{\frac{z}{\pi}}\int_{-\infty}^{\infty} d\omega \int_{-\infty}^{\infty} dk_1 \qquad (3.6.37)$$
$$\cdot \int_{-\infty}^{\infty} d\xi \frac{u_S(\xi,\omega)\sqrt{|k_3|}}{ik_3} e^{2\,[ik_1(x-\xi)-ik_3 z]-i\pi/4\,\mathrm{sgn}\,(\omega)}.$$

3.16 Now, transform this solution to process data for the *reflectivity function, β*, in 2D as we did in 3D and 2.5D in this chapter rather than for the perturbation, α.

a. Follow the earlier discussion in Chapter 3, to transform any of these inversion formulas for α to an inversion for β, by introducing the factor $i\omega/2c_0$ into the operators for α. In particular, apply this modification to the formulas in (3.6.36), to obtain "true amplitude" 2D versions of Stolt's Fourier-type migration. Show that

$$\beta(\boldsymbol{x}) = \frac{4}{\pi}\sqrt{\frac{z}{\pi}}\int_{-\infty}^{\infty} dk_3$$
$$\cdot \int_{-\infty}^{\infty} dk_1 \hat{u}_S(k_1,\omega)\sqrt{|k_3|}e^{2\,[ik_1 x-ik_3 z]-i\pi/4\,\mathrm{sgn}\,(k_3)}$$
$$= \frac{4}{\pi}\sqrt{\frac{z}{\pi}}\int_{-\infty}^{\infty} dk_3 \int_{-\infty}^{\infty} dk_1 \qquad (3.6.38)$$
$$\cdot \int_{-\infty}^{\infty} d\xi u_S(\xi,\omega)\sqrt{|k_3|}e^{2\,[ik_1(x-\xi)-ik_3 z]-i\pi/4\,\mathrm{sgn}\,(k_3)}.$$

b. Now, use this result to derive a Kirchhoff-type inversion formula by applying the method of stationary phase in k_1 to either of these last results. Define the phase

$$\Phi = 2[k_1(x-\xi) - k_3 z], \qquad (3.6.39)$$

and calculate the derivatives with respect to k_1, using the upper equation in (3.6.32).

c. Verify that

$$\frac{\partial\Phi}{\partial k_1} = 2\left[x-\xi+\frac{k_1}{k_3}z\right], \qquad \frac{\partial^2\Phi}{\partial k_1^2} = 2\left[\frac{1}{k_3}+\frac{k_1^2}{k_3^3}\right]z = \frac{2\omega^2 z}{c_0^2 k_3^3}, \qquad (3.6.40)$$

and show that setting the first derivative equal to zero leads to the solution

$$k_1 = -\frac{x-\xi}{\rho}\cdot\frac{\omega}{c_o}, \quad \rightarrow \quad k_3 = \frac{z}{\rho}\cdot\frac{\omega}{c_o}, \quad \rho = \sqrt{(x-\xi)^2+z^2}. \qquad (3.6.41)$$

d. Now show that at the stationary point,

$$\Phi = -2\omega\rho/c_0, \quad \frac{\partial^2\Phi}{\partial k_1^2} = \frac{2c_0\rho^3}{\omega z^2}, \quad \text{sgn}\left[\frac{\partial^2\Phi}{\partial k_1^2}\right] = \text{sgn}\,(\omega).$$

e. With these values, show that the result of applying stationary phase in k_1 in (3.6.38) is β. Note that we must premultiply the integrand by $i\omega/2c_0$:

$$\beta(\boldsymbol{x}) = \frac{4z}{\pi c_0^2}\int_{-\infty}^{\infty}\frac{d\xi}{\rho}\int_{-\infty}^{\infty}|\omega|d\omega u_S(\xi,\omega)e^{-2i\omega\rho/c_o}. \tag{3.6.42}$$

This result should be compared to the 2.5D result, (3.6.16), where the frequency-domain filter is $i\omega$. That is, the frequency-domain filter for inversion of 2D data differs from the filter for 2.5D data. Recall that the input data to 2.5D inversion are really 3D data, whereas the data here are 2D. There really are true 2D inversion problems for which this is the correct filter and inversion formula. Furthermore, it is much easier to generate 2D data than 3D data numerically. If these data are generated in the time domain; then their Fourier transform to the frequency domain will naturally include the frequency-domain factors shown in (3.6.28), whereas 3D data have no such frequency-domain multipliers.

Remark 3.2. Now that we have a "new" type of frequency domain filter for 2D data, we test it on a simple problem to see how it interacts with the frequency dependence of the input data.

3.17 As a final check, consider the simplest example of model data, reflection from a horizontal line at depth L:

$$u_S(\xi,\omega) = R\frac{e^{2i\omega L/c_0 + i\pi/4\,\text{sgn}\,(\omega)}}{4\sqrt{\pi|\omega|L/c_0}}. \tag{3.6.43}$$

Substitute this result into the lower equation in (3.6.38). Note that, for these data, the ξ-dependence of the integrand is totally in the phase, and

$$\frac{1}{\pi}\int_{-\infty}^{\infty}d\xi e^{-2ik_1\xi} = \delta(k_1).$$

Thus, carry out the two integrals in ξ and k_1 to obtain

$$\beta(\boldsymbol{x}) = \frac{R}{\pi}\sqrt{\frac{z}{L}}\int_{-\infty}^{\infty}dk_3 e^{2ik_3[L-z]} = R\sqrt{\frac{z}{L}}\delta(z-L) = R\delta(z-L). \tag{3.6.44}$$

Recall, this is the *most singular part* of the inversion output or the leading-order output at high frequency. The output is the normal-incidence reflection coefficient multiplied by the singular function of the reflection surface. This is the result predicted by the theory, and further confirms this result.

3.18 Now, proceed to verify that the same output arises when the data (3.6.43) are substituted into the Kirchhoff inversion formula, (3.6.42). First, show that the substitution leads to the equation

$$\beta(\boldsymbol{x}) = \frac{z}{\pi c_0^2} \frac{R}{\sqrt{\pi L/c_0}} \cdot \int_{-\infty}^{\infty} \frac{d\xi}{\rho} \int_{-\infty}^{\infty} \sqrt{|\omega|} d\omega e^{2i\omega(L-\rho)/c_o + i\pi/4 \operatorname{sgn}(\omega)}. \tag{3.6.45}$$

3.19 Apply the stationarity contition in ξ to the phase,

$$\Psi = -\rho, \tag{3.6.46}$$

to obtain,

$$\beta(\boldsymbol{x}) = \frac{R}{\pi c_0} \sqrt{\frac{z}{L}} \int_{-\infty}^{\infty} d\omega e^{2i\omega[L-z]/c_0} = R\sqrt{\frac{z}{L}} \delta(z-L) = R\delta(z-L). \tag{3.6.47}$$

That is, obtain the same result as in (3.6.44).

3.7 Testing the Inversion Formula with Kirchhoff Data

In the previous section, a suite of inversion formulas was derived by applying high-frequency asymptotics to a corresponding suite of Fourier inversion formulas. Those formulas were, in turn based on a Born-approximate model for the forward scattering problem. Here, the results of the previous section will be checked by applying them to *Kirchhoff-approximate* data for a single reflector. We will assume the correct wavespeed for the background above the reflector in question. We make no restrictions on the reflection strength of the reflector to be imaged, however. The result will be shown to be linear in the normal-incidence reflection coefficient, which in turn, is a nonlinear function of the change in propagation speed across the unknown reflector.

In this way, the inversion formula will be shown to perform beyond the constraints imposed by the Born approximation on which it is based. That is, while we still require that the error or perturbation in the velocity be small above the reflector in question (taken to be zero in the test problem), we obtain a result that is meaningful for any size jump in reflection strength at the reflector of interest.

3.7.1 The Kirchhoff Approximation

We introduce the Kirchhoff approximation, developed in Appendix E, to represent the upward scattered data from a single reflector, S. Here, we will use the constant-density, zero-offset version of equation (E.8.17). In

this case, $\boldsymbol{x}_g = \boldsymbol{x}_s$ and we use only the latter in this discussion. Then the Kirchhoff-approximate, upward-scattered wavefield is given by

$$u_S(\boldsymbol{x}_s, \omega) = 2i\omega \int_S dS\, R u_I(\boldsymbol{x}_0, \boldsymbol{x}_s, \omega) \tau_{sn} g(\boldsymbol{x}_s, \boldsymbol{x}_0, \omega), \tag{3.7.1}$$

where u_I and g are given by their WKBJ approximations,

$$\begin{aligned} g(\boldsymbol{x}_s, \boldsymbol{x}_0, \omega) &= A(\boldsymbol{x}_0, \boldsymbol{x}_s) e^{i\omega\tau_s(\boldsymbol{x}_s, \boldsymbol{x}_0)}, \\ u_I(\boldsymbol{x}_0, \boldsymbol{x}_s, \omega) &= F(\omega) g(\boldsymbol{x}_s, \boldsymbol{x}_0, \omega), \end{aligned} \tag{3.7.2}$$

with τ_s being the traveltime function in the heterogeneous medium, and A being the corresponding WKBJ amplitude. The τ_s is a solution of the *eikonal equation* and A is a solution of the *transport equation* of geometrical optics as developed in Appendix E. Moreover,

$$\tau_{sn} = \hat{\boldsymbol{n}} \cdot \nabla \tau_s, \tag{3.7.3}$$

with $\hat{\boldsymbol{n}}$ being the upward unit normal vector to the surface, S. We also introduce the normal derivative of the *transmitted phase* on S, defined by

$$\tau_{tn} \equiv \operatorname{sgn}(\tau_{sn}) \left[\tau_{sn}^2 + \frac{1}{c_1^2} - \frac{1}{c_0^2} \right]^{1/2}. \tag{3.7.4}$$

Here c_0 and c_1 denote the wavespeeds above and below S, respectively. With this notation, we can conveniently define the geometrical-optics reflection coefficient, R, in (3.7.1) by the expression

$$R = \frac{\tau_{sn} - \tau_{tn}}{\tau_{sn} + \tau_{tn}}. \tag{3.7.5}$$

The surface S is described in terms of two parameters, $(\sigma_1, \sigma_2) \equiv \boldsymbol{\sigma}$, with $\boldsymbol{x}_0 = \boldsymbol{x}_0(\boldsymbol{\sigma})$. (We reserve the variable, $\boldsymbol{x}$, as the output variable in this discussion.)

For the inverse problem in this chapter, only the case of zero-offset (backscatter) modeling in a homogeneous medium is of interest. In this case,

$$\begin{gathered} \boldsymbol{x}_s = \boldsymbol{\xi} = (\xi_1, \xi_2, 0), \qquad A(\boldsymbol{x}_s, \boldsymbol{x}_0) = 1/4\pi r_0, \qquad \tau_s(\boldsymbol{x}_s, \boldsymbol{x}_0) = r_0/c_0 \\ r_0 = |\boldsymbol{x}_0 - \boldsymbol{\xi}| = \sqrt{(x_{10} - \xi_1)^2 + (x_{20} - \xi_2)^2 + x_{30}^2}, \end{gathered} \tag{3.7.6}$$

and (3.7.1) simplifies to

$$u_S(\boldsymbol{\xi}, \omega) = \int_S \frac{i\omega F(\omega)}{8\pi^2 c_0} R \frac{\hat{\boldsymbol{n}} \cdot \hat{\boldsymbol{r}}_0}{r_0^2} e^{2i\omega r_0/c_0} dS, \tag{3.7.7}$$

with,

$$\hat{\boldsymbol{r}}_0 = \frac{(\boldsymbol{x}_0 - \boldsymbol{\xi})}{r_0}, \quad R = \frac{|\hat{\boldsymbol{n}} \cdot \hat{\boldsymbol{r}}_0|/c_0 - \sqrt{c_1^{-2} - c_0^{-2} + c_0^{-2}(\hat{\boldsymbol{n}} \cdot \hat{\boldsymbol{r}}_0)^2}}{|\hat{\boldsymbol{n}} \cdot \hat{\boldsymbol{r}}_0|/c_0 + \sqrt{c_1^{-2} - c_0^{-2} + c_0^{-2}(\hat{\boldsymbol{n}} \cdot \hat{\boldsymbol{r}}_0)^2}}. \tag{3.7.8}$$

3.7.2 *Asymptotic Inversion of Kirchhoff Data*

The asymptotic inversion formula, (3.6.16), is to be applied to the Kirchhoff data, (3.7.7). In the latter equation, the temporal integral is just the Fourier transform of the observed data, given by (3.7.7). Thus, applying the inversion formula to the data leads to the multifold integral

$$\beta(\boldsymbol{x}) = -\frac{x_3}{\pi^3 c_0^3}\int_\Omega \omega^2 F(\omega)d\omega \int_\Sigma \frac{d^2\xi}{r}\int_S \sqrt{g}\, d^2\sigma \frac{\hat{\boldsymbol{n}}\cdot\hat{\boldsymbol{r}}_0}{r_0^2} Re^{2i\omega(r_0-r)/c_0}. \tag{3.7.9}$$

In this equation, we have introduced the determinant of the first fundamental metric tensor of differential geometry,

$$g \equiv \left|\frac{\partial \boldsymbol{x}_0}{\partial\sigma_1}\times\frac{\partial \boldsymbol{x}_0}{\partial\sigma_2}\right|^2 = \left|\det\left[\frac{\partial \boldsymbol{x}_0}{\partial\sigma_j}\cdot\frac{\partial \boldsymbol{x}_0}{\partial\sigma_k}\right]\right|, \quad j,k=1,2, \tag{3.7.10}$$

to express the surface integral over S in terms of the parametric variables, $\boldsymbol{\sigma}$, describing S. (See Kreyszig [1991], for information on differential geometry.)

The integral (3.7.9) has been written in a form suggestive of the analysis to be carried out. This analysis will be an asymptotic expansion by multidimensional stationary phase in the four variables, $\boldsymbol{\xi}$ and $\boldsymbol{\sigma}$. The phase function is

$$\Phi(\boldsymbol{\xi},\boldsymbol{\sigma}) = r_0 - r, \tag{3.7.11}$$

with first derivatives

$$\frac{\partial\Phi}{\partial\xi_i} = \frac{\xi_i - x_{i0}}{r_0} - \frac{\xi_i - x_i}{r}, \quad \frac{\partial\Phi}{\partial\sigma_i} = \frac{\boldsymbol{x}_0 - \boldsymbol{\xi}}{r_0}\cdot\frac{\partial \boldsymbol{x}_0}{\partial\sigma_i}, \quad i=1,2. \tag{3.7.12}$$

Stationary points in $\boldsymbol{\xi}$ and $\boldsymbol{\sigma}$ are determined by setting these first derivatives equal to zero. Setting $\partial\Phi/\partial\sigma_i$ equal to zero leads to the condition that the unit vector, $(\boldsymbol{x}_0-\boldsymbol{\xi})/r_0$, is orthogonal to two linearly independent tangent vectors in the surface S, meaning that $(\boldsymbol{x}_0-\boldsymbol{\xi})/r_0$ is *normal* to S. Because $\hat{\boldsymbol{n}}$ is an upward normal to S and $(\boldsymbol{x}_0-\boldsymbol{\xi})/r_0$ points downward at S, we conclude that at the stationary point,

$$\hat{\boldsymbol{r}}_0 = (\boldsymbol{x}_0-\boldsymbol{\xi})/r_0 = -\hat{\boldsymbol{n}}. \tag{3.7.13}$$

It follows from this result and the definition of R in (3.7.8) that

$$R = R_n = \frac{c_1 - c_0}{c_1 + c_0}. \tag{3.7.14}$$

Now consider the ξ-derivatives in (3.7.12). The result of setting these derivatives equal to zero implies that two components of two unit vectors must be equal. Magnitudes of the third components are fixed because these are unit vectors. Therefore, these third components could, at most, differ in sign. However, the third components, x_3/r_0 and x_3/r, have the same sign. Hence, these two unit vectors must be equal:

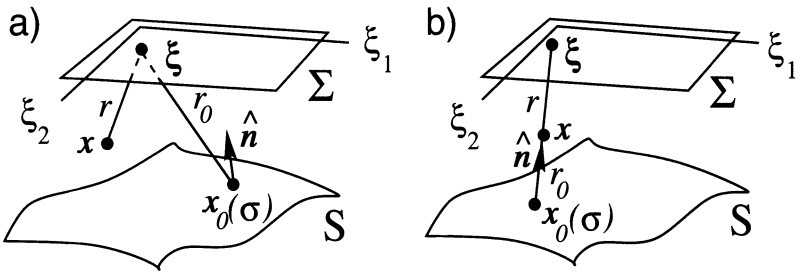

FIGURE 3.5. a) General geometry of the imaging problem. b) Geometry for values of $\boldsymbol{x}$ near the stationary point.

$$(\boldsymbol{x} - \boldsymbol{\xi})/r = \hat{\boldsymbol{r}} = \hat{\boldsymbol{r}}_0. \tag{3.7.15}$$

(see Figure 3.5).

With this information, we can now prescribe a geometrical solution to the condition that the phase be stationary. Given an output point $\boldsymbol{x}$, drop perpendiculars from $\boldsymbol{x}$ to the surface S. Each such perpendicular defines a possible value of $\boldsymbol{\sigma}$ at a stationary point. Extend each normal up to the data surface, $\boldsymbol{\xi}$. For each $\boldsymbol{\xi}$ in the aperture Σ, the pair $\boldsymbol{\xi}, \boldsymbol{\sigma}$ is a stationary point of the fourfold integral (3.7.9). For $\boldsymbol{x}$ "close enough" to S, there will be only one perpendicular from $\boldsymbol{x}$ to S. We continue under the assumption that $\boldsymbol{x}$ is at least this close to the surface. Furthermore, we assume that points at which there are more than one normal to S are at a distance L satisfying our *high-frequency assumption* (3.4.2). This is equivalent to imposing the requirement that the *principal radii of curvature* of S satisfy (3.4.2). Another way of saying this is that we require that there will be no focusing of rays near the recording surface. We further assume that there is a $\boldsymbol{\xi}$ in Σ along the continuation of the surface normal through $\boldsymbol{x}$; that is, we continue under the assumption that there is only one stationary point for the integral (3.7.9).

Because the vectors $\boldsymbol{x}_0 - \boldsymbol{\xi}$ and $\boldsymbol{x} - \boldsymbol{\xi}$ are collinear, the difference of distances defining Φ in (3.7.11) reduces to distance along the normal through $\boldsymbol{x}$. That is,

$$\Phi = r_0 - r = s, \tag{3.7.16}$$

with $s > 0$ when $\boldsymbol{x}$ is above S and $s < 0$ when $\boldsymbol{x}$ is below S, measuring signed distance from S along the normal.

To complete the stationary phase calculation it is necessary to compute the determinant and signature of the matrix of second derivatives,

$$[\Phi_{ij}] = \begin{bmatrix} \dfrac{\partial^2 \Phi}{\partial \xi_i \partial \xi_j} & \dfrac{\partial^2 \Phi}{\partial \xi_i \partial \sigma_j} \\ \dfrac{\partial^2 \Phi}{\partial \sigma_i \partial \xi_j} & \dfrac{\partial^2 \Phi}{\partial \sigma_i \partial \sigma_j} \end{bmatrix}. \tag{3.7.17}$$

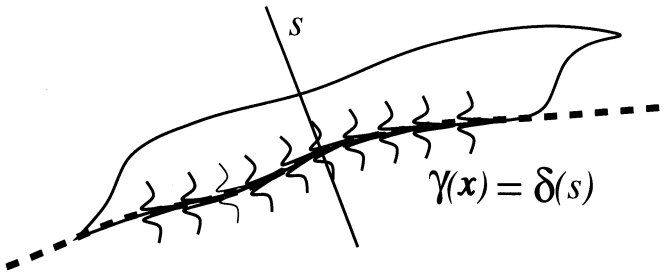

FIGURE 3.6. Cartoon showing the singular function $\gamma(\boldsymbol{x})$ of a reflector surface (viewed edge-on) represented as the bandlimited delta function $\delta_B(s)$, where s is the coordinate normal to the surface.

We defer discussion of this matrix for the present. It will by shown below that for $\boldsymbol{x}$ sufficiently near to S, $\text{sig}\,(\Phi_{ij}) = 0$; the determinant will be denoted by D:

$$D \equiv |\det[\Phi_{ij}]|\,. \tag{3.7.18}$$

The results, (3.7.13), (3.7.14), (3.7.16), and (3.7.18), are used in the stationary phase formul (3.6.3) to evaluate the integral, (3.7.9). The result is

$$\beta(\boldsymbol{x}) = R_n \frac{x_3\sqrt{g}}{rr_0^2\sqrt{D}} \frac{1}{\pi c_0} \int_\Omega d\omega\, F(\omega) e^{2i\omega s/c_0} = R_n \frac{x_3\sqrt{g}}{rr_0^2\sqrt{D}} \delta_B(s). \tag{3.7.19}$$

All variables here are to be evaluated at the stationary point. In the last equality, we have replaced the integral, with proper scale, by the now familiar bandlimited delta function, now of argument equal to the signed normal distance to the reflector. A graph of this function for all $\boldsymbol{x}$ will partially image the reflector because the bandlimited delta function peaks on the reflector surface ($s = 0$). The image is only partial because we obtain this result only when the conditions of stationarity are satisfied. These, in turn, require that there be a normally incident or specular ray from some point on Σ to a point on S. Thus, we can only "see" a point on the reflector surface if we can trace a specularly reflected ray from the source-receiver point to that point on the reflector.

As mentioned earlier, this delta function with support on the surface is called the *singular function* of the surface. We see in the above result that the output $\beta(\boldsymbol{x})$ is the bandlimited singular function scaled by another function of $\boldsymbol{x}$. One factor in this multiplier is the normal-incidence reflection coefficient. The remaining factor is of little interest to us—as long as it is "slowly varying" with respect to two length scales of the problem. The first of these scales is the characteristic wavelength; here we *want* equation (3.4.3) to be violated in the sense that $\lambda << \pi$. The second scale is the width of the main lobe of the singular function; we do *not* want the multiplier to vary significantly over the main lobe, which would diminish or destroy our ability to identify the peak of the delta function. Thus, instead

of computing D everywhere, we be satisfied by computing its value only at $s = 0$, which occurs when $\boldsymbol{x}$ is on S and, consequently, $\boldsymbol{x} = \boldsymbol{x}_0$ at the stationary point.

To compute D, defined by (3.7.17) and (3.7.18), we begin with the result

$$\frac{\partial^2 \Phi}{\partial \xi_i \partial \xi_j} = \frac{\delta_{ij}}{r_0} - \frac{(\xi_i - x_{i0})(\xi_j - x_{j0})}{r_0^3} - \frac{\delta_{ij}}{r} + \frac{(\xi_i - x_i)(\xi_j - x_j)}{r^3}, \tag{3.7.20}$$

$$\text{with } i, j = 1, 2.$$

Here the δ_{ij} is the Kronecker delta symbol, equal to unity when $i = j$ and equal to zero when $i \neq j$. When $\boldsymbol{x} = \boldsymbol{x}_0$, the sum of the four elements here is equal to zero. Consequently, when computing the determinant in (3.7.17), the upper left two-by-two corner is a zero submatrix and

$$D = \left[\det \left[\frac{\partial^2 \Phi}{\partial \sigma_i \partial \xi_j} \right] \right]^2. \tag{3.7.21}$$

The second derivatives here are calculated from the first derivatives in (3.7.12):

$$\frac{\partial^2 \Phi}{\partial \sigma_i \partial \xi_j} = -\frac{\partial \boldsymbol{x}_0}{\partial \sigma_i} \cdot \frac{\hat{\boldsymbol{e}}_j}{r_0}, \tag{3.7.22}$$

$$i, j = 1, 2, \qquad \hat{\boldsymbol{e}}_1 = (1, 0, 0), \quad \hat{\boldsymbol{e}}_2 = (0, 1, 0).$$

Since D is a perfect square, we know that the four eigenvalues must occur in pairs of the same sign. Thus, $\operatorname{sig}(\Phi_{ij}) = \pm 4$ or 0. The first two choices lead to a multiplier of -1 on the result, (3.7.19); the last choice leaves the sign unchanged. Furthermore, the determinant of these four elements is now seen to be the third component of the cross product of the vectors $\partial \boldsymbol{x}_0 / \partial \sigma_1$ and $\partial \boldsymbol{x}_0 / \partial \sigma_2$, multiplied by $1/r_0^2$. That third component can easily be computed by calculating the complete cross product and taking its projection on the vertical. The magnitude of this vector is just $\sqrt{g}$ defined in (3.7.10). The direction of this vector is $\boldsymbol{n}$, with the sign being unimportant as we need only the absolute value of the determinant. Thus, projection onto the vertical is achieved by multiplying the magnitude by the third component of the normal, x_3/r. Therefore, for $\boldsymbol{x}$ on S,

$$\det \left[\frac{\partial^2 \Phi}{\partial \sigma_i \partial \xi_j} \right] = \frac{x_3 \sqrt{g}}{r_0^2 r}, \quad D = \frac{g x_3^2}{r_0^4 r^2}. \tag{3.7.23}$$

We are now prepared to evaluate β at its peak value, that is, for $\boldsymbol{x}$ on S, (see Figure 3.6). We use (3.7.23) and the fact that $r = r_0$ at the peak to obtain

$$\beta_{\text{PEAK}} = R_n \delta_B(0). \tag{3.7.24}$$

That is, for this single reflector model, the reflectivity function has now been confirmed to be asymptotically equal to the singular function of the reflecting surface multiplied by a slowly varying function of $\boldsymbol{x}$. That slowly varying function reduces to the normal-incidence reflection coefficient when $\boldsymbol{x}$ is on S. Thus, the output provides an image of the reflector, while the peak amplitude provides an estimate of the normal-incidence reflection coefficient. In a perfect world, this reflection coefficient could be used to estimate the propagation speed below the reflector in terms of the propagation speed above the reflector.

It remains only to show that the signature of the matrix of second derivatives is equal to zero. Here, again, we limit ourselves initially to the case when $\boldsymbol{x}$ is on S. Note, first, that the determinant, D is nonzero no matter what the values in the lower left-hand corner of the matrix in (3.7.17) are. Therefore, the eigenvalues cannot pass through zero as a function of the values of this submatrix. To determine the signature, then, we might as well consider a case in which this submatrix is particularly simple. This would be the case for a flat reflector. For such a reflector, a reasonable parameterization would be $x_{10} = \sigma_1$, $x_{20} = \sigma_2$, and $x_3 = \text{const.}$, in which case the upper right-hand and lower left-hand two-by-two submatrices in (3.7.17) reduce to diagonal matrices with elements $-1/r_0$, while the lower right two-by-two is a diagonal matrix with elements $1/r_0$. It is then easy to show that the matrix Φ_{ij} has two positive eigenvalues equal to $1/r_0$ and two negative eigenvalues equal to $-1/r_0$. In this case, $\text{sig}\,(\Phi_{ij}) = 0$, as claimed. Because we have explained above why the same result must hold for arbitrary surfaces, we conclude that the signature is zero for $\boldsymbol{x}$ on S for any reflector. We argue, by continuity, that the same must be true in some neighborhood of S. The extent of that neighborhood depends on the curvature of S and on the value of the determinant for $\boldsymbol{x}$ not on S.

This is as far is we will be able to go in subsequent chapters where we consider the corresponding Hessian matrix in variable background for more general source-receiver configurations. In preparation for that, the argument here has been presented as it will be in those later discussions. However, for this relatively simple case, it is possible to carry out the calculation of the determinant D in (3.7.18) and obtain a meaningful result in closed form. The key to doing this calculation with minimal effort is to expand the determinant in two-by-two subdeterminants of the first two rows and their corresponding (two-by-two) minors. Significant reduction in the calculation occurs when one realizes that the determinants of the first two rows are all elements of the cross products of the two surface tangents and the normal with one another. This can be confirmed by expressing the results (3.7.20) and (3.7.21) in terms of these two tangents and normal. Because only first and second components of these vectors appear in the determinant, the subdeterminants are all expressible in terms of the third component of one of the tangents or of the normal vector. After some computation, we find that

$$D = g\frac{x_3^2}{r^4 r_0^2}[1 - s\kappa_1][1 - s\kappa_2]. \tag{3.7.25}$$

In this equation, s is the signed normal distance to the reflector defined by (3.7.16); κ_1 and κ_2 are the signed *principal radii of curvature* at the stationary point. The sign is positive when the reflector is concave-up for the principal curvature in question and negative when the reflector is concave-down for the principal curvature in question. Note that $D = 0$ when $s\kappa_j = 1$, $j = 1, 2$. That is, $D = 0$ at the *center of curvature* associated with one or the other principal curvatures of the reflector. Thus, in order for the asymptotic solution, (3.7.19), to be valid near the reflector, it is necessary that the radii of curvature each satisfy the length scales for which our asymptotic criterion, (3.4.2), is valid for the bandwidth of the observed data.

When (3.7.25) is used in (3.7.19), we obtain the result

$$\beta(\boldsymbol{x}) = \frac{R_n \delta_B(s)}{\sqrt{[1 - s\kappa_1][1 - s\kappa_2].}} \tag{3.7.26}$$

The final result, in the form (3.7.26) or in the form (3.7.19), (3.7.24), confirms the validity of the asymptotic inversion for a single reflector as a leading-order asymptotic result, subject to the existence of the stationary point in the four variables, $\boldsymbol{\xi}, \boldsymbol{\sigma}$. The denominator in this final expression is zero at either of the two centers of principal curvature of the reflector with respect to the stationary point. The ensemble of centers of curvature from every point on S forms two surfaces called the surfaces of centers of S.

The asymptotic expansion, whose leading order term is the right-hand side of equation (3.7.26), breaks down on this surface of centers. By assuming that both of the radii of curvature satisfy the asymptotic criterion (3.4.2), which is the large parameter of the asymptotic expansion, we guarantee that this failure occurs sufficiently far from the recording surface so that (3.7.26) is always valid. It is important to note that near the surfaces of centers, an alternative asymptotic representation exists, called a *uniform asymptotic expansion*; in this case, "uniform" means that the expansion remains valid through a transition region where one of the eigenvalues of the matrix of second derivatives passes through zero. While a discussion of uniform asymptotics is beyond the scope of this text (see Bleistein and Handelsman [1986] for further information), we mention this so that the reader can be aware that stationary phase is not the whole story of the asymptotic expansions of integrals.

In this alternate asymptotic representation, the resulting expansion is not infinite, as suggested by the failure of (3.7.26), but it is larger, typically by a one-sixth power of the large parameter, λ, defined by (3.4.2). This increase in size is due to an increase in the order of stationarity of the phase functions, defined by the number of vanishing derivatives at the

stationary point. Typically, this order increases by 1 on the surfaces of centers. Note that even for $\Lambda = 64 \gg \pi$, the sixth root is only equal to 2. Thus, the asymptotic expansion grows approximately by a factor of 2 from the increasing order of stationarity.

On the other hand, the last integral in ω decays with s, and its decay, by the assumption that the radii of curvature satisfy (3.4.2), is sufficient to compensate for this doubling. That is, the total result remains small on the surfaces of curvature and does not interfere with the imaging predicted by (3.7.26). See Armstrong [1978].

When there is no stationary point in all four variables, the asymptotic contributions are of lower order in ω. Although it is possible to calculate those lower-order results, it is easier to simply demonstrate them with numerical examples.

There will fail to be a stationary point when there is no normal incidence ray from the source-receiver configuration to the scattering surface S; that is, when there is no *specular reflection point* on the surface for any source-receiver point in the region Σ. Thus, this asymptotic inversion images the portion of the reflector for which there are specular returns at the receivers and yields a lower-order contribution when there are none.

Setting $\partial\Phi/\partial\sigma_i = 0$, defines a traveltime $t(\boldsymbol{\xi}) = r_0/c_0$, which is the specular traveltime to the reflector. Then, Φ/c_0 is the difference between the specular traveltime and the two-way traveltime from the source-receiver point to the output point for each $\boldsymbol{\xi}$. Setting the $\partial\Phi/\partial\xi_i$'s equal to zero then determines the envelope of these traveltimes over all values of $\boldsymbol{\xi}$. In particular, $\Phi/c_0 = 0$ determines the reflector as this envelope. In this manner, we see this analysis echoing the discussion of Hagedoorn's graphical migration method discussed in Chapter 1.

The inversion operator is a linear operator on the data. The forward modeling problem is linear in the response to the scattering surfaces, partially as a consequence of neglecting refraction and multiple reflection and transmission through multiple interfaces. Thus, within the range of validity of the linear theory, the method will produce a reflector map of an ensemble of reflectors from observations of the upward-scattered data from those reflectors. In practice, data from multiple reflections will produce (hopefully, weaker) spurious images, while the errors due to refractions will accumulate with depth. Nonetheless, migration/inversion of zero-offset data with a constant background is a first important method of choice for analysis of data, on the way towards more sophisticated migration/inversion methods.

3.7.3 Summary

We have now provided the desired verification of the validity of the inversion procedure. The model data used were Kirchhoff-approximate data for a single reflector, and the background propagation speed used in the test was the correct propagation speed above the reflector. For this test, the imaged

reflector is properly placed and depicted through its bandlimited singular function, and the scaling of the singular function is the normal-incidence geometrical-optics reflection coefficient multiplied by another geometrical factor, which is equal to unity on the reflector. Thus, the peak amplitude of the output provides a means of estimating the propagation speed below the reflector, given the propagation speed above the reflector.

From the analysis, it is apparent that an incorrect background speed in the inversion process will lead to a misplaced (for a planar reflector) and misshapen (for a curved reflector) image, as well as an incorrect value to substitute into the reflection-coefficient output for determination of the propagation speed below the reflector. On the other hand, with correct background, the estimate of the propagation speed below the reflector is not constrained to small perturbations of the speed above, despite the reliance on perturbation theory for the motivating forward model. In that sense, the method has broader validity than its basis in perturbation theory would imply. Indeed, the output is *linear in the reflection coefficient*, which, in turn, is a nonlinear function of the change in propagation speed (and of other medium parameters, when we generalize the forward model).

Exercises

3.20 The purpose of this exercise is to give the reader some practice doing multidimensional stationary phase. The zero-offset Kirchhoff-approximate scattered field due to a point source is given by

$$u_S(\boldsymbol{\xi},\omega) = \int_S \frac{i\omega F(\omega)}{8\pi^2 c_0}\, R \frac{\hat{\boldsymbol{n}}\cdot\hat{\boldsymbol{r}}_0}{r_0^2} e^{2i\omega r_0/c_0}\, dS,$$

with

$$\hat{\boldsymbol{r}}_0 = \frac{(\boldsymbol{x}_0 - \boldsymbol{\xi})}{r_0}, \qquad R = \frac{|\hat{\boldsymbol{n}}\cdot\hat{\boldsymbol{r}}_0|/c_0 - \sqrt{c_1^{-2} - c_0^{-2} + c_0^{-}2(\hat{\boldsymbol{n}}\cdot\hat{\boldsymbol{r}}_0)^2}}{|\hat{\boldsymbol{n}}\cdot\hat{\boldsymbol{r}}_0|/c_0 + \sqrt{c_1^{-2} - c_0^{-2} + c_0^{-2}(\hat{\boldsymbol{n}}\cdot\hat{\boldsymbol{r}}_0)^2}}.$$

The other variables used in this equation are defined in the text.

a. Carry out the two-dimensional stationary phase in the surface parameters, $\boldsymbol{\sigma} = (\sigma_1, \sigma_2)$ introduced in the text. Show that the stationary point(s) are defined as those points on the surface where $\hat{\boldsymbol{r}}_0 = -\hat{\boldsymbol{n}}$ and that

$$\frac{\partial^2\Phi}{\partial\sigma_i\partial\sigma_j} = \frac{1}{r_0}\frac{\partial\boldsymbol{x}}{\partial\sigma_i}\cdot\frac{\partial\boldsymbol{x}}{\partial\sigma_j} - \hat{\boldsymbol{n}}\cdot\frac{\partial^2\boldsymbol{x}}{\partial\sigma_j\partial\sigma_j}, \quad i,j = 1,2.$$

b. To simplify the analysis of the matrix of second derivatives, suppose that σ_1 and σ_2 are locally arclength variables along the directions of principal curvature at the stationary point. In this

case, show that

$$\frac{\partial \boldsymbol{x}}{\partial \sigma_i} \cdot \frac{\partial \boldsymbol{x}}{\partial \sigma_j} = \delta_{ij}, \quad i,j = 1,2,$$

and that

$$\frac{\partial^2 \Phi}{\partial \sigma_1 \partial \sigma_2} = 0, \quad \frac{\partial^2 \Phi}{\partial \sigma_i^2} = \frac{1}{r_0} - \hat{\boldsymbol{n}} \cdot \boldsymbol{\kappa_i}, \quad i = 1,2.$$

In these equations, δ_{ij} is the Kronecker delta, equal to unity when the indices are the same, equal to zero when they are not. Furthermore, the $\boldsymbol{\kappa_i}$'s are the *principal curvatures* of the reflector at the stationary point. We remark that for these variables, $\sqrt{g} = 1$. Also, the final result should be independent of the coordinate system, so the use of an *optimal* coordinate system certainly makes sense.

We leave it as further reading to show that for more general variables, the determinant of the matrix of second derivatives is just the determinant found in this special coordinate system multiplied by g. This latter determinant is exactly what is needed to cancel a corresponding factor in dS when expressed in arbitrary surface coordinates, $\boldsymbol{\sigma}$.

Exercises

3.21 Show, now, that the leading-order contribution from each stationary point is

$$u_S(\boldsymbol{\xi},\omega) \sim -\frac{i\omega F(\omega) R_n}{8\pi r_0 |\omega|} \frac{e^{2i\omega r_0/c_0 + i\pi/4 \operatorname{sgn}(\omega)(\mu_1+\mu_2)}}{\sqrt{|1 - r_0 \hat{\boldsymbol{n}} \cdot \boldsymbol{\kappa}_1||1 - r_0 \hat{\boldsymbol{n}} \cdot \boldsymbol{\kappa}_2|}}.$$

In this equation, R_n is the normal reflection coefficient (3.7.14) and

$$\mu_j = \operatorname{sgn}(1 - r_0 \hat{\boldsymbol{n}} \cdot \boldsymbol{\kappa}_j), \qquad j = 1,2.$$

3.22 For the reflector convex upward, show that $\mu_1 = \mu_2 = +1$, so

$$u_S(\boldsymbol{\xi},\omega) \sim \frac{F(\omega) R_n}{8\pi r_0} \frac{e^{2i\omega r_0/c_0}}{\sqrt{(1 + r_0|\boldsymbol{\kappa}_1|)(1 + r_0|\boldsymbol{\kappa}_2|)}}.$$

3.23 Now suppose that the reflector is flat and obtain the result (3.2.14), with $h = r_0$. Introduce $\rho_j = 1/|\boldsymbol{\kappa}_j|$, $j = 1,2$, setting

$$\frac{1}{(1 + r_0|\boldsymbol{\kappa}_1|)(1 + r_0|\boldsymbol{\kappa}_2|)} = \frac{\rho_1 \rho_2}{(r_0 + \rho_1)(r_0 + \rho_1)}.$$

Then, discuss this factor as a curvature-related amplitude variation due to the local structure at the stationary point.

3.24 Define the dimensionless coordinates, $\boldsymbol{\eta}$, via the expression

$$\boldsymbol{\sigma} = L\boldsymbol{\eta},$$

with $\boldsymbol{\sigma}$ still being arclength on the principal curves through the stationary point. Furthermore, consider the full phase function,

$$\phi(\boldsymbol{\sigma}) = \frac{2\omega r_0(\boldsymbol{\sigma})}{c_0} = \frac{2\omega L}{c_0}\frac{r_0(\boldsymbol{L\eta})}{L} = \lambda\Phi(\boldsymbol{\eta}).$$

Show that, if λ_j is an eigenvalue of the matrix Φ_{ij} (in dimensionless variables) and ν_j is an eigenvalue of the matrix of the matrix ϕ_{ij} (in dimensional variables), then

$$\lambda\lambda_j = L^2\nu_j, \quad j = 1, 2.$$

Here, we use the notation of (3.6.3) for the definitions of Φ_{ij} and ϕ_{ij}.

3.25 Show that

$$\nu_j = \frac{2\omega}{c_0}\left[\frac{1}{r_0} - \hat{\boldsymbol{n}}\cdot\boldsymbol{\kappa}_j\right], \quad j = 1, 2,$$

and hence that the criterion (3.6.7) for validity of the above asymptotic expansion is

$$\min_j\left\{\frac{2|\omega|L^2}{c_0}\left|\frac{1}{r_0} - \hat{\boldsymbol{n}}\cdot\boldsymbol{\kappa}_j\right|\right\} \geq \pi.$$

3.26 There are three relevant length scales in this problem:

- **a.** r_0, the distance from the stationary point in $\boldsymbol{\sigma}$—equivalently, the reflection point in $\boldsymbol{x}$;
- **b.** the two radii of curvature $\rho_j = 1/|\boldsymbol{\kappa}_j|$, $j = 1, 2$.

Thus, show that the asymptotic validity criterion now becomes

$$\left.\begin{array}{l}\left|\dfrac{2\omega r_0}{c_0}\left[1 - r_0\hat{\boldsymbol{n}}\cdot\boldsymbol{\kappa_j}\right]\right| \\ \left|\dfrac{2\omega\rho_j}{c}\left[\dfrac{\rho_j}{r_0} - \operatorname{sgn}\left[\hat{\boldsymbol{n}}\cdot\boldsymbol{\kappa_j}\right]\right]\right|\end{array}\right\} \geq \pi \quad j = 1, 2.$$

Note that all of these restrict the region of validity to avoid the centers of curvature of the reflector. Furthermore, the first of these requires that r_0, the distance between the observation point and the reflection point, be large enough. Finally, the latter pair of criteria warn that the radii of curvature cannot be too small, either; the reflector cannot look like a point diffractor for this asymptotic expansion to be valid.

This last exercise demonstrates how to impose accuracy criteria (3.6.7) on an integral in (dimensional) spatial variables when it is approximated by the method of stationary phase. We review the result of the exercise and expand on it here to close this section.

Let us suppose that we have an integral such as (3.6.1), but in dimensional variables $\boldsymbol{\sigma}$, rather than the dimensionless variables $\boldsymbol{\eta}$ of that equation. In particular, let us assume that the phase, though still dimensionless, has the form

$$\lambda\Phi(\boldsymbol{\eta}) = \omega\phi(\boldsymbol{\sigma}), \quad \boldsymbol{\sigma} = L\boldsymbol{\eta}. \tag{3.7.27}$$

We have seen enough examples, including the discussion in Appendix C, to know that this is a reasonable assumption. Then, simple application of the chain rule tells us that, if λ_j, $j = 1, 2, ..., n$, are the eigenvalues of Φ_{ij}, as defined in (3.6.3), and ν_j, $j = 1, 2, ..., n$, are the eigenvalues of ϕ_{ij}, defined in a completely analogous manner by (3.6.3), then

$$\lambda\lambda_j = L^2\omega\nu_j, \quad j = 1, 2, ..., n. \tag{3.7.28}$$

In this case, the asymptotic criterion (3.6.7) becomes

$$\min_j(L^2|\omega\nu_j|) \geq \pi. \tag{3.7.29}$$

The question arises as to what are the choices of L. In fact, L should be any of the length scales that appear naturally in the phase or the amplitude. The reason for this is that correction terms to the asymptotic expansion will involve derivatives of the amplitude and phase. The dimensional scale of those derivatives will be in inverse powers of those length scales. Hence, not only will the powers of ω increase with each correction term, but so will the powers of the various length scales of the amplitude and phase. More specifically, correction terms will contain progressively higher powers of $L^2\omega\nu_j$, for each L of the amplitude and phase and each ν_j, representing directional derivatives in each of the principal directions defined by ϕ_{ij}. For at least the first correction term in each length scale to be smaller than the leading order contribution obtained by the method of stationary phase, *all* of these correction terms would have to satisfy our asymptotic criterion.

The phases we analyze in spatial integrations are more likely to take the form

$$\lambda\Phi(\boldsymbol{\eta}) = \omega\phi(\boldsymbol{x}(\boldsymbol{\sigma})),$$

with $\boldsymbol{\sigma}$ some arbitrary convenient variable of integration. This general form is more difficult to analyze and we will simply deal with specific examples as they arise.

3.8 Reverse-Time Wave-Equation Migration Deduced from the Kirchhoff Approximation

To complete our discussion of how classical migration formulas follow as special cases of the formalism of this chapter, we will show how *wave-equation migration* (Claerbout, [1970, 1976]; Claerbout and Johnson,

[1971]; Claerbout and Doherty, [1972]) can be derived from the Kirchhoff approximation of the upward-scattered, zero-offset wavefield, (3.7.7).[10] Here, we are using the term "wave-equation migration" to refer exclusively to the technique of applying the wave equation in reverse time, usually via finite-differencing, to migrate zero-offset data. We will see that, contrary to what is widely believed, such wave-equation migration of zero-offset data is not an *exact* technique, but, like other migration/inversion techniques, depends on the validity of high-frequency asymptotic assumptions.

We begin by generalizing the position vector $\boldsymbol{\xi}$, allowing it to have a third variable component ξ_3 and then expressing r_0 in (3.7.6) as

$$r_0 = |\boldsymbol{x}_0 - \boldsymbol{\xi}| = \sqrt{(x_{10} - \xi_1)^2 + (x_{20} - \xi_2)^2 + (x_{30} - \xi_3)^2}. \tag{3.8.1}$$

We propose to apply the Helmholtz operator in $\boldsymbol{\xi}$ to the representation (3.7.7). As in the inversion formalism in Section 3.3, however, we see here that the dependence on r_0 is not quite a Green's function; the denominator has a factor of r_0^2, while we would prefer a factor of r_0. So, we will apply the same "preprocessing" here, as we did there. That is, we set

$$\begin{aligned} v_S(\boldsymbol{\xi}, \omega) &= \frac{\partial}{\partial \omega}\left[\frac{u_S(\boldsymbol{\xi}, \omega)}{i\omega}\right] \\ &= \frac{iF(\omega)}{\pi c_0^2}\int_S R(\hat{\boldsymbol{n}}\cdot\hat{\boldsymbol{r}}_0)\cdot(\hat{\boldsymbol{n}}\cdot\hat{\boldsymbol{r}}_0)\cdot\frac{e^{2i\omega r_0/c_0}}{4\pi r_0}dS. \end{aligned} \tag{3.8.2}$$

Now we see that the rightmost factor of the integrand is a Green's function for the Helmholtz equation—the wave equation in frequency domain—with propagation speed $c_0/2$; that is,

$$\left[\nabla_\xi^2 + \left(\frac{2\omega}{c_0}\right)^2\right]\left[\frac{e^{2i\omega r_0/c_0}}{4\pi r_0}\right] = -\delta(\boldsymbol{\xi} - \boldsymbol{x}_0). \tag{3.8.3}$$

Thus, when we apply this operator to v_S, we find

$$\begin{aligned} \left[\nabla_\xi^2 + \left(\frac{2\omega}{c_0}\right)^2\right] v_S(\xi, \omega) = \frac{iF(\omega)}{\pi c_0^2}\int_S \Bigg\{ &-\delta(\boldsymbol{\xi} - \boldsymbol{x}_0)R(\hat{\boldsymbol{n}}\cdot\hat{\boldsymbol{r}}_0) \\ &+ 2\nabla_\xi\left[\frac{e^{2i\omega r_0/c_0}}{4\pi r_0}\right]\cdot\nabla_\xi\left[R(\hat{\boldsymbol{n}}\cdot\hat{\boldsymbol{r}}_0)\hat{\boldsymbol{n}}\cdot\hat{\boldsymbol{r}}_0\right] \\ &+ \left[\nabla_\xi^2 R(\hat{\boldsymbol{n}}\cdot\hat{\boldsymbol{r}}_0)\right]\frac{e^{2i\omega r_0/c_0}}{4\pi r_0}\Bigg\} dS. \end{aligned} \tag{3.8.4}$$

Let us consider the integration in the first line of this equation. The integrand contains a three-dimensional delta function, but we have a two-

[10] See also Gardner [1985].

dimensional integration to carry out. In order to do this, let us consider a change of coordinates to a system constructed as follows. First, introduce two surface coordinates on S, then introduce, as third coordinate, s, the distance along the normal to the surface. These coordinates become singular on the evolute[11] of S. However, as part of the justification of using asymptotics, we must assume that the principal radii of curvature are at least a few units of reciprocal wavenumber away from S or are choices of L for which (3.4.2) must be satisfied. Observe also that the delta function, as a function of $\boldsymbol{\xi}$, has its support on S. Hence, we only need a coordinate system that is valid near S.

In terms of these new variables, the three-dimensional delta function can now be seen to be a two-dimensional delta function with support on S at the foot of the normal from $\boldsymbol{\xi}$, multiplied by a scalar delta function of s—*the singular function of the scattering surface*, S! We use the two-dimensional delta function to evaluate the remainder of the integrand of the first line at the foot of the normal.[12] At that point, $\hat{\boldsymbol{n}} \cdot \hat{\boldsymbol{r}}_0 = -1$ and $R(\hat{\boldsymbol{n}} \cdot \hat{\boldsymbol{r}}_0) = R_n$, the normal-incidence reflection coefficient. Hence, the first line on the right side of (3.8.4) has integral

$$\frac{iF(\omega)}{\pi c_0^2}\delta(s)R_n.$$

Now, let us consider the second line. First, it is reasonable to ask if we even have to concern ourselves with this term in a leading order asymptotic solution. Except for the common factor, $F(\omega)$, the evaluation above of the first line is order one ($O(1)$) in ω and distributional in space. So, we have to check the order of the second line. Note, first, that the differentiation will introduce a factor of ω. Furthermore, it is at least likely that the phase will have a simple second-order stationary point in its two variables. That would introduce a factor of $1/\omega$, leaving this term of order one in ω as well. In fact, for a higher-order stationary point—singular matrix of second derivatives—this term might be even larger. So we must examine this second line more carefully.

First, note that we can write the elements of the dot product as follows:

$$\nabla_\xi \left[\frac{e^{2i\omega r_0/c_0}}{4\pi r_0}\right] = -\frac{\partial}{\partial r_0}\left[\frac{e^{2i\omega r_0/c_0}}{4\pi r_0}\right]\hat{\boldsymbol{r}}_0$$

and

$$\nabla_\xi \left[R(\hat{\boldsymbol{n}} \cdot \hat{\boldsymbol{r}}_0)\hat{\boldsymbol{n}} \cdot \hat{\boldsymbol{r}}_0\right] = \frac{\partial \left[R(\hat{\boldsymbol{n}} \cdot \hat{\boldsymbol{r}}_0)\hat{\boldsymbol{n}} \cdot \hat{\boldsymbol{r}}_0\right]}{\partial(\hat{\boldsymbol{n}} \cdot \hat{\boldsymbol{r}}_0)}\nabla_\xi \left[\hat{\boldsymbol{n}} \cdot \hat{\boldsymbol{r}}_0\right].$$

Thus, the dot product that we really have to calculate is

---

[11] The evolute is a surface made up of the centers of curvature of S.

[12] Note that we need to know no details of the coordinates on S because $\delta(\cdot,\cdot)dS$ has integral equal to unity for this two-dimensional delta function.

$$\hat{\boldsymbol{r}}_0 \cdot \nabla_\xi \left[\hat{\boldsymbol{n}} \cdot \hat{\boldsymbol{r}}_0\right] = \hat{r}_{0i} \frac{\partial}{\partial \xi_i} \hat{n}_j \hat{r}_{0j}.$$

Here, we sum over repeat indices i, j from 1 to 3. In this notation,

$$\frac{\partial}{\partial \xi_i} \hat{n}_j \hat{r}_{0j} = \hat{n}_j \frac{\partial}{\partial \xi_i} \frac{r_{0j}}{r_0} = -\frac{1}{r_0} \hat{n}_j \left[\delta_{ij} - \frac{r_{0j}}{r_0} \frac{r_{0i}}{r_0}\right].$$

We can reinterpret this equation as

$$\nabla_\xi \left[\hat{\boldsymbol{n}} \cdot \hat{\boldsymbol{r}}_0\right] = \frac{1}{r_0} \left[\hat{\boldsymbol{n}} - (\hat{\boldsymbol{n}} \cdot \hat{\boldsymbol{r}}_0) \hat{\boldsymbol{r}}_0\right],$$

so that

$$\hat{\boldsymbol{r}}_0 \cdot \nabla_\xi \left[\hat{\boldsymbol{n}} \cdot \hat{\boldsymbol{r}}_0\right] = 0.$$

With this factor being zero, the second line in (3.8.4) has integrand zero and, hence, integral equal to zero as well. (We remark that for the variable-background case, this line is no longer identically zero, but it is "smoother" than the distributional result of integrating the first line; hence, lower order in the sense of singular behavior.)

We consider now the last term in (3.8.4). First, note that the Laplacian acting on $\hat{\boldsymbol{r}}_0$ cannot be as singular as the same operator acting on $1/r_0$, which is the part of the operator in the first line that actually produces the delta function. Thus, we would be immediately justified in neglecting this term. However, for this constant-background case, we can go further. With some computational effort (Mathematica™ is a boon here!) we obtain

$$\nabla_\xi^2 \left[\hat{\boldsymbol{n}} \cdot \hat{\boldsymbol{r}}_0\right] = \frac{2\hat{\boldsymbol{n}} \cdot \hat{\boldsymbol{r}}_0}{r_0^2}$$

and conclude that it is this Laplacian that creates the most singular part of the differentiation in the third line. However, the surface-area element is $O(r_0^2)$, which can be confirmed by writing the differential surface area element in terms of polar angles measured from $\boldsymbol{\xi}$. Consequently, as $\omega \to \infty$, this last integral must approach zero. This may be seen by performing a single integration by parts, holding r_0 is constant with respect to the surface coordinates. Therefore, only the first term in the integral on the right-hand side of equation (3.8.4) contributes.

Where the phase r_0 has a simple stationary point on S, this last integral is $O(1/\omega)$. We conclude, therefore, after all of these calculations, that the leading-order source on the right side of (3.8.4) is given by the integration of the first line and

$$\left[\nabla_\xi^2 + \left(\frac{2\omega}{c_0}\right)^2\right] v_S(\xi, \omega) = -\frac{iF(\omega)}{\pi c_0^2} \delta(s) R_n. \tag{3.8.5}$$

We see here that, to leading order, the ensemble of zero offset traces (each coming from a different experiment!) is, itself, a solution of the wave equation, with speed, $c_0/2$, in response to a monopole source distribution,

(delta function with support on S) and intensity in known proportion to the normal-incidence reflection coefficient!

That the ensemble satisfies this wave equation is the basic premise of *wave-equation migration.* Furthermore, that the solution is the response to a source distribution on the reflector is the basic premise of the "exploding reflector model." In this mathematical derivation, however, the relationship between the "strength" of the source distribution and the normal-incidence reflection coefficient is explicitly stated.

There is a technical mathematical detail here that requires further discussion. We have included in this derivation a source signature or filter, $F(\omega)$. Thus, we should have derived a bandlimited result, yet the source distribution on the right side in (3.8.5) is a full-spectrum delta function. It is reasonable to ask how this is possible.

Recall that we have been extremely careful to characterize our sources as being bandlimited in frequency, because that limit imposed a constraint on a derived wavenumber in the domain dual to our unknowns, α and β. On the other hand, in our theory, we have idealized the spatial dependence of the source as being a full-bandwidth delta function, given by $\delta(x)$, in one dimension, or by $\delta(\boldsymbol{x})$ in higher dimensions. Thus, our solutions used the Green's function consistent with these idealized sources in space. If, instead, we had included a spatial distribution of source density, a bandlimited delta function in spatial variables, then we would not have derived a result with a full bandwidth singular function in space in this analysis. Thus, the full-spectrum delta function in the spatial domain is consistent with our modeling and its limitations.

Exercises

3.27 Derive an expression for the surface-area element on S in a polar coordinate system with origin at $\boldsymbol{\xi}$, and confirm that the differential surface-area element is $O(r_0^2)$.

3.28 Write out an expression for the derivative appearing in the third line in (3.8.4) in terms of R' and R'', the derivatives of the reflection coefficient with respect to its argument, $\hat{\boldsymbol{n}} \cdot \hat{\boldsymbol{r}}_0$.

4

Large-Wavenumber Fourier Imaging

In Chapter 1 we discussed the historical aspects of migration. In that context, migration was viewed as the *back propagation* of the recorded data to its "correct" position on the image. This view was modified in Chapters 2 and 3, where we encouraged the reader to view this process as being the solution of an *inverse problem.* In this chapter, we will examine the imaging problem from yet another perspective, that of band- or aperture-limited Fourier transforms. In doing so, we show that there are solid mathematical reasons for choosing to invert for reflectivity. We will also see why extracting smooth information using migration-like techniques will not be easy. (Readers who wish to immediately see the methods of Chapter 3 extended to the problem of inverting seismic data collected with nonzero source-receiver offset in a variable-wavespeed medium, may skip directly to Chapters 5 and 6, and return to this chapter later.)

Originally we formulated the inverse problem by writing a forward modeling formula that was an integral equation for the "scattered" field. By linearizing this integral equation via the Born approximation, and by substituting the constant-wavespeed Green's function, we saw that the resulting integral had the form of a Fourier transform. This meant that we could write the inversion formula as an *inverse* Fourier transform. Our initial formalism yielded a solution for $\alpha(\boldsymbol{x})$—the *wavespeed perturbation* from some assumed background value.

The targets that we chose to image first with this technique were steplike changes in the wavespeed profile. Because seismic data are bandlimited, we found that steplike functions are not well reconstructed using this formulation. We found that we could modify the inversion formula to yield the

solution for $\beta(\boldsymbol{x})$, which we call the *reflectivity function.* The reflectivity function of a single reflector is a bandlimited singular function representing the reflector surface, with amplitude proportional to the specular reflection coefficient. For the zero-offset problems of Chapters 2 and 3, the necessary modification was a simple filter that consisted of multiplying the integrand in the inversion formula by the factor $i\omega/2c_0$. This factor first appeared in Section 2.4 and was seen to be the product $1/4$ times the magnitude of the $\boldsymbol{k}$-vector, which is $k = 2i\omega/c$ assuming two-way wave propagation. This Fourier-domain filter transforms to a simple *directional derivative* operator in the spatial domain. Remarkably, the direction of this derivative was always normal to the discontinuity surface of $\alpha(\boldsymbol{x})$.

Chapters 5 and 6 will deal with the problem of extending the seismic inversion process to more general inversion settings, including those with separated source and receiver, as well as those involving variable-background wavespeed profiles. We will use the same approach to formulating the high-frequency forward and inverse problems as was developed in Chapters 2 and 3. We will create a forward modeling formula written in terms of the perturbation of the wavespeed from an assumed background-wavespeed profile, which will then lead to an inversion formula that solves for this perturbation. To do this, we will employ an approximate Green's function that will more correctly represent wave propagation in variable-wavespeed media than does the constant-wavespeed Green's function used in Chapter 3. Fortunately, we will also be able to find a directional derivative filter that will permit us to solve for the *reflectivity* in these more general problems, as well. Moreover, we will see how such an inversion formula may be extended to address any other inverse-scattering problem, such as variable-density acoustic, as well as elastic or electromagnetic media, though these topics are beyond the scope of our text.

This is possible because the choice of filter is not peculiar to the particular application, but follows from the properties of the Fourier transform. The filter that permits Fourier transform–like inversion formulas to image the reflectors as bandlimited delta functions arises from properties of aperture-limited, large-wavenumber Fourier transforms and their inverses. The objective of this chapter is to present these fundamental ideas about Fourier inversion.

Ultimately, the applications require that we consider something more general than multifold Fourier transforms. While the phase of the integrand will be the phase of a Fourier transform, say, $\boldsymbol{k}\cdot(\boldsymbol{x}-\boldsymbol{x}')$, the amplitude of the integrand will be allowed to depend on both $\boldsymbol{k}$ and $\boldsymbol{x}'$, making the integral resemble an inverse Fourier transform and yet be something different. Thus, a second goal of this chapter will be to investigate the properties of *Fourier transform–like integrals* (as opposed to simple Fourier transforms).

4.1 The Concept of Aperture

Webster's dictionary defines the term "aperture," in its usage in optics, as "the diameter of the stop in an optical system that determines the diameter of the bundle of rays traversing the instrument." Telescopes, cameras, microscopes, and the human eye are all examples optical processing systems that consist, in part, of a spatially limited aperture. In optics, the *resolving power*, which is the ability of an instrument to separate two narrowly spaced light sources, is directly related to the size of the aperture of the instrument. In general, the greater the diameter of the aperture of the objective lens or mirror (at a fixed focal length), the better the resolving power, and hence the better the image quality.[1]

Intuitively, we can see why this is so by considering rays emanating from two narrowly separated light sources. A small lens viewing such a pair of sources does not capture a sufficient number of rays from each source to permit the sources to be distinguished from one another. The large lens, on the other hand, captures rays over a broader range angles, permitting bundles of rays from each source to be uniquely identified with the respective source. Thus, we equate the aperture in optics with a specific range of available ray vectors. The larger the lens, the greater the range of the angular coverage of the source.

So, too, the seismic applications that we discuss have an analogous property that we call "aperture." Correspondingly, there is an issue of "aperture-limiting" that will influence image quality. In the seismic case, the aperture will also be related to the *angular coverage* of the target being imaged. In the inversion formulas we have been studying, this angular coverage is expressed as the angular range of the wavenumber domain. This follows because, in the world of high-frequency asymptotics, *ray* vectors are exactly identifiable with *wavenumber* vectors. Thus, the range of ray angles illuminating a target exactly identifies with the available angular coverage in the wavenumber domain. In addition, the magnitude of all wavenumbers is given by $|\boldsymbol{k}| \equiv 2|\omega|/c$ for two-way propagation in constant-wavespeed media, for the zero-offset source-receiver geometry. This is just the vector sum of the ray vectors pointing from the source and receiver to the point being imaged.

Hence, the property of bandlimiting discussed in Chapter 2 reappears as a restriction in the available *magnitudes* of the $\boldsymbol{k}$ vectors in the wavenumber domain. For nonzero-offset, the effective $\boldsymbol{k}$ vector is still the vector sum of the ray vectors from the source and receiver points to the point being imaged. For constant wavespeed and nonzero offset the magnitude

[1] This is not just a superficial analogy. Lenses have Fourier transforming and phase shifting properties, which make the lens-based optical imaging process similar to the imaging processes we study in this text. See Chapter 5 of Goodman [1996] for more information on the broad subject of Fourier optics.

of the effective wavenumber in inversion formulas will obey the inequality $|\boldsymbol{k}| < 2|\omega|/c$, with $|\boldsymbol{k}| \to 0$ as the angle between incident and reflected rays approaches π. This restriction means that even though we have "high-frequency" waves, we may not have a sufficient range of "large wavenumbers," owing to oblique scattering, to satisfy the validity conditions of our asymptotic inversion formulas. In the extreme case, our formulas can be expected to fail in the case of purely transmitted arrivals for this reason alone.

Thus, the combined limitations of both the angles and magnitudes of the range of ray angles that define the $\boldsymbol{k}$-domain constitute "aperture limiting" in the general problem of Fourier imaging, which includes seismic imaging. To study this phenomenon in greater detail we will consider the aperture-limited Fourier inversion of specific functions in Section 4.3 and generalize these results in Section 4.4.

In Section 4.2 we will discuss the general geometrical problem of aperture. A term that the reader may have encountered, possibly associated with radar imaging, is "synthetic aperture." In the seismic experiment, as in many other imaging technologies, the $\boldsymbol{k}$-domain aperture is built up by combining information collected from many sources illuminating the target zone, with the response recorded on a suite of receivers that usually changes location as the source position is moved. This overlay of responses to an ensemble of sources (and receivers) enhances the aperture beyond that of single source-receiver pairs. The simplest synthetic aperture in seismic application is the common-offset recording geometry, with zero-offset recording being the optimal offset, from the perspective of large-wavenumber asymptotics. Of course, common-offset gathers are obtained by sorting data from overlapping common-source experiments, so an ensemble of such common-source experiments also has an enhanced aperture.

The methods termed "synthetic aperture radar" and "synthetic-aperture focusing technique" (SAFT) derive from this idea, and thus both share mathematical kinship with the seismic inverse problem.

4.2 The Relationship Between Aperture and Survey Parameters

In this section we will provide further motivation and insight into the relevance of Fourier analysis to the inverse-scattering imaging problem, especially as it relates to the generation of reflector images from aperture-limited Fourier data. Here, we rely heavily on the analysis of the application of our Kirchhoff inversion formula to Kirchhoff-approximate data in Section 3.7.2. We will also draw on analogous results for non-zero-offset recording geometries derived in Chapters 5 and 6.

4.2.1 Rays, Fourier Transforms, and Apertures

In Section 3.7.2, we showed an example of the inversion of Kirchhoff-approximate, zero-offset data via the method of stationary phase. From this example, we know that our zero-offset inversion formulas can produce an image of a reflector only when a stationary point exists for the prescribed range of source-receiver positions. Such a stationary point prescribes the condition that points on the reflector surface can be imaged only if a geometrical-optics ray can be traced from the source-receiver position in such a way that the ray is normally incident at the point being imaged. This requirement is embodied in the stationary phase condition (3.7.15), $\hat{\boldsymbol{r}}_0 = \hat{\boldsymbol{r}}$. We will see in Chapters 5 and 6 that for the case of a nonzero offset between source and receiver, we still can produce an image at points only if it is possible to trace a ray from the source to the receiver that reflects specularly off of the point being imaged.

In Chapters 2 and 3 we saw through asymptotic analysis that output points $\boldsymbol{x}$ near the reflector produced the highest amplitudes through the bandlimited delta function in (3.7.19),

$$\delta_B(s) = \frac{1}{\pi c_0} \int_\Omega d\omega \; F(\omega) e^{2i\omega s/c_0}, \tag{4.2.1}$$

which peaks on the reflector under the assumption that the filter, $F(\omega)$, is a symmetric about the origin.

We can interpret these characteristics in terms of Fourier transforms by considering the phase of (3.7.9), and its Taylor series for $\boldsymbol{x}$ "near" the reflector, as well as for points on the reflector in the vicinity of the normal from $\boldsymbol{x}$ to the reflector. We can rewrite the phase as

$$\Phi = \frac{2\omega}{c_0}[r_0 - r] \approx \boldsymbol{k} \cdot [\boldsymbol{x_0} - \boldsymbol{x}], \tag{4.2.2}$$

with

$$\boldsymbol{k} = \nabla_x \Phi = \frac{2\omega}{c_0}\hat{\boldsymbol{r}}. \tag{4.2.3}$$

This result suggests that in the neighborhood of points where the inversion output has its largest values, Φ has the local behavior of the phase of the cascade of a forward and an inverse Fourier transform. The transform variables are $\boldsymbol{x}$ with wavevector, $\boldsymbol{k}$, which is determined by the survey parameters, $\boldsymbol{\xi}$ and ω. Because $\boldsymbol{\xi}$ is limited by the geometry of the survey, the local output near a given reflector is generated by Fourier synthesis over a limited aperture in the $\boldsymbol{k}$-domain. The angular extent of $\boldsymbol{k}$ in that domain is determined by the directions of $\pm\hat{\boldsymbol{r}}$, with the ± 1 coming from the sign of frequency, represented by $\operatorname{sgn}(\omega)$. The range of magnitudes of $\boldsymbol{k}$ is given by $k = |\boldsymbol{k}| = 2|\omega|/c_0$.

If we were to be satisfied with the linear approximation of phase defined by (4.2.2), we could use equation (4.2.3) to define a change of integration

variables from the survey variables $\boldsymbol{\xi}$ and ω to the variables $\boldsymbol{k}$, thus obtaining an *approximate* identification of the imaging process with the process of Fourier synthesis. Yet it is possible to do better than a mere linear approximation. We can change the integration variable to a new variable, $\boldsymbol{\kappa}$, that makes the Taylor expansion in (4.2.2) *exact* when $\boldsymbol{k}$ is replaced by $\boldsymbol{\kappa}$. Thus, we have a true equality between Φ and the dot product of a "wavenumber," $\boldsymbol{\kappa}$ with the difference of spatial coordinates, $[\boldsymbol{x_0} - \boldsymbol{x}]$,

$$\Phi = \frac{2\omega}{c_0}[r_0 - r] = \boldsymbol{\kappa} \cdot [\boldsymbol{x_0} - \boldsymbol{x}],$$

where

$$\boldsymbol{\kappa} = \boldsymbol{k}\,[1 + O(|\boldsymbol{x} - \boldsymbol{x}_0|)]\,.$$

The multifold integral (3.7.9) is recast in the form

$$\beta(\boldsymbol{x}) = \int_K \int_S \mathcal{F}(\boldsymbol{x}, \boldsymbol{x}_0(\boldsymbol{\eta}), \boldsymbol{\kappa}) e^{i\boldsymbol{\kappa}\cdot[\boldsymbol{x}_0(\boldsymbol{\eta}) - \boldsymbol{x}]} d^3k\, dS(\boldsymbol{\eta}). \tag{4.2.4}$$

Here, the details of the function $\mathcal{F}$ are unimportant, except that we require that $\mathcal{F}$ be slowly varying.

To complete our identification of imaging with Fourier synthesis, we must rewrite (4.2.4) as a *volume* integral in $\boldsymbol{x_0}$ rather than as a surface integral in $\boldsymbol{\eta}$. To do so, we need only invoke the definition of the singular function of the surface, introduced earlier, but defined more rigorously below, by equation (4.3.9). Simply put, we introduce a new variable s into the coordinate system $\boldsymbol{\eta}$ on the reflector, S. This variable measures distance normal to S. Then, $ds\, dS$ is a differential volume element, at least near S, and integration of $\delta(s)$ leaves the integral in the previous equation unchanged. It allows us, however, to rewrite (4.2.4) as a volume integral in the $\boldsymbol{x}_0$ coordinates,

$$\beta(\boldsymbol{x}) = \int_K \int \mathcal{F}(\boldsymbol{x}, \boldsymbol{x}_0, \boldsymbol{\kappa}) \delta(s) e^{i\boldsymbol{\kappa}\cdot[\boldsymbol{x}_0 - \boldsymbol{x}]} d^3k\, d^3x_0, \tag{4.2.5}$$

where $\boldsymbol{x}_0 \equiv \boldsymbol{x}_0(\boldsymbol{\eta})$. With this last result, the motivation for studying Fourier-type integrals should be clearer for the reader, independent of whether we are inverting for the steplike perturbation output $\alpha(\boldsymbol{x})$ or for the bandlimited delta function-like output $\beta(\boldsymbol{x})$.

Our analysis will yield more than merely a justification for our choice of inverting for the reflectivity $\beta(\boldsymbol{x})$, rather than for perturbation $\alpha(\boldsymbol{x})$. We will see in later sections why jumps in the wavespeed profile are *preferentially* imaged over smooth variations. In the rest of this section we will see the connection between aperture and our ability to image reflectors of specific dips.

4.2.2 Aperture and Migration Dip

The stationarity condition that governs our ability to image points on a reflector surface may be expressed in two different, but equivalent, ways.

From the viewpoint of geometrical-optics ray tracing, we may think of the ability to image a point on a reflector as being equivalent to having a raypath from the source to the receiver that represents a specular reflection at the point being imaged.

This translates into a restriction on the local reflector orientation, or *reflector dip*. This dip can be characterized by the orientation of the unit vector normal to the reflector $\hat{\boldsymbol{n}}$, at each point. For the zero-offset survey geometry we have a specular reflection when the unit normal vector coaligns with the ray vector that points from the common source-receiver point to the image point. For the case of nonzero offset, we will see in Chapter 5 that the stationarity condition requires that the vector sum of the ray vectors from the source and receiver to the image point must coalign with the normal to the surface at the reflection point, if we are to expect to image the reflector at that point.

The second way of viewing the condition of imaging is in terms of available dips. As was seen in the analysis in Section 3.7.2, the processing produces an image only when the orientation or *dip* of $\hat{\boldsymbol{r}}$ for some source-receiver pair coaligns with the reflector dip (as defined by the normal) at a point on the reflector. The *dip* of $\hat{\boldsymbol{r}}$ has come to be known in the geophysical community as the *migration dip*.

Thus, to complete the story, an image of the reflector is produced at a point of the reflector surface only when the range of migration dips in the survey includes the reflector dip.

Migration Dip Versus Reflector Dip

The reader may be confused at this point. Geologically speaking, we have the natural desire to consider the "dip" of a rock layer as being the vector pointing parallel to the layer (in the downhill direction) oriented in the azimuth of maximum slope. The magnitude of the dip angle will be the same, whether we measure it from the horizontal, in the direction of the sloping layer, or the vertical, in the direction of the normal to the layer. If we do the latter, then we are identifying the reflector dip by a vector oriented 90 degrees respective to the geologists' "dip vector."

The reason this definition is useful relates to the fact that our inversion formulas are Fourier transform–like integrals. We know, a priori, that the Fourier transform of a dipping plane is a plane oriented 90 degrees with respect to the original plane. Thus, we know a priori that the angular range of the $\boldsymbol{k}$-domain, necessary for *imaging* the plane, must contain the plane's normal direction, for the plane to be imaged.

Thus, in terms of our Fourier synthesis analogy, the angular *aperture* in the $\boldsymbol{k}$-domain must include the normal direction to a given point on the reflector surface for that point to be imaged by our inversion formulas. This is just another way of saying that the range of migration dips must contain the reflector dip to permit us to image the reflector.

4.2.3 Migration Dip and Apertures

In Chapters 5 and 6, common-offset and common-shot inversion formulas will be developed for 3D and 2.5D media, respectively. For the constant-wavespeed case we will see that the relevant normal vector direction in these non-constant-offset problems is given by the resultant vector, $\hat{\boldsymbol{r}}_s + \hat{\boldsymbol{r}}_g$, with $\hat{\boldsymbol{r}}_s$ and $\hat{\boldsymbol{r}}_g$ being unit vectors pointing from the source and receiver, respectively, to the output point.

Our analyses in Chapter 5 and 6, particularly as related to equations (5.2.22) and (5.2.23) in Chapter 5 and (6.3.25) and (6.3.26) in Chapter 6, will suggest, analogous to (4.2.3), that we can write the wavenumber in terms of ray directions, which are, in turn, the same as the migration dips that we discussed above. Thus, our wavenumber representation is

$$\boldsymbol{k} = \nabla_x \Phi = \frac{\omega}{c_0} \left[\hat{\boldsymbol{r}}_s + \hat{\boldsymbol{r}}_g \right], \tag{4.2.6}$$

for the more general situation of nonzero offset between source and receiver. Equation (4.2.6) reduces to (4.2.3) when the offset between source and receiver is zero. In the zero-offset case, $\hat{\boldsymbol{r}}_s$ and $\hat{\boldsymbol{r}}_g$ are collinear.

We may use the facts that

$$\left[\hat{\boldsymbol{r}}_s + \hat{\boldsymbol{r}}_g \right]^2 = 2\,(1 + \cos 2\theta) \qquad \text{and} \qquad 2\cos^2\theta = 1 + \cos 2\theta$$

to write, in general, that

$$|\boldsymbol{k}| = 2\frac{|\omega|}{c} \cos\theta, \tag{4.2.7}$$

where 2θ is the angle between $\hat{\boldsymbol{r}}_s$ and $\hat{\boldsymbol{r}}_g$. Figure 4.1a shows how a single range of wavenumbers composing the aperture is related to a single normal direction. Figure 4.1b illustrates the process of aperture synthesis through the combination of contributions from a range of normal directions and, hence, a range of migration dips. In each of these figures, we have drawn only the contribution due to the positive frequencies. The reader should be aware that all $\boldsymbol{k}$-domain apertures are symmetric about $k = 0$.

Common-Offset Apertures

For the case of common-offset surveys (with zero-offset being a special case of common-offset), we might imagine building an aperture out of contributions like those in Figure 4.1a.

In Figure 4.2, the solid horizontal line at the surface represents the range of a zero-offset, two-dimensional survey acquisition line. The points $\boldsymbol{x}_1$ and $\boldsymbol{x}_2$ are two sample output points for the inversion integral. With each point as center of a local $\boldsymbol{k}$-domain coordinate system, the shaded areas depict sample apertures in the $\boldsymbol{k}$-domain. The circular boundaries of the aperture represent the upper and lower limits on the magnitude of the wavenumber k, while the radial sides of the domains depict the angular limits in the $\boldsymbol{k}$-domain. These angular limits are also the limits of migration dip, and hence

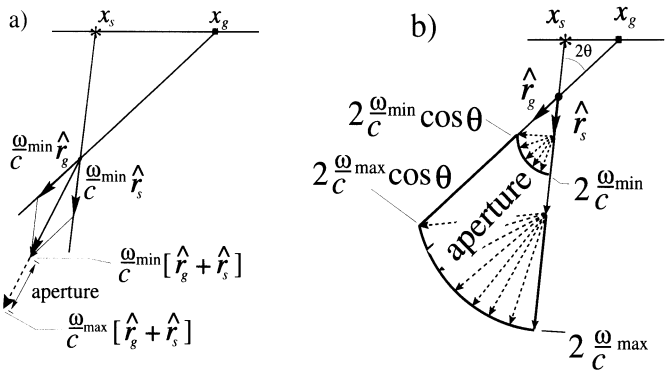

FIGURE 4.1. a) The resultant $\boldsymbol{k}$-vectors representing the aperture for a single source at $\boldsymbol{x}_s$ and a single receiver at $\boldsymbol{x}_g$. The aperture is the line segment between the positions $\omega_{\min}\left[\hat{\boldsymbol{r}}_s+\hat{\boldsymbol{r}}_g\right]/c$ and $\omega_{\max}\left[\hat{\boldsymbol{r}}_s+\hat{\boldsymbol{r}}_g\right]/c$. b) The aperture for the fixed source position at $\boldsymbol{x}_s$, but for receiver positions ranging from $\boldsymbol{x}_s$ to $\boldsymbol{x}_g$, is the area between the two semicircular arcs.

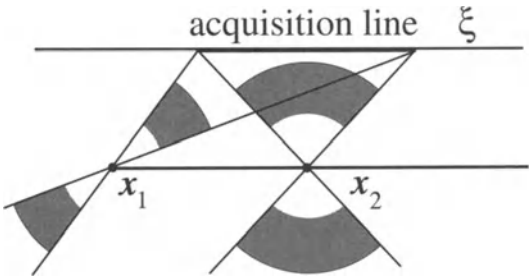

FIGURE 4.2. The $\boldsymbol{k}$-domain apertures at two output points below a data acquisition line for a common-offset survey. The wavenumber domain is restricted to a sector of an annulus in each case. The inside and outside radii of the annulus are given by $2|\omega_{\min}|\cos\theta/c$ and $2|\omega_{\max}|\cos\theta/c$, respectively, where 2θ is the angle between $\hat{\boldsymbol{r}}_s$ and $\hat{\boldsymbol{r}}_g$. The apertures for zero-offset are a special case of this when $\theta=0$. The apertures were computed with the program KAPERTURE.

indicate the range of reflector dips (again, with dip defined by the reflector normal) that can be imaged by our zero-offset, constant-background, high-frequency inversion procedure, either in the Fourier (Stolt) form or in the Kirchhoff (Schneider) form of processing. (Recall that the latter was derived from the former, but a derivation going in the opposite direction is also possible.)

The maximum aperture occurs at points below the center of the recording array, with the size of the aperture diminishing for horizontal positions to the right or left of the array. At extreme distances to the left or right of the source-receiver array, the aperture becomes a vanishingly thin "pie slice" in the $\boldsymbol{k}$-domain. Such narrow domains can only image reflectors over a correspondingly narrow range of corresponding dips.

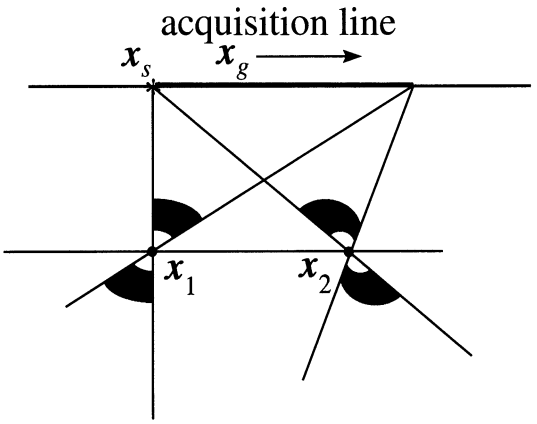

FIGURE 4.3. The $\boldsymbol{k}$-domain apertures at two output points below a data acquisition line for a common-shot survey (computed with KAPERTURE).

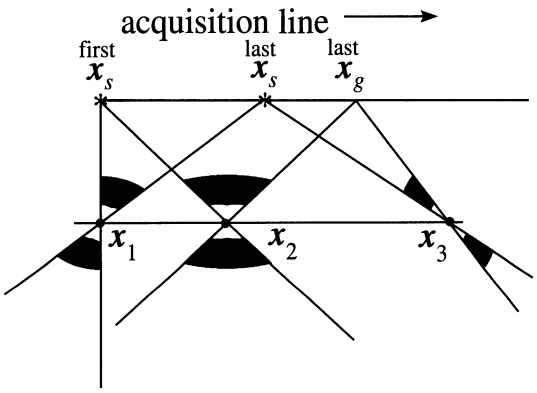

FIGURE 4.4. The $\boldsymbol{k}$-domain apertures at three output points below a data acquisition line for overlapping common-shot surveys. Sources exist from the point labeled **first** $\boldsymbol{x}_s$ to the point labeled **last** $\boldsymbol{x}_s$. Receiver positions exist from **first** $\boldsymbol{x}_s$ to **last** $\boldsymbol{x}_g$. The maximum aperture exists in the region where the overlap of the source and receiver coverage is a maximum. (Apertures computed with KAPERTURE.)

Common-Shot Apertures

In Figure 4.3, we show the $\boldsymbol{k}$-domain apertures at the same two output points, but now for a common-shot experiment in which the source, $\boldsymbol{x}_s$, is fixed at the left end of the survey, but the receiver, $\boldsymbol{x}_g$, ranges to increasing distances to the right, as in the previous example. The vector sum, $\hat{\boldsymbol{r}}_s + \hat{\boldsymbol{r}}_g$, is shown for the extreme positions of $\boldsymbol{x}_g$. The scales of the previous example have been retained here. Now, however, the resultant directions of dip and $\boldsymbol{k}$ are quite different, as depicted by the two skewed annular regions. Note,

also, that this result implies that the range of *magnitudes* of $\boldsymbol{k}$ is different for different dips. This fact follows directly from (4.2.7).

This change in range of values of k also implies a change in resolution of the image. A smaller range of k implies lower resolution, because smaller values of wavenumber translate into longer effective wavelengths. Thus, for example, for the output point at $\boldsymbol{x}_2$, a horizontal reflector would have lower resolution—appear as a thicker bandlimited delta function—than would a reflector inclined downward to the left, but with normal still within the range of migration dips. Of course, a reflector inclined downward to the right would not be imaged by this common-shot survey at all! See, for example, Beylkin et al., [1985].

From the diagrams, it is also apparent that, at each output point, the range of migration dips is smaller for the common-shot survey than for the zero-offset survey. Thus, a single common-shot inversion will provide an image of reflectors for only this smaller range of reflector dips. To be fair, however, the size of the aperture for a survey consisting of *overlapping* common-shot profiles approaches that of a common-offset profile. Such improvement is an example of the benefit of exploiting *aperture synthesis.* Figure 4.4 shows the aperture at three points, located at the same depth, and positions $\boldsymbol{x}_1$, $\boldsymbol{x}_2$, and $\boldsymbol{x}_3$. Sources exist from the point labeled **first** $\boldsymbol{x}_s$ to the point labeled **last** $\boldsymbol{x}_s$. Receiver positions exist from **first** $\boldsymbol{x}_s$ to **last** $\boldsymbol{x}_g$. The maximum aperture exists in the center region where the overlap of the source and receiver coverage is a maximum. An example is the aperture at position $\boldsymbol{x}_2$. The aperture diminishes rapidly with distance outside of the region below the survey as is seen in the aperture at the point $\boldsymbol{x}_3$.

Small Versus Large Offset

In Figure 4.5, we show comparisons of single $\boldsymbol{k}$ vectors for the extreme source and receiver pairs of a common-offset survey. Here, we have used the two subsurface points, $\boldsymbol{x}_1$ and $\boldsymbol{x}_2$, to demonstrate two different features of the analysis of dip for this survey. At $\boldsymbol{x}_1$ and $\boldsymbol{x}_2$ we show the resultant vectors $[\hat{\boldsymbol{r}}_s^+ + \hat{\boldsymbol{r}}_g^+]$ and $[\hat{\boldsymbol{r}}_s^- + \hat{\boldsymbol{r}}_g^-]$. As can be seen in the figure, the further away we are from a source-receiver pair of a given offset, the smaller the opening angle between the two constituent vectors. This yields a larger resultant vector, implying a higher range of values of the effective wavenumber of the survey. Thus, for points far away from a common-offset source-receiver pair, this geometry begins to approximate a zero-offset survey, when considered from the perspective of effective wavenumbers.

If the common-offset survey begins at the location of the $\boldsymbol{x}_s^-$—$\boldsymbol{x}_g^-$ array, and the array is moved in an overlapping fashion until it is coincident with the $\boldsymbol{x}_s^+$—$\boldsymbol{x}_g^+$ array, then the synthetic aperture will consist of the range of dips bounded by the resultants $[\hat{\boldsymbol{r}}_s^+ + \hat{\boldsymbol{r}}_r^+]$ and $[\hat{\boldsymbol{r}}_s^- + \hat{\boldsymbol{r}}_r^-]$, shown as the dashed resultant vectors in Figure 4.5.

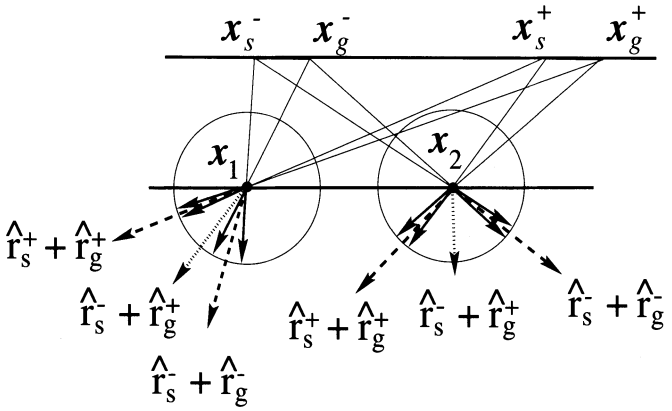

FIGURE 4.5. The $\boldsymbol{k}$-domain apertures at two output points below common-offset surveys. The black arrows are the vectors $\hat{\boldsymbol{r}}_s$ and $\hat{\boldsymbol{r}}_r$, unit vectors for the respective source and receiver raypaths to $\boldsymbol{x}_s^+$, $\boldsymbol{x}_s^-$, $\boldsymbol{x}_g^+$, and $\boldsymbol{x}_g^-$, respectively. The dashed arrows are the resultant vectors, $[\hat{\boldsymbol{r}}_s^+ + \hat{\boldsymbol{r}}_r^+]$ and $[\hat{\boldsymbol{r}}_s^- + \hat{\boldsymbol{r}}_r^-]$, that point in the direction of the associated wavenumber vector, which we associate with a migration dip. The dotted arrows are the resultant vectors representing a large offset between source at $\boldsymbol{x}_s^-$ and receiver $\boldsymbol{x}_g^+$ given by $[\hat{\boldsymbol{r}}_s^- + \hat{\boldsymbol{x}}_g^+]$. Because magnitudes of the $\boldsymbol{k}$ vectors of the aperture are scaled by the magnitudes of these resultants, we see that a wide separation between source and receiver reduces the effective wavenumber of the aperture.

If, on the other hand, we consider the far-offset source-receiver combination of $\boldsymbol{x}_s^-$ paired with $\boldsymbol{x}_g^+$, so that widest possible source-receiver offset is obtained, then the resultant vectors in this case are given by the sum $[\hat{\boldsymbol{r}}_s^- + \hat{\boldsymbol{r}}_g^+]$. These vectors are depicted as the dotted resultant vectors in Figure 4.5. Certainly, this is not a practical situation (unless this is part of a larger survey), but it allows us to make a point about relative offsets. First, note that the difference in lengths of the resultant vectors—the difference in resolution—is much more apparent here. These far-offset resultant vectors are shorter, indicating a lower effective wavenumber, and hence poorer implied resolution.

Common-Midpoint Aperture

We might conceive of forming a collection of source-receiver pairs like this last example, but of varying offsets, each having the same common midpoint—a common-midpoint (CMP) gather. For this example, with the image point directly below the midpoint, all of the resultant vectors—the migration dips—point in the same direction, though they are of different lengths, corresponding to the differing offsets between source and receiver. From the previous discussions of this chapter, we can see that in this case, the Fourier aperture consists of a single line segment. From either the $\boldsymbol{x}$-domain point of view or the $\boldsymbol{k}$-domain point of view, there is no aperture

at all! Thus, even if we could make sense of the integration that produces our seismic images, there is only one reflector dip that could possibly admit imaging—that of the horizontal reflector!

This extreme case should make it apparent to the reader that the range of dips of reflectors for which imaging is possible in a survey tends to diminish with increasing offset, whether we are talking about common-offset or common-shot surveys. Furthermore, if data at different offsets are mapped to zero-offset (via NMO/DMO), or the generalization called TZO in Chapter 7), then not all of the stacked data contains information about all possible reflector dips. The narrow-offset data contain more information than the wide-offset data, from the perspective of relative aperture. Thus, the stacking process will tend to diminish the relative amplitude of reflections from steeper-dipping reflectors compared with the more horizontal reflectors, with the images of these steeper-dipping reflectors potentially being lost in the subsequent processing. While this last issue is off the topic of this chapter, it provides a reason for prestack processing beyond preservation of amplitudes.

VSP and Crosswell Apertures

The issue of aperture becomes critical when Fourier-like formulas are used to process data collected via vertical seismic profiling (VSP) or by crosswell surveys. The angular coverage of points in the subsurface for a typical VSP survey preferentially excludes a large number of dips for most points in the subsurface.

In Figure 4.6, the $\boldsymbol{k}$-domain apertures of a single shot into an array of receivers in a VSP survey are shown. Only those reflectors whose normal vectors fall within the relatively narrow range of dips represented by these apertures will be imaged. Thus, only reflectors dipping from right to left within a narrow range of angles will be imaged. Reflectors of other dips will not be imaged. Because of the large offset between source and receiver, the maximum $|\boldsymbol{k}|$ values (shown by the circles surrounding each aperture in Figure 4.6) are never attained. Indeed, we may be in danger of violating the large-wavenumber assumptions that are inherent in our inversion formulas, in the case of such experiments.

Combining many sources and receivers does little to remedy the problem of angular coverage as can be seen in Figure 4.7. Though the maximum possible wavenumber is attained, the angular coverage still preferentially favors the imaging of reflectors dipping from right to left, and preferentially ignores reflectors of the opposite dip.

This situation is more extreme in the case of crosswell surveys, as may be seen in Figure 4.8. Positions in the subsurface illuminated by wide-angle reflections, as well as transmitted arrivals are poorest candidates for imaging with Fourier transform–like inversion formulas, because of the wide opening angle between source and receiver. Points below the depth of the

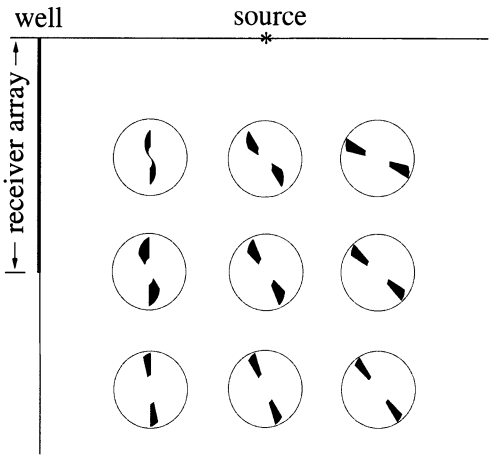

FIGURE 4.6. The $\boldsymbol{k}$-domain apertures at nine output positions in a single-shot VSP profile. Reflectors sloping from right to left and confined to a relatively narrow range of dip angles, will be imaged. Reflectors dipping left-to-right will not be imaged, owing to the preferential orientation of the apertures. In addition, point scatterers will be smeared into left-right dipping line segments. The circles show the maximum possible magnitudes of $\boldsymbol{k}$. (Apertures were computed with KAPERTURE.)

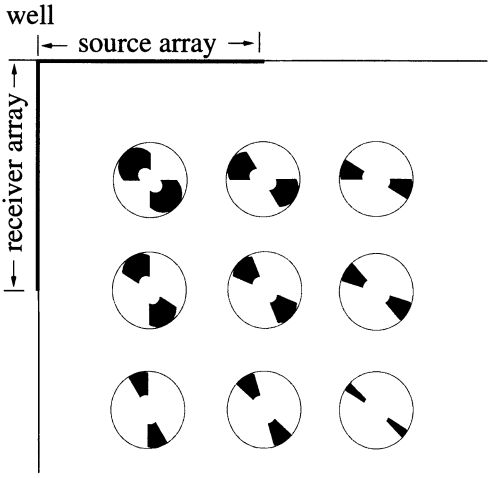

FIGURE 4.7. The $\boldsymbol{k}$-domain apertures at nine output positions in an idealized VSP "walkaway" profile, with many sources at increasing distance from the well, and many receivers at depth in the well. While the maximum $|\boldsymbol{k}|$ value is attained, the angular aperture is not greatly improved over the result from a single source. (Apertures were computed with KAPERTURE.)

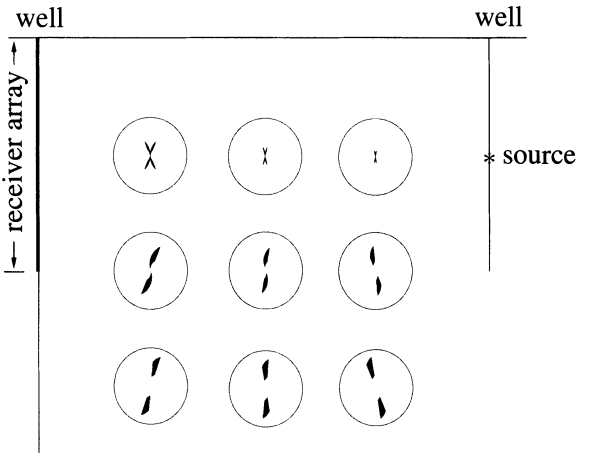

FIGURE 4.8. The $\boldsymbol{k}$-domain apertures at nine output positions in an idealized single common-shot crosswell experiment. (Apertures were computed with KAPERTURE).

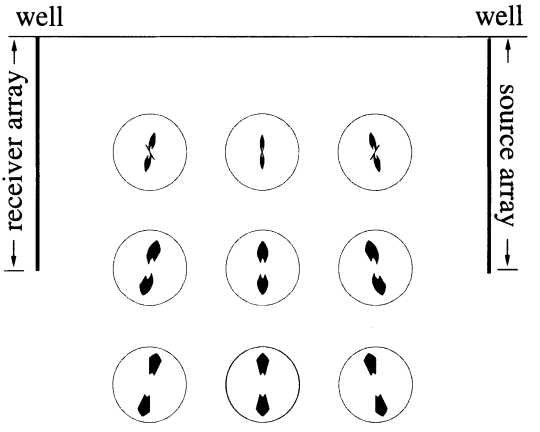

FIGURE 4.9. The $\boldsymbol{k}$-domain apertures at several output points for an idealized common-shot crosswell survey, with many sources and receivers located in two wells. (Apertures were computed with KAPERTURE.)

source and receiver arrays have broader $\boldsymbol{k}$-domain apertures, but still only admit extremely restricted ranges of migration dips. As in the case of VSP, this problem of restricted aperture is not greatly improved by combining many common-source, crosswell experiments, as is shown in Figure 4.9.

4.2.4 Summary

We have introduced the following ideas about reflector imaging via our inversion procedures, which also apply to any traditional migration process, as well.

1. The range of reflector dips and the resolution of the image of the reflector depends on
   - **a.** the location of the output point,
   - **b.** the source-receiver configuration and attendant range of migration dips at the output point, and
   - **c.** the bandwidth.
2. The $\boldsymbol{k}$-domain aperture is determined by the sum of gradients of the traveltimes from source and receiver to the output point, the temporal bandwidth (frequency range), and source signature.
3. The $\boldsymbol{k}$-domain is symmetric with respect to the origin in $\boldsymbol{k}$, but its range in k may vary with migration dip. Hence, even at a single point, reflector resolution is function of reflector dip.
4. In multi-offset surveys, not all common-offset data sets have the same range of migration dips at a given output point.
5. In VSP and crosswell geometries, Fourier transform–based inversion formulas are expected to do a poor job of imaging in most areas of the subsurface, because the geometry of these surveys results in restricted apertures for most points in the subsurface.

4.3 Examples of Aperture-Limited Fourier Inversion

As we have seen, because seismic surveys are limited to small regions on the surface of the Earth, aperture limiting is an important issue in the seismic inverse problem. By studying specific examples of the aperture-limited Fourier inversion of known functions, we hope to learn what is reasonable to expect from seismic inversion formulas. This mode of analysis will reveal other important characteristics of the integrals encountered in high-frequency inversion theory, as well. As noted in the introduction, because we are dealing with these issues totally in the context of Fourier transforms, the results presented here have general application to imaging by Fourier methods and are not limited to the seismic applications that are the main topic of this text.

The general form of the integral to be studied here is the cascade of forward and inverse Fourier transforms acting on a function $f(\boldsymbol{x}')$, written as

$$I(\boldsymbol{x}) = \frac{1}{(2\pi)^3} \int_{D_k} d^3k \int_{D_{x'}} d^3x' f(\boldsymbol{x}') e^{i\boldsymbol{k}\cdot(\boldsymbol{x}-\boldsymbol{x}')}, \tag{4.3.1}$$

where, $\boldsymbol{x}$, $\boldsymbol{x}'$, and $\boldsymbol{k}$ are three-component vectors. The reader will recognize this form as being analogous to the seismic inversion formulas derived in Chapters 2 and 3. The object of the subsections that follow will be to see how well specific functions $f(\boldsymbol{x}')$, are represented by $I(\boldsymbol{x})$ when the domains D_k and $D_{x'}$ are constrained.

In addition to constraints that we might impose on the problem, there are natural constraints imposed on the domain D_k by aspects of the data acquisition. As discussed in the previous section, we recognize that $|\boldsymbol{k}|$, the magnitude of the wavenumber vector, is proportional to $|\omega|$, meaning that the wavenumber domain D_k will derive some of its properties from the bandwidth, that is, from the ω-domain. These properties can be simply represented by a filter, $F(\omega)$ seen in Section 2.5. This filter is symmetric about the origin in the ω-domain, meaning that its k-domain analog will also be symmetric about the origin; that is, if a particular vector, $\boldsymbol{k}_0$, is in the domain, then so is $-\boldsymbol{k}_0$, insuring that the data are real-valued in the space-time domain. Thus, D_k must also be symmetric about the origin. Furthermore, information at $\omega = 0$ is generally not available in seismic data, so we will assume that information at $\boldsymbol{k} = \boldsymbol{0}$ is *always* excluded from the domain D_k, even though the analysis of the previous section showed that a wide opening angle between the source and receiver can create arbitrarily small effective wavenumber magnitude.

In Section 4.4, a generalized form of equation (4.3.1) will be recast in dimensionless variables, just as was done in our analysis of the method of stationary phase in Exercises 3.13 and 3.20. Following the same procedure as was followed in Chapter 3, we will use this scaling to provide a more precise statement of the condition of large wavenumbers in D_k. In the generalization, the function f will also depend on the unit vector, $\hat{\boldsymbol{k}} = \boldsymbol{k}/|\boldsymbol{k}|$. It will also be convenient to represent the domain D_k by the "large-wavenumber bandpass filter factor" $\mathcal{F}(\boldsymbol{k})$. This function will always be taken to be even and nonnegative on D_k, to correspond to the $F(\omega)$ filter discussed above. As stated in (4.3.1), when D_k includes all $\boldsymbol{k}$-vectors, $I(\boldsymbol{x})$ is merely the truncation of $f(\boldsymbol{x})$ to the domain, $D_{x'}$. This means that the interesting features of the analysis of $I(\boldsymbol{x})$ will arise from the shape and extent of D_k, the limiting action of the filter $\mathcal{F}(\boldsymbol{k})$, and the possible dependence of f on $\hat{\boldsymbol{k}}$.

From these investigations we will see what "information" about $f(\boldsymbol{x})$ is, and is not, recoverable from aperture-limited knowledge of its Fourier transform.

4.3.1 Aperture-Limited Inversion of a Dirac Delta Function (A Point Scatterer)

The simplest possible target that we can image is a point scatterer. In seismic imaging, the term "point scatterer" refers to a region in the subsurface

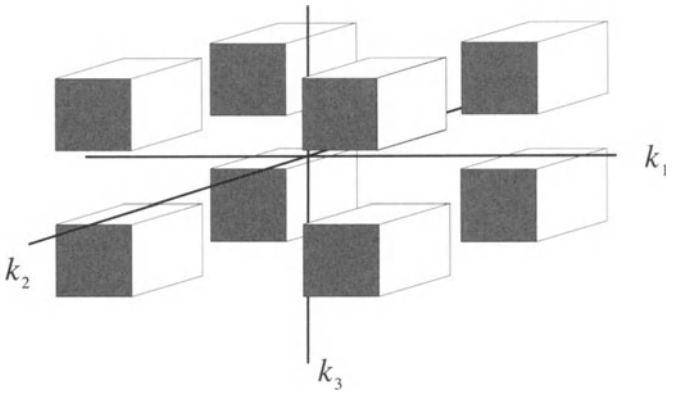

FIGURE 4.10. The domain D_k in equation (4.3.3).

with sufficiently large volume that it is "seen" by the seismic waves, but with sufficiently small volume that it generates only a simple diffraction hyperbola as a seismic response. The result of imaging such a scatterer is a single wave packet on the migrated section.

While the discussion of such point scatterers as a practical matter may become complicated, the simplest realization arises if we suppose that

$$f(\boldsymbol{x}') = A\delta(\boldsymbol{x}' - \boldsymbol{x}_0), \tag{4.3.2}$$

and that $D_{x'}$ includes the point $\boldsymbol{x}_0$. Furthermore, we might consider a simple bandpass filter in the $\boldsymbol{k}$-domain, D_k, which consists of the eight rectangular prisms,

$$D_k: \quad 0 < k_{j-} \leq |k_j| \leq k_{j+}, \quad j = 1, 2, 3. \tag{4.3.3}$$

To calculate $I(\boldsymbol{x})$ in (4.3.1), we first exploit the delta functions in each coordinate direction to carry out all of the integrals in $\boldsymbol{x}'$. The result is

$$I(\boldsymbol{x}) = \frac{1}{(2\pi)^3} \int_{D_k} d^3k e^{i\boldsymbol{k}\cdot(\boldsymbol{x}-\boldsymbol{x}_0)},$$

which can be recast as a product of three integrals of the type (2.4.20), allowing us to express $I(\boldsymbol{x})$ as a product of three sinc functions, (2.4.22), as follows.

$$I(\boldsymbol{x}) = A \prod_{j=1}^{3} \left[\frac{\sin\left[k_j(x_j - x_{j0})\right]}{\pi(x_j - x_{j0})} \Bigg|_{k_j=k_{j-}}^{k_j=k_{j+}} \right] \tag{4.3.4}$$

That is, the aperture-limited Fourier inversion reproduces a product of the differences of scaled sinc functions in each of the coordinate directions. (See Figure 4.11 for a two-dimensional version of this filtering example.) We recognize again that these functions are one-dimensional bandlimited Dirac delta functions, each peaking at the origin of the respective x_j coordinate

axes. The resolution of each bandlimited delta function depends on the bandwidth in the corresponding k_j-variable. The aperture-limited inversion will adequately approximate the function $f(\boldsymbol{x}')$ in (4.3.2), if the bandwidth is large enough. For sufficient bandwidth, the peak value of $I(\boldsymbol{x})$ is given by the expression

$$I_{\text{PEAK}}(\boldsymbol{x}) = A \prod_{j=1}^{3} \frac{k_{j+} - k_{j-}}{\pi}. \tag{4.3.5}$$

Thus, if we had the a priori knowledge that $f(\boldsymbol{x})$ was proportional to a Dirac delta function and we also knew that the support of this delta function was inside D_x, then $\boldsymbol{x}_0$, the support of the delta function $\delta(\boldsymbol{x} - \boldsymbol{x}_0)$, could be determined. (Geophysicists have identified point diffraction events, and their migrated counterparts, on seismograms for decades, so this agrees with experience.)

In addition, we can also determine the amplitude A by taking into account the amplitude scaling due to the bandlimiting of the filter. If a filter factor, $\mathcal{F}(\boldsymbol{k})$, is introduced in the integrand in (4.3.1), the result will remain qualitatively the same as it is here, with the peak value of $I(\boldsymbol{x})$ being modified by the product in (4.3.5) being replaced by the volume integral of the filter in the $\boldsymbol{k}$-domain, divided by $(2\pi)^3$. Thus, by dividing the peak amplitude by $(2\pi)^{-3}$ times the volume of the filter, we can extract A. Similar "volume of the filter" scaling factors will appear in all of the examples we present in this chapter.

Exercises

4.1 Verify equation (4.3.4).
4.2 Verify equation (4.3.5).

4.3.2 Aperture-Limited Inversion of a Singular Function (a Reflecting Plane)

The simple aperture-limited Dirac delta function example of the previous section is not a good model for reflector imaging. In Chapters 2 and 3, we found that the output of our modified inversion operators for the reflectivity, $\beta(\boldsymbol{x})$, yielded the bandlimited singular function of the reflector surface, scaled by the specular reflection coefficient, R. Recall that the singular function of a surface is a delta function with support on the surface. The image of the reflector is described, therefore, as a bandlimited singular function with peak amplitude delineating the reflector surface. Thus, the aperture-limited Fourier inversion of singular functions is of great interest in the seismic inverse problem.

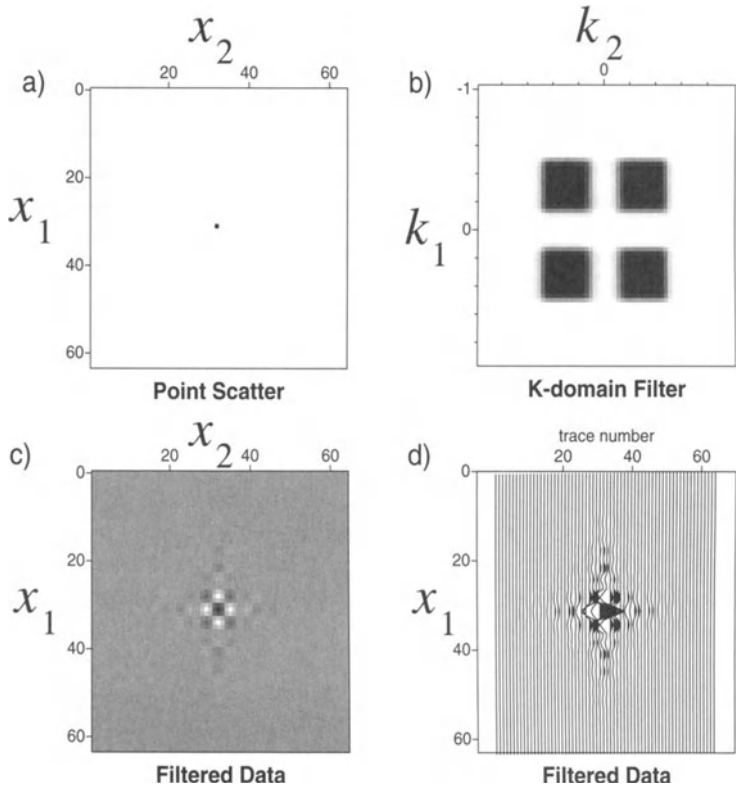

FIGURE 4.11. a) A point scatter in two dimensions. b) A boxlike domain in the (k_1, k_2)-plane, which excludes the origin and the k_1 and k_2 axes. c) An image plot of the spike data with this filter applied. d) Seismic wiggletrace representation of the same output.

The simplest example of a reflector is a horizontal planar surface located at a specific depth, say, x_{30}. Mathematically, we would represent such a reflector as

$$f(\boldsymbol{x}) = A\delta(x_3 - x_{30}). \tag{4.3.6}$$

Unlike the point scatter example of the previous section, this delta function has as its support the entire plane, defined by $x_3 = x_{30}$.

We assume that $D_{x'}$ includes this plane and that D_k includes $k_1 = k_2 = 0$ (that is, that some part of the k_3-axis). Finally, to characterize the bandlimited nature of the problem, we let the intersection of D_k with the k_3-axis include the intervals defined by

$$k_{3-} \leq |k_3| \leq k_{3+}. \tag{4.3.7}$$

The value $k_3 = 0$ is excluded, consistent with the assumption that zero-frequency information is not present in seismic data and, hence, neither is the point $\boldsymbol{k} = \mathbf{0}$. Now, in (4.3.1), we use the fact that

$$\frac{1}{2\pi}\int_{D_k} dk \int_{-\infty}^{\infty} dx' e^{ik(x-x')} = \int_{D_k} dk\, \delta(k) = 1,$$

to carry out the integrations in x_1' and x_2'. Here, the last equality uses the fact that $k_1 = k_2 = 0$ is in D_k for some range of values of k_3. Now, the delta function in the third spatial variable allows us to carry out that integral to obtain

$$I(\boldsymbol{x}) = \frac{A}{2\pi}\int_{k_{3-}\le|k_3|\le k_{3+}} e^{ik_3(x_3-x_{30})}dk_3 = A\frac{\sin\left[k_3(x_3-x_{30})\right]}{\pi(x_3-x_{30})}\Bigg|_{k_3=k_{3-}}^{k_3=k_{3+}}. \tag{4.3.8}$$

As in the previous example, if we knew in advance that $f(\boldsymbol{x}')$ was proportional to the singular function of a surface, then both the support and the peak amplitude of the singular function could be determined from the aperture-limited data by dividing out the scaling factor containing the volume of the filter in the $\boldsymbol{k}$-domain.

If, however, the aperture D_k does not contain a segment of the k_3-axis (assuming $D_{x'}$ covers all space) then $I(x) = 0$! Clearly nothing could be ascertained about the support or amplitude of the singular function from the aperture-limited output in this case. (The case of $D_{x'}$ having finite coverage will be examined in the exercises below.) It should be noted that the direction (0,0,1) of this distinguished line segment is also the direction of the vector normal to the support surface of the singular function, meaning that our inversion formula must contain this normal direction if it is to

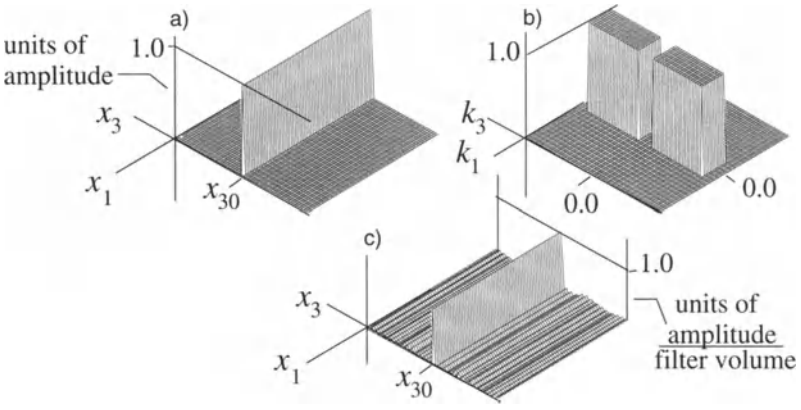

FIGURE 4.12. a) Synthetic data representing the singular function of the line $x = 0$. b) The k-domain containing the direction normal to $x = 0$. c) The inversion of the data using this k-domain *aperture*.

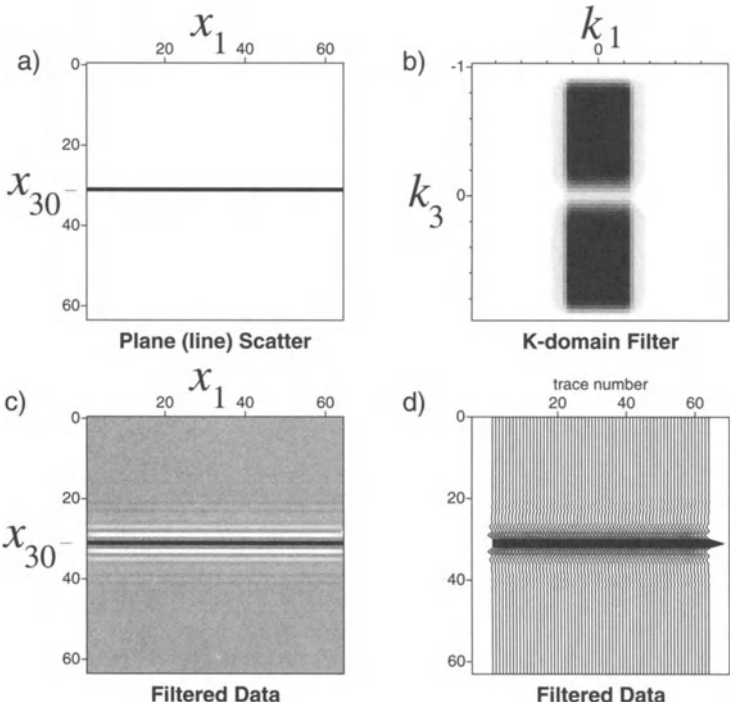

FIGURE 4.13. a) A line scatter in two dimensions. b) A rectangular domain in the (k_1, k_2)-plane, which includes the direction normal to the line scatter. c) An image plot of the line scatter data with this filter applied. d) Seismic wiggletrace representation of the same output.

image the plane. This is consistent with the prediction made in Section 4.2 above.

It is important to recognize that the choice of vertical as the "distinguished direction" for this example is totally arbitrary. If $f(\boldsymbol{x}')$ were chosen to be the singular function of a plane with some other orientation, then the distinguished direction in D_k would lie along the normal direction to that plane, instead. Because D_k is symmetric, it must have an angular range (think of this as a bundle of rays) containing the direction of the two normals $(\pm\hat{\boldsymbol{n}})$ of the given plane. Otherwise, the aperture-limited Fourier inversion will yield a zero result. This dependence of the inversion on nonzero data in the normal direction was demonstrated analytically in two dimensions in Exercise 3.5. In examples below, we will continue to choose vertical as the distinguished direction of the normal, and it will remain the vertical direction that will have to be included in the domain D_k.

The phenomenon described in the paragraph above is demonstrated graphically in two dimensions in Figures 4.12a–c and 4.14a–c. Figure 4.12a shows the singular function of the line $x = 0$, whereas Figure 4.12b shows the k-domain D_k to be used for inversion. Note that this domain includes the normal direction to the line, $x = 0$—"the reflector dip"—of Figure 4.12a. Figure 4.12c shows the aperture-limited inversion. (See Figure 4.13 for a seismic-style plot of similarly filtered data.) The aperture-limited singular function adequately identifies the original function.

Figure 4.14a depicts another k-domain, D_k, for inversion of the same data. Note that this domain does *not* include the reflector dip—normal direction to the line, $x = 0$—although, on a percentage basis, it is much larger than the previous domain. Figure 4.15b is a plot of the aperture-limited inversion for this domain, D_k, on the same scale as Figures 4.12a and 4.12c. Figure 4.14c shows the same output, scaled up by six orders of magnitude. This example demonstrates the necessity of including the dip direction of a surface in the $\boldsymbol{k}$-domain, if the singular function of the surface is recoverable from aperture-limited data.

Exercises

4.3 Repeat the calculation in the previous exercise, assuming that $D_{x'}$ is finite and the wavenumber domain aperture is given by

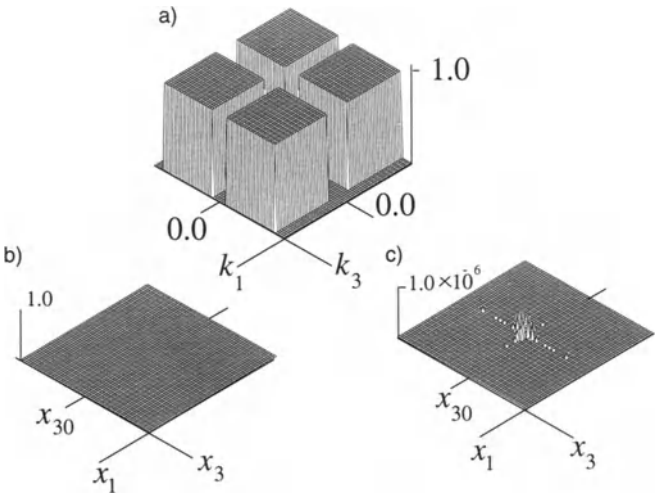

FIGURE 4.14. a) The k-domain excluding the direction normal to $x = 0$. b) The inversion of the data in Figure 4.1a using this k-domain *aperture*. c) The same output as in b), scaled up 6 orders of magnitude.

$$D_k: \quad |k_{j-}| \leq |k_j| \leq |k_{j+}|, \quad j = 1,2,3,$$

that is, that the origin of the $\boldsymbol{k}$-domain is excluded. Show that the result is

$$I(\boldsymbol{x}) = A \frac{k_3 \operatorname{sinc}\left[k_3(x_3 - x_{30})/\pi\right]}{\pi^3}\Bigg|_{k_3=k_{3-}}^{k_3=k_{3+}} \cdot \int_{D_{x'}} d^2x' \left[\prod_{j=1}^{2} k_j \operatorname{sinc}\left[k_j(x_j - x_j')/\pi\right]\Bigg|_{k_j=k_{j-}}^{k_j=k_{j+}}\right].$$

a. Use the 2D version of this expression to explain the small signal seen in Figure 4.14c. Hint: consider the integral of a sinc function to be a bandlimited signum function, with height from zero equal to 1.56223. You may find a symbolic math package helpful for this problem.

4.3.3 Generalization to Singular Functions of Other Types of Surfaces—Asymptotic Evaluation

In the previous sections we saw there is a strong relationship between the normal direction to a plane surface in the $\boldsymbol{x}$-domain and the corresponding direction in the $\boldsymbol{k}$-domain. In particular, we saw that it was necessary to include in D_k the $\boldsymbol{k}$-vector oriented in the direction normal to the plane surface for the image of the plane to be represented by the aperture-limited inversion formula. In the discussion in Section 4.4 we will show that this property persists in the "large-wavenumber limit," when the problem is generalized to that of imaging an arbitrary surface

The first thing we need to do is to define, in a more mathematically formal manner, what we mean by a singular function of a surface. Informally, this is a Dirac delta function of an argument, say s, that measures signed-distance from the surface, so that the support of the delta function is the surface, itself. A more formal definition of a distribution, such as what we desire here, requires that we define the distribution in terms of its action on an appropriate class of test functions (see Appendix A). Therefore, let us define $\gamma(\boldsymbol{x})$ to be the singular function of a surface by taking it to be a distribution having the property that

$$\int_{-\infty}^{\infty} \gamma(\boldsymbol{x}) G(\boldsymbol{x}) d^3x = \int_{S_\gamma} G(\boldsymbol{x}) dS, \tag{4.3.9}$$

for any function $G(\boldsymbol{x})$ that is a member of some appropriate class of test functions. On the right side, S_γ is the support surface of the distribution, $\gamma(\boldsymbol{x})$. The idea is to apply the same aperture-limited Fourier inversion process used in the example of the flat horizontal reflector to the more general singular function. In this way we hope to be able to determine

what parts of the $\boldsymbol{k}$-domain must be present for the singular function of this general surface to be correctly reconstructed.

It is not as easy to compute the results in the general case as it was in the case of a horizontal plane reflector, however. We will be forced to use asymptotic methods to compute an approximate solution to the problem. Because the asymptotic method we will employ is the method of stationary phase, we must recognize a "large parameter" in the formulation. As with the integrals that were evaluated in Chapter 3, the large parameter must compare the wavelength, $2\pi/|\boldsymbol{k}|$, of the waves with the natural length scale of the target being imaged.[2] The minimum wavenumber, $K \equiv \min|\boldsymbol{k}|$, describes the maximum *wavelength* available to image the surface. The principal radii of curvature of S_γ represent the natural length scale of the target being imaged. If L represents the minimum radius of curvature of S_γ, then the product KL is the desired parameter. If we choose $f(\boldsymbol{x}) \equiv \gamma(\boldsymbol{x})$ in (4.3.1), then $KL \gg 1$ will specify the "large-wavenumber" condition.[3]

As we saw in Exercise 3.20 and the discussion following that exercise, the formal large parameter is not the entire story, but only a starting point [Bleistein and Handelsman, 1986]. The eigenvalues of the Hessian—the matrix of second derivatives of the phase—evaluated at the stationary point will also become multipliers of the parameter that ultimately must be large in order that the asymptotic expansions we generate be valid. Nonetheless, we will concentrate on KL and describe *relative* orders of magnitude in terms of this dimensionless parameter.

Order Estimates of Asymptotic Singular Functions

Here is an outline of the results we show below, expressed in dimensionless variables. An asymptotic expansion of $I(\boldsymbol{x})$ will approximate $\gamma(\boldsymbol{x})$ in the following sense. Over most of the $\boldsymbol{x}$-domain, $\gamma(\boldsymbol{x})$ is at most $O(1)$ in KL. However, for some points $\boldsymbol{x}$ on S_γ, $I(\boldsymbol{x})$ is $O(KL)$. At any of these special points, the normal to S_γ defines a direction that is contained in the aperture D_k. In fact, near S_γ, along each line normal to S_γ, $I(\boldsymbol{x})$ is asymptotically a bandlimited delta function, as depicted in Figure 3.6. More precisely, it is the inverse single-variable Fourier transform of the filter in the k-domain along those special directions.

At points on S_γ for which the normal direction defines angles that are not in the angular aperture of $\boldsymbol{k}$-domain, $I(\boldsymbol{x})$ is $O((KL)^{1/2})$ or smaller in KL. Thus, S_γ is imaged only at those points for which its normal is in a direction that is included in the family of directions of $\boldsymbol{k}$-vectors in the domain D_k. See the discussion of Section 4.2.

---

[2]This wavelength relates back to the underlying physical problem that we have studied through the relationship $|\boldsymbol{k}| = 2|\omega|/c$.

[3]Note that this is just our original Rayleigh criterion, $2\pi fL/c \gg 1$, expressed in terms of wavenumber instead of frequency.

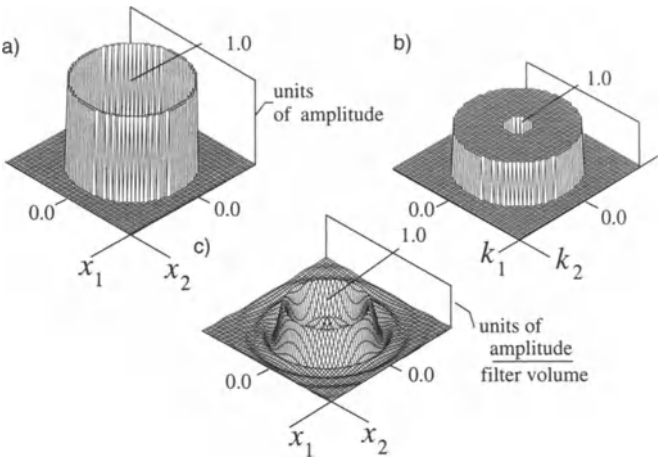

FIGURE 4.15. a) Synthetic data representing the singular function of a circle. b) A k-domain of unrestricted angular aperture, but of restricted magnitude. c) Inversion of the data in a), with the integration range of b).

In the language of asymptotic expansions of integrals, the critical points of the multidimensional Fourier integral are points for which $\boldsymbol{x}-\boldsymbol{x}'$ is normal to S_γ and $\pm\boldsymbol{k}$ lies along the normal. Near S_γ, $I(\boldsymbol{x})$ is a bandlimited delta function whose argument is normal distance to S_γ, provided such critical points are in the domain of integration, $D_x \times D_k$. In this sense, the aperture-limited Fourier inversion provides a partial and approximate reproduction of the distribution $\gamma(\boldsymbol{x})$, with peak amplitude in known proportion to the area under the filter in the k-domain along a particular ray.

We remark, further, that our inversion problems will, in general, have more than one reflector. Hence, $I(\boldsymbol{x})$ will represent a *sum* of singular functions. In order to distinguish these, one from another, *another* length scale—the distance between reflectors—will have to be "large," as well—say, again, $kL \gg 1$, for L the minimum separation between reflectors.

In summary, L will have to be taken to be the minimum among all such length scales in the problem.

The more general case is demonstrated in Figures 4.15a–c (again, in two dimensions). Figure 4.15a depicts the singular function of a circle. Figure 4.15b depicts a k-domain, D_k, in which the angle of $\boldsymbol{k}$ is not restricted, but its magnitude is. Figure 4.15c is the inversion, showing an aperture-limited Dirac delta function along every radial line (every normal to the original curve). Figure 4.16a shows an alternative k-domain, D_k, for which the direction of $\boldsymbol{k}$ is restricted as well. Figure 4.16b shows the inversion. Here, the singular function is adequately defined only for the normal to the circle in the angular aperture of D_k and the output falls off strongly to zero outside of that angular aperture. There is a transition zone that crosses the angular boundary of the $\boldsymbol{k}$-domain boundary. In that transition zone,

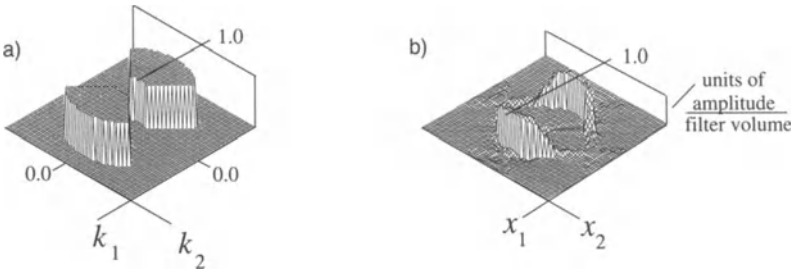

FIGURE 4.16. a) Alternate k-domain restricted both in angle and magnitude. b) The inversion of the data in Figure 4.15a using the restricted aperture in Figure 4.16a.

there is strong interaction of the contribution from the stationary point that produces the delta function and the next order contribution to the asymptotic expansion, arising from the endpoint of integration in the angular direction in $\boldsymbol{k}$. That first derivative appears in the denominator of that contribution and it becomes small as the nearby stationary point approaches the endpoint. When the stationary point is "near enough," the asymptotic expansion in terms of a separate stationary point contribution and an endpoint contribution is invalid. Right at the endpoint, the leading order asymptotic expansion is given by half of the interior stationary point formula. To describe the transition zone adequately, a uniform asymptotic expansion for a stationary point near an endpoint is required.

Exercises

4.4 Let $\gamma(\boldsymbol{x})$ be the singular function of a spherical shell of radius r_0. Show that $\gamma(\boldsymbol{x})$ may be represented by $\delta(r - r_0)$ in spherical coordinates. To do this, you will need to show that the following equality holds:

$$\int_{-\infty}^{\infty} \gamma(\boldsymbol{x}) G(\boldsymbol{x}) d^3x = \int_{S_\gamma} G(\boldsymbol{x}) dS,$$

where S_γ is a spherical shell and $G(\boldsymbol{x})$ is an appropriately chosen test function.

4.5 Let $f(\boldsymbol{x}) = A\gamma(\boldsymbol{x})$, in equation (4.3.1). Show that for the case where $D_{x'}$ includes the support of $\gamma(\boldsymbol{x})$ and when D_k is of infinite extent,

$$I(\boldsymbol{x}) = A\gamma(\boldsymbol{x}).$$

That is, show that the full aperture inversion reconstructs the singular function exactly.

4.6 Let the magnitude of $\boldsymbol{k}$-domain be the annulus $k_- \leq k \leq k_+$, where $k = |\boldsymbol{k}|$. Show that the Fourier inversion of a spherical shell of radius r_0 using this annular aperture is

$$I(\boldsymbol{x}) = \frac{A}{2\pi}\frac{r_0}{r}\left[k\,\mathrm{sinc}\,[k(r-r_0)/\pi] - k\,\mathrm{sinc}\,[k(r+r_0)/\pi]\right]\Bigg|_{k=k_-}^{k=k_+}.$$

Here $r \equiv |\boldsymbol{x}|$.

4.7 (*We intend that this question be used as a point of departure to allow the instructor to bring material in from sources other than our text. It is not necessarily an assignment for students, as is.*) The purpose of this exercise is to answer the following comprehensive exam–type question:

> You are standing at the latitude of the Tropic of Cancer at local noon on the 21st of June. Sketch the representation in $\boldsymbol{k}$-domain of the light that you see coming from the Sun, assuming that the intervening medium has a constant wavespeed and that wave propagation is adequately described by high-frequency asymptotics.

Warning: this is a *thought* experiment. Never look at the Sun!

> Hints: The Sun is directly overhead on this date and appears as a disk in the sky, which subtends an angle of approximately $\frac{1}{2}$ degree. The wavefield emanated from a surface is, in the high-frequency approximation, the Fourier transform of the singular function of that surface, so the wavefield emanated from the Sun is a bandlimited representation of the Fourier transform of the singular function representing the Sun's surface.
>
> We can see why this is so by recalling that ray vectors are identified with wavevectors in the high-frequency approximation. The angular range of the wavenumber domain of the light we see from the Sun is thus given by the angular range of the solar disk. The frequency spectrum of the Sun, and the response of the human eye have certain minimum and maximum frequency values. These, together with the fact that under the high-frequency approximation the magnitude of the wavenumbers is given by $|k| \sim |\omega|/c$, give us the range of magnitudes of the wavenumbers.
>
> Given the ranges of angles and magnitudes of the wavenumbers that we see emanating from the Sun, combined with the fact that the wavenumber domain representation must be symmetric for real values in the spatial domain we can complete the description of the desired wavenumber domain.
>
> For high-frequency waves, the lens of the eye performs a 2D spatial Fourier transform, which is why we see the Sun as a disk!

4.3.4 Relevance to Inverse Scattering

The last example of the previous section has relevance to inverse problems. The surface S_γ could be a reflector, meaning that determination of $\gamma(\boldsymbol{x})$ from aperture-limited Fourier data constitutes mathematical imaging of the reflector. In practice, the singular function of the surface might also be multiplied by a reflection coefficient that is a function of $\hat{\boldsymbol{k}}$. As noted above, $\hat{\boldsymbol{k}}$ is collinear with the normal to S_γ and is therefore also fixed. In Section 4.4, a straightforward method for computing this critical value of $\hat{\boldsymbol{k}}$ is presented. Because of subtleties of the dependence of the reflection coefficient on $\hat{\boldsymbol{k}}$ in applications, the reflection coefficient that is determined need not be the *normal-incidence* reflection coefficient.

4.3.5 Aperture-Limited Fourier Inversion of Smoother Functions

Following are examples of the aperture-limited Fourier inversion of functions that are smoother than those in the previous examples, which involved distributions. By "smoother" we mean a condition on differentiability. A step function is one derivative smoother than a delta function because differentiating a step yields a delta function. A ramp function is two orders smoother than a delta function, and so forth. An infinitely differentiable function may therefore be thought of as being infinitely smooth.

In situations where the function $f(\boldsymbol{x}')$ is related to a wavespeed profile, or the perturbation in a wavespeed, it is typical to think in terms of piecewise-smooth functions whose discontinuity surfaces represent reflectors. Here, it is reasonable to consider a smooth function with support on some domain $D_{x'}$. Note that the $f(\boldsymbol{x}')$ does not necessarily vanish on the boundary of $D_{x'}$. A piecewise-smooth function can then be reconstructed as a "patchwork quilt" of functions of this type.

It will be shown in Section 4.4 that, for smooth functions that are nonzero only in a finite domain, the asymptotic expansion of $I(\boldsymbol{x})$ for large wavenumber is dominated by the boundary values of $f(\boldsymbol{x}')$ at certain critical points, that is, by the value of $f(\boldsymbol{x}')$ on its discontinuity surface(s). In fact, the critical points are exactly those described in the context of the surface S_γ in the previous example, where S_γ is the boundary surface of $D_{x'}$ in this context.

4.3.6 Aperture-Limited Fourier Inversion of Steplike Functions

As a first example of a piecewise-smooth function, consider the box function

$$f(\boldsymbol{x}) = \begin{cases} A, & L \leq x_3 \leq 2L, \\ 0, & \text{otherwise.} \end{cases} \tag{4.3.10}$$

Assume that $D_{x'}$ contains the support of $f(\boldsymbol{x}')$ and that D_k contains some segment of the k_3-axis, that is, some segment of the line, $k_1 = k_2 = 0$. Call that intersection D_3. This function is to be substituted into (4.3.1). Observe that

$$\frac{1}{2\pi}\int\int dx'\, dk\, e^{ik(x-x')} = \int dk\, \delta(k) = 1$$

and use this result to carry out the four integrations in x_1', k_1, x_2', k_2. Then, for the remaining integrals,

$$\begin{aligned} I(\boldsymbol{x}) &= \frac{A}{2\pi}\int_{D_3} dk_3 \int_{L\le x_3'\le 2L} e^{ik_3(x-x')}dx_3' \\ &= \frac{A}{2\pi}\int_{D_3}\frac{dk_3}{ik_3}\left[e^{ik_3(x_3-L)} - e^{ik_3(x_3-2L)}\right]. \end{aligned} \tag{4.3.11}$$

The integral here can be recognized as a difference of bandlimited step functions that define the support of the function $f(\boldsymbol{x})$. Furthermore, the dominant value of $\hat{\boldsymbol{k}}$ here is (0,0,1), which is normal to the boundary of the support domain. (For curved surfaces, the normal would not be a constant vector, nor would the distinguished value of $\hat{\boldsymbol{k}}$ be a constant.)

As discussed in Chapter 2, step functions are not easily reconstructed from bandlimited data that do not contain zero-frequency (or, in this case, zero-wavenumber) information. We could not extract the height of the step in those bandlimited cases. Thus, for example, it would be difficult to estimate the value of A at interior points of D_x, or to locate the boundary of this domain from $I(\boldsymbol{x})$, under the assumption of aperture-limited large-wavenumber data.

Recall that, in applications, it is the aperture-limited Fourier transform of $f(\boldsymbol{x})$ that is known. The specific Fourier inversion kernel to be employed is not a priori specified. Determination of the amplitude A and the discontinuity surfaces of $f(\boldsymbol{x})$ can be facilitated by introducing a new form of the Fourier-like integral equation

$$\bar{I}(\boldsymbol{x}) = \frac{1}{2\pi}\int_{D_k} ik\,\mathrm{sgn}\,(\hat{\boldsymbol{u}}\cdot\hat{\boldsymbol{k}})d^3k \int_{D_{x'}} d^3x' f(\boldsymbol{x}')e^{i\boldsymbol{k}\cdot(\boldsymbol{x}-\boldsymbol{x}')}, \tag{4.3.12}$$

which differs from our original operator only in that a factor of $ik\,\mathrm{sgn}\,(\hat{\boldsymbol{u}}\cdot\hat{\boldsymbol{k}})$ has been introduced in the integrand.[4]

In equation (4.3.12), $\hat{\boldsymbol{u}}$ is a constant vector. In practice, there is usually at least one plane through the origin on which there is little or no data. The

[4]This modification is based on an idea proposed by Bojarski [1967,1968,1982] and has evolved through a series of papers: Mager and Bleistein [1978], Cohen and Bleistein [1979], and Bleistein, [1984]. See also Armstrong [1978] for a related discussion.

vector $\hat{\boldsymbol{u}}$ would be chosen as the normal to this plane. For example, if there were no information about planes perpendicular to the x_3-axis (vertical planes), then, correspondingly, the Fourier transforms of such functions would be of no interest in directions with $k_3 = 0$. In this case, we could set $\hat{\boldsymbol{u}} = (0, 0, \pm 1)$, so that $\operatorname{sgn}(\hat{\boldsymbol{u}} \cdot \hat{\boldsymbol{k}}) = \pm \operatorname{sgn} k_3$. The ambiguity of this function, then, would occur only in a region that is of no interest. The effect of the factor $\operatorname{sgn}(\hat{\boldsymbol{u}} \cdot \hat{\boldsymbol{k}})$ is to make the complete multiplier $ik \operatorname{sgn}(\hat{\boldsymbol{u}} \cdot \hat{\boldsymbol{k}})$ of opposite sign in the two halfspaces defined by the plane through the origin with normal $\hat{\boldsymbol{u}}$. In Section 4.4, we show the somewhat surprising result that, asymptotically, this multiplier produces a normal derivative of $f(\boldsymbol{x}')$ on the boundary surface (the discontinuity surface of $f(\boldsymbol{x}')$), multiplied by $\operatorname{sgn}(\hat{\boldsymbol{u}} \cdot \hat{\boldsymbol{n}})$—$\hat{\boldsymbol{n}}$, a surface normal—*even though the normal direction at each point on the boundary is not known a priori.*

As noted in Section 4.2, in our application of inverting zero-offset seismic data assuming a constant-background wavespeed, $\boldsymbol{k} = 2\omega \hat{\boldsymbol{r}}_0 / c_0$, in which case, $2\omega/c_0 = \pm k$, depending on the sign of ω. Thus, this multiplier that we used in Chapter 3 has exactly the desired property of being positive over half of the $\boldsymbol{k}$-domain ($\omega > 0$) and negative over the other half of the $\boldsymbol{k}$-domain ($\omega > 0$). Note that in the asymptotic analysis of the application of our inversion to Kirchhoff-approximate data, we found that $\hat{\boldsymbol{r}}_0$ was collinear with $\hat{\boldsymbol{n}}$, so that no sign ambiguity arises in the implementation; we care only about $\boldsymbol{k}$ values around the normal direction to the reflector! We will see in the following chapters that this will generalize to data collected with nonzero source-receiver offset, and to variable-wavespeed media as well, in a natural manner. As an indication of what is in store, we point out here that for the nonzero offset, constant-background case, our "normal derivative" filter will merely generalize to $\omega |\hat{\boldsymbol{r}}_s + \hat{\boldsymbol{r}}_g| / c_0$ and will have exactly this same property of being positive on half of the $\boldsymbol{k}$-domain and negative over the other half.

Thus, we view the effect of multiplication by $ik \operatorname{sgn}(\hat{\boldsymbol{u}} \cdot \hat{\boldsymbol{k}})$ as replacing the Fourier inversion of $f(\boldsymbol{x}')$ by the Fourier inversion of the singular function(s) of its boundary surface(s), appropriately scaled. For the specific example under discussion here, at the same level of computation as is implied by (4.3.12), the new operator has an additional factor in the numerator of $i|k_3| \operatorname{sgn}(\hat{\boldsymbol{u}} \cdot \hat{\boldsymbol{k}}) = ik_3 \operatorname{sgn}(u_3)$, (Note that, for this example, $k_1 = k_2 = 0$ and $k = |k_3|$.) Here,

$$\bar{I}(\boldsymbol{x}) = \frac{A \operatorname{sgn} u_3}{\pi} \left[\frac{\sin[k_3(x_3 - L)]}{x_3 - L} - \frac{\sin[k_3(x_3 - 2L)]}{x_3 - 2L} \right] \Bigg|_{k=k_{3-}}^{k_3=k_{3+}} \tag{4.3.13}$$

$$\text{where} \quad |k_{3-}| \leq |k_3| \leq |k_{3+}|.$$

It is apparent that $\bar{I}(\boldsymbol{x})$ is a difference of bandlimited delta functions that peak on the boundary surfaces of D_x. The two delta functions will be distinguishable, which is to say, well separated in the output, as long as $k_3 L$

is "large enough" for "most" of the bandwidth. More simply, if $K \equiv \min |\boldsymbol{k}|$, we require that $KL \gg 1$ for the two delta functions to be well separated and distinguishable.

The peak values of $\bar{I}(\boldsymbol{x})$ are given by the expressions

$$\bar{I}(L) = \frac{A \operatorname{sgn}(u_3)}{\pi} \left[|k_{3+}| - |k_{3-}| - \frac{\sin[k_3 L]}{L} \Big|_{k=k_{3-}}^{k_3=k_{3+}} \right]$$
$$= \frac{A \operatorname{sgn}(u_3)}{\pi} \left[|k_{3+}| - |k_{3-}| \right] \left[1 + O((|k_{3-}|L)^{-1}) \right]$$

and

$$\bar{I}(2L) = -\frac{A \operatorname{sgn} u_3}{\pi} \left[|k_{3+}| - |k_{3-}| - \frac{\sin[k_3 L]}{L} \Big|_{k=k_{3-}}^{k_3=k_{3+}} \right]$$
$$= \frac{A \operatorname{sgn}(u_3)}{\pi} \left[|k_{3+}| - |k_{3-}| \right] \left[1 + O((|k_{3-}|L)^{-1}) \right].$$

For $k_{3\_}L \gg 1$, we can neglect the second term here. This follows the line of discussion in Section 4.3.3. We then obtain the approximate results,

$$\bar{I}(L) \approx \frac{A \operatorname{sgn}(u_3)}{\pi} \left[|k_{3+}| - |k_{3-}| \right], \quad \bar{I}(2L) \approx -\frac{A \operatorname{sgn}(u_3)}{\pi} \left[|k_{3+}| - |k_{3-}| \right]. \tag{4.3.14}$$

Henceforth in this chapter, we will no longer distinguish results of this latter type as being "approximate;" all of our estimates are asymptotic with this type of error in them. Thus, the modified operator (4.3.12) produces a result from which the boundary surfaces and the amplitude of the discontinuity of $f(\boldsymbol{x}')$ across them are more readily determined than from the ordinary Fourier inversion in (4.3.1).

It should be noted that for this example, as for the previous one, if the aperture D_k did not contain some segment of the line $k_1 = k_2 = 0$, then $I(\boldsymbol{x}) = 0$, asymptotically *to this order*. Again, this line in the k-domain is in the direction of the normal to the boundary of D_k.

Exercises

4.8 Verify equation (4.3.13).

4.3.7 Aperture-Limited Fourier Inversion of a Ramplike Function

We expect ramplike functions to be an order smoother than steplike functions, in terms of differentiability. Correspondingly, the next example will

show two additional features of aperture-limited, large-wavenumber Fourier inversion. Consider the function

$$f(\boldsymbol{x}) = \begin{cases} A(1 - x_3/L), & 0 \le x_3 \le L \\ 0, & \text{otherwise.} \end{cases} \tag{4.3.15}$$

with $D_{x'}$ the support of $f(\boldsymbol{x}')$ being unbounded in all variables.

The integrations in x_1', k_1, x_2', k_2, are carried out in the same manner as in the previous example. In this case, that leads to the result,

$$I(\boldsymbol{x}) = \frac{A}{2\pi} \int_{D_3} \frac{dk_3}{ik_3} \left[e^{ik_3 x_3} + \frac{1}{ik_3 L} \left[e^{ik_3(x_3 - L)} - e^{ik_3 x_3} \right] \right]. \tag{4.3.16}$$

If D_3 were the entire line, then the Fourier transform of the first exponential would be a step with support $x_3 > 0$. The next two terms, which correct this step to produce the appropriate finite ramp, are lower order, $O(1/k_3 L)$, for large-wavenumber aperture-limited data. Note that a phase depending on the difference $x_3 - L$ arises only in this lower-order term. The reason for this is that the function defined by (4.3.15) is continuous at $x_3 = 0$.

From aperture-limited large-wavenumber data we cannot reasonably expect to detect the lower order, $O(1/k_3 L)$, contribution to the Fourier transform of $f(\boldsymbol{x}')$. We can only expect to see the leading-order term. To leading order, then, $I(\boldsymbol{x})$ is a bandlimited step function with discontinuity on the discontinuity surface of $f(\boldsymbol{x}')$ and amplitude equal to the amplitude of the discontinuity of $f(\boldsymbol{x}')$. As above, we could use the operator $\bar{I}(\boldsymbol{x})$, defined by (4.3.12), to more easily detect the location of this discontinuity surface and the value A.

Of course, it is possible to use another operator, with multiplier, $[ik \operatorname{sgn}(\hat{\boldsymbol{u}} \cdot \hat{\boldsymbol{k}})]^2 = -k^2$, to detect the jump in the first derivative of $f(\boldsymbol{x}')$. This is equivalent to applying the Laplacian operator to the data. Applying a Laplacian as an "edge-sharpening" operator has a long history in image processing, but is less useful in seismic data processing.

While this will work for synthetic seismic examples, applying a Laplacian would be considerably less reliable with field data and "many" discontinuity surfaces of $f(\boldsymbol{x}')$ and its derivatives. If we had a discontinuity with a known order of smoothness, then it would be profitable to pursue such constructions however, in the absence of a priori information about the smoothness of discontinuities, applying such a formula would be an ad hoc construction, at best. In Earth science, we have little information regarding the order of smoothness of wavespeed discontinuities.

Exercises

4.9 Verify equation (4.3.16).

4.3.8 *Aperture-Limited Inversion of an Infinitely Differentiable Function*

Above, we discussed the cases of discontinuities of finite orders of smoothness, which we relate to finite orders of differentiability. The limiting case of smoothness is infinite smoothness, which implies infinite differentiability. In Exercise 2.15, it was seen that for functions that were infinitely differentiable, their asymptotic expansion was smaller than any inverse power of the large parameter. Here, in the current context, we provide a specific example for which the decay is actually of *exponential* order in the large parameter. That function is defined by

$$f(\boldsymbol{x}) = \begin{cases} 0, & x_3 \leq 0, \\ \sqrt{L/x_3}\exp\left[-L/x_3\right], & x_3 > 0. \end{cases} \tag{4.3.17}$$

We have chosen this somewhat exotic function for this example because we can carry out the details of the calculations in a fairly straightforward manner, to make our point.

Assume that $D_{x'}$ is all space and that D_k is composed of two symmetric domains, as usual, containing segments of the line, $k_1 = k_2 = 0$. As in the previous examples, after integrating in all of the variables except k_3 and x_3' , $I(\boldsymbol{x})$, as defined by (4.3.1), is given by

$$I(\boldsymbol{x}) = \frac{1}{2\pi}\int_{D_3} dk_3 \int_0^\infty dx_3' \sqrt{\frac{L}{x_3'}} e^{ik_3(x_3 - x_3') - L/x_3'},$$

with D_3 the restriction of D_k to the k_3-axis, that is, for the dual range, $k_{3-} \leq |k_3| \leq k_{3+}$. The integration in x_3' can be obtained by using results about the modified Bessel function to be found in Watson [1980] or Abramowitz and Stegun [1965]. Because the details of this derivation are not important to the present discussion, we simply state the result after calculating that integral:

$$I(\boldsymbol{x}) = \frac{L}{\sqrt{\pi}}\int_{D_3} \frac{dk_3}{\eta} e^{[-\eta + ik_3x_3]}. \tag{4.3.18}$$

In this equation,

$$\eta \equiv \sqrt{|k_3|L}\, e^{[i\pi/4\,\mathrm{sgn}\,k_3]} = \eta\sqrt{|k_3|L}[1 + i\,\mathrm{sgn}\,(k_3)]/\sqrt{2}. \tag{4.3.19}$$

It is easy to see, now, that the integrand for each k_3, negative, is just the complex conjugate of its value for k_3, positive. Therefore, we can rewrite this integral as

$$I(\boldsymbol{x}) = 2\sqrt{\frac{2L}{\pi}}\int_{k_{3-}}^{k_{3+}} \frac{dk_3}{\sqrt{k_3}} e^{-\sqrt{k_3 L/2}} \cos\left[\sqrt{k_3 L/2} + k_3x_3 - \pi/4\right].$$

First, note that this integral is not zero for $x_3 \leq 0$. Thus, it is not likely to represent the function well on the negative half-axis. On the other hand,

the exponential decay in this integral depends only on the product $k_3 L$, whereas the exponential decay of the original function, $f(\boldsymbol{x})$ in (4.3.17), for x_3 positive, depends on x_3/L. Therefore, we should at least be suspicious about the ability of this bandlimited inverse Fourier transform to represent the original function there as well. Let us reinforce this last observation more strongly by going further with the analysis.

An upper bound on the absolute value of this last integral can be obtained by replacing the cosine by unity; that is,

$$|I(\boldsymbol{x})| \leq 2\sqrt{\frac{2L}{\pi}} \int_{k_{3-}}^{k_{3+}} \frac{dk_3}{\sqrt{k_3}} e^{-\sqrt{k_3 L/2}}.$$

Note that this integrand is an exact differential, allowing us to carry out the integration in closed form, thus obtaining

$$|I(\boldsymbol{x})| \leq -\frac{8}{\sqrt{\pi}} e^{-\sqrt{k_3 L/2}} \Bigg|_{k_{3-}}^{k_{3+}} \leq \frac{8}{\sqrt{\pi}} e^{-\sqrt{k_{3-} L/2}}.$$

Here, the last inequality is obtained by neglecting the subtraction of a positive, but smaller quantity—the upper limit evaluation—from a larger one—the lower limit evaluation.

If our aperture-limited Fourier transform were to be a good approximation of $f(\boldsymbol{x})$, then, the larger the value of $k_{3-} L$, the better this approximation should be. However, we are free to choose $k_{3-} L$ as large as we like, independent of $\boldsymbol{x}$, or more precisely, independent of x_3. Therefore, in order to show that this aperture-limited inversion does not yield a good approximation of $f(\boldsymbol{x})$, we only need to choose an x_3 for which $f(\boldsymbol{x})$ is of moderate size, and then choose $k_{3-} L$ large enough to make this last estimate of $|I(\boldsymbol{x})|$ small. Therefore, let us choose $x_3 = L$ and choose $k_{3-} L/2 = 16$, so that it is easy to take the square root. We find that

$$f(\boldsymbol{x}) = 0.37, \quad x_3 = L; \qquad |I(\boldsymbol{x})| \leq 0.083, \quad k_{3-} L = 32.$$

Of course, the bound on $|I(\boldsymbol{x})|$ will continue to decrease with increasing $k_{3-} L$, making the disagreement between $f(\boldsymbol{x})$ and $|I(\boldsymbol{x})|$ even worse.

As we will see in the next section, where we generalize the result of Exercise 2.15 to three dimensions, this is typical for infinitely-differentiable functions. The point here is that, if we are limited to "high frequency" reflection data, we should not expect to recover the smooth part of the variations of wavespeed from our data. Indeed, inversion of transmission data—tomography—is usually employed for this purpose. In the context of our approach, this is the extreme case of separated source and receiver in which the opening angle between the incident and "scattered" rays is equal to π. Even if we were to try to apply our theory, equation (4.2.7) would tell us that $|k| = 0$ and we have no bandwidth for imaging.[5]

[5] θ is half the opening angle.

Exercises

4.10 Verify equation (4.3.18).

4.3.9 Summary

Through this hierarchy of examples, our intention has been to make the following points about large-wavenumber, aperture-limited Fourier inversion.

1. Distributions with support at one point or on a surface are well approximated. However, these are less relevant to seismic imaging, as even small-volume, or point, scatterers are not accurately represented as distributions.
2. The output from functions with jump discontinuities (expected in practice) is dominated by function values on the support of the discontinuity surface(s). Even when the function is nonconstant away from the discontinuity surface, the leading-order output is an aperture-limited step function of an arclength variable normal to the discontinuity surface. Detection of the location of the discontinuity surface and the magnitude of the jump is facilitated by multiplying by a factor, $ik\,\mathrm{sgn}\,(\hat{\boldsymbol{u}}\cdot\hat{\boldsymbol{k}})$, before inverting the transform. The output is then an aperture-limited singular function of the discontinuity surface, with peak in known proportion to the magnitude of the jump. This latter result holds at each point on the discontinuity surface at which the normal to the surface is in the aperture of directions from the origin that are in D_k, the support domain of the transform variable.
3. For infinitely smooth functions, the aperture-limited Fourier inversion vanishes faster than any algebraic power of $1/k$ (for the particular example, the decay rate was actually $O(\exp\left\{-\sqrt{kL}\right\})$, making such inversion virtually useless.

In Section 4.4, the method of multidimensional stationary phase will be used to derive these results more generally.

4.4 Aperture-Limited Fourier Identity Operators

In Section 4.3 important ideas regarding aperture-limited Fourier inversion were introduced through several specific examples. In this section, integrals that generalize these ideas will be discussed. To that end, consider the integral

$$I(\boldsymbol{x}) = \frac{1}{(2\pi)^3}\int_{D_k} d^3k \int_{D_{x'}} d^3x' f(\boldsymbol{x}'/L, \hat{\boldsymbol{k}}) e^{i\boldsymbol{k}\cdot(\boldsymbol{x}-\boldsymbol{x}')}. \tag{4.4.1}$$

Here, $\boldsymbol{x}$, $\boldsymbol{x}'$, and $\boldsymbol{k}$ are three-component vectors and $\hat{\boldsymbol{k}}$ is a unit vector. (When we show the division of a vector by a scalar, remember that *each component* of the vector is divided by the scalar, hence $\boldsymbol{x}'/L \equiv (x_1'/L, x_2'/L, x_3'/L)$, denoting that each coordinate direction has the same length scale.) If the domain D_k were infinite in extent, and the function f were independent of $\hat{\boldsymbol{k}}$, then the integral, I, would just be equal to $f(\boldsymbol{x}/L)$ on D_x and zero, outside, for a broad class of functions f. This is just a simple cascade of forward and inverse Fourier transforms. The structure of the analysis, then, comes from the nature of the domain, D_k, and the additional dependence of f on $\hat{\boldsymbol{k}}$. In all of our examples, f was independent of $\hat{\boldsymbol{k}}$. In this generalization, we take f to be an *even* function of $\hat{\boldsymbol{k}}$; that is,

$$f(\boldsymbol{x}'/L, -\hat{\boldsymbol{k}}) = f(\boldsymbol{x}'/L, \hat{\boldsymbol{k}}).$$

The function f is assumed to have as many derivatives as are necessary to carry out all the differentiations in the stationary phase analysis below. For functions that are only sufficiently smooth in a piecewise manner, it is possible to decompose the domain of integration into separate domains whose boundaries include all of the discontinuities of f or the discontinuities of one of the derivatives of f with respect to $\boldsymbol{x}'$. Then, the integral over each subdomain is of the type defined here. It will be seen below that the integral depends asymptotically on the boundary values of the integrand at certain critical points. The way that the critical points are determined will make it clear that, for a sum of such integrals, the output will depend on the *jump* in the integrand across these discontinuity surfaces. Therefore, a critical point on a boundary surface for one integral will simultaneously be a critical point for the other integral sharing the same piece of boundary. The boundary values on the commonly shared portion of boundary will combine to yield the jump in the function or will yield the appropriate discontinuous derivative.

The length scale, L, is assumed to characterize the size of the derivatives of f. Hence, derivatives with respect to $\boldsymbol{y}' = \boldsymbol{x}'/L$ should be comparable in size to f itself. For convenience, the same parameter L is used to characterize the length scales of the bounding surface of $D_{x'}$. For example, L might be a "typical" principal radius of curvature or a lower bound of the principal radii of curvature for the boundary of $D_{x'}$. We know from our discussion of large parameters in Chapter 3 that, in fact, precision about what exactly is the large parameter will come through analysis of the eigenvalues of the Hessian of the phase at the stationary points.

In application to inverse scattering, the domain D_k is symmetric with respect to the origin. That is, whenever $\hat{\boldsymbol{k}}$ is in D_k, so is $-\hat{\boldsymbol{k}}$. The reason for this is that because $\boldsymbol{k}$ is proportional to a frequency, ω, $-\boldsymbol{k}$ is included in D_k whenever $+\boldsymbol{k}$ is also included. Thus, symmetry of D_k will be assumed below, although it is not essential to the analysis. As previously, we assume that D_k does not contain the origin. Let K denote the minimum distance from the origin to the domain D_k. We now introduce the dimensionless

variables

$$\boldsymbol{p} = \frac{\boldsymbol{k}}{K}, \qquad \boldsymbol{y}' = \frac{\boldsymbol{x}'}{L}, \qquad \boldsymbol{y} = \frac{\boldsymbol{x}}{L}, \qquad \text{and} \qquad \lambda \equiv KL. \tag{4.4.2}$$

(Recall that division of a vector by a scalar implies that each component of the vector is divided by the scalar.) Rewriting equation (4.4.1) in spherical coordinates yields

$$I(\lambda, \boldsymbol{y}) = \left[\frac{\lambda}{2\pi}\right]^3 \int_{D_p} p^2 dp \, \sin\theta \, d\theta \, d\phi \int_{D_{y'}} d^3y' f(\boldsymbol{y}', \hat{\boldsymbol{p}}) e^{i\lambda p \hat{\boldsymbol{p}} \cdot (\boldsymbol{y} - \boldsymbol{y}')}. \tag{4.4.3}$$

Here, (p, θ, ϕ) are the components of the $\boldsymbol{p}$ vector in spherical coordinates, with the unit vector, $\hat{\boldsymbol{p}}$, written in terms of θ and ϕ as

$$\hat{\boldsymbol{p}} = (\sin\theta\cos\phi, \sin\theta\sin\phi, \cos\theta). \tag{4.4.4}$$

The domains $D_{y'}$ and D_p are the images of $D_{x'}$ and D_k, respectively, under the scaling (4.4.2). It is important to note that the minimum distance from the origin in $\boldsymbol{p}$ to D_p is now equal to *unity*. (For the original domain D_k it was equal to K.) Evenness of the function f in $\boldsymbol{k}$ translates into evenness of this function in $\boldsymbol{p}$.

Spherical coordinates have a pathology at $\theta = 0$ and $\theta = \pi$, which has nothing to do with the multifold integration, but only to do with the choice of parameterization. This issue will have to be addressed below, by sensible orientation of the coordinate system.

The objective now is to analyze $I(\lambda, \boldsymbol{y})$ asymptotically for large λ as $\boldsymbol{y}$ varies over some domain that includes D_y. This is aperture-limited Fourier-like inversion when the aperture is such that the length scales of f and its support in the x-domain are "many" units of reciprocal wavenumber for all of the available information in the k-domain. Formally, $I(\lambda, \boldsymbol{y})$ is the asymptotic expansion of $f(\lambda, \boldsymbol{y})$ as $\lambda \to \infty$.

The product $\lambda p \geq \lambda$ appears as a "natural" large parameter in the integral. In Section 4.4.1, we will carry out the asymptotic analysis via multidimensional stationary phase in five variables, $(y_1', y_2', y_3', \theta, \phi)$. The product λp will be chosen to be the formal large parameter and the result will be an integral with respect to p that has the form of a causal Fourier transform.

4.4.1 The Significance of the Boundary Values in $D_{y'}$

Let us now look for stationary points of the integral in equation (4.4.3) in all five variables.

If we define the phase of the integrand in (4.4.3) as

$$\Phi = \hat{\boldsymbol{p}} \cdot (\boldsymbol{y} - \boldsymbol{y}'), \tag{4.4.5}$$

then the condition of stationarity will be satisfied when the gradient with respect to all five variables $(y_1', y_2', y_3', \theta, \phi)$ vanishes; that is, when

$$\nabla_{(y',\theta,\phi)}\Phi(y_1', y_2', y_3', \theta, \phi) \equiv \mathbf{0}.$$

However, we may write this gradient as

$$\nabla_{(y',\theta,\phi)}\Phi(\boldsymbol{y}', \theta, \phi) = \left(\nabla_{y'}\left[\hat{\boldsymbol{p}} \cdot (\boldsymbol{y} - \boldsymbol{y}')\right], \nabla_{(\theta,\phi)}\left[\hat{\boldsymbol{p}} \cdot (\boldsymbol{y} - \boldsymbol{y}')\right]\right). \quad (4.4.6)$$

Here, $\nabla_{y'}$ is the gradient with respect to the three variables, (y_1', y_2', y_3'), and $\nabla_{(\theta,\phi)}$ is the gradient with respect to the two variables, (θ, ϕ). Note also that, by the definition in equation (4.4.4), $\hat{\boldsymbol{p}}$ is a function of (θ, ϕ) only. The first three components of this five component vector can never be zero because $\nabla_{y'}\left[\hat{\boldsymbol{p}} \cdot (\boldsymbol{y} - \boldsymbol{y}')\right] \equiv -\hat{\boldsymbol{p}} \neq \mathbf{0}$. Therefore, because *all* of the components of the gradient must be zero for a stationary point to exist in all five variables, the gradient of Φ with respect to the full five variables cannot be zero, either. Thus, there can be no stationary points of the fivefold integral!

We can remedy this situation by recalling that the method of stationary phase is a generalization of the process creating an asymptotic series in inverse powers of λ by repetitive integration by parts. The stationary phase formula is just the first nonzero term of this series when a stationary point exists in each level of the integration by parts process. For multidimensional stationary phase, this translates into a process of repetitive applications of the divergence theorem and testing the resulting phases for stationary points. Again, the first nonvanishing term in the asymptotic series is the stationary phase formula. If there are no stationary points in the interior of the domain of integration, then the only hope for finding an asymptotic solution is that there be stationary points on some *boundary* of the domain of integration. By performing the appropriate integration by parts (application of the divergence theorem), we can replace the integral over the volume by an integral over this boundary with the hope of having stationary points in the new integral.

But what boundary? The integration that we are performing here is a fivefold integral over the combined spatial and wavenumber domain represented by the hypervolume $D_{y'} \times D_{(\theta,\phi)}$. However, only those components of the gradient that are in $D_{y'}$ fail to have zeros. Therefore, we will apply the divergence to the integral over $D_{y'}$ to create a new integral over the new domain $S_{y'} \times D_{(\theta,\phi)}$, where $S_{y'}$ is the boundary of $D_{y'}$.[6]

To do this, first rewrite the integrand as

$$f(\boldsymbol{y}', \hat{\boldsymbol{p}})e^{i\lambda p\Phi} = \frac{-1}{i\lambda p}\left[\nabla_{y'} \cdot \left[\hat{\boldsymbol{p}} f(\boldsymbol{y}', \hat{\boldsymbol{p}})e^{i\lambda p\Phi}\right] + f_1(\boldsymbol{y}', \hat{\boldsymbol{p}})e^{i\lambda p\Phi}\right],$$
$$\text{where} \qquad f_1(\boldsymbol{y}', \hat{\boldsymbol{p}}) = -\nabla_{y'} \cdot [\hat{\boldsymbol{p}} f(\boldsymbol{y}, \hat{\boldsymbol{p}})]. \quad (4.4.7)$$

When this is substituted into (4.4.3) and the divergence theorem is applied to the first term, the result is

---

[6] Even when the domain integral does not have stationary points, the boundary integral will.

$$I(\lambda, \boldsymbol{y}) = I_0(\lambda, \boldsymbol{y}) + \frac{1}{i\lambda} I_1(\lambda, \boldsymbol{y}), \tag{4.4.8}$$

with

$$I_0(\lambda, \boldsymbol{y}) = \frac{i\lambda^2}{[2\pi]^3} \int_{D_p} p \, dp \sin\theta \, d\theta d\phi \int_{S_{y'}} dS_{y'} (\hat{\boldsymbol{n}} \cdot \hat{\boldsymbol{p}}) f(\boldsymbol{y}', \hat{\boldsymbol{p}}) e^{i\lambda p \Phi},$$

$$I_1(\lambda, \boldsymbol{y}) = \left[\frac{\lambda}{2\pi}\right]^3 \int_{D_p} p \, dp \sin\theta \, d\theta d\phi \int_{D_{y'}} d^3 y' f_1(\boldsymbol{y}', \hat{\boldsymbol{p}}) e^{i\lambda p \Phi}. \tag{4.4.9}$$

In this equation, $\hat{\boldsymbol{n}}$ denotes the normal to the boundary, $S_{y'}$, of the domain $D_{y'}$. It should be noted that the integral $I_1(\lambda, \boldsymbol{y})$ is similar to the original integral, $I(\lambda, \boldsymbol{y})$, in that it is an integral over the full domain $D_{y'} \times D_p$. We can see by comparing it with (4.4.8) that it differs from the original integral by a multiplier of $1/i\lambda$. Now consider the effect of repeating this process with $I_1(\lambda, \boldsymbol{y})$. We would again obtain an integral similar to $I_0(\lambda, \boldsymbol{y})$, but multiplied by another power of $1/i\lambda$. Continuing this process recursively N times, we would obtain an asymptotic series of integrals over $S_{y'}$ with an integral over $D_{y'}$ scaled by a $1/(i\lambda)^N$ multiplier.

Thus, it is reasonable to conclude that the leading-order asymptotic expansion of I must come from the analysis of $I_0(\lambda, \boldsymbol{y})$, unless, of course, $f(\boldsymbol{y}', \hat{\boldsymbol{p}})$ were identically zero on $S_{y'}$. This last observation leads to the following result.

Lemma 4.1. *Suppose that $f(\boldsymbol{y}', \hat{\boldsymbol{p}})$ is infinitely differentiable in D_p and vanishes "infinitely smoothly" (that is, f and all of its derivatives vanish smoothly) on the boundary, $S_{y'}$. Then $I(\lambda, \boldsymbol{y})$ is asymptotically zero[7] to all algebraic orders of $1/i\lambda$.*

PROOF. In (4.4.8), $I_0(\lambda, \boldsymbol{y})$ is zero because of the assumptions on f. However, the assumptions on f are true for f_1, as well. Thus, repeat the integration by parts process and obtain another integral similar to $I(\lambda, \boldsymbol{y})$ but multiplied now by $1/(i\lambda)^2$, with an integrand f_2, which also satisfies the conditions placed on f. Repeat the process recursively and obtain any desired algebraic power of $1/i\lambda$ as a multiplier. This completes the proof. □

The point of the lemma is that the integrand has only boundary critical points and then, only if the function $f(\boldsymbol{y}', \hat{\boldsymbol{p}})$ does not vanish infinitely smoothly. This means that the *discontinuities* of f dominate the integration. (A boundary point where f does not vanish infinitely smoothly is a

[7]The example of aperture-limited inversion presented in Section 4.3.8 was a model of this kind of behavior (although, there, the conditional convergence of the Fourier transform at infinity requires a little extra effort). In that example, the decay was actually exponential in a parameter equivalent to $\sqrt{\lambda}$. In general, one can only predict "faster than algebraic" decay.

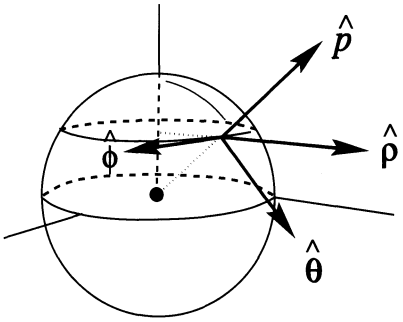

FIGURE 4.17. The polar coordinate unit vectors.

discontinuity of the function because its interior limit is not equal to its exterior limit.) Thus, the large-wavenumber, aperture-limited Fourier integral operator is not an identity operator. For functions that are infinitely differentiable inside the domain, D_p, this operator is one whose output depends only on the discontinuities of f or its derivatives (on the boundary $S_{y'}$ of $D_{y'}$) in a way that we will determine below.

4.4.2 Stationary Phase Analysis for I_0

Through the application of the divergence theorem, and by Lemma 4.1, we have determined that the leading-order asymptotic contribution will arise from the integral $I_0(\lambda, \boldsymbol{y})$, in equation (4.4.9). Again, the phase is given by (4.4.5), except that now $\boldsymbol{y}'$ is a function of two surface parameters that we will call η_1 and η_2.

Our asymptotic analysis of I_0 will, therefore, be fourfold stationary phase in the variables, η_1, η_2, θ, and ϕ. The first derivatives of Φ are given by

$$\frac{\partial \Phi}{\partial \eta_i} = -\hat{\boldsymbol{p}} \cdot \frac{\partial \boldsymbol{y}'}{\partial \eta_i}, \quad i = 1, 2, \quad \frac{\partial \Phi}{\partial \theta} = \hat{\boldsymbol{\theta}} \cdot (\boldsymbol{y} - \boldsymbol{y}'), \quad \frac{\partial \Phi}{\partial \phi} = \hat{\boldsymbol{\phi}} \cdot (\boldsymbol{y} - \boldsymbol{y}') \sin\theta, \tag{4.4.10}$$

$$\hat{\boldsymbol{\theta}} = (\cos\theta\cos\phi, \cos\theta\sin\phi, -\sin\theta), \quad \hat{\boldsymbol{\phi}} = (-\sin\phi, \cos\phi, 0).$$

Note that the vectors $\hat{\boldsymbol{\theta}}$ and $\hat{\boldsymbol{\phi}}$ are orthogonal to $\hat{\boldsymbol{p}}$. See Figure 4.17. Setting these four first derivatives equal to zero has the following geometrical interpretation. At the stationary point, $\hat{\boldsymbol{p}}$ must be orthogonal to two linearly independent tangent vectors in $S_{y'}$ in order that the two derivatives with respect to η_1 and η_2 be zero. Thus, $\hat{\boldsymbol{p}}$ and $\hat{\boldsymbol{n}}$ must be collinear or anticollinear. Note that $\hat{\boldsymbol{n}}$ is a vector in the spatial domain of the input variable $\boldsymbol{y}'$, while $\hat{\boldsymbol{p}}$ is a vector in the wave dual Fourier domain. This stationary phase condition ties together these two vectors in dual domains. Furthermore, $\boldsymbol{y} - \boldsymbol{y}'$ must be orthogonal to two linearly independent tangent vectors on the unit sphere in $\boldsymbol{p}$ at the stationary point in order that the derivatives with respect to θ and ϕ be zero. Therefore, $\hat{\boldsymbol{p}}$ and $\boldsymbol{y} - \boldsymbol{y}'$

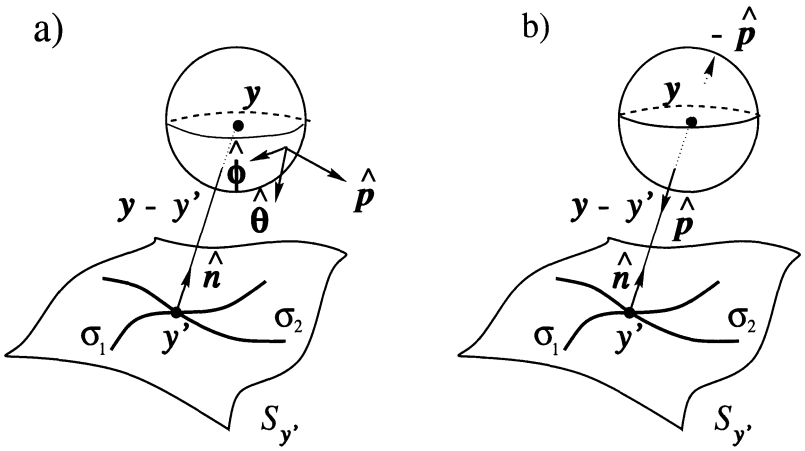

FIGURE 4.18. Geometry of stationarity. a) A point $\boldsymbol{y}'$ is chosen such that $\boldsymbol{y} - \boldsymbol{y}'$ and $\hat{\boldsymbol{n}}$ are collinear. b) The vectors $\hat{\boldsymbol{p}}$ and $-\hat{\boldsymbol{p}}$ are collinear with $\boldsymbol{y} - \boldsymbol{y}'$ and $\hat{\boldsymbol{n}}$ for all stationary points. The distinguished stationary point is at $\boldsymbol{y} = \boldsymbol{y}'$.

are collinear or anticollinear. This condition ties the output variables $\boldsymbol{y}$ to the input spatial variables $\boldsymbol{y}'$ and the Fourier variables $\hat{\boldsymbol{p}}$. In summary, $\hat{\boldsymbol{p}}$, $\hat{\boldsymbol{n}}$, and $\boldsymbol{y} - \boldsymbol{y}'$ must all line up.

Geometrically, the stationary points are determined as functions of $\boldsymbol{y}$ as follows. Given $\boldsymbol{y}$, drop a perpendicular to $S_{y'}$. This determines a point, $\boldsymbol{y}'$, on $S_{y'}$ and a corresponding pair, η_1 and η_2. For this point, $\hat{\boldsymbol{n}}$ and $\boldsymbol{y} - \boldsymbol{y}'$ line up, as in Figure 4.18a. Now choose $\hat{\boldsymbol{p}}$ to line up with these two vectors, as in Figure 4.18b. This determines a choice of θ and ϕ. In total, η_1, η_2, θ, and ϕ are all determined as functions of $\boldsymbol{y}$. Analytically, the relationships among the stationary values of the coordinates are as follows:

$$s = \hat{\boldsymbol{n}} \cdot (\boldsymbol{y} - \boldsymbol{y}') = \operatorname{sgn}\left(\hat{\boldsymbol{n}} \cdot (\boldsymbol{y} - \boldsymbol{y}')\right) |\boldsymbol{y} - \boldsymbol{y}'|, \quad \hat{\boldsymbol{p}} = (\hat{\boldsymbol{n}} \cdot \hat{\boldsymbol{p}})\, \hat{\boldsymbol{n}}, \quad (4.4.11)$$

from which it follows that

$$\Phi = \hat{\boldsymbol{p}} \cdot (\boldsymbol{y} - \boldsymbol{y}') = (\hat{\boldsymbol{n}} \cdot \hat{\boldsymbol{p}})\, \hat{\boldsymbol{n}} \cdot (\boldsymbol{y} - \boldsymbol{y}') = \mu_p s, \quad \mu_p = (\hat{\boldsymbol{n}} \cdot \hat{\boldsymbol{p}}). \quad (4.4.12)$$

Clearly, given the stationary four-tuple $(\eta_1, \eta_2, \theta, \phi)$, a second set, $(\eta_1, \eta_2, \pi - \theta, \phi \pm \pi)$, also satisfies the stationarity conditions, merely replacing the vector $\hat{\boldsymbol{p}}$ in the stationary set of vectors by $-\hat{\boldsymbol{p}}$. (Recall that $-\hat{\boldsymbol{p}}$ is in D_p whenever $\hat{\boldsymbol{p}}$ is.) Thus, there may be none, one, or more than one such pair of stationary points for a given choice of $\boldsymbol{y}$. Those values of $\boldsymbol{y}$ for which there are no stationary points are points where $I_0(\lambda, \boldsymbol{y})$ (and, therefore, $I(\lambda, \boldsymbol{y})$, as well) is asymptotically of lower order than for those points where there are stationary pairs of four-tuples. *Stationary points exist when the aperture in $\hat{\boldsymbol{p}}$ contains the normal from $\boldsymbol{y}$ to one or more points on $S_{y'}$.*

Having determined the possible stationary points, the stationary phase formula (3.6.3) requires the computation of the determinant and signature

of the Hessian of the phase function. For simplicity of notation, introduce

$$\theta = \eta_3 \qquad \text{and} \qquad \phi = \eta_4. \tag{4.4.13}$$

Then, as in (3.6.3), the Hessian at the stationary point $\boldsymbol{\eta}_0$ is expressed as

$$[\Phi_{ij}] = \left[\frac{\partial^2 \Phi(\boldsymbol{\eta}_0)}{\partial \eta_i \partial \eta_j}\right], \qquad \text{where} \qquad i,j = 1,2,3,4. \tag{4.4.14}$$

At the end of this section, the analysis of this matrix is outlined in exercises. Here, we just state the results that we need in order to continue with the discussion of the asymptotic expansion.

The calculation of this determinant is then much like the calculation of the four-by-four determinant in Section 3.7 and is left to the exercises. The result is

$$\det[\Phi_{ij}] = \sqrt{g}(1 - s\kappa_1)(1 - s\kappa_2)\sin^2\theta,$$
$$\text{where} \quad \kappa_1 = \hat{\boldsymbol{n}} \cdot \boldsymbol{\kappa}_1, \quad \kappa_2 = \hat{\boldsymbol{n}} \cdot \boldsymbol{\kappa}_2, \quad \text{and} \quad \text{sig}\,[\Phi_{ij}] = \mu. \tag{4.4.15}$$

In these equations, $\boldsymbol{\kappa}_i$, for $i = 1,2$, are the principal curvature vectors on $S_{y'}$ at the stationary point and κ_i are their signed magnitudes, depending on whether the direction of the curvature vectors are collinear (+) or anticollinear (−) with $\hat{\boldsymbol{n}}$. That is,

$$\kappa_i = \hat{\boldsymbol{n}} \cdot \frac{\partial^2 \boldsymbol{y}}{\partial s_i^2}, \quad \text{where} \quad i = 1,2,$$

with s_i, $i = 1,2$ being arclength variables in the principle directions at the stationary point. Thus, the product $s\kappa_i$ is positive when the observation point $\boldsymbol{y}$ and the center of curvature are on the same side of the surface and negative when they are on opposite sides.

We are interested in the asymptotic expansion for $\boldsymbol{y}$ near the surface $S_{y'}$, or s near zero. One result of the analysis in the exercises is that

$$\mu = 0, \quad (1 - s\kappa_i) > 0, \quad \text{where} \quad i = 1,2.$$

That is, the signature is always zero for a stationary point sufficiently close to the surface, $S_{y'}$.

We can also see, in (4.4.15), the effects of the singular behavior of the coordinate system, through the presence of the factor of $\sin^2\theta$ as a multiplier. If we were unfortunate enough that the stationary value of θ were 0 or π, then this determinant would be zero. Recall that the square root of this determinant appears in the denominator of the stationary phase contribution. However, it is also true that the integrand has a corresponding multiplier of $\sin\theta$ in the numerator, so that we really arrive at an indeterminate result. In fact, analysis of subsequent terms in the asymptotic expansion would reveal that like powers of $\sin\theta$ always appear in the numerator and the denominator. The problem is with the coordinate system. With hindsight, we propose the following "cure" for this problem. In the plane where $\theta = \pi/2$, rotate the coordinate system around the line orthogonal to the stationary

value of ϕ so that the stationary points are *always* at $\theta = \pi/2$; then set $\sin\theta = 1$! The resulting asymptotic expansion is unchanged, but we avoid dealing with a peculiarity of the coordinate system by this device.

Now, the asymptotic expansion of $I_0(\lambda, \boldsymbol{y})$ in (4.4.9) consists of a sum of contributions over stationary points as follows.

$$I_0(\lambda, \boldsymbol{y}) = \frac{1}{2\pi} \sum \frac{i}{\sqrt{|1 - s\kappa_1||1 - s\kappa_2)|}} \int_{d_p} \frac{dp}{p} (\hat{\boldsymbol{n}} \cdot \hat{\boldsymbol{p}}) f(\boldsymbol{y}', \hat{\boldsymbol{p}}) e^{i\lambda p \hat{\boldsymbol{n}} \cdot \hat{\boldsymbol{p}} s + i\mu\pi/4}.$$

In this equation, d_p is the dual domain—two line segments—associated with two stationary points pointing in opposite directions and the summation is to be taken over all such pairs of stationary points. On these two domains, $\hat{\boldsymbol{n}} \cdot \hat{\boldsymbol{p}} = \pm 1$, respectively. Thus, we can rewrite this result as

$$I_0(\lambda, \boldsymbol{y}) = \frac{1}{2\pi} \sum \frac{if(\boldsymbol{y}', \hat{\boldsymbol{p}})}{\sqrt{|1 - s\kappa_1||1 - s\kappa_2)|}} \cdot \int_{d_{p+}} \frac{dp}{p} \left[e^{i\lambda ps + i\mu\pi/4} - e^{-i\lambda ps - i\mu\pi/4} \right].$$

Here, d_{p+} is the line segment of d_p on which $\hat{\boldsymbol{n}} \cdot \hat{\boldsymbol{p}} = +1$. Further, we have used the fact (to be verified in the exercises) that the eigenvalues are of opposite sign for these two contributions. Finally, we have used the evenness of $f(\boldsymbol{y}', \hat{\boldsymbol{p}})$ in $\hat{\boldsymbol{p}}$ to take this factor out from under the integral sign.

Now, the result can be recast in terms of a bandlimited step function; we need only replace p by $-p$ in the second integral. Then, the integration range for this integral is just the reflection of d_{p+} through $p = 0$ and the previous result is replaced by

$$I(\lambda, \boldsymbol{y}) \sim \sum G(\boldsymbol{y}, \boldsymbol{y}', \hat{\boldsymbol{p}}) J(\lambda, \boldsymbol{y}). \tag{4.4.16}$$

In this equation,

$$J(\lambda, \boldsymbol{y}) = \frac{1}{2\pi} \int F(p) \frac{dp}{ip} e^{i\lambda ps + i\mu\pi/4}. \tag{4.4.17}$$

and

$$G(\boldsymbol{y}, \boldsymbol{y}', \hat{\boldsymbol{p}}) = -\frac{f(\boldsymbol{y}, \hat{\boldsymbol{p}})}{\sqrt{|1 - s\kappa_1|\,|1 - s\kappa_2|}}. \tag{4.4.18}$$

The function $F(p)$ is the filter that restricts the domain of integration to the two intervals defined by d_{p+} and its reflection through the origin.

For s near zero, $\mu = 0$ and the function $J(\lambda, \boldsymbol{y})$ can be recognized as the bandlimited step function that first arose in Chapter 2, equation (2.4.12). Note also that right on the surface $S_{y'}$ there is one pair of stationary points for which $\boldsymbol{y}' = \boldsymbol{y}$ and $G(\boldsymbol{y}, \boldsymbol{y}', \hat{\boldsymbol{p}}) = f(\boldsymbol{y}, \hat{\boldsymbol{p}})$, as long as the normal direction to the surface, $S_{y'}$, is contained in the aperture, D_p. That is, there is one pair of stationary points for which the contribution to the asymptotic expansion of $I((\lambda, \boldsymbol{y})$ is just the value of f at the boundary, multiplied by

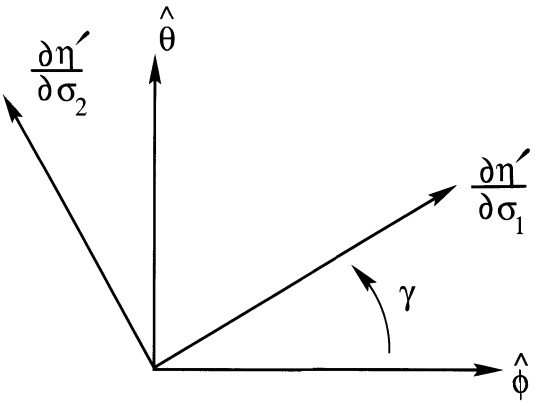

FIGURE 4.19. The angle γ.

a bandlimited step function. This is the extent to which the asymptotic identity operator approximates the function f, restricted to the domain $D_{y'}$.

Exercises

4.11 The purpose of this exercise is to carry out the analysis leading to (4.4.15) for the case in which η_1 and η_2 are arclength variables. In this case,

$$\left.\frac{\partial \boldsymbol{y}}{\partial \eta_i} \cdot \frac{\partial \boldsymbol{y}}{\partial \eta_j}\right|_{\boldsymbol{\eta}=\boldsymbol{\eta}_0} = \delta_{ij} = \begin{cases} 1, & i = j \\ 0, & i \neq j \end{cases}, \quad i,j = 1,2.$$

Furthermore, in (4.4.9), for $\boldsymbol{\eta} = \boldsymbol{\eta}_0$,

$$dS_{y'} = \sqrt{g}\, d\eta_1 d\eta_2, \quad g = \det\left[\frac{\partial \boldsymbol{y}}{\partial \eta_i} \cdot \frac{\partial \boldsymbol{y}}{\partial \eta_j}\right] = \left|\frac{\partial \boldsymbol{y}}{\partial \eta_1} \times \frac{\partial \boldsymbol{y}}{\partial \eta_2}\right|^2 = 1.$$

Also, the exercise derives the evaluation of μ for s near zero.

a. Use the first derivatives in (4.4.10) and assume that the coordinates, η_1 and η_2 are arclength coordinates in the principal directions at the stationary point to verify the following evaluations of second derivatives. All indices i, j range over the values 1 and 2 in this exercise, unless otherwise indicated.

b. Show that

$$\frac{\partial^2 \Phi}{\partial \eta_i \partial \eta_j} = -\hat{\boldsymbol{p}} \cdot \frac{\partial^2 \boldsymbol{y}'}{\partial^2 \eta_i} \delta_{ij} = -\left(\hat{\boldsymbol{n}} \cdot \hat{\boldsymbol{p}}\, \hat{\boldsymbol{n}}\right) \cdot \left(\hat{\boldsymbol{n}} \cdot \boldsymbol{\kappa}_i\, \hat{\boldsymbol{n}}\right) \delta_{ij} = -\mu_p \kappa_i \delta_{ij}.$$

Here, μ_p is defined in (4.4.12).

c. Verify that

$$\frac{\partial^2 \Phi}{\partial \eta_i \partial \theta} = -\hat{\boldsymbol{\theta}} \cdot \frac{\partial \boldsymbol{y}'}{\partial \eta_i} = \begin{cases} -\sin\gamma, & i = 1, \\ -\cos\gamma, & i = 2; \end{cases}$$

$$\frac{\partial^2 \Phi}{\partial \eta_i \partial \phi} = \hat{\boldsymbol{\phi}} \cdot \frac{\partial \boldsymbol{y}'}{\partial \eta_i} = \begin{cases} -\cos\gamma \sin\theta, & i = 1, \\ \sin\gamma \sin\theta, & i = 2. \end{cases}$$

Here, the angle γ is defined in Figure 4.19. Also, we have used the fact that all four of the indicated vectors are orthogonal to two collinear vectors, $\hat{\boldsymbol{n}}$ and $\hat{\boldsymbol{p}}$, and therefore can be viewed as coplanar, even though they reside in different domains.

d. Show that

$$\frac{\partial^2 \Phi}{\partial \theta^2} = -\hat{\boldsymbol{p}} \cdot (\boldsymbol{y} - \boldsymbol{y}') = -\mu_p s, \quad \frac{\partial^2 \Phi}{\partial \theta \partial \phi} = 0,$$

$$\frac{\partial^2 \Phi}{\partial \phi^2} = -\hat{\boldsymbol{\rho}} \cdot (\boldsymbol{y} - \boldsymbol{y}') \sin\theta = -\mu_p s \sin^2\theta,$$

with μ_p defined in equation (4.4.12) and

$$\rho = (\cos\phi, \sin\phi, 0).$$

See Figure 4.17.

4.12 In this exercise, we show that the fundamental result is only slightly modified if the η's are *not* arclength variables on the surface. Let us assume this to be the case and introduce the variables, s_i, $i = 1, 2$ and $\boldsymbol{s} = (s_1, s_2)$. These are assumed to be arclength variables in the principal directions at the stationary point.

a. Show that

$$\frac{\partial \Phi}{\partial \eta_i} = \frac{\partial \Phi}{\partial s_p} \frac{\partial s_p}{\partial \eta_i}, \quad \frac{\partial^2 \Phi}{\partial \eta_i \partial \eta_j} = \frac{\partial^2 \Phi}{\partial s_p \partial s_q} \frac{\partial s_p}{\partial \eta_i} \frac{\partial s_q}{\partial \eta_j} + \frac{\partial \Phi}{\partial s_p} \frac{\partial^2 s_p}{\partial \eta_i \partial \eta_i}.$$

Here, sum over the repeated indices, p and q, from 1 to 2.

b. Show that a stationary point in $\boldsymbol{\eta}$ implies a stationary point in $\boldsymbol{s}$ and, hence, that

$$\frac{\partial^2 \Phi}{\partial \eta_i \partial \eta_j} = \frac{\partial^2 \Phi}{\partial s_p \partial s_q} \frac{\partial s_p}{\partial \eta_i} \frac{\partial s_q}{\partial \eta_j}$$

at the stationary point.

c. Introduce the 4×4 matrix, Γ, made up of 2×2 submatrices as follows:

$$\Gamma = \begin{bmatrix} \left[\dfrac{\partial s_p}{\partial \eta_i}\right] & 0 \\ 0 & I \end{bmatrix},$$

with I being the 2×2 identity matrix. Further, denote by $\tilde{\Phi}_{ij}$ the matrix Φ_{ij}, but with $\boldsymbol{\eta}$ replaced by $\boldsymbol{s}$. Show that

$$\Phi_{ij} = \Gamma \tilde{\Phi}_{ij} \Gamma^T,$$

with Γ^T being the transpose of the matrix Γ. Thus, conclude that

$$\det [\Phi_{ij}] = \det \left[\tilde{\Phi}_{ij}\right] [\det[\Gamma]]^2 .$$

d. Show that

$$[\det[\Gamma]]^2 = \left| \frac{d\boldsymbol{s}}{d\eta_1} \times \frac{d\boldsymbol{s}}{d\eta_2} \right|^2 = \left| \frac{d\boldsymbol{x}}{d\eta_1} \times \frac{d\boldsymbol{x}}{d\eta_2} \right|^2 = g.$$

Here, the first cross product is in the two-dimensional space of $\boldsymbol{s}$, while the second cross product is in the three-dimensional space of $\boldsymbol{y}$. Also, g is, as usual, the determinant of the first fundamental tensor of differential geometry, as defined by the previous term in the string of equalities. (See Kreyszig [1991] for information on differential geometry.)

e. Verify (4.4.15).

4.13 a. In (4.4.15), set $\sin\theta = 1$ and do the same in all of the second derivatives, above. Then, rewrite (4.4.15) as

$$[\Phi_{ij}] = (1 - s\kappa_1)(1 - s\kappa_2) = (1 - \mu_p s \mu_p \kappa_1)(1 - \mu_p s \mu_p \kappa_2)$$

and conclude that the eigenvalues, λ_j, $j = 1, 2, 3, 4$, must satisfy the equation

$$(1 - (\mu_p s + \lambda_j)(\mu_p \kappa_1 + \lambda_j))\,(1 - (\mu_p s + \lambda_j)(\mu_p \kappa_2 + \lambda_j)) = 0.$$

Hint: It is not necessary to recompute the determinant.

b. Show that the four eigenvalues come in pairs, corresponding to κ_1 and κ_2 as follows:

$$\lambda_{j\pm} = \frac{1}{2}\left[-\mu_p(\kappa_j + s) \pm \sqrt{(\kappa_j - s)^2 + 4}\right], \quad j = 1, 2.$$

c. Check that for $s = 0$, each pair, $\lambda_{j\pm}$, have opposite signs and thus conclude that

$$\text{sig } [\Phi_{ij}] = \mu = 0.$$

d. Show that the solution for the eigenvalues can also be written in these alternative ways:

$$\begin{aligned} \lambda_{j\pm} &= -\frac{\mu_p}{2}\left[(\kappa_j + s) \pm \sqrt{(\kappa_j - s)^2 + 4}\right] \\ &= -\frac{\mu_p \,\text{sgn}\,(\kappa_j + s)}{2}\left[|\kappa_j + s| \pm \sqrt{(\kappa_j - s)^2 + 4}\right]. \end{aligned}$$

e. Explain why the eigenvalue of minimum absolute value must be chosen from $|\lambda_{j-}|$ in this final form, and that

$$|\lambda_{j-}| = \frac{2|1 - s\kappa_j|}{|\kappa_j + s| + \sqrt{(\kappa_j - s)^2 + 4}}.$$

4.14 Verify equations (4.4.17) and (4.4.18).

4.4.3 The Near-Surface Condition

Consider the integral (4.4.17) when $\boldsymbol{y}$ approaches the surface $S_{y'}$. For the nearest stationary point, the phase approaches zero in this limit. (There may be other stationary points further away on $S_{y'}$ for which the limit is not zero.) For this distinguished stationary point, $J(\lambda, \boldsymbol{y})$ is $O(1)$ in λ in this limit, whereas it is $O(1/\lambda)$ for all other stationary points. Thus, $J(\lambda, \boldsymbol{y})$ changes its order in λ when $\boldsymbol{y}$ is actually on $S_{y'}$ and it is reasonable to expect the sum to be dominated by this nearest stationary point.

From its definition in (4.4.16), J can be recognized as a bandlimited step function, for $\boldsymbol{y}$ on $S_{y'}$, $\mu = 0$. The magnitude of the step can be determined by evaluating $G(\boldsymbol{y}, \boldsymbol{y}', \hat{\boldsymbol{p}})$ in the limit when $\boldsymbol{y}$ is on $\partial S_{y'}$. The result is

$$G_{\text{PEAK}} = f(\boldsymbol{y}, \hat{\boldsymbol{p}}), \quad \boldsymbol{y} \text{ on } S_{y'}. \tag{4.4.19}$$

That is, the magnitude of the step is just the value of $f(\boldsymbol{y}, \hat{\boldsymbol{p}})$, which is the magnitude of the discontinuity of f across the surface $S_{y'}$ at the stationary value of $\hat{\boldsymbol{p}}$. For two integrals over domains sharing the same segment of boundary surface, the stationary point is shared as well. The only differences in evaluation of the integral arise from the different values of the amplitude function, $G(\boldsymbol{y}, \boldsymbol{y}', \hat{\boldsymbol{p}})$ in the two integrands and the fact that $\hat{\boldsymbol{n}}$ has opposite direction in the two integrals. Thus, the sum of the integrals will yield a difference of function values that reduces to just the jump in the function f when $\boldsymbol{y}$ is actually on the surface $S_{y'}$ and for the same value of $\hat{\boldsymbol{p}}$. This is the main result regarding the asymptotic identity operator (4.4.3).

4.4.4 Extracting Information About f on $S_{y'}$

In applications of this analysis to inverse problems, the aperture-limited information about $f(\boldsymbol{x}/L, \hat{\boldsymbol{k}})$ *in the Fourier domain* constitutes the known data and the objective is to extract information about the function $f(\boldsymbol{x}/L, \hat{\boldsymbol{k}})$ in the spatial domain. The analysis presented here suggests that, from large-wavenumber aperture-limited data, at best, information about the boundary values of $f(\boldsymbol{x}/L, \hat{\boldsymbol{k}})$ can be extracted at some as yet unknown value of $\hat{\boldsymbol{k}}$. More generally, one might hope to determine the value of the jump in $f(\boldsymbol{x}/L, \hat{\boldsymbol{k}})$ across its discontinuity surfaces in the $\boldsymbol{x}'$-domain at a yet-to-be-determined value of $\hat{\boldsymbol{k}}$.

Two issues need to be addressed. The first is the question of how to easily extract information about the height of the step. As we saw in Chapter 2, bandlimited step functions are not as easy to recognize in numerical representations as they are in analytic expressions. We want to be able to extract both the location and the magnitude of the step. In the asymptotic representation (4.4.17) we see that the amplitude of the bandlimited step function is actually equal to zero at its discontinuity, significantly mitigating the effect of growth of the integral I from $O(1/\lambda)$ to $O(1)$ in this region. This serves to strengthen our conviction that searching for the midpoint of a bandlimited step is not the best approach to the problem of inverting for surfaces of discontinuity.

In addition to the issue of extracting information about f, there is the issue of how to determine the *distinguished* value of $\hat{\boldsymbol{p}}$ that must be addressed. These issues will be addressed in the next subsection. Note, however, that neither of the solutions to these problems is new. We have already seen hints at the solution to these questions in the previous chapter, in the context of the zero-offset inverse problem.

4.4.5 *Processing for a Scaled Singular Function of the Boundary Surface $S_{y'}$*

With a minor change of the kernel, the integral operator in (4.4.1) can be transformed into an integral operator yielding a bandlimited delta function, rather than a bandlimited step, as its output. This delta function will have its support on the surface, $S_{y'}$. This function is the *singular function* of the surface $S_{y'}$, as defined by (4.3.9). Thus, we can expect an output whose peak value defines the surface $S_{y'}$ and whose amplitude is proportional to $f(\boldsymbol{x}/L, \hat{\boldsymbol{k}})$ on $S_{y'}$.

To transform the integral $I(\lambda, \boldsymbol{y}))$ in (4.4.16) into a bandlimited delta function, we need to introduce a multiplier that cancels the factor $(\hat{\boldsymbol{n}} \cdot \hat{\boldsymbol{p}})/ip$ present in the integrand. Thus, we need a multiplier of ip on half of the p-domain and $-ip$ on the image of that domain through the origin. As suggested in the previous section, the multiplier $ik \operatorname{sgn}(\hat{\boldsymbol{u}} \cdot \hat{\boldsymbol{k}})$, with $\hat{\boldsymbol{u}}$ a constant unit vector, will do the trick. When this factor is inserted into the integrand in (4.4.1), it will have exactly the desired effect. After rescaling,

$$ik \operatorname{sgn}(\hat{\boldsymbol{u}} \cdot \hat{\boldsymbol{k}}) = i\lambda p \operatorname{sgn}(\hat{\boldsymbol{u}} \cdot \hat{\boldsymbol{p}}). \tag{4.4.20}$$

For a closed convex body and full aperture information, this multiplier is not defined in the plane through the origin with $\hat{\boldsymbol{u}}$ as normal. In most applications, however, there is at least one plane of directions in which there is no information, so the domain D_k will exclude some plane through the origin. Choose $\hat{\boldsymbol{u}}$ as the unit normal to that plane.

In the applications to inversion, the choice of sign is straightforward. Typically, $k = |\boldsymbol{k}|$ is proportional to $|\omega|$, with $\operatorname{sgn}\omega = \operatorname{sgn}(\hat{\boldsymbol{u}} \cdot \hat{\boldsymbol{k}})$ for some

undetermined $\hat{\boldsymbol{u}}$. Therefore, instead of multiplying by $|\omega|$ to compute k, we multiply by ω to compute $k\,\mathrm{sgn}\,(\hat{\boldsymbol{u}}\cdot\hat{\boldsymbol{k}})$, *even though the corresponding* $\hat{\boldsymbol{u}}$ *is never determined.*

Proceeding with this idea, in place of the integral (4.4.1) consider

$$\bar{I} = \frac{i}{(2\pi)^3}\int_{D_k} k\,\mathrm{sgn}\,(\hat{\boldsymbol{u}}\cdot\hat{\boldsymbol{k}})\,d^3k\int_{D_{x'}} d^3x' f(\boldsymbol{x}'/L,\hat{\boldsymbol{k}})e^{i\boldsymbol{k}\cdot(\boldsymbol{x}-\boldsymbol{x}')}. \tag{4.4.21}$$

The integral (4.4.3), obtained after scaling, is replaced by

$$\bar{I}(\lambda,\boldsymbol{y}) = \frac{i\lambda^4}{(2\pi)^3}\int_{D_p} p^2\,\mathrm{sgn}\,(\hat{\boldsymbol{u}}\cdot\hat{\boldsymbol{p}})\,dp\,\sin\theta\,d\theta d\phi\int_{D_{y'}} d^3y' f(\boldsymbol{y}',\hat{\boldsymbol{p}})e^{i\lambda p\hat{\boldsymbol{p}}\cdot(\boldsymbol{y}-\boldsymbol{y}')} \tag{4.4.22}$$

and the integral $I_0(\lambda,\boldsymbol{y})$ in (4.4.8) and (4.4.9) is now replaced by

$$\bar{I}_0(\lambda,\boldsymbol{y}) = \left[\frac{\lambda}{2\pi}\right]^3\int_{D_p} p^2\,\mathrm{sgn}\,(\hat{\boldsymbol{u}}\cdot\hat{\boldsymbol{p}})\,dp\,\sin\theta\,d\theta d\phi \cdot\int_{S_{y'}} dS_{y'}(\hat{\boldsymbol{n}}\cdot\hat{\boldsymbol{p}})f(\boldsymbol{y}',\hat{\boldsymbol{p}})e^{i\lambda p\Phi}. \tag{4.4.23}$$

The asymptotic analysis of this integral proceeds as for $I_0(\lambda,\boldsymbol{y})$, yielding in place of (4.4.15) and (4.4.16) the results

$$\bar{I}(\lambda,\boldsymbol{y}) \sim \sum G(\boldsymbol{y},\boldsymbol{y}',\hat{\boldsymbol{p}})\bar{J}(\lambda,\boldsymbol{y}) \tag{4.4.24}$$

and

$$\bar{J}(\lambda,\boldsymbol{y}) = \frac{\lambda\mu_3}{2\pi}\int dp\,e^{[i\lambda ps+i\mu\pi/4]}, \quad \text{where} \quad \mu_3 = (\hat{\boldsymbol{n}}\cdot\hat{\boldsymbol{p}})\,\mathrm{sgn}\,(\hat{\boldsymbol{u}}\cdot\hat{\boldsymbol{p}}) = \mathrm{sgn}\,(\hat{\boldsymbol{n}}\cdot\hat{\boldsymbol{u}}). \tag{4.4.25}$$

In other words, μ_3 does not depend on the direction of $\hat{\boldsymbol{p}}$. Except for the new parameter μ_3 (which takes on the values of (± 1), only) the constituent functions and parameters here are still defined by (4.4.17) and (4.4.14).

For $\boldsymbol{y}$ on $S_{y'}$ there is one stationary point in $\boldsymbol{y}'$, with $\boldsymbol{y}' = \boldsymbol{y}$ as long as $\hat{\boldsymbol{n}}$ is a direction in D_k. For this stationary point, $\bar{J} = O(\lambda)$, whereas for all other stationary points, or for $\boldsymbol{y}$ not on $S_{y'}$, $\bar{J} = O(1)$ in λ. Thus, as $\boldsymbol{y}$ approaches $S_{y'}$, one stationary point dominates the value of $I(\lambda,\boldsymbol{y})$, and the function value is larger by $O(\lambda)$ than the value for $\boldsymbol{y}$ bounded away from $S_{y'}$. As noted earlier, for this distinguished stationary point, $\mu = 0$. Recalling that we must sum over the two stationary points $\pm\hat{\boldsymbol{p}}$, the integral $\bar{J}$ becomes

$$\bar{J}(\lambda,\boldsymbol{y}) = \frac{\lambda\mu_3}{2\pi}\int_{-p_+}^{-p_-} + \int_{p_-}^{p_+} dp\,e^{i\lambda p|\boldsymbol{y}-\boldsymbol{y}'|}. \tag{4.4.26}$$

The limits of integration, p_- and p_+ are the intersections of the ray from the origin in the stationary direction $\hat{\boldsymbol{p}}$ with the domain D_p. In the k-domain, that is, undoing the scaling defined by (4.4.2),

$$\bar{J}(\lambda, \boldsymbol{y}) = \frac{2\mu_3}{2\pi} \left(\int_{-k_+}^{-k_-} + \int_{k_-}^{k_+} \right) dk e^{ikd},$$
$$d = |\boldsymbol{x} - \boldsymbol{x}'| \operatorname{sgn}(\hat{\boldsymbol{k}} \cdot (\boldsymbol{x} - \boldsymbol{x}')). \tag{4.4.27}$$

Here, $k_\pm$ have definitions completely analogous to $p_\pm$. In either form, $\bar{J}$ can be recognized as a symmetric bandlimited delta function with support at $|\boldsymbol{y} - \boldsymbol{y}'| = 0$, ($|\boldsymbol{x} - \boldsymbol{x}'| = 0$), which occurs when $\boldsymbol{y}$ is on $S_{y'}$ (or $\boldsymbol{x}$ is on an equivalent surface in the x-domain, $S_{x'}$). In this limit, the dominant term in (4.4.23) is readily evaluated with the aid of (4.4.18):

$$\bar{I}(\lambda, \boldsymbol{y}) \sim \lambda(p_+ - p_-)\mu_3 \frac{f(\boldsymbol{y}, \hat{\boldsymbol{p}})}{\pi} = (k_+ - k_-)\mu_3 \frac{f(\boldsymbol{x}/L, \hat{\boldsymbol{k}})}{\pi}, \quad \boldsymbol{y} \text{ on } S_{y'}. \tag{4.4.28}$$

Thus, the value of $\bar{I}$ on $S_{y'}$ is proportional to the interval width in the k-domain along an appropriate ray, multiplied by $\mu_3 f(\boldsymbol{x}/L, \hat{\boldsymbol{k}})/\pi$. If the integrand contained a filter factor, $F(\boldsymbol{k}) = F(K\boldsymbol{p})$, then the factor $p_+ - p_-$ is replaced by the area under the filter function in the stationary direction of $\hat{\boldsymbol{p}}$.

Qualitatively, for $\boldsymbol{x}$ near $S_{x'}$, the dominant term in the sum in (4.4.23) has the form of an aperture-limited singular function scaled by a slowly varying function. The scale factor becomes the jump in the function f multiplied by μ_3 when $\boldsymbol{x}$ is on S_x, and the aperture-limited singular function becomes the area under the bandpass filter in a distinguished direction, divided by 2π.

4.4.6 The Normal Direction

It remains to show how to determine the direction of the normal at the stationary point. Equivalently, we need only determine the distinguished value of $\hat{\boldsymbol{p}}$ at the stationary point. To simplify further, we must determine $\sin\theta$ or $\cos\theta$ and $\sin\phi$ or $\cos\phi$ at the stationary point. Note from (4.4.4) that

$$\cos\theta = \frac{k_3}{k} = \frac{p_3}{p}, \quad \cos\phi = \frac{k_1}{\sqrt{k_1^2 + k_2^2}} = \frac{p_1}{\sqrt{p_1^2 + p_2^2}}. \tag{4.4.29}$$

Suppose that we define two new integral operators with these factors introduced into the kernels of the operator $\bar{I}$. That is, starting from (4.4.20), define

$$\bar{I}_\theta = \int_{D_k} d^3k \, k_3 \operatorname{sgn}(\hat{\boldsymbol{u}} \cdot \hat{\boldsymbol{k}}) \int_{D_{x'}} d^3x' f(\boldsymbol{x}'/L, \hat{\boldsymbol{k}}) e^{i\boldsymbol{k}\cdot(\boldsymbol{x}-\boldsymbol{x}')}, \tag{4.4.30}$$

$$\bar{I}_\phi = \int_{D_k} d^3k \frac{k \, k_1 \operatorname{sgn} k_3}{\sqrt{k_1^2 + k_2^2}} \int_{D_{x'}} d^3x' f(\boldsymbol{x}'/L, \hat{\boldsymbol{k}}) e^{i\boldsymbol{k}\cdot(\boldsymbol{x}-\boldsymbol{x}')}. \tag{4.4.31}$$

Let us now consider the asymptotic analysis of $\bar{I}_\theta$ and $\bar{I}_\phi$. Clearly, it will proceed exactly as in Section 4.4.4, with only the amplitudes of the results being influenced by the changes introduced here. Thus, the peak values of these new integral operators can also be predicted. They will differ from the result for $\bar{I}$ itself, by the factors $\cos\theta$, $\cos\phi$, *each evaluated at the distinguished stationary point.* That is,

$$\cos\theta = \frac{\bar{I}_{\theta\text{PEAK}}}{\bar{I}_{\text{PEAK}}}, \qquad \cos\phi = \frac{\bar{I}_{\phi\text{PEAK}}}{\bar{I}_{\text{PEAK}}}, \qquad \boldsymbol{y} \text{ on } S_{y'}. \tag{4.4.32}$$

Clearly, $\sin\phi$ can be determined this way as well, while $\sin\theta$ can be defined in terms of $\cos\theta$, taking the positive square root ($0 \leq \theta \leq \pi$). Given these values at the distinguished stationary point, $\hat{\boldsymbol{p}}$ is determined there.

Thus, we have found a way to extract information about the orientation of a reflector as a parameter that we invert for, rather than relying merely on the appearance in an image. In Chapters 5 and 6 we will apply these ideas to solve the problem of determining reflectivity as a function of angle, with the angle of incidence determined via an inversion process of this type.

4.4.7 Integrands with Other Types of Singularities

It should be noted that the multiplier $ik\,\text{sgn}\,(\hat{\boldsymbol{u}}\cdot\hat{\boldsymbol{k}})$ is a "best choice" only because $f(\boldsymbol{x}'/L,\hat{\boldsymbol{p}})$ was assumed to be smooth but not to vanish smoothly on the boundary of its domain of definition. In contrast, the original operator, I, will optimally depict a function that is a (sum of) Dirac delta function(s) as was shown in the first example of the previous section (equation (4.3.2) and the discussion below it). Furthermore, the second example, equation (4.3.6), suggests that $I(\boldsymbol{x})$ will also be a better operator than $\bar{I}$ for singular functions. That can readily be verified now, as follows. Let us consider the application of I as defined by (4.4.1) to the function

$$f(\boldsymbol{x}'/L,\hat{\boldsymbol{k}}) = \gamma(\boldsymbol{x}'/L), \tag{4.4.33}$$

with $\gamma(\boldsymbol{y}')$, the singular function of a surface, $S_{y'}$, as defined in equation (4.3.9) of the previous section and the related discussion. Substitution of this function into (4.4.1) and use of the change of variables defined by (4.4.2) and (4.4.4) leads to the result

$$I(\lambda,\boldsymbol{y}) = \left[\frac{\lambda}{2\pi}\right]^3 \int_{D_p} p^2 dp \sin\theta d\theta d\phi \int_S dS e^{i\lambda p\Phi}, \tag{4.4.34}$$

with Φ defined by (4.4.5).

Thus, without introducing an additional multiplier to modify the operator I to $\bar{I}$, this integral is exactly like the integral $\bar{I}_0(\lambda,\boldsymbol{y})$ defined by (4.4.22), with the amplitude of that integral, $\text{sgn}\,(\hat{\boldsymbol{u}}\cdot\hat{\boldsymbol{p}}) = \hat{\boldsymbol{n}}\cdot\hat{\boldsymbol{p}} = f(\boldsymbol{y}',\hat{\boldsymbol{p}}) = \mu_3 f(\boldsymbol{y}',\hat{\boldsymbol{p}})$ replaced by unity. Consequently, the asymptotic analysis for this

integral has already been done. The output will be an aperture-limited version of $\gamma(\boldsymbol{y}')$. That is, it will be a bandlimited delta function along each normal that is a direction from the origin to D_k. The structure of the delta function will depend on the extent of that ray in the k-domain and also on any smoothing that might be applied through the introduction of a large-wavenumber bandpass filter along that ray.

Asymptotically, then, the large-wavenumber, aperture-limited Fourier inversion of data for a singular function behaves just as the exact result did for a planar surface.

Minor Extension

In the applications of interest, the function f depends on $\boldsymbol{x}$, in addition to the other dependencies indicated in (4.4.1). This does not change the results stated here, since $\boldsymbol{x}$ merely acts as a parameter with respect to the integrations in (4.4.1).

A Form that Arises in the Analysis of Kirchhoff Data for the Inverse-Scattering Formalism

A last extension to be considered here is the case in which the integrand has both a singular function and a smoother amplitude function. Modify equation (4.3.1) by replacing $f(\boldsymbol{x}'/L, \hat{\boldsymbol{k}})$ with $f(\boldsymbol{x}'/L, \boldsymbol{x}/L, \hat{\boldsymbol{k}})\gamma(\boldsymbol{x}'/L)$. Then, after exploiting the sifting property of the singular function, the integral (4.3.1) becomes

$$I = \frac{1}{(2\pi)^3} \int_{D_k} d^3k \int_{S_{x'}} dS' f(\boldsymbol{x}'/L, \boldsymbol{x}/L, \hat{\boldsymbol{k}}) e^{i\boldsymbol{k}\cdot(\boldsymbol{x}-\boldsymbol{x}')}, \tag{4.4.35}$$

or, in dimensionless variables,

$$I = \left[\frac{\lambda}{2\pi}\right]^3 \int_{D_p} d^3p \int_{S_{y'}} dS_{y'} f(\boldsymbol{y}', \boldsymbol{y}, \hat{\boldsymbol{p}}) e^{i\lambda p\Phi}. \tag{4.4.36}$$

Here, Φ is defined by (4.4.5). Except for the fact that we have not used polar coordinates, the integral is of the same form as (4.4.22) with the amplitude $(\hat{\boldsymbol{n}} \cdot \hat{\boldsymbol{p}}) \operatorname{sgn}(\hat{\boldsymbol{u}} \cdot \hat{\boldsymbol{p}}) f(\boldsymbol{y}', \hat{\boldsymbol{p}}) = \mu_3 f(\boldsymbol{y}', \hat{\boldsymbol{p}})$ replaced by $f(\boldsymbol{y}', \boldsymbol{y}, \hat{\boldsymbol{p}})$. The analysis proceeds as before, with the extra dependence on $\boldsymbol{y}$ in f merely playing the role of a parameter as regards the asymptotic analysis of the integral.

Consequently, the asymptotic expansion of the integral in (4.4.36) is given by (4.4.23), with the following insertions. The function $G(\boldsymbol{y}, \boldsymbol{y}', \hat{\boldsymbol{p}})$ is defined by (4.4.17), except that $f(\boldsymbol{y}, \hat{\boldsymbol{p}})$ is replaced by $f(\boldsymbol{y}', \boldsymbol{y}, \hat{\boldsymbol{p}})$ and $\bar{J}$ is given by (4.4.24), (4.4.25), or (4.4.26) with μ_3 replaced by unity. In particular, for $\boldsymbol{y}$ near S, the asymptotic expansion is dominated by a scaled bandlimited singular function. When $\boldsymbol{y}$ is on S, the scale factor is just the amplitude, $f(\boldsymbol{y}'/L, \boldsymbol{y}/L, \hat{\boldsymbol{k}})$, evaluated at the stationary point and determinable as described in the discussion above for determination of $\hat{\boldsymbol{p}}$. That is,

$$\bar{I}(\lambda, \boldsymbol{y}) = f(\boldsymbol{y}, \boldsymbol{y}, \hat{\boldsymbol{p}}) \cdot \frac{1}{2\pi} \int dp, \quad \boldsymbol{y} \text{ on } S, \tag{4.4.37}$$

where the domain of integration is the range of values of p in the direction of $\hat{\boldsymbol{p}}$. Thus, the amplitude is the value of $f(\boldsymbol{y}, \boldsymbol{y}, \hat{\boldsymbol{p}})$, which in a real-life application would be a reflection coefficient, multiplied by the area under the filter in the $\boldsymbol{p}$-domain in the direction of the stationary value of $\hat{\boldsymbol{p}}$.

Lower-Order Contributions

The results obtained so far assume the existence of at least one pair of stationary points. It is important to note here that such stationary point(s) can exist only if the normal direction to $S_{y'}$ is a direction in the k-domain aperture, D_k. When this is not the case, the integral is asymptotically of lower order and the results obtained here do not apply.

4.4.8 Summary

We have shown here that the large-wavenumber, aperture-limited Fourier inversion of the Fourier transform of a piecewise-smooth function is dominated by the function values on the discontinuity surface. The inversion is approximately a bandlimited step function of normal distance from each point on the discontinuity surface. The amplitude of the step function is proportional to the jump in the function across the surface at the point in question. By modifying the inversion operator, the output can be transformed into the singular function(s) of the discontinuity surface(s) of the original function, again scaled by the jump in the original function at each point of the discontinuity surface. This change facilitates the numerical identification of the discontinuity surface(s) and the amplitude of the jump at each point on the surface(s). Aperture-limited inversion of data for a singular function of a surface was shown to produce an aperture-limited approximation of the singular function.

In the language of asymptotic expansions of integrals, given an output point, $\boldsymbol{x}$, the large-wavenumber, aperture-limited Fourier inversion of a piecewise-smooth function or of the singular function of a surface is dominated by certain critical points that can be determined as functions of $\boldsymbol{x}$. A critical point consists of a location $\boldsymbol{x}'$ in the spatial domain and a direction $\hat{\boldsymbol{k}}$ in the dual Fourier domain. When $\boldsymbol{x}$ is on a discontinuity surface of the smooth function or on the support surface of the singular function, and the normal to the surface in question is a direction $\hat{\boldsymbol{k}}$ in the aperture D_k, the output is at least $O(\lambda)$ larger than it is otherwise. This increase in order can be exploited to detect the discontinuity surface(s) or support surface(s) and estimate an amplitude function on the surface(s). When the normal direction at $\boldsymbol{x}$ on $S_{x'}$ is not a direction in D_k, there is no stationary point and the results described above do not apply. In this case, no information

about the discontinuity surface can be determined. This was seen in the computer outputs of the previous section.

4.4.9 Modern Mathematical Issues

In Section 2.5.1, we mentioned that both our Born-approximate modeling formula and our proposed inversion formula, which are both Fourier-like integrals, are members of a special class of operators—the elliptic pseudodifferential operators. These operators have the properties of being invertible and of preserving the singular support of the data, which for us is the reflector location and reflectivity. If our Born-approximate modeling formulas are reasonable approximations of the wavefield, then our choice of inversion formulas will accurately represent the reflector information. In this chapter, we have discussed aperture limiting, and we must conclude from the discussion here that, at best, we are talking about *aperture-limited* pseudodifferential operators.

To deal with the issue of aperture limiting in a modern mathematical setting requires an extension of our concept of singular support, one that incorporates the new concepts of reflector and migration dips. In the theory of pseudodifferential operators, the singular support of a distribution, combined with the family of normal directions to the region of singular support, is called the *wavefront set* of the distribution. For a singular function, this concept is a generalization of the concept of singular support—one which does, indeed, take into account the idea migration dip. Thus, to reconstruct a reflector, in mathematical terms, we must reconstruct its wavefront set.[8]

Thus, the results of this section can be stated as follows. For the class of piecewise-smooth functions, large-wavenumber aperture-limited Fourier data can be used to determine the wavefront sets of the given function on a subset for which the directions of the normals lie in the Fourier domain aperture. For the geophysicist, this is important because we now have a coherent mathematical justification supporting the idea that we can extract reflectivity information from *aperture-limited* data, albeit for only those portions of the reflector that are illuminated.

---

[8]In advanced mathematical literature, the terms *tangent bundle* and *cotangent bundle* appear. For us, the set of reflector dips constitutes the tangent bundle of the reflectors, whereas the set of migration dips constitute the reflectors' cotangent bundle. In the literature of *microlocal analysis*, which is the topic of mathematical analysis in conical neighborhoods of points, imaging problems are said to be "formulated on the cotangent bundle." We would say, equivalently, that migration formulas are "formulated in terms of migration dips."

5

Inversion in Heterogeneous Media

In Chapter 3, we created our first inversion formulas for the three-dimensional inverse-scattering imaging problem. We formulated the problem for the special case of data collected with a zero-offset recording geometry, and assumed a constant-background wavespeed. The formulas we derived yielded a bandlimited representation of the *singular function* of a reflector surface scaled by the *normal-incidence reflection coefficient* of the reflector—*the reflectivity function*—$\beta(\boldsymbol{x})$. These formulas were further shown to correspond to the classic Fourier transform–based migration formula created by Stolt [1978] and the Kirchhoff-based formula created by Schneider [1978], with the latter deduced from the former.

Our inversion/migration formalisms are aperture-limited Fourier-like integrals. This fact motivated the discussion of the general theory of large-wavenumber Fourier imaging presented in Chapter 4. There we found that many of the attributes of the constant-wavespeed inversion formulas are really general properties of Fourier-like integrals, rather than being characteristics specific to the particular case that we studied in Chapter 3. Because the results of Chapter 4 rest on solid mathematical foundations, and because the attributes appear to be robust, these results serve to strengthen our confidence in the high-frequency theory we have developed thus far.

Our satisfaction with these results is short-lived, however. The inversion formulas we have created to this point are not general enough to permit us to deal with real-world imaging problems. We still need to develop a more general formalism that will yield inversion formulas that are applicable to the more complicated recording geometries and more realistic

variable-wavespeed profiles encountered in seismic exploration. Therefore, the motivation for this chapter will be to derive such an inversion formalism.

This new formalism will permit inversion of data resulting from wave propagation in variable-wavespeed media and will naturally accommodate many of the practical source-receiver configurations that were discussed in Chapter 1. We will also be able to extend this formalism to deal with models having a variable-background *density*, as well. Further extensions to isotropic and anisotropic media have also been carried out. These extensions are possible through the application of the methods of high-frequency asymptotics.

The inversion formulas will be aperture-limited, Fourier-like integrals of the type studied in Chapter 4. The integrand of these integrals will contain a determinant that will characterize the viability of inverting a particular data set. This determinant is part of a Jacobian that depends both on the background propagation parameters and on the source-receiver configuration. As a result, the problem of extending the inversion formula to new recording geometries is reduced to a problem of computing the value of the determinant associated with a specific geometry [Cohen, Hagin and Bleistein, 1986; Bleistein, 1986a].

In Chapter 6, the asymptotic formalism developed here will be extended to the two-and-one-half-dimensional inverse-scattering inversion problem.

5.1 Asymptotic Inversion of the Born-Approximate Integral Equation—General Results

The discussion of asymptotic inversion will begin with the Born-approximate integral equation representing the scattered field, originally presented as equation (3.2.1):

$$u_S(\boldsymbol{x}_g, \boldsymbol{x}_s, \omega) = \omega^2 \int_D \frac{\alpha(\boldsymbol{x})}{c^2(\boldsymbol{x})} u_I(\boldsymbol{x}, \boldsymbol{x}_s, \omega) g(\boldsymbol{x}_g, \boldsymbol{x}, \omega) d^3x. \tag{5.1.1}$$

In Chapter 3, the sources and receivers were assumed to be coincident, with the recording surface being a horizontal plane. Our interest in this chapter is the more general problem of inverting seismic data collected with nonzero offset between sources and receivers. Furthermore, the sources and receivers may be located on a surface that is not necessarily horizontal or even planar. Therefore, we must represent source and/or receiver locations in a more general way than was done in Chapter 3.

5.1.1 Recording Geometries

To this end, we will assume that either the source or the receiver locations range over some surface (the surface of the Earth, in seismic reflection

applications). That surface will be parameterized by the vector $\boldsymbol{\xi} = (\xi_1, \xi_2)$. In the most general case, each (x_1, x_2, x_3) is a function of ξ_1 and ξ_2. For example, a common- (single-) source experiment will be described by $\boldsymbol{x}_s =$ constant, $\boldsymbol{x}_g = \boldsymbol{x}_g(\boldsymbol{\xi})$. For the common-receiver experiment, the roles of $\boldsymbol{x}_s$ and $\boldsymbol{x}_g$ would be reversed.

The common- (constant-) offset experiment will be described by introducing a function $\boldsymbol{f}(\boldsymbol{\xi})$ parameterizing the surface. Offset in the $\boldsymbol{\xi}$ coordinates is then represented by introducing a vector $\boldsymbol{h} = (h_1, h_2)$, representing the common offset. The coordinates, (x_1, x_2, x_3), are, in general, functions of h_1 and h_2. Finally we set $\boldsymbol{x}_s(\boldsymbol{\xi}) = \boldsymbol{f}(\boldsymbol{\xi} - \boldsymbol{h})$, and $\boldsymbol{x}_g(\boldsymbol{\xi}) = \boldsymbol{f}(\boldsymbol{\xi} + \boldsymbol{h})$. If the surface described by $\boldsymbol{f}$ is not planar, then choosing a constant vector $\boldsymbol{h}$ (a constant offset in $\boldsymbol{\xi}$) does not constitute a constant-offset experiment between $\boldsymbol{x}_s$ and $\boldsymbol{x}_g$. (The zero-offset experiment is a special case of the common-offset experiment with $\boldsymbol{h} = \boldsymbol{0}$.) For a generally nonplanar surface, such a common-offset geometry may be difficult to achieve. In principle, we may choose the respective source and receiver coordinates $\boldsymbol{x}_s(\boldsymbol{\xi}) = \boldsymbol{f}(\boldsymbol{\xi} - \boldsymbol{h}_+(\boldsymbol{\xi}))$ and $\boldsymbol{x}_g(\boldsymbol{\xi}) = \boldsymbol{f}(\boldsymbol{\xi} - \boldsymbol{h}_-(\boldsymbol{\xi}))$, with $\boldsymbol{h}_+(\xi)$ and $\boldsymbol{h}_-(\boldsymbol{\xi})$ being such that the source and receiver positions fall equally spaced on a planar (but not necessarily horizontal) datum surface. While such a geometry may be attainable by judicious data selection, this is not what happens in real surveys. On land, data are commonly collected with a constant spacing between receiver positions, measured on the surface of the Earth, within seismic lines, but lines need not (and generally are not) be separated by the same offset . At sea, fluctuations in currents cause *cable feathering*, the horizontal variation of the location of the hydrophone streamer.

Thus, topographic variations (on land) and feathering (at sea) cause nonuniformity in the absolute separation of receivers and between sources and receivers. The functions $\boldsymbol{h}_+(\xi)$ and $\boldsymbol{h}_-(\boldsymbol{\xi})$ would have to track that variation. However, it may not be possible in practice to find appropriate $\boldsymbol{h}_+$ and $\boldsymbol{h}_-$ such that this may be done, and some compromises in accuracy might have to be made.[1]

---

[1]Such topographic variations can introduce large time shifts on individual seismic traces. On land, the near surface of the Earth usually consists of a low-velocity *weathering layer*. The time shifts are introduced because of variations in the thickness of the weathering layer caused by variations in the topography, as well as by the fact that the bottom of the weathering layer is not planar. In seismic exploration the term "statics" is applied to the problem of removing these time shifts. We will assume that the data have been corrected for these static shifts in the analysis that follows. A process called wave-equation datuming may be applied to eliminate larger distortions due to topography [Berryhill, 1979, 1984 and Bevc, 1995, 1999]. Data may also be migrated taking topography into account, see, for example, Gray and Marfurt [1995].

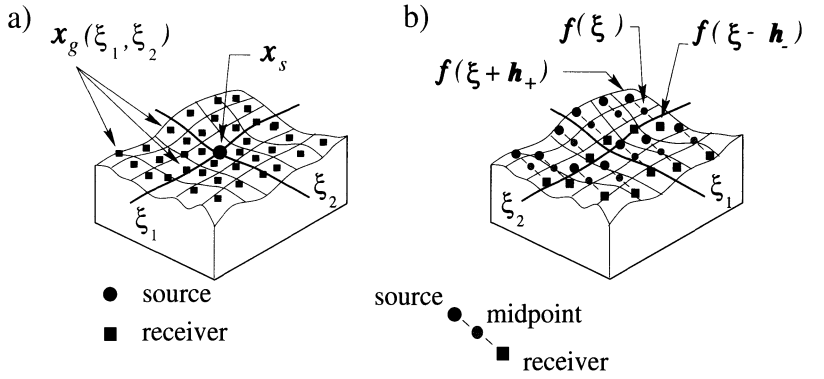

FIGURE 5.1. Generalized source and receiver positions. The surface is parameterized by $\boldsymbol{\xi}$, with a) representing the generalized common-source experiment and b) the generalized common-offset geometry.

Binning and Stacking

A common way of creating an approximate zero-offset 3D data set is to perform the 3D equivalent of common-midpoint stacking. One possible generalization of the common-midpoint gather in 3D is achieved by a process called *binning*. Binning involves defining a rectangular grid on the surface of the Earth. Data having source-receiver pairs whose midpoint coordinates fall into a specific grid are assigned to the central point of that grid. The data are then NMO corrected and stacked, creating the approximate 3D zero-offset data set. Bin-stacking is, therefore, an extension of the common-midpoint (CMP) method with similar advantages and disadvantages. The advantages of bin-stacking are that it reduces the size of the data set and uses the redundancy of the data to enhance the signal and suppress noise in the data. The disadvantages of bin-stacking are similar to the disadvantages of CMP stacking, which is that amplitude information, particularly at the higher frequencies, is lost owing to the averaging that occurs when the traces are stacked. Both methods have intrinsic value, in that *velocity analysis* is performed as part of the process, to find the appropriate *stacking velocities* required to flatten the arrivals in the gathers prior to stacking.

Other Geometries

Some important source-receiver configurations do not fit the criterion of having a surface spread of sources and receivers. Included among these are surface surveys carried out on a single line, single vertical seismic profile (VSP) experiments, and crosswell experiments involving only two wells. Furthermore, a suite of VSP experiments with the sources arrayed along a radial line away from the well, or a suite of well-to-well experiments with all the sources in one well and all the receivers in another, are special cases of

arrays confined to a single vertical plane. Such dimensionally constrained data sets do not provide sufficient coverage for a full three-dimensional inversion. Discussion of these cases must be postponed until the problem of two-and-one-half-dimensional inversion is considered in Chapter 6.

5.1.2 *Formulation of the 3D, Variable-Background, Inverse-Scattering Problem*

If the incident field u_I is represented by

$$u_I(\boldsymbol{x}, \boldsymbol{x}_s, \omega) = F(\omega) g(\boldsymbol{x}, \boldsymbol{x}_s, \omega), \tag{5.1.2}$$

then equation (5.1.1) is recast as an integral with two Green's functions,

$$u_S(\boldsymbol{x}_g, \boldsymbol{x}_s, \omega) = \omega^2 F(\omega) \int_D \frac{\alpha(\boldsymbol{x})}{c^2(\boldsymbol{x})} g(\boldsymbol{x}, \boldsymbol{x}_s, \omega) g(\boldsymbol{x}_g, \boldsymbol{x}, \omega) d^3x. \tag{5.1.3}$$

The key to high-frequency inversion here is to invoke high-frequency asymptotics at the very beginning of the analysis. To do this, we replace the Green's functions in this equation by the WKBJ (ray theoretic) Green's function. (See Appendix E for a discussion of ray theory).[2] These approximations take the form

$$g(\boldsymbol{x}, \boldsymbol{x}_0, \omega) \sim A(\boldsymbol{x}, \boldsymbol{x}_0) e^{i\omega\tau(\boldsymbol{x}, \boldsymbol{x}_0)}.$$

Here, τ is the traveltime from $\boldsymbol{x}_0$ to $\boldsymbol{x}$ and $A(\boldsymbol{x}, \boldsymbol{x}_0)$ is the corresponding ray-theoretic amplitude, derived by solving the eikonal equation

$$\nabla\tau \cdot \nabla\tau = \frac{1}{c^2(\boldsymbol{x})}, \qquad \tau(\boldsymbol{x}_0, \boldsymbol{x}_0) = 0, \tag{5.1.4}$$

and the (first) transport equation

$$2\nabla\tau \cdot \nabla A + A\nabla^2\tau = 0, \tag{5.1.5}$$

subject to the condition

$$4\pi A|\boldsymbol{x} - \boldsymbol{x}_0| \to 1 \qquad \text{as} \quad |\boldsymbol{x} - \boldsymbol{x}_0| \to 0. \tag{5.1.6}$$

See Appendix E for the details of these computations. Substitution of the WKBJ Green's functions into (5.1.3) yields

$$u_S(\boldsymbol{x}_g, \boldsymbol{x}_s, \omega) \approx \omega^2 F(\omega) \int d^3x \frac{\alpha(\boldsymbol{x})}{c^2(\boldsymbol{x})} a(\boldsymbol{x}, \boldsymbol{\xi}) e^{i\omega\phi(\boldsymbol{x}, \boldsymbol{\xi})}, \tag{5.1.7}$$

where

---

[2] See also Gray [1986, 1988, 1992, 1997, 1998], Gray and May [1994], Ratcliff, Jacewitz, and Gray, [1994], and Červený, and de Castro [1993] for discussions of the applications of ray-theoretic Green's functions in migration algorithms.

$$\phi(\boldsymbol{x},\boldsymbol{\xi}) = \tau(\boldsymbol{x},\boldsymbol{x}_s(\boldsymbol{\xi})) + \tau(\boldsymbol{x}_{\boldsymbol{g}}(\boldsymbol{\xi}),\boldsymbol{x}),$$
$$a(\boldsymbol{x},\boldsymbol{\xi}) = A(\boldsymbol{x},\boldsymbol{x}_s(\boldsymbol{\xi}))A(\boldsymbol{x}_g(\boldsymbol{\xi}),\boldsymbol{x}). \tag{5.1.8}$$

The care we have taken in specifying the order of arguments in $g(\boldsymbol{x}_g,\boldsymbol{x},\omega)$ is unnecessary for this particular problem because the constant-density scalar wave operator is *self-adjoint*. Other wave operators (for example, the variable-density acoustic wave operator) are not self-adjoint, however. In those cases, (5.1.7) has the proper structure; only the amplitude factor of the WKBJ Green's function is asymmetric in its arguments in the non-self-adjoint problem. The traveltime does not depend on the direction in which a ray is traced, meaning that the order of the arguments of τ is unimportant, even in the non-self-adjoint problem. Equation (5.1.8) is consistent with these characteristics.

We remark that this formulation can also accommodate modeling of mode-converted scalar components of elastic waves by requiring that the traveltime and amplitude to the geophone satisfy the appropriate eikonal and transport equations, different from the eikonal and transport equation for the traveltime and amplitude from the source. Because this is a *scalar* representation, however, it cannot account for all of the vector aspects of elastic wave propagation and scattering [Sumner, 1988].

The structure of previously derived inversion formulas will serve as a guide in the construction of the more general inversion formalism that we present here. Previously derived inversion formulas were Fourier-like integrals over frequency and over the source-receiver array with an integration kernel that was derived either exactly or asymptotically. The kernels of those inversion formulas all contained a phase function that was of the opposite sign of the phase function in the kernel of the respective forward-modeling formula. An important difference between forward-modeling formulas and their respective inversion formulas results from the distinction that was made between the Earth model variables, $\boldsymbol{x}$, and the output variables, $\boldsymbol{y}$. The phase of the forward-modeling integrand was a function of the input variables, $(\boldsymbol{x}_s,\boldsymbol{x}_g,\omega)$, or, now, $(\boldsymbol{\xi},\omega)$, and the earth modeling variables, $\boldsymbol{x}$, whereas the phase of the inversion kernel in the simpler problems was a function of both the input and output variables. Following this example, our inversion operators should include a phase functions of the form $-i\omega\phi(\boldsymbol{y},\boldsymbol{\xi})$. This is an example of what is often called *matched filtering*.

The amplitude of the inversion kernel could also be a function of the input variables, $(\boldsymbol{\xi},\omega)$, and the output variables, $\boldsymbol{y}$. In the three-dimensional example of Chapter 3, we found that there was no ω-dependence in the inversion kernel for the wavespeed perturbation α. The ω-dependence of the inversion kernel for the corresponding reflectivity function β consisted only of a multiplication by a factor of $i\omega$. Consequently, we will assume that the new inversion formulas for α and β that we are creating here will have the same dependence, and verify that this assumption is correct later.

Combining these ideas, we conclude that the inversion operator should have the form

$$\alpha(\boldsymbol{y}) = \int d\omega \int d^2\xi \; B(\boldsymbol{y},\boldsymbol{\xi}) e^{-i\omega\phi(\boldsymbol{y},\boldsymbol{\xi})} u_S(\boldsymbol{x}_g,\boldsymbol{x}_s,\omega), \tag{5.1.9}$$

where the kernel $B(\boldsymbol{y},\boldsymbol{\xi})$ is to be determined.

There are three approaches to the solution of this problem; see Beylkin [1985], Cohen and Hagin [1985], and Sullivan and Cohen [1987]. All three methods lead to the same inversion formula for $\alpha(\boldsymbol{y})$. The method developed here is a synthesis of these three approaches. Only the leading-order inversion operator is of interest because we have already restricted the problem to leading-order asymptotics in our approximations of the Green's functions. We substitute the data given in (5.1.7) into (5.1.9), to obtain the cascade of the forward-modeling formula and the associated inversion formula

$$\alpha(\boldsymbol{y}) = \int \omega^2 F(\omega) d\omega \int d^2\xi \; B(\boldsymbol{y},\boldsymbol{\xi}) \cdot \int d^3x \; e^{i\omega\{\phi(\boldsymbol{x},\boldsymbol{\xi})-\phi(\boldsymbol{y},\boldsymbol{\xi})\}} C(\boldsymbol{x},\boldsymbol{\xi})\alpha(\boldsymbol{x}), \tag{5.1.10}$$

where

$$C(\boldsymbol{x},\boldsymbol{\xi}) \equiv \frac{a(\boldsymbol{x},\boldsymbol{\xi})}{c^2(\boldsymbol{x})}. \tag{5.1.11}$$

Let us think of this sixfold integral as a threefold integral in $\boldsymbol{x}$ of $\alpha(\boldsymbol{x})$ times some kernel function, yielding $\alpha(\boldsymbol{y})$. If this is to be true, then the kernel function must, in some asymptotic sense, have the same sifting property as the Dirac delta function, $\delta(\boldsymbol{y}-\boldsymbol{x})$ in the integral

$$\alpha(\boldsymbol{y}) \sim \int d^3x \; \delta(\boldsymbol{x}-\boldsymbol{y})\alpha(\boldsymbol{x}).$$

We conclude, then, that the integration over $\boldsymbol{\xi}$ and ω in (5.1.10), with all of the factors except $\alpha(\boldsymbol{x})$, must produce a Dirac delta function, at least asymptotically. That is,

$$\delta(\boldsymbol{x}-\boldsymbol{y}) \sim \int \omega^2 F(\omega) d\omega \int d^2\xi \; B(\boldsymbol{y},\boldsymbol{\xi}) e^{i\omega\{\phi(\boldsymbol{x},\boldsymbol{\xi})-\phi(\boldsymbol{y},\boldsymbol{\xi})\}} C(\boldsymbol{x},\boldsymbol{\xi}). \tag{5.1.12}$$

To understand why this might be so, we must remember that the integral in (5.1.10) or in (5.1.12) is to be evaluated in a high-frequency asymptotic limit, where one might suspect that $\boldsymbol{x}=\boldsymbol{y}$ is a dominant critical point of the integrand. We note that the complex exponential part of the integrand in those equations is an oscillatory function, whose phase is identically zero for $\boldsymbol{x}=\boldsymbol{y}$, lending plausibility to the dominant critical-point idea. Intuitively, we might expect that the $\boldsymbol{\xi}$ integration would yield a larger result when the oscillations of the phase function are absent—that is, when $\boldsymbol{x}=\boldsymbol{y}$—as compared to the value of the $\boldsymbol{\xi}$ integration when $\boldsymbol{x}\neq\boldsymbol{y}$. It will be verified

later that the dominance of this critical point is, indeed, correct. Therefore, we are interested in approximating this integral for $\boldsymbol{x}$ in a neighborhood of $\boldsymbol{y}$.

Formally, in (5.1.12), we may expand the amplitude function $C(\boldsymbol{x}, \boldsymbol{\xi})$ and the phase function $i\omega \{\phi(\boldsymbol{x}, \boldsymbol{\xi}) - \phi(\boldsymbol{y}, \boldsymbol{\xi})\}$ into the Taylor series about the point $\boldsymbol{x} = \boldsymbol{y}$. Approximating the amplitude function by the first term of its Taylor series, we have

$$C(\boldsymbol{x}, \boldsymbol{\xi}) \approx C(\boldsymbol{y}, \boldsymbol{\xi}) = \frac{a(\boldsymbol{y}, \boldsymbol{\xi})}{c^2(\boldsymbol{y})},$$

while the difference in the phase has the approximation

$$\phi(\boldsymbol{x}, \boldsymbol{\xi}) - \phi(\boldsymbol{y}, \boldsymbol{\xi}) \approx \nabla_x \phi(\boldsymbol{x}, \boldsymbol{\xi}) \Big|_{\boldsymbol{x}=\boldsymbol{y}} \cdot (\boldsymbol{x} - \boldsymbol{y}) + \ldots,$$

yielding the following:

$$i\omega \{\phi(\boldsymbol{x}, \boldsymbol{\xi}) - \phi(\boldsymbol{y}, \boldsymbol{\xi})\} \approx i\boldsymbol{k} \cdot (\boldsymbol{x} - \boldsymbol{y}). \tag{5.1.13}$$

Here, $\omega \nabla \phi$ is interpreted as a wave vector $\boldsymbol{k}$, through the identity:[3]

$$\boldsymbol{k} \equiv \omega \nabla_y \phi(\boldsymbol{y}, \boldsymbol{\xi}) \equiv \omega \nabla_x \phi(\boldsymbol{x}, \boldsymbol{\xi}) \Big|_{\boldsymbol{x}=\boldsymbol{y}}. \tag{5.1.14}$$

We have approximated the total phase function by the first nonvanishing term of its Taylor series. This equation defines a change of variables of integration from $(\omega, \boldsymbol{\xi})$ to $\boldsymbol{k}$. In terms of the new variables of integration, (5.1.12) becomes

$$\delta(\boldsymbol{x} - \boldsymbol{y}) \sim \int d^3k \, B(\boldsymbol{y}, \boldsymbol{\xi}) \omega^2(\boldsymbol{k}) F(\omega(\boldsymbol{k})) \frac{a(\boldsymbol{y}, \boldsymbol{\xi})}{c^2(\boldsymbol{y})} \left| \frac{\partial(\omega, \boldsymbol{\xi})}{\partial(\boldsymbol{k})} \right| e^{i\boldsymbol{k} \cdot (\boldsymbol{x} - \boldsymbol{y})}. \tag{5.1.15}$$

The function $\omega(\boldsymbol{k})$ is defined via the expression (5.1.14) formally as

$$\omega(\boldsymbol{k}) = \frac{\boldsymbol{k} \cdot \nabla_y \phi(\boldsymbol{y}, \boldsymbol{\xi})}{|\nabla_y \phi(\boldsymbol{y}, \boldsymbol{\xi})|^2}. \tag{5.1.16}$$

The reciprocal of the Jacobian appearing in equation (5.1.15) is easier to calculate than the function $\partial(\boldsymbol{k})/\partial(\omega, \boldsymbol{\xi})$. To do so, it is sufficient to compute the necessary derivatives directly from the definition of $\boldsymbol{k}$ in (5.1.14). That result is

$$\frac{\partial(\boldsymbol{k})}{\partial(\omega, \boldsymbol{\xi})} = \omega^2 h(\boldsymbol{y}, \boldsymbol{\xi}),$$

---

[3] For $\boldsymbol{y}$ "near enough" to $\boldsymbol{x}$, there exists an exact change of variables from ω, $\boldsymbol{\xi}$ to $\boldsymbol{k}$ for which equation (5.1.13) is exact, (5.1.14) is the leading term of the Taylor series for $\boldsymbol{k}$, and (5.1.17) is the Jacobian of the change of variables at $\boldsymbol{x} = \boldsymbol{y}$. See Lemma 5.2 in Section 5.5.

$$h(\boldsymbol{y},\boldsymbol{\xi}) = \det \begin{bmatrix} \nabla_y \phi(\boldsymbol{y},\boldsymbol{\xi}) \\ \dfrac{\partial}{\partial \xi_1} \nabla_y \phi(\boldsymbol{y},\boldsymbol{\xi}) \\ \dfrac{\partial}{\partial \xi_2} \nabla_y \phi(\boldsymbol{y},\boldsymbol{\xi}) \end{bmatrix}, \tag{5.1.17}$$

so that $\omega^2 \partial(\omega,\boldsymbol{\xi})/\partial(\boldsymbol{k})$ is seen to be a function of $\boldsymbol{y}$ and $\boldsymbol{\xi}$ only.

The right side of (5.1.15) is seen to have the form of a forward and inverse Fourier transform with two exceptions. First, note from (5.1.15) that $\boldsymbol{\xi}$ is a function of the two independent variables in $\hat{\boldsymbol{k}} = \boldsymbol{k}/k$, because

$$\hat{\boldsymbol{k}} = \operatorname{sgn}(\omega) \nabla_y \phi(\boldsymbol{y},\boldsymbol{\xi}) / |\nabla_y \phi(\boldsymbol{y},\boldsymbol{\xi})|$$

relates these variables independent of the choice of $|\omega|$. Thus, the function $a(\boldsymbol{y},\boldsymbol{\xi})$, written in the new variables, depends on both $\hat{\boldsymbol{k}} = \boldsymbol{k}/k$ and $\boldsymbol{y}$. Second, the amplitude of the integrand depends on $\boldsymbol{y}$, as well as on $\boldsymbol{k}$.[4] Indeed, if (5.1.15) were an exact result, then the entire amplitude would have to be equal to $1/8\pi^3$. At the very least, if $F(\omega)$ were not identically equal to unity, this could not be an exact inverse transform. Thus, we should expect that, at best, this integral will be the cascade of an *asymptotic* forward and inverse transform. So, let us pose the problem more mildly; we ask only that the entire integrand should reduce to $1/8\pi^3$ for $F(\omega) = 1$. That is,

$$\frac{B(\boldsymbol{y},\boldsymbol{\xi}) a(\boldsymbol{y},\boldsymbol{\xi})}{|h(\boldsymbol{y},\boldsymbol{\xi})| c^2(\boldsymbol{y})} = \frac{1}{8\pi^3},$$

implying that

$$B(\boldsymbol{y},\boldsymbol{\xi}) = \frac{1}{8\pi^3} \frac{|h(\boldsymbol{y},\boldsymbol{\xi})| c^2(\boldsymbol{y})}{a(\boldsymbol{y},\boldsymbol{\xi})}. \tag{5.1.18}$$

With this value in place, (5.1.9) provides the high-frequency inversion of the observed data for the wavespeed perturbation as

$$\alpha(\boldsymbol{y}) = \frac{1}{8\pi^3} \int d^2\xi \, \frac{|h(\boldsymbol{y},\boldsymbol{\xi})| c^2(\boldsymbol{y})}{a(\boldsymbol{y},\boldsymbol{\xi})} \int d\omega \, e^{-i\omega\phi(\boldsymbol{y},\boldsymbol{\xi})} u_S(\boldsymbol{x}_g, \boldsymbol{x}_s, \omega). \tag{5.1.19}$$

Implicit in this inversion is an identification of a Fourier wave vector, $\boldsymbol{k}$ in (5.1.14) as a function of both frequency, and of a gradient vector that depends on the particular source-receiver configuration and the location of

---

[4]This is exactly the kind of integral considered in the Chapter 4. It should be expected that a justification of the approximations made here will be based on the theory developed in that chapter. While such a justification will not be presented in detail in this text, it has been carried out [Bleistein, 1988] and will be briefly discussed later. Note, however, that for this definition of $\hat{\boldsymbol{k}}$, positive and negative values of ω pick out vectors in both of the directions, $\pm\nabla_y \phi(\boldsymbol{y},\boldsymbol{\xi})/|\nabla_y \phi(\boldsymbol{y},\boldsymbol{\xi})|$, as anticipated by the theory of the last chapter.

the output point. This is what we claimed in the discussion in Section 4.2. As in that discussion, we tie this identification back to something more familiar. Recall that for the constant-background, zero-offset inversion of Chapter 3, the sum of traveltimes, $\phi(\boldsymbol{y}, \boldsymbol{\xi})$ as defined by (5.1.8) is just the two-way traveltime $2r/c_0 = 2|\boldsymbol{y} - \boldsymbol{x}_s|/c_0$, for which $\boldsymbol{k} = 2\omega\hat{\boldsymbol{r}}/c_0$. This is just the stationary phase result, (3.6.11), except for the detail of the special treatment of k_3 in the analysis of that section. Likewise, the $\omega(\boldsymbol{k})$ that is defined in equation (5.1.16) reduces to the formula for ω of the zero-offset, constant-background case treated in Chapter 3.

The direction, $\hat{\boldsymbol{k}}$, of the vector, $\boldsymbol{k}$, is the *migration dip*, (discussed in Chapter 4). We can think of a particular survey as sweeping out an area of migration dips on the unit sphere—a suite of directions—as the sources and receivers range over the acquisition surface. This sweep varies with the location of the output point $\boldsymbol{y}$, as well as with the range of sources and receivers of the given experiment.

The determinant, $h(\boldsymbol{y}, \boldsymbol{\xi})$ in (5.1.17), must be finite and nonzero for the identification of the cascaded model and inversion integral (5.1.10) as an approximate Fourier integral (5.1.15). Thus, we could use the value of this matrix to characterize whether or not given source-receiver configurations provide invertible data by this formalism at an output point $\boldsymbol{y}$. In particular, we require that this determinant be finite and nonzero for some range of $\boldsymbol{\xi}$ values at any $\boldsymbol{y}$ where the high-frequency inversion is to be computed.

The expression of the spatial weighting in terms of this one determinant for any source-receiver configuration and background propagation speed is a major contribution of Beylkin's [1985] approach to high-frequency inversion.[5] For this reason, we will henceforth refer to this object as the *Beylkin determinant.*

5.1.3 Inversion for a Reflectivity Function

Equation (5.1.15) is a Fourier-like integral of the type discussed in Chapter 4. The perturbation function $\alpha(\boldsymbol{y})$ will be assumed to be piecewise-smooth, but also to have discontinuity surfaces that behave as reflectors. Because data must be assumed to be band- and aperture-limited, we know

[5]The lasting contribution of Beylkin [1985] was the identification of Fourier-like inverse-scattering inversion formulas of the type we discuss throughout this text with the mathematical objects known as *elliptic pseudodifferential operators.* The importance of this contribution stems from the fact that mathematicians have created a set of well defined rules describing an *algebra* for this class of operators. That is, the multiplication, division, and composition (which is to say, cascading) of elliptic pseudodifferential operators is well defined. We are, therefore, justified in constructing inverses of such operators as in Chapters 2 through 6, and in the cascading (composing) of such operators, as we do in Chapter 7. See the discussions in Sections 2.5.1 and 4.4.9.

from the results of Chapter 4 that inverting for $\alpha(\boldsymbol{x})$ will produce band- and aperture-limited step functions acting at the positions of the reflector surfaces. However, such band- or aperture-limited step functions are not ideal reflector images for parameter estimation because they are doublet-like waveforms with zero-crossings at the reflector positions. Therefore, as in Chapters 2 and 3 we will modify equation (5.1.15) to invert for the reflectivity function $\beta(\boldsymbol{y})$ so that the reflector surfaces will be delineated by band- and aperture-limited impulses, instead.

In Chapter 4, such a modification was obtained by applying a symmetric filter in the $\boldsymbol{k}$-domain. We will apply the same filter to (5.1.15) to create an inversion formula to invert for the reflectivity. This filter is a simple multiplication by ik in one half of the $\boldsymbol{k}$-domain, and a multiplication by $-ik$ in the other half of the $\boldsymbol{k}$-domain.

The magnitude of the wave vector $\boldsymbol{k}$, as defined by (5.1.14), is simply $k = |\omega||\nabla_y \phi(\boldsymbol{y}, \boldsymbol{\xi})|$. It follows that the symmetric filter in $\boldsymbol{k}$-domain can be taken to be $i\omega|\nabla_y \phi(\boldsymbol{y}, \boldsymbol{\xi})|$ where $\operatorname{sgn}(\omega)$ expresses the desired change of sign in the two halves of the $\boldsymbol{k}$-domain. Thus, we obtain the reflectivity function $\tilde{\beta}$,

$$\tilde{\beta}(\boldsymbol{y}) = \int d^2\xi \; B(\boldsymbol{y}, \boldsymbol{\xi}) |\nabla_y \phi(\boldsymbol{y}, \boldsymbol{\xi})| \cdot \int i\omega \; d\omega \; e^{-i\omega\phi(\boldsymbol{y}, \boldsymbol{\xi})} u_S(\boldsymbol{x}_g, \boldsymbol{x}_s, \omega), \tag{5.1.20}$$

which is the first inversion formula that we have deduced by applying the theory of Chapter 4 to equation (5.1.9). Other reflectivity functions will follow in this chapter.

Up to this point, we only expect a result in the form of a bandlimited singular function $\gamma(\boldsymbol{x})$ of the reflector(s)—discontinuity surface(s)—scaled by the jump across the reflector. However we should anticipate, as in our earlier inversion formulas, that the asymptotic output is proportional to some reflection coefficient. This reflection coefficient will be a function of the jump in material parameters (wavespeed, wavespeed and density, or impedance) that is localized to the values of $\boldsymbol{x}$ where $\gamma(\boldsymbol{x})$ acts. Recall that in the one-dimensional inversion results, as well as in the higher-dimensional zero-offset (constant-background wavespeed) problems, division by 4 yielded an output that was the reflection coefficient times a singular function. In the next section we show that the correct divisor in this case is the dimensionless expression, $c^2(\boldsymbol{y})|\nabla_y \phi(\boldsymbol{y}, \boldsymbol{\xi})|^2$, which reduces to a divisor of 4 in the case of zero offset. This more exotic divisor will be seen to account for *obliquity*—an additional amplitude factor due to the angular separation of rays traced from the output point to the source and receiver—in the non-zero-offset inversion process. Thus, using equation (5.1.18), equation (5.1.20), and this new divisor, the inversion for a new reflectivity function is proposed. This new inversion formula is

$$\beta(\boldsymbol{y}) = \frac{1}{8\pi^3} \int d^2\xi \frac{|h(\boldsymbol{y},\boldsymbol{\xi})|}{a(\boldsymbol{y},\boldsymbol{\xi})|\nabla_y \phi(\boldsymbol{y},\boldsymbol{\xi})|} \cdot \int i\omega \, d\omega \, e^{-i\omega\phi(\boldsymbol{y},\boldsymbol{\xi})} u_S(\boldsymbol{x}_g, \boldsymbol{x}_s, \omega). \qquad (5.1.21)$$

5.1.4 *Summary of Asymptotic Verification*

As in Chapter 3, this formula will be analytically tested by applying it to Kirchhoff-approximate data representing the scattered field from a single reflector, S, in a medium with a known background wavespeed. This analysis is the subject of Section 5.4. For the reader who prefers to skip the details of that analysis, we state the main results in Sections 5.1.6 through 5.1.7.

5.1.5 *Inversion in Two Dimensions*

While this chapter is devoted to the formulation of inversion in models with 3D wavespeed variability, models with 2D variability are equally important. In Chapter 6, we will present results for inversion in models with 2D variability, but still with waves experiencing 3D (spherical) geometrical spreading—which is to say *2.5D models.*

Though less physically relevant, inversions of *fully* 2D data (with waves experiencing cylindrical, instead of spherical, spreading) are still important for comparison. Because of the computer-intensive nature of fully 3D seismic modeling, particularly for generating synthetics using finite-difference solutions to the wave equation, the geophysical community has relied on purely 2D methods for many seismic modeling applications. We will not present a comprehensive study of 2D inversion, but we will make use of the 3D results derived in this section to point the way, via a set of exercises, to the 2D inversion formulas corresponding to those results.

Therefore, the purpose of this next series of exercises is to derive a 2D inversion formula following the discussion in this section. Essentially, the steps of the previous 3D derivation are repeated, except that the derivation begins with a 2D modeling formula, involving 2D Green's functions. The point of these exercises is to get the powers of ω right. Thus, we consider a two-dimensional model in which data acquired along a line or curve on one side of a halfspace (the interior of the "2D Earth," for example). Equivalently, we can think of line sources in 3D along lines parallel to the generators of a "cylindrical Earth."

The discussion of asymptotic inversion will begin with the Born-approximate integral equation for the scattered field that was originally presented as equation (3.2.1).

Exercises

5.1 Explain why the shift from 3D to 2D leads to the integral equation

$$u_S(\boldsymbol{x}_g, \boldsymbol{x}_s, \omega) = \omega^2 \int_D \frac{\alpha(\boldsymbol{x})}{c^2(\boldsymbol{x})} u_I(\boldsymbol{x}, \boldsymbol{x}_s, \omega) g(\boldsymbol{x}_g, \boldsymbol{x}, \omega) d^2x, \quad (5.1.22)$$

which is the same as the previous 3D Born modeling formula result, with the exception of the integration being two-dimensional, and D being a two-dimensional domain.

Here, in keeping with our preference of maintaining z or x_3 as the depth variable, we take $\boldsymbol{x} = (x, z)$ or $\boldsymbol{x} = (x_1, x_3)$, with similar definitions for $\boldsymbol{x}_s$, $\boldsymbol{x}_g$, and any other spatial and wave vectors that will arise.

The sources and receivers may be located on a curve; they need not be restricted to a horizontal line. Therefore, as in the development above, we represent the sources more generally, with the position vectors, $\boldsymbol{x}_s$, $\boldsymbol{x}_s$, now functions of a scalar parameter, ξ. The ideas here follow the ideas there and will not be repeated in this brief discussion.

5.2 If the incident field u_I is represented by

$$u_I(\boldsymbol{x}, \boldsymbol{x}_s, \omega) = F(\omega) g(\boldsymbol{x}, \boldsymbol{x}_s, \omega), \quad (5.1.23)$$

then verify that equation (5.1.22) is recast as an integral with two Green's functions,

$$u_S(\boldsymbol{x}_g, \boldsymbol{x}_s, \omega) = \omega^2 F(\omega) \int_D \frac{\alpha(\boldsymbol{x})}{c^2(\boldsymbol{x})} g(\boldsymbol{x}, \boldsymbol{x}_s, \omega) g(\boldsymbol{x}_g, \boldsymbol{x}, \omega) d^2x. \quad (5.1.24)$$

5.3 Again, we invoke high frequency asymptotics at the very beginning of the analysis. To do this, we replace the Green's functions in this equation by their WKBJ (ray-theoretic) approximations. Explain why, for two-dimensional problems, these Green's functions take the form

$$g(\boldsymbol{x}, \boldsymbol{x}_0, \omega) \sim \frac{e^{i\pi/4 \operatorname{sgn}(\omega)}}{\sqrt{|\omega|}} A(\boldsymbol{x}, \boldsymbol{x}_0) e^{i\omega\tau(\boldsymbol{x}, \boldsymbol{x}_0)}.$$

Here, as for the 3D problems, τ is the traveltime from $\boldsymbol{x}_0$ to $\boldsymbol{x}$ and $A(\boldsymbol{x}, \boldsymbol{x}_0)$ is the corresponding ray-theoretic amplitude, derived by solving the eikonal equation

$$\nabla\tau \cdot \nabla\tau = \frac{1}{c^2(\boldsymbol{x})}, \qquad \tau(\boldsymbol{x}_0, \boldsymbol{x}_0) = 0, \quad (5.1.25)$$

and the (first) transport equation

$$2\nabla\tau \cdot \nabla A + A\nabla^2\tau = 0, \quad (5.1.26)$$

subject now to the condition

$$2\sqrt{2\pi|\boldsymbol{x} - \boldsymbol{x}_0|/c} A \to 1, \qquad \text{as} \quad |\boldsymbol{x} - \boldsymbol{x}_0| \to 0. \quad (5.1.27)$$

Hint:

Consider the case of a constant-background medium. Show that the Green's function in this case is $iH_0^{(1)}(\omega r/c)/4$, with r being radial distance from the source and $H_0^{(1)}$ the Hankel function of the first kind (consistent with our choice of temporal Fourier transform). Then, use the asymptotic expansion of this Green's function (Appendix E) to verify the spatial and frequency structure of the general Green's function defined above.

5.4 Show that substitution of the WKBJ Green's functions into (5.1.24) yields

$$u_S(\boldsymbol{x}_g, \boldsymbol{x}_s, \omega) \approx i\omega F(\omega) \int d^2x \frac{\alpha(\boldsymbol{x})}{c^2(\boldsymbol{x})} a(\boldsymbol{x}, \xi) e^{i\omega\phi(\boldsymbol{x},\boldsymbol{\xi})}, \tag{5.1.28}$$

where

$$\begin{aligned} \phi(\boldsymbol{x}, \xi) &= \tau(\boldsymbol{x}, \boldsymbol{x}_s(\xi)) + \tau(\boldsymbol{x_g}(\xi), \boldsymbol{x}), \\ a(\boldsymbol{x}, \xi) &= A(\boldsymbol{x}, \boldsymbol{x}_s(\xi)) A(\boldsymbol{x}_g(\xi), \boldsymbol{x}). \end{aligned} \tag{5.1.29}$$

Hint:

Here, use

$$\begin{aligned} \omega^2 \left[\frac{e^{i\pi/4 \operatorname{sgn}(\omega)}}{\sqrt{|\omega|}} \right]^2 &= |\omega|^2 \left[\frac{e^{i\pi/4 \operatorname{sgn}(\omega)}}{\sqrt{|\omega|}} \right]^2 \\ &= |\omega| e^{i\pi/2 \operatorname{sgn}(\omega)} = i\omega. \end{aligned}$$

5.5 Follow the discussion of the 3D derivation to conclude that the inversion operator should have the form

$$\alpha(\boldsymbol{y}) = \int d\omega f(\omega) \int d^2\xi \, B(\boldsymbol{y}, \xi) e^{-i\omega\phi(\boldsymbol{y},\boldsymbol{\xi})} u_S(\boldsymbol{x}_g, \boldsymbol{x}_s, \omega), \tag{5.1.30}$$

where the kernel $B(\boldsymbol{y}, \xi)$ and the function $f(\omega)$ are to be determined. Explain why we have included a possible frequency domain filter here that was absent in the 3D derivation.

5.6 Verify that the cascade of the forward-modeling formula and the inversion formula yields the representation

$$\begin{aligned} \alpha(\boldsymbol{y}) = \int i\omega f(\omega) F(\omega) d\omega \int d\xi \, B(\boldsymbol{y}, \xi) \\ \cdot \int d^2x \, e^{i\omega\{\phi(\boldsymbol{x},\boldsymbol{\xi}) - \phi(\boldsymbol{y},\boldsymbol{\xi})\}} C(\boldsymbol{x}, \xi) \alpha(\boldsymbol{x}), \end{aligned} \tag{5.1.31}$$

where

$$C(\boldsymbol{x},\xi) \equiv \frac{a(\boldsymbol{x},\xi)}{c^2(\boldsymbol{x})}. \tag{5.1.32}$$

5.7 Explain why the asymptotic structure of this equation must have the form

$$\alpha(\boldsymbol{y}) \sim \int d^2x\, \delta(\boldsymbol{x}-\boldsymbol{y})\alpha(\boldsymbol{x}),$$

or

$$\delta(\boldsymbol{x}-\boldsymbol{y}) \sim \int i\omega f(\omega)F(\omega)d\omega \cdot \int d\xi\, B(\boldsymbol{y},\xi)e^{i\omega\{\phi(\boldsymbol{x},\boldsymbol{\xi})-\phi(\boldsymbol{y},\boldsymbol{\xi})\}}C(\boldsymbol{x},\xi). \tag{5.1.33}$$

5.8 Explain why we may use the approximations

$$C(\boldsymbol{x},\xi) \approx C(\boldsymbol{y},\xi)$$

and

$$\phi(\boldsymbol{x},\xi)-\phi(\boldsymbol{y},\xi) \approx \nabla_x\phi(\boldsymbol{x},\xi)\Big|_{\boldsymbol{x}=\boldsymbol{y}} \cdot (\boldsymbol{x}-\boldsymbol{y}) + \ldots.$$

5.9 Show that this last approximation leads to the introduction of a local wave vector, $\boldsymbol{k}$, as follows:[6]

$$i\omega\{\phi(\boldsymbol{x},\xi)-\phi(\boldsymbol{y},\xi)\} \approx i\boldsymbol{k}\cdot(\boldsymbol{x}-\boldsymbol{y}). \tag{5.1.34}$$

$$\boldsymbol{k} \equiv \omega\nabla_y\phi(\boldsymbol{y},\xi) \equiv \omega\nabla_x\phi(\boldsymbol{x},\xi)\Big|_{\boldsymbol{x}=\boldsymbol{y}}. \tag{5.1.35}$$

5.10 Show that

$$\hat{\boldsymbol{k}} = \boldsymbol{k}/k = \operatorname{sgn}(\omega)\nabla_y\phi(\boldsymbol{y},\xi)/|\nabla_y\phi(\boldsymbol{y},\xi)|,$$

relates ξ to $\hat{\boldsymbol{k}}$, independent of ω, except for the trivial dependence on sign. Thus, the direction of $\boldsymbol{k}$ is completely determined by the acquisition geometry through the directions of the rays from source and receiver at the imaging point; that is, it is a function of $\boldsymbol{x}_s(\xi)$, $\boldsymbol{x}_g(\xi)$, and $\boldsymbol{y}$. As noted in the text in the discussion of 3D inversion, this direction is called the *migration dip*.

---

[6] As noted above in the discussion of 3D inversion, for $\boldsymbol{y}$ "near enough" to $\boldsymbol{x}$, there exists an exact change of variables from ω, ξ to $\boldsymbol{k}$ for which the result here is the leading term of a Taylor series for $\boldsymbol{k}$. See Lemma 5.2 in Section 5.5.

5.11 Show that, with $\boldsymbol{k}$ replacing the variables ξ and ω, (5.1.33) becomes

$$\delta(\boldsymbol{x}-\boldsymbol{y}) \sim \int d^2k\, B(\boldsymbol{y},\xi) i\omega(\boldsymbol{k}) f(\omega(\boldsymbol{k})) \cdot F(\omega(\boldsymbol{k})) \frac{a(\boldsymbol{y},\xi)}{c^2(\boldsymbol{y})} \left| \frac{\partial(\omega,\xi)}{\partial(\boldsymbol{k})} \right| e^{i\boldsymbol{k}\cdot(\boldsymbol{x}-\boldsymbol{y})}. \quad (5.1.36)$$

Here, the function $\omega(\boldsymbol{k})$ is defined via the expression (5.1.35) formally as

$$\omega(\boldsymbol{k}) = \frac{\boldsymbol{k}\cdot\nabla_y\phi(\boldsymbol{y},\xi)}{|\nabla_y\phi(\boldsymbol{y},\xi)|^2}. \quad (5.1.37)$$

5.12 It is easier to calculate the reciprocal of the Jacobian appearing in equation (5.1.36), that is, the function, $\partial(\boldsymbol{k})/\partial(\omega,\xi)$. To do so, it is sufficient to compute the necessary derivatives directly from the definition of $\boldsymbol{k}$ in (5.1.35). Show that

$$\frac{\partial(\boldsymbol{k})}{\partial(\omega,\xi)} = \omega H(\boldsymbol{y},\xi) \quad (5.1.38)$$

$$H(\boldsymbol{y},\xi) = \det \begin{bmatrix} \nabla_y\phi(\boldsymbol{y},\xi) \\ \dfrac{\partial}{\partial\xi}\nabla_y\phi(\boldsymbol{y},\xi) \end{bmatrix}.$$

5.13 Verify that $\omega[\partial(\omega,\xi)/\partial(\boldsymbol{k})]$ is a function of $\boldsymbol{y}$ and ξ, only. However, note that the absolute value of this function appears in (5.1.36), so we need to take some care to account for this in our analysis, below.

5.14 Follow the arguments of this section to conclude that

$$f(\omega) i\,\mathrm{sgn}\,(\omega) \frac{B(\boldsymbol{y},\xi)a(\boldsymbol{y},\xi)}{|H(\boldsymbol{y},\xi)|c^2(\boldsymbol{y})} = \frac{1}{4\pi^2},$$

implying that

$$B(\boldsymbol{y},\xi) = \frac{1}{4\pi^2}\frac{|H(\boldsymbol{y},\xi)|c^2(\boldsymbol{y})}{a(\boldsymbol{y},\xi)} \qquad \text{and} \qquad f(\omega) = -i\,\mathrm{sgn}\,(\omega). \quad (5.1.39)$$

5.15 Show that, with this value in place, (5.1.30) provides the high-frequency inversion of the observed data for the wavespeed perturbation as

$$\alpha(\boldsymbol{y}) = \frac{-1}{4\pi^2}\int d\xi\, \frac{|H(\boldsymbol{y},\xi)|c^2(\boldsymbol{y})}{a(\boldsymbol{y},\xi)} \cdot \int i\,\mathrm{sgn}\,(\omega) d\omega\, e^{-i\omega\phi(\boldsymbol{y},\boldsymbol{\xi})} u_S(\boldsymbol{x}_g,\boldsymbol{x}_s,\omega). \quad (5.1.40)$$

We remark that the frequency domain filter, $-i\,\mathrm{sgn}\,(\omega)$, is equivalent to extracting the *Hilbert transform* of the temporal data. See Section A.7.1.

5.16 Explain why the discussion that leads to the derivation of β remains unchanged. However, show that the revised expression for β is as follows.

$$\beta(\boldsymbol{y}) = \frac{1}{4\pi^2}\int d\xi \frac{|H(\boldsymbol{y},\xi)|}{a(\boldsymbol{y},\xi)|\nabla_y\phi(\boldsymbol{y},\xi)|} \cdot \int |\omega|\, d\omega\, e^{-i\omega\phi(\boldsymbol{y},\boldsymbol{\xi})} u_S(\boldsymbol{x}_g,\boldsymbol{x}_s,\omega). \quad (5.1.41)$$

5.1.6 *General Inversion Results, Stationary Triples, and* $\cos\theta_s$

In Section 5.4, we will present a detailed asymptotic analysis of the application of the inversion formula, (5.1.21), to Kirchhoff approximate data for a single reflector, paralleling the analysis of Section 3.7. The essential details of that derivation arise from asymptotic analysis of the combined phase that arises from the cascade of the modeling and inversion integrals. Here, we provide a synopsis of that analysis with some qualitative remarks about the details of the analysis.

The dominant contribution to the asymptotic expansion occurs when there are "stationary triples." A stationary triple consists of a source point $\boldsymbol{x}_s$, a receiver position $\boldsymbol{x}_g$, and a reflection point $\boldsymbol{x}$, located on the scattering surface such that the law of reflection is satisfied at $\boldsymbol{x}$ for the given source-receiver pair. Furthermore, the output point $\boldsymbol{y}$ is tied to this triple through a requirement on the gradients of the traveltimes to source and receiver points from $\boldsymbol{y}$ to the upper surface (see Figure 5.2). This latter condition takes on a slightly different form for each of the source-receiver configurations of

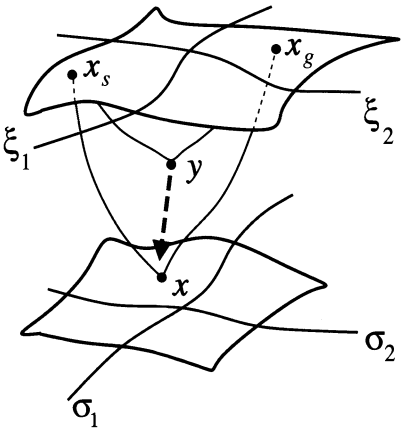

FIGURE 5.2. The graphical representation of the "stationary triple" composed of the source position $\boldsymbol{x}_s$, receiver position $\boldsymbol{x}_g$, and reflection point $\boldsymbol{x}$ on the reflecting surface.

interest. However, by associating $\boldsymbol{y}$ with the stationary triple, this condition defines each of those points as functions of the output point $\boldsymbol{y}$.

In terms of the vector $\boldsymbol{k}$ defined by (5.1.14), the stationarity condition requires that the stationary value of $\boldsymbol{k}$ be the wavenumber vector pointing normal to the surface S. For each output point $\boldsymbol{y}$ on the reflector, as ω and $\boldsymbol{\xi}$ vary over their domains, (5.1.14) defines a mapped $\boldsymbol{k}$-domain. For a prescribed output point the only reflectors that could possibly be imaged are those for which the normal vector to the surface points in direction supported in the mapped $\boldsymbol{k}$-domain. When there is no stationary triple for the given $\boldsymbol{y}$, the output is asymptotically of lower order (and, presumably, smaller) at that output point.

We characterize the inclination of the tangent plane of the reflector at each point by its normal, introducing the term *reflector normal dip* or, more succinctly, *reflector dip*. Then, we can state the condition that we just described for our inversion formula to yield an image at a particular point as follows.

> A stationary point in $\boldsymbol{x}$ and $\boldsymbol{\xi}$ exists for a given output point $\boldsymbol{y}$ on the reflector when the migration dip equals the reflector dip at that point.

Alternatively,

> An image will only be produced at points where the sweep of migration dips includes the reflector dip.

The first form here focuses on the asymptotic analysis; the second form implies a need to design the source/receiver array with an eye towards the range of dips of reflectors to be expected in the region of interest in the Earth.

When the stationary triple does exist, the output is shown to be proportional to the bandlimited singular function of the surface, introduced in Chapter 4, denoted by $\gamma_B(\boldsymbol{y})$ or $\delta_B(s)$. That is,

$$\beta(\boldsymbol{y}) \sim f(\boldsymbol{y}) R(\boldsymbol{x}, \theta_s) \gamma_B(\boldsymbol{y}), \tag{5.1.42}$$

where θ_s is the angle of incidence (or reflection) for a *specularly incident* ray. In this equation, $f(\boldsymbol{y})$ is a slowly varying function of $\boldsymbol{y}$, which is equal to unity when $\boldsymbol{y}$ is on the reflector, S. Furthermore, $R(\boldsymbol{x}, \theta_s)$ is the geometrical-optics reflection coefficient at the incidence angle θ_s determined by the stationary triple.[7] For $\boldsymbol{y}$ on S, $\boldsymbol{x} = \boldsymbol{y}$ and $\gamma_B(\boldsymbol{y}) = \delta_B(\boldsymbol{0})$, where this latter function is easily expressed in terms of the filter and the

---

[7]The subscript s is used to indicate that this is the angle that the incident or reflected ray makes with the vertical (and is, therefore, $\frac{1}{2}$ the opening angle between the incident and reflected rays) for the special case of a *specularly* reflected ray. The reader should note that when $\cos\theta$ appears in an inversion formula, the θ is a ray theoretic estimate of half the angle between two rays traced to a

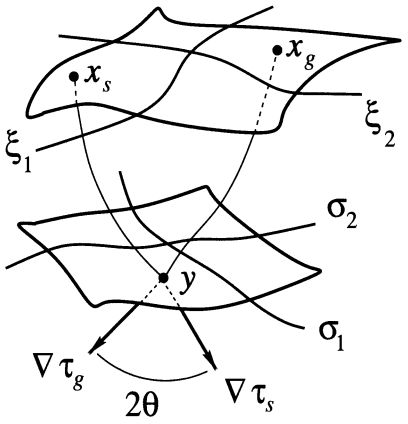

FIGURE 5.3. When the stationary triple exists, the output point $\boldsymbol{y}$ is also the stationary point $\boldsymbol{x}$ on the reflector. The ray direction from the output point to the source is along $\nabla\tau_s \equiv \nabla_y\tau(\boldsymbol{y}, \boldsymbol{x}_s)$. The ray direction from the output point to the receiver is along $\nabla\tau_g \equiv \nabla_y\tau(\boldsymbol{y}, \boldsymbol{x}_g)$. The opening angle, $2\theta_s$, is the angle between these two vectors for the special case of a specularly reflected ray.

same θ_s. This leads to the result

$$\begin{aligned}\beta_{\text{PEAK}}(\boldsymbol{y}) &\sim R(\boldsymbol{y}, \theta_s)\delta_B(0) \\ &\sim R(\boldsymbol{y}, \theta_s)\frac{1}{2\pi}\int_{-\infty}^{\infty} \tilde{F}(k)\, dk, \quad \tilde{F}(k) = F(ck/2cos\theta_s).\end{aligned}$$

But we show further that the transformation from a k-integral to an ω-integral leads to the result

$$\beta_{\text{PEAK}} \sim R(\boldsymbol{y}, \theta_s)\frac{\cos\theta_s}{\pi c(\boldsymbol{y})}\int_{-\infty}^{\infty} F(\omega)d\omega, \quad \text{for} \quad \boldsymbol{y} \quad \text{on} S. \tag{5.1.43}$$

That is, the peak value of β for $\boldsymbol{y}$ on S is the geometrical-optics reflection coefficient multiplied by $2\cos\theta_s/c(\boldsymbol{y})$ times $1/2\pi$, further multiplied by the area under the filter in the ω-domain.

Determination of $\cos\theta_s$

For $\boldsymbol{y}$ not on S, the angle θ is defined by the equation

$$\nabla_y\tau(\boldsymbol{y}, \boldsymbol{x}_s) \cdot \nabla_y\tau(\boldsymbol{y}, \boldsymbol{x}_g) = \frac{\cos 2\theta}{c^2(\boldsymbol{y})}, \tag{5.1.44}$$

which follows from the eikonal equation and the definition of the dot product of two vectors. By computing $\nabla\phi(\boldsymbol{y}, \boldsymbol{\xi})\cdot\nabla\phi(\boldsymbol{y}, \boldsymbol{\xi})$, we may apply (5.1.44) and the eikonal equation to show that

---

particular subsurface location using the given background-wavespeed profile, and does not, in general, represent a specular reflection angle.

$$|\nabla_y \phi(\boldsymbol{y}, \boldsymbol{\xi})|^2 = |\nabla_y \tau(\boldsymbol{y}, \boldsymbol{x}_s)|^2 + |\nabla_y \tau(\boldsymbol{y}, \boldsymbol{x}_g)|^2 + 2\nabla_y \tau(\boldsymbol{y}, \boldsymbol{x}_s) \cdot \nabla_y \tau(\boldsymbol{y}, \boldsymbol{x}_g)$$
$$= \frac{1}{c^2(\boldsymbol{y})} \{1 + 2\cos 2\theta\} = \frac{4\cos^2 \theta}{c^2(\boldsymbol{y})}. \tag{5.1.45}$$

Thus,

$$\cos\theta = \frac{c(\boldsymbol{y})}{2|\nabla_y \phi(\boldsymbol{y}, \boldsymbol{\xi})|}. \tag{5.1.46}$$

In particular, for $\boldsymbol{y}$ on S, this provides a means for estimating $\cos\theta_s$, through the introduction of another inversion operator, differing from β by one power of $|\nabla_y \phi|$:

$$\beta_1(\boldsymbol{y}) = \frac{1}{8\pi^3} \int d^2\xi \frac{|h(\boldsymbol{y}, \boldsymbol{\xi})|}{a(\boldsymbol{y}, \boldsymbol{\xi}) |\nabla_y \phi(\boldsymbol{y}, \boldsymbol{\xi})|^2} \cdot \int i\omega \, d\omega \, e^{-i\omega\phi(\boldsymbol{y}, \boldsymbol{\xi})} u_S(\boldsymbol{x}_g, \boldsymbol{x}_s, \omega). \tag{5.1.47}$$

The asymptotic analysis of β_1 proceeds exactly as for $\beta(\boldsymbol{y})$. The introduction of the extra divisor of $|\nabla_y \phi|$, however, introduces this divisor in the asymptotic amplitudes of the result, as well. In particular, using (5.1.43) and (5.1.45), we conclude that

$$\beta_{1\text{PEAK}}(\boldsymbol{y}) \sim R(\boldsymbol{y}, \theta_s) \frac{1}{2\pi} \int F(\omega) \, d\omega, \quad \text{for } \boldsymbol{y} \text{ on } S. \tag{5.1.48}$$

The fact that these two operators differ by a factor of $2\cos\theta / c(\boldsymbol{y})$ allows us to estimate $\cos\theta_s$ from the ratio of the outputs *without ever having to determine the specular source-receiver pair that produced the distinguished value of* θ_s*!* This, in turn, allows us to determine $R(\boldsymbol{y}, \theta_s)$ from either output. With knowledge of θ_s and the background-wavespeed $c(\boldsymbol{y})$, it is conceivable, within the limits of the accuracy of the data, that we should be able to estimate the jump in the propagation speed across S using the formula for the geometrical-optics reflection coefficient. At the very least, we would have a value of the reflection coefficient as a function of angle for the amplitude, versus, offset (AVO) analysis.

We note also, here, that computation of β by (5.1.21) involves computation of a square root, $|\nabla_y \phi|$ for each $\boldsymbol{\xi}$, whereas the computation of β_1, above, involves computation of the square of the gradient—no square root. Now that we understand the role of factors of $|\nabla_y \phi|$ in the amplitude, we could conceive of *another* inversion operator, say β_2, with *no* factor of $|\nabla_y \phi|$ in the integrand. The output from this new operator would differ from β_1 by a factor of $4\cos^2 \theta_s / c^2(y)$. The ratio of the two outputs, β_1 and β_2, could just as easily be used to determine $\cos\theta_s$ as the ratio proposed above. The advantage in computing β_1 and β_2 is that there is no square root necessary in the calculation. (Such computations do not require multiple migrations of the data. They require only that two different multiplications occur in

the innermost loop of the migration/inversion algorithm. Thus, one pass at the migration could generate both the β_1 and β_2 outputs.)

Despite this observation, for theoretical purposes, we will continue to develop the theory in terms of β and β_1.

When Things Go Wrong

In heterogeneous media, it is possible that the ray Jacobian that defines one or the other of the amplitudes in (5.1.8) might be zero for some choice of $(\boldsymbol{y}, \boldsymbol{\xi})$. (See (E.3.9).) The actual Green's function is not infinite there, but the simple structure $A \exp\{i\omega\tau\}$ is no longer valid in such a region. Fortunately, such events occur at isolated points (a "set of measure zero," in mathematical jargon), and thus make a minor contribution to the integration process. Furthermore, the limit of the integrand in this case is zero, provided h remains finite at such a point. Thus, we can expect only small errors in the analytical integration through such points, even if we continue to use the asymptotic expressions for the Green's functions in a regime where they are not valid. Because such errors are a characteristic of the approximations we are using for the Green's functions, we could consider replacing our classical WKBJ asymptotics with a more appropriate asymptotic expansion. A *uniform expansion*, for example, would produce a large, though not infinite, amplitude at such a point, but because the points are all isolated, this would result, again, in only a small contribution to the total integral. In practice, there is little reason to go to such lengths for this reason.

When the integral is transformed into a sum, one simply needs a criterion to skip points where the Jacobian, on which the amplitude is based, is too small. Alternatively, one could explicitly write the amplitude in terms of the Jacobian. Then, the integrand would be zero at such points, because the amplitudes vary inversely with the square root of the Jacobian.

The zeros of the Jacobian indicate that the geometrical optics ray is passing through an envelope or *caustic* of the ensemble of rays of the Green's function, such as might happen when rays propagate through a low-velocity lens on their path from $\boldsymbol{y}$ to source or receiver. With the caustic passing through the data-acquisition surface, on one side or the other of the surface point where there is a caustic, the caustic will be below the surface. At that point, the rays shall have passed through this caustic on their trajectory to the surface. The amplitude of the Green's function must then be adjusted with a phase shift to account for the passage through the caustic. We will not address such cases in the text, but the extension of these methods to deal with caustics with some degree of complexity is possible. See, for example, de Hoop [1998].

There is also the possibility that the Beylkin determinant might be infinite or zero. Again, if this occurs at isolated points, it indicates that the basic premises of the theory have broken down, but the contribution to the

overall sum or integral of more accurate representations of the integrand at such isolated points will be negligible.

The only time either of these pathologies is a serious problem for the basic theory is if the particular value of $\boldsymbol{\xi}$ corresponds to the specular source/receiver pair—or is "near" the specular value, for the given $\boldsymbol{y}$. Then the theory really does break down.

In Section 5.3, we show that the Beylkin determinants for common-source or common-receiver inversion are proportional to the squares of the amplitudes of the corresponding Green's functions. So the quotient, $h/a = h/A^2$ depends on simpler relationships between the coordinates that describe the ray directions and their relationship to the surface coordinates. This suggests that the quotient can actually remain finite when both functions approach zero.

The situation is more complicated for common-offset inversion, owing to the structure of the Beylkin determinant for this case. Still, singularities of amplitude or of the Beylkin determinant do not cause serious error in the output, except when that choice of $\boldsymbol{y}$ and $\boldsymbol{\xi}$ is nearly a specular reflection point.

Except for this case, an isolated violation of the basic hypotheses of the theory has a mild influence on the output that we obtain. Usually, the primary influence is on amplitude, while phase—which changes reflector location—is not affected nearly as much. That is, the reflector map remains intact, but parameter estimation might suffer.

Similarly, if a small part of the bandwidth, say, 25%, fails to satisfy our high-frequency criterion, then, again, amplitude degrades more than reflector location.

Other Geometrical Attributes

The basic idea used to determine $\cos\theta_s$ can be used to determine other attributes of the ray geometry for reflections at the specular reflection angle. For example, consider another reflectivity function whose integrand differed from the one in β_1 by the factor, $\phi(\boldsymbol{y}, \boldsymbol{\xi})$. Then, the output of these two reflectivities will differ by a factor equal to the total traveltime from source to specular point to receiver. Similarly, one could determine the separate traveltimes by using factors of $\tau(\boldsymbol{y}, \boldsymbol{x}_s)$ or $\tau(\boldsymbol{y}, \boldsymbol{x}_g)$. Other useful information might be the direction of the normal, the specular source coordinates, the specular receiver coordinates, and so on. All can be determined exactly as we determined $\cos\theta_s$ at specular, above; see the exercises and Geoltrain and Chovet [1991].

Exercises

5.17 Show that an equivalent expression for β_1 in 2D is given by

$$\beta_1(\boldsymbol{y}) = \frac{-1}{4\pi^2} \int d\xi \frac{|H(\boldsymbol{y},\xi)|}{a(\boldsymbol{y},\xi)|\nabla_y \phi(\boldsymbol{y},\xi)|^2} \cdot \int |\omega|\, d\omega\, e^{-i\omega\phi(\boldsymbol{y},\boldsymbol{\xi})} u_S(\boldsymbol{x}_g, \boldsymbol{x}_s, \omega). \quad (5.1.49)$$

5.1.7 *An Alternative Derivation: Removing the Small-Perturbation Restriction at the Reflector*

Our method of deriving inversion formulas so far has been to create a forward model using perturbation theory. A result of this has been that we have set the goal of inverting for the perturbation in wavespeed $\alpha(\boldsymbol{x})$ that was part of this formulation. Contained in these choices is the implication that the results are valid only if the jumps in wavespeed are "small perturbations" from a known background-wavespeed profile.

The robustness of the seismic method in actual applications, even when the background wavespeed is not well determined, suggests that the seismic method is not really constrained to imaging small perturbations only. In fact, geophysical common sense would indicate that the reverse is true—that stronger reflectors will be imaged *better* than weaker ones. Mathematically, the results of this section show that the output of our linearized inversion formulas, when evaluated in the neighborhood of a reflector, is an estimate of the *reflectivity*—a linear function of the specular reflection coefficient (which is a nonlinear function of the perturbation in wavespeed). The fact that we are seeing the fully nonlinear reflectivity function, rather than merely a linearized approximation to the reflectivity, suggests that the small perturbation constraint is an artifact of the derivation instead of being an actual limitation on the inversion formulas.

It is, therefore, reasonable to try to derive our inversion formulas by starting with a forward model that is not restricted to small perturbations across reflecting surfaces. Again, we will assume that the background propagation speed is known accurately down to the neighborhood of a given reflecting surface. We choose to derive an inversion operator that images the reflector, while yielding an estimate of its specular reflection coefficient. Note that we are no longer inverting for the perturbation $\alpha(\boldsymbol{x})$, but are going directly for the reflectivity.

To do this, we start with a different forward model of the reflected wave—a model that is not restricted to small perturbations. The *Kirchhoff modeling formula*

$$u_S(\boldsymbol{x}_g, \boldsymbol{x}_s, \omega) \sim i\omega F(\omega) \int_S R(\boldsymbol{x}, \boldsymbol{x}_s) a(\boldsymbol{x}, \boldsymbol{\xi}) \cdot (\hat{\boldsymbol{n}} \cdot \nabla_x \phi(\boldsymbol{x}, \boldsymbol{\xi}))\, e^{i\omega\phi(\boldsymbol{x},\boldsymbol{\xi})} dS. \quad (5.1.50)$$

derived in Section E.8, is just such a representation. While the Kirchhoff modeling formula *is* restricted to *high frequencies*, it has no restriction in the size of the jump in material parameters across a given reflector. Of course, above the reflector, we must assume that the background wavespeed is close to the true wavespeed, both for locating the reflector in its correct output position and for estimating the reflection coefficient correctly.. Furthermore, this is still a primaries-only theory in which multiple reflections are neglected.[8] Both of these omitted features of the seismic experiment still require that the perturbations in the wavefield above the reflector of interest be small, in some sense.

As a first step, we want to rewrite (5.1.50) in a form that will allow us to recast this surface integral as a volume integral. Recall that all we want to recover is the reflector itself, and an estimate of R. In the forward model, then, we only care about the main contribution to the integral at high frequency, which is to say, the contribution produced by the method of stationary phase. While we do not want to carry out that analysis completely and have to make conjectures about the Hessian and its signature at stationarity, we can rewrite the integral in a somewhat simpler form by taking account of some of the consequences of stationarity.

In particular, we know that at the stationary point, the normal and the gradient of the traveltime are anticollinear, the surface normal pointing upward and the gradient pointing downward, but in the normal direction. Consequently,

$$\hat{\boldsymbol{n}} \cdot \nabla_x \phi(\boldsymbol{x}, \boldsymbol{\xi}) = -|\nabla_x \phi(\boldsymbol{x}, \boldsymbol{\xi}))|, \tag{5.1.51}$$

at stationarity. Thus, in (5.1.50), we could replace the factor $\hat{\boldsymbol{n}} \cdot \nabla_x \phi(\boldsymbol{x}, \boldsymbol{\xi})$ by the right side of (5.1.51) and still have the same leading-order asymptotic result for the specularly-reflected wave. Similarly, we can replace the pointwise reflection coefficient in (5.1.50) by its specular value. Without changing notation, let us assume, below, that this has also been done.

Then, (5.1.50) can be recast as follows:

$$\begin{aligned} u_S(\boldsymbol{x}_g, \boldsymbol{x}_s, \omega) \sim -i\omega F(\omega) \int_S dS\, R(\boldsymbol{x}, \boldsymbol{x}_s) \gamma(\boldsymbol{x}) \\ \cdot a(\boldsymbol{x}, \boldsymbol{\xi}) |\nabla_x \phi(\boldsymbol{x}, \boldsymbol{\xi}))|\, e^{i\omega\phi(\boldsymbol{x}, \boldsymbol{\xi})}. \end{aligned} \tag{5.1.52}$$

It is fairly straightforward to transform equation (5.1.52) into a volume integral, similar to (5.1.7). We introduce a new coordinate system in place of $\boldsymbol{x}$, consisting of the two parameters on the surface S, and the normal distance to this surface. This transformation will break down at the *evolute* of the reflector (which is to say, the surface made up of centers of

[8] See, for example, Hill, Dragoset, and Weglein [1999], and the follow-up articles of that special section for a survey of current results on multiple attenuation.

principal curvature of the reflector surface), but will be good closer to the surface than the evolute. That is, in a neighborhood of S, $dSdn_r = d^3x$ (the differential surface element multiplied by the differential normal element) is exactly the differential volume needed to create a volume integral representation. We rewrite (5.1.52) as

$$u_S(\boldsymbol{x}_g, \boldsymbol{x}_s, \omega) \sim -i\omega F(\omega) \int d^3x\, R(\boldsymbol{x}, \boldsymbol{x}_s)\gamma(\boldsymbol{x}) \cdot a(\boldsymbol{x}, \boldsymbol{\xi})|\nabla_x \phi(\boldsymbol{x}, \boldsymbol{\xi})|\, e^{i\omega\phi(\boldsymbol{x},\boldsymbol{\xi})}. \tag{5.1.53}$$

Here, the integral is over the entire region $x_3 \geq 0$; $\gamma(\boldsymbol{x})$ is the singular function of the reflecting surface. Clearly, we need some well-behaved extension of R off the reflecting surface; the particular choice of extension is not important, as long as it allows for our asymptotic analysis to proceed. In practice, our inversion will create a bandlimited singular function. For this function, it is necessary to require that the evolute be "many wavelengths" from the reflector so that the breakdown in the coordinate system occurs in a region where the contribution to the total integral is asymptotically small. Under this restriction, we may proceed without regard to the breakdown of the coordinate system. This latter assumption is merely the requirement that the principal radii of curvature of the reflector at each point are among the length scales that must conform to the high-frequency criterion of Section 3.4.

The product, $R(\boldsymbol{x}, \boldsymbol{x}_s)\gamma(\boldsymbol{x})$, is exactly our *reflectivity function*, $\beta(\boldsymbol{x})$. Thus, we rewrite the previous result one more time, as

$$u_S(\boldsymbol{x}_g, \boldsymbol{x}_s, \omega) \sim -i\omega F(\omega) \int d^3x\, \beta(\boldsymbol{x}) a(\boldsymbol{x}, \boldsymbol{\xi}) \cdot |\nabla_x \phi(\boldsymbol{x}, \boldsymbol{\xi})|\, e^{i\omega\phi(\boldsymbol{x},\boldsymbol{\xi})}. \tag{5.1.54}$$

We now have an integral equation that is similar to equation (5.1.7). We make the following identifications between that equation and the representation (5.1.54).

$$\begin{aligned} u_S(\boldsymbol{x}_g, \boldsymbol{x}_s, \omega) &\to i\omega u_S(\boldsymbol{x}_g, \boldsymbol{x}_s, \omega), \\ \alpha(\boldsymbol{x}) &\to \beta(\boldsymbol{x}), \\ a(\boldsymbol{x}, \boldsymbol{\xi})/c^2(\boldsymbol{x}), &\to a(\boldsymbol{x}, \boldsymbol{\xi})|\nabla_x \phi(\boldsymbol{x}, \boldsymbol{\xi})|, \\ \phi(\boldsymbol{x}, \boldsymbol{\xi}) &\to \phi(\boldsymbol{x}, \boldsymbol{\xi}). \end{aligned} \tag{5.1.55}$$

We could, at this point, proceed with the derivation of the asymptotic inversion of (5.1.55) exactly as we did in Section 5.1 to invert (5.1.7). However, there is no need to do so. The same result can be obtained by making the identifications (5.1.54) in the inversion formula, (5.1.10),

$$\beta(\boldsymbol{x}) = \frac{1}{8\pi^3} \int d^2\xi \frac{|h(\boldsymbol{y},\boldsymbol{\xi})|}{a(\boldsymbol{y},\boldsymbol{\xi})|\nabla_x \phi(\boldsymbol{x},\boldsymbol{\xi}))|} \cdot \int i\omega \, d\omega \, e^{-i\omega\phi(\boldsymbol{y},\boldsymbol{\xi})} u_S(\boldsymbol{x}_g, \boldsymbol{x}_s, \omega). \quad (5.1.56)$$

This formula should be compared to (5.1.21) for $\beta(\boldsymbol{y})$. We see that the right sides agree. Thus, with some hand-waving, we have obtained the same result as before, without making the small perturbation assumption. This result will be verified by asymptotic analysis in the next section.

5.1.8 Discussion

In Section 5.1.7 we found that starting with the Kirchhoff modeling formula provides a quicker path to an imaging formula that yields the reflectivity function of a given reflector. We have said that we have "removed the small-perturbation assumption," yet the result is still a *linearized* inversion formula. What we actually have done is shifted the emphasis of the process of linearization from "linearization in wavespeed perturbation" to "linearization in reflection coefficient." Most assuredly, in the presence of strong reflectors (such as volcanic layers), multiples will be generated, likely masking the data. Even if such multiples could be successfully removed through a preprocessing step, there may not be sufficient energy penetrating into the subsurface beneath a strong reflector to give the inversion formula anything to image. Thus, the concept of seismic imaging contains a built-in "small-perturbation requirement." We have removed only the small-perturbation assumption at the reflector of interest, which was an artifact of our derivation.

Exercises

5.18 The approximation $C(\boldsymbol{x},\boldsymbol{\xi}) \sim C(\boldsymbol{y},\boldsymbol{\xi})$, for $\boldsymbol{x}$ near $\boldsymbol{y}$, was used as part of the derivation of equation (5.1.19). Justify this approximation for $\boldsymbol{x} \neq \boldsymbol{y}$ by examining the relative sizes of the terms in the Taylor series expansion of $C(\boldsymbol{x},\boldsymbol{\xi})$ defined by (5.1.11) for a constant wavespeed medium.

5.19 Consider the four reflectivity functions,

$$(\tilde{\beta}_1(\boldsymbol{y}), \tilde{\beta}_2(\boldsymbol{y}), \tilde{\beta}_3(\boldsymbol{y})) = \int d^2\xi \left(\frac{\partial\phi(\boldsymbol{y},\boldsymbol{\xi})}{\partial y_1}, \frac{\partial\phi(\boldsymbol{y},\boldsymbol{\xi})}{\partial y_2}, \frac{\partial\phi(\boldsymbol{y},\boldsymbol{\xi})}{\partial y_3} \right) \cdot \int i\omega \, d\omega \, e^{-i\omega\phi(\boldsymbol{y},\boldsymbol{\xi})} u_S(\boldsymbol{x}_g, \boldsymbol{x}_s, \omega)$$

and

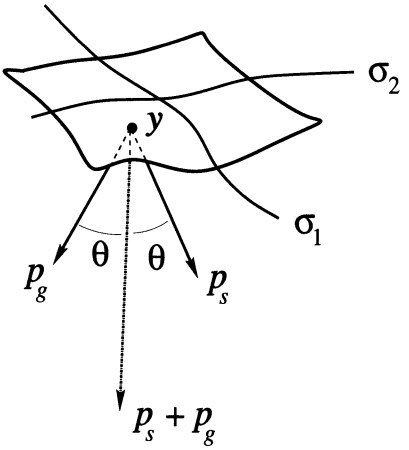

FIGURE 5.4. Geometry of the slowness vectors, $\boldsymbol{p}_g$ and $\boldsymbol{p}_s$. The opening angle, 2θ, is the angle between these two vectors, and the direction of the vector $\boldsymbol{p}_s + \boldsymbol{p}_g$ is normal to the reflector surface when the output point, $\boldsymbol{y}$, describes a specular reflection point.

$$\tilde{\beta}_4(\boldsymbol{y}) = \int d^2\xi \int i\omega \, d\omega \, e^{-i\omega\phi(\boldsymbol{y},\boldsymbol{\xi})} u_S(\boldsymbol{x}_g, \boldsymbol{x}_s, \omega).$$

Explain why the ratios

$$(\tilde{\beta}_1(\boldsymbol{y}), \tilde{\beta}_2(\boldsymbol{y}), \tilde{\beta}_3(\boldsymbol{y}))/\tilde{\beta}_4(\boldsymbol{y})$$

yield an estimate of the normal to the reflector, S, when evaluated on the reflector. How do you know where the reflector is?

5.2 The Beylkin Determinant h, and Special Cases of 3D Inversion

An important consequence of the formulation that we have created is that the influence of source-receiver geometry is completely described by the Beylkin determinant $h(\boldsymbol{y}, \boldsymbol{\xi})$. It is therefore worthwhile to examine the specific structure of this determinant.

Recalling that

$$\nabla_y \phi(\boldsymbol{y}, \boldsymbol{\xi}) \equiv \nabla_y \tau(\boldsymbol{y}, \boldsymbol{x}_s) + \nabla_y \tau(\boldsymbol{x}_g, \boldsymbol{y}),$$

we will use the notations

$$\boldsymbol{p}_s = \nabla_y \tau(\boldsymbol{y}, \boldsymbol{x}_s), \qquad \boldsymbol{p}_g = \nabla_y \tau(\boldsymbol{y}, \boldsymbol{x}_g), \qquad \nabla_y \phi(\boldsymbol{y}, \boldsymbol{\xi}) = \boldsymbol{p}_s + \boldsymbol{p}_g.$$

Rewriting equation (5.1.17) using these definitions yields an expression for the Beylkin determinant

$$h(\boldsymbol{y},\boldsymbol{\xi}) = \det \begin{bmatrix} \boldsymbol{p}_s + \boldsymbol{p}_g \\ \dfrac{\partial(\boldsymbol{p}_s + \boldsymbol{p}_g)}{\partial \xi_1} \\ \dfrac{\partial(\boldsymbol{p}_s + \boldsymbol{p}_g)}{\partial \xi_2} \end{bmatrix}, \tag{5.2.1}$$

in terms of the slowness vectors $\boldsymbol{p}_s$ and $\boldsymbol{p}_g$ and their derivatives with respect to the surface coordinates (ξ_1, ξ_2). The reader should be aware that these vector quantities are evaluated at the output point $\boldsymbol{y}$.

5.2.1 *General Properties of the Beylkin Determinant*

Some general properties of the quantities that compose the Beylkin determinant can be exploited for simplification purposes. Several properties that will prove to be useful in future computations are

$$\boldsymbol{p}_s^2 = \boldsymbol{p}_g^2 = \frac{1}{c^2(\boldsymbol{y})} \qquad \text{(the eikonal equation)}, \tag{5.2.2}$$

$$\boldsymbol{p}_s \cdot \frac{\partial \boldsymbol{p}_s}{\partial \xi_i} = \frac{1}{2}\frac{\partial(\boldsymbol{p}_s \cdot \boldsymbol{p}_s)}{\partial \xi_i} = \frac{1}{2}\frac{\partial(1/c^2(\boldsymbol{y}))}{\partial \xi_i} = 0, \tag{5.2.3}$$

$$\boldsymbol{p}_g \cdot \frac{\partial \boldsymbol{p}_g}{\partial \xi_i} = \frac{1}{2}\frac{\partial(\boldsymbol{p}_g \cdot \boldsymbol{p}_g)}{\partial \xi_i} = \frac{1}{2}\frac{\partial(1/c^2(\boldsymbol{y}))}{\partial \xi_i} = 0 \qquad \text{for } i = 1, 2, \tag{5.2.4}$$

with the last two results following because $c(\boldsymbol{y})$ is not a function of ξ_1 or ξ_2.[9] The last two relations here state that a given slowness vector is orthogonal to the vector obtained by taking its ξ_i derivative, which we see is a consequence of the fact that the length of the slowness vector is independent of $\boldsymbol{\xi}$. The notation may be simplified further by defining the quantities for $\boldsymbol{v}_s$, $\boldsymbol{v}_g$, $\boldsymbol{w}_s$, and $\boldsymbol{w}_g$,

$$\boldsymbol{v}_s \equiv \frac{\partial \boldsymbol{p}_s}{\partial \xi_1}, \quad \boldsymbol{v}_g \equiv \frac{\partial \boldsymbol{p}_g}{\partial \xi_1}, \quad \boldsymbol{w}_s \equiv \frac{\partial \boldsymbol{p}_s}{\partial \xi_2}, \quad \text{and} \quad \boldsymbol{w}_g \equiv \frac{\partial \boldsymbol{p}_g}{\partial \xi_2}. \tag{5.2.5}$$

Using these new notations, the Beylkin determinant may be written as

$$h(\boldsymbol{y},\boldsymbol{\xi}) = \det \begin{bmatrix} \boldsymbol{p}_s + \boldsymbol{p}_g \\ \boldsymbol{v}_s + \boldsymbol{v}_g \\ \boldsymbol{w}_s + \boldsymbol{w}_g \end{bmatrix} \equiv (\boldsymbol{p}_s + \boldsymbol{p}_g) \cdot [(\boldsymbol{v}_s + \boldsymbol{v}_g) \times (\boldsymbol{w}_s + \boldsymbol{w}_g)],$$

where the expression on the far right is the representation of the determinant as a triple scalar product of three vectors.

Using the relations in equation (5.2.5), it follows that the vectors defined by the cross products $\boldsymbol{v}_s \times \boldsymbol{w}_s$ and $\boldsymbol{v}_g \times \boldsymbol{w}_g$ point in the same direction as

[9] In the anisotropic case, the wavespeed will be a function of the direction of the ray, ultimately characterized by $\boldsymbol{\xi}$. In that case, this simplification does not occur.

$\boldsymbol{p}_s$ and $\boldsymbol{p}_g$, respectively, implying that

$$\begin{aligned} \boldsymbol{v}_s \times \boldsymbol{w}_s &\equiv \mu_s \hat{\boldsymbol{p}}_s |\boldsymbol{v}_s \times \boldsymbol{w}_s| = \mu_s c(\boldsymbol{y})\, \boldsymbol{p}_s |\boldsymbol{v}_s \times \boldsymbol{w}_s|, \\ \boldsymbol{v}_g \times \boldsymbol{w}_g &\equiv \mu_g \hat{\boldsymbol{p}}_g |\boldsymbol{v}_g \times \boldsymbol{w}_g| = \mu_g c(\boldsymbol{y})\, \boldsymbol{p}_g |\boldsymbol{v}_g \times \boldsymbol{w}_g|. \end{aligned} \tag{5.2.6}$$

Here, μ_s, $\mu_g = \pm 1$, according to whether the respective cross products are collinear or anticollinear with $\hat{\boldsymbol{p}}_s$ and $\hat{\boldsymbol{p}}_g$, respectively. This result implies the following triple scalar product forms

$$\boldsymbol{p}_s \cdot \boldsymbol{v}_s \times \boldsymbol{w}_s = \frac{\mu_s}{c(\boldsymbol{y})} |\boldsymbol{v}_s \times \boldsymbol{w}_s| \qquad \text{and} \qquad \boldsymbol{p}_g \cdot \boldsymbol{v}_g \times \boldsymbol{w}_g = \frac{\mu_g}{c(\boldsymbol{y})} |\boldsymbol{v}_g \times \boldsymbol{w}_g|. \tag{5.2.7}$$

Figure 5.4 shows the geometry of the $\boldsymbol{p}_g$ and $\boldsymbol{p}_s$ vectors. We may define the angle θ via the dot product of these two vectors as

$$\boldsymbol{p}_s \cdot \boldsymbol{p}_g = \frac{1}{c^2(\boldsymbol{y})} \cos 2\theta. \tag{5.2.8}$$

Equation (5.1.45) now takes the form

$$\begin{aligned} |\boldsymbol{p}_s + \boldsymbol{p}_g|^2 &= (\boldsymbol{p}_s + \boldsymbol{p}_g) \cdot (\boldsymbol{p}_s + \boldsymbol{p}_g) = \boldsymbol{p}_s \cdot \boldsymbol{p}_s + 2\boldsymbol{p}_s \cdot \boldsymbol{p}_g + \boldsymbol{p}_g \cdot \boldsymbol{p}_g \\ &= \frac{2}{c^2(\boldsymbol{y})}(1 + \cos 2\theta) = \frac{4\cos^2\theta}{c^2(\boldsymbol{y})}, \end{aligned}$$

and (5.1.46) becomes

$$|\boldsymbol{p}_s + \boldsymbol{p}_g| = \frac{2\cos\theta}{c(\boldsymbol{y})}. \tag{5.2.9}$$

Furthermore, (5.2.7) allows us to write the following triple scalar product relations:

$$\begin{aligned} \boldsymbol{p}_g \cdot \boldsymbol{v}_s \times \boldsymbol{w}_s &= \mu_s c(\boldsymbol{y})(\boldsymbol{p}_g \cdot \boldsymbol{p}_s)|\boldsymbol{v}_s \times \boldsymbol{w}_s| = \frac{\mu_s \cos 2\theta}{c(\boldsymbol{y})} |\boldsymbol{v}_s \times \boldsymbol{w}_s| \\ \boldsymbol{p}_s \cdot \boldsymbol{v}_g \times \boldsymbol{w}_g &= \mu_g c(\boldsymbol{y})(\boldsymbol{p}_s \cdot \boldsymbol{p}_g)|\boldsymbol{v}_g \times \boldsymbol{w}_g| = \frac{\mu_g \cos 2\theta}{c(\boldsymbol{y})} |\boldsymbol{v}_g \times \boldsymbol{w}_g|. \end{aligned} \tag{5.2.10}$$

With these relations and the identity

$$1 + \cos 2\theta = 2\cos^2\theta, \tag{5.2.11}$$

which we have used extensively, we are ready to write simplified forms of the Beylkin determinant for several common geophysical recording geometries.

Exercises

5.20 Verify the following identities

$$\boldsymbol{p}_s \cdot \boldsymbol{v}_s \times \boldsymbol{w}_g = \frac{\mu_s}{c|\boldsymbol{v}_s \times \boldsymbol{w}_s|} \left[|\boldsymbol{v}_s|^2 (\boldsymbol{w}_s \cdot \boldsymbol{w}_g) - (\boldsymbol{v}_s \cdot \boldsymbol{w}_g)(\boldsymbol{v}_s \cdot \boldsymbol{w}_s) \right],$$

$$\boldsymbol{p}_s \cdot \boldsymbol{v}_g \times \boldsymbol{w}_s = \frac{\mu_s}{c|\boldsymbol{v}_s \times \boldsymbol{w}_s|} \left[|\boldsymbol{w}_s|^2 (\boldsymbol{v}_s \cdot \boldsymbol{v}_g) - (\boldsymbol{v}_s \cdot \boldsymbol{w}_s)(\boldsymbol{w}_s \cdot \boldsymbol{v}_g) \right],$$

$$\boldsymbol{p}_g \cdot \boldsymbol{v}_s \times \boldsymbol{w}_g = \frac{\mu_g}{c|\boldsymbol{v}_g \times \boldsymbol{w}_g|} \left[|\boldsymbol{w}_g|^2 (\boldsymbol{v}_g \cdot \boldsymbol{v}_s) - (\boldsymbol{v}_g \cdot \boldsymbol{w}_g)(\boldsymbol{v}_g \cdot \boldsymbol{w}_s) \right],$$

$$\boldsymbol{p}_g \cdot \boldsymbol{v}_g \times \boldsymbol{w}_s = \frac{\mu_g}{c|\boldsymbol{v}_g \times \boldsymbol{w}_g|} \left[|\boldsymbol{v}_g|^2 (\boldsymbol{w}_g \cdot \boldsymbol{w}_s) - (\boldsymbol{v}_g \cdot \boldsymbol{w}_s)(\boldsymbol{w}_g \cdot \boldsymbol{v}_g) \right].$$

5.21 Use the eikonal equation, (5.2.2), to eliminate derivatives of p_3 and show that

$$\boldsymbol{p}_s \cdot \boldsymbol{v}_s \times \boldsymbol{w}_s = \frac{1}{c^2(\boldsymbol{y}) p_{s3}} \det \left[\frac{\partial p_{si}}{\partial \xi_j} \right], \quad i,j = 1,2,$$

and

$$\boldsymbol{p}_g \cdot \boldsymbol{v}_g \times \boldsymbol{w}_g = \frac{1}{c^2(\boldsymbol{y}) p_{g3}} \det \left[\frac{\partial p_{gi}}{\partial \xi_j} \right], \quad i,j = 1,2.$$

Here, p_{sj}, $j = 1,2,3$, is the j-th component of the vector $\boldsymbol{p}_s$, and likewise for p_{gj}. Thus, the three component cross produces of (5.2.7) are replaced by 2×2 determinants, with the sign explicitly carried by the sign of those determinants. (Unfortunately, the cross products of mixed source and receiver vectors do not simplify in this manner.)

5.2.2 Common-Shot Inversion

In the common-shot geometry, the shotpoint is fixed and the receiver positions vary in space. Thus $\boldsymbol{p}_s$ is independent of the surface parameters $\boldsymbol{\xi}$, because the source position is held constant. The Beylkin determinant in (5.1.17) simplifies to

$$h(\boldsymbol{y}, \boldsymbol{\xi}) = \det \begin{bmatrix} \boldsymbol{p}_s + \boldsymbol{p}_g \\ \dfrac{\partial \boldsymbol{p}_g}{\partial \xi_1} \\ \dfrac{\partial \boldsymbol{p}_g}{\partial \xi_2} \end{bmatrix}. \tag{5.2.12}$$

Using the new notations defined above,

$$\det \begin{bmatrix} \boldsymbol{p}_s + \boldsymbol{p}_g \\ \boldsymbol{v}_g \\ \boldsymbol{w}_g \end{bmatrix} = (\boldsymbol{p}_s + \boldsymbol{p}_g) \cdot \boldsymbol{v}_g \times \boldsymbol{w}_g = \boldsymbol{p}_s \cdot \boldsymbol{v}_g \times \boldsymbol{w}_g + \boldsymbol{p}_g \cdot \boldsymbol{v}_g \times \boldsymbol{w}_g. \tag{5.2.13}$$

The expression on the far right can be further simplified using equations (5.2.6), (5.2.10), and (5.2.11):

$$(\boldsymbol{p}_s + \boldsymbol{p}_g) \cdot (\boldsymbol{v}_g \times \boldsymbol{w}_g) = \frac{\mu_g}{c(\boldsymbol{y})} (1 + \cos 2\theta) \, |\boldsymbol{v}_g \times \boldsymbol{w}_g|$$

$$= \frac{2\mu_g \cos^2\theta}{c(\boldsymbol{y})} |\boldsymbol{v}_g \times \boldsymbol{w}_g|$$
$$= 2\mu_g \cos^2\theta \, \boldsymbol{p}_g \cdot (\boldsymbol{v}_g \times \boldsymbol{w}_g). \tag{5.2.14}$$

Translating this back in our original notation, we have

$$h(\boldsymbol{y},\boldsymbol{\xi}) = 2\cos^2\theta \det \begin{bmatrix} \boldsymbol{p}_g \\ \dfrac{\partial \boldsymbol{p}_g}{\partial \xi_1} \\ \dfrac{\partial \boldsymbol{p}_g}{\partial \xi_2} \end{bmatrix} \equiv 2\cos^2\theta \, h_g(\boldsymbol{y},\boldsymbol{\xi}). \tag{5.2.15}$$

Thus, for a fixed source point, we have reduced the computation of $h(\boldsymbol{y},\boldsymbol{\xi})$ to the calculation of the determinant $h_g(\boldsymbol{y},\boldsymbol{\xi})$ and the opening angle of the rays from source and receiver, θ. By using this result and (5.1.45) in (5.1.21) and (5.1.47), the following two formulas are obtained for common-shot inversion in a constant-density medium with background propagation speed that can be a function of all three spatial variables:

$$\beta(\boldsymbol{y}) = \frac{c(\boldsymbol{y})}{8\pi^3} \int d^2\xi \, \frac{\cos\theta |h_g(\boldsymbol{y},\boldsymbol{\xi})|}{a(\boldsymbol{y},\boldsymbol{\xi})} \cdot \int i\omega \, d\omega \, e^{-i\omega\phi(\boldsymbol{y},\boldsymbol{\xi})} u_S(\boldsymbol{x}_g,\boldsymbol{x}_s,\omega), \tag{5.2.16}$$

and

$$\beta_1(\boldsymbol{y}) = \frac{c^2(\boldsymbol{y})}{16\pi^3} \int d^2\xi \, \frac{|h_g(\boldsymbol{y},\boldsymbol{\xi})|}{a(\boldsymbol{y},\boldsymbol{\xi})} \cdot \int i\omega \, d\omega \, e^{-i\omega\phi(\boldsymbol{y},\boldsymbol{\xi})} u_S(\boldsymbol{x}_g,\boldsymbol{x}_s,\omega). \tag{5.2.17}$$

Note that the scaling by $2\cos\theta/c(\boldsymbol{y})$, which allows us to determine the distinguished angle of incidence θ_s for a point on a reflector, is now seen explicitly as the ratio of the integrands of $\beta(\boldsymbol{y})$ and $\beta_1(\boldsymbol{y})$. However, this is symbolic; one must still compute this scaling factor for each $\boldsymbol{\xi}$, $\boldsymbol{y}$ by using the definition (5.1.45).

To specialize further, assume that $c(\boldsymbol{y}) =$ constant. In this case,

$$\begin{aligned} \boldsymbol{r}_s &= \boldsymbol{y} - \boldsymbol{x}_s, \quad r_s = |\boldsymbol{r}_s|, \quad \hat{\boldsymbol{r}}_s = \boldsymbol{r}_s/r_s, \\ \boldsymbol{r}_g &= \boldsymbol{y} - \boldsymbol{x}_g, \quad r_g = |\boldsymbol{r}_g|, \quad \hat{\boldsymbol{r}}_g = \boldsymbol{r}_g/r_g, \\ 1/a(\boldsymbol{y},\boldsymbol{\xi}) &= 16\pi^2 r_s r_g, \quad \phi(\boldsymbol{y},\boldsymbol{\xi}) = [r_s + r_g]/c. \end{aligned} \tag{5.2.18}$$

We leave it as an exercise to show that, in this case,

$$h_g(\boldsymbol{y},\boldsymbol{\xi}) = \frac{1}{c^3 r_g^2} \det \begin{bmatrix} \hat{\boldsymbol{r}}_g \\ \dfrac{\partial \boldsymbol{x}_g}{\partial \xi_1} \\ \dfrac{\partial \boldsymbol{x}_g}{\partial \xi_2} \end{bmatrix}. \tag{5.2.19}$$

Furthermore, for a planar horizontal upper surface with $x_{g_1} = \xi_1$ and $x_{g_2} = \xi_2$, our representation for h_g further simpifies to:

$$h_g(\boldsymbol{y}, \boldsymbol{\xi}) = \frac{y_3}{c^3 r_g^3}. \tag{5.2.20}$$

The full Beylkin determinant is, therefore

$$h(\boldsymbol{y}, \boldsymbol{\xi}) = 2\cos^2\theta \frac{y_3}{c^3 r_g^3}. \tag{5.2.21}$$

The corresponding formulas for $\beta(\boldsymbol{y})$ and $\beta_1(\boldsymbol{y})$ become

$$\beta(\boldsymbol{y}) = \frac{2y_3}{\pi c^2} \int d^2\xi \, \frac{r_s}{r_g^2} \cos\theta \int i\omega \, d\omega \, e^{-i\omega[r_s + r_g]/c} u_S(\boldsymbol{x}_g, \boldsymbol{x}_s, \omega) \tag{5.2.22}$$

and

$$\beta_1(\boldsymbol{y}) = \frac{y_3}{\pi c} \int d^2\xi \, \frac{r_s}{r_g^2} \int i\omega \, d\omega \, e^{-i\omega[r_s + r_g]/c} u_S(\boldsymbol{x}_g, \boldsymbol{x}_s, \omega). \tag{5.2.23}$$

In practice, we use the fact that $\cos\theta \equiv 1/2\,|\hat{\boldsymbol{r}}_s + \hat{\boldsymbol{r}}_g|$, to carry out the integration in equation (5.2.22).

The results for the *common-receiver* geometry follow from similar arguments to those above. (For a discussion of other approaches to amplitude-preserving, common-shot migration, see Hanitzsch [1995, 1997].)

Exercises

5.22 Verify equation (5.2.19). Hint: Gaussian elimination.
5.23 Verify equations (5.2.20), (5.2.22), and (5.2.23).
5.24 Compute the Beylkin determinant $h(\boldsymbol{y}, \boldsymbol{\xi})$ and the respective formulas for $\beta(\boldsymbol{y})$ and $\beta_1(\boldsymbol{y})$ for the *common-receiver* geometry.

5.2.3 Common-Offset Inversion

The first difficulty is to define what we mean by "common-offset" geometry when dealing with a 3D data set. As was discussed in Section 5.1, we will treat the simple case in which the source and receiver positions are referenced to a general surface coordinate $\boldsymbol{\xi}$ through constant vector $\boldsymbol{h}$ (see Figure 5.1b), such that

$$\boldsymbol{x}_s(\boldsymbol{\xi} - \boldsymbol{h}) = \boldsymbol{x}_s(\xi_1 - h_1, \xi_2 - h_2), \qquad \boldsymbol{x}_g(\boldsymbol{\xi} + \boldsymbol{h}) = \boldsymbol{x}_g(\xi_1 + h_1, \xi_2 + h_2).$$

If the recording surface is planar, then $\boldsymbol{x}_s$, $\boldsymbol{\xi}$, and $\boldsymbol{x}_g$ are collinear. This implies that the data set has been sorted into a collection of parallel source-receiver pairs separated by a distance of $2|\boldsymbol{h}|$. Because all of the source-receiver pairs are separated by a constant *vector*, the orientation of that vector is a distinguished direction in the problem. Thus, we may take the

orientation of the common-offset vector to be the ξ_1-direction, permitting the following to be written:

$$\boldsymbol{x}_s \equiv \boldsymbol{x}_s(\boldsymbol{\xi}_1 - |\boldsymbol{h}|, \boldsymbol{\xi}_2) \qquad \boldsymbol{x}_g \equiv \boldsymbol{x}_g(\boldsymbol{\xi}_1 + |\boldsymbol{h}|, \boldsymbol{\xi}_2).$$

The general form of the Beylkin determinant can be written for an arbitrary source-receiver geometry as

$$\begin{aligned} h(\boldsymbol{y}, \boldsymbol{\xi}) &= (\boldsymbol{p}_s + \boldsymbol{p}_g) \cdot (\boldsymbol{v}_s + \boldsymbol{v}_g) \times (\boldsymbol{w}_s + \boldsymbol{w}_g) \\ &= (\boldsymbol{p}_s + \boldsymbol{p}_g) \cdot \boldsymbol{v}_g \times \boldsymbol{w}_g + (\boldsymbol{p}_s + \boldsymbol{p}_g) \cdot \boldsymbol{v}_s \times \boldsymbol{w}_s \\ &\quad + (\boldsymbol{p}_s + \boldsymbol{p}_g) \cdot \boldsymbol{v}_g \times \boldsymbol{w}_s + (\boldsymbol{p}_s + \boldsymbol{p}_g) \cdot \boldsymbol{v}_s \times \boldsymbol{w}_g. \end{aligned} \tag{5.2.24}$$

The first two terms can be recognized as being the Beylkin determinants for the common-shot and common-receiver geometries (see the discussion in the previous section). We may write the Beylkin determinant as

$$h(\boldsymbol{y}, \boldsymbol{\xi}) = 2\cos^2\theta\,[h_s(\boldsymbol{y}, \boldsymbol{\xi}) + h_g(\boldsymbol{y}, \boldsymbol{\xi})] + (\boldsymbol{p}_s + \boldsymbol{p}_g) \cdot [\boldsymbol{v}_g \times \boldsymbol{w}_s + \boldsymbol{v}_s \times \boldsymbol{w}_g], \tag{5.2.25}$$

where $h_g(\boldsymbol{y}, \boldsymbol{\xi})$ is the determinant defined in equation (5.2.19) and $h_s(\boldsymbol{y}, \boldsymbol{\xi})$ is the corresponding determinant describing the triple scalar product, $\boldsymbol{p}_s \cdot \boldsymbol{v}_s \times \boldsymbol{w}_s$. Unfortunately, the term on the far right contains the cross products, $\boldsymbol{v}_s \times \boldsymbol{w}_g$ and $\boldsymbol{v}_g \times \boldsymbol{w}_s$, which are not easily simplified.

Another way of writing the Beylkin determinant is

$$\begin{aligned} h(\boldsymbol{y}, \boldsymbol{\xi}) &= 2\cos^2\theta\,[h_s(\boldsymbol{y}, \boldsymbol{\xi}) + h_g(\boldsymbol{y}, \boldsymbol{\xi})] \\ &\quad + h_a(\boldsymbol{y}, \boldsymbol{\xi}) + h_b(\boldsymbol{y}, \boldsymbol{\xi}) + h_c(\boldsymbol{y}, \boldsymbol{\xi}) + h_d(\boldsymbol{y}, \boldsymbol{\xi}), \end{aligned} \tag{5.2.26}$$

where the respective h_a, h_b, h_c and h_d are defined by

$$\begin{aligned} h_a(\boldsymbol{y}, \boldsymbol{\xi}) &\equiv \boldsymbol{p}_s \cdot \boldsymbol{v}_s \times \boldsymbol{w}_g, \qquad & h_b(\boldsymbol{y}, \boldsymbol{\xi}) &\equiv \boldsymbol{p}_s \cdot \boldsymbol{v}_g \times \boldsymbol{w}_s, \\ h_c(\boldsymbol{y}, \boldsymbol{\xi}) &\equiv \boldsymbol{p}_g \cdot \boldsymbol{v}_s \times \boldsymbol{w}_g, \qquad & h_d(\boldsymbol{y}, \boldsymbol{\xi}) &\equiv \boldsymbol{p}_g \cdot \boldsymbol{v}_g \times \boldsymbol{w}_s. \end{aligned} \tag{5.2.27}$$

Unfortunately, we cannot write the general common-offset Beylkin determinant in a form that has a common multiplier of $\cos^2\theta$. This means that we can do no better than the general forms of the inversion formula for $\beta(\boldsymbol{y})$ and $\beta_1(\boldsymbol{y})$ given by equations (5.1.21) and (5.1.47).

However, for the special case of constant wavespeed, with a generally nonplanar surface, some simplification is possible. Application of Gaussian elimination produces the following simplified forms for h_a, h_b, h_c, and h_d

$$\begin{aligned} h_a(\boldsymbol{y}, \boldsymbol{\xi}) &\equiv \frac{-1}{c^2 r_s} \hat{\boldsymbol{r}}_s \cdot \frac{\partial \boldsymbol{x}_s}{\partial \xi_1} \times \frac{\partial \boldsymbol{p}_g}{\partial \xi_2}, \qquad & h_b(\boldsymbol{y}, \boldsymbol{\xi}) &\equiv \frac{-1}{c^2 r_s} \hat{\boldsymbol{r}}_s \cdot \frac{\partial \boldsymbol{p}_g}{\partial \xi_1} \times \frac{\partial \boldsymbol{x}_s}{\partial \xi_2}, \\ h_c(\boldsymbol{y}, \boldsymbol{\xi}) &\equiv \frac{-1}{c^2 r_g} \hat{\boldsymbol{r}}_g \cdot \frac{\partial \boldsymbol{p}_s}{\partial \xi_1} \times \frac{\partial \boldsymbol{x}_g}{\partial \xi_2}, \qquad & h_d(\boldsymbol{y}, \boldsymbol{\xi}) &\equiv \frac{-1}{c^2 r_g} \hat{\boldsymbol{r}}_g \cdot \frac{\partial \boldsymbol{x}_g}{\partial \xi_1} \times \frac{\partial \boldsymbol{p}_s}{\partial \xi_2}. \end{aligned} \tag{5.2.28}$$

For the special case of constant wavespeed, with a planar horizontal recording surface, h_s, h_g, h_a, h_b, h_c, and h_d become

$$h_g \equiv \frac{y_3}{c^3 r_g^3}, \qquad h_s \equiv \frac{y_3}{c^3 r_s^3}, \qquad h_a \equiv \frac{y_3}{c^3 r_s^2 r_g},$$
$$h_b \equiv \frac{y_3 \cos 2\theta}{c^3 r_s r_g^2}, \qquad h_c \equiv \frac{y_3 \cos 2\theta}{c^3 r_s^2 r_g}, \qquad h_d \equiv \frac{y_3}{c^3 r_s r_g^2}. \tag{5.2.29}$$

Substituting these results into equation (5.2.25), the full expression for the Beylkin determinant may be written as

$$h(\boldsymbol{y}, \boldsymbol{\xi}) = 2\cos^2\theta \, \frac{y_3}{c^3} \left[\frac{(r_s + r_g)(r_s^2 + r_g^2)}{r_s^3 r_g^3} \right]. \tag{5.2.30}$$

The corresponding formulas for $\beta(\boldsymbol{y})$ and $\beta_1(\boldsymbol{y})$ for 3D common-offset, constant-wavespeed, and with a planar horizontal recording surface become

$$\beta(\boldsymbol{y}) = \frac{2y_3}{\pi c^2} \int d^2\xi \left[\frac{(r_s + r_g)(r_s^2 + r_g^2)}{r_s^2 r_g^2} \right] \cdot \cos\theta \int i\omega \, d\omega \, e^{-i\omega[r_s + r_g]/c} u_S(\boldsymbol{x}_g, \boldsymbol{x}_s, \omega) \tag{5.2.31}$$

and

$$\beta_1(\boldsymbol{y}) = \frac{y_3}{\pi c} \int d^2\xi \left[\frac{(r_s + r_g)(r_s^2 + r_g^2)}{r_s^2 r_g^2} \right] \cdot \int i\omega \, d\omega \, e^{-i\omega[r_s + r_g]/c} u_S(\boldsymbol{x}_g, \boldsymbol{x}_s, \omega). \tag{5.2.32}$$

Equation (5.2.31) exactly matches equation (30) in Sullivan and Cohen [1987], which was derived using a slightly different approach. For a computer implementation of this theory for $v(z)$ media, see Xu [1996a, 1996b]. See, also, Cohen and Hagin [1985].

Exercises

5.25 Verify equations (5.2.28).
5.26 Verify equations (5.2.29) and (5.2.30).
5.27 Verify equations (5.2.31) and (5.2.32).

5.2.4 Zero-Offset Inversion

A number of simplifications occur when the offset between the source and receiver is zero. For this geometry,

$$\tau(\boldsymbol{y}, \boldsymbol{x}_s) = \tau(\boldsymbol{y}, \boldsymbol{x}_g), \quad \phi(\boldsymbol{y}, \boldsymbol{\xi}) = 2\tau(\boldsymbol{y}, \boldsymbol{x}_s), \quad |\nabla_y \phi(\boldsymbol{y}, \boldsymbol{\xi})| = 2/c(\boldsymbol{y}),$$
$$\boldsymbol{p}_s = \boldsymbol{p}_g \equiv \boldsymbol{p}, \qquad \boldsymbol{v}_s = \boldsymbol{v}_g \equiv \boldsymbol{v}, \qquad \boldsymbol{w}_s = \boldsymbol{w}_g \equiv \boldsymbol{w}, \tag{5.2.33}$$

making

$$h(\boldsymbol{y},\boldsymbol{\xi}) = 8h_s(\boldsymbol{y},\boldsymbol{\xi}) = 8h_g(\boldsymbol{y},\boldsymbol{\xi}) = 8\det\begin{bmatrix} \boldsymbol{p} \\ \dfrac{\partial \boldsymbol{p}}{\partial \xi_1} \\ \dfrac{\partial \boldsymbol{p}}{\partial \xi_2} \end{bmatrix} = 8\det\begin{bmatrix} \boldsymbol{p} \\ \boldsymbol{v} \\ \boldsymbol{w} \end{bmatrix}. \tag{5.2.34}$$

Now, there is no need to use both (5.1.21) and (5.1.47), because $\theta = 0$ and no new information can be gained by computing both inversions. Because of the simple form of (5.1.48), we choose to use the inversion formula for $\beta_1(\boldsymbol{y})$ in (5.1.47) for this case:

$$\beta_1(\boldsymbol{y}) = \frac{c^2(\boldsymbol{y})}{4\pi^3}\int d^2\xi\,\frac{|h_s(\boldsymbol{y},\boldsymbol{\xi})|}{A^2(\boldsymbol{y},\boldsymbol{x}_s)}\int i\omega\, d\omega\, e^{-2i\omega\tau(\boldsymbol{y},\boldsymbol{x}_s)}u_S(\boldsymbol{x}_g,\boldsymbol{x}_s,\omega). \tag{5.2.35}$$

In this equation, $A(\boldsymbol{y},\boldsymbol{x}_s)$ is the ray-theoretic amplitude defined by (5.1.4). Of course, for this case, $\beta(\boldsymbol{y})$ differs from $\beta_1(\boldsymbol{y})$ only through a factor of $2/c(\boldsymbol{y})$. We leave it as an exercise for the reader to check that for constant background the formula for $\beta(\boldsymbol{y})$ obtained here agrees with (3.6.15).

Exercises

5.28 Show that the inversion formula (5.2.35) agrees with inversion formula (3.6.15).

5.3 Beylkin Determinants and Ray Jacobians in the Common-Shot and Common-Receiver Configurations

In the previous sections, we presented general results for Beylkin determinants, and results for the special case of constant wavespeed and horizontal planar recording surfaces. In this section, we will explore ray-theoretic forms of Beylkin determinants for the common-shot and common-receiver configurations.

Such a set of results was presented by Najmi [1997]. In particular, his results relate the Beylkin determinant to the corresponding ray Jacobians for amplitude variations along a ray starting from point sources. These are the amplitudes for the corresponding Green's functions that we have denoted

by $A(\boldsymbol{x}, \boldsymbol{x}_s)$ and $A(\boldsymbol{x}_g, \boldsymbol{x})$. The significance of these results is that they simplify the total calculation of the weighting functions in the corresponding inversion formulas, such as (5.2.16) and (5.2.17).

Najmi's result is restricted to horizontal planar upper surfaces. Here, we generalize that result to a curved surface, reflecting the generality in our acquisition surface geometry implicit in the representation $\boldsymbol{x}_s(\boldsymbol{\xi})$ and $\boldsymbol{x}_g(\boldsymbol{\xi})$.

We focus on the common-shot Beylkin determinant here. Recall that, in this case, the shot position is constant and the general Beylkin determinant reduces to a determinant that depends only on the variation in the receiver position. That determinant was denoted by $h_g(\boldsymbol{y}, \boldsymbol{\xi})$ and defined implicitly in equation (5.2.15) by

$$h_g(\boldsymbol{y}, \boldsymbol{\xi}) = \det \begin{bmatrix} \boldsymbol{p} \\ \dfrac{\partial \boldsymbol{p}}{\partial \xi_1} \\ \dfrac{\partial \boldsymbol{p}}{\partial \xi_2} \end{bmatrix}. \tag{5.3.1}$$

We have dropped the subscript g in $\boldsymbol{p}_g$ for this discussion, because we will need to examine specific components of this vector, and we want to limit the proliferation of subscripts here.

We will not start from this determinant. Instead, we begin our analysis by considering the ray Jacobian[10] associated with the propagation between the point $\boldsymbol{x}_g$ and $\boldsymbol{x}$. Let us denote that Jacobian by

$$J_g(\boldsymbol{x}, \boldsymbol{x}_g) = \frac{\partial(\boldsymbol{x})}{\partial(\boldsymbol{\sigma})} = \det \begin{bmatrix} \dfrac{\partial \boldsymbol{x}}{\partial \sigma_1} \\ \dfrac{\partial \boldsymbol{x}}{\partial \sigma_2} \\ \dfrac{\partial \boldsymbol{x}}{\partial \sigma_3} \end{bmatrix}, \quad \boldsymbol{\sigma} = (\sigma_1, \sigma_2, \sigma_3). \tag{5.3.2}$$

In this equation, we think of a family of rays as being set off at the source point $\boldsymbol{x}_s$ and arriving at a generic point $\boldsymbol{x}$. Later, we will evaluate our determinants at the specific point $\boldsymbol{y}$. The rays are labeled by the parameters (σ_1, σ_2), representing the initial directions of their trajectory. These could be the polar angles of the initial directions of the rays, for example, or any other parameter that characterizes these initial directions.

The third parameter, σ_3 is a running parameter along the ray. The different choices of σ_3 characterize different scalings between this running parameter and arclength along the rays. For example, we could choose a parameter $\sigma = \sigma_3$, for which the equations of the rays are

[10]The reader unfamiliar with ray theory should review Appendix E.

$$\frac{d\boldsymbol{x}}{d\sigma} = \boldsymbol{p} = \nabla_x \tau(\boldsymbol{x}, \boldsymbol{x}_g), \quad \frac{d\boldsymbol{p}}{d\sigma} = \frac{1}{2}\nabla_x \left[\frac{1}{c^2(\boldsymbol{x})}\right], \quad \frac{d\tau}{d\sigma} = \frac{1}{c^2(\boldsymbol{x})}. \tag{5.3.3}$$

In Appendix E, we show that σ is related to arclength, s, along the ray through the equation

$$d\sigma = c(\boldsymbol{x})ds.$$

As we shall see in the next chapter, this is a particularly useful choice in 2.5D analysis. On the other hand, one might as easily want to use traveltime as a parameter, or even one of the coordinates, such as z, when the wavespeed depends only on z—a good and practical first approximation in many applications.

We will have need of a notation for derivatives of the traveltime, $\tau(\boldsymbol{x}, \boldsymbol{x}_g)$, with respect to the surface variables $\boldsymbol{x}_g$. Thus, we introduce the notation

$$\nabla_{x_g} \tau = \boldsymbol{q} \tag{5.3.4}$$

and observe that

$$\frac{\partial q_i}{\partial x_j} = \frac{\partial p_j}{\partial x_{gi}}.$$

This just represents an interchange of orders of integration between the independent variables on the upper surface and the variables at depth.

The particular endpoint, $\boldsymbol{y}$, in (5.3.1) and (5.3.2) is associated with a particular ray, that is, with a particular choice of the parameters (σ_1, σ_2) and a value of the running parameter (σ_3, in general—σ, in our particular example, above), for which the ray passes through $\boldsymbol{y}$. Here, we are assuming that there is only a single ray trajectory that connects the points, $\boldsymbol{y}$ and $\boldsymbol{x}_g$. Indeed, we have assumed this throughout our analysis, for simplicity, but the theory can accommodate more complicated situations with multiple travel paths and multiple arrivals, as well.

In the Jacobian defined by (5.3.2), we want to make two changes of variables. First, we want to replace σ_3 by the traveltime τ and, second, we want to replace the arbitrary parameters, (σ_1, σ_2) by the specific parameters, (q_1, q_2). We do this by using the chain rule for functions of more than one variable, that is, by multiplying appropriate Jacobians together, as follows.

$$\begin{aligned} J_g(\boldsymbol{x}, \boldsymbol{x}_g) &= \frac{\partial(\boldsymbol{x})}{\partial(\sigma_1, \sigma_2, \tau)} \cdot \frac{\partial(\sigma_1, \sigma_2, \tau)}{\partial(\sigma_1, \sigma_2, \sigma_3)} \\ &= \frac{\partial(\boldsymbol{x})}{\partial(q_1, q_2, \tau)} \cdot \frac{\partial(q_1, q_2, \tau)}{\partial(\sigma_1, \sigma_2, \tau)} \cdot \frac{\partial(\sigma_1, \sigma_2, \tau)}{\partial(\sigma_1, \sigma_2, \sigma_3)} \\ &= \frac{\partial(\boldsymbol{x})}{\partial(q_1, q_2, \tau)} \cdot \frac{\partial(q_1, q_2)}{\partial(\sigma_1, \sigma_2)} \cdot \frac{\partial \tau}{\partial \sigma_3}. \end{aligned} \tag{5.3.5}$$

In the first line, we have exchanged σ_3, the generic running parameter along the ray with a specific ray parameter, the traveltime τ. In the next line, we

have exchanged the generic parameters, σ_1 and σ_2, that label the ray, with the specific parameters, q_1 and q_2. (At the end of this section, we discuss alternatives to this formulation, such as using q_1, q_3, when appropriate.) Finally, in the last line, we reduce the middle factor of the previous line to a 2×2 Jacobian, and the last factor to a simple derivative. We know this last derivative from the ray equations. For the particular example $\sigma_3 = \sigma$, in (5.3.3), this factor is just $1/c^2(\boldsymbol{x})$. In any case, it is always known.

Let us now focus on the first factor in the second line of (5.3.6) and observe that

$$\frac{\partial(\boldsymbol{x})}{\partial(\tau, q_1, q_2)} = \frac{1}{\tilde{h}(\boldsymbol{x}, x_{g1} x_{g2})}, \tag{5.3.6}$$

where

$$\tilde{h}(\boldsymbol{x}, x_{g1}, x_{g2}) = \frac{\partial(\tau, q_1, q_2)}{\partial(\boldsymbol{x})} = \det \begin{bmatrix} \boldsymbol{p} \\ \nabla_x q_1 \\ \nabla_x q_2 \end{bmatrix} = \det \begin{bmatrix} \boldsymbol{p} \\ \dfrac{\partial \boldsymbol{p}}{\partial x_{g1}} \\ \dfrac{\partial \boldsymbol{p}}{\partial x_{g2}} \end{bmatrix}. \tag{5.3.7}$$

Here, we have interchanged derivatives with respect to $\boldsymbol{x}$ and with respect to x_{g1}, x_{g2}.

Note that, if the upper surface were a horizontal plane and the parameters that we chose to describe this surface were

$$\boldsymbol{\xi} = (\xi_1, \xi_2) = (x_{g1}, x_{g2}),$$

then $\tilde{h}(\boldsymbol{y}, \boldsymbol{\xi})$ would be exactly the Beylkin determinant, $h_g(\boldsymbol{y}, \boldsymbol{\xi})$, defined in (5.3.1). This is Najmi's result. That is, for a horizontal and planar upper surface, we have related the Beylkin determinant to the ray Jacobian for common-source data, in a variable-wavespeed medium.

Now we wish to go further and relate these two determinants when the acquisition surface is more general. That is, we want to relate J_g to the determinant h_g in (5.3.1). We see there that the differentiation in the second and third rows is with respect to ξ_1, ξ_2, whereas the differentiation here is with respect to the explicit first two coordinates, x_{g1}, x_{g2}. Transforming from one set of variables to the other requires more than just another 2×2 Jacobian. To see why, think of the differentiation with respect to each ξ_i as being carried out by using the chain rule, first differentiating $\partial\tau/\partial x_k$ with respect to x_{gj} and then multiplying by $\partial x_{gj}/\partial \xi_i$ and summing on j. That result *includes a derivative with respect to* x_{g3}, which does not appear in our result, (5.3.7), above. Thus, in (5.3.1), we must find a way to eliminate derivatives with respect to x_{g3} in order to have a chance of relating that result with the determinant $\tilde{h}$ and subsequently to J_g. That is what we will proceed to do here.

Below, we sum over repeated indices. We will have occasion to carry out some sums over the indices, 1, 2, and other sums over 1, 2, 3. We will use capital indices for the former range, lowercase indices for the latter range.

We begin by setting

$$\begin{aligned} \frac{\partial}{\partial \xi_I}\frac{\partial \tau}{\partial x_j} &= \frac{\partial^2 \tau}{\partial x_{gk}\partial x_j}\frac{\partial x_{gk}}{\partial \xi_I} \\ &= \frac{\partial q_k}{\partial x_j}\frac{\partial x_{gk}}{\partial \xi_I}. \end{aligned} \tag{5.3.8}$$

Here, the first line is just a statement of the chain rule. In the second line, we have first interchanged the order of differentiation between x_j and x_{gk}.

Now, we eliminate the differentiation with respect to x_{g3} in this equation by using the eikonal equation in the form

$$q_3 = -\sqrt{1/c^2(\boldsymbol{x}_g) - q_1^2 - q_2^2}$$

and then setting

$$\frac{\partial q_3}{\partial x_j} = \frac{\partial}{\partial x_j}\sqrt{1/c^2(\boldsymbol{x}_g) - q_1^2 - q_2^2} = -\frac{q_K}{q_3}\frac{\partial q_K}{\partial x_j}. \tag{5.3.9}$$

We use this result in (5.3.8) to write

$$\begin{aligned} \frac{\partial}{\partial \xi_I}\frac{\partial \tau}{\partial x_j} &= -\left[\frac{\partial q_K}{\partial x_j}\frac{\partial x_{gK}}{\partial \xi_I} - \frac{q_K}{q_3}\frac{\partial q_K}{\partial x_j}\right] \\ &= \left[\frac{\partial}{\partial x_{gK}}\frac{\partial \tau}{\partial x_j}\frac{\partial x_{g3}}{\partial \xi_I}\right]\left[\frac{\partial x_{gK}}{\partial \xi_I} - \frac{q_K}{q_3}\frac{\partial x_{g3}}{\partial \xi_I}\right]. \end{aligned} \tag{5.3.10}$$

Recall that the indices $I = 1, 2$ in this equation form the elements of the second and third row of the matrix on the right side of (5.3.1), while the indices $J = 1, 2$ form the elements of the second and third rows of the matrix on the right side of (5.3.8). This last equation states that the last two rows of the former matrix are *linear combinations* of the last two rows of the latter matrix. It is a general rule of matrix multiplication that one can carry out such a summation as a product of matrices by performing the same linear combination on the columns of the identity matrix and then premultiplying the given matrix by this modified identity matrix. That is, we write

$$\begin{bmatrix} \boldsymbol{p} \\ \dfrac{\partial \boldsymbol{p}}{\partial \xi_1} \\ \dfrac{\partial \boldsymbol{p}}{\partial \xi_2} \end{bmatrix} = \begin{bmatrix} 1 & 0 & 0 \\ 0 & \dfrac{\partial x_{g1}}{\partial \xi_1} - \dfrac{q_1}{q_3}\dfrac{\partial x_{g3}}{\partial \xi_1} & \dfrac{\partial x_{g2}}{\partial \xi_1} - \dfrac{q_2}{q_3}\dfrac{\partial x_{g3}}{\partial \xi_1} \\ 0 & \dfrac{\partial x_{g1}}{\partial \xi_2} - \dfrac{q_1}{q_3}\dfrac{\partial x_{g3}}{\partial \xi_2} & \dfrac{\partial x_{g2}}{\partial \xi_2} - \dfrac{q_2}{q_3}\dfrac{\partial x_{g3}}{\partial \xi_2} \end{bmatrix} \begin{bmatrix} \boldsymbol{p} \\ \dfrac{\partial \boldsymbol{p}}{\partial x_{g1}} \\ \dfrac{\partial \boldsymbol{p}}{\partial x_{g2}} \end{bmatrix}. \tag{5.3.11}$$

The left side here is just the matrix whose determinant is h_g, defined by (5.3.1), while the determinant of the rightmost matrix is just $\tilde{h}$ defined by (5.3.7). Hence, we need only calculate the determinant of the middle matrix. Let us carry out the direct multiplication and proceed to simplify the result:

$$\begin{aligned} \frac{h_g}{\tilde{h}} &= \left[\frac{\partial x_{g1}}{\partial \xi_1} - \frac{q_1}{q_3}\frac{\partial x_{g3}}{\partial \xi_1}\right]\left[\frac{\partial x_{g2}}{\partial \xi_2} - \frac{q_2}{q_3}\frac{\partial x_{g3}}{\partial \xi_2}\right] \\ &\qquad - \left[\frac{\partial x_{g2}}{\partial \xi_1} - \frac{q_2}{q_3}\frac{\partial x_{g3}}{\partial \xi_1}\right]\left[\frac{\partial x_{g1}}{\partial \xi_2} - \frac{q_1}{q_3}\frac{\partial x_{g3}}{\partial \xi_2}\right] \\ &= \frac{\partial(x_{g1}, x_{g2})}{\partial(\xi_1, \xi_2)} + \frac{q_2}{q_3}\frac{\partial(x_{g3}, x_{g1})}{\partial(\xi_1, \xi_2)} + \frac{q_1}{q_3}\frac{\partial(x_{g2}, x_{g3})}{\partial(\xi_1, \xi_2)} \\ &= \frac{1}{q_3}\det\begin{bmatrix} \boldsymbol{p} \\ \dfrac{\partial \boldsymbol{x}_g}{\partial \xi_1} \\ \dfrac{\partial \boldsymbol{x}_g}{\partial \xi_2} \end{bmatrix} = \frac{1}{q_3}\boldsymbol{p} \cdot \left\{\frac{\partial \boldsymbol{x}_g}{\partial \xi_1} \times \frac{\partial \boldsymbol{x}_g}{\partial \xi_2}\right\} \\ &= \frac{\cos\theta_g \sqrt{g_g}}{q_3\, c(\boldsymbol{x}_g)}. \end{aligned} \tag{5.3.12}$$

In this last equation, we have used θ_g for the angle between the gradient vector $\boldsymbol{p}$ and the normal to the acquisition surface S_a with direction determined by the direction of the cross product.[11] Similarly, we have used g_g to denote the determinant of the first fundamental tensor of differential geometry of the acquisition surface; that is, the differential surface element on S_a is related to the differentials in $\boldsymbol{\xi}$ through the equation

$$dS_a = \sqrt{g_g}\, d\xi_1 d\xi_2 = \left|\frac{\partial \boldsymbol{x}_g}{\partial \xi_1} \times \frac{\partial \boldsymbol{x}_g}{\partial \xi_2}\right| d\xi_1 d\xi_2.$$

(See Kreyszig [1991], for information on differential geometry.) We can see from the last form in (5.3.12) that this derivation will break down if the normal to the acquisition surface and the gradient of the traveltime

[11] We do not really care about the sign of this dot product as we will ultimately use only the absolute value in our inversion formula.

or, equivalently, the ray direction, are parallel. Furthermore, the derivation breaks down if $q_3 = 0$. This is a consequence of having singled out $x_{g1}(\boldsymbol{\sigma}), x_{g2}(\boldsymbol{\sigma})$ in the original Najmi derivation. This makes sense if the acquisition surface is the upper surface. However, in the next chapter, we will consider 2.5D inversion, which is also applicable to VSP or well-to-well diffraction tomography. (We are referring to the usage of this term as in Devaney and Oristaglio, [1984]). In those cases, it makes more sense to think of x_{g2} and x_{g3} as the independent variables. This will lead to a corresponding requirement that $q_1 \neq 0$ and a result like (5.3.12), with q_3 replaced by q_1 and derivatives with respect to x_{g1} on the right replaced by derivatives with respect to x_{g3}.[12]

Throughout the derivation, we have used a generic final point, $\boldsymbol{x}$, along the ray, as we needed to examine the variation with respect to σ_1, σ_2 as well as σ_3 in order to introduce the ray Jacobian, J_g. Now, we need only evaluate our result at $\boldsymbol{x} = \boldsymbol{y}$ in order to relate the ray Jacobian to the Beylkin determinant. To do so, we need to use (5.3.12) in our earlier results, (5.3.6), and (5.3.7), to obtain our final result,

$$J_g(\boldsymbol{y}, \boldsymbol{\xi}) \cdot h_g(\boldsymbol{y}, \boldsymbol{\xi}) = \frac{\partial \tau}{\partial \sigma_{g3}} \cdot \frac{\partial(q_{g1}, q_{g2})}{\partial(\sigma_{g1}, \sigma_{g2})} \cdot \frac{\cos\theta_g \sqrt{g_g}}{q_{g3}\, c(\boldsymbol{x}_g)}. \tag{5.3.13}$$

Here, we have restored the subscripts g to all variables to distinguish them from the result below for the relationship between J_s and h_s.

We remark that the Jacobian is related to the ray-theoretic Green's function amplitude, $A_g(\boldsymbol{y}, \boldsymbol{\xi})$, through the equation

$$A_g^2(\boldsymbol{y}, \boldsymbol{\xi}) = \frac{K_g(\sigma_{g1}, \sigma_{g2})}{J_g(\boldsymbol{y}, \boldsymbol{\xi})}, \tag{5.3.14}$$

with $K_g(\sigma_1, \sigma_2)$ a constant along the ray that depends on the specific choice of parameters (σ_1, σ_2). Thus, we can as easily write h_g in terms of this amplitude as

$$h_g(\boldsymbol{y}, \boldsymbol{\xi}) = \frac{A_g^2(\boldsymbol{y}, \boldsymbol{\xi})}{K_g(\sigma_{g1}, \sigma_{g2})} \cdot \frac{\partial \tau}{\partial \sigma_{g3}} \cdot \frac{\partial(q_{g1}, q_{g2})}{\partial(\sigma_{g1}, \sigma_{g2})} \cdot \frac{\cos\theta_g \sqrt{g_g}}{q_{g3}\, c(\boldsymbol{x}_g)}. \tag{5.3.15}$$

In summary, we compute the Beylkin determinant for common-shot inversion from the same constituents that we need for the Green's function: raytrace-based traveltime and amplitude, plus additional factors that depend on the parameterizations of the acquisition geometry $\boldsymbol{x}_g(\boldsymbol{\xi})$ and of the rays $\boldsymbol{x}(\boldsymbol{\sigma})$. Clearly, the same result could be derived for the relationship between the Beylkin determinant h_s and the corresponding ray Jacobian. That is,

---

[12] We will see that further simplifications are possible, as well. All functions will be evaluated in the x_1, x_3-plane and these 3×3 matrices will be replaced by 2×2 matrices.

$$J_s(\boldsymbol{y},\boldsymbol{\xi}) \cdot h_s(\boldsymbol{y},\boldsymbol{\xi}) = \frac{\partial \tau}{\partial \sigma_{s3}} \cdot \frac{\partial(q_{s1}, q_{s2})}{\partial(\sigma_{s1}, \sigma_{s2})} \cdot \frac{\cos\theta_s \sqrt{g_s}}{q_{s3}\, c(\boldsymbol{x}_s)} \tag{5.3.16}$$

and

$$h_s(\boldsymbol{y},\boldsymbol{\xi}) = \frac{A_s^2(\boldsymbol{y},\boldsymbol{\xi})}{K_s(\sigma_{s1}, \sigma_{s2})} \cdot \frac{\partial \tau}{\partial \sigma_{s3}} \cdot \frac{\partial(q_{s1}, q_{s2})}{\partial(\sigma_{s1}, \sigma_{s2})} \cdot \frac{\cos\theta_s \sqrt{g_s}}{q_{s3}\, c(\boldsymbol{x}_s)}. \tag{5.3.17}$$

5.4 Asymptotic Inversion of Kirchhoff Data for a Single Reflector

The purpose of this section is to check the validity of the inversion formulas, (5.1.21) and (5.1.47). This will be done in two different ways. First, as in Chapter 3, the inversion formulas will be checked by applying them to Kirchhoff-approximate, upward-scattered data for a single reflector. We will assume that the background propagation speed above the reflector is known and is continued in some smooth but arbitrary way through the reflector. This approach repeats the method of Chapter 3, but now for a far more general inversion formula, allowing variable-background propagation speed and a variety of source-receiver configurations. In this approach, multidimensional stationary phase is applied to the integral over the source-receiver configuration and to the Kirchhoff integral over the reflecting surface, under the assumption of high-frequency data. The remaining frequency-domain integral will then be identified as a bandlimited delta function—the singular function of the reflecting surface—scaled by a factor that reduces to the appropriate multiple of the reflection coefficient, depending on whether the integral for $\beta(\boldsymbol{y})$ or $\beta_1(\boldsymbol{y})$ is being analyzed.

Second, the method of Chapter 4 will be applied. More precisely, we will show that the inversion integral applied to Kirchhoff data for a single reflector is asymptotically dominated by the integration over a small region containing the output point and a nearby section of the reflector. When this region is small enough, the change of variables (5.1.13) can be made exact and the inversion integral applied to Kirchhoff data is reduced to forward and inverse Fourier-type integration of a scaled singular function of a surface. The theory of Chapter 4 can then be applied directly to this integral to yield the desired result.

In both of these methods, it is assumed that the Beylkin determinant, $h(\boldsymbol{y},\boldsymbol{\xi})$, defined by (5.1.17), is nonzero in some neighborhood of the reflector, S. In the first approach, this assumption will isolate the support of the singular function to the surface, S. In the second method, it will allow for the exact change of variables needed to reduce the multifold integral to an integral of Fourier type treated in the previous chapter. The first method shows the crucial role that physically meaningful principles—such as the reflection principle—relate to the asymptotic processing of model

data. The second method shows the close tie to Fourier inversion suggested by the formal analysis of the previous chapter.

In addition to the rigorous asymptotic justification of the inversion formalism, the reader should come away with the idea that the tie between the Fourier domain and the spatial/frequency domain, implicit in (5.1.14), is an asymptotically dominant reality. In particular, the range of observations provided by the source-receiver configuration and the bandwidth provide a description of a Fourier domain over which parameter information can be deduced.

5.4.1 *Stationary Phase Analysis of the Inversion of Kirchhoff Data*

We first apply (5.1.21) to Kirchhoff-approximate data for the upward-scattered field from a single reflector in response to a point source. We then evaluate the resulting integral asymptotically by the method of stationary phase. The Kirchhoff approximate wavefield is given by (E.8.17). In the constant-density case, in the notation used here, that representation is

$$u_S(\boldsymbol{x}_g, \boldsymbol{x}_s, \omega) \sim i\omega F(\omega) \int_S R(\boldsymbol{x}, \boldsymbol{x}_s) a(\boldsymbol{x}, \boldsymbol{\xi}) (\hat{\boldsymbol{n}} \cdot \nabla_x \phi(\boldsymbol{x}, \boldsymbol{\xi}))\, e^{i\omega\phi(\boldsymbol{x},\boldsymbol{\xi})} dS. \tag{5.4.1}$$

In this equation, $\phi(\boldsymbol{x}, \boldsymbol{\xi})$ and $a(\boldsymbol{x}, \boldsymbol{\xi})$ are defined by (5.1.8) and $R(\boldsymbol{x}, \boldsymbol{x}_s)$ is the geometrical-optics reflection coefficient given by (E.4.23). We repeat that result here:

$$R(\boldsymbol{x}, \boldsymbol{x}_s) = \frac{\left|\frac{\partial}{\partial n}\tau(\boldsymbol{x}, \boldsymbol{x}_s)\right| - \left\{1/c_+^2(\boldsymbol{x}) - 1/c^2(\boldsymbol{x}) + \left[\frac{\partial}{\partial n}\tau(\boldsymbol{x}, \boldsymbol{x}_s)\right]^2\right\}^{1/2}}{\left|\frac{\partial}{\partial n}\tau(\boldsymbol{x}, \boldsymbol{x}_s)\right| + \left\{1/c_+^2(\boldsymbol{x}) - 1/c^2(\boldsymbol{x}) + \left[\frac{\partial}{\partial n}\tau(\boldsymbol{x}, \boldsymbol{x}_s)\right]^2\right\}^{1/2}}. \tag{5.4.2}$$

The unit normal $\hat{\boldsymbol{n}}$ points upward and $\partial/\partial n = \hat{\boldsymbol{n}} \cdot \nabla_x$; $c_+(\boldsymbol{x})$ is the propagation speed below the reflector.

This result is to be substituted into equation (5.1.21); specifically, the inversion for $\beta(\boldsymbol{y})$ will be analyzed and then the second inversion operator, $\beta_1(\boldsymbol{y})$, will be discussed. The substitution of (5.4.1) into (5.1.21) leads to the following multifold integral representation of the output $\beta(\boldsymbol{y})$ when applied to these synthetic data:

$$\beta(\boldsymbol{y}) \sim -\frac{1}{8\pi^3} \int \omega^2 d\omega F(\omega) \int_{S_\xi} d^2\xi \int_{S_x} dS \frac{|h(\boldsymbol{y}, \xi)|}{a(\boldsymbol{y}, \boldsymbol{\xi}) |\nabla_y \phi(\boldsymbol{y}, \boldsymbol{\xi})|} \cdot R(\boldsymbol{x}, \boldsymbol{x}_s) a(\boldsymbol{x}, \boldsymbol{\xi}) (\hat{\boldsymbol{n}} \cdot \nabla_x \phi(\boldsymbol{x}, \boldsymbol{\xi}))\, e^{i\omega\Phi(\boldsymbol{y},\boldsymbol{x},\boldsymbol{\xi})}. \tag{5.4.3}$$

In this equation,

$$\Phi(\boldsymbol{y}, \boldsymbol{x}, \boldsymbol{\xi}) = \phi(\boldsymbol{x}, \boldsymbol{\xi}) - \phi(\boldsymbol{y}, \boldsymbol{\xi}) \tag{5.4.4}$$

is the difference of traveltimes. These are, respectively, the traveltime from the source point to the scattering point $\boldsymbol{x}$ (on the reflector) to the receiver point, minus traveltime from the source point to the output point $\boldsymbol{y}$ to the receiver point. The surface S is described parametrically in terms of two parameters (σ_1, σ_2) by an equation of the form

$$\boldsymbol{x} = \boldsymbol{x}(\boldsymbol{\sigma}), \quad \boldsymbol{\sigma} = (\sigma_1, \sigma_2). \tag{5.4.5}$$

As in Section 3.7, in terms of these parameters,

$$dS = \sqrt{g} d\sigma_1 d\sigma_2, \tag{5.4.6}$$

with g being the determinant of the first fundamental metric tensor (of differential geometry) for S,

$$g = \left| \frac{\partial \boldsymbol{x}}{\partial \sigma_1} \times \frac{\partial \boldsymbol{x}}{\partial \sigma_2} \right|^2 = \left| \det \left[\frac{\partial \boldsymbol{x}}{\partial \sigma_k} \cdot \frac{\partial \boldsymbol{x}}{\partial \sigma_m} \right] \right|, \quad k, m = 1, 2. \tag{5.4.7}$$

Here, $\times$ denotes the vector cross product. (Again, we refer the reader to Kreyszig [1991], for information on the topic of differential geometry.)

The method of stationary phase in the four variables $(\boldsymbol{\xi}, \boldsymbol{\sigma})$ will be applied to equation (5.4.4) under the assumption that $F(\omega)$ constrains the bandwidth of the data to "high frequency," as discussed in Chapters 2 and 3. The phase $\Phi(\boldsymbol{y}, \boldsymbol{x}, \boldsymbol{\xi})$ is a function of these variables through the dependence of $\boldsymbol{x}$ on $\boldsymbol{\sigma}$ and the dependence of $\boldsymbol{x}_s$ and $\boldsymbol{x}_g$ on ξ. Equation (5.4.4) is used to write the four first derivatives of $\Phi(\boldsymbol{y}, \boldsymbol{x}, \boldsymbol{\xi})$ in terms of the derivatives of the traveltimes:

$$\begin{aligned} \frac{\partial \Phi}{\partial \xi_m} &= \nabla_s \left[\tau(\boldsymbol{x}, \boldsymbol{x}_s) - \tau(\boldsymbol{y}, \boldsymbol{x}_s) \right] \cdot \frac{\partial \boldsymbol{x}_s}{\partial \xi_m} \\ &\quad + \nabla_g \left[\tau(\boldsymbol{x}, \boldsymbol{x}_g) - \tau(\boldsymbol{y}, \boldsymbol{x}_g) \right] \cdot \frac{\partial \boldsymbol{x}_g}{\partial \xi_m}, \\ \frac{\partial \Phi}{\partial \sigma_m} &= \nabla_x \left[\phi(\boldsymbol{x}, \boldsymbol{\xi}) \right] \cdot \frac{\partial \boldsymbol{x}}{\partial \sigma_m}, \quad \text{for} \quad m = 1, 2. \end{aligned} \tag{5.4.8}$$

In this equation, ∇_s is a gradient with respect to the variables $\boldsymbol{x}_s$; similarly, ∇_g is a gradient with respect to $\boldsymbol{x}_g$.

The stationary points in $(\boldsymbol{\xi}, \boldsymbol{\sigma})$ are determined by requiring that these first derivatives all be equal to zero. Note that $\partial \Phi / \partial \sigma_m = 0$, $m = 1, 2$, is just a statement of the law of reflection; that is, the sum of the gradients of the traveltime being orthogonal to two tangents in the surface S is equivalent to the condition that the angles of incidence and reflection with respect to the surface normal be equal. Equivalently, the sum of gradients must lie along the normal at the stationary point. In this second form, the stationarity condition generalizes to the case in which the reflection being modeled is a scalar representation of mode conversion, involving two different propagation speeds characterizing the traveltime from the source

to the reflector and from the reflector to the receiver. If, for a given point on S, there is no source-receiver pair for which the sum of gradients is normal at the point, then there will be no stationary point in all four variables; the asymptotic order (in ω) will be lower and, presumably, smaller in magnitude than in the case where there is a stationary point.

For $\boldsymbol{y}$ on S, one stationary point is easy to identify. Set $\boldsymbol{x} = \boldsymbol{y}$, with $\boldsymbol{\sigma}$ chosen accordingly. Note that, in this case, $\partial\Phi/\partial\xi_m \equiv 0$ because the traveltimes from $\boldsymbol{x}$ and $\boldsymbol{y}$, respectively, to $\boldsymbol{x}_s$ and $\boldsymbol{x}_g$ are the same, making the differences in the first line in (5.4.8) identically zero. Thus, we need only to find a "specular" source-receiver pair, that is, a source and receiver for which the law of reflection is satisfied at $\boldsymbol{y}$. This determines $\boldsymbol{\xi}$. Further, it confirms our earlier claim: imaging is achieved if, for some source/receiver pair in the survey, migration dip equals reflector dip.

When the conditions of stationarity are satisfied, $\boldsymbol{\xi}$ and $\boldsymbol{\sigma}$ are determined as functions of $\boldsymbol{y}$ as in the specific discussion here. Thus, $\boldsymbol{x}_s, \boldsymbol{x}_g$, and $\boldsymbol{x}$ are determined as functions of $\boldsymbol{y}$. These are the geometrical coordinates of interest, while $\boldsymbol{\xi}$ and $\boldsymbol{\sigma}$ characterize only a particular parameterization of the source-receiver surface and the reflection surface. We think of the former three vectors as being more fundamental than the latter two. Thus, below, we focus on the *stationary triple*, $\boldsymbol{x}_s, \boldsymbol{x}_g$, and $\boldsymbol{x}$, where the two sets of derivatives in (5.4.8) are zero, rather than on the values of the parameters $\boldsymbol{\xi}$ and $\boldsymbol{\sigma}$ that make these derivatives equal zero.

Furthermore, we are most interested in the asymptotic analysis for $\boldsymbol{y}$ near S and in the stationary triple that reduces to our special example above when $\boldsymbol{y}$ is on S. That is, we focus our attention on this stationary point, which has the limit $\boldsymbol{x} = \boldsymbol{y}$ as $\boldsymbol{y}$ approaches S. The interest in this particular type of stationary point should remind the reader of the asymptotic analysis of the previous chapter for the case of a scaled singular function, Section 4.4.5. Recall that, for $\boldsymbol{y}$ on the support S of the singular function, the asymptotic inversion was significantly larger, $O(\lambda)$, than for points $\boldsymbol{y}$ not on S. It is this asymptotically-dominant contribution that will produce an image of the reflector.

We proceed under the assumption that a distinguished stationary triple has been determined for $\boldsymbol{y}$ near S and that the corresponding values of $\boldsymbol{\sigma}$ and $\boldsymbol{\xi}$ are interior points of their respective domains of integration.

The result of applying the method of stationary phase to equation (5.4.4) is the following:

$$\beta(\boldsymbol{y}) \sim -R(\boldsymbol{x}, \boldsymbol{x}_s)\frac{a(\boldsymbol{x}, \boldsymbol{\xi})}{a(\boldsymbol{y}, \boldsymbol{\xi})}\frac{|h(\boldsymbol{y}, \xi)|}{\sqrt{|\det[\Phi_{\xi\sigma}]|}}\frac{\hat{\boldsymbol{n}} \cdot \nabla_x \phi(\boldsymbol{x}, \boldsymbol{\xi})}{|\nabla_y \phi(\boldsymbol{y}, \boldsymbol{\xi})|}\sqrt{g}\, I(\boldsymbol{y}). \tag{5.4.9}$$

In this equation, g is defined by equation (5.4.7), and

$$I(\boldsymbol{y}) = \frac{1}{2\pi}\int F(\omega) e^{i\omega\Phi(\boldsymbol{y}, \boldsymbol{x}, \boldsymbol{\xi}) + i(\operatorname{sgn}(\omega))(\pi/4)\operatorname{sig}[\Phi_{\xi\sigma}]} d\omega. \tag{5.4.10}$$

This integral, as well as the entire right side of equation (5.4.9), are functions of $\boldsymbol{y}$ alone, because $\boldsymbol{x}, \boldsymbol{x}_s$, and $\boldsymbol{x}_g$ are determined as functions of $\boldsymbol{y}$ from the stationarity conditions; $[\Phi_{\xi\sigma}]$ is the 4×4 matrix

$$[\Phi_{\xi\sigma}] = \begin{bmatrix} \dfrac{\partial^2\Phi}{\partial\xi_k\partial\xi_m} & \dfrac{\partial^2\Phi}{\partial\xi_k\partial\sigma_m} \\ \dfrac{\partial^2\Phi}{\partial\xi_k\partial\sigma_m} & \dfrac{\partial^2\Phi}{\partial\sigma_k\partial\sigma_m} \end{bmatrix}, \quad k, m = 1, 2; \tag{5.4.11}$$

$\det[\Phi_{\xi\sigma}]$ denotes the determinant of this matrix and $\operatorname{sig}[\Phi_{\xi\sigma}]$ denotes the signature of the matrix.

Because it is expected that $\beta(\boldsymbol{y})$ peaks for $\boldsymbol{y}$ on S, we are interested in evaluating equation (5.4.9) for $\boldsymbol{y}$ near S. First consider the behavior of the matrix $[\Phi_{\xi\sigma}]$ in equation (5.4.11) when $\boldsymbol{y}$ is on S. In this case, $\boldsymbol{\sigma}$ can be fixed *before* evaluating the second derivatives with respect to ξ_k and ξ_m. In that limit, $\Phi = 0$; the entire 2×2 matrix in the upper left-hand corner of $[\Phi_{\xi\sigma}]$ is a matrix of zeroes and the determinant of $[\Phi_{\xi\sigma}]$ is just the square of the determinant of the 2×2 matrix in the upper right-hand corner:

$$\det[\Phi_{\xi\sigma}] = \left[\det\left[\frac{\partial^2\Phi}{\partial\xi_k\partial\sigma_m}\right]\right]^2 = \left[\det\left[\frac{\partial^2\phi(\boldsymbol{x},\boldsymbol{\xi})}{\partial\xi_k\partial\sigma_m}\right]\right]^2, \quad k, m = 1, 2, \tag{5.4.12}$$

with $\boldsymbol{x}$ evaluated at the stationary point $\boldsymbol{y}$ on S and $\boldsymbol{x}_s$ and $\boldsymbol{x}_g$ evaluated to complete the stationary triple.

From this result, the determinant is seen to be positive, meaning that the eigenvalues of each sign must occur in pairs. Thus, the only choices for $\operatorname{sig}[\Phi_{\xi\sigma}]$ are ± 4 and 0 and the only effect that the signature factor can have on the result in equations (5.4.9) and (5.4.10) is a multiplication by -1 or $+1$, respectively. We show below that the signature is zero and the multiplier is $+1$. By continuity, if this signature is equal to zero for $\boldsymbol{y}$ on S, then it must be equal to zero for $\boldsymbol{y}$ in some neighborhood of S, and it is assumed that this neighborhood is at least a few units of reciprocal wavenumber at the frequencies within the bandwidth of the data. Then, the depiction of the output described below will hold in a region around S sufficiently wide for the reflector to be detected. With $\operatorname{sig}[\Phi_{\xi\sigma}] = 0$, the integral $I(\boldsymbol{y})$ defined by equation (5.4.7) becomes

$$I(\boldsymbol{y}) = \frac{1}{2\pi}\int F(\omega)e^{i\omega\Phi(\boldsymbol{y},\boldsymbol{x},\boldsymbol{\xi})}d\omega. \tag{5.4.13}$$

By assumption, the function $F(\omega)$, is the spectrum of a bandlimited delta function. Thus, it can be seen that $I(\boldsymbol{y})$ is a bandlimited delta function of the argument $\Phi(\boldsymbol{y}, \boldsymbol{x}, \boldsymbol{\xi})$. Therefore, set

$$I(\boldsymbol{y}) = \delta_B\left[\Phi(\boldsymbol{x}, \boldsymbol{y}, \boldsymbol{\xi})\right], \tag{5.4.14}$$

where, as in earlier applications, the subscript B is used to represent the bandlimiting.

The function Φ is equal to zero on the surface S. Thus, the support of this delta function includes S. This is the only zero in the neighborhood of S. To see why this is so, take the gradient of Φ with respect to $\boldsymbol{y}$, with $\boldsymbol{x}$, $\boldsymbol{x}_s$, and $\boldsymbol{x}_r$ defined by the stationarity conditions:

$$\frac{d\Phi}{dy_j} = \frac{\partial \Phi}{\partial y_j} + \sum_k \left[\frac{\partial \Phi}{\partial \sigma_k} \frac{\partial \sigma_k}{\partial y_j} + \frac{\partial \Phi}{\partial \xi_k} \frac{\partial \xi_k}{\partial y_j} \right], \quad j = 1, 2, 3. \tag{5.4.15}$$

In this equation, $\partial\Phi/\partial\sigma_k = \partial\Phi/\partial\xi_k = 0$, because these *are* the conditions of stationarity. Thus, the total derivative with respect to y_j is just the partial derivative with respect to the explicit y_j in Φ. The condition of stationarity was that this gradient be normal to the reflector at this stationary point. Normality would be trivially satisfied if the actual magnitude of the gradient were zero; this would require that the incident and reflected ray actually be tangent to the reflector at the stationary point. We reject this case as one in which the entire theory breaks down; the gradient is the first line of the matrix forming the Beylkin determinant and was assumed to be nonzero. Consequently, the surface S is an isolated zero of the argument of the bandlimited delta function (5.4.14).

By standard rules about delta functions, we can now write $I(\boldsymbol{y})$ in terms of a delta function of arclength along a curve normal to S. Denoting that arclength by s,

$$I(\boldsymbol{y}) = \frac{\delta_B(s)}{|\nabla_y \Phi(\boldsymbol{y}(\boldsymbol{x}), \boldsymbol{\xi})|} = \frac{\delta_B(s)}{|\nabla_y \Phi(\boldsymbol{y}, \boldsymbol{\xi})|}\bigg|_{\boldsymbol{\xi}=\boldsymbol{\xi}(\boldsymbol{y})} \equiv \frac{\gamma_B(\boldsymbol{y})}{|\nabla_y \Phi(\boldsymbol{y}, \boldsymbol{\xi})|}. \tag{5.4.16}$$

The delta function, $\delta(s) = \gamma(\boldsymbol{x})$, with support on S, is the singular function of the surface S; its bandlimited counterpart is $\delta_B(s) = \gamma_B(\boldsymbol{x})$. This result provides a partial confirmation of the asymptotic validity of the inversion formalism. That is, $\beta(\boldsymbol{y})$ has been shown to be proportional to a bandlimited singular function of the reflecting surface under reasonable conditions on the background propagation speed. This confirms that the processing proposed here constitutes mathematical imaging of the reflector and that graphic output will provide a visual image of the reflector. At this point, we have confirmed that our inversion operator is at least a migration operator. Further, this result suggests that if one just gets the phase right in the Kirchhoff operator and uses a "reasonable" amplitude function, then imaging is guaranteed when migration dip equals reflector dip.

It remains now to study the amplitude to determine how its value on the reflector is related to the reflection coefficient. By using the result (5.4.16) in (5.4.9) with $\delta_B(s)$ replaced by $\gamma_B(\boldsymbol{x})$, we obtain

$$\beta(\boldsymbol{y}) \sim -R(\boldsymbol{x}, \boldsymbol{x}_s) \frac{a(\boldsymbol{x}, \boldsymbol{\xi})}{a(\boldsymbol{y}, \boldsymbol{\xi})} \frac{|h(\boldsymbol{y}, \boldsymbol{\xi})|}{|\det[\Phi_{\xi\sigma}]|^{1/2}} \frac{\hat{\boldsymbol{n}} \cdot \nabla_x \phi(\boldsymbol{x}, \boldsymbol{\xi})}{|\nabla_y \phi(\boldsymbol{y}, \boldsymbol{\xi})|^2} \sqrt{g} \gamma_B(\boldsymbol{x}). \tag{5.4.17}$$

Recall now the definition of θ in (5.1.44). Similarly, define an angle, θ_x, for the corresponding x-gradients and note that the two gradients make

equal angles with the normal at stationarity. Therefore,

$$\hat{\boldsymbol{n}} \cdot \nabla_x \phi(\boldsymbol{x}, \xi) = -\frac{2\cos\theta_x}{c(\boldsymbol{x})} \tag{5.4.18}$$

and

$$|\nabla_x \phi(\boldsymbol{x}, \boldsymbol{\xi})| = \frac{2\cos\theta_x}{c(\boldsymbol{x})}. \tag{5.4.19}$$

Note that for $\boldsymbol{y}$ on S, $\theta_x = \theta_s$, the specular reflection angle. Furthermore, we will show in Section 5.4.5 that

$$\frac{|h(\boldsymbol{y}, \boldsymbol{\xi})|}{|\det[\Phi_{\xi\sigma}]|^{1/2}} \sqrt{g} = |\nabla_y \phi(\boldsymbol{y}, \boldsymbol{\xi})| \Rightarrow \frac{2\cos\theta_s}{c(\boldsymbol{y})}, \quad \boldsymbol{y} \text{ on } S. \tag{5.4.20}$$

By inserting the results given by equations (5.4.18)–(5.4.20) into equation (5.4.17), we obtain

$$\beta_{\text{PEAK}}(\boldsymbol{y}) \sim R(\boldsymbol{y}, \boldsymbol{x}_s)\delta_B(0), \quad \boldsymbol{y} \text{ on } S. \tag{5.4.21}$$

In this equation, we return to the notation $\delta_B(0)$, because the representation $\gamma_B(\boldsymbol{y})$ does not easily lend itself to the evaluation of this function for $\boldsymbol{y}$ on S. Modulo the few results that were postponed to later subsections, this confirms the claim that the inversion operator (5.1.21), applied to Kirchhoff-approximate data, (5.4.1), yields an asymptotic output that is the bandlimited singular function of the reflecting surface multiplied by a "slowly varying function" whose value on the reflector is the geometrical-optics reflection coefficient.

5.4.2 Determination of $\cos\theta_s$ *and* c_+

We now explain the need for the operator $\beta_1(\boldsymbol{y})$, defined by (5.1.47), to determine $\cos\theta_s$ and the change in propagation speed across the reflector. First, note from (5.4.21), that it is necessary to evaluate $\delta_B(0)$ to determine the peak value of $\beta_{\text{PEAK}}(\boldsymbol{y})$. To do so, use (5.4.16) to relate $\delta_B(0)$ to $I(\boldsymbol{y})$ and then (5.4.13) to evaluate $I(\boldsymbol{y})$ for $\boldsymbol{y}$ on S. Then use (5.4.19) to evaluate the sum of the gradients and conclude that

$$\beta_{\text{PEAK}}(\boldsymbol{y}) \sim \frac{2\cos\theta_s}{c(\boldsymbol{y})} R(\boldsymbol{y}, \boldsymbol{x}_s) \frac{1}{2\pi} \int F(\omega) d\omega, \quad \boldsymbol{y} \text{ on } S. \tag{5.4.22}$$

This equation shows that the numerical value at the peak depends on the area under the filter in the frequency domain, the opening angle θ_s between the normal and each of the rays from $\boldsymbol{x}_s$ to $\boldsymbol{y}$ on S and from $\boldsymbol{x}_g$ to $\boldsymbol{y}$ on S, and the reflection coefficient at that opening angle. We know the filter and, hence, the area under the filter, but the separate elements θ_s and c_+ remain coupled in this equation.

First, consider θ_s. Note that the factor of $2\cos\theta_s/c(\boldsymbol{y})$ is a result of quotients of factors of $|\nabla_x \phi(\boldsymbol{x}, \boldsymbol{\xi})|$, $\hat{\boldsymbol{n}} \cdot \nabla_x \phi(\boldsymbol{x}, \boldsymbol{\xi})$, and $|\nabla_y \phi(\boldsymbol{y}, \boldsymbol{\xi})|$ at the stationary point, along with the results (5.4.18), (5.4.19), and (5.1.45).

Among these factors, the user has control over the power of the last of these appearing in the inversion operator (5.1.21). By changing the power of this factor in that operator, it is possible to change the power of the multiplicative factor $2\cos\theta_s/c(\boldsymbol{y})$ at the peak of the output of the inversion operator. Therefore, in addition to processing the data with the inversion operator in equation (5.1.21), one can apply the inversion operator (5.1.47) to produce the output $\beta_1(\boldsymbol{y})$. The asymptotic analysis of this inversion operator proceeds exactly as above for $\beta(\boldsymbol{y})$. This function also produces the bandlimited singular function $\gamma_B(\boldsymbol{y})$ scaled by a different factor. At the peak, that scale factor differs from the scale for $\beta(\boldsymbol{y})$ by $|\nabla\phi(\boldsymbol{y},\boldsymbol{\xi})|^{-1}$ evaluated at the stationary point on S. By using (5.1.45), we conclude that

$$\beta_1(\boldsymbol{x}) \sim R(\boldsymbol{x},\boldsymbol{x}_s)\frac{1}{2\pi}\int F(\omega)d\omega, \qquad \boldsymbol{x} \quad \text{on} \quad S, \tag{5.4.23}$$

and

$$\frac{\beta_{\text{PEAK}}(\boldsymbol{x})}{\beta_{1\text{PEAK}}(\boldsymbol{x})} \sim \frac{2\cos\theta_s}{c(\boldsymbol{x})}, \quad \boldsymbol{x} \quad \text{on} \quad S. \tag{5.4.24}$$

Consequently, when both inversion operators are applied to the data, the locations of the peaks of either of them determine the reflector, and then the ratio of the peak values determines $\cos\theta_s$. When we use multiple-offset data to determine more than one inversion output, the estimates of incidence angles provide the necessary additional tool for AVA analysis.[13][14]

Once $\cos\theta_s$ is determined, either peak amplitude, β_{PEAK} or $\beta_{1\text{PEAK}}$, provides a single equation for the remaining unknown, $c_+(\boldsymbol{y})$. To see how this works out in detail, first rewrite the reflection coefficient in equation (5.4.2) in terms of θ_s and $\boldsymbol{x} = \boldsymbol{y}$ on S. Note first that, from the stationarity conditions,

$$\left|\frac{\partial\tau(\boldsymbol{x},\boldsymbol{x}_s)}{\partial n}\right|\Bigg|_{\boldsymbol{x}=\boldsymbol{y}} = \frac{\cos\theta_s}{c(\boldsymbol{y})}. \tag{5.4.25}$$

---

[13]In numerical experiments, such as in Sullivan and Cohen [1987] and in Bleistein et al. [1988], the estimates of the cosine of the incidence angle tend to be an order of magnitude better than the estimates of the reflection coefficient itself. We believe that this occurs because the numerical processing in the numerator and the denominator is quite similar, with errors likely trending in the same direction; hence, a tendency towards cancellation of error and increased accuracy in the calculation of the quotient of integrals, as compared to either integral itself.

[14]In Kirchhoff migration the amplitude of the operator is simpler than the amplitude of our inversion operator. Nonetheless, the output produces an accurate image of the reflector. Furthermore, this quotient-of-integrals trick can still be used in any Kirchhoff migration operator. In the simplest case, it is only necessary to get the phase right and use a crude amplitude normalization to get an accurate quotient. Then one can produce an estimate of the cosines of incidence angles, or any of a variety of geometrical attributes of the data; see Geoltrain and Chovet [1991] and Exercise 5.19.

With a slight abuse of notation, using arguments $\boldsymbol{y}$ and θ_s for R, rather than $\boldsymbol{x}$ and $\boldsymbol{x}_s$, equation (5.4.2) can be rewritten as follows:

$$R(\boldsymbol{y},\theta_s)=\frac{\cos\theta_s/c(\boldsymbol{y})-\left[1/c_+^2(\boldsymbol{y})-\sin^2\theta_s/c^2(\boldsymbol{y})\right]^{1/2}}{\cos\theta_s/c(\boldsymbol{y})+\left[1/c_+^2(\boldsymbol{y})-\sin^2\theta_s/c^2(\boldsymbol{y})\right]^{1/2}}. \tag{5.4.26}$$

Suppose that both operators $\beta(\boldsymbol{y})$ and $\beta_1(\boldsymbol{y})$ have been computed for a data set. Furthermore, a particular point $\boldsymbol{y}$ has been identified as being a peak of the bandlimited singular functions depicting the reflecting surface. Then $\cos\theta_s$ is determined from the ratio of the outputs. Furthermore, dividing the peak value of $\beta_1(\boldsymbol{y})$ by the area under the filter in the frequency domain provides a value for the left side of equation (5.4.26) at $\boldsymbol{y}$. The solution of this equation for $c_+(\boldsymbol{y})$ is most easily expressed in terms of the squared slowness. That is,

$$\frac{1}{c_+^2(\boldsymbol{y})}=\frac{1}{c^2(\boldsymbol{y})}\left[1-\frac{4R\cos^2\theta_s}{(1+R)^2}\right]. \tag{5.4.27}$$

This completes the determination of $c_+(\boldsymbol{y})$. This expression is consistent with the angularly dependent geometrical-optics reflection coefficient.

Variable Density; Mode Conversion

It is possible to show that if the appropriate asymptotic Green's functions are used, the results derived here generalize to variable-density acoustic media and scalar mode-converted observations in elastic media—both isotropic and anisotropic [Geoltrain, 1989; de Hoop and Bleistein, 1997, 1998]. In these cases, output at one incidence angle is not sufficient to determine the change in earth parameters across the reflector; one must use multi-offset data and attempt to derive parameter changes to provide a "best fit," say, in a least-squares sense to the *amplitude versus angle* estimates of the reflection coefficient(s).

5.4.3 Finding Stationary Points

The existence of stationary points for $\Phi(\boldsymbol{y},\boldsymbol{x},\boldsymbol{\xi})$, (5.4.4), will be considered further here for the most important cases of common-shot and common-offset data sets. In the discussion, above, it was noted that for $\boldsymbol{y}$ on S, a stationary triple would exist for $\boldsymbol{x}=\boldsymbol{y}$ if, in addition, there existed a source-receiver pair in the data set for which the geometrical-optics rays from those points satisfied the law of reflection; that is, the incidence angles of these rays at $\boldsymbol{x}=\boldsymbol{y}$ made equal angles with the normal at that point. This turned out to be the distinguished stationary point that produced the peak value on the reflector that provided an image of the reflector through the bandlimited singular function. Here, we propose to consider such stationary points when $\boldsymbol{y}$ is not on S, but nearby.

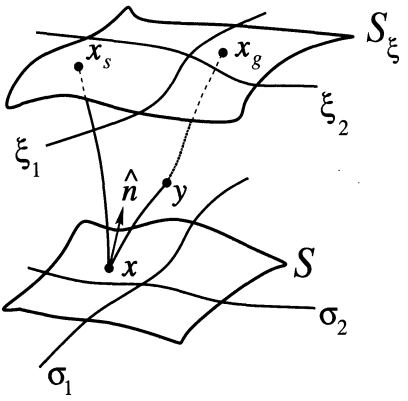

FIGURE 5.5. Stationary triple for common-shot inversion.

Consider, first, a common-source experiment. It is fairly straightforward to describe geometrically how a stationary triple would be determined. We start from the law of reflection, obtained by setting the second line in (5.4.8) equal to zero:

$$\nabla_x \left[\phi(\boldsymbol{x}, \boldsymbol{\xi})\right] \cdot \frac{\partial \boldsymbol{x}}{\partial \sigma_m} = 0, \quad m = 1, 2. \tag{5.4.28}$$

Given $\boldsymbol{y}$ and the fixed source point, $\boldsymbol{x}_s$, find a point on S for which the geometrical-optics rays from $\boldsymbol{y}$ and $\boldsymbol{x}_s$ satisfy the law of reflection at $\boldsymbol{x}$. Then, continue the ray from $\boldsymbol{x}$ through $\boldsymbol{y}$ up to the upper surface, S_ξ, and choose $\boldsymbol{x}_g$ to be the emergence point of this ray on the upper surface. This choice of $\boldsymbol{x}$ and $\boldsymbol{x}_g$ completes the stationary triple. See Figure 5.5.

To see why this is so, note first that, for the common-shot case, $\boldsymbol{x}_s$ is independent of $\boldsymbol{\xi}$. Consequently, from (5.4.8), stationarity in $\boldsymbol{\xi}$ for this case means that

$$\nabla_g \left[\tau(\boldsymbol{x}, \boldsymbol{x}_g) - \tau(\boldsymbol{y}, \boldsymbol{x}_g)\right] \cdot \frac{\partial \boldsymbol{x}_g}{\partial \xi_m} = 0, \quad m = 1, 2. \tag{5.4.29}$$

The ray from $\boldsymbol{x}$ to $\boldsymbol{x}_g$ overlays the ray from $\boldsymbol{y}$ to $\boldsymbol{x}_g$; the gradients appearing in this equation are identical and their difference is zero. Hence, this stationarity condition is satisfied. By the choice of $\boldsymbol{x}$ on S, (5.4.28) is satisfied as well. If such a pair $\boldsymbol{x}$ and $\boldsymbol{x}_g$ cannot be found for the given $\boldsymbol{y}$ (which is to say that there is no specular reflection point), then the asymptotic order in ω of the integrals in $\boldsymbol{\xi}$ and $\boldsymbol{\sigma}$ will be lower than when such a pair exists.

Now consider the common-offset case. In particular, let us consider the traveltime surface, $\phi(\boldsymbol{x}, \boldsymbol{\xi})$, as a function of $\boldsymbol{\xi}$, constrained by the stationarity condition, (5.4.28). That is, for each source-receiver pair, identify the point(s) $\boldsymbol{x}$ on S for which the reflection law is satisfied. While this might be a multisheeted surface, in general, the value of $\phi(\boldsymbol{x}, \boldsymbol{\xi})$ on this surface will be finite.

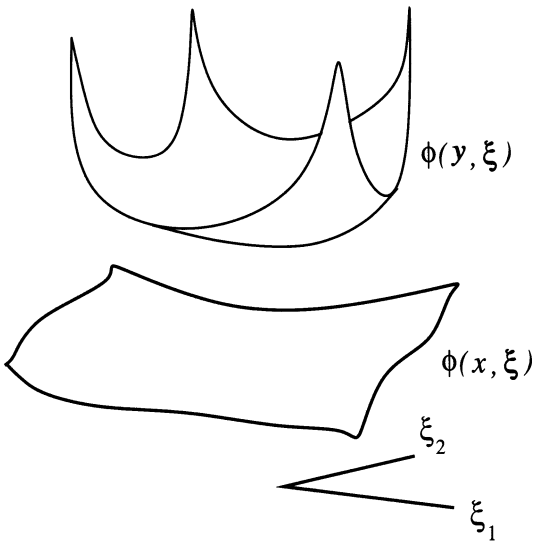

FIGURE 5.6. The traveltime surfaces $\phi(\boldsymbol{x},\boldsymbol{\xi})$ and $\phi(\boldsymbol{y},\boldsymbol{\xi})$ with the former subject to the stationarity condition, (5.4.28).

On the other hand, consider the traveltime surface $\phi(\boldsymbol{y},\boldsymbol{\xi})$ as a function of $\boldsymbol{\xi}$ for fixed $\boldsymbol{y}$. For an unbounded source-receiver surface, this function is unbounded and must attain one or more interior minima. See Figure 5.6. Under the assumption that the condition, (5.4.28) is satisfied, stationarity in $\boldsymbol{\xi}$ is equivalent to seeking the extrema of the difference in these two traveltime functions. Because one function is bounded while the other is not, we argue that one or more internal local minima must exist. That is, at least one stationary triple, $\boldsymbol{x}$, $\boldsymbol{x}_s$, and $\boldsymbol{x}_g$, must exist.

This argument requires an unbounded source-receiver domain. In practice, that is not the case. For finite source-receiver domains, the stationary triple might not exist for the given $\boldsymbol{y}$, and $\beta(\boldsymbol{y})$ will be asymptotically of lower order at such choices of $\boldsymbol{y}$ than it will be when a stationary triple does exist.

It is somewhat unsatisfactory that a constructive demonstration of the stationary triple is not available in this case as it was for the previous case. However, for the simple example of a constant-background medium, with a horizontal, planar acquisition surface over a horizontal planar reflector, it is possible to be more explicit. Given $\boldsymbol{y}$, drop a perpendicular to S. This defines the point $\boldsymbol{x}$. Now pass a plane through that normal, parallel to the offset vector $2\boldsymbol{h}$, and consider the line of intersection of that plane with the upper surface. Find the source-receiver pair along that line for which the rays to $\boldsymbol{x}$ make equal incidence angles at that point. See Figure 5.7. For that pair, (5.4.28) is satisfied. Moreover, for that pair, $\nabla_s\tau(\boldsymbol{x},\boldsymbol{x}_s)$ and $\nabla_g\tau(\boldsymbol{x},\boldsymbol{x}_g)$ have projections of equal magnitude but opposite direction on the data surface, S_ξ. The same is true for $\nabla_s\tau(\boldsymbol{y},\boldsymbol{x}_s)$ and $\nabla_g\tau(\boldsymbol{y},\boldsymbol{x}_g)$. Thus,

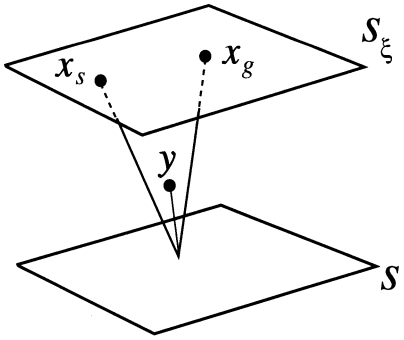

FIGURE 5.7. The stationary triple for the common-offset case, planar reflector, planar source-receiver surface, and constant-background wavespeed.

.

$\partial\Phi/\partial\xi_m = 0$, $m = 1, 2$ in (5.4.8) because the separate pairs of derivatives with arguments $\boldsymbol{x}$ and $\boldsymbol{y}$ are each zero.

In the two-and-one-half-dimensional inversion in the next chapter, the out-of-plane integration in the inversion operators will be approximated by the method of stationary phase. Analysis of the stationary points for the remaining in-plane modeling and inversion reduces to a two-dimensional integral in the two scalar variables, ξ and σ. The arguments used in the above discussion carry over to that simpler case. Hence, no further analysis is needed.

As noted earlier, VSP and well-to-well inversion are special cases of two-and-one-half-dimensional, common-shot inversion in which the datum line(s) or curve(s) need not be the upper surface. Nonetheless, the same arguments apply in those cases.

5.4.4 Determination of the Matrix Signature

We will show here that the signature of the matrix $[\Phi_{\xi\sigma}]$, defined by (5.4.11), is equal to zero. Consider first the special case in which the background sound speed $c(\boldsymbol{x})$ in the region between the upper surface and the reflecting surface is constant, the reflector is planar, and there is zero offset between sources and receiver. For this case, the analysis of $\text{sig}\,[\Phi_{\xi\sigma}]$ was carried out in Section 3.7 and it was shown that the signature was, indeed, zero for $\boldsymbol{y}$ near S.

Now consider deforming this constant-background, zero-offset model into the true model. Think first about changing the background wavespeed. If the signature is to change as the wavespeed model is deformed, then at some point in the deformation at least one eigenvalue must be zero. In fact, exactly two eigenvalues would have to be zero at this point and both would have to change sign because $\det[\Phi_{\xi\sigma}]$ at stationarity is a perfect square and hence is positive. Because the signature was zero to begin with, it remains

zero after two eigenvalues change sign. This might happen repeatedly as the wavespeed model is deformed from constant background to the true variable background. The same argument can be applied to the progressive separation of source and receiver. In the next subsection, we show that $\det[\Phi_{\xi\sigma}]$ is proportional to $h(\boldsymbol{y},\boldsymbol{\xi})$. It has been assumed that $h(\boldsymbol{y},\boldsymbol{\xi})$ is nonzero for the true model. Therefore, right at the wavespeed model and offset under analysis, $\det[\Phi_{\xi\sigma}]$ is different from zero—positive—and therefore its signature is zero.

Cases in which $\det[\Phi_{\xi\sigma}]$ is allowed to be near zero are currently under study. For the present, we content ourselves with the knowledge that, for experiments and background models for which the Beylkin determinant is different from zero, the signature is zero.

5.4.5 *The Quotient* $h/|\det[\Phi_{\xi\sigma}]|^{1/2}$

Equation (5.4.20) remains to be verified. As a first step, introduce the notation

$$\boldsymbol{p}(\boldsymbol{y},\boldsymbol{x}_s) = \nabla_y \tau(\boldsymbol{y},\boldsymbol{x}_s), \quad \boldsymbol{p}(\boldsymbol{y},\boldsymbol{x}_g) = \nabla_y \tau(\boldsymbol{y},\boldsymbol{x}_g) \tag{5.4.30}$$

and then set

$$h(\boldsymbol{y},\boldsymbol{\xi}) = \det \begin{vmatrix} \boldsymbol{p}(\boldsymbol{y},\boldsymbol{x}_s) + \boldsymbol{p}(\boldsymbol{y},\boldsymbol{x}_g) \\ \dfrac{\partial}{\partial \xi_1}\left[\boldsymbol{p}(\boldsymbol{y},\boldsymbol{x}_s) + \boldsymbol{p}(\boldsymbol{y},\boldsymbol{x}_g)\right] \\ \dfrac{\partial}{\partial \xi_2}\left[\boldsymbol{p}(\boldsymbol{y},\boldsymbol{x}_s) + \boldsymbol{p}(\boldsymbol{y},\boldsymbol{x}_g)\right] \end{vmatrix}. \tag{5.4.31}$$

To calculate this determinant, the matrix is multiplied by a matrix whose determinant is known:

$$K = \left[\frac{d\boldsymbol{x}}{d\sigma_1}, \frac{d\boldsymbol{x}}{d\sigma_2}, \frac{d\boldsymbol{x}}{dn}\right], \tag{5.4.32}$$

where each vector represents a column of K. Note that

$$|\det K| = \left|\hat{\boldsymbol{n}} \cdot \frac{d\boldsymbol{x}}{d\sigma_1} \times \frac{d\boldsymbol{x}}{d\sigma_2}\right| = \sqrt{g}. \tag{5.4.33}$$

Now, in multiplying K by the matrix in equation (5.4.31), the first two elements of the first row are both zero by equation (5.4.28), while the third element is given by

$$[\boldsymbol{p}(\boldsymbol{x},\boldsymbol{x}_s) + \boldsymbol{p}(\boldsymbol{x},\boldsymbol{x}_g)] \cdot \hat{\boldsymbol{n}} = \frac{2\cos\theta}{c(\boldsymbol{y})}, \tag{5.4.34}$$

which is just (5.4.18) rewritten in the notation of this subsection and using $\boldsymbol{x} = \boldsymbol{y}$. Thus, in expanding the determinant of the product by the first row, it is necessary to consider only the lower left 2×2 matrix after multiplication. A typical term is

$$\frac{\partial}{\partial \xi_k}\left[\boldsymbol{p}(\boldsymbol{y},\boldsymbol{x}_s)+\boldsymbol{p}(\boldsymbol{y},\boldsymbol{x}_g)\right]\cdot\frac{d\boldsymbol{x}}{d\sigma_m}\bigg|_{\boldsymbol{x}=\boldsymbol{y}} = \frac{\partial}{\partial \xi_k}\frac{\partial}{\partial \sigma_m}\left[\tau(\boldsymbol{y},\boldsymbol{x}_s)+\tau(\boldsymbol{y},\boldsymbol{x}_g)\right]\bigg|_{\boldsymbol{x}=\boldsymbol{y}} \tag{5.4.35}$$

$$= \frac{\partial^2\Phi}{\partial\xi_k\partial\sigma_m}\bigg|_{\boldsymbol{x}=\boldsymbol{y}} \qquad k,m=1,2.$$

It now follows that if the matrix in equation (5.4.31) is multiplied by the matrix K before calculating the determinant, the following result is obtained:

$$|h(\boldsymbol{y},\boldsymbol{\xi})|\sqrt{g} = \frac{2\cos\theta_s}{c(\boldsymbol{y})}\left|\det\left[\Phi_{\xi\sigma}\right]\right|^{1/2}, \tag{5.4.36}$$

for $\boldsymbol{x}=\boldsymbol{y}$ on S.

This verifies our claim, (5.4.20).

Exercises

5.29 The purpose of this exercise is to provide an alternative derivation of the result (5.4.20), with some added interpretation of the close tie between h and $\Phi_{\xi\sigma}$. We will start by considering a matrix closely related to the one in the rightmost expression in (5.4.12), which is to say,

$$\phi_{\xi s} = \frac{\partial^2\phi(\boldsymbol{x},\boldsymbol{\xi})}{\partial\xi_k\partial s_m}, \quad k,m=1,2.$$

Here, $\boldsymbol{s}=(s_1,s_2)$ are arclength variables along the principle directions at the stationary point in $\boldsymbol{\sigma}$. Extend the variables $\boldsymbol{s}$ to three orthogonal variables, $(\boldsymbol{s},s_3)$, by introducing s_3 as a variable in the normal direction in such a manner that $(\boldsymbol{s},s_3)$ forms a right-handed coordinate system. Finally, set

$$\boldsymbol{P} = \nabla_s\phi(\boldsymbol{x},\boldsymbol{\xi}).$$

Here, $\boldsymbol{P}$ is the representation of the gradient of ϕ in the coordinates $(\boldsymbol{s},s_3)$.

a. Consider the cross product

$$\frac{\partial}{\partial\xi_1}\boldsymbol{P}\times\frac{\partial}{\partial\xi_2}\boldsymbol{P}.$$

Explain why

$$\left|\det\left[\phi_{\xi s}\right]\right| = \left|\frac{\partial}{\partial\xi_1}\boldsymbol{P}\times\frac{\partial}{\partial\xi_2}\boldsymbol{P}\right|_3,$$

where the subscript 3 denotes the third component or normal component of the cross product.

b. Show that

$$|\det[\phi_{\xi s}]| = \left|\hat{\boldsymbol{n}} \cdot \frac{\partial}{\partial \xi_1}\boldsymbol{P} \times \frac{\partial}{\partial \xi_2}\boldsymbol{P}\right|.$$

c. Explain why

$$|\det[\phi_{\xi s}]| = \left|\hat{\boldsymbol{n}} \cdot \frac{\partial}{\partial \xi_1}\boldsymbol{p} \times \frac{\partial}{\partial \xi_2}\boldsymbol{p}\right|,$$

where, now, $\boldsymbol{p}$ is just the representation of the gradient in the usual Cartesian variables, $\boldsymbol{x}$.

d. Show that, at stationarity,

$$|\det[\phi_{\xi s}]| = \left|\frac{\boldsymbol{p}}{|\boldsymbol{p}|} \cdot \frac{\partial}{\partial \xi_1}\boldsymbol{p} \times \frac{\partial}{\partial \xi_2}\boldsymbol{p}\right|.$$

e. Show that, if $\boldsymbol{s} = \boldsymbol{\sigma}$, then (5.4.20) is verified.

5.30 We continue the previous exercise for the case when $\boldsymbol{s} \neq \boldsymbol{\sigma}$. Introduce the matrix

$$\mathcal{G} = \left[\frac{\partial s_i}{\partial \sigma_j}\right], \quad i,j = 1,2.$$

a. Show that

$$[\phi_{\xi s}]\,\mathcal{G} = [\phi_{\xi \sigma}].$$

b. Show that

$$|\det \mathcal{G}| = \left|\frac{\partial \boldsymbol{x}}{\partial \sigma_1} \times \frac{\partial \boldsymbol{x}}{\partial \sigma_2}\right| = g,$$

the determinant of the metric tensor of differential geometry as in (5.4.6).

c. Show that

$$|\det[\phi_{\xi s}]|\, g = |\det[\phi_{\xi \sigma}]|.$$

d. Use this result and the previous exercise to confirm (5.4.20) for arbitrary parameters $\boldsymbol{\sigma}$.

5.5 Verification Based on the Fourier Imaging Principle

The purpose of this section is to verify the validity of the inversion formula (5.1.21) applied to Kirchhoff data for a single reflector based on the Fourier imaging theory of Chapter 4. Again, then, the formula of interest is (5.4.3) with the attendant definitions of the variables involved. However, we make one minor further assumption—that the integrand vanishes smoothly at

the boundaries of S and S_ξ. This avoids details of analysis associated with "edge effects" that are of no interest here.

Let us suppose now that $\boldsymbol{y}$ is near S. Introduce a neutralizer function, $N(\boldsymbol{y}, \boldsymbol{x})$, which is identically equal to unity in some ball, say $|\boldsymbol{y} - \boldsymbol{x}| \leq r_1$, identically equal to zero outside some larger ball, $|\boldsymbol{y} - \boldsymbol{x}| \geq r_2 > r_1$, and is infinitely differentiable everywhere. We will prove the following lemma.

Lemma 5.1. *Consider the integrals obtained from (5.4.3) by introducing the neutralizer functions $N(\boldsymbol{y}, \boldsymbol{x})$ and $N^\star(\boldsymbol{y}, \boldsymbol{x}) = 1 - N(\boldsymbol{y}, \boldsymbol{x})$ as multipliers in the integrand. Call the first integral $\beta_N(\boldsymbol{y})$ and the second integral $\beta_N^\star(\boldsymbol{y})$. Then $\beta_N^\star(\boldsymbol{y}) = o(\omega^{-m})$, where m is limited only by the smoothness of the integrand.*

PROOF. The fourfold integral $\beta_N^\star(\boldsymbol{y})$ in $\boldsymbol{\xi}$ and $\boldsymbol{\sigma}$ is of the form

$$\beta_N^\star(\boldsymbol{y}) = \int_{D_\eta} G(\boldsymbol{\eta}) e^{i\omega\Phi_1(\boldsymbol{\eta})} d\eta_1 d\eta_2 d\eta_3 d\eta_4. \tag{5.5.1}$$

In this equation, the four variables $\boldsymbol{\eta}$ are just the variables $(\xi_1, \xi_2, \sigma_1, \sigma_2)$, renamed to make the discussion below easier. The phase Φ_1 is just the phase Φ in the newly-named variables, while G is the (tapered) amplitude of (5.4.3) multiplied by $N^\star(\boldsymbol{y}, \boldsymbol{x})$. The domain, D_η, is just the pair of domains in $\boldsymbol{\xi}$ and $\boldsymbol{\sigma}$: $S_\xi \times S_\sigma$, and the dependence of the integrand on $\boldsymbol{y}$ has been suppressed.

For $\boldsymbol{y}$ on S, the stationary point requires that $\boldsymbol{x} = \boldsymbol{y}$. Choose the support of the function $N(\boldsymbol{y}, \boldsymbol{x})$ so that the stationary value of $\boldsymbol{x}$ remains in the support of this function. Then, the integrand in (5.5.1) has no stationary points in D_η and vanishes C^∞ smoothly on its boundary. Therefore, the integrand can be expanded as follows in preparation for integration by parts (the divergence theorem):

$$G(\boldsymbol{\eta}) e^{i\omega\Phi_1(\boldsymbol{\eta})} = \frac{1}{i\omega} \left[\nabla_\eta \cdot \left[\frac{\nabla\Phi_1}{|\nabla\Phi_1|^2} G(\boldsymbol{\eta}) e^{i\omega\Phi_1} \right] + G_1(\boldsymbol{\eta}) e^{i\omega\Phi_1} \right], \tag{5.5.2}$$

$$G_1(\boldsymbol{\eta}) = -\nabla_\eta \cdot \left[\frac{\nabla\Phi_1}{|\nabla\Phi_1|^2} G(\boldsymbol{\eta}) \right].$$

Substitute this identity into the previous equation and use the divergence theorem to replace the first integral over D_η by an integral over the boundary of this domain. Because the integrand vanishes on the boundary, this first integral is zero and

$$\beta_N^\star(\boldsymbol{x}) = \frac{1}{i\omega} \int_{D_\eta} G_1(\boldsymbol{\eta}) \exp\left[i\omega\Phi_1(\boldsymbol{\eta})\right] d\eta_1 d\eta_2 d\eta_3 d\eta_4. \tag{5.5.3}$$

This process can be repeated recursively, as long as the integrand has derivatives in D_η. Each time, another power of $1/i\omega$ is introduced as a

multiplier of the integrand while the integral itself remains finite. Thus, the claim of the lemma is confirmed. This ends the proof. □

Now consider the integral $\beta_N(\boldsymbol{y})$. This integral can be reduced to an aperture-limited Fourier identity operator of the type discussed in Chapter 4. To do so, we must first make the approximation (5.1.13), (5.1.14) exact, in the support of $N(\boldsymbol{y}, \boldsymbol{x})$. The following lemma does the trick.

Lemma 5.2. *In some neighborhood of $\boldsymbol{x}$ there exists a change of variables from $(\omega, \boldsymbol{\xi})$ to $\boldsymbol{k} = (k_1, k_2, k_3)$ with nonvanishing Jacobian, having the following properties:*

$$\boldsymbol{k} = \omega \left[\nabla_x \left[\tau(\boldsymbol{x}, \boldsymbol{x}_s) + \tau(\boldsymbol{x}, \boldsymbol{x}_g)\right] + O\left(|\boldsymbol{x} - \boldsymbol{y}|\right)\right] \tag{5.5.4}$$

and

$$\frac{\partial(\boldsymbol{k})}{\partial(\omega, \boldsymbol{\xi})} = \omega^2 H(\boldsymbol{y}, \boldsymbol{x}, \boldsymbol{\xi}) = \omega^2 \left[h(\boldsymbol{x}, \boldsymbol{\xi}) + O\left(|\boldsymbol{x} - \boldsymbol{y}|\right)\right]. \tag{5.5.5}$$

PROOF. Write the Taylor series for $\phi(\boldsymbol{x}, \boldsymbol{\xi}) = \tau(\boldsymbol{x}, \boldsymbol{x}_g) + \tau(\boldsymbol{x}, \boldsymbol{x}_g)$ as follows:

$$\phi(\boldsymbol{x}, \boldsymbol{\xi}) = \phi(\boldsymbol{y}, \boldsymbol{\xi}) + \nabla_y \phi(\boldsymbol{y}, \boldsymbol{\xi}) \cdot (\boldsymbol{x} - \boldsymbol{y}) + \sum_{n=2}^{\infty} \sum_{||\boldsymbol{\nu}||=n} \frac{1}{\boldsymbol{\nu}!} \frac{\partial^n \phi(\boldsymbol{y}, \boldsymbol{\xi})}{\partial \boldsymbol{y}^{\boldsymbol{\nu}}} (\boldsymbol{x} - \boldsymbol{y})^{\boldsymbol{\nu}}. \tag{5.5.6}$$

In this equation,

$$\begin{aligned} \boldsymbol{\nu} &= (\nu_1, \nu_2, \nu_3, \nu_4), \\ ||\boldsymbol{\nu}|| &\equiv \nu_1 + \nu_2 + \nu_3 + \nu_4, \\ \boldsymbol{\nu}! &\equiv \nu_1! \nu_2! \nu_3! \nu_4!, \\ (\boldsymbol{x} - \boldsymbol{y})^{\boldsymbol{\nu}} &\equiv (x_1 - y_1)^{\nu_1} (x_2 - y_2)^{\nu_2} (x_3 - y_3)^{\nu_3}, \\ \partial \boldsymbol{y}^{\boldsymbol{\nu}} &\equiv \partial y_1^{\nu_1} \partial y_2^{\nu_2} \partial y_3^{\nu_3} \partial y_4^{\nu_4}, \end{aligned} \tag{5.5.7}$$

with the ν_j's being nonnegative integers.

Now define the vector $\boldsymbol{k}$ by

$$k_j = \omega p_j, \tag{5.5.8}$$

$$p_j = \frac{\partial \phi(\boldsymbol{y}, \boldsymbol{\xi})}{\partial y_j} + \sum_{n=2}^{\infty} \sum_{\substack{||\boldsymbol{\nu}||=n \\ \nu_j \neq 0}} \frac{\nu_j}{||\boldsymbol{\nu}||} \frac{1}{\boldsymbol{\nu}!} \frac{\partial^n \phi(\boldsymbol{y}, \boldsymbol{\xi})}{\partial \boldsymbol{x}^{\boldsymbol{\nu}}} \frac{(\boldsymbol{y} - \boldsymbol{x})^{\boldsymbol{\nu}}}{(x_j - y_j)}, \quad j = 1, 2, 3.$$

One can check that $\boldsymbol{k} \cdot (\boldsymbol{y} - \boldsymbol{x}) = \omega \phi(\boldsymbol{y}, \boldsymbol{\xi})$ by multiplying p_j by $\omega(x_j - y_j)$ and summing on j to obtain the series in (5.5.6) multiplied by ω. Note that the radius of convergence of each of the series in (5.5.8) is the same as for the series in (5.5.6). Furthermore, (5.5.4) follows by direct computation. Thus, in some neighborhood of $\boldsymbol{x}$, the transformation from $(\omega, \boldsymbol{\xi})$ to $\boldsymbol{k}$ is one-to-one with the transformation to the Fourier-type phase function

being *exact*. Indeed, with hindsight, choose the support of $N(\boldsymbol{y}, \boldsymbol{x})$ to be small enough that $H(\boldsymbol{y}, \boldsymbol{x}, \boldsymbol{\xi})$ is nonvanishing on the support of $N(\boldsymbol{y}, \boldsymbol{x})$.

This completes the proof. □

It is interesting to note that the regularity of the transformation does not depend on ω, but only on the spatial variables. Furthermore,

Lemma 5.3. *The wavenumber* $\hat{\boldsymbol{k}} = \boldsymbol{k}/|\boldsymbol{k}|$ *is a function of* $\boldsymbol{\xi}\,\mathrm{sgn}\,(\omega)$ *with nonvanishing Jacobian. Conversely, for each choice of* $\mathrm{sgn}\,(\omega)$, $\boldsymbol{\xi}$ *is a function of* $\hat{\boldsymbol{k}}$.

Remark 5.4. That is, if we were to pick two parameters, such as the first two components of $\hat{\boldsymbol{k}}$ (or the polar angles of $\hat{\boldsymbol{k}}$) with respect to some set of axes, then these variables are functions of $\boldsymbol{\xi}$ (and only the sign of ω) with nonvanishing Jacobian wherever $H(\boldsymbol{x}, \boldsymbol{\xi})$ is nonvanishing.

PROOF. This follows from the proof of Lemma 3. □

This result has an important implication with regard to the aperture of $\boldsymbol{k}$ values in the domain of integration after transformation to these variables. The directions of the $\boldsymbol{k}$-vectors in the domain of integration are solely a function of the source-receiver configuration. The approximate form of the transformation in (5.5.4) suggests further that this angular aperture is completely determined by the sum of the gradients of the traveltimes at $\boldsymbol{x}$. Again, see Section 4.2. Equivalently, this is the sum of the tangents to the rays from the source and receiver. In Beylkin, Oristaglio, and Miller [1985] and Miller, Oristaglio, and and Beylkin [1987], extensive use is made of this fact. For our purposes here, the significance of this observation is what it implies about the integrand of (5.4.3) after transformation. Specifically, the integral takes the form

$$\beta(\boldsymbol{y}) \sim \frac{1}{8\pi^3} \int_{D_k} d^3k F(\omega(\boldsymbol{k})) \int_S dS f(\boldsymbol{x}, \boldsymbol{y}, \hat{\boldsymbol{k}}) e^{i\boldsymbol{k}\cdot(\boldsymbol{x}-\boldsymbol{x}')}. \tag{5.5.9}$$

In this equation,

$$f(\boldsymbol{x}, \boldsymbol{y}, \hat{\boldsymbol{k}}) = -R(\boldsymbol{x}, \boldsymbol{x}_s) \frac{a(\boldsymbol{x}, \boldsymbol{\xi}) \hat{\boldsymbol{n}} \cdot \nabla_x \phi(\boldsymbol{x}, \boldsymbol{\xi}) |h(\boldsymbol{y}, \boldsymbol{\xi})|}{a(\boldsymbol{y}, \boldsymbol{\xi}) |\nabla \phi(\boldsymbol{y}, \boldsymbol{\xi})|\, |H(\boldsymbol{y}, \boldsymbol{x}, \boldsymbol{\xi})|}. \tag{5.5.10}$$

The integral (5.5.9) is of the form (4.4.35), with certain changes, as listed below.

1. The variables $\boldsymbol{x}'$ and $\boldsymbol{x}$ of the former result are replaced by $\boldsymbol{x}$ and $\boldsymbol{y}$, respectively, in this discussion.
2. The aperture limiting in $\boldsymbol{k}$ is partially characterized here by the function $F(\omega(\boldsymbol{k}))$.
3. The function $f(\boldsymbol{x}'/L, \boldsymbol{x}/L, \hat{\boldsymbol{k}})$ of the former result is replaced by $f(\boldsymbol{x}, \boldsymbol{y}, \hat{\boldsymbol{k}})$ in this discussion.

The first of these is just a change of variables; the second is a matter of replacing one slowly varying function of the variables by a different func-

tion, which will not alter the asymptotic analysis applied to the integral, (4.4.35). The third amounts to neglecting explicit scaling in the arguments of the function f.

The condition that the wavenumber be large for the results of the previous section to apply, first requires that $\nabla_y \phi(\boldsymbol{y}, \boldsymbol{\xi})$ be nonzero on the support of $N(\boldsymbol{y}, \boldsymbol{x})$. (Note that this gradient vanishes when the rays from $\boldsymbol{x}_s$ and $\boldsymbol{x}_g$ are tangent at $\boldsymbol{y}$. That is, they are both part of a single ray from $\boldsymbol{x}_s$ to $\boldsymbol{x}_g$. Such raypaths would naturally arise in transmission tomography. This theory does not apply to such cases. That this sum of gradients does not vanish is assured by the assumption that $h(\boldsymbol{y}, \boldsymbol{\xi})$ be nonzero, because this vector is the first row of the determinant in (5.1.17). Once the minimum magnitude of this vector is determined, and the natural length scale L for the integral (5.4.3) is established, the burden of "large wavenumber" is put on the frequency parameter. In seismic applications, frequencies as low as 4 Hz will prove to be high enough for the corresponding parameter, $\lambda = KL$, to be large. Thus, the theory of Chapter 4, particularly Section 4.4, applies in seismic applications. It follows from the analysis of that chapter, particularly the analysis of (4.4.35), that the output of (5.5.9) is proportional to a bandlimited singular function of the reflecting surface. The proportionality factor may be constructed from (5.5.10) and (4.4.17). When $\boldsymbol{y}$ is on S, this factor reduces to $f(\boldsymbol{y}, \boldsymbol{y}, \hat{\boldsymbol{k}})$, which we can evaluate from (5.5.10). In that equation, the quotient of a's is equal to one in this limit. Furthermore, it was shown above, (5.5.5), that the quotient h/H is equal to 1 in this limit. It only remains to evaluate the quotient of derivatives in that equation.

We already know that the distinguished value of $\hat{\boldsymbol{k}}$ must be $\pm\hat{\boldsymbol{n}}$ by applying stationarity to the derivatives in (4.4.10). (This is just the reflection law, as in the discussion in Section 5.1.7.) From the approximate form of $\boldsymbol{k}$ in (5.5.4), it is apparent that $\hat{\boldsymbol{k}}$ must point *downward*, while the normal to S, $\hat{\boldsymbol{n}}$, in the Kirchhoff representation of u_S is an *upward* normal. Consequently, in (5.5.10),

$$\hat{\boldsymbol{n}} \cdot \nabla_x \phi(\boldsymbol{x}, \boldsymbol{\xi}) \Big|_{\boldsymbol{x}=\boldsymbol{y}} = -\left|\nabla_y \phi(\boldsymbol{y}, \boldsymbol{\xi})\right|. \tag{5.5.11}$$

Furthermore, from (5.5.5),

$$H(\boldsymbol{x}, \boldsymbol{x}, \boldsymbol{\xi}) = h(\boldsymbol{x}, \boldsymbol{\xi}).$$

Thus, when the distinguished point, $\boldsymbol{y}$ on S, is in a region where there is a stationary point,

$$f(\boldsymbol{y}, \boldsymbol{x}, \hat{\boldsymbol{k}}) = R(\boldsymbol{y}, \boldsymbol{x}_s). \tag{5.5.12}$$

In this equation, $\boldsymbol{x}_s$ is fixed by the stationarity conditions. This is an angularly dependent reflection coefficient.

We need not go any further. From (4.4.37), the multiplier of f is the area under the filter, for which we have previously introduced the notation $\delta_B(0)$. The verification is now complete.

In summary, for a single reflector and for $\boldsymbol{y}$ near enough to S, we have shown that (5.4.3) can be asymptotically reduced to a Fourier-like integral operator of the type treated in Chapter 4. Then, the theory of that chapter yields the desired result. Along the way, we have shown that the approximate definition of $\boldsymbol{k}$, introduced in (5.1.13) can be made exact in a neighborhood of the reflecting surface S.

5.6 Variable Density

So far in this chapter, we have developed inversion formulas for the 3D constant-density acoustic problem. The formalism presented here, however, is extendible to the variable-density problem as well.

Recall that the Helmholtz or reduced form of the variable-density (acoustic) wave equation may be written as

$$\rho(\boldsymbol{x})\nabla\cdot\left[\frac{1}{\rho(\boldsymbol{x})}\nabla g(\boldsymbol{x},\boldsymbol{x}_s,\omega)\right]+\frac{\omega^2}{c^2(\boldsymbol{x})}g(\boldsymbol{x},\boldsymbol{x}_s,\omega)=-\delta(\boldsymbol{x}-\boldsymbol{x}_s). \quad (5.6.1)$$

The variable-density Helmholtz equation is not self-adjoint. The corresponding adjoint equation may be written as

$$\nabla\cdot\left[\frac{1}{\rho(\boldsymbol{x})}\nabla\left(\rho(\boldsymbol{x})g^\star(\boldsymbol{x},\boldsymbol{x}_g,\omega)\right)\right]+\frac{\omega^2}{c^2(\boldsymbol{x})}g^\star(\boldsymbol{x},\boldsymbol{x}_g,\omega)=-\delta(\boldsymbol{x}-\boldsymbol{x}_g), \quad (5.6.2)$$

where $g^\star(\boldsymbol{x},\boldsymbol{x}_g,\omega)$ is the adjoint Green's function. By the theorem of reciprocity, the equality

$$g^\star(\boldsymbol{x},\boldsymbol{x}_g,\omega)=g(\boldsymbol{x}_g,\boldsymbol{x},\omega)$$

follows.

The necessary WKBJ Green's functions is derived in Section E.6.1. In particular, the necessary adjustment of amplitude is given by (E.6.8), so that

$$g(\boldsymbol{x},\boldsymbol{x}_0,\omega)\sim A(\boldsymbol{x},\boldsymbol{x}_0)\sqrt{\frac{\rho(\boldsymbol{x})}{\rho(\boldsymbol{x}_0)}}e^{i\omega\tau(\boldsymbol{x},\boldsymbol{x}_0)}. \quad (5.6.3)$$

Here, $A(\boldsymbol{x},\boldsymbol{x}_0)$ is the ray theoretic amplitude for constant density equal to 1. Substitution of the WKBJ Green's functions into (5.1.3) yields

$$u_S(\boldsymbol{x}_g,\boldsymbol{x}_s,\omega)\approx\omega^2F(\omega)\int d^3x\frac{\alpha^{vd}(\boldsymbol{x})}{c^2(\boldsymbol{x})}\sqrt{\frac{\rho(\boldsymbol{x}_s)}{\rho(\boldsymbol{x}_g)}}a(\boldsymbol{x},\boldsymbol{\xi})e^{i\omega\phi(\boldsymbol{x},\boldsymbol{\xi})}, \quad (5.6.4)$$

where

$$\phi(\boldsymbol{x},\boldsymbol{\xi}) = \tau(\boldsymbol{x},\boldsymbol{x}_s(\boldsymbol{\xi})) + \tau(\boldsymbol{x}_g(\boldsymbol{\xi}),\boldsymbol{x}), \quad a(\boldsymbol{x},\boldsymbol{\xi}) = A(\boldsymbol{x},\boldsymbol{x}_s(\boldsymbol{\xi}))A(\boldsymbol{x}_g(\boldsymbol{\xi}),\boldsymbol{x}). \tag{5.6.5}$$

Note that we are being purposely vague about what we mean by the "perturbation" $\alpha^{vd}(\boldsymbol{x})$. Certainly, there is the possibility of both a perturbation in wavespeed and density or possibly a perturbation in bulk modulus and density.

We can still formally solve for an inversion formula for this perturbation to create an equation similar to equation (5.1.9),

$$\alpha^{vd}(\boldsymbol{y}) = \int d\omega \int d^2\xi \sqrt{\frac{\rho(\boldsymbol{x}_s)}{\rho(\boldsymbol{x}_g)}} \cdot B(\boldsymbol{y},\boldsymbol{\xi}) e^{-i\omega\phi(\boldsymbol{y},\boldsymbol{\xi})} u_S(\boldsymbol{x}_g,\boldsymbol{x}_s,\omega). \tag{5.6.6}$$

The only difference between equation (5.6.6) and equation (5.1.9) is the ratio of the square roots of density at the source and receiver position.

Thus, a derivation similar to that in Section 5.1 may be created, yielding a formal result for $\alpha^{vd}(\boldsymbol{y})$:

$$\alpha^{vd}(\boldsymbol{y}) = \frac{1}{8\pi^3} \int d^2\xi \, \frac{|h(\boldsymbol{y},\boldsymbol{\xi})| c^2(\boldsymbol{y})}{a(\boldsymbol{y},\boldsymbol{\xi})} \cdot \sqrt{\frac{\rho(\boldsymbol{x}_s)}{\rho(\boldsymbol{x}_g)}} \int d\omega \, e^{-i\omega\phi(\boldsymbol{y},\boldsymbol{\xi})} u_S(\boldsymbol{x}_g,\boldsymbol{x}_s,\omega), \tag{5.6.7}$$

which is analogous to equation (5.1.19).

5.6.1 *Variable-Density Reflectivity Inversion Formulas*

By inspection, we may write inversion formulas for reflectivity in variable-density media that are analogous to equations (5.2.16) and (5.2.17), respectively:

$$\beta(\boldsymbol{y}) = \frac{c(\boldsymbol{y})}{8\pi^3} \int d^2\xi \, \frac{\cos\theta |h_g(\boldsymbol{y},\boldsymbol{\xi})|}{a(\boldsymbol{y},\boldsymbol{\xi})} \cdot \sqrt{\frac{\rho(\boldsymbol{x}_s)}{\rho(\boldsymbol{x}_g)}} \int i\omega \, d\omega \, e^{-i\omega\phi(\boldsymbol{y},\boldsymbol{\xi})} u_S(\boldsymbol{x}_g,\boldsymbol{x}_s,\omega) \tag{5.6.8}$$

and

$$\beta_1(\boldsymbol{y}) = \frac{c^2(\boldsymbol{y})}{16\pi^3} \int d^2\xi \, \frac{|h_g(\boldsymbol{y},\boldsymbol{\xi})|}{a(\boldsymbol{y},\boldsymbol{\xi})} \cdot \sqrt{\frac{\rho(\boldsymbol{x}_s)}{\rho(\boldsymbol{x}_g)}} \int i\omega \, d\omega \, e^{-i\omega\phi(\boldsymbol{y},\boldsymbol{\xi})} u_S(\boldsymbol{x}_g,\boldsymbol{x}_s,\omega). \tag{5.6.9}$$

All other variations of the reflectivity formulas for constant-density media have corresponding variable-density analogs that differ from the constant-

density formulas only by the factor $\sqrt{\rho(\boldsymbol{x}_s)/\rho(\boldsymbol{x}_g)}$ that is present in the integrand. This may appear to be a counterintuitive result. If the density is the same at the source and receiver positions, it appears that there is no change in the output due to density. This is not the case, however, as we will see in the next subsection.

5.6.2 *The Meaning of the Variable-Density Reflectivity Formulas*

Finally, following our analogy between the constant-density and variable-density problems, we can parallel the discussion of Section 5.4 by substituting Kirchhoff approximate data into the inversion formula. There are only two differences in the analysis.

The first of these is that the Kirchhoff modeling formula

$$u_S(\boldsymbol{x}_g, \boldsymbol{x}_s, \omega) \sim i\omega F(\omega) \sqrt{\frac{\rho(\boldsymbol{x}_g)}{\rho(\boldsymbol{x}_s)}} \int_S R^{vd}(\boldsymbol{x}, \boldsymbol{x}_s) a(\boldsymbol{x}, \boldsymbol{\xi}) \cdot (\hat{\boldsymbol{n}} \cdot \nabla_x \phi(\boldsymbol{x}, \boldsymbol{\xi}))\, e^{i\omega\phi(\boldsymbol{x},\boldsymbol{\xi})} dS. \tag{5.6.10}$$

differs from the constant-density Kirchhoff modeling formula (5.4.1) only by a factor of $\sqrt{\rho(\boldsymbol{x}_g)/\rho(\boldsymbol{x}_s)}$, which exactly cancels the factor of $\sqrt{\rho(\boldsymbol{x}_s)/\rho(\boldsymbol{x}_g)}$, seen in the variable-density inversion formulas.

In this equation, $\phi(\boldsymbol{x}, \boldsymbol{\xi})$ and $a(\boldsymbol{x}, \boldsymbol{\xi})$ are defined by (5.6.5) and $R^{vd}(\boldsymbol{x}, \boldsymbol{x}_s)$ is the variable-density geometrical-optics reflection coefficient given by (E.6.13), which is to say,

$$R^{vd}(\boldsymbol{x}, \boldsymbol{x}_s) = \frac{\frac{1}{\rho(\boldsymbol{x})}\left|\frac{\partial\tau}{\partial n}\right| - \frac{1}{\rho_+(\boldsymbol{x})}\left\{1/c_+^2(\boldsymbol{x}) - 1/c^2(\boldsymbol{x}) + \left[\frac{\partial\tau}{\partial n}\right]^2\right\}^{1/2}}{\frac{1}{\rho(\boldsymbol{x})}\left|\frac{\partial tau}{\partial n}\right| + \frac{1}{\rho_+(\boldsymbol{x})}\left\{1/c_+^2(\boldsymbol{x}) - 1/c^2(\boldsymbol{x}) + \left[\frac{\partial\tau}{\partial n}\right]^2\right\}^{1/2}}, \tag{5.6.11}$$

where $\tau \equiv \tau(\boldsymbol{x}, \boldsymbol{x}_s)$. As in the constant-density problem, the unit normal vector $\hat{\boldsymbol{n}}$ points upward and $\partial/\partial n = \hat{\boldsymbol{n}} \cdot \nabla_x$; $c_+(\boldsymbol{x})$ and $\rho_+(\boldsymbol{x})$ are the propagation speed and density below the reflector.

All other parts of the stationary phase analysis in Section 5.4 are the same, yielding the same peak value as in equation (5.4.21):

$$\beta_{\text{PEAK}}(\boldsymbol{y}) \sim R^{vd}(\boldsymbol{y}, \boldsymbol{x}_s)\delta_B(0), \quad \boldsymbol{y} \text{ on } S, \tag{5.6.12}$$

with the only difference being that R^{vd} is the variable-density reflectivity. All other discussions in Section 5.1.3 follow analogously.

Exercises

5.31 Using Green's theorem and the variable-density acoustic Helmholtz equation (5.6.1) find the adjoint equation (5.6.2).

5.32 Discuss an approach to deriving an inversion formula for elastic media following the logic that has been used in this chapter.

5.7 Discussion of Results and Limitations

We have developed a formalism for creating high-frequency asymptotic inversion formulas for the imaging/migration/parameter estimation problem in 3D variable-wavespeed and variable-density media. The technique is general enough to permit inversion of data gathered from experiments whose source-receiver geometry is compatible with the high-frequency assumptions inherent in our formalism.

When the geometry of a source-receiver pair is not compatible with these assumptions, however, the inversion formalism presented here will fail in ways that may be mild to catastrophic. Catastrophic failure occurs when a particular Jacobian of transformation, which we call the Beylkin determinant, becomes infinite. This determinant is a necessary ingredient for writing high-frequency modeling and inversion formulas as Fourier-like integrals, because it permits us to convert frequencies and survey coordinates into wavenumbers. Fortunately, in most of the seismic applications that we consider, such failures happen only at isolated positions away from the area of interest. Milder failure of the method occurs at output locations where the WKBJ approximation of the Green's function amplitude becomes infinite (such as in cusps of caustics), or where the Beylkin determinant vanishes. A reasonably coherent image in the vicinity of such output positions can still be obtained, at the expense of errors in the amplitude information. Thus, for traditional reflection experiments aimed at imaging deep targets, there may only be isolated points where there are problems.

In contrast, the Beylkin determinant will always be equal to zero for purely *transmitted* raypaths, such as those in crosswell and vertical seismic profile (VSP) surveys. Our formulas will not be able to image points that are sampled by purely transmitted energy (with no scattering), for this reason alone. Yet there is still need for our formalism for creating formulas to invert data collected from such "near-transmission" surveys. Not all of the energy in these surveys consists of purely transmitted arrivals; some arrivals experience scattering, albeit at wider angles than in surface reflection–seismic experiments. If such scattered waves can be identified, then the application of Fourier-like methods is still appropriate.

Aperture Limiting

We expect lower resolution and increased image distortion in crosswell and VSP surveys, even under the best of circumstances, because of the naturally limited aperture in these recording geometries. Recall that the k-domain aperture is scaled by $\cos\theta$, where θ is the half-angle between rays from source and receiver as measured at the point being imaged. In VSP and crosswell applications, that angle is often nearer to $\pi/2$ than in surface experiments, causing lower resolution for a given bandwidth. In addition, as we saw in Chapter 4, the angular restriction of the $\boldsymbol{k}$-domain apertures restricts the range of reflector dips that can be recovered, distorting the image at these points. (See Section 4.2.3 for details.)

The trade-off is that the shorter propagation paths of waves in such experiments allow for the use of higher frequencies than are possible in traditional surface reflection seismic experiments aimed at imaging deeper structures. Thus, restrictions on the opening angle alone are not the whole story. In the literature, the application of Fourier-like inversion or migration appears under the name *diffraction tomography.* (Here, we are using this term as in Devaney and Oristaglio [1984].)

Endpoint Artifacts

Yet another source of image degradation results from the finiteness of the survey line, or equivalently, finiteness of the data within a line. Recall that all of our asymptotic analyses have assumed that the dominant contribution to the image output is from stationary-point contributions. To be valid, such analysis requires that contributions from the endpoints of integration be small when compared to contributions from stationary point

Implied in this requirement is the assumption that the stationary points are far from the endpoints when measured in units of reciprocal wavenumber or when the length scale L in (3.4.4) is the distance between the stationary point and the endpoint. The separation of these contributions is even better when the integrand vanishes at the endpoints of integration.

For us, the endpoints of integration are naturally the ends of the survey lines, provided that the data are continuous along the survey, so that the latter condition cannot, in general, be relied upon to make our stationary point contribution dominate the output. Indeed, if there are discontinuities in the data, such as gaps, or points that are poorly illuminated in the subsurface, such as the bottoms of sharp synclines, then effectively our formulas perform "piecewise integrations," putting potential "endpoints of integration" inside the survey, with contributions from these endpoints possibly being comparable in size to the stationary point contributions. The result is that we see artifacts commonly called *diffraction smiles* on output near the location of such terminations of the data. The diffraction smile can be viewed as a pseudoreflector created by the inversion formalism to characterize a discontinuous data set. In other words, the diffraction smile

is the "reflector" required to produce the data discontinuity; all of the reflections from the diffraction smile arrive back at the point of discontinuity. We will see examples of diffraction smiles in the next chapter.

The discussion of artifacts could easily fill a textbook on its own and therefore we cannot tell the whole story here. Nevertheless, this beginning is provided to at least make the reader aware of these types of issues as they fall within the theoretical approach we employ.

Failure of Ray Theory

As noted in the preface, we have also avoided extensions of our method to the case in which there are caustics in the ray-family associated with point sources. In those cases, the Jacobian of the amplitude passes through zero and usually changes sign. The correct WKBJ solutions for the Green's function must include appropriate phase shift factors (the KMAH index[15] [Lewis, 1965; Ludwig, 1966; Kravtsov and Orlov, 1990; Ziolkowski and Deschamps, 1980, 1984; Červený, 1995, 2000]), or the Green's function must be represented by functions of more general form than $A\exp\{i\omega\tau\}$. These extensions are in process at the time of this writing, with some results available in the literature. However, these more recent approaches are beyond the scope of this text.

5.7.1 Summary

In summary, we have provided a formalism for imaging reflectors in the Earth and estimating reflection coefficients. The formalism allows for a wide variety of source-receiver configurations and reasonable complexity of the the Earth environment. Our operators can be described as appropriately weighted Kirchhoff migration operators with those weights arising from the underlying inversion theory. The method lends itself to extensions with even greater complexity, both in the medium–leading to more general descriptions of the underlying Green's functions—and to multicomponent inversion, both isotropic and anisotropic elastic media, as well as to electromagnetic radiation, which we do not address at all.

[15]The KMAH index keeps track of the phase shifts experienced by waves as rays pass through caustics.

6

Two-and-One-Half-Dimensional Inversion

The formulas of Chapter 5 were derived for general 3D data sets, but, as we have mentioned in previous chapters, a large amount of oil industry seismic data is still in the form of seismograms collected along single lines. In Chapter 3, we introduced the concept of the two-and-one-half-dimensional (2.5D) geometry to compensate for the fewer degrees of freedom available in such single-line experiments. The two-and-one-half-dimensional formulas will allow for the inversion of a single line of data while accounting for many aspects of three-dimensional wave propagation. It is the method of choice when data are gathered along a line in a direction of dominant lateral changes in the subsurface (dip direction), providing an amplitude-consistent inversion of the medium in the vertical plane containing the source-receiver line. The method cannot, however, account for scattered energy that arrives from outside the vertical plane, except by imaging these arrivals at equivalent, but incorrect, in-plane locations. It is also possible to perform 2.5D migration/inversion on lines making oblique angles with the dip direction [French, 1975], again, as long as that direction is fixed in the subsurface. The main point to be stressed is that the two-and-one-half-dimensional assumption allows a reduction of the processing of the three-dimensional inversion of Chapter 5, just as it did for the simpler constant-background, zero-offset inversion of Chapter 3. (See Bleistein, Cohen, and Hagin [1987].)

Indeed, the reader may want to review the discussion of Section 3.5 before proceeding further in this chapter.

As described in Section 3.5, given one line of experiments in the dip direction of a 2.5D model, parallel lines of otherwise identical experiments

will produce identical data sets. We denote the surface parameter in the out-of-plane direction by ξ_2, and recognize that the data are independent of this variable. Therefore, in the integrals in (5.1.21) and (5.1.47), the only dependence on ξ_2 is in the known amplitude and phase of the inversion operator. Thus, just as in the reductions of Section 3.5, the integration in ξ_2 can be approximated by the method of stationary phase. We will see below that this reduction leads to an inversion operator whose constituent elements can all be computed in terms of in-plane variables, reducing the two-and-one-half-dimensional inversion to purely two-dimensional computations. Because these 2D computations characterize in-plane propogation of waves from point sources in 3D, they are a closer representation of reality than a completely 2D theory that does not recognize the out-of-plane geometrical spreading of waves.

We introduce 2.5D ray theory for modeling in the next section, restating the conditions and thought experiment that lead to in-plane processing of 3D point-source data. In Section 6.2, we use these results to derive processing formulas for in-plane lines of sources and receivers, but with 3D geometrical spreading in the Green's functions and data. We then discuss implementation for familiar 2.5D source/receiver configurations and provide some examples of processing of numerically generated data.

6.1 2.5D Ray Theory and Modeling

Because our methods depend on introducing ray-theoretic approximate Green's functions, a discussion of 2.5D ray theory [Cohen and Bleistein, 1983; Bleistein, 1986b] is necessary. The discussion here will be somewhat brief. A more comprehensive discussion is contained in Appendix E, with Section E.5 being devoted to the derivation of 2.5D ray-theoretic results.

6.1.1 Two-and-One-Half-Dimensional Ray Theory

Our mental picture of the symmetry of a two-and-one-half-dimensional problem consists of the concept of raypaths confined to the vertical plane containing the source(s) and receiver(s), as depicted in Figure 6.1 for the special case of a common-shot geometry. At the end of this section are exercises that cover most of the concepts and results of ray theory that the reader will need in order to understand the applications in this chapter.

Recall that the traveltimes and amplitudes in the inversion formulas (5.1.21) and (5.1.47) satisfy the eikonal and transport equations (5.1.4). The eikonal equation is solved by the *method of characteristics*, where the *characteristics*, or rays, are a solution of the system of ordinary differential equations (ODEs)

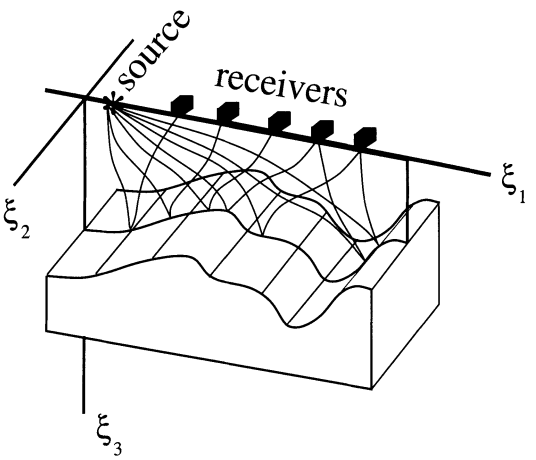

FIGURE 6.1. Schematic showing rays propagating in a 2.5D, in-plane fashion in a common-shot experiment.

$$\frac{d\boldsymbol{x}}{d\sigma} = \boldsymbol{p}, \qquad \frac{d\boldsymbol{p}}{d\sigma} = \frac{1}{2}\nabla\left[\frac{1}{c^2(\boldsymbol{x})}\right], \qquad \frac{d\tau}{d\sigma} = \frac{1}{c^2(\boldsymbol{x})}, \tag{6.1.1}$$

where $\boldsymbol{p} \equiv \nabla\tau$. These formulas are called the *ray equations*. In spite of the compact notation, the first (vector) ray equation, which relates $\boldsymbol{x}$ to $\boldsymbol{p}$, represents three ODEs for three-dimensional wave propagation. The second (vector) ray equation also is a system of three ODEs. Thus, with the third formula appearing in (6.1.1), which is a single ODE, the ray equations are a system of *seven* ordinary differential equations for the problem of determining the rays (the first six equations) and the propagation of the traveltime along them (the seventh equation) in 3D media.

The most straightforward problem for such a system of ODE's is an initial-value problem. To model propagation from a point source, the initial value of $\boldsymbol{x}$ is the source point $\boldsymbol{x}_0$, which, in the notation of (5.1.4), is either $\boldsymbol{x}_s$ or $\boldsymbol{x}_g$, depending on the application. The initial value of $\boldsymbol{p}$ on a ray is restricted in magnitude by the eikonal equation itself,

$$\boldsymbol{p} \cdot \boldsymbol{p} = \frac{1}{c^2(\boldsymbol{x})}, \tag{6.1.2}$$

but its direction is unspecified. From the first ray equation, we see that changing the direction of $\boldsymbol{p}$ changes the initial direction of the geometrical-optics ray. Thus, by selecting the desired initial point on the ray, and the specified direction, we may "shoot" rays in the model.[1]

[1]In practice, we need the solution for rays propagating from a specified initial point to a specified endpoint. This system of equations does not lend itself to simple solution techniques for such problems. Instead, we shoot a suite of rays, by varying the initial direction, then search for solutions with rays that pass near

For each solution of the six equations for $\boldsymbol{x}$ and $\boldsymbol{p}$, the traveltime τ can be determined along each ray be solving the third equation in (6.1.1),

$$\frac{d\tau}{d\sigma} = \frac{1}{c^2(\boldsymbol{x})}. \tag{6.1.3}$$

The appropriate initial value for the traveltime in the point-source problem is $\tau(\boldsymbol{x}_0) = 0$.

The special feature of the two-and-one-half-dimensional problem is that the medium parameters—both the background and the unknown perturbation—are independent of the out-of-plane variable, x_2. Thus, in particular, $c(\boldsymbol{x}) = c(x_1, x_3)$ and $\partial c(\boldsymbol{x})/\partial x_2 = 0$. Consequently, in (6.1.1), the derivative of p_2, the second component of $\boldsymbol{p}$, is equal to zero, from which it follows that p_2 is a *constant* on each ray. Then, the equation that relates x_2 to p_2 through the first expression in (6.1.1) has the simple solution

$$x_2 - x_{20} = p_2\sigma. \tag{6.1.4}$$

In-Plane Wave Propagation

Let us consider the rays that propagate in the vertical plane below the source line, that is, the rays for which $x_2 = x_{20}$. We see from (6.1.4) that this ray trajectory occurs only for $p_2 = 0$.

For this in-plane propagation, (6.1.1) is reduced from seven equations to five and the traveltime is determined from (6.1.3) in terms of the solutions for (x_1, x_3), independent of the choice of x_{20}, because $c(\boldsymbol{x})$ is independent of x_2. Consequently, analysis of in-plane ray trajectories in the two-and-one-half-dimensional medium becomes much simpler than analysis of three-dimensional rays.

Amplitude Along the Ray

To determine the amplitude along a ray, we cannot yet completely abandon out-of-plane considerations. Recall that the amplitude is proportional to a Jacobian that characterizes the cross-sectional area of a tube of rays. We must, therefore, consider out-of-plane rays, but only those passing near the $x_2 = 0$ plane.

The value of x on the rays can be described in terms of the running variable σ, the parameter p_2 that characterizes the out-of-plane propagation of the ray, and a third parameter, say σ_1, which characterizes the initial in-plane direction of the ray. Typical choices of σ_1 are the initial value of p_1 or p_3 or an initial reference angle for which p_1 and p_3 are proportional to sine and cosine of the angle. The particular choice of σ_1 is not important here. What is important, however, is that the amplitude $A(\boldsymbol{x}, \boldsymbol{x}_0)$ has the

---

the final point of interest. The final step is to interpolate between known rays bracketing a particular endpoint to find the actual solution that we seek.

form

$$A(\boldsymbol{x}, \boldsymbol{x}_0) = \frac{\text{const.}}{\sqrt{|J|}}, \tag{6.1.5}$$

where the constant depends on the choice of σ_1 and

$$J = \det \begin{bmatrix} \dfrac{d\boldsymbol{x}}{d\sigma} \\ \dfrac{d\boldsymbol{x}}{d\sigma_1} \\ \dfrac{d\boldsymbol{x}}{dp_2} \end{bmatrix}. \tag{6.1.6}$$

Again, some simplification occurs when the amplitude is to be evaluated in-plane. In this limit, the second element of the first row, which, from (6.1.1), is just p_2 itself, is equal to zero. Also, the second element of the second row is zero. This can be seen from the solution (6.1.4) for x_2, which is independent of the variable σ_1. Thus, for in-plane evaluation, the determinant of this 3×3 matrix can be expanded by this middle column and thereby be reduced to the determinant of a 2×2 matrix multiplied by $\partial x_2 / \partial p_2$. We now determine the last element of this column by differentiating (6.1.4) implicitly with respect to p_2,

$$\frac{\partial x_2}{\partial p_2} = \sigma,$$

and setting $p_2 = 0$. Here, we use the fact that σ and p_2 are independent variables in the suite of solutions of the ray equations. Therefore, we find that

$$J = \sigma \det \begin{bmatrix} \dfrac{d\boldsymbol{x}}{d\sigma} \\ \dfrac{d\boldsymbol{x}}{d\sigma_1} \end{bmatrix} = \sigma J_{2D}. \tag{6.1.7}$$

In this equation, J_{2D} is the determinant of the 2×2 matrix of the middle equation, while $\boldsymbol{x} = (x_1, x_3)$ is a solution of the four equations in (6.1.1) resulting from disregarding the pair of equations in x_2, p_2 and setting $p_2 = 0$. (J_{2D} is, in fact, the ray Jacobian for purely 2D ray amplitudes.) Thus, the amplitude and phase are determined by in-plane computations, with the out-of-plane spreading determined by the scaling $\sqrt{\sigma}$ when (6.1.7) is substituted into (6.1.5).

The variable σ is somewhat of a hybrid ray parameter. More familiar parameters are arclength on the ray or traveltime. From (6.1.1), we can easily define the relationship between σ and arclength s by noting that

$$\frac{d\boldsymbol{x}}{d\sigma} \cdot \frac{d\boldsymbol{x}}{d\sigma} = \left[\frac{ds}{d\sigma}\right]^2 = \boldsymbol{p} \cdot \boldsymbol{p} = \frac{1}{c^2(\boldsymbol{x})}, \tag{6.1.8}$$

with ds being differential arclength along the ray. Thus, σ is seen to be a ray parameter with dimension of [length]^2/[time].

We now have the machinery in place for reducing the three-dimensional inversion formulas (5.1.21) and (5.1.47) to two-and-one-half-dimensional inversion formulas for a line of data gathered in the dip direction over a medium with two-dimensional variation.

The exercises that follow are intended to familiarize the reader with the concepts of ray theory. The reader will find a comprehensive overview of the subject in Appendix E, which includes the 2.5D results that are not discussed in traditional treatments of ray theory. We also recommend that the reader consult Kravtsov and Orlov [1990] for a more detailed treatment of the subject of ray theory in heterogeneous media.

Exercises

6.1 Consider the case of in-plane wave propagation when $c =$ constant.

a. From (6.1.1), show that, in this case, p_1 and p_3 are constants that we can take to be of the form

$$p_1 = \frac{\sin\beta}{c}, \qquad p_3 = \frac{\cos\beta}{c},$$

with β a constant.

b. Further, show that

$$x_1 - x_{10} = \frac{\sigma\sin\beta}{c}, \qquad x_3 - x_{30} = \frac{\sigma\cos\beta}{c}.$$

c. Consider the point-source problem in which (x_{10}, x_{30}) is fixed, and identify β as the second parameter, σ_1, in (6.1.7). Calculate the determinant in that equation and show that the solution to (6.1.5) is

$$A(\boldsymbol{x}, \boldsymbol{x}_0) = \frac{\text{const.}}{\sigma/c}.$$

d. Compare this result with the exact solution,

$$A(\boldsymbol{x}, \boldsymbol{x}_0) = \frac{1}{4\pi r}, \qquad r = \sqrt{(x_1 - x_{10})^2 + (x_3 - x_{30})^2},$$

and conclude that, for this choice of the parameter σ_1, the constant in (6.1.5) is equal to $1/4\pi$.

Remark 6.1. For variable c, we argue that the constant depends only on c in the neighborhood of $\boldsymbol{x}_0$, where $c(\boldsymbol{x}) \approx c(\boldsymbol{x}_0)$. Thus, we use the same constant for the solution with variable c. That is, we set

$$A(\boldsymbol{x}, \boldsymbol{x}_0) = \frac{1}{4\pi\sqrt{\sigma|J_{2D}|}}, \quad J_{2D} = \det \begin{bmatrix} \dfrac{d\boldsymbol{x}}{d\sigma} \\ \dfrac{d\boldsymbol{x}}{d\beta} \end{bmatrix}. \tag{6.1.9}$$

6.2 For a depth-dependent propagation speed $c(x_3)$, it makes more sense to rewrite the ray equations (6.1.1) and the eikonal equation (6.1.3) with x_3 as the independent variable. We do this by dividing the equations in σ by the equation for $dx_3/d\sigma$,

$$\frac{dx_3}{d\sigma} = p_3.$$

a. Show that the resulting equations are

$$\frac{dx_1}{dx_3} = \frac{p_1}{p_3}, \qquad \frac{d\tau}{dx_3} = \frac{1}{c^2(x_3)p_3},$$

$$\frac{d\sigma}{dx_3} = \frac{1}{p_3}, \qquad \frac{dp_1}{dx_3} = 0, \qquad \frac{dp_3}{dx_3} = -\frac{c'(x_3)}{c^3(x_3)p_3},$$

where $c'(x_3)$ denotes the x_3-derivative of c.

b. Conclude from these equations that p_1 is a constant that we can take to be $\sin\beta/c(x_{30})$, and then conclude from the eikonal equation itself that

$$p_3^2 = \frac{1}{c^2(x_3)} - \frac{\sin^2\beta}{c^2(x_{30})}.$$

For the remainder of this exercise, let us consider rays moving in the direction of increasing x_3, and choose p_3 to be positive so that the traveltime increases as x_3 does.

c. Derive the results

$$x_1 - x_{10} = \sin\beta \int_{x_{30}}^{x_3} \frac{dz}{\sqrt{n^2(z) - \sin^2\beta}}, \quad n^2(z) = \frac{c^2(x_{30})}{c^2(z)},$$

$$\tau(\boldsymbol{x}) - \tau(\boldsymbol{x}_0) = \frac{1}{c(x_{30})} \int_{x_{30}}^{x_3} \frac{n^2(z)dz}{\sqrt{n^2(z) - \sin^2\beta}},$$

$$\sigma(\boldsymbol{x}) - \sigma(\boldsymbol{x}_0) = c(x_{30}) \int_{x_{30}}^{x_3} \frac{dz}{\sqrt{n^2(z) - \sin^2\beta}}.$$

In all of these results, we assume that $n^2(z) > \sin^2(\beta)$ over the whole range of integration.

d. Consider the point-source problem, as in the previous exercise. The objective now is to determine the amplitude A. To do so, we must compute the 2×2 Jacobian, J_{2D}. To this end, we remind

the reader that J_{2D} is a Jacobian of a transformation between variables x_1, x_3 and variables σ, β, and use the rules of Jacobian multiplication to conclude that

$$|J_{2D}| = \frac{\partial(x_1, x_3)}{\partial(\sigma, \beta)} = \frac{\partial(x_1, x_3)}{\partial(\beta, x_3)} \frac{\partial(x_3, \beta)}{\partial(\sigma, \beta)} = \left| \frac{\partial x_1}{\partial \beta} \frac{\partial x_3}{\partial \sigma} \right|.$$

Compute the two derivatives in the last expression to conclude that

$$|J_{2D}| = \sqrt{n^2(x_3) - \sin^2 \beta} \frac{\cos \beta}{c(x_{30})} \int_{x_{30}}^{x_3} \frac{n^2(z) dz}{\left[n^2(z) - \sin^2 \beta\right]^{3/2}}.$$

6.3 The purpose of this exercise is to determine the constant of the amplitude in (6.1.5) for arbitrary choice of the parameter, σ_1. We know that, even for variable background, the singular behavior of the source near the source point must be the same as for the constant-coefficient case, because it has to yield the correct distributional behavior near the source point. That is,

$$A(\boldsymbol{x}, \boldsymbol{x}_0) \approx \frac{1}{4\pi r},$$

with r being the distance from the source.

a. Show that

$$\text{const.} = \lim_{r \to 0} \frac{\sqrt{\sigma |J_{2D}(\boldsymbol{x}, \boldsymbol{x}_0)|}}{4\pi r}.$$

b. For small r, show that the solution of the ray equations,

$$\boldsymbol{x} \approx \boldsymbol{p}_0 \sigma = \boldsymbol{p}_0 c(\boldsymbol{x}_0) r,$$

where $\boldsymbol{p}_0$ is the initial value of the p-vector at $\sigma = 0$.

c. Conclude, then, that the equation for the Jacobian, (6.1.7), simplifies to

$$J_{2D} = \sigma \det \begin{bmatrix} \boldsymbol{p}_0 \\ \dfrac{d\boldsymbol{p}_0}{d\sigma_1} \end{bmatrix} = r c(\boldsymbol{x}_0) \det \begin{bmatrix} \boldsymbol{p}_0 \\ \dfrac{d\boldsymbol{p}_0}{d\sigma_1} \end{bmatrix}.$$

d. The vector $\boldsymbol{p}_0$ has constant length. By differentiating the dot product of this vector with itself, show that $\boldsymbol{p}_0$ is orthogonal to its σ_1-derivative.

e. Conclude that

$$|J_{2D}| = r \left| \frac{d\boldsymbol{p}_0}{d\sigma_1} \right|. \tag{6.1.10}$$

f. Now use this result to evaluate the constant of the solution as

$$\text{const.} = \frac{1}{4\pi} \sqrt{c(\boldsymbol{x}_0) \left| \frac{d\boldsymbol{p}_0}{d\sigma_1} \right|} \tag{6.1.11}$$

and, therefore, that

$$A(\boldsymbol{x}, \boldsymbol{x}_0) = \frac{1}{4\pi}\sqrt{\frac{c(\boldsymbol{x}_0)}{\sigma|J_{2D}(\boldsymbol{x}, \boldsymbol{x}_0)|}\left|\frac{d\boldsymbol{p}_0}{d\sigma_1}\right|}. \tag{6.1.12}$$

Remark 6.2. Note that the amplitude is a symmetric function of the two endpoints in this simple acoustic, constant-density case. However, the constant's dependence on the initial point produces a representation in an asymmetric form. The conclusion has to be that the asymmetry of J balances the distinguished dependence on the initial point in this representation, so that the entire expression is, indeed, symmetric.

6.2 2.5D Inversion and Ray Theory

Suppose that the medium being investigated has only two-dimensional variation, say in the directions (x_1, x_3). Suppose that source(s) and receiver(s) are arrayed in some vertical plane parallel to the x_1, x_3-plane, at constant x_2. Experimental configurations could be common-source, common-receiver, common-offset, well-to-well or VSP (surface-to-well). Consider now an identical set of experiments in a plane at a different constant x_2. By the nature of the experiment, the data are identical with the data for the experiment that was actually carried out. Therefore, by assuming the same data values in all planes parallel to the plane where the actual experiments were done, we fill out a surface array of data as required by the formulas (5.1.21) and (5.1.47).

Parametrically, the data surface(s) take on the special form

$$\boldsymbol{x}_s(\boldsymbol{\xi}) = (x_{1s}(\xi_1), \xi_2, x_{3s}(\xi_1)), \quad \boldsymbol{x}_g(\boldsymbol{\xi}) = (x_{1g}(\xi_1), \xi_2, x_{3g}(\xi_1)). \tag{6.2.1}$$

Consider first (5.1.21). The data are independent of ξ_2, by assumption, thus, are a function only of ξ_1 and ω. Therefore, for such data, the integral in ξ_2 can be computed once and for all.

Fortunately, we can carry out this integration by the method of stationary phase, for any choice of source/receiver configuration. The phase is still defined by (5.1.8), with the formal large parameter being $-\omega$. The first derivative of the phase is

$$\frac{\partial\phi}{\partial\xi_2} = \frac{\partial}{\partial\xi_2}\left[\tau(\boldsymbol{y}, \boldsymbol{x}_s) + \tau(\boldsymbol{y}, \boldsymbol{x}_g)\right] = p_2(\boldsymbol{x}_s, \boldsymbol{y}) + p_2(\boldsymbol{x}_g, \boldsymbol{y}). \tag{6.2.2}$$

Note that the values of p_2 are those for the ray starting at $\boldsymbol{y}$ and terminating at $\boldsymbol{x}_s$ or $\boldsymbol{x}_g$, because the derivative is with respect to the second coordinate of the source or receiver variable. Because p_2 is constant on a ray, these values are just the negatives of the values on the rays directed from $\boldsymbol{x}_s$ or $\boldsymbol{x}_g$ to $\boldsymbol{y}$.

This derivative has to be zero at the stationary point. Analysis of the second component of the ray equations (6.1.4) for each of the rays of interest

here will help us determine the stationary value of ξ_2. From (6.1.4) and the fact that $x_{2s} = x_{2g} = \xi_2$, the equation of propagation for this component of each of these rays is given by

$$\xi_2 - y_2 = p_2(\boldsymbol{x}_s, \boldsymbol{y})\sigma_s, \quad \xi_2 - y_2 = p_2(\boldsymbol{x}_g, \boldsymbol{y})\sigma_g. \tag{6.2.3}$$

Here, we have been careful to show $\boldsymbol{y}$ as the initial point on the rays and $\boldsymbol{x}_s$ or $\boldsymbol{x}_g$ as the final point. We can do this, because the derivatives are with respect to ξ_2, the out-of-plane Cartesian coordinate for both traveltimes. Because σ_s and σ_g are positive, it is necessary that the two p_2's in this equation have the same sign. Therefore, the only way that the derivative in (6.2.2) can be zero is if each of these variables is separately equal to zero. In this case, $\xi_2 = y_2$ at stationarity.

Now, the theory of the previous subsection comes into play. At stationarity,

- the propagation is in-plane;
- the amplitude and phase of the inversion operator are independent of y_2;
- the amplitude and phase of the WKBJ Green's functions in the inversion operator are determined by two-dimensional calculations, with the scaling by $\sqrt{\sigma_s}$ and $\sqrt{\sigma_g}$ characterizing the out-of-plane spreading of the Green's functions.

We need to calculate the second derivative of the phase at stationarity. That is, we need to calculate the derivatives of $p_2(\boldsymbol{x}_s, \boldsymbol{y})$ and $p_2(\boldsymbol{x}_g, \boldsymbol{y})$ with respect to ξ_2 and evaluate them when these two variables are equal to zero and $\xi_2 = y_2$. The easiest way to do this is by differentiating each of the relationships in (6.2.3) with respect to ξ_2 and evaluating at the stationary point. There is some subtlety here. Although we have used the ray equations, we cannot think of σ_s and σ_g as independent variables. The reason is that, in this calculation, we are considering rays that are solutions of the two-point—initial and final—problem, rather than solutions of the initial value problem, and we are varying the second coordinate of the final point, $\boldsymbol{x}_s$ or $\boldsymbol{x}_g$. Thus, we must consider the derivatives of both σ_s and σ_g when differentiating (6.2.3) with respect to ξ_2. Let us carry out that differentiation without regard for subscripts s or g in (6.2.3):

$$\begin{aligned} 1 &= \frac{\partial p_2(\boldsymbol{x}, \boldsymbol{y})}{\partial \xi_2}\sigma + p_2(\boldsymbol{x}, \boldsymbol{y})\frac{\partial \sigma}{\partial \xi_2} \\ &= \frac{\partial^2 \tau(\boldsymbol{y}, \boldsymbol{x})}{\partial \xi_2^2}\sigma + p_2(\boldsymbol{x}, \boldsymbol{y})\frac{\partial \sigma}{\partial \xi_2}. \end{aligned}$$

We see, here, that $\partial\sigma/\partial\xi_2$ is multiplied by p_2, which is zero whether we evaluate with subscript s or with subscript g. Furthermore, σ_s and σ_g are symmetric functions of $\xi_2 - y_2$ and, hence, their derivatives are zero at $\xi_2 = y_2$. Thus, the result of this differentiation is

$$\frac{\partial^2\tau(\boldsymbol{y},\boldsymbol{x}_s)}{\partial\xi_2^2}\sigma_s = \frac{\partial^2\tau(\boldsymbol{y},\boldsymbol{x}_g)}{\partial\xi_2^2}\sigma_g = 1,$$

$$\frac{\partial^2\phi(\boldsymbol{y},\boldsymbol{\xi})}{\partial\xi_2^2} = \frac{1}{\sigma_s} + \frac{1}{\sigma_g} = \frac{\sigma_s+\sigma_g}{\sigma_s\sigma_g},$$

$$\text{and} \quad \operatorname{sgn}\left(\frac{\partial^2\phi(\boldsymbol{y},\boldsymbol{\xi})}{\partial\xi_2^2}\right) = +1. \tag{6.2.4}$$

6.2.1 *The 2.5D Beylkin Determinant*

As might be expected from the analysis above, the Beylkin determinant, (5.1.17), also simplifies in the in-plane, two-and-one-half-dimensional limit. In that determinant, note that the element in the first row, second column is zero. To see why this is so, first note that in the notation introduced in (6.2.2)

$$\frac{\partial^2\phi(\boldsymbol{y},\boldsymbol{\xi})}{\partial y_2} = p_2(\boldsymbol{y},\boldsymbol{x}_s) + p_2(\boldsymbol{y},\boldsymbol{x}_g) = -p_2(\boldsymbol{x}_s,\boldsymbol{y}) - p_2(\boldsymbol{x}_g,\boldsymbol{y}), \tag{6.2.5}$$

as was mentioned above. This can also be seen by simply rewriting the ray equations, (6.2.3), as equations for $y_2 - \xi_2$ and concluding that the change in sign on the right side implies a change in sign in each p_2 when differentiation is carried out on τ with respect to the y_2 variable, rather than with respect to x_{2s} or x_{2g}. In any case, because the second set of p_2's in (6.2.5) is zero at the stationary point, so is the first set. Hence, this element of the Beylkin determinant is equal to zero. Similarly, differentiation of (6.2.3) with respect to ξ_1, evaluated at $\xi_2 = y_2$ and $p_2 = 0$, reveals that the element in the $(2,2)$ position in the Beylkin determinant is zero, as well. The differentiation of the ray equation in (6.2.1) for $p_2(\boldsymbol{x}_s,\boldsymbol{y})$, for example, goes as follows.

$$0 = \frac{\partial p_2(\boldsymbol{x}_s,\boldsymbol{y})}{\partial\xi_1}\sigma_s + p_2(\boldsymbol{x}_s,\boldsymbol{y})\frac{\partial\sigma_s}{\partial\xi_1}.$$

Now, for $p_2 = 0$, the second term is equal to zero and so, then, the first term must be equal to zero as well. Because σ_s is not zero, the derivative of p_2 with respect to ξ_1 must be zero.

The remaining element of this second column of the Beylkin determinant, which is to say, the $(2,3)$ element, can be calculated by using the same trick as above and by using the relationship between the first derivatives with respect to ξ_2 and y_2, noted in the previous equation. That is,

$$\frac{\partial^2\phi(\boldsymbol{y},\boldsymbol{\xi})}{\partial\xi_2\partial y_2} = \frac{\partial p_2(\boldsymbol{y},\boldsymbol{x}_s)}{\partial\xi_2} + \frac{\partial p_2(\boldsymbol{y},\boldsymbol{x}_g)}{\partial\xi_2} = -\frac{\partial p_2(\boldsymbol{x}_s,\boldsymbol{y})}{\partial\xi_2} - \frac{\partial p_2(\boldsymbol{x}_g,\boldsymbol{y})}{\partial\xi_2}. \tag{6.2.6}$$

We have already computed the last derivatives above in (6.2.4) to be $1/\sigma_s$ and $1/\sigma_g$. Therefore,

$$h(\boldsymbol{y},\boldsymbol{\xi}) = -\left[\frac{\sigma_s+\sigma_g}{\sigma_s\sigma_g}\right] H(\boldsymbol{y},\xi_1),$$

(6.2.7)

$$H(\boldsymbol{y},\xi_1) = \det \begin{bmatrix} \nabla_y \phi(\boldsymbol{y},\xi_1,0) \\ \dfrac{\partial}{\partial \xi_1} \nabla_y \phi(\boldsymbol{y},\xi_1,0) \end{bmatrix}.$$

In this equation, the gradient is to be reinterpreted as a two-component derivative including differentiations in y_1 and y_3 only. Because the variable ξ_2 has been set equal to zero, $\boldsymbol{\xi} = (\xi_1, 0)$ and there is no longer a need for either the vector $\boldsymbol{\xi}$ or the subscript 1. Consequently, we write $H(\boldsymbol{y},\xi)$, $\phi(\boldsymbol{y},\xi)$, etc., with ξ denoting the variable ξ_1 of the vector $\boldsymbol{\xi}$.

In summary, applying the method of stationary phase to (5.1.21) amounts to the following.

1. Evaluate the phase and amplitude by computations in-plane as defined by (6.1.5) and (6.1.7).
2. Evaluate the second derivative at the stationary point by (6.2.3).
3. Introduce $\xi = \xi_1$; there is no longer a need for the subscript.
4. Evaluate $h(\boldsymbol{y},\xi)$ by in-plane computations only, as noted in (6.2.6).
5. Interpret $\boldsymbol{y} = (y_1, y_3)$, and interpret the gradient as a two-component operator in the same variables.

6.2.2 *The General 2.5D Inversion Formulas for Reflectivity*

With these items in place, we can directly derive the general variable-background, 2.5D inversion formulas for reflectivity, corresponding to the 3D formula (5.1.21) for $\beta(\boldsymbol{y})$, reflectivity multiplied by $\cos\theta_s$, and that corresponding to equation (5.1.47) for $\beta_1(\boldsymbol{y})$, which was reflectivity without the cosine multiplier.

The stationary phase formula applied to (5.1.21) now yields

$$\beta(\boldsymbol{y}) = \frac{1}{[2\pi]^{5/2}} \int d\xi \, \frac{|H(\boldsymbol{y},\xi)|}{a(\boldsymbol{y},\xi)|\nabla_y \phi(\boldsymbol{y},\xi)|} \frac{\sqrt{\sigma_s + \sigma_g}}{\sqrt{\sigma_s \sigma_g}} \cdot \int \sqrt{|\omega|} d\omega e^{-i\omega\phi(\boldsymbol{y},\xi) + i\pi/4 \operatorname{sgn}(\omega)} u_S(\boldsymbol{x}_g, \boldsymbol{x}_s, \omega). \quad (6.2.8)$$

Similarly, the inversion for β_1 in two-and-one-half dimensions is obtained by applying stationary phase to equation (5.1.47):

$$\beta_1(\boldsymbol{y}) = \frac{1}{[2\pi]^{5/2}} \int d\xi \frac{|H(\boldsymbol{y},\xi)|}{a(\boldsymbol{y},\xi)|\nabla \phi_y(\boldsymbol{y},\xi)|^2} \frac{\sqrt{\sigma_s + \sigma_g}}{\sqrt{\sigma_s \sigma_g}} \cdot \int \sqrt{|\omega|} d\omega e^{-i\omega\phi(\boldsymbol{y},\xi) + i\pi/4 \operatorname{sgn}(\omega)} u_S(\boldsymbol{x}_g, \boldsymbol{x}_s, \omega). \quad (6.2.9)$$

The resultant exponent $i\pi/4 \operatorname{sgn}(\omega)$ arises from two factors. First, $i\omega$ in the earlier formulas (5.1.21) and (5.1.47) is rewritten as $|\omega| \exp\{i\pi/2 \operatorname{sgn}(\omega)\}$,

and this exponential is combined with a corresponding factor, $\exp\{-i\pi/4\,\mathrm{sgn}\,(\omega)\}$, arising from the stationary phase formula, to yield the final result.

These two inversion formulas provide a basis for inverting data gathered on a dip line on the surface of the Earth or with the sources and/or the receivers in a borehole (well-to-well or VSP).

Exercises

6.4 Suppose that the subsurface has only one dimensional variation and that a single zero-offset data set is available.

a. Create the appropriate "thought experiment" to allow the application of equation (5.1.21) to determine the reflectivity in this case.

b. Following along the lines of the derivation of a 2.5D inversion in this section, apply the method of stationary phase in the transverse directions and show that one only needs to consider the three-dimensional wavefield on the vertical ray below the source/receiver point.

c. Use the same logic as in this section to show that the elements of the matrix of second derivatives at the stationary point are

$$\phi_{ij} = \delta_{ij}/\sigma, \quad i,j = 1,2.$$

d. Show that the Beylkin determinant is given by

$$h = \frac{4}{c(z)\sigma^2}.$$

Show that the amplitude of the Green's function on the stationary ray is given by

$$A = \frac{\sqrt{c(z)c(0)}}{4\pi\sigma}.$$

e. Show that

$$\beta(z) = \frac{8\sigma}{c(z)c(0)} \int u_s((0),\omega) e^{-i\omega\tau(z)} d\omega.$$

Here,

$$\tau(z) = \int_0^z \frac{dz'}{c(z')}.$$

f. Specialize to constant background and compare to the result, (3.2.16).

6.5 In Chapter 3, we set down criteria under which it could be expected that a stationary phase result would provide a reasonable numerical result for the purposes of forward modeling and inversion. For a

one-dimensional integral in dimensionless variables, the criterion was given by (3.6.5), and for such an integral in dimensional variables, with the dimension of length, such as our ξ_2 here, we use (3.6.25) as well, to require that

$$L^2\omega\frac{d^2\phi(x)}{d\xi_2^2} \geq \pi.$$

a. Use this criterion and (6.2.4) to conclude that the accuracy of the asymptotic analysis that led to (6.2.8) and (6.2.9) requires that

$$\omega L^2\left[\frac{1}{\sigma_s}+\frac{1}{\sigma_g}\right] \geq \pi.$$

b. Specialize this result to a constant background medium and show that the criterion becomes

$$\frac{\omega L}{c}L\left[\frac{1}{r_s}+\frac{1}{r_g}\right] \geq \pi,$$

with the r's being the distances between the output point and the source or the receiver as indicated by the subscript.

c. The relevant length scales of this problem are r_s and r_g. Thus, conclude that

$$\frac{\omega r_s}{c}\left[1+\frac{r_s}{r_g}\right] \geq \pi$$

and

$$\frac{\omega r_g}{c}\left[1+\frac{r_g}{r_s}\right] \geq \pi.$$

d. Explain why these criteria will always be satisfied when the underlying WKBJ approximation of the Green's functions is valid.

6.6 The purpose of this exercise is to derive a 2.5D Kirchhoff modeling formula for the upward-scattered field from a single surface. This derivation will use equation (5.4.1) for 3D Kirchhoff modeling as a point of departure.

Consistent with the 2.5D concept, we consider a cylindrical reflector whose mathematical description is essentially independent of the out-of-plane variable. Thus, let us define the reflecting surface by an in-plane parametric curve,

$$\boldsymbol{x} = (x_1(\ell), x_2, x_3(\ell)).$$

A fixed value of ℓ, that is, a fixed $x_1 = x_1(\ell)$, $x_3 = x_3(\ell)$, and x_2 free to vary, defines a straight line. The family of straight lines through the in-plane curve are the *generators* of the cylindrical surface. For this choice of parameters, dS in (5.4.1) is replaced by $dx_2\, d\ell$. Furthermore,

it is necessary to assume that the source and receiver are in-plane; that is,

$$\boldsymbol{x}_s(\boldsymbol{\xi}) = (x_{1s}(\xi_1), \xi_2, x_{3s}(\xi_1)), \quad \boldsymbol{x}_g(\boldsymbol{\xi}) = (x_{1g}(\xi_1), \xi_2, x_{3g}(\xi_1)).$$

It is further necessary to assume that the propagation speed, c, is independent of x_2, as in the discussion above, in this section.
With these changes, (5.4.1) can be further simplified by carrying out stationary phase in the x_2-direction. It is that analysis that will be outlined here as a series of exercises.

a. Consider the phase in (5.4.1), defined through (5.1.8) as

$$\phi(\boldsymbol{x}, \boldsymbol{\xi}) = \tau(\boldsymbol{x}, \boldsymbol{x}_s(\boldsymbol{\xi})) + \tau(\boldsymbol{x}_g(\boldsymbol{\xi}), \boldsymbol{x}).$$

Show that this phase is stationary when

$$\frac{\partial \phi}{\partial x_2} = \frac{\partial \tau(\boldsymbol{x}, \boldsymbol{x}_s(\boldsymbol{\xi}))}{\partial x_2} + \frac{\partial \tau(\boldsymbol{x}_g(\boldsymbol{\xi}), \boldsymbol{x})}{\partial x_2} = p_{2s} + p_{2g} = 0.$$

b. Suppose that $\xi_2 \neq x_2$. Consider the geometrical-optics rays from $\boldsymbol{x}$ to $\boldsymbol{x}_s(\boldsymbol{\xi})$ and to $\boldsymbol{x}_g(\boldsymbol{\xi})$, respectively. Explain why p_{2s} and p_{2g} must be constant on the rays and of the same sign, which is to say, the sign of the difference, $\xi_2 - x_2$.

c. Explain why the phase can be stationary only when

$$p_{2s} = p_{2g} = 0,$$

and that this corresponds to the phase being stationary for the choice $x_2 = \xi_2$.

d. Write down an equation of the form, (6.1.4) for the second component of rays from $\boldsymbol{x}$ to $\boldsymbol{x}_s(\boldsymbol{\xi})$ and to $\boldsymbol{x}_g(\boldsymbol{\xi})$, respectively, with the two choices of σ distinguished as σ_s and σ_g, respectively. Differentiate those equations explicitly and evaluate at $p_{2s} = p_{2g} = 0$ to conclude that

$$\frac{\partial p_{2s}}{\partial x_2} = \frac{1}{\sigma_s}, \quad \frac{\partial p_{2g}}{\partial x_2} = \frac{1}{\sigma_g}$$

at the stationary point.

e. Thus, show that

$$\frac{\partial^2 \phi}{\partial x_2^2} = \frac{1}{\sigma_s} + \frac{1}{\sigma_g} = \frac{\sigma_s + \sigma_g}{\sigma_s \sigma_g}, \quad \operatorname{sgn}\left\{\frac{\partial^2 \phi}{\partial x_2^2}\right\} = +1,$$

at the stationary point.

f. Now, use the stationary phase formula (3.6.4) to conclude that

$$u_S(\boldsymbol{x}_g,\omega) = -\sqrt{|\omega|}e^{-i\pi\,\mathrm{sgn}\,(\omega)/4}F(\omega)$$
$$\cdot \int R(\boldsymbol{x},\boldsymbol{x}_s)(\hat{\boldsymbol{n}}\cdot\nabla_x)\phi(\boldsymbol{x},\xi) \tag{6.2.10}$$
$$\cdot\, a_I(\boldsymbol{x},\xi)\frac{\sqrt{\sigma_s(\boldsymbol{x},\xi)\sigma_g(\boldsymbol{x},\xi)}}{\sqrt{\sigma_s(\boldsymbol{x},\xi)+\sigma_g(\boldsymbol{x},\xi)}}e^{i\omega\phi(\boldsymbol{x},\xi)}d\ell.$$

In this equation, there is no longer any dependence on x_2 and ξ_2 and no longer a need for a subscript on the remaining variable, ξ_1, which has now been redefined as ξ. Thus,

$$\boldsymbol{x}(\ell) = (x_1(\ell), x_3(\ell)), \qquad \boldsymbol{x}_s(\xi) = (x_{1s}(\xi), x_{3s}(\xi)),$$
$$\boldsymbol{x}_g(\xi) = (x_{1g}(\xi), x_{3g}(\xi)).$$

Furthermore, we have set

$$i\omega\frac{e^{i\pi\,\mathrm{sgn}\,\omega/4}}{\sqrt{|\omega|}} = \sqrt{|\omega|}e^{3i\pi\,\mathrm{sgn}\,\omega/4} = -\sqrt{|\omega|}e^{-i\pi\,\mathrm{sgn}\,\omega/4}.$$

g. Show that the constraint on parameters for use of this 2.5D Kirchhoff approximation (6.2.10) is as in the previous exercise.

6.3 The Beylkin Determinant H and Special Cases of 2.5D Inversion

In this section, we specialize the inversion formulas, (6.2.8) and (6.2.9), to the cases of common-shot, VSP, well-to-well, and common-offset inversion. In each case, the details of the inversions operators will change slightly, but all are special cases of these two equations. This discussion will follow along the general lines of the 3D case, Section 5.2. Recall, then, that

$$\nabla_y\phi(\boldsymbol{y},\xi) \equiv \nabla_y\tau(\boldsymbol{y},\boldsymbol{x}_s) + \nabla_y\tau(\boldsymbol{x}_g,\boldsymbol{y}),$$

with the gradient now being two-dimensional in the variables $\boldsymbol{x} = (x_1, x_3)$. Of course, we will continue to use the notation

$$\boldsymbol{p}_s = \nabla_y\tau(\boldsymbol{y},\boldsymbol{x}_s), \qquad \boldsymbol{p}_g = \nabla_y\tau(\boldsymbol{y},\boldsymbol{x}_g), \qquad \nabla_y\phi(\boldsymbol{y},\xi) = \boldsymbol{p}_s + \boldsymbol{p}_g.$$

6.3.1 General Properties of the Beylkin Determinant

As in Section 5.2, we introduce

$$\boldsymbol{v}_s \equiv \frac{\partial \boldsymbol{p}_s}{\partial\xi}, \quad \boldsymbol{v}_g \equiv \frac{\partial \boldsymbol{p}_g}{\partial\xi}, \tag{6.3.1}$$

and rewrite H, as defined in (6.2.7), as

$$H(\boldsymbol{y},\xi) = \det \begin{bmatrix} \boldsymbol{p}_s + \boldsymbol{p}_g \\ \boldsymbol{v}_s + \boldsymbol{v}_g \end{bmatrix}. \tag{6.3.2}$$

The elementary relationships among the vectors $\boldsymbol{p}_s$, $\boldsymbol{p}_g$, $\boldsymbol{v}_s$, and $\boldsymbol{v}_g$ are essentially unchanged from what they were in Section 5.2.1. We list them here, without rederiving them:

$$\boldsymbol{p}_s^2 = \boldsymbol{p}_g^2 = \frac{1}{c^2(\boldsymbol{y})}, \quad \boldsymbol{p}_s \cdot \boldsymbol{v}_s = \boldsymbol{p}_g \cdot \boldsymbol{v}_g = 0, \tag{6.3.3}$$

$$\boldsymbol{p}_s \cdot \boldsymbol{p}_g = \frac{1}{c^2(\boldsymbol{y})} \cos 2\theta, \quad |\boldsymbol{p}_s + \boldsymbol{p}_g| = \frac{2\cos\theta}{c(\boldsymbol{y})}. \tag{6.3.4}$$

We use the orthogonality in (6.3.3) to define a relative orientation between each $\boldsymbol{p}$ and $\boldsymbol{v}$. Let us define μ_s and μ_g, such that $\boldsymbol{v}_s\mu_s$ and $\boldsymbol{v}_g\mu_g$ are the respective right-hand rotations through angle $\pi/2$ from $\boldsymbol{p}_s$ and $\boldsymbol{p}_g$. In the simple situation of a flat horizontal reflector, constant-background wavespeed, and source or receiver x_1-coordinate increasing with ξ, then $\mu_s = 1$ or $\mu_g = 1$, respectively. Let us further define $\boldsymbol{e}_1$ and $\boldsymbol{e}_3$ as unit vectors along the respective x_1 and x_3 axes, and then set

$$\boldsymbol{e}_2 = \boldsymbol{e}_1 \times \boldsymbol{e}_3.$$

Note that $\boldsymbol{e}_2$ is defined opposite to the right-hand convention to suit the unusual choice of singling out the clockwise rotation from the $\boldsymbol{p}$'s as special. With this convention,

$$\boldsymbol{p}_s \times \boldsymbol{v}_s = \frac{1}{c(\boldsymbol{y})} |\boldsymbol{v}_s| \mu_s \boldsymbol{e}_2, \quad \boldsymbol{p}_g \times \boldsymbol{v}_g = \frac{1}{c(\boldsymbol{y})} |\boldsymbol{v}_g| \mu_g \boldsymbol{e}_2 \tag{6.3.5}$$

$$\boldsymbol{p}_s \times \boldsymbol{v}_g = \frac{\cos 2\theta}{c(\boldsymbol{y})} |\boldsymbol{v}_g| \boldsymbol{e}_2 \mu_g, \quad \boldsymbol{p}_g \times \boldsymbol{v}_s = \frac{\cos 2\theta}{c(\boldsymbol{y})} |\boldsymbol{v}_s| \boldsymbol{e}_2 \mu_s. \tag{6.3.6}$$

Using these results, we are prepared to write down the general Beylkin determinant by first interpreting it as a two-dimensional cross product:

$$\begin{aligned} |H(\boldsymbol{y},\xi)| &= \left|(\boldsymbol{p}_s + \boldsymbol{p}_g) \times (\boldsymbol{v}_s + \boldsymbol{v}_g)\right| \\ &= \left|\boldsymbol{p}_s \times \boldsymbol{v}_s + \boldsymbol{p}_g \times \boldsymbol{v}_s + \boldsymbol{p}_g \times \boldsymbol{v}_g + \boldsymbol{p}_g \times \boldsymbol{v}_s\right| \\ &= \left|\frac{1}{c(\boldsymbol{y})} |\boldsymbol{v}_s| \mu_s (1 + \cos 2\theta) + \frac{1}{c(\boldsymbol{y})} |\boldsymbol{v}_g| \mu_g (1 + \cos 2\theta)\right| \\ &= \frac{2\cos^2\theta}{c(\boldsymbol{y})} \left| |\boldsymbol{v}_s| \mu_s + |\boldsymbol{v}_g| \mu_g \right| \\ &= 2\cos^2\theta \, |H_s(\boldsymbol{y},\xi) + H_g(\boldsymbol{y},\xi)| \,. \end{aligned} \tag{6.3.7}$$

In this last line, we have set

$$H_s(\boldsymbol{y},\xi) = \frac{1}{c(\boldsymbol{y})} |\boldsymbol{v}_s| \mu_s \quad \text{and} \quad H_g(\boldsymbol{y},\xi) = \frac{1}{c(\boldsymbol{y})} |\boldsymbol{v}_g| \mu_g. \tag{6.3.8}$$

6.3.2 *Common-Shot Inversion*

For common-shot inversion, $\tau(\boldsymbol{y}, \boldsymbol{x}_s)$ is independent of ξ, and $\boldsymbol{v}_s = \boldsymbol{0}$. Then, using (6.3.3) through (6.3.7), we find that the respective inversion formulas for $\beta(\boldsymbol{y})$ and $\beta_1(\boldsymbol{y})$ are

$$\beta(\boldsymbol{y}) = \frac{1}{[2\pi]^{5/2}} \int d\xi \frac{\cos\theta}{a(\boldsymbol{y},\xi)} \left| \frac{\partial \boldsymbol{p}_g}{\partial \xi} \right| \frac{\sqrt{\sigma_s + \sigma_g}}{\sqrt{\sigma_s \sigma_g}} \cdot \int \sqrt{|\omega|} d\omega e^{-i\omega\phi(\boldsymbol{y},\xi) + i\pi/4 \operatorname{sgn}(\omega)} u_S(\boldsymbol{x}_g, \boldsymbol{x}_s, \omega) \quad (6.3.9)$$

and

$$\beta_1(\boldsymbol{y}) = \frac{c(\boldsymbol{y})}{2[2\pi]^{5/2}} \int d\xi \frac{1}{a(\boldsymbol{y},\xi)} \left| \frac{\partial \boldsymbol{p}_g}{\partial \xi} \right| \frac{\sqrt{\sigma_s + \sigma_g}}{\sqrt{\sigma_s \sigma_g}} \cdot \int \sqrt{|\omega|} d\omega e^{-i\omega\phi(\boldsymbol{y},\xi) + i\pi/4 \operatorname{sgn}(\omega)} u_S(\boldsymbol{x}_g, \boldsymbol{x}_s, \omega). \quad (6.3.10)$$

In these equations, the factor $2\cos\theta/c(\boldsymbol{y})$, which allows us to identify the incidence angle for $\boldsymbol{y}$ on S, appears explicitly. That is, the first integrand can be obtained from the second by multiplying the latter by $2\cos\theta/c(\boldsymbol{y})$. However, it should be noted that this factor is really defined by (6.3.4).

6.3.3 *A Numerical Example—Extraction of Reflectivity from a Common-Shot Inversion*

Figure 6.2 shows a test of these formulas using synthetic 2.5D data generated on a simple two-plane model, with a vertical slice through the model shown in Figure 6.2a. The source point is at the center of the model, with receivers spread along a single line on the upper surface in both directions. Figure 6.2b shows the 2.5D model data, created with CSHOT [Docherty, 1987, 1988, and 1991].

The additional plots are the demonstration outputs that come with the code CXZCS [Dong, 1990, and Dong et al. 1991]. Figure 6.2c shows the inversion of the data in Figure 6.2b for $\beta(\boldsymbol{y})$; Figure 6.2c shows the inversion of these data for $\beta_1(\boldsymbol{y})$. In processing the data to obtain these outputs, the correct background velocity, $c(\boldsymbol{x})$, was used. In both of these figures, we can see the loss of resolution away from the center of the model. With increasing offset, $\cos\theta_s$ decreases and we know from the theory of the previous chapter that the normal wave vector is proportional to $\cos\theta_s$:

$$k_{normal} = |\boldsymbol{k}| = \frac{2|\omega|\cos\theta_s}{c(\boldsymbol{y})}.$$

With a decreasing spatial bandwidth of the image in the normal direction, resolution degrades. It is easy to check from the geometry, here, that $\cos\theta_s$ is less than 0.3 at the widest offset, and that the widths of the lobes of the output wavelet are more than triple at this offset compared to their widths

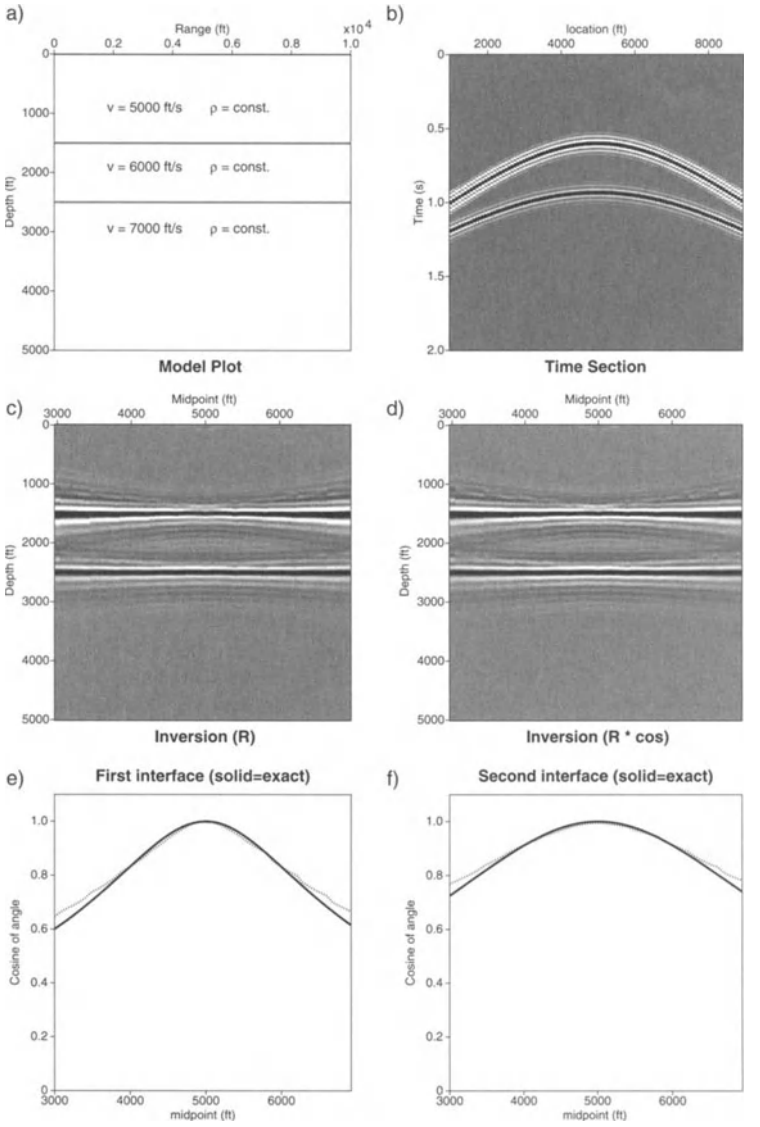

FIGURE 6.2. a) The two-plane model, and b) common-shot seismic section across the model generated with the program CSHOT. c) Inversion for the reflectivity function using equation (6.3.9), and d) for the reflectivity multiplied times $\cos\theta$, using equation (6.3.9) with the exact wavespeed profile with program CXZCS. e) Values of $\cos\theta_s$ on the first layer extracted from the amplitudes of the seismic inversion compared with computed values. f) Values of $\cos\theta_s$ on the second layer extracted from the amplitudes of the seismic inversion compared with computed values.

at zero offset. More subtle is the degradation of resolution of the image of the second reflector at zero offset compared to the resolution of the first reflector, just above. Here, it is the increased value of $c(\boldsymbol{y})$ that causes the degradation. On the other hand, due to the refractions at the first interface, θ_s does not increase quite as fast with offset at the second reflector and the relative degradation with offset can be seen not to increase as fast on this reflector as it does on the first reflector.

Figures 6.2e and 6.2f show comparisons of numerically computed estimates of $\cos\theta_s$ for the upper and lower reflector, respectively, with their theoretically determined counterparts. Recall that this estimate must come from a ratio of *peak* values of the two outputs β and β_1. In this calculation, the local maxima were used for the peak values. We see a falloff in accuracy accompanying the falloff in resolution with increasing offset. The failure of agreement is small for this synthetic data set, but for real data more careful "peak correction" may be required. There is more than one way to perform such peak corrections. The most accurate way is by interpolating the data points with sinc functions. A less computationally expensive, but nearly as accurate, way is by picking the nearest output points around the peak and then correcting those values to the nearest parabolic peak. Either technique would produce optimal results, with errors usually less than 1%. We can rarely justify the increased effort required for extracting amplitudes with this degree of precision from real data, however.

6.3.4 Constant-Background Propagation Speed

For a constant-background propagation speed, we use the following notation to simplify the integrands in (6.3.9) and 6.3.10):

$$\begin{aligned} \boldsymbol{r}_s &\equiv \boldsymbol{y} - \boldsymbol{x}_s, & \boldsymbol{r}_g &\equiv \boldsymbol{y} - \boldsymbol{x}_g, \\ r_s &\equiv |\boldsymbol{y} - \boldsymbol{x}_s|, & r_g &\equiv |\boldsymbol{y} - \boldsymbol{x}_g|, \\ \hat{\boldsymbol{r}}_s &\equiv \boldsymbol{r}_s/r_s, & \hat{\boldsymbol{r}}_g &\equiv \boldsymbol{r}_g/r_g, \\ \sigma_s &\equiv cr_s, & \sigma_g &\equiv cr_g. \end{aligned} \tag{6.3.11}$$

In terms of these variables,

$$\begin{aligned} &\tau(\boldsymbol{y},\boldsymbol{x}_s) = r_s/c, \qquad \tau(\boldsymbol{y},\boldsymbol{x}_g) = r_g/c, \qquad \phi(\boldsymbol{y},\xi) = [r_s + r_g]/c, \\ &1/a(\boldsymbol{y},\xi) = (4\pi)^2 r_s r_g, \qquad \boldsymbol{p}_s = \hat{\boldsymbol{r}}_s/c, \qquad \boldsymbol{p}_g = \hat{\boldsymbol{r}}_g/c, \\ &\qquad\qquad H_g(\boldsymbol{y},\xi) = \frac{1}{c^2}\left|\frac{\partial \hat{\boldsymbol{r}}_g}{\partial \xi}\right|, \end{aligned} \tag{6.3.12}$$

which follows from (6.3.8) and the definition of $\boldsymbol{v}_g$ in (6.3.1).

For a horizontal planar upper surface, the determinant in the last line simplifies even further,

$$H_g(\boldsymbol{y},\xi) = \frac{y_3}{c^2 r_g^2}, \quad \boldsymbol{x}_g = (\xi, 0), \tag{6.3.13}$$

and the common-shot inversion formulas for a constant-background wavespeed and horizontal planar upper surface are obtained by substituting these results into (6.3.9) and (6.3.10). The results are

$$\beta(\boldsymbol{y}) = \frac{4y_3}{\sqrt{2\pi c^3}} \int d\xi \frac{\sqrt{r_s + r_g}\sqrt{r_s}}{r_g^{3/2}} \cos\theta \cdot \int \sqrt{|\omega|} d\omega e^{-i\omega\phi(\boldsymbol{y},\xi)+i\pi/4\,\mathrm{sgn}\,(\omega)} u_S(\boldsymbol{x}_g, \boldsymbol{x}_s, \omega) \quad (6.3.14)$$

and

$$\beta_1(\boldsymbol{y}) = \frac{2y_3}{\sqrt{2\pi c}} \int d\xi \frac{\sqrt{r_s + r_g}\sqrt{r_s}}{r_g^{3/2}} \cdot \int \sqrt{|\omega|} d\omega e^{-i\omega\phi(\boldsymbol{y},\xi)+i\pi/4\,\mathrm{sgn}\,(\omega)} u_S(\boldsymbol{x}_g, \boldsymbol{x}_s, \omega).$$

Remark 6.3. The operator, $\beta_1(\boldsymbol{y})$ yields as peak value the area under the filter multiplied by the reflection coefficient. For constant background, there is no need to multiply by $2\cos\theta/c$ as in the inversion operator $\beta(\boldsymbol{y})$, when what we really need is $\cos\theta = \sqrt{1 + \hat{\boldsymbol{r}}_s \cdot \hat{\boldsymbol{r}}_g}/2$. In fact, an operator differing from $\beta_1(\boldsymbol{y})$ by exactly this factor is recommended. In the theoretical discussions here, we will continue to list $\beta(\boldsymbol{y})$ and $\beta_1(\boldsymbol{y})$.

6.3.5 Vertical Seismic Profiling

Vertical seismic profiling (VSP) is a special case of the common-shot geometry in which the source is on the upper surface and the receivers are in a well [Dong and Bleistein, 1990]. Three-dimensional inversion from a single VSP experiment is not possible. A two-and-one-half-dimensional inversion is possible, however, and meaningful only when the earth environment and the source-receiver configuration allow for the 2.5D in-plane propagation assumption to be made. First, the source-receiver array must (at least, nearly) define a vertical plane. Second, the out-of-plane variations should be minimal.[2] Third, there must be scattered arrivals. A typical application for VSP is the determination of interval velocities in the subsurface from the direct arrivals on the seismogram. The theory we have developed, however, requires that scattered energy be present. This is, of course, the case with the majority of VSP profiles, but this also means that we de-emphasize the importance of the direct arrivals.

For the mathematical model, it is assumed that the source-receiver array is in a vertical plane and that the propagation speed varies only in

[2]Clearly, this basic idea admits an extension to an "oblique" plane in a medium with two-dimensional variation in another plane making an acute angle with the plane of the survey.

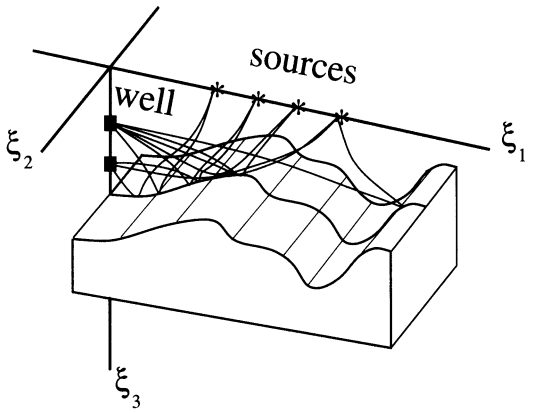

FIGURE 6.3. A schematic of a VSP survey in a 2.5D model. Only rays representing scattered energy are drawn.

that plane. See Figure 6.3. The "thought experiment" for development of the two-and-one-half-dimensional inversion for this problem is to consider identical VSP planes, defined by identical wells, recording lines, and transmitted and reflected ray paths. Only the out-of-plane coordinate of the sources and receivers characterizes these planes as being different.

In this case, the suite of experiments is exactly like the suite of surface common-source experiments used above to reduce the three-dimensional inversion to the two-and-one-half-dimensional, common-shot inversions. Consequently, the inversion formulas (6.3.9) and (6.2.2) apply also to VSP inversion, with the specification to VSP carried in the description of the source-receiver configuration and the consequent evaluation of the functions in the integrand of those equations. Note that these formulas allow for a deviated borehole—in-plane, at least—through the equations that describe $\boldsymbol{x}_g(\xi)$.

The specialization to VSP becomes more apparent when the inversion formulas (6.3.9) and (6.2.2) are further specialized to constant background. For example, set

$$\boldsymbol{x}_s = (-h, 0), \quad \boldsymbol{x}_g = (h, \xi). \tag{6.3.15}$$

For this parameterization, the major change from the computation above for the surface common-source inversion is that now

$$\frac{\partial \boldsymbol{x}_g}{\partial \xi} = (0, 1), \tag{6.3.16}$$

whereas previously the right side was $(1, 0)$. The results (6.3.11) and (6.3.12) remain unchanged, but, in place of (6.3.13), we find in this case that

$$H_g(\boldsymbol{y}, \xi) = -\frac{y_1 - h}{c^2 r_g^2}, \quad \boldsymbol{x}_g = (0, \xi). \tag{6.3.17}$$

That is, the total change in the formulas (6.3.14) and (6.3.15) for the case of VSP is merely that the factor of y_3 is replaced by $y_1 - h$. Therefore, for VSP,

$$\beta(\boldsymbol{y}) = \frac{4|y_1 - h|}{\sqrt{2\pi c^3}} \int d\xi \frac{\sqrt{r_s + r_g}\sqrt{r_s}}{r_g^{3/2}} \cdot \cos\theta \int \sqrt{|\omega|} d\omega e^{-i\omega\phi(\boldsymbol{y},\xi)+i\pi/4\,\mathrm{sgn}\,(\omega)} u_S(\boldsymbol{x}_g, \boldsymbol{x}_s, \omega) \quad (6.3.18)$$

and

$$\beta_1(\boldsymbol{y}) = \frac{2|y_1 - h|}{\sqrt{2\pi c}} \int d\xi \frac{\sqrt{r_s + r_g}\sqrt{r_s}}{r_g^{3/2}} \cdot \int \sqrt{|\omega|} d\omega e^{-i\omega\phi(\boldsymbol{y},\xi)+i\pi/4\,\mathrm{sgn}\,(\omega)} u_S(\boldsymbol{x}_g, \boldsymbol{x}_s, \omega). \quad (6.3.19)$$

6.3.6 *Well-to-Well Inversion*

The two-and-one-half-dimensional inversion of well-to-well data is similar to the VSP case above [Dong and Bleistein, 1990]. The only difference is that the source, as well as the receivers, is at depth. Thus, for example, (6.3.15) would be replaced by

$$\boldsymbol{x}_s = (-h, \eta), \quad \boldsymbol{x}_g = (h, \xi). \quad (6.3.20)$$

Here, η denotes the depth of the receiver in the well. Except for this change, the formulas of the discussion of VSP inversion apply to this case as well.

6.3.7 *Invert for What?*

We have written down inversion formulas for VSP and well-to-well configurations as if the requirements of the formalism developed above apply here as easily as they do for the surface experiments of the earlier discussions. In fact, they do not and some caution is necessary.

In these experiments, it is often the case (for example, classical tomographic inversion) that the raypath from the source to the output point, and that from the output point to the receiver, are nearly two segments of a single trajectory from source to receiver. This can occur because the reflection is at an oblique angle, or because the ray is bent, rather than scattered. For such trajectories, the two gradients $\nabla_y\tau(\boldsymbol{y}, x_s)$ and $\nabla_y\tau(\boldsymbol{y}, x_g)$ are pointed nearly opposite to one another. Thus, $\nabla_y\phi(\boldsymbol{y}, \xi) = \nabla_y\tau(\boldsymbol{y}, x_s) + \nabla_y\tau(\boldsymbol{y}, x_s)$ is nearly zero. So the approximation (5.1.13), (5.1.14) is not very good (we need second-order terms in the Taylor series, at least), and the first row of the matrix in (5.1.17) is nearly zero. While it may be possible to stabilize

the inversion formulas, the limited aperture and effective wavenumbers associated with such near-transmission geometry (discussed in Section 4.2) is not possible to fix.

These indicators should all cause the reader to question the validity of the application of this method in the near-forward scattering direction suggested by the configurations described here. That is, in the direction for which traditional tomographic methods are applicable, the inversion technique proposed here breaks down. It should be noted, however, that tomographic methods invert either perturbations in traveltime data or amplitude attenuation data to characterize the medium. In the context of the high-frequency inversion discussed here, these are inversions in the "slower" scales, which are assumed to be "many" units of reciprocal wavenumber. Thus, these are the inversion techniques for low-resolution or large-length scale characterization of the propagating medium.

On the other hand, for source-receiver pairs and output points $\boldsymbol{y}$ where $\nabla_y \phi$ is bounded away from zero (smaller values of θ, as in reflection from targets beneath both source and receiver), one should expect that the method will work as well as it does for surface surveys. Because of the similarity of the source-receiver configurations for (traveltime or transmission) tomography and common-shot, well-to-well migration or inversion, the latter is what we have been referring to as "diffraction tomography." See Devaney and Oristaglio [1984].

6.3.8 Common-Offset Inversion

For common-offset inversion, in contrast to the common-source inversion above, both $\boldsymbol{x}_s$ and $\boldsymbol{x_g}$ are functions of ξ and we need both terms in (6.3.7).

By using these results in (6.3.9) and (6.3.10), we find that the formulas for $\beta(\boldsymbol{y})$ and $\beta_1(\boldsymbol{y})$ become, respectively,

$$\beta(\boldsymbol{y}) = \frac{c(\boldsymbol{y})}{[2\pi]^{5/2}} \int d\xi \frac{\cos\theta}{a(\boldsymbol{y},\xi)} [|H_s(\boldsymbol{y},\xi) + H_g(\boldsymbol{y},\xi)|] \frac{\sqrt{\sigma_s + \sigma_g}}{\sqrt{\sigma_s \sigma_g}} \cdot \int \sqrt{|\omega|} d\omega e^{-i\omega\phi(\boldsymbol{y},\xi)+i\pi/4\,\mathrm{sgn}\,(\omega)} u_S(\boldsymbol{x}_g, \boldsymbol{x}_s, \omega) \quad (6.3.21)$$

and

$$\beta_1(\boldsymbol{y}) = \frac{c^2(\boldsymbol{y})}{2[2\pi]^{5/2}} \int d\xi \frac{1}{a(\boldsymbol{y},\xi)} [|H_s(\boldsymbol{y},\xi) + H_g(\boldsymbol{y},\xi)|] \frac{\sqrt{\sigma_s + \sigma_g}}{\sqrt{\sigma_s \sigma_g}} \cdot \int \sqrt{|\omega|} d\omega e^{-i\omega\phi(\boldsymbol{y},\xi)+i\pi/4\,\mathrm{sgn}\,(\omega)} u_S(\boldsymbol{x}_g, \boldsymbol{x}_s, \omega). \quad (6.3.22)$$

(See Sullivan and Cohen [1987] for comparison.)

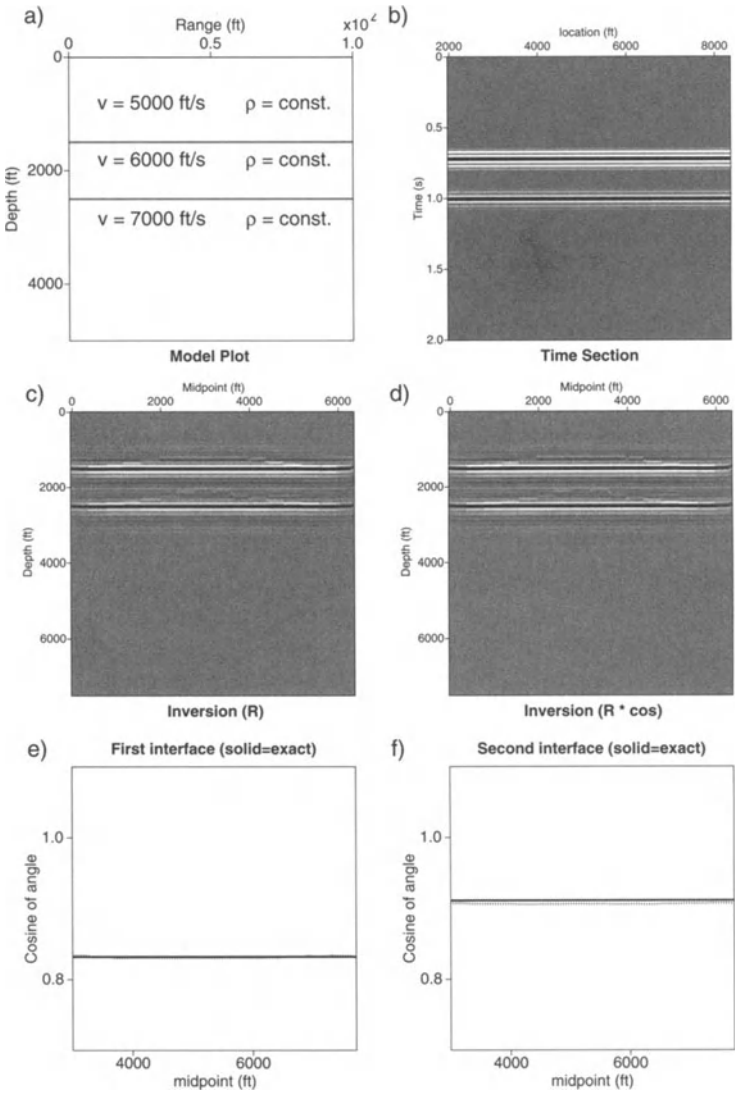

FIGURE 6.4. a) The two-plane model, and b) common-offset seismic section across the model generated with the program CSHOT. c) Inversion for the reflectivity function using equation (6.3.9), and d) for the reflectivity multiplied times $\cos\theta$, using equation (6.3.9) with the exact wavespeed profile with program CXZCO [Hsu, 1992]. e) Comparison of reflectivities extracted from the seismic data for the first layer with computed values. f) Comparison of reflectivities extracted from the seismic data for the second layer with computed values.

6.3.9 *A Numerical Example—Extraction of the Reflection Coefficient and* $\cos\theta_s$ *from a Common-Offset Inversion*

Figure 6.4a shows a test of these formulas for the same model as in Figure 6.2a. Again, data generated by CSHOT is shown in Figure 6.4b. In this case, θ_s is constant at each level. Thus, we see no relative changes in resolution at each reflector in the outputs in Figures 6.4c 6.4d. Figure 6.4e and Figure 6.4f, show estimates of the reflectivity, β, for the two reflectors. The inversion is performed with the program CXZCO [Hsu, 1992]. (These plots are based on demos that are included with the code.) Again, no peak corrections were carried out. The greater accuracy of the reflectivity relative to theory in Figure 6.4e compared to Figure 6.4f is serendipitous. For the parameters chosen for this model, for the first reflector, the peak sample was closer to the peak of the continuous sinc function than it was for the second reflector. The result for the second reflector could be improved significantly using sinc interpolation to resample the output, and then picking the peak of the interpolated data.

6.3.10 *A Numerical Example—Imaging a Syncline with Common-offset Inversion*

Figure 6.5a shows a test of equation (6.3.9) using a synthetic data set generated over a model similar to that represented by Figure 1.1. Figure 6.5b shows the data generated numerically, again using CSHOT. The offset between source and receiver for this model is 40 m, with source-receiver midpoint spacing of 12 m. The bandwidth of the data was a trapezoid with corner frequencies of 10, 15, 45, and 50 Hz. Thus, this model represents a near-offset seismic geometry.

Figure 6.5c shows the output, β, for these data, again computed with CXZCO. This output shows several "diffraction smile" artifacts. As was discussed at the end of the last chapter, diffraction smiles are integration endpoint contributions. One way of viewing this phenomenon is that the inversion (or migration, for that matter) is creating a reflector for which the data stops abruptly. Such a reflector would have to turn upward in such a manner as to "aim" the specular arrival to one side of the abrupt end of the data stream at the upper surface. Here, one can see one such smile entering the figure from the left; the synthetic data was sufficiently close to the left end of the output domain for the endpoint contribution to be significant compared to the (interior) stationary point contribution that produced the reflector image.

Furthermore, CSHOT, being a raytrace-based modeling code, does not correctly represent the terminations of the "bow-tie" events representing the synclines. In full-waveform data (either real or synthetic) such bow-tie events taper smoothly to zero over a greater distance than what we see in the CSHOT model data. This failure to correctly model the bow-tie

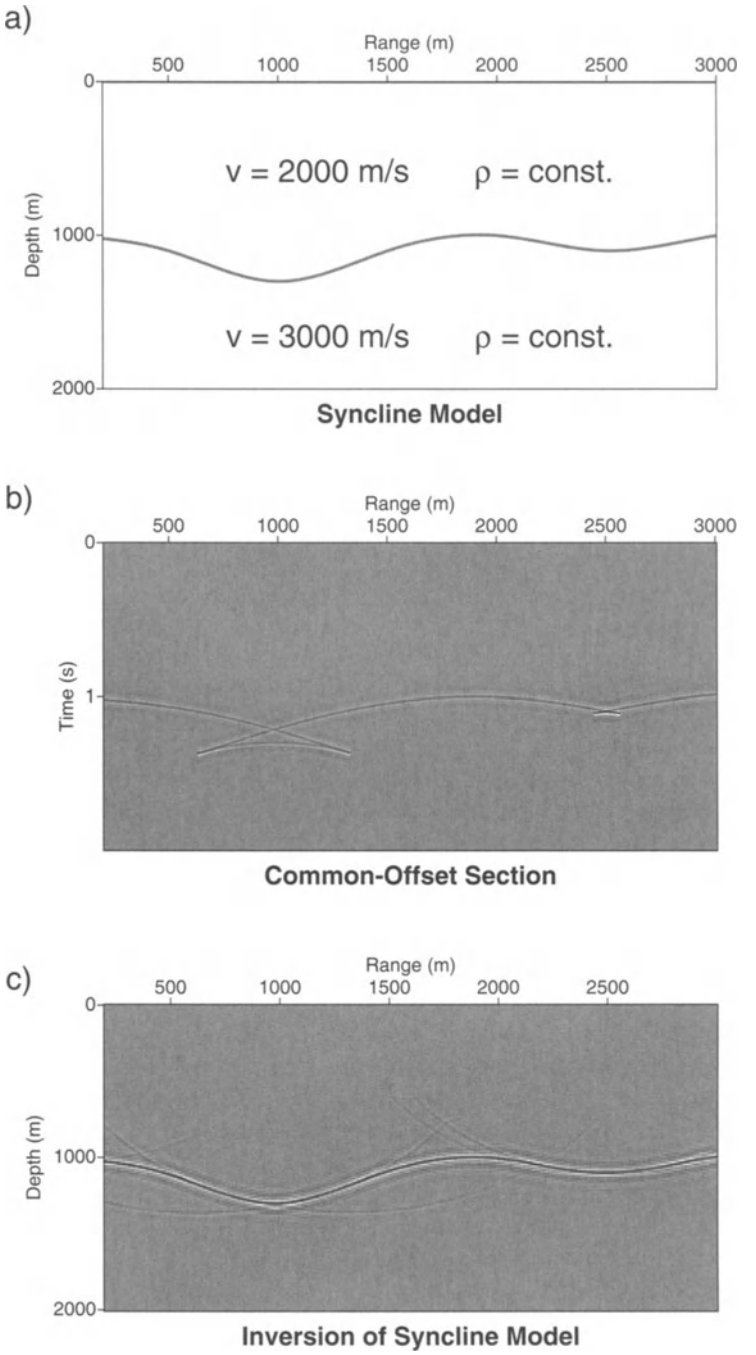

FIGURE 6.5. a) The simple syncline model with piecewise-constant wavespeeds and densities, and b) common-shot seismic section across the model generated with the program CSHOT. c) Inversion for the reflectivity using equation (6.3.9), assuming the exact wavespeed profile as the background, showing diffraction smiles at points poorly represented by raytracing.

events leads to a discontinuous wavefield, easily observed in Figure 6.5b at about 1.4 seconds at 600 m and 1200 m, and again at about 1.1 seconds at 2450 m and 2550 m. The former pair produces two diffraction smiles that are clearly visible and well separated in Figure 6.5c, tangent to the reflector image on the two sides of the syncline at about 1000 m. The latter pair produces two nearby smiles that are most visible above the reflector between 1500 m and 2000 m. The inversion of correctly modeled bow-tie features would not have such diffraction-smile artifacts.

6.3.11 Constant Background Inversion

For constant-background wavespeed and a horizontal planar upper surface, set

$$\boldsymbol{x}_s = (\xi - h, 0), \quad \boldsymbol{x}_g = (\xi + h, 0). \tag{6.3.23}$$

With this choice, the results in (6.3.11) and (6.3.12) remain unchanged. In the last line, $\partial \boldsymbol{x}_g / \partial \xi = (1, 0)$, as does $\partial \boldsymbol{x}_s / \partial \xi$, which we need for calculating the analogous determinant, $H_s(\boldsymbol{y}, \xi)$. In fact, $H_g(\boldsymbol{y}, \xi)$ is again given by (6.3.13) with $\boldsymbol{x}_g$ now given by (6.3.23) and $H_s(\boldsymbol{y}, \xi)$, obtained by replacing the subscript g by the subscript s. Thus, we have

$$H_g(\boldsymbol{y}, \xi) = \frac{y_3}{c^2 r_g^2}, \quad H_s(\boldsymbol{y}, \xi) = \frac{y_3}{c^2 r_s^2}. \tag{6.3.24}$$

With these expressions substituted into (6.3.21) and (6.3.22), the common-offset, constant-background inversion formulas become, respectively,

$$\beta(\boldsymbol{y}) = \frac{4y_3}{\sqrt{2\pi c^3}} \int d\xi \sqrt{r_s + r_g} \frac{r_s^2 + r_g^2}{(r_s r_g)^{3/2}} \cdot \cos\theta \int \sqrt{|\omega|} d\omega e^{-i\omega[r_s + r_g] + i\pi/4 \operatorname{sgn}(\omega)} u_S(\boldsymbol{x}_g, \boldsymbol{x}_s, \omega) \tag{6.3.25}$$

and

$$\beta_1(\boldsymbol{y}) = \frac{2y_3}{\sqrt{2\pi c}} \int d\xi \sqrt{r_s + r_g} \frac{r_s^2 + r_g^2}{(r_s r_g)^{3/2}} \cdot \int \sqrt{|\omega|} d\omega e^{-i\omega[r_s + r_g] + i\pi/4 \operatorname{sgn}(\omega)} u_S(\boldsymbol{x}_g, \boldsymbol{x}_s, \omega). \tag{6.3.26}$$

6.3.12 Zero-Offset Inversion

Finally, we consider the specialization to zero offset. Now, $\tau(\boldsymbol{y}, \boldsymbol{x}_g) = \tau(\boldsymbol{y}, \boldsymbol{x}_s)$, so $\phi(\boldsymbol{y}, \boldsymbol{\xi}) = 2\tau(\boldsymbol{y}, \boldsymbol{x}_s)$, with a similar doubling occurring with all of the subscripted variables in (6.3.21) and (6.3.22). Consequently,

$$\beta(\boldsymbol{y}) = \frac{c(\boldsymbol{y})}{2\pi^{5/2}} \int d\xi \frac{|H_s(\boldsymbol{y}, \xi)|}{\sqrt{\sigma_s} A^2(\boldsymbol{y}, x_s)} \cdot \int \sqrt{|\omega|} d\omega e^{-2i\omega\tau(\boldsymbol{y}, \boldsymbol{x}_s) + i\pi/4 \operatorname{sgn}(\omega)} u_S(\boldsymbol{x}_s, \boldsymbol{x}_s, \omega). \quad (6.3.27)$$

In this equation, $A(\boldsymbol{y}, \boldsymbol{x}_s)$ is the two-and-one-half-dimensional, ray-theoretic amplitude defined by (6.1.5) and (6.1.7). This would be the inversion formula of choice for poststack, two-and-one-half-dimensional inversion in a variable background. Of course, for this case, the formula for $\beta(\boldsymbol{y})$ will differ from this one by only a factor of $2/c(\boldsymbol{y})$ because $\theta = 0$. We leave it as an exercise for the reader to verify that the further specialization to constant background of the current formula for $\beta(\boldsymbol{y})$ agrees with the zero-offset, two-and-one-half-dimensional, constant-background inversion result, (3.6.24).

Exercises

6.7 To obtain a zero-offset, constant-background inversion formula, β, start from (6.3.25), set $r_s = r_g = r$ and $\cos\theta = 1$. Show that the result agrees with (3.6.24), except for notational differences.

7

The General Theory of Data Mapping

Throughout this text we have treated the seismic imaging problem as an inverse problem. To realize the goal of creating inversion formulas, we began with a simple idea. We created approximate forward modeling formulas, which we wrote as Fourier-like integrals. We then deduced their inverses, relying on the invertibility property of the Fourier transform. The inversion formulas that we obtained were also Fourier-like integrals owing to this procedure, with many of the classical Fourier-based migration techniques "falling out" as special cases of these more general formulas.

Anyone familiar with seismic data processing should be aware of *other* integral equation–based processing techniques that bear a similarity in appearance to migration formulas. Many of these are Fourier-like integral operators, but with amplitude factors differing from those that appear in migration formulas. Classical examples of such formulas are those for performing *dip-moveout* (DMO) and *wave-equation datuming.* More modern examples are the formulas for performing *offset continuation*, and those for *data regularization.* It is our goal in this chapter to show that these traditional techniques, as well as their more modern cousins, are members of a general family that we refer to as "data-mapping" formulas.

Our plan is to present a *general prescription* that not only unifies the classical methods, but is sufficiently general to permit many other related formulas to be generated as needed. The reader should realize that this is a *research* chapter. Here we present results that are close to the cutting edge of a branch of geophysical research that is active at the time we are writing. Thus, we are not presenting "cut-and-dried" results, but rather a snapshot of research in progress.

7.1 Introduction to Data Mapping

Geophysicists have always strained existing computational resources by processing increasingly large volumes of data, recorded in ever more complicated acquisition geometries. Accordingly, data have been preprocessed to remove a variety of undesirable characteristics, either to reduce data volume or to make data suitable for further processing, usually with codes designed for simpler geometries.

With the move to acquire seismic data in increasingly hostile environs, geophysicists must expect that data will be collected with a nonuniform trace spacing, and on a recording surfaces that are neither flat nor horizontal. While preprocessing techniques for remedying specific distortions of data differ for specific applications, all share common attributes in that they operate by remapping the data to an approximation of the data that would have been collected in a simpler setting. In the subsections that follow, we discuss specific examples of such data-mapping techniques.

Normal NMO and Dip Moveout (DMO)

The classical method of applying the *normal moveout correction* followed by stacking (the NMO-stack), and the related method of bin-stacking for 3D data, are the most primitive techniques for mapping data to zero offset. Such methods are based on the simplistic assumption that the Earth consists of a single constant-wavespeed medium overlying a single flat horizontal reflector.

A more sophisticated approach to this operation called *dip moveout* (DMO) has been an important seismic data preprocessing technique for years. Because NMO fails to truly map dipping events in the data to zero offset, dip moveout was conceived as a way of mapping NMO-corrected data to *true zero offset*. Thus, NMO-DMO represent data mapping to zero-offset.[1] In the course of performing the NMO-DMO correction, a process called "velocity analysis" is performed. That is to say, the appropriate background-wavespeed model is found, such that NMO-DMO produces "flattened" shot gathers that are suitable for stacking. This estimate can serve as an approximation of the background-wavespeed profile needed for the final migration of the data. Thus, even with the availability of more powerful computers, as well as prestack migration codes, the NMO-DMO process has an intrinsic value. (See Byun [1990] for important papers on the topic of velocity analysis.) Therefore, understanding NMO-DMO in the context of data mapping to zero offset is a worthy endeavor.

---

[1]See Hale [1995] for important papers on the topic DMO. Among the more relevant of these are Artley and Hale [1994], Black et al. [1993], Gardner and Forel [1988, 1995], Hale [1984], Hale and Artley [1993], Liner [1990, 1991], and Dietrich and Cohen [1993].

Wave-Equation Datuming

Seismic data, particularly those acquired in land-based surveys, may have significant traveltime and amplitude distortions due to variations in local topography. Similar distortions owing to hydrophone streamer feathering in ocean surveys may also be seen. Migration codes traditionally have not directly accounted for these topographic and feathering influences, however. To remove the time shifts due to nonuniformity in recording surface elevation, techniques for "downward continuing" seismic data, called *datuming*, were invented [Berryhill, 1979, 1984 and Bevc, 1995, 1999]. The idea is to remap data collected in a source-receiver geometry with topographic variations to the equivalent data set that would have been collected had the survey been conducted at a particular "datum" depth in the absence of topographic variations. (This datum elevation may be above or below the actual elevation of the topography, so the continuation need not be "downward" in all cases.) In this way, datuming produces output that is suitable for migration with a code that does not account for variations of topography.

Offset Continuation and Data Regularization

Traditional migration codes also have not accounted for nonuniform source-receiver spacing within a survey. Such nonuniformity can result from obstacles on the surface of the Earth, the inability to record near a source, dead traces due to mechanical failure of receivers, or naturally nonuniform recording geometry, as in 3D surveys. Indeed, such convenient geometries as common offset, which may be straightforward to obtain in line surveys, may be difficult to realize in 3D data sets. Even if source-receiver pairs with the same offset can be found, there is no guarantee that such pairs will all be oriented in the same direction, as was assumed in our discussion of 3D common-offset inversion in Section 5.1.

The name *offset continuation* is applied to any process that extrapolates data beyond source-receiver positions in a survey, or that rotates data to new source-receiver orientations. Such processes are closely related to *data regularization*, which is the term applied to processing intended to fill in gaps where data are missing, or that are intended correct data for nonuniform source-receiver spacing. These processes, too, fall into the classification of what we call "data mapping."

Fourier Integral Operations That Are *Not* Data Mapping

Not all integral equation–based seismic data preprocessing operations are "data mappings," in the sense we intend to convey. Such processes as *deconvolution*, $\boldsymbol{k}$-domain filtering, τ-p or *slant-stack domain* filtering may, indeed, modify or map data in some sense via a Fourier-like or migration-

like process, but these operations are not wave equation–based and, as such, are not data mappings of the variety we discuss here.

7.1.1 Kirchhoff Data Mapping (KDM)

How can we represent such *data mapping* operations in the theoretical setting developed in the first six chapters of this text? The simple answer is to consider *inverting* the data, via one of our inversion formulas, followed by a process of *remodeling* via an approximate modeling formula of the type that we used as the beginning of our inversion formula derivations. If we have the correct background-wavespeed profile, the output of the cascade of inversion and forward modeling should be expected to have the appropriately corrected amplitude for the new geometry, taking into account all point-source geometrical spreading effects, for example.

Furthermore, because the traveltime curvature contains information about the reflector curvature [Hubral, Tygel, and Schleicher, 1995], we have good reason to expect that our formula will correct for the influence of reflector curvature on the geometrical spreading as well. Indeed, we confirm this expectation in the sequel. Less apparent is the question of what happens to the reflection coefficient as a result of this process. As we show below, the reflection coefficient *does not change.* The reflection coefficient of the input data is preserved in the output data.

This basic idea of cascading two operations is clumsy. In practice, we do not want to perform the cascade of integrals of an inversion formula, followed by an equal number of integrals of a forward-modeling formula. This would be computationally impractical. Indeed, the classical Fourier transform–based DMO method of Hale [1984] has only the form similar to a Kirchhoff migration formula, which is just a single set of integrations (one integration in 2D). Thus, we are justified in expecting something similar for our data mapping formulations as well.

Our intuition from previous problems provides a possible plan of attack. First, we can guess that our final formulas should merely be an integration over the recording surface, meaning that we will assume the form of a Kirchhoff-like integral for the final mapping formula. To this end, we suspect that the method of stationary phase will provide a means of creating estimates of some of the integrals involved, thus reducing the total number of integrations to the desired smaller number. Because we are beginning with a cascade of Kirchoff modeling and inversion formulas, we will naturally call the outcome of such a procedure *Kirchhoff Data Mapping* or KDM.

Our term, KDM, does not describe a single formula, but rather a *general* prescription for transforming data from one prescribed source-receiver configuration and wavespeed profile to another acquisition geometry and possibly different wavespeed model. The specific configurations and/or models dictate the final form of the KDM-based formulas. Note that, in

this description, the wavespeed profile that is assumed for the inversion need *not* be the same as that used for the subsequent remodeling, meaning that KDM has the potential of creating a broad range of different final formulas, covering both geometric and model-based possibilities.

7.1.2 Amplitude Preservation

A point we have stressed throughout the text is the value of amplitude-preserving processing formulas; we make no exception to this rule in this chapter. We consider the preservation of amplitudes in data to be a critical issue with KDM as well. We can expect KDM to be a "true amplitude" process in the following sense.

1. Traveltime and point-source geometrical spreading for the input configuration are transformed to those for the output configuration.
2. Geometrical spreading associated with reflector curvature of the input configuration is transformed to that of the output configuration.

The angularly-dependent reflection coefficient of the input configuration, however, is left unchanged by KDM in the output data, despite the fact that the incidence angle of specular rays is typically changed by the mapping process.

On the other hand, as in Section 5.4.3, the formalism provides a mechanism for determining both the input and the output geometrical-optics incidence angles of the reflection process in these applications. Thus, we have a basis for amplitude-versus-angle (AVA) analysis. Both of these transformations are model consistent, which is to say that they depend on the input and output physical models assumed for the processing. Therefore, if the inversion step is carried out using a background model that does not adequately describe the "true" Earth model, the resulting reflector map will be in error. If the modeling step is carried out with respect to an inaccurate background model, the placement of reflection events on the output trace, as well as their amplitudes, will result in an inaccurate data mapping. Thus, we expect that data mapping will require accurate background models to produce meaningful output. In this sense, data mapping is also model consistent.

7.1.3 A Rough Sketch of the Formulation of the KDM Platform

As mentioned above, the basic idea of the formulation of data mapping is to operate on the data with a cascade of an inversion formula followed by a remodeling formula.

We must take great care to distinguish the input variables $\boldsymbol{\xi}_I$ and ω_I of the original data, from the coordinates of position within the model

produced by the inversion $\boldsymbol{x}$ and, in turn to distinguish these from the final output variables $\boldsymbol{\xi}_O$ and ω_O of the new data. Thus, the inversion part of the process takes data in $\boldsymbol{\xi}_I$ and ω_I and produces an output model in the $\boldsymbol{x}$-variables. The remodeling part of the process converts these model coordinates into new data in the $\boldsymbol{\xi}_O$ and ω_O variables.

While the input data set depends only on the variables of the acquisition geometry and the initial frequency content of the data—the variables $\boldsymbol{\xi}_I$ and ω_I—the full data-mapping operator is a function of the input and output parameters, as well as the reflectivity model variables. That is, data mapping depends on all of the variables introduced above. The idea, then, is to carry out the integration over the Earth modeling variables $\boldsymbol{x}$, asymptotically, to obtain a weight that is a function of the input and output variables only. This weight is then applied to the input data set to produce the output data set. It is this asymptotic analysis alone that can be partially carried out in the absence of an explicit KDM implementation. This is why we use the word "platform," to describe the general form of KDM.

We conduct our formulation in the frequency domain, as we have for all of the formulations of this text.[2] See Bleistein and Jaramillo [2000]. In Chapters 2, 3, and 5, we used the Born-approximate modeling formula to begin our derivations. We found that we had to perform additional analysis to "patch up" the result, to give reflectivity as the output. The reason for this difficulty is that the amplitude of the Born formulation is linearized in the wavespeed perturbation. In Section 5.1.7 we found that the Kirchhoff modeling formula is a better starting point, because the amplitudes in this formula are linearized in terms of the reflection coefficient, directly.[3] For this reason, our remodeling formula will be the Kirchhoff modeling formula.

Our derivation below is based on a single reflector model, requiring a good estimate of the Earth parameters above the reflector of interest. It neglects multiple reflections, as do all methods for data mapping (including classic DMO) to date. The approach used here *does* allow for larger jumps in medium parameters across the reflector of interest than would the Born approximation, however. In the absence of multi-pathing,[4] the interpretation of the output in terms of the geometrical-optics reflection coefficient is direct and immediate in this approach.

---

[2]See Tygel et al. [1998], Jaramillo [1998], and Jaramillo and Bleistein [1998, 1999] for a time-domain formulation of data mapping.

[3]The reader should remember, however, that the reflection coefficient, itself is a *nonlinear* function of the medium parameter perturbations.

[4]Multi-pathing refers to the situation in which more than one raypath from a point at depth reaches the same point in the source receiver domain, on either input or output. Multi-pathing is neglected in the discussion here, as it has been in the rest of the text.

7.1.4 Possible Kirchhoff Data Mappings

We use the term "macro-model" to denote the background-wavespeed profile(s) used for the respective inversion and remodeling phases of the data mapping process. The reason for this choice of terminology is that we wish to make a distinction between these "models," and the "model" that is the output of the inversion process.

Below is a list some possible mappings of data sets from an input macro-model and a given source-receiver configuration, to an output macro-model and new source-receiver configuration. We expect that all of these operations can be carried out in 2D, 2.5D, and 3D:

1. **Offset continuation and TZO.** KDM is not limited to transforming nonzero offset data to zero-offset; the formula lends itself to analysis of the transformation of data from one offset to another, with TZO as a special case. That is, (7.2.6) and (7.3.4), below, provide a platform for *offset continuation* along the lines of Fomel [1995a,b, 1996, 1997] and Fomel et al. [1996]. However, as soon as we apply the type of asymptotic analysis that leads to the classical NMO/DMO-type data mapping formulas to the platform equations, the mapping requires "large" (in units of reciprocal wavenumber) change in offset to be valid.
2. **Transformation of common-offset data to common-shot data.** In this case, the transformed data represent the response from a single shot at an array of receivers covering the upper surface, except for the fact that the reflection coefficient has the wrong incidence angle for the common-shot data. This could be corrected by processing data from all offsets, estimating input and output reflection coefficient, and matching them—that is, extracting the output data from the input data at an offset that makes the input and output incidence angles be the same. Such data have the advantage that they are the solution of the wave equation, whereas common-offset (and zero-offset) data are a collection of single responses to an ensemble of wave equations, one for each shot. These ensemble data do not constitute a solution of the wave equation, although they are treated as such in certain types of *wave-equation migration*, under the assumption that the data were generated at exploding reflectors. See Section 3.8.
3. **Mapping of data from variable-background propagation parameters to constant-background parameters.** Time sections in constant-background media are easier to interpret. It is not clear to us at this point, however, how multi-paths will map, nor how data from vertical and overhanging reflectors will map; we do not treat these cases here, but propose them in this list as open research topics. We expect singularities of the mapping process for such cases. On the other hand, where the method works, it opens the mapped data set to a much broader suite of applicable migration/inversion programs and related analysis techniques.

4. **"Unconverting" mode-converted waves.** For example, one could map the scalar components of P-SV data to the scalar components of P-P data [Chen and Stewart, 1996]. If the "true" P-P data were available, a comparison of this latter data set with the mapped data set could provide a check on the assumptions made in the macro-model for the converted wave propagation. Furthermore, again, there are many more processing options available for P-P data than for mode-converted data. This mapping would provide a means of extending the range of processing options once the data are mapped.
5. **Velocity analysis.** When data from a suite of offsets are all mapped to zero-offset, events should line up. To the extent that they do not, they provide the same type of information about velocity errors as does a common trace gather of a suite of prestack migrations/inversions.
6. **Wave-equation datuming.** The acquisition surface can be changed for both the sources and receivers. Downward continuation of sources and receivers or mapping from irregular acquisition topography to a planar topography, are two potential datuming applications for this platform [Sheaffer and Bleistein 1998]. For small increments in depth, the implementation of KDM provides an alternative to phase shift migration [Gazdag and Sguazzero, 1984], while for larger increments in depth, the implementation of KDM provides an alternative to wave equation datuming [Berryhill 1979, 1984, and Bevc 1995, 1999].
7. **Data regularization.** Data collected with uneven source-receiver spacing could be converted to equivalent uniformly spaced data.
8. **Mapping of swath data to a single line at zero azimuth.** Swath shooting is a process whereby multiple lines of receivers are used with a single shot, as might occur if a boat were to tow more than one line of hydrophones. The data from the separate lines could each be mapped to a single line that could be "straightened" to be along the line of the survey—given sufficient information about the deviation of the swath survey from that line and about the path of the boat [Biondi and Chemingui, 1994].
9. **Combinations of the above.** For example, consider the application of downward continuation of receivers (or sources). The continuation process always yields output data over a shorter line than that of the input data. Starting from a prescribed shot gather with a given cable length of receivers, the cable length of asymptotically accurately mapped data decreases from the input cable length with increasing depth. On the other hand, consider first creating a single common-shot data set from the full array of common-offset gathers. This new data set effectively has a "cable length" equal to the length of the survey, typically much longer than the cable length for each shot. Now, the range of validity of the downward continuation of receivers "shrinks" from an initial length equal to the survey length. One can expect that the data could be continued much deeper into the subsurface while adequately maintaining

properly transformed geometrical spreading and traveltime corrections over a cable length that will be of sufficient length to make further processing possible. As a second example of cascading, consider the process of first downward continuing the receivers and then downward continuing the sources. This should provide the equivalent of true amplitude, simultaneous downward-continuation of sources and receivers.

In part, the reader should view this as a statement of what we plan to present in the rest of the chapter. In part, however, this is a "wish list," based on what we believe are reasonable expectations based on our current familiarity with this type of problem. We have a few examples worked out in great detail, which we do present. Others simply have not been addressed, as yet. Furthermore, because this is relatively new material, we must investigate and justify the methods we use. We present these justifications as well. The reader must remember that we are avoiding some important issues. These include the influences of multi-pathing, multiple scattering, and the differences between (anisotropic) elastic wave theory and the scalar wave theory we employ.

Accordingly, this chapter proceeds as follows. In the next section, we derive the fundamental three dimensional KDM platform equation, discussing both the spatial and frequency structure of the resulting formula, and derive formulas for determining the cosine of the incidence angles in the input and output geometries.

In Section 7.3, we specialize our KDM platform to 2.5D. In the next section we test our results on Kirchhoff data, presenting details of the asymptotic analysis of our results. In Section 7.5 we present an example of KDM applied to the problem of datuming common-shot data. We discuss 2.5D transformation to zero-offset (TZO), deriving formulas similar to the dip moveout formulas of Hale and of Gardner and Forel. In Section 7.7 we return to our 3D formulation of KDM and derive 3D TZO representations, concluding our exposition.

7.2 Derivation of a 3D Kirchhoff Data Mapping Formula

Here, we derive the fundamental equation for space-frequency domain KDM in 3D. This will be done by cascading a Kirchhoff-approximate forward modeling formula with an inversion formula. Crucial to this analysis is the representation of the Kirchhoff modeling formula as a *volume* integral in which the only unknown from the point of view of the inverse problem will be the reflectivity function described in the introduction. That modeling formula was developed in Section 5.1.7, specifically equation (5.1.54). However, we need to rewrite that equation in the variables of the type described above.

The Remodeling Formula

The Kirchhoff modeling representation we will use is

$$u_O(\boldsymbol{\xi}_O, \omega_O) \sim -i\omega_O F(\omega_O) \int a_O(\boldsymbol{x}, \boldsymbol{\xi}_O) |\nabla_x \tau_O(\boldsymbol{x}, \boldsymbol{\xi}_O)| \beta(\boldsymbol{x}) e^{i\omega_O \tau_O(\boldsymbol{x}, \boldsymbol{\xi}_O)} d^3x. \tag{7.2.1}$$

In this equation, the subscript O is used to denote output variables. Below, input variables with subscript I will be introduced. The two-component vector $\boldsymbol{\xi}_O$ is used to parameterize the source and receiver locations $\boldsymbol{x}_s(\boldsymbol{\xi}_O)$ and $\boldsymbol{x}_g(\boldsymbol{\xi}_O)$, respectively, and ω_O denotes the frequency of the output wave. The traveltime and amplitude are given by

$$\begin{aligned} \tau_O(\boldsymbol{x}, \boldsymbol{\xi}_O) &= \tau(\boldsymbol{x}, \boldsymbol{x}_s(\boldsymbol{\xi}_O)) + \tau(\boldsymbol{x}, \boldsymbol{x}_g(\boldsymbol{\xi}_O)), \\ a_O(\boldsymbol{x}, \boldsymbol{\xi}_O) &= A(\boldsymbol{x}, \boldsymbol{x}_s(\boldsymbol{\xi}_O)) \cdot A(\boldsymbol{x}, \boldsymbol{x}_g(\boldsymbol{\xi}_O)), \end{aligned} \tag{7.2.2}$$

with the separate traveltimes and amplitudes being solutions of appropriate eikonal and transport equations, respectively, for initial point $\boldsymbol{x}_s$ or $\boldsymbol{x}_g$ and final point $\boldsymbol{x}$. We choose not to be more specific here, allowing for different propagation speeds in the eikonal equations (including mode conversions) and transport equations appropriate to the degree of generality of the propagation model under consideration. The amplitudes can also include products of transmission coefficients arising from interfaces above the reflecting surface.

The Inversion Formula

We now want to use an inversion formula for $\beta(\boldsymbol{x})$, but express the result in terms of the input acquisition geometry and data. The formula we need is given in equation (5.1.56). Written in a set of variables consistent with this discussion, the reflectivity function is given by

$$\beta(\boldsymbol{x}) = \frac{1}{8\pi^3} \int d^2\xi_I \frac{|h(\boldsymbol{x}, \boldsymbol{\xi}_I)|}{a_I(\boldsymbol{x}, \boldsymbol{\xi}_I) |\nabla_x \tau_I(\boldsymbol{x}, \boldsymbol{\xi}_I)|} \int i\omega_I \, d\omega_I \, e^{-i\omega_I \tau_I(\boldsymbol{x}, \boldsymbol{\xi}_I)} u_I(\boldsymbol{\xi}_I, \omega_I). \tag{7.2.3}$$

In this equation, the subscript I is used to denote input variables (that is, the variables of the original acquisition geometry and data). The two-component vector $\boldsymbol{\xi}_I$ is used to parameterize the respective source and receiver of the input data, $\boldsymbol{y}_s(\boldsymbol{\xi}_I)$ and $\boldsymbol{y}_g(\boldsymbol{\xi}_I)$. In addition, ω_I denotes the frequency of the input wave. The traveltime and amplitude are given by

$$\begin{aligned} \tau_I(\boldsymbol{x}, \boldsymbol{\xi}_I) &= \tau(\boldsymbol{x}, \boldsymbol{y}_s(\boldsymbol{\xi}_I)) + \tau(\boldsymbol{x}, \boldsymbol{y}_g(\boldsymbol{\xi}_I)); \\ a_I(\boldsymbol{x}, \boldsymbol{\xi}_I) &= A(\boldsymbol{x}, \boldsymbol{y}_s(\boldsymbol{\xi}_I)) \cdot A(\boldsymbol{x}, \boldsymbol{y}_g(\boldsymbol{\xi}_I)). \end{aligned} \tag{7.2.4}$$

The traveltimes and amplitudes are again solutions of the eikonal and transport equations, except that now the initial points will be chosen to be $\boldsymbol{y}_s(\boldsymbol{\xi}_I)$ and $\boldsymbol{y}_g(\boldsymbol{\xi}_I)$. Furthermore,

$$h(\boldsymbol{x}, \boldsymbol{\xi}_I) = \det \begin{bmatrix} \nabla_x \tau(\boldsymbol{x}, \boldsymbol{\xi}_I) \\ \dfrac{\partial}{\partial \xi_{I1}} \nabla_x \tau(\boldsymbol{x}, \boldsymbol{\xi}_I) \\ \dfrac{\partial}{\partial \xi_{I2}} \nabla_x \tau(\boldsymbol{x}, \boldsymbol{\xi}_I) \end{bmatrix} \tag{7.2.5}$$

is the Beylkin [1985] determinant of equation (5.1.17), rewritten in variables appropriate to this discussion.

The Kirchhoff Data-Mapping Platform Formula

Now, we are prepared to write down a formula to map data from the input variables $(\boldsymbol{\xi}_I, \omega_I)$, to the output variables, $(\boldsymbol{\xi}_O, \omega_O)$. To achieve this, the inversion formula that describes the physical model in terms of the input variables, (7.2.3), is substituted into the data modeling formula in the output variables (7.2.1). The result is the following representation for the mapping of data from any input source-receiver configuration and background model to an alternative output source-receiver configuration and background model:

$$\begin{aligned} u_O(\boldsymbol{\xi}_O, \omega_O) \sim -\frac{i\omega_O}{8\pi^3} \int i\omega_I \, d\omega_I \, d^2\xi_I \, u_I(\boldsymbol{\xi}_I, \omega_I) \\ \cdot \int \frac{a_O(\boldsymbol{x}, \boldsymbol{\xi}_O)}{a_I(\boldsymbol{x}, \boldsymbol{\xi}_I)} \frac{|\nabla_x \tau_O(\boldsymbol{x}, \boldsymbol{\xi}_O)|}{|\nabla_x \tau_I(\boldsymbol{x}, \boldsymbol{\xi}_I)|} \\ \cdot |h(\boldsymbol{x}, \boldsymbol{\xi}_I)| e^{[i\omega_O \tau_O(\boldsymbol{x}, \boldsymbol{\xi}_O) - i\omega_I \tau_I(\boldsymbol{x}, \boldsymbol{\xi}_I)]} d^3x. \end{aligned} \tag{7.2.6}$$

Note that the input data in the first line here are independent of the Earth-modeling variables $\boldsymbol{x}$. Hence, for each choice of input and output Earth model and each choice of input and output source-receiver configuration, the integrations over $\boldsymbol{x}$ in the second and third lines could be carried out to obtain an operator kernel that is a function of $\boldsymbol{\xi}_I$, ω_I, $\boldsymbol{\xi}_O$, and ω_O. Indeed, we anticipate carrying out those integrations by analytical methods, including asymptotic methods, such as multidimensional stationary phase. Numerical integration is out of the question, owing to the large computational effort required. There are $O(n^3)$ coordinates of integration, with $O(n^3)$ input variables and $O(n^3)$ output variables. Clearly, the n's are different, but this is still an intractably large set of variables. The processing of this formula would require an integration over $O(n^6)$ for each choice of $O(n^3)$ output variables.

A better choice is to employ asymptotic analysis to the volume integral represented by the second and third line to obtain an analytically explicit kernel that depends only on the input and output variables, $\boldsymbol{\xi}_I$, ω_I, $\boldsymbol{\xi}_O$, and ω_O. However, we cannot proceed with that analysis until we know more about the source-receiver configurations and the background models, for

both input and output. It is in this sense that (7.2.6) is only a platform—a point of departure for further analysis for specific data mappings.

In the specific example of 2.5D DMO [Bleistein et al., 1999], data mapping did *not* transform the reflection coefficient of the input data configuration to the reflection coefficient of the output configuration, so this should not be expected in the general result here, either. We do anticipate, however, that geometrical spreading and curvature effects for the input configuration will be transformed to the correct behavior for the output configuration, as was true for the case of 2.5D DMO. [5]

7.2.1 Spatial Structure of the KDM Operator

There is a certain amount of symmetry, some of which could have been predicted in advance, in the spatial structure of the KDM operator. The geometrical spreading of the input data is "undone" by the division by a_I, while the geometrical spreading of the output is introduced through the multiplication by a_O. Similarly, the obliquity factor in the input data, expressed through the factor $|\nabla_x \tau_I(\boldsymbol{x}, \boldsymbol{\xi}_I)|$ is undone by the division in (7.2.6), while the obliquity of the output data is introduced through multiplication by a similar gradient factor in the numerator.

Because our representation is in the frequency domain, the arrival time of the input data manifests itself in the phase of the exponentials. This is undone by the multiplication by the negative of the input traveltime times the input frequency in the phase of the operator. Similarly, the positive product of output frequency and output traveltime in the phase of the operator introduces the "correct" arrival time on output. All of these variables are evaluated at stationarity of the integrand. In the simplest of such evaluations, the determinant of the Hessian (the matrix of second derivatives) evaluated at the stationary point, will correct for the influence of curvature from input to output data.

The symmetry that we see here is undone only by the Beylkin determinant and the powers of ω_I and ω_O. The key to seeing this result in symmetric form is to exploit the interpretation of h as a Jacobian of a transformation of coordinates between $(\omega_I, \boldsymbol{\xi}_I)$ and a local wave vector $\boldsymbol{k}$ as described in Section 5.1, equations, (5.1.13) through (5.1.17).

Similarly, then, in (7.2.3), the inversion is asymptotically a Fourier inversion with respect to some wave vector $\boldsymbol{k}$, although the integration is over variables $\boldsymbol{\xi}_I$ and ω_I. Thus, in (7.2.3) and in (7.2.6) the factor of h arises through the identity

$$d^3k = \left| \frac{\partial(\boldsymbol{k})}{\partial(\boldsymbol{\xi}, \omega_I)} \right| d^2\, \xi_I\, d\omega_I = \omega_I^2\, |h(\boldsymbol{x}, \boldsymbol{\xi}_I)|\; d^2\xi_I\, d\omega_I.$$

---

[5] In fact, this has been proven by Tygel et al. [1998], using a somewhat different (time-domain) approach to the same problem.

In fact, if h in (7.2.6) is replaced by the Jacobian appearing on the right side of this equation, then the remaining frequency dependence of the operator becomes ω_O/ω_I and has the same quotient symmetry and explanation as do the spatial factors discussed above. That is,

$$u_O(\boldsymbol{\xi}_O,\omega_O) \sim -\frac{1}{8\pi^3}\int \frac{\omega_O}{\omega_I} u_I(\boldsymbol{\xi}_I,\omega_I)d^3k \cdot \int \frac{a_O(\boldsymbol{x},\boldsymbol{\xi}_O)}{a_I(\boldsymbol{x},\boldsymbol{\xi}_I)} \frac{|\nabla_x \tau_O(\boldsymbol{x},\boldsymbol{\xi}_O)|}{|\nabla_x \tau_I(\boldsymbol{x},\boldsymbol{\xi}_I)|} \cdot e^{[i\omega_O\tau_O(\boldsymbol{x},\boldsymbol{\xi}_O)-i\omega_I\tau_I(\boldsymbol{x},\boldsymbol{\xi}_I)]}d^3x, \tag{7.2.7}$$

with the change of variables from $\boldsymbol{\xi}_I, \omega_I$ to $\boldsymbol{k}$ defined above. Note also that the Beylkin determinant has been "absorbed" into the definition of $\boldsymbol{k}$ and no longer explicitly appears in this form. That is, if we were to distribute the sources, receivers and frequency samples over a grid that was uniform in $\boldsymbol{k}$, there would be no need for the Beylkin determinant, in either the inversion formulas or the data mapping formulas!

Unfortunately, data generally are not uniform in this fashion, and it is not likely that such full data sets of this form will become available in the near future. Nevertheless, we might consider forming "common-$\boldsymbol{k}$," *common-angle*, or *common image-point* gathers in data sets with sufficient coverage. This would likely be done for specific purposes, such as amplitude versus angle (AVA) analysis, or to study localized regions in the subsurface. The issue becomes one of being able to sort data efficiently, because the drawback is that a different data sorting is needed for each output point in the image [de Hoop and Brandesberg-Dahl, 2000]; [de Hoop, Spencer, and Burridge, 1999].

7.2.2 Frequency Structure of the Operator and Asymptotic Preliminaries

We can anticipate an aspect of the asymptotic analysis from the form of result (7.2.6) alone. On the right side of the equation, there are two factors of frequency, $\omega_O \cdot \omega_I$—crudely speaking, the right side is explicitly quadratic in frequency. The amplitude of 3D point-source data has no power of frequency in its asymptotic (WKBJ) representation, and the same should be true for the output. So, the left side of the equation is of zero order in frequency. The two sides should balance.

Each spatial integral on the right that is carried out by stationary phase will produce an inverse power of the square root of frequency, if they are approximated by simple[6] stationary point contributions. There are five

[6] A stationary point of a single integral is simple if the first derivative is zero, but the second derivative is not. In higher dimensions, all first derivatives are zero, but the matrix of second derivatives must have nonzero determinant.

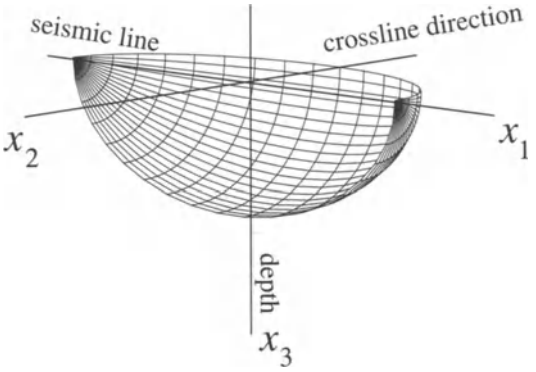

FIGURE 7.1. Example of an isochron surface: constant-background, offset source and receiver. This isochron would arise in common-offset or common-shot source-receiver configurations.

such integrations to be performed. If all were approximated by the method of stationary phase, the resulting divisor would be of order 5/2 in frequency. Taking account the explicit quadratic frequency dependence of the integrand, that leads to a result that is of order $-1/2$ in frequency, not balancing the frequency dependence of the left side (order zero). Thus, *not all of the spatial integrals can be estimated by simple stationary point contributions* because the resulting power of ω on the two sides of the equation will not match. Clearly, then, some other method besides stationary phase must play a role in the analysis of this integral operator.[7]

Isochrons

The natural geometry of the problem comes into play. We express this natural geometry through the interaction of the *isochrons*, that is to say, the surfaces of equal traveltime, associated with the respective inversion and remodeling formulas that we have cascaded to form the data mapping. See Figure 7.1.

Suppose, for the moment, that the first two integrals are carried out by the method of stationary phase, with the last integral in the direction of increasing traveltime analyzed separately. In general, an isochron of τ_I is cut by the isochrons of τ_O. It is fairly straightforward[8] to show that

[7]It is in this context that Tygel et al. [1998] employ a different approach. Consider the integral over the interior variables, represented by the differential d^3x. Ultimately, this integral is recast as an integral over the isochrons of the input configuration, say, $\tau_I(\boldsymbol{x}, \boldsymbol{\xi}_O) = \text{constant} = t_I$, followed by integration over t_I. See Figure 7.2.

[8]This is shown in 2.5D in Section 7.4.2 and in 3D in Section 7.7.1

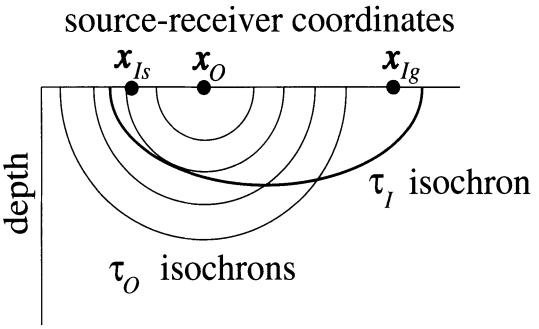

FIGURE 7.2. A 2.5D example of an isochron of the input source-receiver configuration intersected by isochrons of the output source-receiver configuration. Here, we have used the ellipse and circles of TZO, the transformation of common-offset data to zero-offset data, with a constant-background wavespeed.

stationarity occurs when the normals of the two traveltimes line up; that is, the phase is stationary when *the isochron of τ_O is tangent to the isochron of τ_I*. See Figure 7.2 for an example. Suppose, for some such stationary point, there was a reflector at that point in space whose normal also lines up with this common normal of the two isochrons. The matching of the reflector normal and the isochron normal (for either the input or output data set) is equivalent to the law of reflection for the incident and reflected rays in either the input or output source receiver configuration. Thus, if we always map data through the rule that the isochron normals must be collinear, we assure that a specular return in the input configuration will always be mapped—at least kinematically—to a specular return in the output configuration. This observation generalizes a known feature of NMO/DMO processing.

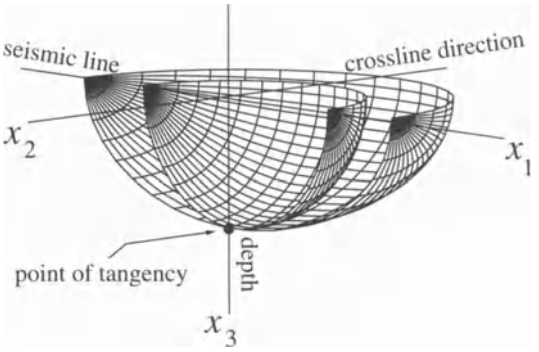

FIGURE 7.3. A point of tangency of isochrons from two traveltime functions, corresponding to a simple stationary point in the integration over an isochron.

Figure 7.3 depicts this tangency occurring at a single point at the center of the front edge of the two isochrons. This corresponds to a simple stationary point in the integral over the isochron, and the estimates of the asymptotic order of the stationary phase evaluation proceed as described above. In the simplest of situations, however, offset continuation and TZO/DMO in constant-background, this is not what occurs. In such a medium, the isochrons are surfaces of revolution. They can be determined by taking the isochron in the vertical plane below the source and receiver and rotating about the line containing the source and receiver.

Failure of Stationary Phase

For constant-background KDM, consider the mapping from input to output source-receiver configurations along parallel lines. In Section 7.7.3, we consider this special case of KDM and show that there are no stationary points unless the out-of-plane input and output variables are the same, which is to say, $\xi_{I2} = \xi_{O2}$; that analysis is the same for all such mappings. Now, the input and output sources and receivers will all lie along the same line. In this case, the isochrons are surfaces of revolution with the same axis, $\xi_{I2} = \xi_{O2}$. If the normals to the isochrons are collinear at one point, they will remain collinear along the entire *curve* of revolution through that point and there is an entire *curve* of stationary points, rather an isolated stationary point.

In this case, the ordinary method of stationary phase in two dimensions will not apply. In fact, all directional derivatives in the direction of the curve of revolution at the stationary point will vanish if the first derivative vanishes. See Figure 7.4. Thus, asymptotically, the ξ_{I2} integration behaves like a delta function and the integration in the direction of the generating curve of revolution. The order of the stationary point in this case is infinite. This is a manifestation of a known fact about 3D DMO/TZO in constant-background (but now stated for a more general class of data mappings):

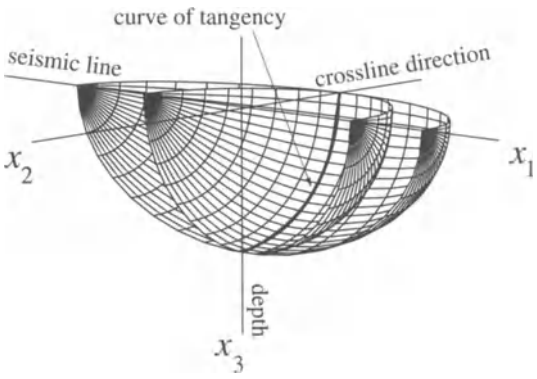

FIGURE 7.4. Tangency of isochrons along a curve of revolution.

while the kinematics of 3D DMO/TZO are straightforward, its dynamics are not, and determination of amplitude dependence of the operator requires great care.

Where Uniform Asymptotics is Required

This also should serve as a warning about 3D processing for nonconstant background. Suppose that the propagation speeds of the model are nearly constant. Then, formally, the straightforward multidimensional stationary phase described at the beginning of this section will seem to work. However, with all derivatives vanishing in the limit of zero gradient in the direction of the curve of near-revolution, in particular, the second derivative in that direction will be small; indeed, it approaches zero with the gradient of the propagation speeds. In this case, the validity of the asymptotic expansion in terms of simple stationary points relies on that second derivative being bounded away from zero. Thus, there will be some lower bound on this second derivative, and hence also a lower bound on the gradient of the propagation speed, beyond which the asymptotic expansion in terms of simple stationary points will no longer be valid in the sense that the derived amplitude will be inaccurate (although the mapping of traveltimes will still be correct). Thus, to obtain a data mapping formula that yields accurate dynamics as well as accurate kinematics, with decreasing gradient of the propagation speeds, *uniform asymptotic analysis* is required.

More generally, for the problem of offset continuation, a similar pathology occurs. If the offset difference is small, then the two isochrons are quite similar. Again, near-total contact at stationarity will imply a small determinant of the matrix of second derivatives arising in the denominator of the stationary phase formula. In this case, the asymptotics break down again, yielding a result for which the kinematics is right, but the dynamics is not. For example, TZO or its constant-background equivalent, NMO/DMO, is an asymptotic result that requires this type of stationary phase calculation. Thus, true amplitude offset continuation through small offsets cannot be achieved through the same process that produces this constant background results. Here, at the time of this writing, the alternative method for offset continuation of Fomel [1995a,b, 1996, 1997] and Fomel et al. [1996] is the method of choice.

7.2.3 Determination of Incidence Angle

When the input data are dominated by isolated specular reflection returns, the output will be dominated by such returns, as well. Asymptotically, in this case, the cascade of integrals is dominated by stationary phase contributions where the isochrons of the input and output traveltimes are tangent and share the same normal direction. This direction is also normal to the reflector at the specular point. In the absence of mode conversion,

at this specular point,

$$|\nabla_x \tau_I(\boldsymbol{x}, \boldsymbol{\xi}_I)| = \frac{2\cos\theta_I}{c(\boldsymbol{x})}, \qquad |\nabla_x \tau_O(\boldsymbol{x}, \boldsymbol{\xi}_O)| = \frac{2\cos\theta_O}{c(\boldsymbol{x})},$$

where $2\theta_I$ and $2\theta_O$ are the opening angles between the incident rays of the input and output source/receiver configurations at the point $\boldsymbol{x}$. Thus, we introduce two other KDM operators,

$$\cos_I = -\frac{1}{8\pi^3}\int |\nabla_x \tau_I(\boldsymbol{x}, \boldsymbol{\xi}_I)|(\cdots), \qquad \cos_O = -\frac{1}{8\pi^3}\int |\nabla_x \tau_O(\boldsymbol{x}, \boldsymbol{\xi}_O)|(\cdots).$$

Here, $(\cdots)$ denotes the three lines of (7.2.6) beyond the integral sign. Then, the ratios of outputs,

$$\frac{\cos_I}{u_I(\boldsymbol{\xi}_O, \omega_O)}, \qquad \frac{\cos_O}{u_O(\boldsymbol{\xi}_O, \omega_O)},$$

will provide asymptotic estimates of $2\cos\theta_I/c_I(\boldsymbol{x})$ and $2\cos\theta_O/c_O(\boldsymbol{x})$, thereby providing estimates of θ_I and θ_O, respectively. This is simply a repeat of the method introduced in Section 5.1.6, except that we have allowed for the possibility that the background wavespeed for the input model and the output model might be different.

7.3 2.5D Kirchhoff Data Mapping

In this section, we discuss the specialization of our KDM platform for 2.5D processing. We begin by recalling the appropriate *thought experiment* from which to derive this 2.5D counterpart of (7.2.6).

> Consider a medium in which the propagation speed and other medium parameters are independent of one transverse direction, say x_2. It is further assumed that the input data is gathered on lines of constant x_2, say, $x_2 = \xi_{I2}$. Finally, consider an output source-receiver configuration that is also confined to lines of constant value of this out-of-plane coordinate. In this case, the input data are independent of the out-of-plane variable, ξ_{I2}, and the integration in ξ_{I2} and in x_2 can be carried out by the method of stationary phase.

Actually, it is easiest to apply the stationary phase analysis in ξ_{I2} first, and then in x_2 as iterated integrals, rather than to do them together as a two-dimensional stationary phase calculation. The analysis has already been carried out in Section 6.2, so we need only briefly describe the main features in this modified application of the same technique [Bleistein et al., 1999].

For the integration in ξ_{I2}, the phase to be considered is $\tau_I(\boldsymbol{x}, \boldsymbol{\xi}_I)$. The stationary point in ξ_{I2} is at $\xi_{I2} = x_2$, and the second component of the gradient of the phase is zero at this point. Furthermore, similar to the result in (6.2.4),

$$\left.\frac{\partial^2 \tau_I}{\partial \xi_{I2}^2}\right|_{\xi_{I2}=x_2} = \frac{1}{\sigma_{Is}} + \frac{1}{\sigma_{Ig}}. \tag{7.3.1}$$

In this equation, σ_{Is} (σ_{Ig}) is a running ray parameter along the ray from the source (receiver) to the scattering point $\boldsymbol{x}$.

When this value of ξ_{I2} is substituted into the phase $\tau_I(\boldsymbol{x}, \boldsymbol{\xi}_I)$, the resulting phase is independent of x_2. This makes the second stationary phase analysis easier, because we only have to consider the phase, $\tau_O(\boldsymbol{x}, \boldsymbol{\xi}_O)$. The analysis on this phase again proceeds as described in Section 6.2. In this case, stationarity requires that $x_2 = \xi_{O2}$, essentially eliminating the out-of-plane coordinates from further consideration. All second component variables take on the same value. Note that this is exactly as occurred in the derivation of the 2.5D inversion in Section 6.2.

Finally, the Beylkin determinant, (7.2.5), also becomes simpler in this case, as in (6.2.7). It is given by

$$h(\boldsymbol{x}, \boldsymbol{\xi}_I) = \left[\frac{1}{\sigma_{Is}} + \frac{1}{\sigma_{Ig}}\right] H(\boldsymbol{x}, \xi_I), \tag{7.3.2}$$

with

$$H(\boldsymbol{x}, \xi_I) = \det \begin{bmatrix} \nabla_x \tau(\boldsymbol{x}, \xi_I) \\ \dfrac{\partial}{\partial \xi_I} \nabla_x \tau(\boldsymbol{x}, \xi_I) \end{bmatrix}. \tag{7.3.3}$$

In this last equation, the gradient is a two-component operator in (x_1, x_3) and ξ_I is a scalar variable.

Applying the method of stationary phase to the integral in (7.2.6) in both variables and taking account of the results stated above leads to the following 2.5D analog of that earlier result:

$$\begin{aligned} u_O(\xi_O, \omega_O) \sim \frac{\sqrt{|\omega_O|} e^{-i\pi \operatorname{sgn}(\omega_O)/4}}{4\pi^2} \int \sqrt{|\omega_I|} e^{i\pi \operatorname{sgn}(\omega_I)/4} d\omega_I d\xi_I u_I(\xi_I, \omega_I) \\ \cdot \int \frac{a_O(\boldsymbol{x}, \xi_O)}{a_I(\boldsymbol{x}, \xi_I)} \frac{|\nabla_x \tau_O(\boldsymbol{x}, \xi_O)|}{|\nabla_x \tau_I(\boldsymbol{x}, \xi_I)|} \frac{\sqrt{\sigma_{Is} + \sigma_{Ig}}}{\sqrt{\sigma_s + \sigma_g}} \frac{\sqrt{\sigma_s \sigma_g}}{\sqrt{\sigma_{Is} \sigma_{Ig}}} \\ \cdot |H(\boldsymbol{x}, \xi_I)| \cdot e^{[i\omega_O \tau_O(\boldsymbol{x}, \xi_O) - i\omega_I \tau_I(\boldsymbol{x}, \xi_I)]} d^2x. \end{aligned} \tag{7.3.4}$$

In this equation, we have rewritten ξ_I for ξ_{I1} and ξ_O for ξ_{O1}, because the second component is no longer in the representation and the formerly two component vectors are now scalars.

Equation (7.3.4) provides a platform for mapping data from any (curvi)linear input source-receiver configuration and input medium parameters to data from a (curvi)linear output source-receiver configuration and output medium parameters. It is a 2.5D transformation, meaning that it accounts for 3D geometrical spreading, but assumes modeling parameters that are only 2D, in that they do not depend on the out-of-plane variable.

As with the 3D data mapping formula, (7.2.6), we view this result as a platform for further analysis when a particular data mapping is prescribed. As in the former 3D result, for each choice of source-receiver configuration and medium parameters of input and output, this integral should be carried out in advance, preferably analytically, invoking asymptotic methods as appropriate. Then, for a given data set, one would only need to process the line of data by carrying out the integrals in the first line employing the simplified weighting function obtained by the preprocessing analysis of the second and third lines. This is the usual form of TZO (NMO/DMO), for example.

Exercises

7.1 Carry out the details of the derivation of (7.3.4) from (7.2.6) by the method outlined in the text. Draw liberally on the 2.5D calculations in Chapter 6.

7.2 Derive a 2.5D version of the forward modeling formula (7.2.1). Rewrite the inversion formula (6.2.8) in the appropriate output variables, analogous to the result (7.2.3). Then, substitute this representation for β into the 2.5D modeling result previously derived and obtain (7.3.4).

7.3.1 Determination of Incidence Angle

Because 2.5D processing is really a special case of 3D processing, the technique that we proposed in the previous section works here as well. The changes that must be made are as follows. First, the processing for the cosines must be based on (7.3.4), above. That means we must introduce two new 2.5D integral operators,

$$\begin{aligned} \cos_I &= \frac{\sqrt{|\omega_O|}e^{-i\pi\,\mathrm{sgn}\,(\omega_O)/4}}{4\pi^2}\int |\nabla_x \tau_I(\boldsymbol{x},\boldsymbol{\xi}_I)|(\cdots), \\ \cos_O &= \frac{\sqrt{|\omega_O|}e^{-i\pi\,\mathrm{sgn}\,(\omega_O)/4}}{4\pi^2}\int |\nabla_x \tau_O(\boldsymbol{x},\boldsymbol{\xi}_O)|(\cdots), \end{aligned} \tag{7.3.5}$$

with $(\cdots)$ now representing everything beyond the integral sign in (7.3.4).

Then, again, the ratios of outputs, $\cos_I/u_I(\boldsymbol{\xi}_O,\omega_O)$, $\cos_O/u_O(\boldsymbol{\xi}_O,\omega_O)$, will provide asymptotic estimates of $2\cos\theta_I/c$ and $2\cos\theta_O/c$, respectively. Thereafter, the discussion proceeds as at the end of the last section.

7.4 Application of KDM to Kirchhoff Data in 2.5D

In this section, we analyze the application of the 2.5D KDM platform equation (7.3.4) to 2.5D Kirchhoff data. That application leads to 2.5D Kirchhoff data again, but with the input variables of the test data transformed to output variables. In the earlier discussion, below equation (7.2.6), we claimed that it was only the leading-order asymptotic output of our integral processing that would provide the output data mapping we seek. That is what we show here by using the method of stationary phase to examine the cascade of the data mapping platform formula to Kirchhoff-approximate data. We do so only for the 2.5D case, equation (7.3.4), because the analysis is simpler, but shows the essence of this asymptotic analysis.

To begin, define the reflector S_R through the curve,

$$\boldsymbol{x} = \boldsymbol{x}_R(\ell), \quad \boldsymbol{x}_R = (x_{R1}, x_{R3}). \tag{7.4.1}$$

Here, with no loss of generality, ℓ can be taken to be arclength along this curve, which defines the reflector. The 2.5D Kirchhoff approximate data for the upward reflected field was derived in Chapter 6, in Exercise 6.6 given by equation (6.2.10). With appropriate modifications of notation to reflect the discussion above, that representation is

$$\begin{aligned} u_I(\xi_I, \omega_I) = -\sqrt{|\omega_I|}e^{-i\pi\,\mathrm{sgn}\,(\omega_I)/4}F(\omega_I)\int R(\boldsymbol{x}_R(\ell), \boldsymbol{x}_s(\xi_I)) \\ \cdot \hat{\boldsymbol{n}}_R \cdot \nabla_x \tau_I(\boldsymbol{x}_R(\ell), \xi_I) a_I(\boldsymbol{x}_R, \xi_I) \\ \cdot \frac{\sqrt{\sigma_{Is}(\boldsymbol{x}_R, \xi_I)\sigma_{Ig}(\boldsymbol{x}_R, \xi_I)}}{\sqrt{\sigma_{Is}(\boldsymbol{x}_R, \xi_I) + \sigma_{Ig}(\boldsymbol{x}_R, \xi_I)}} e^{i\omega_I \tau_I(\boldsymbol{x}_R, \xi_I)]} d\ell. \end{aligned} \tag{7.4.2}$$

In this equation, $F(\omega_I)$ represents the source signature and $\hat{\boldsymbol{n}}_R$ is the upward unit normal on the reflector. Other expressions are defined as in earlier equations except that now one of the points is $\boldsymbol{x}_R(\ell)$ on the reflecting surface.

This upward scattered field is inserted into (7.3.4). The result is

$$u_O(\boldsymbol{\xi}_O, \omega_O) = -\sqrt{|\omega_O|}e^{-i\pi\,\mathrm{sgn}\,(\omega_O)/4}\int |\omega_I| d\omega_I d\xi_I d\ell d^2x\; \mathcal{G}\; e^{i\Psi}. \tag{7.4.3}$$

In this equation,

$$\Psi = \omega_O \tau_O(\boldsymbol{x}, \xi_O) - \omega_I \tau_I(\boldsymbol{x}, \xi_I) + \omega_I \tau_I(\boldsymbol{x}_R(\ell), \xi_I) \tag{7.4.4}$$

and

$$\begin{aligned} \mathcal{G} = \frac{R(\boldsymbol{x}_R(\ell), \boldsymbol{x}_s(\xi_I))}{4\pi^2} \hat{\boldsymbol{n}}_R \cdot \nabla_x \tau_I(\boldsymbol{x}_R(\ell), \xi_I) a_I(\boldsymbol{x}_R, \xi_I) \\ \cdot \frac{\sqrt{\sigma_{Is}(\boldsymbol{x}_R, \xi_I)\sigma_{Ig}(\boldsymbol{x}_R, \xi_I)}}{\sqrt{\sigma_{Is}(\boldsymbol{x}_R, \xi_I) + \sigma_{Ig}(\boldsymbol{x}_R, \xi_I)}} \frac{a_O(\boldsymbol{x}, \xi_O)}{a_I(\boldsymbol{x}, \xi_I)} \frac{|\nabla_x \tau_O(\boldsymbol{x}, \xi_O)|}{|\nabla_x \tau_I(\boldsymbol{x}, \xi_I)|} \\ \cdot \frac{\sqrt{\sigma_{Is}(\boldsymbol{x}, \xi_I) + \sigma_{Ig}(\boldsymbol{x}, \xi_I)}}{\sqrt{\sigma_s(\boldsymbol{x}, \xi_I) + \sigma_g(\boldsymbol{x}, \xi_I)}} \frac{\sqrt{\sigma_s(\boldsymbol{x}, \xi_I)\sigma_g(\boldsymbol{x}, \xi_I)}}{\sqrt{\sigma_{Is}(\boldsymbol{x}, \xi_I)\sigma_{Ig}(\boldsymbol{x}, \xi_I)}} |H(\boldsymbol{x}, \xi_I)| \end{aligned} \tag{7.4.5}$$

is the cascade of the integrands of (7.4.2) and (7.3.4), exclusive of the explicit frequency dependence appearing in (7.4.3).

The method of stationary phase in the variable ℓ will be applied to this representation. The phase of interest is

$$\Phi_1(\ell) = \tau_I(\boldsymbol{x}_R(\ell), \xi_I). \tag{7.4.6}$$

To carry out the method of stationary phase, we need the derivatives

$$\begin{aligned} \frac{\partial \Phi_1}{\partial \ell} &= \nabla_x \tau_I(\boldsymbol{x}_R, \xi_I) \cdot \frac{d\boldsymbol{x}_R}{d\ell}, \\ \frac{\partial^2 \Phi_1}{\partial \ell^2} &= \frac{\partial^2 \tau_R}{\partial x_{Ri} \partial x_{Rj}} \frac{dx_{Ri}}{d\ell} \frac{dx_{Rj}}{d\ell} + \frac{\partial \tau_R}{\partial x_{Ri}} \frac{d^2 x_{Ri}}{d\ell^2}. \end{aligned} \tag{7.4.7}$$

In our convention of always using x_3 or z as the depth coordinate, the indices i, j, only take on the values 1 and 3. In these equations and those below, summation over the repeated indices is to be understood, with their values being 1 and 3. Setting the first derivative of Φ_1 equal to zero picks out the specular reflection point as the stationary point. Denote the stationary value of ℓ by $\bar{\ell} = \bar{\ell}(\xi_I)$. Detailed analysis of the second derivative is deferred for the moment. After stationary phase in ℓ, (7.4.3) becomes

$$\begin{aligned} u_O(\boldsymbol{\xi}_O, \omega_O) = &-\sqrt{2\pi|\omega_O|} e^{-i\pi \operatorname{sgn}(\omega_O)/4} \\ &\cdot \int \sqrt{|\omega_I|} F(\omega_I) e^{-i\pi \operatorname{sgn}(\omega_I \Phi_1'')/4} \mathcal{G} \frac{e^{i\Psi}}{\sqrt{|\Phi_1''|}} d^2x \, d\omega_I \, d\xi_I, \\ &\text{where} \quad \ell = \bar{\ell}(\xi_I). \end{aligned} \tag{7.4.8}$$

Here, Φ_1'' denotes the value of the second derivative at the stationary point,

$$\Phi_1'' = \left. \frac{\partial^2 \Phi(\ell)}{\partial \ell^2} \right|_{\ell = \bar{\ell}}, \tag{7.4.9}$$

assumed bounded away from zero in the sense discussed in Section 3.6.1. As in Exercise 3.20, this restriction assures us that any caustic or focus of the reflected rays is bounded away from the observation surface. On the other hand, it does not tell us what the sign of this second derivative is. That would depend on how many caustics the arriving ray has passed through on its way to the observation surface. These are caustics arising from the geometry of the surface. The case in which point-source rays have caustics has been excluded, initially, by not including a KMAH index [Lewis, 1965; Ludwig, 1966; Kravtsov and Orlov 1990; Ziolkowski and Deschamps 1980, 1984; Červený, 1995, 2000] in our original Green's functions in the modeling and inversion formulas.

Finding the Stationary Points

Stationary phase in ξ_I is now to be applied to the integral in (7.4.8). The ξ_I-dependent part of the phase is

$$\Phi_2 = \tau_I(\boldsymbol{x}_R(\bar{\ell}(\xi_I)), \xi_I) - \tau_I(\boldsymbol{x}, \xi_I), \tag{7.4.10}$$

and the derivatives of this expression with respect to ξ_I are given by

$$\begin{aligned}
\frac{\partial \Phi_2}{\partial \xi_I} &= \frac{\partial \tau_I(\boldsymbol{x}_R(\bar{\ell}(\xi_I)), \xi_I)}{\partial \xi_I} - \frac{\partial \tau_I(\boldsymbol{x}, \xi_I)}{\partial \xi_I} + \nabla_x \tau_I(\boldsymbol{x}_R(\bar{\ell}(\xi_I)), \xi_I) \cdot \frac{d\boldsymbol{x}_R}{d\bar{\ell}} \frac{d\bar{\ell}}{d\xi_I}, \\
\frac{\partial^2 \Phi_2}{\partial \xi_I^2} &= \frac{\partial^2 \tau_I(\boldsymbol{x}_R(\bar{\ell}(\xi_I)), \xi_I)}{\partial \xi_I \partial x_{Rj}} \frac{d\boldsymbol{x}_{Rj}}{d\bar{\ell}} \frac{d\bar{\ell}}{d\xi_I} + \Delta\tau_I,
\end{aligned} \tag{7.4.11}$$

where

$$\Delta\tau_I = \frac{\partial^2 \tau_I(\boldsymbol{x}_R(\bar{\ell}(\xi_I)), \xi_I)}{\partial \xi_I^2} - \frac{\partial^2 \tau_I(\boldsymbol{x}, \xi_I^2)}{\partial \xi_I^2}. \tag{7.4.12}$$

In the first line in (7.4.11), the last term is zero because the dot product there was set equal to zero to obtain the stationary point of Φ_1 in the variable ℓ. In the second line, summation over the repeated index j, for $j = 1, 3$, is understood.

Consider the condition that the first derivative of Φ_2 is equal to zero. The first traveltime in Φ_2 is just the time for the specular raypath from source to S_R to the receiver. This traveltime remains finite as ξ varies. On the other hand, the second term represents the traveltime from the source to a fixed point at depth to a receiver. If the source-receiver array were of infinite extent, this traveltime would increase beyond all bounds as the source-receiver pair moves off towards infinity in either direction. Nevertheless, this traveltime would achieve at least one local extremum (a minimum) at some finite value of ξ_I. Thus, the traveltime difference will approach $-\infty$ at the extremes and reach some finite maximum for some value(s) ξ_I. If such a ξ_I is in the range of integration, that is, in the range of source-receiver pairs for which data were collected, then the integral has a stationary point. If no such ξ is in the range, then, for that choice of $\boldsymbol{x}$, there is no stationary point, and the contribution to the total integral is of lower order. We proceed as if there is an interior stationary point, $\xi_I = \xi_I(\boldsymbol{x})$.

Note that if $\boldsymbol{x}$ is on the reflector, then the ξ_I (and, therefore, $\bar{\ell}(\xi_I)$, for which $\boldsymbol{x}_R(\bar{\ell}(\xi_I)) = \boldsymbol{x}$ is the specular reflection point) satisfies both stationary phase conditions. An easy way to see this is to note that in this case, the rays from $\boldsymbol{x}$ and $\boldsymbol{x}_R(\ell)$ to the source and receiver are the same and are specular. See Figure 7.5.

The fact that the rays are specular makes Φ_1 stationary; the fact that these two points are the same makes their derivatives with respect to ξ_I

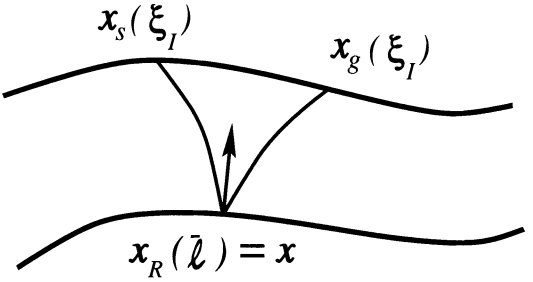

FIGURE 7.5. Stationary point in ξ_I when $\boldsymbol{x}$ is on S_R. ξ_I is chosen so that $\boldsymbol{x}_R(\bar{\ell}(\xi_I)) = \boldsymbol{x}$.

the same and the difference of derivatives appearing in $\partial\Phi_2/\partial\xi_I$ is then equal to zero. It is for this reason that the difference of second derivatives is combined into the expression $\Delta\tau_I$. This difference is equal to zero on the reflector and, therefore, near zero for $\boldsymbol{x}$ near the reflector. This will be important below.

Finding the Second Derivatives of the Phase, at Stationarity

In order to determine the second derivative at stationarity, the first derivative of $\bar{\ell}$ with respect to ξ_I is needed. This derivative is determined by first setting $\partial\Phi_1/\partial\ell = 0$ in (7.4.7) and then differentiating implicitly with respect to ξ_I. That is, we set

$$\nabla_x \tau_I(\boldsymbol{x}_R(\bar{\ell}(\xi_I)), \xi_I) \cdot \frac{d\boldsymbol{x}_R}{d\ell} = \frac{\partial \tau_I(\boldsymbol{x}_R(\bar{\ell}(\xi_I)), \xi_I)}{\partial x_{Rj}} \frac{dx_{Rj}}{d\ell}\bigg|_{\ell=\bar{\ell}(\xi_I)} = 0,$$

and then differentiate:

$$\frac{\partial^2 \tau_I(\boldsymbol{x}_R(\bar{\ell}(\xi_I)), \xi_I)}{\partial x_{Rj}\partial x_{Rk}} \frac{dx_{Rj}}{d\ell}\frac{dx_{Rk}}{d\ell}\frac{d\bar{\ell}(\xi_I)}{d\xi_I} + \frac{\partial^2 \tau_I(\boldsymbol{x}_R(\bar{\ell}(\xi_I)), \xi_I)}{\partial x_{Rj}\xi_I}\frac{dx_{Rj}}{d\ell}\,|_{\ell=\bar{\ell}(\xi_I)} = 0.$$

The summation over j and k in the first term here is recognized as just Φ_1'', as defined by (7.4.9). Therefore, we find that

$$\frac{d\bar{\ell}}{d\xi_I} = -\frac{\partial^2 \tau_I(\boldsymbol{x}_R(\bar{\ell}(\xi_I)), \xi_I)}{\partial\xi_I \partial x_{Rj}}\frac{dx_{Rj}}{d\ell}\,[\Phi_1'']^{-1}. \tag{7.4.13}$$

With this result, (7.4.11) is replaced by

$$\frac{\partial^2\Phi_2}{\partial\xi_I^2} = -\left[\frac{\partial^2 \tau_I(\boldsymbol{x}_R(\bar{\ell}(\xi_I)), \xi_I)}{\partial\xi_I \partial x_{Rj}}\frac{d\boldsymbol{x}_{Rj}}{d\bar{\ell}}\right]^2 [\Phi_1'']^{-1} + \Delta\tau_I. \tag{7.4.14}$$

The summation in first factor on the right, is just a dot product, allowing the simplification

$$\left|\frac{\partial^2 \tau_I(\boldsymbol{x}_R(\bar{\ell}(\xi_I)),\xi_I)}{\partial \xi_I \partial x_{Rj}} \frac{d\boldsymbol{x}_{Rj}}{d\bar{\ell}}\right| = \left|\frac{\partial \nabla_x \tau_I}{\partial \xi_I} \cdot \frac{d\boldsymbol{x}_R}{d\bar{\ell}}\right| = \left|\frac{\partial \nabla_x \tau_I}{\partial \xi_I} \times \hat{\boldsymbol{n}}_R\right| \tag{7.4.15}$$

$$= \frac{\left|\frac{\partial \nabla_x \tau_I}{\partial \xi_I} \times \nabla_x \tau_I\right|}{|\nabla_x \tau_I|} = \frac{|H(\boldsymbol{x}_R,\xi_I)|}{|\nabla_x \tau_I|}.$$

In the second equality, we have exploited the fact that in two dimensions the magnitude of the dot product with the tangent is the same as the magnitude of the cross product with the orthogonal vector, which is to say, the normal. In the next equality, starting the second line the collinearity (within a sign) of the surface normal and the traveltime gradient at stationarity is used. The last equality, in turn, rewrites this two-dimensional cross product as a determinant, the same Beylkin determinant as appears in the inversion formula. Here, however, it is evaluated at the point, $\boldsymbol{x}_R$ on the reflector, subject to the two stationarity conditions, above. Now (7.4.14) can be rewritten as

$$\Phi_2'' = -\left|\frac{|H(\boldsymbol{x}_R,\xi_I)|}{|\nabla_x \tau_I|}\right|^2 [\Phi_1'']^{-1} + \Delta\tau_I. \tag{7.4.16}$$

As with Φ_1, the notation, Φ_2'', is introduced for the evaluation of the second derivative at the stationary point. We remark that for $\boldsymbol{x}$ near the reflector, this second derivative is dominated by the first term and

$$\operatorname{sgn}(\Phi_2'') = -\operatorname{sgn}(\Phi_1''),$$

while this sign might change when $\boldsymbol{x}$ is "sufficiently far" from the reflector, presumably more than three units of reciprocal wavenumber away, for the sake of asymptotic analysis. The discussion of this possible latter region is postponed until later, and the analysis proceeds in the restricted range where the signs of the second derivatives satisfy the above relationship.

Applying Stationary Phase to Equation (7.4.8)

In this case, application of the method of stationary phase to (7.4.8) leads to the result

$$u_O(\boldsymbol{\xi}_O,\omega_O) = -2\pi\sqrt{|\omega_O|}e^{-i\pi \operatorname{sgn}(\omega_O)/4}\int F(\omega_I)d\omega_I d^2x\, \mathcal{G}\frac{e^{i\Psi}}{\sqrt{|\Phi_1''\Phi_2''|}}. \tag{7.4.17}$$

Here, the amplitude and the phase are to be evaluated at the dual stationary points in ℓ and ξ_I.

The dependence on ω_I has now become particularly simple. There is the linear dependence in Ψ, as defined by (7.4.4), and also the amplitude factor, $F(\omega_I)$. If $F = 1$, the ω_I-integration yields a delta function. We take the point of view that F is a filter that leads to a bandlimited version of the delta function that we will denote by δ_B :

$$\delta_B(t) = \frac{1}{2\pi}\int F(\omega)e^{-i\omega t}d\omega. \tag{7.4.18}$$

By using this identity to carry out the ω_I integration in (7.4.17), we obtain

$$u_O(\boldsymbol{\xi}_O,\omega_O) = -4\pi^2\sqrt{|\omega_O|}e^{-i\pi\,\mathrm{sgn}\,(\omega_O)/4} \cdot \int d^2x\, \mathcal{G}\frac{e^{i\Psi}}{\sqrt{|\Phi_1''\Phi_2''|}}\delta_B(\tau_I(\boldsymbol{x}_R(\bar{\ell}),\xi_I) - \tau_I(\boldsymbol{x},\xi_I)). \tag{7.4.19}$$

The last factor here is a scalar delta function. Its argument is zero when $\boldsymbol{x}$ is on the reflector where the stationary phase conditions yield $\boldsymbol{x} = \boldsymbol{x}_R$ and the value of ξ_I makes the corresponding source-receiver pair specular. Furthermore, this zero is isolated; the gradient of the argument is just the gradient of the traveltime, which is normal to the reflector. Thus, the direction of maximal change of argument of the delta function is initially normal to the reflector. Within a scale factor, then, this delta function is the *singular function of the surface*, S_R. The scale factor is just the magnitude of the gradient of the traveltime; that is,

$$\begin{aligned}\delta_B(\tau_I(\boldsymbol{x}_R(\bar{\ell}),\xi_I) - \tau_I(\boldsymbol{x},\xi_I)) &= \delta_B(n_R)\frac{d\tau_I}{dn_R} = \delta(n_R)\left|\nabla_x\tau_I(\boldsymbol{x}_R(\bar{\ell}),\xi_I)\cdot\hat{\boldsymbol{n}}_R\right| \\ &= \delta(n_R)|\nabla_x\tau_I(\boldsymbol{x}_R(\bar{\ell}),\xi_I)|.\end{aligned} \tag{7.4.20}$$

As an asymptotic approximation, we will replace the bandlimited delta function by the delta function, itself. In this case, we can evaluate all amplitude factors on the reflector, S_R. In particular, Φ_2'' in (7.4.16) is evaluated on S_R. As noted above, the last term in that equation, $\Delta\tau_I$, defined by (7.4.12), is zero on S_R, so that

$$\Phi_2'' = -\left|\frac{|H(\boldsymbol{x}_R,\xi_I)|}{|\nabla_x\tau_I|}\right|^2[\Phi_1'']^{-1}$$

on S_R. In this case, (7.4.19) can be rewritten as

$$u_O(\boldsymbol{\xi}_O,\omega_O) = -4\pi^2\sqrt{|\omega_O|}e^{-i\pi\,\mathrm{sgn}\,(\omega_O)/4}\int d\ell\,\mathcal{G}\frac{e^{i\Psi}}{\sqrt{|\Phi_1''\Phi_2''|}|\nabla_x\tau_I(\boldsymbol{x}_R(\ell),\xi_I)|}. \tag{7.4.21}$$

In this equation, the stationarity conditions define $\xi_I = \xi_I(\ell)$, choosing the value of ξ_I for which the input source-receiver pair are specular at $\boldsymbol{x}_R(\ell)$. Now, the amplitude in this equation must be evaluated at stationarity and for $\boldsymbol{x} = \boldsymbol{x}_R$. In this limit, from (7.4.5),

$$\begin{aligned}\mathcal{G} = \frac{R(\boldsymbol{x}_R(\ell),\boldsymbol{x}_s(\xi_I))}{4\pi^2}a_O(\boldsymbol{x}_R,\xi_O)\hat{\boldsymbol{n}}_R\cdot\nabla_x\tau_I(\boldsymbol{x}_R(\ell),\xi_I) \\ \cdot\frac{|\nabla_x\tau_O(\boldsymbol{x}_R,\xi_O)|}{|\nabla_x\tau_I(\boldsymbol{x}_R,\xi_I)|}\frac{\sqrt{\sigma_s(\boldsymbol{x}_R,\xi_O)\sigma_g(\boldsymbol{x}_R,\xi_O)}}{\sqrt{\sigma_s(\boldsymbol{x}_R,\xi_O)+\sigma_g(\boldsymbol{x}_R,\xi_O)}}|H(\boldsymbol{x},\xi_I)|.\end{aligned} \tag{7.4.22}$$

Furthermore, with the term $\Delta\tau_I$ now equal to zero, and the simplification of Φ_2'' above,

$$\sqrt{|\Phi_1''\Phi_2''|} = \frac{|H(\boldsymbol{x}_R, \xi_I)|}{|\nabla_x \tau_I|}. \tag{7.4.23}$$

Obtaining the Kirchhoff Integral Equation Result

These results are used in (7.4.21) to obtain

$$\begin{aligned} u_O(\boldsymbol{\xi}_O, \omega_O) = &-\sqrt{|\omega_O|}e^{-i\pi \operatorname{sgn}(\omega_O)/4} \\ &\cdot \int d\ell\, R(\boldsymbol{x}_R(\ell), \boldsymbol{x}_s(\xi_I)) a_O(\boldsymbol{x}_R, \xi_O) \\ &\cdot \hat{\boldsymbol{n}}_R \cdot \nabla_x \tau_I(\boldsymbol{x}_R(\ell), \xi_I) \frac{|\nabla_x \tau_O(\boldsymbol{x}_R, \xi_O)|}{|\nabla_x \tau_I(\boldsymbol{x}_R, \xi_I)|} \\ &\cdot \frac{\sqrt{\sigma_s(\boldsymbol{x}_R, \xi_O)\sigma_g(\boldsymbol{x}_R, \xi_O)}}{\sqrt{\sigma_s(\boldsymbol{x}_R, \xi_O) + \sigma_g(\boldsymbol{x}_R, \xi_O)}} e^{i\omega_O \tau_O(\boldsymbol{x}_R, \xi_O)}. \end{aligned} \tag{7.4.24}$$

Because the integrand is evaluated subject to the stationarity relation between ℓ and ξ_I,

$$\hat{\boldsymbol{n}}_R \cdot \nabla_x \tau_I(\boldsymbol{x}_R(\ell), \xi_I) = -|\nabla_x \tau_I(\boldsymbol{x}_R, \xi_I)|. \tag{7.4.25}$$

Just as in (7.4.25), we set

$$|\nabla_x \tau_O(\boldsymbol{x}_R, \xi_O)| = -\hat{\boldsymbol{n}}_R \cdot \nabla_x \tau_O(\boldsymbol{x}_R(\ell), \xi_O). \tag{7.4.26}$$

With these substitutions,

$$\begin{aligned} u_O(\xi_O, \omega_O) = &-\sqrt{|\omega_O|}e^{-i\pi \operatorname{sgn}(\omega_O)/4} \\ &\cdot \int R(\boldsymbol{x}_R(\ell), \boldsymbol{x}_s(\xi_I)) \hat{\boldsymbol{n}}_R \cdot \nabla_x \tau_O(\boldsymbol{x}_R(\ell), \xi_O) a_O(\boldsymbol{x}_R, \xi_O) \\ &\cdot \frac{\sqrt{\sigma_s(\boldsymbol{x}_R, \xi_O)\sigma_g(\boldsymbol{x}_R, \xi_O)}}{\sqrt{\sigma_s(\boldsymbol{x}_R, \xi_O) + \sigma_g(\boldsymbol{x}_R, \xi_O)}} e^{i\omega_O \tau_O(\boldsymbol{x}_R, \xi_O)]} d\ell. \end{aligned} \tag{7.4.27}$$

This is the formula for the "Kirchhoff data" remapped via 2.5D KDM.

Interpreting the Result

Now compare (7.4.27) with (7.4.2). The Kirchhoff representation in the input source-receiver coordinates has been transformed into the Kirchhoff representation in the output source-receiver coordinates. In obtaining this result, a region of the $\boldsymbol{x}$-domain integration where $\operatorname{sgn}(\Phi_2'') = \operatorname{sgn}(\Phi_1'')$ has been neglected. In this region, the signature factor in the method of stationary phase becomes $\exp\{i\pi/2 \operatorname{sgn}(\omega_I) \operatorname{sgn}(\Phi_2'')\}$, whose Fourier transform is the Cauchy principal-value-$1/t$ function, $PV - 1/t$. Thus, the delta function that confined the support of the volume integral to the reflecting surface is now replaced by this $PV - 1/t$ function in the residual part

of the $\boldsymbol{x}$-domain integration. As with the delta function, this function is singular at the zero of its argument—on the reflecting surface. However, we use this function in a spatial region that is bounded away from the reflector. In that region, the amplitude $1/t$ is relatively small compared to its value in the neighborhood of $t = 0$. In fact, in the Fourier domain, the function that is equal to $\pm i$ for $\pm\omega$ "large," produces the singular behavior of $PV - 1/t$, while the part of the function that is equal to $\pm i$ near zero produces the slowly decaying tail of $1/t$. However, as noted above, this combination of signs, $\text{sgn}\,(\Phi_2'') = \text{sgn}\,(\Phi_1'')$, only occurs "far"—a few units of reciprocal wavenumber away—from the reflector and produces some low frequency—presumably, small amplitude contribution to the total asymptotic expansion. Thus, any contribution that might be obtained from this integration over ω_I and the integration over $\boldsymbol{x}$ in a region bounded away from the reflector will be of lower order asymptotically than the result given here. In this sense, Kirchhoff-approximate input data is mapped to Kirchhoff-approximate output data.

We lack a proof in the most general case that the Kirchhoff integral provides the leading-order WKBJ approximate expansion of the return from specular reflections; this is always the case in asymptotic expansions that can be carried out explicitly. This is the basis of our claim that traveltime and all geometrical spreading and curvature effects, including effects of "buried foci"—caustics produced by synclines—will be properly transformed by the KDM process. Where the caustic pierces the upper surface, the arrival time is expected to be accurate, but no claims are made about the accuracy of the amplitude. The factor Φ_1'' is zero in this case and the asymptotic analysis is invalid. Nevertheless, it produces an integrable singularity in the Kirchhoff integral, with the correct traveltimes in the phase, hence, our claim that the arrival time is correct, but the amplitude need not be.

For edge-diffracted returns, the Kirchhoff integral produces the correct arrival time, but an inaccurate diffraction coefficient, except at the shadow boundary of the last reflected ray. The reason is that the asymptotic expansion of the diffracted wave arises from an endpoint contribution of the data-modeling integral. The traveltime from that endpoint to the observation point is just the diffraction raypath traveltime. Even in the region covered by specular reflections, this endpoint contribution is a next order term in the asymptotic expansion; it is often visible, somewhat dimmer than the reflection response. Thus, the mapped data are expected to contain mapped diffraction arrival times with inaccurate amplitudes. The amplitudes are inaccurate because the Kirchhoff approximations of the original forward model underlying the derivation are themselves inaccurate in a region close to the diffracting edge.

There is another source of "error" in the amplitude. Note that, in (7.4.27), the reflection coefficient is evaluated at an incidence angle associated with the input source-receiver configuration, through its dependence

on the stationary value of ξ_I. For mapped data, we would prefer to have this dependence mapped to ξ_O, so that the reflection coefficient is mapped to its value in the output configuration and at the output incidence angle. Unfortunately, this is not the case. The input reflection coefficient is preserved, not mapped. This is known from the TZO case and is therefore not surprising in this general result.

As in Section 5.1.6, we can see here how the additional integral operators $\cos_I$ and $\cos_O$ of Section 7.2.3, produce estimates of the incidence angles in the input and output configurations. Because the entire integrand of each of the operators $\cos_I$ and $\cos_O$, is evaluated at its stationary value, this is true, in particular, for the traveltime gradients appearing in these integral kernels. Those stationary values are, indeed, just $2\cos\theta/c(\boldsymbol{x})$, subscripted either I or O. Hence the ratio of operators is, asymptotically, as claimed.

In summary, we have shown that the leading-order asymptotic input data are mapped to the leading-order asymptotic output data, except for the reflection coefficient, which maintains its input value everywhere. Clearly, the same sort of analysis could be carried out in 3D, starting from (7.2.6) and applying this operator to the 3D Kirchhoff data, (7.2.1). While the details of the higher-dimensional stationary phase analysis would be more difficult, analogous to the proof in Chapter 6 for the basic inversion formula, the analysis would proceed exactly along the lines presented in this simpler 2.5D case, here. Thus, we forego that more difficult analysis.

7.4.1 Asymptotic Analysis of 2.5D KDM

The 2.5D KDM platform formula (7.3.4) is somewhat easier to analyze than is the 3D formula (7.2.6). As noted earlier, the first approach will be to apply stationary phase in so-called *isochron coordinates*, and that analysis is simpler in 2.5D than in 3D. See Figure 7.1. In this approach, we integrate over a running parameter on a fixed isochron and then over a second coordinate, the temporal coordinate that moves us from one isochron to another. We will see that the first integration, the one along the isochron, can always be carried out by the method of stationary phase, subject to the second derivative of the phase being "large enough" for the method of stationary phase to be valid. At that point, one particular data mapping application will require special handling, while a more global approach in the frequency domain will apply to all others. The method applied to the exceptional case proves to be a time-domain method applicable to all cases for which the stationary phase method applied to the first integration is valid.

Thus, we begin by introducing those new coordinates, one of which is the input traveltime $\tau_I(\boldsymbol{x}, \boldsymbol{\xi}_I)$, defined in (7.2.4), and the other is a running parameter along each curve of constant τ_I, that is, on the isochrons of τ_I. Let us call that second parameter, γ. See Figure 7.6. For simplicity, we

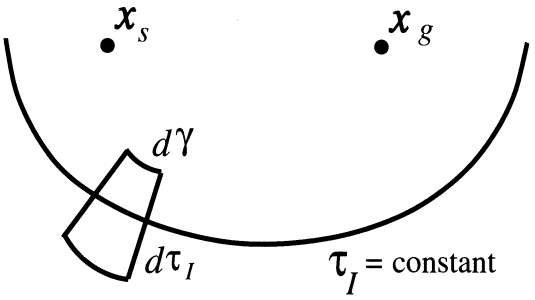

FIGURE 7.6. Isochron coordinate system.

choose the level curves of γ to be orthogonal trajectories to the isochrons.

We remark that now $\boldsymbol{x} = \boldsymbol{x}(\gamma, t_I)$ and that

$$t_I \equiv \tau_I(\boldsymbol{x}(\gamma, t_I), \xi_I), \tag{7.4.28}$$

with

$$d^2x = d\gamma dt_I \left| \frac{\partial(\boldsymbol{x})}{\partial(\gamma, t_I)} \right|.$$

Because coordinate curves are orthogonal to one another, the Jacobian appearing here is just the product of the magnitudes of the derivatives appearing in each row. That is,

$$d^2x = d\gamma dt_I \left| \frac{\partial \boldsymbol{x}}{\partial \gamma} \right| \left| \frac{\partial \boldsymbol{x}}{\partial t_I} \right|.$$

Now, $|\partial \boldsymbol{x}/\partial t_I|$ is just the directional derivative of $\boldsymbol{x}$ in the direction of increasing traveltime. To simplify this expression, observe first that

$$\left| \frac{\partial \boldsymbol{x}}{\partial t_I} \cdot \nabla \tau_I \right| = \left| \frac{\partial x_i}{\partial t_I} \frac{\partial \tau_I}{\partial x_i} \right| = \frac{d\tau_I}{dt_I} = 1.$$

Here, we use summation convention in the first equality and obtain the next equality by observing that this sum is just the chain rule for differentiating τ_I with respect to t_I. However, because t_I is just the value of τ_I on each isochron, this derivative is equal to 1, which is the last equality. The two vectors in the first expression both point in the direction orthogonal to the isochron. Hence, this dot product is really the product of their magnitudes. On the other hand, the last result makes them reciprocals of one another. That is,

$$\left| \frac{\partial \boldsymbol{x}}{\partial t_I} \right| = \frac{1}{|\nabla \tau_I|}.$$

Next, observe that

$$\left| \frac{\partial \boldsymbol{x}}{\partial \gamma} \right| = \sqrt{\left[\frac{\partial x_1}{\partial \gamma}\right]^2 + \left[\frac{\partial x_2}{\partial \gamma}\right]^2 + \left[\frac{\partial x_3}{\partial \gamma}\right]^2}$$

$$= \lim_{\Delta\gamma\to 0} \sqrt{\left(\frac{\Delta x_1}{\Delta\gamma}\right)^2 + \left(\frac{\Delta x_2}{\Delta\gamma}\right)^2 + \left(\frac{\Delta x_3}{\Delta\gamma}\right)^2}$$

$$= \lim_{\Delta\gamma\to 0} \frac{\sqrt{(\Delta x_1)^2 + (\Delta x_2)^2 + (\Delta x_3)^2}}{\Delta\gamma} = \left|\frac{\partial s}{\partial\gamma}\right|.$$

Collecting these results, we can write

$$d^2x = \frac{d\gamma dt_I}{|\nabla\tau_I(\boldsymbol{x},\xi)|}\left|\frac{\partial s}{\partial\gamma}\right|, \tag{7.4.29}$$

with s being arclength along the isochron.

With this change of variables of integration, (7.3.4) becomes

$$\begin{aligned} u_O(\xi_O,\omega_O) \sim{}& \frac{\sqrt{|\omega_O|}e^{-i\pi\,\mathrm{sgn}\,(\omega_O)/4}}{4\pi^2} \\ &\cdot \int \sqrt{|\omega_I|}e^{i\pi\,\mathrm{sgn}\,(\omega_I)/4} d\omega_I d\xi_I u_I(\xi_I,\omega_I) \\ &\cdot \int \frac{a_O(\boldsymbol{x},\xi_O)}{a_I(\boldsymbol{x},\xi_I)} \frac{|\nabla\tau_O(\boldsymbol{x},\xi_O)|}{|\nabla\tau_I(\boldsymbol{x},\xi_I)|^2} \frac{\sqrt{\sigma_{Is}+\sigma_{Ig}}}{\sqrt{\sigma_s+\sigma_g}} \frac{\sqrt{\sigma_s\sigma_g}}{\sqrt{\sigma_{Is}\sigma_{Ig}}} \\ &\cdot |H(\boldsymbol{x},\xi_I)| \cdot e^{[i\omega_O\tau_O(\boldsymbol{x},\xi_O)-i\omega_I\tau_I(\boldsymbol{x},\xi_I)]} d\gamma dt_I \left|\frac{\partial s}{\partial\gamma}\right|. \end{aligned} \tag{7.4.30}$$

7.4.2 Stationary Phase Analysis in γ

We will now apply the method of stationary phase, in the variable γ, to this last integral. Thus, we consider the phase function

$$\Phi = \tau_O(\boldsymbol{x}(\gamma,t_I),\xi_O). \tag{7.4.31}$$

The derivatives of this phase are

$$\begin{aligned} \frac{d\Phi}{d\gamma} &= \nabla\tau_O \cdot \frac{\partial\boldsymbol{x}}{\partial\gamma} = \frac{\partial\tau_O}{\partial x_i}\frac{\partial x_i}{\partial\gamma}, \\ \frac{d^2\Phi}{d\gamma^2} &= \frac{\partial^2\tau_O}{\partial x_i\partial x_j}\frac{\partial x_i}{\partial\gamma}\frac{\partial x_j}{\partial\gamma} + \frac{\partial\tau_O}{\partial x_i}\frac{\partial^2 x_i}{\partial\gamma^2}. \end{aligned} \tag{7.4.32}$$

In these equations, the repeated indices are, again, to be summed over 1 and 3. The same will be true for repeated indices that arise below.

The phase is stationary when the first derivative here is equal to zero:

$$\nabla\tau_O \cdot \frac{\partial\boldsymbol{x}}{\partial\gamma} = 0. \tag{7.4.33}$$

We see here that the gradient of τ_O is required to be orthogonal to the tangent vector to the isochron, $\tau_I = t_I$. This is as predicted earlier and is depicted in Figure 7.2.

Now, we must evaluate the second derivative of the phase in (7.4.32). First, let us address the second term in that derivative. In the exercises below, we outline the derivation of the result

$$\frac{\partial \tau_O}{\partial x_i}\frac{\partial^2 x_i}{\partial \gamma^2} = -\left|\nabla \tau_O(\boldsymbol{x}, \xi_O)\right| \kappa_I \left[\frac{ds}{d\gamma}\right]^2. \tag{7.4.34}$$

Here, κ_I is the curvature of the isochron, $\tau_I = t_I$, with the sign determined by the implied dot product on the left side, which is

$$\operatorname{sgn}\left(\nabla \tau_O(\boldsymbol{x}, \xi_O) \cdot \frac{d^2\boldsymbol{x}}{ds^2}\right) = -1. \tag{7.4.35}$$

This follows from the fact that, in the absence of multi-pathing, the gradient faces downward, while the curvature vector faces upward, toward the concave side of the isochron of τ_I.

Analysis of the first term on the right side of (7.4.32) requires more discussion. Let us denote by t_O the value of the traveltime τ_O at stationarity. Now, consider the isochron of τ_O defined by $\tau_O = t_O$. Denote the equation of that isochron by $\boldsymbol{x} = \boldsymbol{x}'(\gamma')$. Then, by implicit differentiation,

$$\begin{aligned} 0 &= \frac{\partial \tau_O}{\partial x_i}\frac{\partial x_i'}{\partial \gamma'}, \\ 0 &= \frac{\partial^2 \tau_O}{\partial x_i' \partial x_j'}\frac{\partial x_i'}{\partial \gamma'}\frac{\partial x_j'}{\partial \gamma'} + \frac{\partial \tau_O}{\partial x_i'}\frac{\partial^2 x_i'}{\partial \gamma'^2}. \end{aligned} \tag{7.4.36}$$

In this equation, the first line is simply a statement that the traveltime gradient and the tangent to the isochron are orthogonal. In the second line, we can make the first term agree with the first term of $d^2\Phi/d\gamma^2$ at the stationary point if we choose γ' as a local function of γ for which

$$\frac{d\gamma'}{d\gamma} = 1$$

at the stationary point. Then,

$$\frac{\partial^2 \tau_O}{\partial x_i \partial x_j}\frac{\partial x_i}{\partial \gamma}\frac{\partial x_j}{\partial \gamma} = \frac{\partial^2 \tau_O}{\partial x_i' \partial x_j'}\frac{\partial x_i'}{\partial \gamma'}\frac{\partial x_j'}{\partial \gamma'}.$$

That is, the two tangent vectors appearing as second factors, here, now agree, as do the first factors, at the stationary point. The orthogonality in the first line of (7.4.36) leads us to conclude, as above, that

$$\frac{\partial \tau_O}{\partial x_i'}\frac{\partial^2 x_i'}{\partial \gamma'^2} = \frac{\partial \tau_O}{\partial x_i}\frac{\partial^2 x_i}{\partial \gamma^2} = -\left|\nabla \tau_O(\boldsymbol{x}, \xi_O)\right| \kappa_O \left[\frac{ds'}{d\gamma'}\right]^2.$$

One can see here that we have obtained the same sort of expression as above, except that the curvature in question is now the curvature of the isochron of τ_O, which is tangent to the isochron of τ_I at stationarity. Combining these results, we find that

$$\frac{\partial^2 \tau_O}{\partial x_i \partial x_j}\frac{\partial x_i}{\partial \gamma}\frac{\partial x_j}{\partial \gamma} = \frac{\partial^2 \tau_O}{\partial x_i' \partial x_j'}\frac{\partial x_i'}{\partial \gamma'}\frac{\partial x_j'}{\partial \gamma'} = -\frac{\partial \tau_O}{\partial x_i'}\frac{\partial^2 x_i'}{\partial \gamma'^2}$$
$$= \frac{\partial \tau_O}{\partial x_i}\frac{\partial^2 x_i}{\partial \gamma^2} = |\nabla \tau_O(\boldsymbol{x}, \xi_O)|\,\kappa_O \left[\frac{ds'}{d\gamma'}\right]^2$$
$$= |\nabla \tau_O(\boldsymbol{x}, \xi_O)|\,\kappa_O \left[\frac{ds}{d\gamma}\right]^2 .$$

With these results, the expression for the second derivative of Φ in (7.4.32) becomes

$$\frac{d^2\Phi}{d\gamma^2} = |\nabla \tau_O(\boldsymbol{x}, \xi_O)| \left[\frac{ds}{d\gamma}\right]^2 (\kappa_O - \kappa_I), \quad \operatorname{sgn}\left(\frac{d^2\Phi}{d\gamma^2}\right) = \operatorname{sgn}(\kappa_O - \kappa_I). \tag{7.4.37}$$

We use these results to compute the leading-order approximation by the method of stationary phase in γ applied to the integral in (7.4.30). The result is

$$u_O(\xi_O, \omega_O) \sim \frac{e^{i\pi \operatorname{sgn}(\omega_O)/4[\operatorname{sgn}(\kappa_O - \kappa_I) - 1]}}{[2\pi]^{3/2}}$$
$$\cdot \int \sqrt{|\omega_I|} e^{i\pi \operatorname{sgn}(\omega_I)/4} u_I(\xi_I, \omega_I) d\omega_I \, d\xi_I$$
$$\cdot \int \frac{a_O(\boldsymbol{x}, \xi_O)}{a_I(\boldsymbol{x}, \xi_I)} \frac{\sqrt{|\nabla \tau_O(\boldsymbol{x}, \xi_O)|}}{|\nabla \tau_I(\boldsymbol{x}, \xi_I)|^2} \frac{|H(\boldsymbol{x}, \xi_I)|}{\sqrt{|\kappa_O - \kappa_I|}}$$
$$\cdot \frac{\sqrt{\sigma_{Is} + \sigma_{Ig}}}{\sqrt{\sigma_s + \sigma_g}} \frac{\sqrt{\sigma_s \sigma_g}}{\sqrt{\sigma_{Is}\sigma_{Ig}}} dt_I e^{i\omega_O \tau_O(\boldsymbol{x}, \xi_O) - i\omega_I t_I}. \tag{7.4.38}$$

Here, $\boldsymbol{x} = \boldsymbol{x}(\gamma, t_I)$ defined by the change of variable of integration; γ is further defined as a function of ξ_I, ξ_O, t_I at the stationary point, obtained by setting the first γ-derivative of the phase equal to zero, (7.4.33). This condition should be familiar to readers who have experience with constant-background DMO. There, as in Figure 7.2, the common-offset isochrons are ellipses, while the zero-offset isochrons are circles. For each t_I, there is a corresponding isochron of τ_O, which satisfies the stationary phase condition or, its equivalent, the tangency condition between isochrons. In the absence of multi-pathing, there is only one stationary point for each fixed value of ξ_I, ξ_O, t_I; at that stationary point, $\boldsymbol{x}$, t_O and γ are determined as functions of these variables.

Exercises

7.3 The purpose of this exercise is to verify (7.4.34). We begin by considering the isochron

$$\tau_I(\boldsymbol{x}(\gamma, t_I), \xi_O) \equiv t_I,$$

and represent it as $\boldsymbol{x} = \boldsymbol{x}(s(\gamma))$, with s being arclength on the isochron.

a. Differentiate this equation with respect to γ to conclude that

$$\begin{aligned} \frac{d\boldsymbol{x}}{d\gamma} &= \frac{d\boldsymbol{x}}{ds}\frac{ds}{d\gamma}, \\ \frac{d^2\boldsymbol{x}}{d\gamma^2} &= \frac{d^2\boldsymbol{x}}{ds^2}\left[\frac{ds}{d\gamma}\right]^2 + \frac{d\boldsymbol{x}}{ds}\frac{d^2s}{d\gamma^2} \end{aligned}$$

b. Let $\boldsymbol{n}$ be a unit normal to this isochron and explain why

$$\boldsymbol{n} \cdot \frac{d^2\boldsymbol{x}}{d\gamma^2} = \boldsymbol{n} \cdot \frac{d\boldsymbol{x}}{ds}\frac{d^2s}{d\gamma^2} = \boldsymbol{n} \cdot \boldsymbol{\kappa}_I \frac{d^2s}{d\gamma^2}.$$

That is, the normal projection of the second derivative with respect to γ is proportional to the *curvature* vector of the curve, $\boldsymbol{x} = \boldsymbol{x}(\gamma, t_I)$.

c. Now verify (7.4.34).

7.4.3 Validity of the Stationary Phase Analysis

It can be seen from this last result that the amplitude of the integrand becomes infinite when the two curvatures are equal. The curvature difference arose through the evaluation of the second derivative of the phase in (7.4.37). Indeed, in Section 3.6.1, we discuss the asymptotic validity of the method of stationary phase. The essence of that result is that, in appropriate dimensionless variables, $\omega_O d^2\Phi/d\gamma^2$ must be "large," say, greater than π. The appropriate length and time scales for this calculation should be the "slow" scales over which the amplitude and traveltime varies, rather than the "fast" scales associated with wavelength and period.

The form of (7.4.37), in terms of an arbitrary parameter, γ, lends itself to an easy identification of the second derivative in terms of an appropriate slow length scale. To do so, let us define L to be the length along the raypath from output source to receive; in the constant background case, for example, $L = ct_O$. Then, let us define

$$\gamma = s/L,$$

where s is arclength along the isochron. In this case,

$$\left[\frac{ds}{d\gamma}\right]^2 = L^2$$

and we can then calculate

$$\omega_O \frac{d^2\Phi}{d\gamma^2} = \frac{4\pi f_O L^2}{c_O} \cos\theta_O \, |\kappa_O - \kappa_I|$$

$$= \frac{4\pi f_O L}{c_O} \cos\theta_O \, L|\kappa_O - \kappa_I| \geq \pi. \tag{7.4.39}$$

Here, c_O is an "average" propagation speed in the output medium; f_O is the frequency in Hz; θ_O is the half-opening angle of the rays associated with τ_O at the output point $\boldsymbol{x}$. In the final form, we have written the inequality as 4π times three dimensionless factors. The first factor is the travel distance measured in wavelengths; the second factor is the half-opening angle between the rays from source and receiver to the stationary point, $\boldsymbol{x}$; the third factor is the curvature difference on the isochrons normalized by the slow length scale. This result should be compared to the dimensionless large parameter, (3.6.5), for inversion. The new feature here is that the curvature difference on the input and output isochrons plays a role in the asymptotic validity of the result.

We can see from (7.4.39) that validity of the asymptotic expansion requires that

- the output travel distance must be a "few units of reciprocal wavenumber" from the output acquisition points;
- the half-opening angle between the rays cannot be too near to $\pi/2$;
- the curvature difference cannot be too small, when measured in units of inverse travel distance along the output rays from source to stationary point to receiver.

Effects of Relative Isochron Curvature

In this list of requirements, the last observation is worth further discussion. In (7.4.39), the presence of the last factor, the difference of isochron curvatures, presents an important limitation on simplifications of the data mapping platform (7.4.30) that are arrived at by carrying out the stationary phase computation, above. For example, for offset continuation through small offsets, or transformation to zero-offset from a small initial offset, any result produced through further analysis of (7.4.30) would not be valid.[9] We remark that the classic NMO/DMO sequence arises from exactly this type of asymptotic analysis. Hence, this is one of the processes that is constrained as we have described here. While NMO/DMO is a kinematically accurate mapping from small offset to zero-offset, it will be dynamically inaccurate, unable to produce the true amplitude predicted in the introduction. That will be shown, below, in Section 7.6.

We see, also, that the sign of the curvature difference influences the processing formula for u_O in (7.4.38). If the curvature difference is positive, the total phase shift represented by the outside multiplier on the right side

[9] Actually, the kinematics would be right, but the dynamics would not. That is, the transformation of traveltime, or phase, would be accurate, but the output amplitude would not properly transform the geometrical spreading effects from input to output.

of that equation is zero. On the other hand, if the curvature difference is negative, the integration output on the right hand side is multiplied by

$$e^{i\pi \operatorname{sgn}(\omega_O)/4[\operatorname{sgn}(\kappa_O-\kappa_I)-1]} = -i \operatorname{sgn}(\omega_O).$$

The inverse transform of this factor is $-1/\pi t$; as a convolutional operator in the time domain, this is the Hilbert transform. See (A.7.1) in Appendix A. Thus, if the output of the integral operations on the right side would normally produce a bandlimited delta function in the time domain, the result of this operator would be to transform the output into a bandlimited $1/t$ function, a form of doublet (different from a bandlimited $\delta'(t)$, for example). In summary, the relative curvature of the isochrons changes the character of the output data in the time domain.

In Figure 7.2, the input isochrons are depicted as having larger radii of curvature (smaller curvatures) than the output isochrons. In fact, in that figure, the isochrons are just the ellipse and circles of the constant-background TZO, or NMO/DMO, data mapping. In this case, the curvature difference appearing in the phase shift multiplier preceding the integral sign in the first line of (7.4.38) is positive and the total phase shift represented by that factor is zero. On the other hand, suppose the processes were reversed, that is, mapping from zero-offset to finite offset. In this case, these phase shifts produce a multiplier of $-i \operatorname{sgn}(\omega_O)$, as noted above. This is the Fourier transform of the Hilbert transform kernel, $1/t$, back in the time domain. Thus, given an input source signature in the time domain, a data mapping of this type requires transforming that source signature to its Hilbert transform on output.

As a second example, consider the mapping from common-offset to common-shot. Now for input offset greater than the separation between source and receiver of the output, there is no phase shift due to curvature. However, when the input offset is less than the output offset, the curvature difference is negative and we are in the second case; there is a phase shift due to curvature. Thus, the smaller offset part of the output data set requires no Hilbert transform, while the latter part of the data set, larger output offset, *does* require a Hilbert transform.

Computing the Isochron Curvatures

We remark that each of the isochron curvatures, κ_O and κ_I, appearing in (7.4.38) can be written in terms of the separate curvatures for the traveltimes from source or receiver, respectively, to the point at depth. That is,

$$\begin{aligned}
\kappa_I &= \frac{\cos\theta_I}{2}\left[\kappa_{Is} + \kappa_{Ig} + \tan^2\theta_I \nabla c \cdot \nabla \tau_I\right], \\
\kappa_O &= \frac{\cos\theta_O}{2}\left[\kappa_{Os} + \kappa_{Og} + \tan^2\theta_O \nabla c \cdot \nabla \tau_O\right].
\end{aligned} \tag{7.4.40}$$

Here, as always, θ_I and θ_O are the half-angles between the rays from the source and receiver meeting at the isochron in input and output configurations, respectively. The importance of this result is that the separate isochron curvatures can be computed along the rays at the same time that other ray quantities are.

Note that for constant background, the gradient terms in (7.4.40) are absent, and the individual isochrons are circles. In this case, each radius of curvature is just the radius of the corresponding circle and the total curvature is just the average of the individual curvatures—or the average of the reciprocal radii—multiplied by $\cos\theta_I$ or $\cos\theta_O$, respectively:

$$\kappa_I = \frac{\cos\theta_{Is}}{2}\left[\frac{1}{r_{Is}} + \frac{1}{r_{Ig}}\right],$$
$$\kappa_O = \frac{\cos\theta_{Os}}{2}\left[\frac{1}{r_{Os}} + \frac{1}{r_{Og}}\right]. \tag{7.4.41}$$

The gradient terms in (7.4.40) provide corrections that takes account of the component of the background propagation speed in the direction normal to the isochron of τ_I or τ_O, respectively. The result, (7.4.40), will be derived at the end of the chapter.

We would propose to proceed from this point by carrying out the integration in the variable, t_I by the method of stationary phase applied to the phase function

$$\omega_O \tau_O(\boldsymbol{x}(\gamma, t_I), \xi_O) - \omega_I t_I,$$

with γ further defined as a function of ξ_I, ξ_O, t_I through the above stationary phase analysis. In fact, there is one case in which the phase is *linear* in t_I and, hence, the method of stationary phase cannot be applied. Before proceeding to the next stationary phase analysis, then, we will pause to consider this implementation.

7.5 Common-Shot Downward Continuation of Receivers (or Sources)

Here we consider a the problem of performing the KDM form of datuming on a common-shot data set. The objective is to move the receivers from one datum surface to another. For example, we might want to move the receivers from an irregular acquisition surface to a regular one, or simply move the receivers to a different depth. (By reciprocity, we could do the same thing to sources by considering a common-receiver gather.)

For this case, it is easy to explain the stationary phase condition (7.4.33) geometrically. Draw the ray from the input receiver through the output receiver and down to the isochron $\tau_I = t_I$. Draw the ray from that intersection

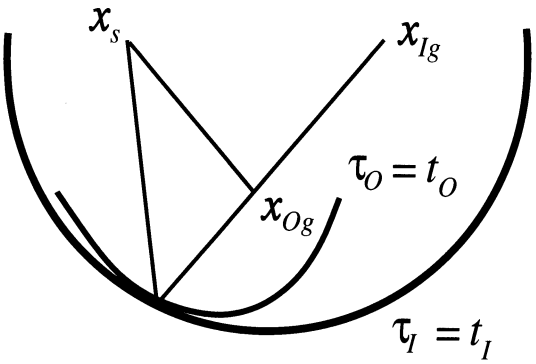

FIGURE 7.7. Geometry of the stationary phase analysis in γ for downward continuation of receivers in a constant-background medium.

point to the common source point. The input and output traveltimes share the same traveltime from source to isochron and then from isochron to the output receiver. In fact, they differ only by the traveltime from the input receiver to the output receiver, which is a constant in time for fixed input and output receiver location. Because the input and output rays overlay one another at the isochron, the two traveltime gradients are identical and the isochrons are tangent. This also means that the opening angles, $2\theta_I$ and $2\theta_O$, between the rays from source and receiver at the isochron, are identical. That is,

$$|\nabla_x \tau_O(\boldsymbol{x}, \xi_O)| = |\nabla \tau_I(\boldsymbol{x}, \xi_I)| = 2\cos\theta/c. \tag{7.5.1}$$

Here, we no longer distinguish between input and output opening angles because they are the same. Consequently, the reflection coefficient at input incidence angle is also the reflection coefficient at output incidence angle; that is, the reflection coefficient *is preserved* in this mapping. Furthermore, for this case, the output traveltime is less than the input traveltime; is radius of curvature at stationarity is smaller than the corresponding radius on the input isochron and, therefore, the curvature difference is positive; hence, we lose the phase factor from (7.4.38).

It is now straightforward to transform (7.4.38) to the time domain by multiplying by $\exp\{-i\omega_O t_O\}\ /2\pi$ and integrating on both sides. The only ω_O-dependence on the right is now in the phase, producing a delta function in time, $\delta(t_O - \tau_O)$, thereby allowing us to carry out the time domain integration as well. The result is,

$$U_O(\xi_O, t_O) \sim \frac{1}{[2\pi]^{3/2}} \int \frac{D_{1/2}(\xi_I, t_I)}{|\nabla \tau_I(\boldsymbol{x}, \xi_I)|^{3/2}} \frac{A(\boldsymbol{x}, \boldsymbol{x}_g(\xi_O))}{A(\boldsymbol{x}, \boldsymbol{x}_g(\xi_I))} \cdot \frac{\sqrt{\sigma_{Is} + \sigma_{Ig}}}{\sqrt{\sigma_s + \sigma_g}} \frac{\sqrt{\sigma_g}}{\sqrt{\sigma_{Ig}}} \frac{|H(\boldsymbol{x}, \xi_I)|}{\sqrt{|\kappa_O - \kappa_I|}} d\xi_I. \tag{7.5.2}$$

Here,

$$D_{1/2}(\xi,t) = \frac{1}{2\pi}\int \sqrt{|\omega|}e^{i\pi\,\mathrm{sgn}\,(\omega)/4-i\omega t}u_I(\xi,\omega)d\omega \tag{7.5.3}$$

is the Hilbert transform of the half-derivative of the input data. In the frequency domain, the product

$$e^{i\pi/2\,\mathrm{sgn}\,(\omega_I)}\cdot\sqrt{|\omega_I|}e^{-i\pi\,\mathrm{sgn}\,(\omega_I)/4} = i\,\mathrm{sgn}\,(\omega_I)\cdot\sqrt{-i\omega_I},$$

commutes, but their temporal counterparts, Hilbert transform and half-derivative, respectively, *do not.* The reason is that fractional derivatives can be applied to causal functions only; application of the Hilbert transform to a causal function does *not* yield a causal function. Hence, we must take care to keep track of the order in which these operators are applied in the time domain.

In (7.5.2), $t_I = t_I(t_O,\xi_I,\xi_O)$, through the stationary phase condition that fixes the input and output traveltime isochrons to be tangent. This type of mapping between input and output traveltimes is similar to the mapping of input to output traveltimes in DMO. Given t_O,ξ_I,ξ_O, we draw the isochron $\tau_O = t_O$ and find the isochron of τ_I that is tangent to it. This determines t_I and we can proceed to evaluate the integrand. In Sheaffer and Bleistein [1998], the constant-background implementation of this result is discussed in greater detail.

We remark that the Beylkin determinant and the ray-theoretic amplitudes appearing in (7.5.2) admit some simplification because we are dealing with a 2.5D implementation. For the Beylkin determinant, we use (6.3.2); that is, we set

$$|H(\boldsymbol{x},\xi_I)| = \frac{4\cos^2\theta}{c(\boldsymbol{x})}\left|\frac{\partial p((x),\boldsymbol{x}_g(\xi_I))}{\partial\xi_I}\right| = |\nabla\tau_I|^2\left|\frac{\partial p((x),\boldsymbol{x}_g(\xi_I))}{\partial\xi_I}\right|.$$

Furthermore, the 2.5D amplitudes are given by (6.1.5) and (6.1.7). The amplitudes appearing in 7.5.2) can each be expressed in the form (6.1.12). Of course, the σ's and the $\boldsymbol{p}_0$'s have to be chosen appropriately for the computation; they depend on the initial and final points along the ray.

7.5.1 *Time-Domain Data Mapping for Other Implementations*

The technique we used in the previous discussion—inverse Fourier transform from ω_O to t_O—will always provide a mapping to output data in space-time. However, we have to account for the possibility that $\mathrm{sgn}\,(\kappa_O - \kappa_I) = -1$, leading to a nontrivial phase-shift in the first line of (7.4.38). To do so, we rewrite (7.4.38) as follows. First, set

$$u_O(\xi_O,\omega_O) = e^{i\pi\,\mathrm{sgn}\,(\omega_O)/4[\,\mathrm{sgn}\,(\kappa_O-\kappa_I)-1]}d_O(\xi_O,\omega_O), \quad \text{with}$$

$$d_O(\xi_O,\omega_O) = \frac{1}{[2\pi]^{3/2}} \int \sqrt{|\omega_I|} e^{i\pi \operatorname{sgn}(\omega_I)/4} u_I(\xi_I,\omega_I) d\omega_I \, d\xi_I$$
$$\cdot \int \frac{a_O(\boldsymbol{x},\xi_O)}{a_I(\boldsymbol{x},\xi_I)} \frac{\sqrt{|\nabla\tau_O(\boldsymbol{x},\xi_O)|}}{|\nabla\tau_I(\boldsymbol{x},\xi_I)|^2} \frac{|H(\boldsymbol{x},\xi_I)|}{\sqrt{|\kappa_O - \kappa_I|}}$$
$$\cdot \frac{\sqrt{\sigma_{Is}+\sigma_{Ig}}}{\sqrt{\sigma_s+\sigma_g}} \frac{\sqrt{\sigma_s\sigma_g}}{\sqrt{\sigma_{Is}\sigma_{Ig}}} dt_I e^{i\omega_O\tau_O(\boldsymbol{x},\xi_O) - i\omega_I t_I}. \tag{7.5.4}$$

Now, we can treat the inverse Fourier transform on the right side as the transform of a product, leading to a convolution in the time domain. Let us focus on the inverse transform of $d_O(\xi_O,\omega_O)$:

$$D_O(\xi_O,t_O) = \frac{1}{2\pi} \int d_O(\xi_O,\omega_O) e^{-i\omega_O t_O} d\omega_O. \tag{7.5.5}$$

Observe that the only dependence on ω_O in $d_O(\xi_O,\omega_O)$ is through the phase factor $i\omega_O\tau_O(\boldsymbol{x},\xi_O)$ and, further, that

$$\frac{1}{2\pi} \int e^{i\omega_O\{\tau_O(\boldsymbol{x},\xi_O) - t_O\}} d\omega_O = \delta(\tau_O(\boldsymbol{x},\xi_O) - t_O).$$

We will use this delta function to carry out the integration in t_I. Recall that the time $\tau_O(\boldsymbol{x},\xi_O)$ is related to the time t_I It is easier to carry out the temporal integral in t_O than in t_I. To do so, observe that

$$dt_I = \frac{dt_I}{d\tau_I} d\tau_I = \frac{d\tau_I}{d\tau_O} d\tau_O$$
$$= \frac{|\nabla\tau_I(\boldsymbol{x},\xi_I)|}{|\nabla\tau_O(\boldsymbol{x},\xi_O)|} \frac{d\tau_O}{dt_O} dt_O = \frac{|\nabla\tau_I(\boldsymbol{x},\xi_I)|}{|\nabla\tau_O(\boldsymbol{x},\xi_O)|} dt_O.$$

Here, to obtain the second equality, we have set $dt_I/d\tau_I = 1$ and used the chain rule to replace $d\tau_I$ by a scale factor multiplying $d\tau_O$. In the next line, we have written the derivative $d\tau_I/d\tau_O$ as a quotient of gradients and replaced $d\tau_O$ by a scale factor multiplying dt_O. Finally, for the last equality, we have replaced that final scale factor by unity.

Therefore, exploiting the delta function to carry out the t_I integral requires that we introduce this quotient of gradients as a scale factor in the amplitude on the right side of (7.4.38). (Note, from (7.5.1), that this scale factor is equal to unity in the downward continuation example, above.)

The final result, then, depends on the value of the phase shift. We find that

$$\begin{aligned} U_O(\xi_O,t_O) &= D_O(\xi_O,t_O), \quad \kappa_O > \kappa_I, \\ U_O(\xi_O,t_O) &= \mathcal{H}[D_O(\xi_O,t_O)] \\ &= \frac{1}{\pi} \int_0^\infty \frac{D_O(\xi_O,t)}{t - t_O} dt, \quad \kappa_O < \kappa_I. \end{aligned} \tag{7.5.6}$$

Here, $\mathcal{H}$ denotes the Hilbert transform. See Section A.7.1 in Appendix A.

Thus, we see that the output might involve a last Hilbert transform after the processing by integration over the variables, ξ_I and ω_I, depending on the relative curvatures of the isochrons. For example, when mapping from finite offset to zero-offset, $\text{sgn}\,(\kappa_O - \kappa_I) - 1 = 0$, and $D_O(\xi_O, t_O)$ produces a formula for the data U_O themselves. When mapping from zero-offset to finite offset, $\text{sgn}\,(\kappa_O - \kappa_I) - 1 = -2$ and the output, $D_O(\xi_O, t_O)$, requires a further Hilbert transform to arrive at $U_O(\xi_O, t_O)$.

When mapping from common-offset to common-shot, D_O represents the data, themselves, when the output source and receiver are closer than the input common-offset; D_O represents the Hilbert transform of the data when the output source and receiver are further apart than the input source and receiver. When *upward* continuing receivers in a common-shot gather, again, D_O is the Hilbert transform of the data U_O.

7.5.2 Stationary Phase in t_I

Let us now continue the asymptotic analysis of the integral in (7.4.38) under the assumption that the traveltime τ_O is *not* a linear function of t_I. In other implementations, this is true and we can apply the method of stationary phase to the t_I integral in (7.4.38). In this case, we will continue the asymptotic analysis by applying the method of stationary phase in t_I to the phase of that integral,

$$\Phi(t_I, \cdots) = \omega_O \tau_O(\boldsymbol{x}(\gamma(\xi_I, \xi_O, t_I,), t_I, \xi_O) - \omega_I t_I. \tag{7.5.7}$$

Here, $\cdots$ denotes other variables in Φ. On the other hand, we have taken care to note on the right side that τ_O depends explicitly on t_I, and also implicitly on t_I, through the stationary phase analysis of the γ-integration, in particular, equation (7.4.33). This expression must be differentiated with respect to t_I, in order to determine the condition under which it is stationary in that variable:

$$\frac{d\Phi}{dt_I} = \omega_O \left[\frac{\partial \tau_O}{\partial t_I} + \frac{\partial \tau_O}{\partial \gamma} \frac{\partial \gamma}{\partial t_I} \right] - \omega_I.$$

Here, the first term represents the differentiation of τ_O with respect to its explicit t_I dependence, while the second term arises from the above-mentioned dependence of γ on t_I through stationarity. In fact, this second term is identically zero, again due to stationarity; the left side of equation (7.4.33) is merely a chain rule representation of the derivative of τ_O with respect to γ.

To proceed, then, we apply the chain rule to the first term to obtain

$$\frac{d\Phi}{dt_I} = \omega_O \left[\frac{\partial \tau_O}{\partial x_j} \frac{\partial x_j}{\partial t_I} \right] - \omega_I. \tag{7.5.8}$$

Here, summation over j over the values 1 and 3 is to be understood; the summation process, then, is just the dot product of two vectors. The first

vector is the gradient of the total traveltime, τ_O; therefore, it is a vector pointing normal to the isochrons of τ_O, with magnitude $\cos\theta_O/c(\boldsymbol{x})$. The second vector is just the derivative of the $\boldsymbol{x}$-vector with respect to the traveltime t_I, and therefore is directed orthogonal to the isochron of τ_I. Of course, both of these vectors are to be evaluated at stationarity of γ, *which means that these two isochrons are collinear.* Hence, we need only determine the magnitude of the second vector in order to find a simpler expression for this dot product.

To do so, introduce arclength, s_I, in the direction of t_I and then write

$$\frac{\partial \boldsymbol{x}}{\partial t_I} = \frac{\partial \boldsymbol{x}}{\partial s_I}\frac{\partial s_I}{\partial t_I} = \boldsymbol{n}_I \left|\nabla \tau_I\right|^{-1} = \boldsymbol{n}_I \frac{c(\boldsymbol{x})}{2\cos\theta_I}.$$

In this equation, $\boldsymbol{n}_I$ is the unit normal vector in the direction of increasing t_I; that is, this vector is the unit normal along the mutual gradient direction of the isochrons of τ_I and τ_O (again, because everything is evaluated at the stationary value of γ). Clearly, this vector and $\nabla\tau_O$ are collinear. Thus, we obtain the result that

$$\frac{d\Phi}{dt_I} = \omega_O \frac{\cos\theta_O}{\cos\theta_I} - \omega_I, \tag{7.5.9}$$

from which we conclude that the phase will be stationary when[10]

$$\frac{\omega_O}{\omega_I} = \frac{\cos\theta_I}{\cos\theta_O}. \tag{7.5.10}$$

This equation can be viewed as defining a scaling between input and output frequencies. This is familiar from migration/inversion outputs, as well as from DMO processing, where the change in resolution is observed. This rescaling actually assures that the final image resolution in the direction of the reflector-normal after inversion or migration will be the same, whether the input or output data are processed.

To find a stationary point, here, one must examine the stationary points in γ for each t_I. At each such point, and for given values of ω_I and ω_O, it is necessary to check the ratio of cosines, $\cos\theta_I/\cos\theta_O$. If a t_I can be found for which this ratio satisfies (7.5.10), then that is the stationary value of t_I.

For a stationary point to exist, ω_I and ω_O must have the same sign. Furthermore, when mapping from a larger offset to a smaller offset—$\cos\theta_I < \cos\theta_O$—then $\omega_O/\omega_I < 1$; when mapping from a smaller offset to a larger offset—$\cos\theta_I > \cos\theta_O$—then $\omega_O/\omega_I > 1$. Thus, the range of integration in ω_I is restricted by the condition that the phase be stationary in t_I. For either choice of ratio $\cos\theta_I/\cos\theta_O$, either greater than unity or less than unity, there is a range of integration in ω_I for which we can expect to

---

[10]When the wavespeeds are different, this result becomes $\frac{\omega_O}{\omega_I} = \frac{\cos\theta_I}{\cos\theta_O}\frac{c_O(\boldsymbol{x})}{c_I(\boldsymbol{x})}$. We will not mention this extension below.

find a stationary point in t_I and a complementary ratio, less than unity or greater than unity, respectively, where there are no stationary point in t_I. For this complementary range of integration, the contribution to the total integral is smaller, less than leading order in ω_O. Because this is a leading-order asymptotic theory, we neglect those contributions and restrict the domain of integration in ω_I to assure the existence of a stationary point.

When the ratio ω_O/ω_I is near to unity, the two cosines must be nearly equal; this will occur deep in the data set when there is little distinction in incidence directions for input and output rays. When mapping from larger offset to smaller offset, we can expect that the input offset will allow θ_I to approach $\pi/2$ "up shallow" while θ_O is bounded away from that value. That is, up shallow, the ratio of frequencies in (7.5.10) will become small, which can occur only if ω_I approaches infinity with the same sign as ω_O. Hence, formally, we can think of the range of integration in ω_I, in this case, being $\operatorname{sgn}(\omega_O)(1,\infty)$, corresponding to traveltimes ranging from large to small. On the other hand, when mapping to larger offset, it is θ_O that could approach $\pi/2$ while θ_I does not. In this case, it is necessary that ω_I become small in magnitude. Hence, now, the range of ω_I is $\operatorname{sgn}(\omega_O)(0,1)$, corresponding to traveltimes ranging from small to large with increasing magnitude of ω_I.

We proceed to express the result of evaluating the right side of (7.4.38) by the method of stationary phase. The result is

$$
\begin{aligned}
u_O(\xi_O,\omega_O) \sim\; & e^{i\pi \operatorname{sgn}(\omega_O)\operatorname{sgn}(\kappa_O-\kappa_I)/4} \\
& \cdot \frac{1}{2\pi}\int_\Omega \sqrt{|\omega_I|}e^{i\pi \operatorname{sgn}(K)/4} d\omega_I\, d\xi_I\, u_I(\xi_I,\omega_I) \\
& \cdot \frac{a_O(\boldsymbol{x},\xi_O)}{a_I(\boldsymbol{x},\xi_I)} \frac{\sqrt{|\nabla\tau_O(\boldsymbol{x},\xi_O)|}}{|\nabla\tau_I(\boldsymbol{x},\xi_I)|} \frac{|H(\boldsymbol{x},\xi_I)|}{\sqrt{|(\kappa_O-\kappa_I)K|}} \\
& \cdot \frac{\sqrt{\sigma_{Is}+\sigma_{Ig}}}{\sqrt{\sigma_s+\sigma_g}} \frac{\sqrt{\sigma_s\sigma_g}}{\sqrt{\sigma_{Is}\sigma_{Ig}}} e^{i\omega_O t_O - i\omega_I t_I}.
\end{aligned}
\tag{7.5.11}
$$

In this equation, Ω is the restricted interval of integration imposed by stationarity. We have also used the fact that

$$\operatorname{sgn}(\omega_I) = \operatorname{sgn}(\omega_O)$$

to eliminate the $\pi/4$ phase shifts arising from the factors

$$e^{-i\pi/4\operatorname{sgn}(\omega_O)} \quad \text{and} \quad e^{i\pi/4\operatorname{sgn}(\omega_I)}$$

in (7.4.38). The traveltimes t_O and t_I are functions of $\xi_I,\omega_I,\xi_O,\omega_O$, defined by the two stationarity conditions above. That is, first consider the points of tangency between isochrons for given input and output source and receiver locations. Among those, find the one for which the ratio of cosines of incidence angles satisfies (7.5.10). That determines the traveltimes in this formula. Also, K is related to the second derivative of the

phase with respect to t_I, evaluated at stationarity. In the discussion of traveltime curvatures below, we show that

$$K = \frac{\omega_O \sin^2 \theta_O}{c} \{\kappa_{Os} + \kappa_{Og} - \nabla c \cdot \nabla \tau_O\} - \frac{\omega_I \sin^2 \theta_I}{c} \{\kappa_{Is} + \kappa_{Ig} - \nabla c \cdot \nabla \tau_I\}. \quad (7.5.12)$$

As above, the κ's are the curvatures of the separate isochrons of the traveltimes from source or receiver to scattering point and for input or output variables, subscripted appropriately. It is interesting to note that the second derivative in the direction orthogonal to the isochrons can be expressed in terms of the curvatures of the isochrons. This is peculiar to two dimensions; the three-dimensional case is much more complicated.

7.6 2.5D Transformation to Zero-Offset (TZO)

It is this application that was the primary motivator for this general theory of data mapping. As we have discussed at the beginning of this chapter, a standard preprocessing step in migration is to gather up data from multi-offset experiments into equivalent zero-offset data, consistent with some assumed known background propagation speed. This is done approximately through the NMO-stacking or bin-NMO-stacking procedure, or via a combination of NMO-DMO. From our discussions above, it is reasonable to conclude that this procedure is a data mapping.

Two important observations:

1. it is possible to modify the amplitude of the combined NMO/DMO operator so that it becomes a true amplitude operator in the sense of this chapter—this is just a special case of data mapping;
2. for more general background propagation speeds, application of the platform for data mapping *does not* produce a process that decomposes into a cascade of processes.

Because of this last observation, we use a different name entirely for the true amplitude processing that we propose here, which is *transformation to zero-offset* (TZO).[11]

[11]The term MZO, *migration to zero-offset* is also used [Tygel, Hubral, and Schleicher, 1996; Tygel, Schleicher, and Hubral, 1995a,b; Tygel, Schleicher, and Hubral, 1996a,b; and Tygel, Filpo, and Oliveira, 1997; Tygel, Schleicher, and Santos, 1998].

7.6.1 TZO in the Frequency Domain

We must specialize (7.5.11) to obtain the result we seek. For arbitrary variable-background media, there is little to be done with this general formula, except to specialize the Beylkin determinant to the common-offset case. That is, we use (6.3.7) and (6.3.8) for H. Here, however, we have made the additional assumption that there are no caustics. In this case, the two determinants H_1 and H_2 have the same sign. Therefore,

$$|H(\boldsymbol{x},\xi_I)| = \frac{2\cos^2\theta_I}{c(\boldsymbol{x})}\left|\frac{\partial}{\partial\xi_I}(\boldsymbol{p}_{Is}+\boldsymbol{p}_{Ig})\right|. \tag{7.6.1}$$

In this equation,

$$\boldsymbol{p}_{Is} = \nabla_x\tau(\boldsymbol{x},\boldsymbol{x}_s(\xi_I)), \quad \boldsymbol{p}_{Ig} = \nabla_x\tau(\boldsymbol{x},\boldsymbol{x}_g(\xi_I)). \tag{7.6.2}$$

Until we specialize to constant-background or to a depth-dependent background, where more can be done with the general equation, there is little more to do, except to note that the stationarity condition (7.5.10) simplifies to

$$\frac{\omega_O}{\omega_I} = \cos\theta_I, \tag{7.6.3}$$

because, on output, the source and receiver rays are coincident and $\theta_O = 0$.

Therefore, let us turn to the constant-background case, with a horizontal acquisition surface, where a significantly simpler formula will be developed in the specialization of (7.5.11). We can also simplify our notation here because we are dealing with the mapping of data to zero-offset. We do so with the help of Figure 7.8. There, the midpoint of the common-offset data is labeled by its x-coordinate, ξ_I, and the zero-offset point by its x-coordinate, ξ_O. In particular, $\theta_O = 0$ in this case and therefore we can dispense with the subscript on θ_I and set

$$\theta_I = \theta \tag{7.6.4}$$

for the remainder of this section and the related exercises. We can further simplify the notation as follows. We set

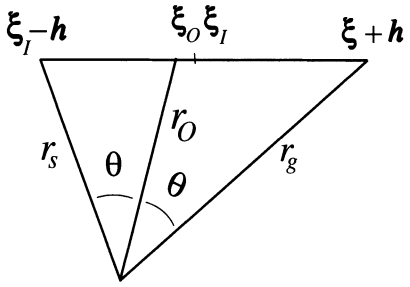

FIGURE 7.8. The geometry of the rays for transforming finite offset data to zero-offset.

$$r_{Os} = r_{Og} = r_0, \quad r_{Is} = r_s, \quad r_{Ig} = r_g. \tag{7.6.5}$$

That is, we have exploited the fact that at zero-offset, the rays from $\boldsymbol{x}$ to $\boldsymbol{x}_{Os}$ and $\boldsymbol{x}_{Og}$ are the same ray, so we can simplify the subscripting for the elements of the output ray tracing. Once the subscripts s and g are deleted from the output notation, leaving only the subscript O, we no longer need the subscript I to distinguish the input variables.

Now, we can list some of the simplifications of the variables that appear in (7.5.11). The reader should also refer to Section 6.3.8 on common-offset inversion, as we use results and notational conventions from this section. For traveltime and amplitude, we find

$$t_O = \frac{2r_0}{c}, \quad t_I = \frac{(r_s + r_g)}{c}, \quad a_O = \frac{1}{16\pi^2 r_0^2}, \quad a_I = \frac{1}{16\pi^2 r_s r_g}. \tag{7.6.6}$$

The gradients of the traveltimes are

$$\begin{aligned} \nabla\tau_I &= \frac{\hat{\boldsymbol{r}}_s + \hat{\boldsymbol{r}}_g}{c}, \quad |\nabla\tau_I| = \frac{2\cos\theta}{c}, \\ \nabla\tau_O &= \frac{2\hat{\boldsymbol{r}}_0}{c}, \quad |\nabla\tau_O| = \frac{2}{c}. \end{aligned} \tag{7.6.7}$$

Here, the unit vectors, $\hat{\boldsymbol{r}}_0$, $\hat{\boldsymbol{r}}_s$, $\hat{\boldsymbol{r}}_g$, point downward from the upper surface towards the stationary point where all the rays intersect.

Next, note that $\sigma = rc$, with the subscripts corresponding in each case, so that

$$\frac{\sqrt{\sigma_{Is} + \sigma_{Ig}}}{\sqrt{\sigma_s + \sigma_g}} \frac{\sqrt{\sigma_s \sigma_g}}{\sqrt{\sigma_{Is}\sigma_{Ig}}} = \frac{\sqrt{r_s + r_g}}{\sqrt{2r_0}} \frac{r_0}{\sqrt{r_s r_g}}. \tag{7.6.8}$$

We take the Beylkin determinant from the discussion in Section 6.3.8:

$$H = \frac{2z\cos^2\theta}{c^2}\left[\frac{1}{r_s^2} + \frac{1}{r_g^2}\right]. \tag{7.6.9}$$

For the isochron curvatures, we use the constant propagation speed result, (7.4.41), but specialize to the case where the output mapping is at zero-offset:

$$\kappa_O = \frac{1}{r_0}, \quad \kappa_I = \frac{\cos\theta}{2}\left[\frac{1}{r_s} + \frac{1}{r_g}\right]. \tag{7.6.10}$$

The latter result admits further simplification because of the special geometry of the stationary point. Note that the two interior angles of the triangles at ξ_O are supplementary. By using this fact and the law of sines in those triangles, one can show that

$$\frac{1}{r_s} + \frac{1}{r_g} = \frac{2\cos\theta}{r_0}. \tag{7.6.11}$$

Consequently, evaluating the curvature difference appearing in (7.5.11), we find that

$$\kappa_O - \kappa_I = \frac{1}{r_0}\left[1 - \cos^2\theta\right] = \frac{\sin^2\theta}{r_0}, \quad \operatorname{sgn}(\kappa_O - \kappa_I) = +1. \tag{7.6.12}$$

We see here that the curvature difference, $\kappa_O - \kappa_I$ is positive, which is as predicted for TZO; the curvature of the elliptical finite offset isochron is less than the curvature of the circular zero-offset isochron.

We also have to evaluate the factor K, using (7.5.12). In this case, with $\theta_O = 0$, the first expression on the right in that equation is also zero, so that

$$K = -\frac{\omega_I \sin^2\theta}{c}\left[\frac{1}{r_s} + \frac{1}{r_g}\right] = -\frac{2\omega_I \sin^2\theta\cos\theta}{cr_0},$$
$$\operatorname{sgn}(K) = -\operatorname{sgn}(\omega_I) = -\operatorname{sgn}(\omega_O). \tag{7.6.13}$$

Let us now collect all of the results obtained so far and write down an expression for the TZO specialization of (7.5.11) to the constant-background, horizontal planar acquisition surface case. The result is

$$u_O(\xi_O,\omega_O) \sim \frac{1}{\pi c}\int_\Omega d\omega_I\, d\xi_I\, u_I(\xi_I,\omega_I)\frac{zr_sr_g}{r_0}\frac{\cos\theta}{\sin^2\theta}\left[\frac{1}{r_s^2} + \frac{1}{r_g^2}\right] e^{i\omega_O t_O - i\omega_I t_I}. \tag{7.6.14}$$

In the stationary phase calculations that we carried out, the fixed independent variables were ξ_I, ξ_O, ω_I, and ω_O. Thus, it remains to be shown how all of the variables appearing here can be written in terms of those four variables. That is, we must find expressions for r_s, r_g, r_0, t_I, t_O, and $\cos\theta$, in terms of the four variables listed above. Of course, the traveltimes are related to the distances through (7.6.6), so that we need only find the travel distances in order to find the traveltimes.

One expression is particularly easy, this is the equation for $\cos\theta$, because it is given by the stationarity condition, (7.5.10). Thus, we can be content to leave the trigonometric functions in place, because their replacement is straightforward. We will find below that the signed distance between the midpoint of the input coordinates and the zero-offset point of the output coordinates arises naturally in our analysis. Therefore, we set

$$\delta = \xi_I - \xi_O, \tag{7.6.15}$$

and turn now to the task of determining the relevant distance functions in terms of the fundamental variables listed above. We need three equations for the three unknowns, r_s, r_g, r_0, and we find them in the law of cosines applied to each of the smaller triangles in Figure 7.8 and to the larger triangle. Those laws are

$$4h^2 = r_s^2 + r_g^2 - 2r_sr_g\cos 2\theta,$$
$$(h-\delta)^2 = r_s^2 + r_0^2 - 2r_sr_0\cos\theta,$$
$$(h+\delta)^2 = r_g^2 + r_0^2 - 2r_gr_0\cos\theta.$$

We use one other auxiliary result that will make the computation easier. This one comes from using the law of sines, again, in the two smaller triangles, but now with r_s, r_g, and the two pieces of the offset line. Again, we use the fact that the angles at the shared vertex are supplementary to conclude that

$$\frac{r_s}{h-\delta} = \frac{r_g}{h+\delta}. \tag{7.6.16}$$

This result allows us to rewrite the first equation in (7.6.16) as an equation in r_s^2 or r_g^2 alone, solve that one, and then use the above equation to find the other. The result is

$$r_s = \frac{h(h-\delta)}{L}, \quad r_g = \frac{h(h+\delta)}{L}, \tag{7.6.17}$$

with

$$L = \sqrt{h^2 \sin^2\theta + \delta^2 \cos^2\theta} = \sqrt{h^2 - (h^2 - \delta^2)\cos^2\theta}. \tag{7.6.18}$$

It is now fairly straightforward to show, also, that

$$\frac{1}{r_s^2} + \frac{1}{r_g^2} = 2\frac{L^2}{h^2}\frac{h^2+\delta^2}{(h^2-\delta^2)^2}. \tag{7.6.19}$$

We can also use (7.6.17) and (7.6.11) to find that

$$r_0 = \frac{h^2-\delta^2}{L}\cos\theta. \tag{7.6.20}$$

We need an expression for z. This one is somewhat indirect. First, we write out the definitions of the distance functions,

$$r_s^2 = (x - \xi_I + h)^2 + z^2, \quad r_g^2 = (x - \xi_I - h)^2 + z^2,$$

and take the difference to find that

$$x - \xi_I = \frac{r_s^2 - r_g^2}{4h}.$$

Now, we can use the definition

$$r_0^2 = (x - \xi_O)^2 + z^2 = (x - \xi_I + \delta)^2 + z^2,$$

to obtain an equation for z in terms of quantities that we already know:

$$z^2 = r_0^2 - \left[\frac{r_s^2 - r_g^2}{4h} + \delta\right]^2.$$

After much algebra, this expression can be simplified to yield

$$z = \frac{h(h^2-\delta^2)}{L^2}\sin\theta\cos\theta. \tag{7.6.21}$$

Finally, we turn to the evaluation of the phase. By using the definitions of the distances, above, we find that

$$\begin{aligned}\omega_O t_O - \omega_I t_I &= 2\frac{\omega_O}{c}\frac{h^2-\delta^2}{L}\cos\theta - 2\frac{\omega_I}{c}\frac{h^2}{L} \\ &= 2\frac{\omega_I}{Lc}\left[h^2\cos^2\theta - h^2 - \delta^2\cos^2\theta\right] \qquad (7.6.22) \\ &= -2\frac{\omega_I L}{c}.\end{aligned}$$

When we gather up all of the results derived here and substitute into (7.6.14), we obtain

$$u_O(\xi_O,\omega_O) \sim \frac{2}{\pi c}\int_\Omega d\omega_I\, d\xi_I\, u_I(\xi_I,\omega_I)\cot\theta\,\frac{h}{L}\frac{h^2+\delta^2}{h^2-\delta^2}e^{-2i\omega_I L/c}. \quad (7.6.23)$$

The integrand, here, has two apparent singularities—one when $\theta = 0$ and the other when $\delta = h$. In fact, neither of the singularities is in the domain of integration. First, note that $\theta = 0$ could occur everywhere if $h = 0$, in which case we would not be mapping from finite offset to zero-offset. We eliminate all other possibilities by requiring that there is some minimum depth, above which there are no reflectors:

$$z \geq z_{\min} > 0. \qquad (7.6.24)$$

Then, from (7.6.21), we see $\delta = h$ and $\theta = 0$ (as well as $\theta = \pi/2$—transmitted rays) are precluded at stationary points. However, we can at best obtain a coupled lower bound on θ and upper bound on δ. We will need to do better.

Another lower bound on θ arises in a different manner. With increasing depth, this opening angle between the rays from offset source and receiver again approaches zero. If we combine some maximum time on the data record with the minimum depth, $z_{\min}$, we arrive at another possible lower bound for θ. In order to include all possible stationary points, we define $\theta_{\min}$ to be the lesser of these two possible bounds and then,

$$\theta \geq \theta_{\min} > 0, \quad \delta \leq \delta_{\max} < h.$$

However, as noted above, these limits might be interdependent at this point and we need to obtain at least one of them independent of the other. Below we will obtain such an independent bound for δ, as well as the bounds on the domain of integration in ω_I. Then, (7.6.21) will provide an independent choice for the lower bound on θ, as well. With that in place, $\theta_{\min}$ will also be well defined.

First, from (7.6.3), and the bound on θ,

$$\frac{1}{\cos\theta_{\min}} = \frac{\omega_{I\,\min}}{\omega_O} \leq \frac{\omega_I}{\omega_O},$$

with the left expression defining $\omega_{I\,\min}$ in the middle expression.

We next consider the upper bound on ω_I/ω_O. We begin by considering one of the consequences of stationarity, (7.6.17). By adding the two

equations there and solving for L, we find that

$$L = \frac{2h}{r_s + r_g} h, \tag{7.6.25}$$

where $(r_s + r_g)/c$ can be viewed as the input traveltime on the stationary ellipse for the given values of the variables, ξ_I, ξ_O, ω_I, and ω_O. We would argue that there is some smallest ellipse on which data are nonzero; this ellipse corresponds to the minimum traveltime for which data are nonzero. Furthermore, the traveltime on that ellipse has to be larger than $2h/c$, implying that

$$L \leq \gamma h, \quad \gamma = \frac{2h}{\min\{r_s + r_g\}} < 1. \tag{7.6.26}$$

We rewrite the first inequality here as $L^2 \leq \gamma^2 h^2$, then use the second form of L in (7.6.18) with $\cos\theta = \omega_O/\omega_I$, from (7.6.3). After some algebra, this inequality can be rewritten as

$$(1 - \gamma^2)\frac{\omega_I^2}{\omega_O^2} + \frac{\delta^2}{h^2} \leq 1. \tag{7.6.27}$$

In this inequality, ω_I^2 can only assume its maximum when $\delta = 0$. We then find that

$$\frac{1}{\cos^2\theta_{\min}} \leq \frac{\omega_I^2}{\omega_O^2} \leq \frac{1}{1 - \gamma^2}. \tag{7.6.28}$$

Now, let us consider the lower bound, $\omega_I^2/\omega_O^2 = 1/\cos^2\theta_I \geq 1$. We use the absolute lower bound, one, in order to obtain an upper bound on δ^2 from (7.6.27) that is independent of $\theta_{\min}$:

$$\delta^2 \leq \gamma^2 h^2. \tag{7.6.29}$$

Thus, the range of integration in δ is

$$0 \leq \delta^2 \leq \gamma^2 h^2 < h^2. \tag{7.6.30}$$

Further refinement is possible, but there is no need. We have assured a domain of integration in which the amplitude is not singular. The inequalities (7.6.28) and (7.6.30) redefine the domain of integration, Ω, in (7.6.23) as a domain in both variables and as a domain that excludes the singular values of the integrand but includes all of the possible stationary points of our analysis above. In summary, Ω in (7.6.23) is defined by

$$\Omega : \begin{cases} \omega_{I\min}/\omega_O \leq \omega_I/\omega_O \leq 1/\sqrt{1-\gamma^2}, \\ \\ -h\sqrt{1-(1-\gamma^2)\omega_I^2/\omega_O^2} \leq \xi_I - \xi_O \leq h\sqrt{1-(1-\gamma^2)\omega_I^2/\omega_O^2} \end{cases} . \tag{7.6.31}$$

7.6.2 A Hale-Type TZO

Hale [1984] developed transformation to zero-offset (Hale DMO) that uses input data in a wavenumber/frequency domain, but produces a space/frequency result, as we have here. That result can be derived from (7.6.23) by using the definition

$$u_I(\xi_I, \omega_I) = \frac{1}{2\pi} \int U_I(k, t_I) e^{ik\xi_I + i\omega_I t} dk dt_I, \tag{7.6.32}$$

reintroducing t_I as the input time. When this representation is substituted into (7.6.23), only the operator depends on the variables, ξ_I and ω_I, while the data do not depend on these variables. We can then approximate the integrals in these variables by the method of stationary phase, applied to the cascaded phase,

$$\begin{aligned} \Phi &= k\xi_I + \omega_I t - \frac{2}{c}\omega_I L \\ &= k\xi_I + \omega_I t - \frac{2}{c}\,\mathrm{sgn}\,(\omega_O)\sqrt{h^2\omega_I^2 + \delta^2\omega_O^2}. \end{aligned} \tag{7.6.33}$$

We leave to the exercises to verify that the stationary values of ξ_I and ω_I are given by

$$\begin{aligned} \delta &= \frac{kh^2}{\omega_O t_n A}, & \omega_I &= \frac{\omega_O t_I}{A t_n}, \\ A &= \sqrt{1 + \frac{k^2 h^2}{\omega_O^2 t_n^2}}, & t_n &= \sqrt{t_I^2 - \frac{4h^2}{c^2}}, \end{aligned} \tag{7.6.34}$$

with the auxiliary results

$$\cos\theta = \frac{A t_n}{t_I}, \qquad L = \frac{2h^2}{c t_n}. \tag{7.6.35}$$

The time t_n is the *normal moveout time*. For a horizontal reflector at depth H, the plot of t_I as a function of h is a hyperbola,

$$t_I^2 = \frac{4h^2}{c^2} + \frac{4H^2}{c^2},$$

so that

$$t_n = \frac{2H}{c},$$

is constant. That is, t_n is independent of h; the plot of t_n as a function of h is a horizontal line for a horizontal reflector (in a homogeneous medium, c = constant).

We also leave as an exercise the evaluation by the method of stationary phase for the operator (7.6.23), with u_I replaced by (7.6.32). The result is

$$u_O(\xi_O, \omega_O) \sim \frac{1}{2\pi} \int \frac{dk\, dt_n}{A} \left[1 + \frac{2k^2h^2}{\omega_O^2 t_n^2}\right] U_I(k, t_I) e^{i\Theta}. \tag{7.6.36}$$

Here,

$$\Theta = k\xi_O + \omega_O t_n A. \tag{7.6.37}$$

We see here, that the integration variable has been changed to the NMO time, t_n, while we have written the data in terms of the input time, t_I. The transformation of the data,

$$\tilde{U}_I(k, t_n) = U_I(k, t_I(t_n)),$$

amounts to NMO processing. The result here differs from the Hale DMO formula by the factor in square brackets. In fact, using the definition of A in (7.6.34), we can write

$$1 + \frac{2k^2h^2}{\omega_O^2 t_n^2} = A^2 + \frac{k^2h^2}{\omega_O^2 t_n^2},$$

with the last term being exactly the quotient needed to determine A^2 itself. Hence, including this new factor requires an additional add and multiply in the summation process that approximates this integral. Thus, it is fairly straightforward to transform any Hale DMO algorithm into one that is "true amplitude" in the sense of this chapter. If this is not done, then the classic Hale DMO will produce results with substantial amplitude differences from the one above when the second term in the brackets is significant.

We can associate k-values with dips on the input data—equivalently, slopes of reflection events. Thus, for steep events at moderate times, the term in square brackets will differ significantly from unity. The shallower the event (smaller $\omega_O t_n$), the more significant will be this difference. On the other hand, for deep reflections—large t_n measured in units of period ($\omega_O t_n$), this extra factor will be near unity for most dips.

Exercises

7.4 Define an output time by

$$t_O = 2r_O/c.$$

Use (7.6.20) to write r_O in terms of L and then use (7.6.35) to write L in terms of the variables of Hale DMO to conclude that

$$t_O = \frac{t_n}{A}.$$

7.5 The purpose of this exercise is to verify the calculations that lead to the Hale-type TZO.

a. Show that when (7.6.32) is substituted into (7.6.23), the resulting phase of the integral operator is given by the phase Φ defined in (7.6.31).

b. For this phase, show that the first derivatives are given by

$$\frac{\partial \Phi}{\partial \xi_I} = k - \frac{2\omega_O^2 \delta \operatorname{sgn}(\omega_O)}{c\sqrt{h^2\omega_I^2 + \delta^2\omega_O^2}}, \quad \frac{\partial \Phi}{\partial \omega_I} = t - \frac{2h^2\omega_I \operatorname{sgn}(\omega_O)}{c\sqrt{h^2\omega_I^2 + \delta^2\omega_O^2}}.$$

c. Set these first derivatives equal to zero and solve for δ and ω_I to verify (7.6.34). Hint: Equate the two expression for $\sqrt{h^2\omega_I^2 + \delta^2\omega_O^2}$ to obtain a linear relationship between δ and ω_I. Then substitute into either equation to obtain an equation in just one unknown.

d. Show that

$$\det \begin{bmatrix} \dfrac{\partial^2 \Phi}{\partial \xi_I^2} & \dfrac{\partial^2 \Phi}{\partial \xi_I \partial \omega_I} \\ \dfrac{\partial^2 \Phi}{\partial \xi_I \partial \omega_I} & \dfrac{\partial^2 \Phi}{\partial \omega_I^2} \end{bmatrix} = -\frac{c^2 k^4 A^4}{4}$$

and use this result to verify (7.6.36).

7.6.3 Gardner/Forel-Type TZO

Gardner and Forel [1988, 1995] proposed a transformation to zero-offset that mapped space-time data to space-time data. Here, we can specialize (7.5.4) to obtain a version of that transformation consistent with the present theory. We remind the reader that we are still dealing with TZO, for which the input isochron is an ellipse and the output isochron is a circle. Because the circle fits inside the ellipse at tangency (stationarity), the circle's radius of curvature is smaller than that of the ellipse. Correspondingly,

$$\kappa_O > \kappa_I$$

and, therefore, we use the first form in that equation, with D_O defined by (7.5.4) and (7.5.5).

For the specialization to constant-background, many of the results that we already derived become useful here. From our computations above, (7.5.4) simplifies as follows:

$$U_O(\xi_O, t_O) \sim \frac{1}{2(2\pi)^{3/2}\sqrt{c}} \int z\, D_{1/2}(\xi_I, t_I) \frac{\sqrt{r_s r_g}}{r_0} \frac{\sqrt{\cos\theta}}{\sin\theta} \cdot \sqrt{r_s + r_g} \left[\frac{1}{r_s^2} + \frac{1}{r_g^2}\right] d\xi_I. \quad (7.6.38)$$

The independent variables here are ξ_I, ξ_O and t_O. Thus, it remains to show how all other variables can be expressed in terms of just these three. The reader is reminded that we have all of the equations that arise from the stationary phase conditions in γ. We outline the necessary calculations below and leave the details as an exercise for the reader.

First, note that

$$r_0 = ct_O/2, \tag{7.6.39}$$

so that we can use either r_O or t_O as an independent variable. Below, we will use them interchangeably, as the need arises.

We next substitute the second form of L, given in (7.6.18), into (7.6.20) to solve for $\cos\theta$. The result is

$$\cos\theta = \frac{r_0}{\sqrt{h^2-\delta^2}\sqrt{h^2-\delta^2+r_0^2}}. \tag{7.6.40}$$

Because r_0 and δ are given (linear) functions of ξ_I, ξ_O and t_O, $\cos\theta$ is now determined in terms of those independent variables.

Now, we can return to the definition of L in (7.6.18) to write

$$L = \frac{h\sqrt{h^2-\delta^2}}{\sqrt{h^2-\delta^2+r_0^2}}. \tag{7.6.41}$$

With L determined, we now can write expressions for r_s and r_g by using (7.6.17):

$$r_s = \sqrt{h^2-\delta^2+r_0^2}\sqrt{\frac{h-\delta}{h+\delta}}, \quad r_g = \sqrt{h^2-\delta^2+r_0^2}\sqrt{\frac{h+\delta}{h-\delta}}. \tag{7.6.42}$$

Now, by summing these two, we obtain an expression for t_I,

$$t_I = \frac{r_s+r_g}{c} = \frac{2h}{c}\frac{\sqrt{h^2-\delta^2+r_0^2}}{\sqrt{h^2-\delta^2}}. \tag{7.6.43}$$

Finally, we obtain z by using (7.6.21). The result is

$$z = \frac{r_0}{h^2-\delta^2}\sqrt{(h^2-\delta^2)^2-\delta^2 r_0^2}. \tag{7.6.44}$$

The list is now complete. For each choice of the variables, ξ_I, ξ_O and t_O, we know the traveltime and input spatial coordinate at which to evaluate $D_{1/2}(\xi_I, t_I)$. Furthermore, we have given a formula for each of the spatial variables appearing in the kernel of the operator in (7.6.36).

When all of these results are substituted into (7.6.36), the final result takes on a much simpler form,

$$U_O(\xi_O, t_O) \sim \frac{h\sqrt{t_O}}{(2\pi)^{3/2}} \int D_{1/2}(\xi_I, t_I)\frac{h^2+\delta^2}{(h^2-\delta^2)^2} d\xi_I. \tag{7.6.45}$$

Here, the domain of integration in ξ_I is as defined in (7.6.31).

Exercises

7.6 Verify the results stated in equations (7.6.39) through (7.6.44).

7.6.4 *On the Simplification of the Second Derivatives of the Phase*

Equation (7.4.40) expresses the isochron curvature in terms of the separate curvatures of the isochrons of the wavefronts from the source and receiver. This, in turn, provides an expression for the second derivative of the phase in (7.3.4) with respect to γ, a parameter along the isochron of τ_I, at the point where the phase is stationary. Equation (7.5.12) provides a corresponding simplification of the derivative of the phase at stationarity with respect to t_I, after the first stationary phase condition with respect to γ is applied. The significance of these two results is that they provide expressions for these second derivatives in terms of quantities that can be computed along the rays from the source and receiver, respectively, and in terms of the half-opening angle between those rays where they meet. Here, we derive those simplifications.

The reader who is not interested in these derivations could skip this section with no loss of information as regards the main theme of this chapter, which is to say, derivation of various specializations of the data mapping platform to applications of interest in seismic data processing.

Isochron Curvature

Here, we derive (7.4.40). Thus, we consider a single isochron, with the objective of expressing its curvature in terms of the curvatures of the separate source and receiver isochrons that intersect with the given isochron at the stationary point.

Because the derivation will apply to both τ_O and τ_I, the subscripts O and I will be omitted, for the moment. Thus, we begin with an equation of the form (7.4.28), but with the simplifications that the subscripts I are not used and the dependence of the traveltime on ξ_I is unnecessary, as well. That is, the relationship between the isochron traveltime t, the orthogonal variable γ on the isochrons, and the Cartesian coordinates $\boldsymbol{x}$ is simply given by

$$t \equiv \tau(\boldsymbol{x}(\gamma, t)). \tag{7.6.46}$$

For the purpose of the analysis of derivatives along the isochron for a fixed choice of t, the variable γ can be chosen as arclength along the isochron. We apply the chain rule to this equation, with the objective of determining relationships between derivatives with respect to γ:

$$\begin{aligned} 0 &= \frac{\partial \tau}{\partial x_i} \frac{\partial x_i}{\partial \gamma}, \\ 0 &= \frac{\partial^2 \tau}{\partial x_i \partial x_j} \frac{\partial x_i}{\partial \gamma} \frac{\partial x_j}{\partial \gamma} + \frac{\partial \tau}{\partial x_i} \frac{\partial^2 x_i}{\partial \gamma^2}. \end{aligned} \tag{7.6.47}$$

Here and below, summation over repeated indices is to be understood, with $i, j, \ldots$ assuming the values 1 and 3,.

In the second line, above, the second term can now be recognized as the dot product of the gradient of the total traveltime with the curvature vector of the isochron. Both of these vectors are normal to the isochron. The gradient of the traveltime points towards increasing traveltime, which would generally be the downward direction. In the absence of multi-pathing, the isochron is a convex-up curve, such as the DMO-ellipse; its curvature vector points in that upward direction. Thus, the curvature vector and the gradient point in opposite directions. That is,

$$\frac{\partial \tau}{\partial x_i} \frac{\partial^2 x_i}{\partial \gamma^2} = -|\nabla \tau| \kappa = -\frac{2\cos\theta}{c} \kappa.$$

In this equation, the second equality follows, as usual, from our knowledge of the magnitude of the gradient of the traveltime, with 2θ still the opening angle between the rays from the source and receiver in the input geometry—equation (6.3.3). Thus, we can solve for the second term in the second line of equation (7.6.47) as

$$|\nabla \tau| \kappa = \frac{2\cos\theta}{c} \kappa = \frac{\partial^2 \tau}{\partial x_i \partial x_j} \frac{\partial x_i}{\partial \gamma} \frac{\partial x_j}{\partial \gamma}. \tag{7.6.48}$$

We have now related the quadratic form in second derivatives of the traveltime τ to the curvature of the isochron. Next, we will relate this quadratic form to corresponding expressions in the traveltime from the source τ_s and the receiver. See Figure 7.9. Recall that $\tau = \tau_s + \tau_g$ and, hence,

$$\frac{\partial^2 \tau}{\partial x_i \partial x_j} \frac{\partial x_i}{\partial \gamma} \frac{\partial x_j}{\partial \gamma} = \frac{\partial^2 \tau_s}{\partial x_i \partial x_j} \frac{\partial x_i}{\partial \gamma} \frac{\partial x_j}{\partial \gamma} + \frac{\partial^2 \tau_g}{\partial x_i \partial x_j} \frac{\partial x_i}{\partial \gamma} \frac{\partial x_j}{\partial \gamma}. \tag{7.6.49}$$

Therefore, let us consider the isochron of the wavefront from the source point passing through the stationary point. Let t_s denote the time on this isochron, and $\tau_s(\boldsymbol{x})$ denote the traveltime function itself. Further, let γ_s denote arclength on the isochron and n_s denote signed arclength on a curve normal to the isochron, measured from the isochron and positive in the

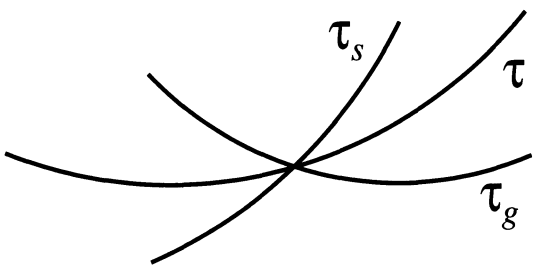

FIGURE 7.9. The three isochrons of τ, τ_s, and τ_g, crossing at the stationary point.

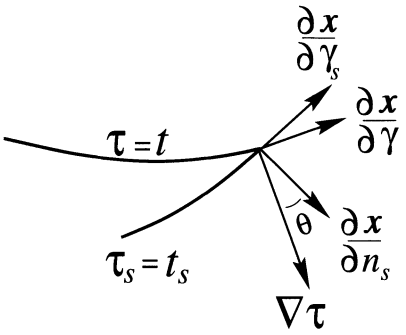

FIGURE 7.10. The tangents and normals to the intersecting isochrons of τ and τ_s. All are unit vectors except for $\nabla\tau$.

direction of increasing time. Then, $\boldsymbol{x} = \boldsymbol{f}_s(\gamma_s, n_s)$ defines a local coordinate system near this isochron. In particular, the isochron, itself, is given by

$$t_s = \tau_s(\boldsymbol{f}_s(\gamma_s, 0)). \tag{7.6.50}$$

Below, we will use the derivatives $d\boldsymbol{x}/d\gamma_s$ and $d\boldsymbol{x}/dn_s$, where it is to be understood that these derivatives are calculated by differentiating the function $\boldsymbol{f}_s(\gamma_s, n_s)$.

There are four vectors of interest to us in the analysis below: the unit tangent and normal to the isochron of τ_s, the unit tangent to the isochron of τ, and the normal to that isochron, $\nabla\tau$. They are all depicted in Figure 7.10. From the diagram, it is straightforward to check that

$$\frac{\partial \boldsymbol{x}}{\partial \gamma} = \frac{\partial \boldsymbol{x}}{\partial \gamma_s}\cos\theta + \frac{\partial \boldsymbol{x}}{\partial n_s}\sin\theta. \tag{7.6.51}$$

Using this result, the first expression on the right side in (7.6.49) can be rewritten as

$$\frac{\partial^2 \tau_s}{\partial x_i \partial x_j}\frac{\partial x_i}{\partial \gamma}\frac{\partial x_j}{\partial \gamma} = \frac{\partial^2 \tau_s}{\partial x_i \partial x_j}\left[\frac{\partial x_i}{\partial \gamma_s}\frac{\partial x_j}{\partial \gamma_s}\cos^2\theta + 2\frac{\partial x_i}{\partial \gamma_s}\frac{\partial x_j}{\partial n_s}\cos\theta\sin\theta + \frac{\partial x_i}{\partial n_s}\frac{\partial x_j}{\partial n_s}\sin^2\theta\right], \tag{7.6.52}$$

where all expressions are to be evaluated at the stationary point; in particular, $n_s = 0$ there.

The first double sum appearing on the right, here, is exactly the first term in the second line of (7.6.47), except for the subscripts, s. In fact, both lines of (7.6.47) are true for τ_s, with parameter γ replaced by γ_s. Consequently, (7.6.48), is true for τ_s as well, except that now $|\nabla\tau_s| = 2/c$. Therefore

$$\frac{\partial^2 \tau_s}{\partial x_i \partial x_j}\frac{\partial x_i}{\partial \gamma_s}\frac{\partial x_j}{\partial \gamma_s} = \frac{\kappa_s}{c}. \tag{7.6.53}$$

In this equation, κ_s is the curvature of the isochron of τ_s at the stationary point. With this result, the first summation on the right side of (7.6.52) has been expressed in terms of an isochron curvature and the background velocity.

Now, we turn to the two more difficult sums in that equation. The key here, is to relate the derivatives in the direction of n_s to derivatives along the rays associated with the eikonal equation that τ_s satisfies. In fact, with n_s being arclength in the direction normal to τ_s, we might as well take n_s to be the arclength variable on the ray through the isochron at the point in question. In this case, we can use the ray equations in arclength variables in Appendix E, which is to say, (E.2.13); that is, we can set

$$\frac{\partial \boldsymbol{x}}{\partial n_s} = \hat{\boldsymbol{p}}_s, \quad \frac{\partial \boldsymbol{p}_s}{\partial n_s} = -\frac{\nabla c}{c^2}, \quad \frac{\partial \tau_s}{\partial n_s} = \frac{1}{c}, \quad \boldsymbol{p}_s \equiv \nabla \tau_s, \quad \hat{\boldsymbol{p}}_s = c\boldsymbol{p}_s. \tag{7.6.54}$$

We use these results to write

$$\frac{\partial \tau_s}{\partial n_s} = \frac{1}{c} = \frac{\partial \tau_s}{\partial x_i} \frac{\partial x_i}{\partial n_s}. \tag{7.6.55}$$

By taking a second derivative with respect to n_s, here, we can obtain two alternative expressions for the second derivative of τ_s, one from differentiating $1/c$, and the other from differentiating the last expression. Of course, both differentiations are carried out using the chain rule, allowing us to relate the second derivative with respect to n_s to derivatives with respect to $\boldsymbol{x}$. As a first step, then,

$$\frac{\partial^2 \tau_s}{\partial n_s^2} = \frac{\partial^2 \tau_s}{\partial x_i \partial x_j} \frac{\partial x_i}{\partial n_s} \frac{\partial x_j}{\partial n_s} + \frac{\partial \tau_s}{\partial x_i} \frac{\partial^2 x_i}{\partial n_s^2}. \tag{7.6.56}$$

Note that the last term here is just the dot product of the gradient of the traveltime with the curvature vector of the ray. However, the gradient of the traveltime points along the ray, while the curvature vector is orthogonal to the ray. Thus, those two vectors are orthogonal, making the dot product equal to zero. Therefore,

$$\frac{\partial^2 \tau_s}{\partial n_s^2} = \frac{\partial^2 \tau_s}{\partial x_i \partial x_j} \frac{\partial x_i}{\partial n_s} \frac{\partial x_j}{\partial n_s}.$$

Now, let us obtain the second derivative of τ_s by differentiating $1/c$ in (7.6.55):

$$\frac{\partial^2 \tau_s}{\partial n_s^2} = -\frac{1}{c^2} \frac{\partial c}{\partial x_i} \frac{\partial x_i}{\partial n_s} = -\frac{\nabla c}{c^2} \cdot \frac{\partial \boldsymbol{x}}{\partial n_s} = -\frac{\nabla c}{c} \cdot \nabla \tau_s.$$

By equating our two expressions for the second derivative of τ_s, we find that

$$\frac{\partial^2 \tau_s}{\partial x_i \partial x_j} \frac{\partial x_i}{\partial n_s} \frac{\partial x_j}{\partial n_s} = -\frac{\nabla c}{c} \cdot \nabla \tau_s. \tag{7.6.57}$$

This is a representation of the third sum on the right side of (7.6.52) in terms of ray quantities and the underlying velocity function $c(\boldsymbol{x})$.

Now, we need to address the middle sum in (7.6.52). We can start again from (7.6.55), except that now we need to differentiate that equation with respect to γ_s. That is,

$$\frac{\partial^2 \tau_s}{\partial n_s \partial \gamma_s} = \frac{\partial^2 \tau_s}{\partial x_i \partial x_j} \frac{\partial x_i}{\partial n_s} \frac{\partial x_j}{\partial \gamma_s} + \frac{\partial \tau_s}{\partial x_i} \frac{\partial^2 x_i}{\partial \gamma_s \partial n_s} = -\frac{1}{c^2} \frac{\partial c}{\partial x_i} \frac{\partial x_i}{\partial \gamma_s} = -\frac{\nabla c}{c^2} \nabla c \cdot \frac{\partial \boldsymbol{x}}{\partial \gamma_s}. \tag{7.6.58}$$

We claim that

$$\frac{\partial \tau_s}{\partial x_i} \frac{\partial^2 x_i}{\partial \gamma_s \partial n_s} = 0.$$

To see why this is so, observe that the first factor here is just the gradient of the traveltime and is therefore orthogonal to the isochron of τ_s. The derivative, $\partial \boldsymbol{x}/\partial n_s$, is a unit vector in the same direction. Hence, the derivative of this vector with respect to γ_s is orthogonal to the vector itself, and thus also orthogonal to the gradient. Therefore, the claim follows.

In summary, then,

$$\frac{\partial^2 \tau_s}{\partial x_i \partial x_j} \frac{\partial x_i}{\partial n_s} \frac{\partial x_j}{\partial \gamma_s} = -\frac{1}{c^2} \frac{\partial c}{\partial x_i} \frac{\partial x_i}{\partial \gamma_s} = -\frac{\nabla c}{c^2} \cdot \frac{\partial \boldsymbol{x}}{\partial \gamma_s}. \tag{7.6.59}$$

This simplifies the middle sum in (7.6.52).

Now, we have all the terms we need to rewrite (7.6.52) in simpler form. We use results (7.6.53), (7.6.57), and (7.6.59) to do this, obtaining

$$\frac{\partial^2 \tau_s}{\partial x_i \partial x_j} \frac{\partial x_i}{\partial \gamma} \frac{\partial x_j}{\partial \gamma} = \frac{\kappa_s}{c} \cos^2 \theta - 2 \frac{\nabla c}{c^2} \cdot \frac{\partial \boldsymbol{x}}{\partial \gamma_s} \cos \theta \sin \theta - \frac{\nabla c}{c} \cdot \nabla \tau_s \sin^2 \theta. \tag{7.6.60}$$

Recall that our objective is to use (7.6.49) to arrive at a relationship between the curvature of the isochron of τ and the curvatures of the separate isochrons of τ_s and τ_g. Equation (7.6.48) gives the left side of (7.6.49) in terms of the curvature of τ; equation (7.6.60) gives the first term on the right in (7.6.49) in terms of the curvature of the isochron of τ_s. Now, we need an analogous relationship between the second term on the right in (7.6.49) and the curvature of the isochron of τ_g. That requires that we repeat the analysis immediately above for the traveltime function τ_g, but, of course, it will not be necessary to do this in detail. The corresponding result for τ_g can be deduced from the result above by making the following replacements:

$$\tau_s,\ \gamma_s,\ n_s,\ \kappa_s \longrightarrow \tau_g,\ \gamma_g,\ n_g,\ \kappa_g, \quad \text{respectively,}$$

$$\theta_s \longrightarrow -\theta_g.$$

Here, the last replacement follows from the fact that the gradients of τ_s and τ_g fall on sides of opposite of the gradient of τ, or, equivalently, that the

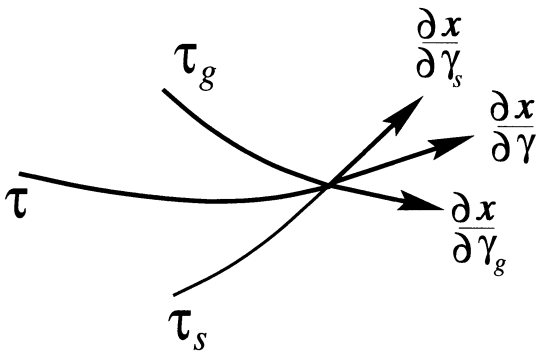

FIGURE 7.11. The intersection point of the three isochrons of τ_s, τ_g, and τ, with their respective tangent vectors.

tangents to the isochrons of τ_s and τ_g fall on opposite sides of the tangent to the isochron of τ as in Figure 7.11. Thus, the corresponding result to (7.6.60) for τ_g is

$$\frac{\partial^2 \tau_g}{\partial x_i \partial x_j} \frac{\partial x_i}{\partial \gamma} \frac{\partial x_j}{\partial \gamma} = \frac{\kappa_g}{c} \cos^2\theta + 2\frac{\nabla c}{c^2} \cdot \frac{\partial \boldsymbol{x}}{\partial \gamma_g} \cos\theta \sin\theta - \frac{\nabla c}{c} \cdot \nabla \tau_g \sin^2\theta. \tag{7.6.61}$$

We now use (7.6.48) and (7.6.49) to conclude that

$$\kappa = \cos\theta \frac{\kappa_s + \kappa_g}{2} + \frac{\nabla c}{c} \cdot \left[\frac{\partial \boldsymbol{x}}{\partial \gamma_g} - \frac{\partial \boldsymbol{x}}{\partial \gamma_s}\right] \sin\theta - \frac{\nabla c}{2} \cdot [\nabla \tau_g + \nabla \tau_s] \frac{\sin^2\theta}{\cos\theta}. \tag{7.6.62}$$

Further simplification is possible here. From Figure 7.11, one can see that the tangents to the isochrons of τ_s and τ_g have the same projection on the tangent to the isochron of τ. Hence, the difference of those two vectors, appearing in this equation, has no projection on the last tangent and, instead, is a vector along $\nabla\tau$. Furthermore, it is easy to see that the magnitude of that normal vector is $2\sin\theta$; that is,

$$\frac{\partial \boldsymbol{x}}{\partial \gamma_g} - \frac{\partial \boldsymbol{x}}{\partial \gamma_s} = \frac{c\nabla\tau}{2\cos\theta} 2\sin\theta = c\nabla\tau \tan\theta. \tag{7.6.63}$$

Here, the middle expression is written as the product of a unit vector in the direction of $\nabla\tau$ and the deduced magnitude of the sum of tangents. Therefore, the middle term in (7.6.62) becomes

$$\frac{\nabla c}{c} \cdot \left[\frac{\partial \boldsymbol{x}}{\partial \gamma_g} - \frac{\partial \boldsymbol{x}}{\partial \gamma_s}\right] \sin\theta = \nabla\tau \cdot [\nabla \tau_g + \nabla \tau_s] \frac{\sin^2\theta}{\cos\theta},$$

while the last term in (7.6.62) is just half that same quantity. Therefore, the last two terms in (7.6.62) combine, leading to the result

$$\kappa = \frac{\cos\theta}{2} \left[\kappa_s + \kappa_g + \nabla c \cdot \nabla\tau \tan^2\theta\right]. \tag{7.6.64}$$

This verifies claim (7.4.40), except, of course, that we have dropped the subscripts O and I for this discussion. The same derivation applies to both. Note that the result is an even function of θ. Thus, although we started with a particular orientation of source and receiver—thereby assigning θ to the former and $-\theta$ to the latter—we see, here, that the result is independent of that orientation and remains unchanged (as it should) if the source and receiver positions are reversed.

The Second Derivative of the Phase with Respect to t_I

We turn now to the verification of (7.5.12), where K is the second derivative of the phase Φ, (7.5.7), whose first derivative is given by (7.5.8). Then, as above, chain rule differentiation leads to the result

$$\frac{\partial^2 \Phi}{\partial t_I^2} = \omega_O \left[\frac{\partial \tau_O}{\partial x_i} \frac{\partial^2 x_i}{\partial t_I^2} + \frac{\partial^2 \tau_O}{\partial x_i \partial x_j} \frac{\partial x_i}{\partial t_I} \frac{\partial x_j}{\partial t_I} \right]. \tag{7.6.65}$$

Our next objective is to make a substitution that replaces the second derivatives of the x_i's with second derivatives of a traveltime. To this end, we write the identity

$$\frac{\partial \tau_I}{\partial x_i} \frac{\partial x_i}{\partial t_I} = 1$$

The factor, $\partial x_i / \partial t_I$, treats the x_i's as functions of t_I (and γ_I), while the factor, $\partial \tau_I / \partial x_i$, recasts the traveltime as a function of $\boldsymbol{x}$. Differentiation of this expression with respect to t_I leads to two terms:

$$\begin{aligned} 0 &= \frac{\partial \tau_I}{\partial x_i} \frac{\partial^2 x_i}{\partial t_I^2} + \frac{\partial}{\partial t_I} \left[\frac{\partial \tau_I}{\partial x_i} \right] \frac{\partial x_i}{\partial t_I} \\ &= \frac{\partial \tau_I}{\partial x_i} \frac{\partial^2 x_i}{\partial t_I^2} + \frac{\partial^2 \tau_I}{\partial x_i \partial x_j} \frac{\partial x_i}{\partial t_I} \frac{\partial x_j}{\partial t_I}. \end{aligned}$$

The second form follows from the chain rule and leads to the conclusion

$$\frac{\partial^2 x_i}{\partial t_I^2} \frac{\partial \tau_I}{\partial x_i} = - \frac{\partial^2 \tau_I}{\partial x_i \partial x_j} \frac{\partial x_i}{\partial t_I} \frac{\partial x_j}{\partial t_I}.$$

Note that the gradient of τ_I on the left side of this equation is parallel to the gradient of τ_O at the stationary point where all of these functions are being evaluated. In fact, the only difference between them is a ratio of cosines, leading to the conclusion,

$$\frac{\partial^2 x_i}{\partial t_I^2} \frac{\partial \tau_O}{\partial x_i} \frac{\cos \theta_I}{\cos \theta_O} = - \frac{\partial^2 \tau_I}{\partial x_i \partial x_j} \frac{\partial x_i}{\partial t_I} \frac{\partial x_j}{\partial t_I}.$$

The summation on the left side of this last equation is the same as that appearing as the first term on the right side of (7.6.65). Thus, we conclude that

$$\frac{\partial^2 \Phi}{\partial t_I^2} = \omega_O \frac{\partial^2 \tau_O}{\partial x_i \partial x_j} \frac{\partial x_i}{\partial t_I} \frac{\partial x_j}{\partial t_I} - \omega_I \frac{\partial^2 \tau_I}{\partial x_i \partial x_j} \frac{\partial x_i}{\partial t_I} \frac{\partial x_j}{\partial t_I}.$$

Here, we have also used stationarity condition (7.5.10) to eliminate the ratio of cosines. This expression contains two gradient vectors that we now replace by unit vectors. To do so, we introduce n as arclength in that gradient direction and rewrite this last equation as

$$\frac{\partial^2 \Phi}{\partial t_I^2} = \frac{c^2}{4\cos^2 \theta_I} \left[\omega_O \frac{\partial^2 \tau_O}{\partial x_i \partial x_j} - \omega_I \frac{\partial^2 \tau_I}{\partial x_i \partial x_j} \right] \frac{\partial x_i}{\partial n} \frac{\partial x_j}{\partial n}. \tag{7.6.66}$$

Now, it is necessary to carry out an analysis similar to that following (7.6.49). There, the tangent $(d\boldsymbol{x}/d\gamma)$ to the isochron, τ (τ_O or τ_I) was expressed in terms of the tangent and normal to respective isochrons τ_s and τ_g. We were then able to derive simpler expressions for the quadratic forms in the second derivatives of these separate isochron functions, equations (7.6.53), (7.6.57) and (7.6.59). Here, the same sort of decomposition has to be carried out for the normal vector, $d\boldsymbol{x}/dn$. This will lead to exactly the same quadratic forms as above, but in different linear combination reflecting the difference between the quadratic form in second derivatives with tangent vector components (previously) and the second derivatives with normal vector components (here).

As in the previous analysis, we dispense with the subscripts I and O for the following discussion. In either case, it is necessary to first write the quadratic form on the right side of (7.6.66) in terms of the quadratic forms in τ_s and τ_g, completely analogously to (7.6.49). That is,

$$\frac{\partial^2 \tau}{\partial x_i \partial x_j} \frac{\partial x_i}{\partial n} \frac{\partial x_j}{\partial n} = \frac{\partial^2 \tau_s}{\partial x_i \partial x_j} \frac{\partial x_i}{\partial n} \frac{\partial x_j}{\partial n} + \frac{\partial^2 \tau_g}{\partial x_i \partial x_j} \frac{\partial x_i}{\partial n} \frac{\partial x_j}{\partial n}. \tag{7.6.67}$$

With the aid of Figure 7.11, we set

$$\frac{\partial x_i}{\partial n} = \frac{\partial x_i}{\partial n_s} \cos\theta - \frac{\partial x_i}{\partial \gamma_s} \sin\theta \tag{7.6.68}$$

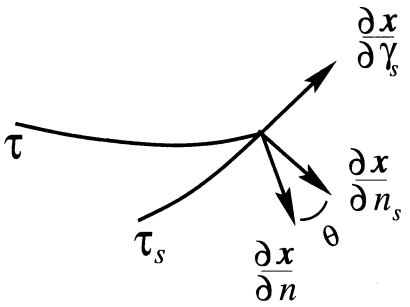

FIGURE 7.12. The intersection point of the isochrons τ_s and τ with the relevant unit vectors.

$$= \frac{\partial x_i}{\partial n_g}\cos\theta - \frac{\partial x_i}{\partial \gamma_g}\sin\theta.$$

The first line should be compared to (7.6.51); the second line follows from the replacement of θ by $-\theta$.

Now, as in the earlier analysis, we focus on the expression in τ_s and write

$$\frac{\partial^2\tau_s}{\partial x_i \partial x_j}\frac{\partial x_i}{\partial n}\frac{\partial x_j}{\partial n} = \frac{\partial^2\tau_s}{\partial x_i \partial x_j}\frac{\partial x_i}{\partial n_s}\frac{\partial x_j}{\partial n_s}\cos^2\theta$$

$$- 2\frac{\partial^2\tau_s}{\partial x_i \partial x_j}\frac{\partial x_i}{\partial n_s}\frac{\partial x_j}{\partial \gamma_s}\cos\theta\sin\theta + \frac{\partial^2\tau_s}{\partial x_i \partial x_j}\frac{\partial x_i}{\partial \gamma_s}\frac{\partial x_j}{\partial \gamma_s}\sin^2\theta \tag{7.6.69}$$

$$= -\frac{\nabla c}{c}\cdot\nabla\tau_s\cos^2\theta + 2\frac{\nabla c}{c^2}\cdot\frac{\partial \boldsymbol{x}}{\partial \gamma_s}\cos\theta\sin\theta + \frac{\kappa_s}{c}\sin^2\theta.$$

Here, to obtain the second equation, we used equations (7.6.53), (7.6.57), and (7.6.59).

There is no need to redo the analysis for τ_g; as previously, we can extrapolate that result from this one:

$$\frac{\partial^2\tau_g}{\partial x_i \partial x_j}\frac{\partial x_i}{\partial n}\frac{\partial x_j}{\partial n} = -\frac{\nabla c}{c}\cdot\nabla\tau_g\cos^2\theta - 2\frac{\nabla c}{c^2}\cdot\frac{\partial \boldsymbol{x}}{\partial \gamma_g}\cos\theta\sin\theta + \frac{\kappa_g}{c}\sin^2\theta. \tag{7.6.70}$$

We now combine these last two results to obtain the right side of (7.6.67). That result is

$$\frac{\partial^2\tau}{\partial x_i \partial x_j}\frac{\partial x_i}{\partial n}\frac{\partial x_j}{\partial n} = -\frac{\nabla c}{c}\cdot\nabla\tau\cos^2\theta - 2\frac{\nabla c}{c^2}\cdot\left[\frac{\partial \boldsymbol{x}}{\partial \gamma_g} - \frac{\partial \boldsymbol{x}}{\partial \gamma_s}\right]\cos\theta\sin\theta$$

$$+ \frac{\kappa_s + \kappa_g}{c}\sin^2\theta. \tag{7.6.71}$$

Finally, use the result (7.6.63) to obtain

$$\frac{\partial^2\tau}{\partial x_i \partial x_j}\frac{\partial x_i}{\partial n}\frac{\partial x_j}{\partial n} = -\frac{\nabla c}{c}\cdot\nabla\tau\left[1+\sin^2\theta\right] + \frac{\kappa_s + \kappa_g}{c}\sin^2\theta. \tag{7.6.72}$$

Here, we have also simplified the combination of trig functions in the first expression.

Recall that our objective is to obtain an expression for the second derivative of the phase function in (7.6.66) in terms of ray quantities. To do so, this last result must be applied to τ_O and to τ_I, leading to the expression

$$\frac{\partial^2\Phi}{\partial t_I^2} = \frac{c^2}{4\cos^2\theta_I}\left[\omega_O\left\{-\frac{\nabla c}{c}\cdot\nabla\tau_O\left[1+\sin^2\theta_O\right] + \frac{\kappa_s+\kappa_g}{c}\sin^2\theta_O\right\}\right. \tag{7.6.73}$$

$$\left. - \omega_I\left\{-\frac{\nabla c}{c}\cdot\nabla\tau_I\left[1+\sin^2\theta_I\right] + \frac{\kappa_{Is}+\kappa_{Ig}}{c}\sin^2\theta_I\right\}\right].$$

Note, however, that

$$\frac{c^2}{4\cos^2\theta_I} = \frac{1}{|\nabla\tau_I|^2}.$$

Also, recall that, at stationarity, the two gradients are parallel and that (7.5.10) is satisfied; that is,

$$\omega_O \nabla\tau_O = \omega_I \nabla\tau_I.$$

By using these two results in (7.6.73), we obtain the conclusion

$$\frac{\partial^2\Phi}{\partial t_I^2} = \frac{1}{|\nabla\tau_I|^2} K, \tag{7.6.74}$$

with K given by (7.5.12).

7.7 3D Data Mapping

We return now to the 3D data mapping platform, equation (7.2.6). The results obtained above for 2.5D data maps provide a guide to 3D applications. For example, again we can perform asymptotic analysis in traveltime variables. There is much to be learned from stationary phase analysis along the isochron, and that will be our first approach to 3D processing. Thus, we begin the analysis of this section by introducing the 3D version of the isochron variables in (7.4.28). That is, we introduce two coordinates on the traveltime surface $\boldsymbol{\gamma} = (\gamma_1, \gamma_2)$, with $\boldsymbol{x} = \boldsymbol{x}(\boldsymbol{\gamma})$ on the isochron, and the traveltime itself as the third variable as shown in Figure 7.13. That is,

$$t_I \equiv \tau_I(\boldsymbol{x}(\boldsymbol{\gamma}, \boldsymbol{\xi_I})), \tag{7.7.1}$$

with

$$d^3x = d\gamma_1 d\gamma_2 dt_I \left|\frac{\partial(\boldsymbol{x})}{\partial(\boldsymbol{\gamma}, t_I)}\right| = d\gamma_1 d\gamma_2 dt_I \left|\frac{\partial(\boldsymbol{x})}{\partial(\boldsymbol{\gamma})}\right| \left|\frac{\partial \boldsymbol{x}}{\partial t_I}\right|$$

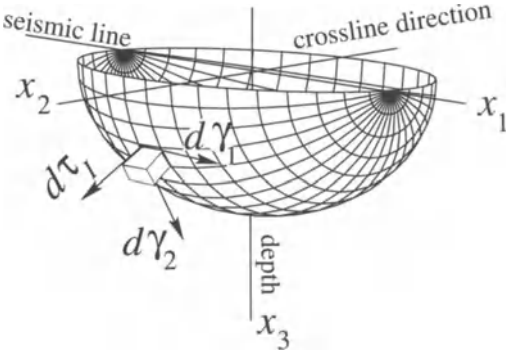

FIGURE 7.13. Isochron and coordinate system for 3D data mapping.

$$= d\gamma_1 d\gamma_2 dt_I \frac{\sqrt{g_I}}{|\nabla_x \tau_I|}. \tag{7.7.2}$$

In this equation, the second equality follows from the fact that the surface defined by $\boldsymbol{x} = \boldsymbol{x}(\boldsymbol{\gamma})$ is orthogonal to the direction of increasing t_I. In the next equality, g_I^2 is the determinant of the elements in the first fundamental tensor of differential geometry for the isochron surface(s) of τ_I:

$$g_I^2 = \det \left| \frac{d\boldsymbol{x}}{d\gamma_i} \cdot \frac{d\boldsymbol{x}}{d\gamma_j} \right| = \left| \frac{\partial(\boldsymbol{x})}{\partial(\boldsymbol{\gamma})} \right|^2.$$

Here, with $i, j = 1, 2$, the first equality is a definition and the second is a derivable result that can be found in any text on differential geometry, such as Kreyszig [1991]. Alternatively, one can obtain result (7.7.2) by observing that the surface area element of a basic parallelogram on the isochron, due to differential increments in γ_1 and γ_2, is given by

$$dS = \left| \frac{\partial(\boldsymbol{x})}{\partial\gamma_1} \times \frac{\partial(\boldsymbol{x})}{\partial\gamma_2} \right| d\gamma_1 d\gamma_2.$$

With these new variables, the 3D KDM platform equation (7.2.6) becomes

$$\begin{aligned} u_O(\boldsymbol{\xi}_O, \omega_O) \sim -\frac{i\omega_O}{8\pi^3} \int i\omega_I \, d\omega_I \, d^2\xi_I \, u_I(\boldsymbol{\xi}_I, \omega_I) \\ \cdot \int \frac{a_O(\boldsymbol{x}, \boldsymbol{\xi}_O)}{a_I(\boldsymbol{x}, \boldsymbol{\xi}_I)} \frac{|\nabla_x \tau_O(\boldsymbol{x}, \boldsymbol{\xi}_O)|}{|\nabla_x \tau_I(\boldsymbol{x}, \boldsymbol{\xi}_I)|^2} |h(\boldsymbol{x}, \boldsymbol{\xi}_I)| \\ \cdot e^{i\omega_O \tau_O(\boldsymbol{x}, \boldsymbol{\xi}_O) - i\omega_I t_I} \sqrt{g_I} d\gamma_1 d\gamma_2 dt_I. \end{aligned} \tag{7.7.3}$$

7.7.1 Stationary Phase in $\boldsymbol{\gamma}$

We can now apply the method of stationary phase in $\boldsymbol{\gamma}$. As in (7.4.31), we consider the phase function

$$\Phi = \tau_O(\boldsymbol{x}(\boldsymbol{\gamma}), \boldsymbol{\xi}_O). \tag{7.7.4}$$

The derivatives of this phase are

$$\begin{aligned} \frac{\partial\Phi}{\partial\gamma_p} &= \nabla_x \tau_O \cdot \frac{\partial \boldsymbol{x}}{\partial\gamma_p} = \frac{\partial\tau_O}{\partial x_i} \frac{\partial x_i}{\partial\gamma_p}, \quad p = 1, 2, \\ \frac{\partial^2\Phi}{\partial\gamma_p \partial\gamma_q} &= \frac{\partial^2\tau_O}{\partial x_i \partial x_j} \frac{\partial x_i}{\partial\gamma_p} \frac{\partial x_j}{\partial\gamma_q} + \frac{\partial\tau_O}{\partial x_i} \frac{\partial^2 x_i}{\partial\gamma_p \partial\gamma_q}, \quad p, q = 1, 2. \end{aligned} \tag{7.7.5}$$

In these equations, summation over the indices i, j from 1 to 3 is to be understood.

The phase will be stationary when the two first derivatives in the first line of the last equation are both zero. This requires that the gradient of the traveltime τ_O be orthogonal to two independent tangent vectors in the

isochron surface of τ_I. That is, the gradients of the two traveltimes $\nabla_x \tau_I$ and $\nabla_x \tau_O$ must be parallel at the stationary point, or, equivalently, the two isochrons must be tangent at the stationary point. We might think of Figures 7.2 and 7.3 as showing slices of the isochron surface of τ_I being cut by the isochrons of τ_O with tangency occurring at a point. For the moment, we will proceed with the analysis here as if there is a single, identifiable stationary point.

If $\hat{\boldsymbol{n}}$ denotes the upward unit normal common to both isochrons at the stationary point, then we can write

$$\begin{aligned} \nabla_x \tau_I &= -\hat{\boldsymbol{n}} |\nabla_x \tau_I| = -\hat{\boldsymbol{n}} \cos\theta_I / c(\boldsymbol{x}), \\ \nabla_x \tau_O &= -\hat{\boldsymbol{n}} |\nabla_x \tau_O| = -\hat{\boldsymbol{n}} \cos\theta_O / c(\boldsymbol{x}), \end{aligned} \tag{7.7.6}$$

and we can set

$$\frac{\partial \tau_O}{\partial x_i} \frac{\partial^2 x_i}{\partial \gamma_p \partial \gamma_q} = -\hat{\boldsymbol{n}} \cdot \frac{\partial^2 \boldsymbol{x}}{\partial \gamma_p \partial \gamma_q} |\nabla_x \tau_O| = -B^I_{pq} |\nabla_x \tau_O|, \quad p, q = 1, 2. \tag{7.7.7}$$

Here, B^I_{pq} introduces the standard notation for the dot product in the middle expression. These are the elements of the *second* fundamental tensor of differential geometry. As in the analysis of the isochron *curve* in the 2.5D data mapping, above, this tensor characterizes the curvature of the isochron surface. We will say more about these coefficients below.

In analogy with the 2.5D discussion, we now relate the second derivative of τ_O in (7.7.5) to the second fundamental tensor associated with the isochron of the stationary value of τ_O. As in the discussion leading to (7.4.36), we denote the equation of this isochron by $\boldsymbol{x} = \boldsymbol{x}'(\boldsymbol{\gamma}')$. Then, by implicit differentiation,

$$\begin{aligned} 0 &= \frac{\partial \tau_O}{\partial x_i} \frac{\partial x'_i}{\partial \gamma'_p}, \quad p = 1, 2 \\ 0 &= \frac{\partial^2 \tau_O}{\partial x_i \partial x_j} \frac{\partial x'_i}{\partial \gamma'_p} \frac{\partial x'_i}{\partial \gamma'_q} + \frac{\partial \tau_O}{\partial x_i} \frac{\partial^2 x'_i}{\partial \gamma'_p \partial \gamma'_q}, \quad p, q = 1, 2. \end{aligned} \tag{7.7.8}$$

The first equation here is again a statement of the orthogonality of the gradient of τ_O to each of two independent tangents in the isochron surface, equivalent to the orthogonality of the gradient to the isochron surface. In the second equation, we can make the first term on the right agree with the first term in the second derivative of Φ in (7.7.5) by taking the variables $\boldsymbol{\gamma}'$ to agree with the variables $\boldsymbol{\gamma}$, at least at the stationary point. Then, using (7.7.6), we find that

$$\begin{aligned} \frac{\partial^2 \tau_O}{\partial x_i \partial x_j} \frac{\partial x'_i}{\partial \gamma_p} \frac{\partial x'_i}{\partial \gamma_q} &= -\frac{\partial \tau_O}{\partial x_i} \frac{\partial^2 x'_i}{\partial \gamma_p \partial \gamma_q} \\ &= \hat{\boldsymbol{n}} \cdot \frac{\partial^2 \boldsymbol{x}'}{\partial \gamma_p \partial \gamma_q} |\nabla_x \tau_O| \end{aligned} \tag{7.7.9}$$

$$= B^O_{pq} |\nabla_x \tau_O|, \qquad p, q = 1, 2.$$

That is, the second derivatives of τ_O are related to elements of the second fundamental tensor of the isochron of the stationary value of τ_O.

By combining this result with our previous result about the second term of the second derivatives of Φ in (7.7.5), we find that

$$\frac{\partial^2 \Phi}{\partial \gamma_p \partial \gamma_q} = \left[B^I_{pq} - B^O_{pq}\right] |\nabla_x \tau_O|, \qquad p, q = 1, 2. \tag{7.7.10}$$

7.7.2 Discussion of the Second Derivatives of the Phase

We are now prepared to discuss the second derivatives of the phase function. The matrix of second derivatives will be expressed in terms of the derivatives of the second fundamental tensors for the isochron surfaces. Recall that the determinant of the matrix of second derivatives of Φ (the Hessian) and the signature of this matrix of second derivatives are given by

$$\det\left[\frac{\partial^2 \Phi}{\partial \gamma_p \partial \gamma_q}\right] = |\nabla_x \tau_O|^2 \det\left[B^I_{pq} - B^O_{pq}\right], \quad \mu = \operatorname{sgn}\left[\frac{\partial^2 \Phi}{\partial \gamma_p \partial \gamma_q}\right]. \tag{7.7.11}$$

This determinant and signature appear in the application of the method of stationary phase to (7.7.3). In particular, from (3.6.7), for the method of stationary phase to yield a computationally acceptable result, it is necessary that

$$\frac{|\omega_O| L^4}{{g_I}^2} \min_j(|\lambda_j|) \geq \pi.$$

In this equation, the λ_j's are the eigenvalues of the matrix

$$\left[\frac{\partial^2 \Phi}{\partial \gamma_p \partial \gamma_q}\right], \quad p, q = 1, 2.$$

We see here, that the eigenvalues of $B^I_{pq} - B^O_{pq}$, the difference of second fundamental tensors of the traveltimes appearing in (7.7.11), play a crucial role in the asymptotic validity and utility of the application of the method of stationary phase to the $\boldsymbol{\gamma}$-integration in (7.7.3).

Let us now discuss the second fundamental tensors appearing in (7.7.10). If we view the second fundamental tensor as a 2×2 matrix, then the symmetry of the matrix assures that there exists an orthogonal transform that diagonalizes this matrix. In this diagonal form, the elements on the main diagonal are given by

$$\hat{\boldsymbol{n}} \cdot \boldsymbol{\kappa}_p \left[\frac{ds}{d\tilde{\gamma}_p}\right]^2, \quad p = 1, 2.$$

Here, we do not sum over p. Each $\tilde{\gamma}_p$ is a local linear rotation of the original γ's. On the other hand, the $\boldsymbol{\kappa}_p$'s are the *principal curvatures* of the isochron.

They are collinear with $\hat{\boldsymbol{n}}$ (within a sign) and their values are the minimum and maximum of the this dot product on normal slices through the isochron at the given point.

Thus, if the principal directions of the isochrons were collinear, then the Hessian determinant here would just be a product of the differences of curvatures, a simple generalization of (7.4.37). This provides an insight into the possibility of failure of the method of stationary phase for the analysis of data mapping. In this simple case, where the principal directions are collinear, the Hessian will be zero (and the simple stationary phase formula will not provide a valid asymptotic expansion of the data mapping integral) if one or the other pairs of the principal curvatures are equal. This generalizes the results of the 2.5D discussion, where the matching of the isochron *curves* would cause the method of stationary phase to fail.

More generally, when the principal directions of the two fundamental tensors do not agree, the eigenvalues of the matrix of the difference of fundamental tensors must be bounded away from zero.

There is one particular case where we know that: (i) the principal directions coincide and (ii) the curvatures of the isochrons in at least one of the principal directions agree. In this case, the Hessian is zero and we will require an alternative method to approximate the data mapping integral. That is the subject of the next section.

Barring these pitfalls occurring, we can apply the 2D stationary phase formula to (7.7.3) to obtain

$$\begin{aligned} u_O(\boldsymbol{\xi}_O, \omega_O) &\sim e^{i\,\mathrm{sgn}\,(\omega_O)\mu\pi/4} d_O(\boldsymbol{\xi}_O, \omega_O), \quad \text{with} \\ d_O(\boldsymbol{\xi}_O, \omega_O) &= \frac{1}{4\pi^2} \int \omega_I \, d\omega_I \, d^2\xi_I \, u_I(\boldsymbol{\xi}_I, \omega_I) \\ &\quad \cdot \int \frac{a_O(\boldsymbol{x}, \boldsymbol{\xi}_O)}{a_I(\boldsymbol{x}, \boldsymbol{\xi}_I)} \frac{|h(\boldsymbol{x}, \boldsymbol{\xi}_I)|}{|\nabla_x \tau_I(\boldsymbol{x}, \boldsymbol{\xi}_I)|^2} \frac{\sqrt{g_I}}{\sqrt{\left|\det\left[B^O_{pq} - B^I_{pq}\right]\right|}} \\ &\quad \cdot e^{[i\omega_O \tau_O(\boldsymbol{x}, \boldsymbol{\xi}_O) - i\omega_I t_I]} dt_I. \end{aligned} \tag{7.7.12}$$

In this equation, $\boldsymbol{\gamma} = \boldsymbol{\gamma}(\boldsymbol{\xi}_I, \boldsymbol{\xi}_O, t_I)$, is determined by the stationarity of Φ, setting the first derivatives in (7.7.5) equal to zero. Correspondingly, $\boldsymbol{x} = \boldsymbol{x}(\boldsymbol{\gamma}(\boldsymbol{\xi}_I, \boldsymbol{\xi}_O, t_I), t_I)$ as a result of its definition as a function of $\boldsymbol{\gamma}$.

As a further consequence,

$$\tau_O(\boldsymbol{x}, \boldsymbol{\xi}_O) = \tau_O(\boldsymbol{x}(\boldsymbol{\gamma}(\boldsymbol{\xi}_I, \boldsymbol{\xi}_O, t_I), t_I, \boldsymbol{\xi}_O).$$

That is, the output traveltime is coupled to the input traveltime and to the geometry of sources, receivers and rays through the stationary phase evaluation.

Time-Domain Processing

It is fairly straightforward to write down the formula for a general 3D time-domain processing by taking the inverse Fourier transform with respect to

ω_O. This follows the derivation in Section 7.5.1 for time-domain processing in 2.5D. Of course, the result becomes useful only when particular input and output source-receiver configurations and background wavespeeds are defined. Nonetheless, we proceed. One need only observe the simple time-frequency dependence in the definition of d_O in (7.7.12) to realize that the inverse transform from ω_O to t_O will yield a delta function in time, allowing us to carry out the integration in t_I, as well. This is exactly as was done in Section 7.5.1. That is,

$$\begin{aligned} D_O(\boldsymbol{\xi}_O, t_O) &= \int d_O(\boldsymbol{\xi}_O, \omega_O) e^{-i\,\mathrm{sgn}\,(\omega_O)\mu\pi/4 - i\omega_O t_O} d\omega_O \\ &= \frac{1}{4\pi^2} \int \omega_I \, d\omega_I \, d^2\xi_I \, u_I(\boldsymbol{\xi}_I, \omega_I) \\ &\quad \cdot \int \frac{a_O(\boldsymbol{x}, \boldsymbol{\xi}_O)}{a_I(\boldsymbol{x}, \boldsymbol{\xi}_I)} \frac{|h(\boldsymbol{x}, \boldsymbol{\xi}_I)|}{|\nabla_x \tau_I(\boldsymbol{x}, \boldsymbol{\xi}_I)|^2} \frac{\sqrt{g_I}}{\sqrt{|\det\left[B^O_{pq} - B^I_{pq}\right]|}} \\ &\quad \cdot e^{-i\omega_I t_I} \delta(t_O - \tau_O(\boldsymbol{x}, \boldsymbol{\xi}_O)) dt_I. \end{aligned} \tag{7.7.13}$$

As in Section 7.5.1, to carry out the next integration, we need only realize that

$$dt_I = dt_O \frac{dt_I}{dt_O} = dt_O \frac{|\nabla_x \tau_I|}{|\nabla_x \tau_O|}.$$

This allows us to transform the integration over t_I into an integration over t_O and immediately evaluate that integral exploiting the delta function.

The result is

$$\begin{aligned} D_O(\boldsymbol{\xi}_O, t_O) = \frac{1}{2\pi} \int \frac{a_O(\boldsymbol{x}, \boldsymbol{\xi}_O)}{a_I(\boldsymbol{x}, \boldsymbol{\xi}_I)} \frac{D_I(\boldsymbol{\xi}_I, t_I)|h(\boldsymbol{x}, \boldsymbol{\xi}_I)|}{|\nabla_x \tau_I(\boldsymbol{x}, \boldsymbol{\xi}_I)||\nabla_x \tau_O(\boldsymbol{x}, \boldsymbol{\xi}_O)|} \\ \cdot \frac{\sqrt{g_I}}{\sqrt{|\det\left[B^O_{pq} - B^I_{pq}\right]|}} d^2\xi_I. \end{aligned} \tag{7.7.14}$$

Here,

$$D_I(\boldsymbol{\xi}_I, t_I) \equiv \frac{1}{2\pi} \int \omega_I \, d\omega_I u_I(\boldsymbol{\xi}_I, \omega_I) e^{-i\omega_I t_I}, \tag{7.7.15}$$

and the coupling between the traveltimes is determined by the geometry of the stationary phase condition that requires that the isochrons of $\tau_I = t_I$ and $\tau_O = t_O$ be tangent.

Now it is a matter of relating this result for $D_O(\boldsymbol{\xi}_O, t_O)$ to a corresponding result for $U_O(\boldsymbol{\xi}_O, t_O)$ by using the relationship between the two functions as defined in (7.7.13). The final result, then, depends on μ, which is defined in (7.7.11) to be the signature of the matrix of second derivatives. The possible choices of this signature are ± 2 when the eigenvalues have the same sign, and zero when the eigenvalues have opposite signs. In the later case, $D_O = U_O$; in the former case, they are related through Hilbert transform. That is,

$$U_O(\boldsymbol{\xi}_O, t_O) = \begin{cases} D_O(\boldsymbol{\xi}_O, t_O), & \mu = 0, \\ \\ \mp\mathcal{H}[D_O(\boldsymbol{\xi}_O, t_O)], & \mu = \pm 2. \end{cases} \tag{7.7.16}$$

In this equation, $\mathcal{H}$ denotes the Hilbert transform, (A.7.6).

7.7.3 3D Constant-Background TZO

In this section, we consider the case of 3D constant-background TZO, an implementation of the data mapping platform for which the above asymptotic analysis does not apply. It will be seen below why this is so.

We assume that data are gathered along parallel lines, say constant value of the coordinate ξ_{I2}, at constant offset from a midpoint ξ_{I1}, placing the source and receiver at $(\xi_{I1} \mp h, \xi_{I2}, 0)$. The input traveltimes are then given by

$$\begin{aligned} \tau(\boldsymbol{x}, \boldsymbol{\xi}_I) &= [r_s + r_g]/c, \\ r_s &= \sqrt{(x - \xi_{O1} + h)^2 + (y - \xi_{O2})^2 + z^2}, \\ r_g &= \sqrt{(x - \xi_{O1} - h)^2 + (y - \xi_{O2})^2 + z^2}. \end{aligned} \tag{7.7.17}$$

Here, $2h$ is the offset between source and receiver, and r_s and r_g are the respective distances from the source and receiver to the point at depth. As in the case of 2.5D TZO, we dispense with the subscripts I on the distances associated with the input ray lengths. We retain the notation r_O for the present, reserving the notation r_0 for a simplification of this variable after the analysis below. The isochrons are ellipsoids on which $\tau_I = t_I$, a constant, described parametrically, with parameters γ_1 and γ_2, as follows:

$$x_1 - \xi_{I1} = a\cos\gamma_1, \quad x_2 - \xi_{I2} = b\sin\gamma_1\sin\gamma_2, \quad x_3 = b\sin\gamma_1\cos\gamma_2, \tag{7.7.18}$$

$$a = ct_I/2, \quad b = \sqrt{a^2 - h^2}.$$

The lower half of these ellipsoids are covered by γ_1 in the range $(0, \pi)$ and γ_2 in the range, $(-\pi/2, \pi/2)$. Similarly, the output isochrons are hemispheres, centered at $\boldsymbol{\xi}_O = (\xi_{O1}, \xi_{O2}, 0)$:

$$t_O = \tau_O(\boldsymbol{x}, \boldsymbol{\xi}_O) = 2\sqrt{(x_1 - \xi_{O1})^2 + (x_2 - \xi_{O2})^2 + x_3^2}/c = 2r_O/c. \tag{7.7.19}$$

We will start from (7.7.3). We leave it as an exercise to the reader to show that, for this case,

$$\sqrt{g_I} = \rho b\sin\gamma_1, \quad \rho = \sqrt{a^2\sin^2\gamma_1 + b^2\cos^2\gamma_1}. \tag{7.7.20}$$

The specialization of (7.7.3) to constant-background follows along the lines of the discussion of Section 7.6. We leave it as an exercise for the reader to verify that, for this case, that formula reduces to

$$u_O(\boldsymbol{\xi}_O, \omega_O) = -\frac{i\omega_O}{8\pi^3} \int i\omega_I d\omega_I d^2\xi_I u_I(\boldsymbol{\xi}_I, \omega_I) B(\gamma_1, \boldsymbol{\xi}_I) e^{2i\omega_O r_O/c - i\omega_I t_I} \cdot \frac{b \sin\gamma_1 \cos\gamma_2}{r_O^2} d\gamma_1 d\gamma_2 dt_I. \tag{7.7.21}$$

In this equation,

$$B(\gamma_1, \boldsymbol{\xi}_I) = \frac{\rho b \sin\gamma_1}{c^2} \frac{(r_s + r_g)(r_s^2 + r_g^2)}{r_s^2 r_g^2}. \tag{7.7.22}$$

We propose, first, to examine the possibility of applying the method of stationary phase. For this example, the phase, Φ of (7.7.4) is given by

$$\Phi = \tau_O = \frac{2r_O}{c} = \frac{2}{c}\sqrt{(\delta_1 + a\cos\gamma_1)^2 + b^2 \sin^2\gamma_1 + \delta_2^2 + 2\delta_2 b \sin\gamma_1 \sin\gamma_2}, \tag{7.7.23}$$

with

$$\delta_1 = \xi_{I1} - \xi_{O1}, \text{ and } \delta_2 = \xi_{I2} - \xi_{O2}. \tag{7.7.24}$$

Then consider the derivatives with respect to $\boldsymbol{\gamma}$:

$$\frac{\partial\Phi}{\partial\gamma_1} = \frac{2}{cr_O}\left[-a\sin\gamma_1(\delta_2 + a\cos\gamma_1) + b\cos\gamma_1(b\sin\gamma_1 + \delta_2\sin\gamma_2)\right], \tag{7.7.25}$$

$$\frac{\partial\Phi}{\partial\gamma_2} = \frac{2}{c}\frac{\partial r_O}{\partial\gamma_2} = \frac{2}{cr_O} b\delta_2 \sin\gamma_1 \cos\gamma_2.$$

For δ_2 nonzero, the derivative with respect to γ_2 is zero for $\gamma_1 = 0$, π, or $\gamma_2 = \pm\pi/2$, both of which place the stationary point at the upper surface. On the one hand, this is an unphysical choice of stationary point; on the other hand, the amplitude of the integrand in (7.7.21) is zero there anyway. Thus, the leading-order asymptotic contribution will not arise from a simple stationary point contribution. Now, when δ_2 *is* zero, this derivative is identically zero. Indeed, the phase, Φ, is independent of γ_2 for $\delta_2 = 0$.

This should bring to mind a phase of the form, $i\omega_O\delta_2\gamma_2$, which also has the property of a nonzero derivative with respect to γ_2 when δ_2 is nonzero, but is independent of γ_2 (actually, zero) when $\delta_2 = 0$. We know that integrals with this latter phase will lead to delta functions when the amplitude is constant (or *nearly* constant). In our case, in the high-frequency limit, we need only that the amplitude be nearly constant on the length scale of reciprocal wavenumber associated with ω_O, c/ω_O. This suggests that we search for an asymptotic delta function in the structure of the integrand of (7.7.21).

7.7.4 The γ_2 Integral As a Bandlimited Delta Function

Note that we have written (7.7.21) in a form in which the part of the mapping kernel that depends on γ_2 explicitly appears in the integral, while

B is independent of γ_2. Therefore, to analyze the γ_2 integration in that equation, we introduce the integral

$$I = \int_{-\pi/2}^{\pi/2} \frac{b \sin\gamma_1 \cos\gamma_2}{r_O^2} e^{2i\omega_O r_O/c} d\gamma_2. \tag{7.7.26}$$

The amplitude of the integrand here differs from the γ_2-derivative of the phase in (7.7.26) by an extra power of r_O in the denominator. On the other hand,

$$\frac{\partial I}{\partial \omega_O} = \frac{2i}{c} \int_{-\pi/2}^{\pi/2} \frac{b \sin\gamma_1 \cos\gamma_2}{r_O} e^{2i\omega_O r_O/c} d\gamma_2. \tag{7.7.27}$$

From (7.7.25), we see that the amplitude is now proportional to the γ_2-derivative of the phase, allowing us to carry out the integration in γ_2 to obtain

$$\frac{\partial I}{\partial \omega_O} = \frac{e^{2i\omega_O r_O/c}}{\omega_O \delta_2}\Bigg|_{-\pi/2}^{\pi/2} = \frac{e^{2i\omega_O r_+/c} - e^{2i\omega_O r_-/c}}{\omega_O \delta_2}.$$

Here,

$$r_\pm = \sqrt{(a\cos\gamma_1 + \delta_1)^2 + (b\sin\gamma_1 \pm \delta_2)^2}$$

are just the values of r_O at the limits of integration.

Now, define

$$\bar{r} \equiv \frac{r_+ + r_-}{2}, \quad \tilde{r} \equiv \frac{r_+ - r_-}{2},$$
$$r_0 \equiv \sqrt{(a\cos\gamma_1 + \delta_1)^2 + b^2 \sin^2\gamma_1},$$

and observe for future reference that

$$\bar{r} = r_0 + O(\delta_2^2), \quad \tilde{r} = \frac{\delta_2 b \sin\gamma_2}{r_0} + O(\delta_2^2).$$

(Note that r_0—"r sub zero"—is different from r_O—"r sub cap O"—used above.) With these new variables, (7.7.27) can be rewritten as

$$\frac{\partial I}{\partial \omega_O} = e^{2i\omega_O \bar{r}/c} \frac{2i\tilde{r}}{\omega_O \delta_2} \frac{\sin\{2\omega_O \tilde{r}/c\}}{\tilde{r}}. \tag{7.7.28}$$

The last factor here is of the form $\sin\{\lambda x\}/x$, where we can think of λ being large in the high-frequency limit, because of the scaling by ω_O. This is one of the forms that leads to the delta function; that is,

$$\lim_{\lambda\to\infty} \int_{-\infty}^{\infty} f(x) \frac{\sin\lambda x}{x} dx = \pi f(0),$$

for $f(x)$ in an appropriate class of test functions. (See, for example, Sneddon [1972].) In fact, the integral need not extend from $-\infty$ to ∞ for this result to be valid, but the interval of integration must include the origin. On the

other hand, for finite λ, the right hand side will be a reasonable approximation (to leading order in ω_O) only for the frequency "high enough"—again, an asymptotic result requiring that the interval of integration extend at least a few units of reciprocal wavenumber left and right of the origin at the given frequency. Therefore, asymptotically, we set

$$\frac{\sin\{2\omega_O\tilde{r}/c\}}{\tilde{r}} \sim \operatorname{sgn}(\omega_O)\pi\delta(\tilde{r}) = \frac{\delta(\delta_2)}{\frac{d\tilde{r}}{d\delta_2}} = \operatorname{sgn}(\omega_O)\pi\delta(\delta_2)\frac{r_0}{b\sin\gamma_1}.$$

Here, in the last factor, the derivative of $\tilde{r}$ has been evaluated at $\delta_2 = 0$. In fact, we can now do this in the other terms in (7.7.28) to obtain the result

$$\frac{\partial I}{\partial\omega_O} = \operatorname{sgn}(\omega_O)\frac{2\pi i}{\omega_O}e^{2i\omega_O r_0/c}\delta(\delta_2). \tag{7.7.29}$$

This is the result we need to simplify (7.7.21).

The integral I, equation (7.7.26), can be seen as a part of the integration on the right side of (7.7.21). However, we analyzed not I, but its derivative with respect to ω_O. Before we can proceed, then, we need to recast (7.7.21) as an equation in which the γ_2 dependence matches that of the result we just calculated. To do so, in (7.7.21) we must

i) divide by ω_O and
ii) differentiate both sides of that equation with respect to ω_O.

In doing so, on the left side, we restrict this operation to the leading-order asymptotic result by taking

$$\frac{\partial}{\partial\omega_O}\left[\frac{u_O(\boldsymbol{\xi}_O,\omega_O)}{\omega_O}\right] \sim \frac{1}{\omega_O}\frac{\partial u_O(\boldsymbol{\xi}_O,\omega_O)}{\partial\omega_O}.$$

We find now that

$$\frac{\partial u_O(\boldsymbol{\xi}_O,\omega_O)}{i\partial\omega_O} = \frac{-i\operatorname{sgn}(\omega_O)}{4\pi^2}\int i\omega_I d\omega_I d^2\xi_I u_I(\boldsymbol{\xi}_I,\omega_I)B(\gamma_1,\boldsymbol{\xi}_I) \cdot e^{2i\omega_O r_0/c - i\omega_I t_I}\delta(\delta_2)d\gamma_1 dt_I. \tag{7.7.30}$$

The seemingly superfluous factors of i, here, lend to the simple interpretation back in the time domain. On the left side, the operator $\partial/i\partial\omega_O$ is equivalent to multiplication by t_O. On the right side, the operator, $-i\operatorname{sgn}(\omega_O)$ transforms into convolution with $-1/\pi t_O$; that is, the *Hilbert transform* of the remainder of the right side transformed to the time domain. See Section A.7.1.

As a next step in this analysis, we can now exploit the delta function to carry out the integration in ξ_{I2}. From the definition of δ_2 in (7.7.24), we see that this amounts to evaluating the integrand at $\xi_{I2} = \xi_{O2}$. Thus, asymptotically, the leading-order contribution to the TZO mapping arises only from the line of input data that contains the zero-offset output point. We proceed to carry out this evaluation to obtain

$$\frac{\partial u_O(\boldsymbol{\xi}_O,\omega_O)}{i\partial\omega_O} = \frac{-i\,\mathrm{sgn}\,(\omega_O)}{4\pi^2}\int i\omega_I d\omega_I d\xi_{I1} u_I(\xi_{I1},\xi_{O2},\omega_I) B(\gamma_1,\xi_{I1},\xi_{O2}) \cdot e^{2i\omega_O r_0/c - i\omega_I t_I} d\gamma_1 dt_I. \tag{7.7.31}$$

7.7.5 *Space/Frequency TZO in Constant Background*

At this point, we have eliminated two integrations in the 3D TZO operator (7.7.21) to end up with an integral with much the same structure as (7.4.30), as regards the variables over which integrations are to be carried out. In particular, the integration over γ_1 here is exactly like the integration over γ there. The stationary phase condition (7.4.33) requires that the geometry of the rays be related as in Figure 7.8. Furthermore, the asymptotic analysis of the γ-integral there follows along the same lines here. In addition, we can apply all of the specializations of constant-background 2.5D DMO, Section 7.6, to this case. Indeed, our notation, r_s, r_g, and r_0 was chosen to facilitate the analogy with that section.

In particular, to apply the method of stationary phase here, we must evaluate the second derivative in (7.4.37); for this case, we already know that $\mathrm{sgn}\,(\kappa_O - \kappa_I) = 1$. In that evaluation, it is straightforward to show from (7.7.18), with $\gamma_2 = \pm\pi/2$, that

$$\frac{ds}{d\gamma_1} = \rho,$$

with the latter defined by (7.7.20). For the curvature factor in the second derivative, we use (7.6.12) and for $|\nabla\tau_O|$ we use (7.4.37).

With these results, we can evaluate the γ_1 integral by the method of stationary phase. The result is

$$\frac{\partial u_O(\boldsymbol{\xi}_O,\omega_O)}{i\partial\omega_O} = \frac{-i\,\mathrm{sgn}\,(\omega_O) e^{i\pi\,\mathrm{sgn}\,(\omega_O)/4}}{(2\pi)^{3/2}\sqrt{2|\omega_O|/c}}\int i\omega_I d\omega_I d\xi_{I1} u_I(\xi_{I1},\xi_{O2},\omega_I) \cdot \frac{\sqrt{r_0} B(\gamma_1,\xi_{I1},\xi_{O2})}{\rho\sin\theta} e^{2i\omega_O r_0/c - i\omega_I t_I} dt_I. \tag{7.7.32}$$

This last integral has the same structure as the 2.5D result, (7.4.38), in that it is an integral over the input source-receiver parameter, the input frequency, and the input time. It also has the same type of phase. In this integral, there is an additional fixed out-of-plane variable, ξ_{O2}, but this variable will play no role at all in the further analysis of the right side. Rather than redoing the stationary phase analysis in t_I for the integral above, we want to extrapolate from the result that we previously obtained to derive the frequency-domain data mapping for this example. Recall that the previous analysis led to (7.5.11), and it was this result that we used to derive the 2.5D TZO formula (7.6.23).

If we knew the specialization of (7.4.38) to constant-background TZO, then by comparing the integral operator in that specialization to (7.7.32), above, we could determine how to modify the earlier result, (7.6.23), to produce the result of stationary phase analysis in t_I here. Fortunately, we wrote out all of the specializations of the elements of the integrand in (7.4.38) when deriving (7.6.23). They can be found in equations (7.6.6), (7.6.7), (7.6.8), (7.6.9), and (7.6.12).

It is a fairly straightforward calculation, much like the one carried out in Section 7.6.1, to show that the specialization of (7.4.38) to constant-background yields the following equation:

$$\frac{\partial u_O(\boldsymbol{\xi}_O, \omega_O)}{i\partial\omega_O} \sim \frac{1}{2[2\pi]^{3/2}\sqrt{c}} \int \sqrt{|\omega_I|} e^{i\pi \operatorname{sgn}(\omega_I)/4} u_I(\xi_I, \omega_I) d\omega_I \, d\xi_I \tag{7.7.33}$$

$$\cdot \int \frac{z\sqrt{r_s r_g}\sqrt{r_s + r_g}}{r_0 \sin\theta} \frac{r_s^2 + r_g^2}{r_s^2 r_g^2} dt_I e^{2i\omega_O r_0/c - i\omega_I t_I}.$$

Our objective now is to rewrite this result to look more like (7.7.32). We proceed as follows:

$$\frac{\partial u_O(\boldsymbol{\xi}_O, \omega_O)}{i\partial\omega_O} \sim \frac{1}{2[2\pi]^{3/2}\sqrt{c}} \int \sqrt{|\omega_I|} e^{i\pi \operatorname{sgn}(\omega_I)/4} u_I(\xi_I, \omega_I) d\omega_I \, d\xi_I$$

$$\cdot \int \frac{\sqrt{r_s r_g}\sqrt{r_s + r_g}}{r_0 \sin\theta} \frac{c^2 B}{\rho(r_s + r_g)} dt_I e^{2i\omega_O r_0/c - i\omega_I t_I}$$

$$\sim \frac{1}{2}\left[\frac{c}{2\pi}\right]^{3/2} \int \frac{i\omega_I}{\sqrt{|\omega_I|} e^{i\pi \operatorname{sgn}(\omega_I)/4}} u_I(\xi_I, \omega_I) d\omega_I \, d\xi_I$$

$$\cdot \int \frac{\sqrt{r_s r_g}}{r_0^{3/2}\sqrt{r_s + r_g}} \frac{\sqrt{r_0} B}{\rho \sin\theta} dt_I e^{2i\omega_O r_0/c - i\omega_I t_I}.$$

In the first line here, B was introduced through its definition, (7.7.22). In the second line, the frequency dependence was rewritten to appear as a multiplier on the frequency dependence in (7.7.32).

Now, a comparison of this result with (7.7.32) reveals that this integrand can be transformed into the latter one by introducing the multiplier

$$M = 2\left[\frac{c}{2\pi}\right]^{-3/2} \frac{r_0^{3/2}\sqrt{r_s + r_g}}{\sqrt{r_s r_g}} \sqrt{|\omega_I|} e^{i\pi \operatorname{sgn}(\omega_I)/4} \left[\frac{-i \operatorname{sgn}(\omega_O) e^{i\pi \operatorname{sgn}(\omega_O)/4}}{(2\pi)^{3/2}\sqrt{2|\omega_O|/c}}\right] \tag{7.7.34}$$

$$= \frac{\sqrt{2} r_0^{3/2}\sqrt{r_s + r_g}}{c\sqrt{r_s r_g}} \sqrt{\frac{|\omega_I|}{|\omega_O|}} e^{i\pi[\operatorname{sgn}(\omega_I) - \operatorname{sgn}(\omega_O)]/4}.$$

Next, we use the results of Section 7.6.1. In particular, from (7.6.11),

$$\frac{\sqrt{2}r_0^{3/2}\sqrt{r_s+r_g}}{c\sqrt{r_s r_g}} = \frac{2r_0}{c}\sqrt{\cos\theta} = \frac{2r_0}{c}\sqrt{\frac{|\omega_O|}{|\omega_I|}}$$

and, from (7.6.3),

$$\text{sgn}\,(\omega_I) = \text{sgn}\,(\omega_O).$$

Thus, we obtain for M the surprisingly simple result,

$$M = \frac{2r_0}{c} = 2\cos\theta\frac{h^2-\delta_1^2}{cL}. \tag{7.7.35}$$

The last equality follows from (7.6.20).

It is now a matter of using this multiplier in (7.6.23) to obtain the right side of (7.7.32) after the t_I integral is approximated by the method of stationary phase. The result is

$$\frac{\partial u_O(\boldsymbol{\xi}_O,\omega_O)}{i\partial\omega_O} = \frac{4}{\pi c^2}\int_\Omega d\omega_I d\xi_I u_I(\xi_{I1},\xi_{O2},\omega_I) \cdot\cot\theta\ \cos\theta\frac{h}{L^2}(h^2+\delta_1^2)e^{-2i\omega_I L/c} \tag{7.7.36}$$

Here, the domain of integration is defined by inequalities (7.6.26) and (7.6.31). Also, we remind the reader that

$$\cos\theta = \omega_O/\omega_I, \quad \delta_1 = \xi_{I1}-\xi_{O1},$$

and L is given by (7.6.18) with δ replaced by δ_1.

Although this is a fairly simple result, we can do even better. On the right side, we have multiplied by $2r_0/c = t_O$. On the left side, we have the Fourier transform of $t_O U_O(\boldsymbol{\xi}_O, t_O)$. Thus, after transforming to the time domain, *we would just cancel the common factors of* t_O *on both sides of the equation*! We can achieve the same result by *not* introducing the extra multiplier, $2r_0/c = t_O$, on the right and *not* taking the derivative with respect to frequency on the left! Thus, we need only reinterpret this *and all of our 2.5D* constant-background TZO operators, in terms of the corresponding variables of the 3D data mapping, to obtain the 3D TZO operators. For example, we must replace the coordinate pairs (ξ_I,ω_I) by the coordinate triple $(\xi_{I1},\xi_{O2},\omega_I)$ and the coordinate pair (ξ_O,ω_O) by the triple, $(\xi_{O1},\xi_{O2},\omega_O)$. Then, we find that the 3D constant-background TZO operator deduced from (7.6.23) is

$$u_O(\boldsymbol{\xi}_O,\omega_O) \sim \frac{2}{\pi c}\int_\Omega d\omega_I\, d\xi_{I1}\, u_I(\xi_{I1},\xi_{O2},\omega_I)\cot\theta\,\frac{h}{L}\frac{h^2+\delta_1^2}{h^2-\delta_1^2}e^{-2i\omega_I L/c}. \tag{7.7.37}$$

7.7.6 A Hale-Type 3D TZO

As noted earlier in Section 7.6.2, Hale's DMO is a transformation between input data in wavenumber and time and output data in space and fre-

quency. In 2.5D, the TZO analog of Hale DMO was given in (7.6.36). Again, we need only reinterpret the variables of that result in terms of our 3D variables. We find that

$$u_O(\boldsymbol{\xi}_O, \omega_O) \sim \frac{1}{2\pi} \int \frac{dk dt_n}{A} \left[1 + \frac{2k^2 h^2}{\omega_O^2 t_n^2} \right] U_I(k, \xi_{O2}, t_I) e^{i\Theta}. \qquad (7.7.38)$$

Now, to account for the extra dimension, we modify the definition of Θ in (7.6.37) to be

$$\Theta = k\xi_{O1} + \omega_O t_n A. \qquad (7.7.39)$$

Gardner/Forel-type 3D TZO

It is now a straightforward calculation to rewrite (7.6.45) as a 3D TZO operator. The result is

$$U_O(\boldsymbol{\xi}_O, t_O) \sim \frac{h\sqrt{t_O}}{(2\pi)^{3/2}} \int D_{1/2}(\xi_{I1}, \xi_{O2}, t_I) \frac{h^2 + \delta_1^2}{(h^2 - \delta_1^2)^2} d\xi_{I1}. \qquad (7.7.40)$$

Exercises

7.7 Verify this last result.

7.8 Summary and Conclusions

We have derived platforms for 3D and 2.5D KDM for the mapping of scalar wavefields. Our formalism assumes knowledge of a physical model for both the input and output data and prescribed input and output source-receiver configurations. By cascading an inversion formula with a modeling formula, we obtain the KDM platform formula. This cascade is a single-reflector formalism in the absence of multiple reflections and multi-pathing, and for the simplified model of acoustic wave propagation. In this sense, our results may seem somewhat limited, being restricted to the level of generality of standard migration or DMO formalisms.

In the absence of a specific application, the formula includes a multifold integration over the physical model space that must be evaluated asymptotically for each example of KDM to permit the derivation of a *computationally feasible* formalism for implementation. Application of this formalism in constant-background 2.5D DMO produces the same formula as was derived in Bleistein et al. [1999].

On the other hand, we show how Kirchhoff-approximate model data in a given input configuration is mapped to Kirchhoff data in a different output configuration for the 2.5D case. We have done this in great generality, without specifying any particular configuration transformation. From this

result, we conclude that the traveltime and geometrical spreading of the input model are properly mapped to their counterparts in the output model, without altering the values of the angularly dependent reflection coefficient.

In doing this, we have presented an approach that unifies a broad collection of classical data mapping representations, demonstrated through the derivation of downward continuation (datuming), and the various approaches to dip moveout, which we recognize as transformation to zero offset (TZO). Further, we have introduced two additional operators that allow us to estimate the cosine of the specular reflection angle of a reflection event as a ratio of integral operators on the data. While we have not found everything on our "wish list" of possible data mappings outlined in Section 7.1.4, the results of this chapter certainly point the way for attacking those problems, and others like them.

Appendix A
Distribution Theory

We expect the reader to have some familiarity with the topics of distribution theory and Fourier transforms, as well as the theory of functions of a complex variable. However, to provide a bridge between texts that deal with these topics and this textbook, we have included several appendices. It is our intention that this appendix, and those that follow, perform the function of outlining our notational conventions, as well as providing a guide that the reader may follow in finding relevant topics to study to supplement this text. As a result, some precision in language has been sacrificed in favor of understandability through heuristic descriptions.

Our main goals in this appendix are to provide background material as well as mathematical justifications for our use of "singular functions" and "bandlimited delta functions," which are distributional objects not normally discussed in textbooks.

A.1 Introduction

Distributions provide a mathematical framework that can be used to satisfy two important needs in the theory of partial differential equations.

First, quantities that have point duration and/or act at a point location may be described through the use of the traditional "Dirac delta function" representation. Such quantities find a natural place in representing energy sources as the forcing functions of partial differential equations. In this usage, distributions can "localize" the values of functions to specific spatial

and/or temporal values, representing the position and time at which the source acts in the domain of a problem under consideration.

The second important role of distributions is to extend the process of differentiability to functions that fail to be differentiable in the classical sense at isolated points in their domains of definition. In this role, distributions may localize the singular behavior of the derivatives of functions—for example, the singularities of the derivative caused by jump discontinuities.

In a related role, the process of differentiation itself may be localized via distributions to specific positions and/or temporal values in a domain of interest. For example, dipole sources may be distributionally represented by localizing the derivative operation to a point. Or, an "exploding reflector" may be represented by localizing the derivative normal to a given surface to points on that surface.

A.2 Localization via Dirac Delta functions

The classical definition of the Dirac delta "function" originally used by physicists was

$$\delta(x) \stackrel{def}{=} \begin{cases} 0 & \text{for } |x| \neq 0 \\ \infty & \text{for } x = 0, \end{cases} \tag{A.2.1}$$

with the property that the "delta function" would not introduce any scaling of its own if it appeared in an integral. This second property is expressed by the integral

$$\int_{-\infty}^{\infty} \delta(x)dx = 1,$$

where we may think of $\delta(x)$ as being integrated with a function (not shown) whose value is unity near $x = 0$. The definition and property above are contradictory as written, because any function that is nonzero at only a finite number of isolated points has an integral that vanishes, even if the nonzero values of the function are arbitrarily large.

The modern approach to distributions, based on the work of Laurent Schwartz [Schwartz, 1950–1951], follows from a consideration of the theory of topological vector spaces. One result of this theory identifies $\delta(x)$ as a "measure."

(A measure is a weight applied in the Lebesgue formulation of the integral.) Such modern treatments may be found in other, more advanced texts [Friedlander, 1982; Petersen, 1983; Hörmander, 1983]; Treves, 1967; and Treves, 1980]. While this material is far outside the scope of our book, the exposition we present does, in fact, depend on these more advanced results. In particular, we need to have the ability to approximate functions and distributions, to an arbitrary degree of precision, with sequences of

smooth functions. This ability is guaranteed by theorems that are beyond the scope of our text.

We will take a more classical approach through so-called "delta sequences." Such sequences of functions are discussed in mathematical physics and applied mathematics texts, such as Butkov [1968], Nussenzveig [1972], and Stakgold [1979]. This is the "generalized function" approach to describing distributions, and is also largely founded on the work of Schwartz.

Distributions As the Limits of Delta Sequences

The basic idea is to consider distributions to be a generalization of the concept of function. The way this is done is to consider a distribution, or rather the result of integration of a function with a distribution, as being a "linear functional." A functional is an operator that assigns a number to each function of a particular class of test functions. (The operation is linear because the linear combination of values assigned to several functions is the same as the value assigned to a linear combination of the same functions.)

We then create a sequence of linear functionals, defined as integration with elements of a sequence of functions $\{S_n(x)\}$, in such a way that as $n \to \infty$, the limiting functional behaves the same way that the distribution in question would behave. In this way, the limiting functional can make sense even though the pointwise limit of the sequence $\{S_n(x)\}$ as $n \to \infty$ does not exist as an ordinary function. This is one way to arrive at distributions such as $\delta(x)$. The properties of distributions can be determined only through integration with a "sufficiently well behaved" test function out of an appropriate class.

For example, the reader may have already encountered the "box sequence." The graph of each function in the sequence is a box, with the integral of each function being equal to one. As n increases, the width of each successive box decreases towards zero, while the height, necessarily, must increase beyond all bounds. If we allow infinity as a limiting value, then this sequence leads back to the "function" introduced in (A.2.1). Furthermore,

$$\lim_{n\to\infty} \int_{-\infty}^{\infty} f(x) S_n(x) dx = f(0),$$

for any $f(x)$ in an appropriate class of test functions. This is the "sifting property" of the Dirac delta function.

As a second example, and one that arises in various forms in the text, we introduce the sequence,

$$S_n(x) = \begin{cases} \dfrac{\sin(n\pi x)}{\pi x}, & x \neq 0, \\ \dfrac{n}{\pi} & x = 0, \end{cases} \qquad n = 1, 2, \cdots .$$

This sequence of functions does not have pointwise limits (except for infinity at $x = 0$), yet it can be shown that this sequence has the same sifting property as did the sequence of the previous example [Sneddon, 1972].

Let us now address the question of the appropriate class of test functions. From the standard theory of distributions, these are defined to be those functions that are infinitely differentiable and have "compact support," meaning that each function is nonzero on a closed and bounded interval, but is zero everywhere else. Formally, test functions having both of these properties are called C_0^∞ test functions. Such a function and all of its derivatives will vanish smoothly (that is to say, without singularities) outside of some closed and bounded interval. In fact, the name "test function" is reserved exclusively for the C_0^∞ functions in much of the mathematical literature that deals with the subject of partial differential equations.

By restricting the test functions to be extraordinarily well-behaved, an extremely wide range of entities can act as "distributions" because a broad class of functions, and other mathematical objects, including all delta sequence functions and their limits, can be integrated with a C_0^∞ function. The reader may have some question as to the validity of this approach, however. Is it not our interest to create distributions that will operate on ordinary functions? The answer to this question is that it is a standard trick in functional analysis to derive results for extremely well-behaved functions and then extend those results to "ordinary" functions by showing that ordinary functions may be approximated by the well-behaved ones. The validity of such approximations depends on powerful theorems from functional analysis that show that well-behaved functions exist "arbitrarily closely" to any ordinary function that we may choose. One such result is that any continuous function $f(x)$ with compact support can be uniformly approximated on a finite interval by C_0^∞ functions.

For example, if $\phi_n(x)$ represents a delta sequence, that is, it behaves like $\delta(x)$ as $n \to \infty$, and is nonzero in the domain of support of $f(x)$, then it is possible to write

$$\psi_n(x) = \int_{-\infty}^{\infty} f(\xi)\phi_n(x - \xi)\, d\xi. \tag{A.2.2}$$

This is just the convolution of our original function with an appropriately chosen test function. There exists an n such that the C_0^∞ function $\psi_n(x)$ approximates $f(x)$ to any desired order of accuracy. This process of building smoother approximate functions through convolution with a test function is called "regularization" in the language of mathematical analysis. In the language of signal processing, this process is equivalent to applying a "smoothing filter" that preserves the values of the function on some part of its domain. That is, in the frequency domain, we multiply by a function that is (nearly) equal to unity over some bandwidth and then tapers smoothly to zero. We use the term "neutralizer" for such functions in several places in the text. In mathematical literature, these functions

are often referred to as "mollifiers," "approximate identity functions," or "partitions of unity."[1]

All of the properties of the delta function (really, the Dirac distribution) that are implied by the physicist's original formal[2] definition may now be derived, with the primary property being the sifting property, introduced above,

$$\phi(0) = \int_D dx\ \phi(x)\delta(x). \tag{A.2.3}$$

Here, $\phi(x)$ is the "test function" with support contained in the domain D with $x = 0$ being a point inside of D. Other properties follow, directly. For example, the effect of translation on the delta function is to make

$$\phi(x_0) = \int_D dx\ \phi(x)\delta(x - x_0), \tag{A.2.4}$$

where x_0 is a point inside the domain D. If x_0 is not in D then the result of the integration is zero, whereas, letting $x_0 \to 0$ gives us (A.2.3) back. This property expresses the localization of $\phi(x)$ to the point x_0.

Localizing Derivatives with Distributions

Derivatives of $\phi(x)$ may be similarly localized through the expression

$$(-1)^m \phi^{(m)}(x_0) = \int_D dx\ \phi(x)\delta^{(m)}(x - x_0), \tag{A.2.5}$$

again provided that the point x_0 lies in the domain D. The quantity, $\delta^{(m)}(x - x_0)$, may be imprecisely described as the "mth derivative of a delta

---

[1]The last term refers to a common technique used in analysis, which we also employ in this text. Suppose that we want to study a function $f(\omega)$ with support on some (not necessarily finite) interval of the real line. We begin by partitioning the interval of support into a collection subintervals that have relevance to our study; for example, the function may have critical points at one or more locations. We may then define a series of neutralizers, each an infinitely differentiable function with support on a given subinterval, in such a way that the sum of all of the neutralizers is just the unit function on the entire interval. This is a partition of unity.

We then multiply $f(\omega)$ by the series of neutralizers, which produces a series of smoothly tapering functions, each with support on one of the respective subintervals. Because the sum of the neutralizers is unity, the sum of the resulting series of smooth functions equals $f(\omega)$. The effect is to isolate the points or subintervals of interest of $f(\omega)$ so that they may be treated separately. This is useful because often different techniques of analysis must be applied to the different points of interest in the support of the function being studied.

[2]In mathematical language, the word "formal" means the same as "symbolic," and generally refers to steps that are performed by allowing the notation to operate mechanically, possibly carrying us farther than the original intent of the notation. The second step in any formal discussion is usually to show that there is additional justification for believing such an extension.

function," but it is more precise to say that this distribution "localizes the mth derivative" of $\phi(x)$ to the point x_0. The reader may verify (A.2.5) formally, via repeated integration by parts, treating $\delta^{(m)}(x - x_0)$ formally as the "m-th derivative of the delta function," and by the application of equation (A.2.3).

Additional properties of the delta function may be revealed by considering its argument to be a function that may be zero at one or more points. That is to say, we are interested in $\delta(g(x))$, with $g(x_a) = 0$ at one or more points x_a, but

$$\left.\frac{dg(x)}{dx}\right|_{x=x_a} \equiv \frac{dg(x_a)}{dx} \neq 0.$$

Then, changing the variable of integration to $u = g(x)$, locally, in the neighborhood of each point, x_a, introduces this derivative into the denominator of the integrand. The sifting property of the delta function then leads to the result

$$\int_D dx\ \phi(x)\delta\left(g(x)\right) = \sum_a \frac{\phi(x_a)}{\left|\frac{dg(x_a)}{dx}\right|}. \tag{A.2.6}$$

This result suggests the identity

$$\delta\left(g(x)\right) = \sum_a \frac{\delta(x - x_a)}{\left|\frac{dg(x_a)}{dx}\right|}. \tag{A.2.7}$$

Here, as with all distributional equalities, the "=" denotes that the distributions have the same action under integration with a test function.

Higher Dimensions

The sifting property extends naturally to the higher-dimensional domain D via the expression

$$\phi(\boldsymbol{x}_0) = \int_D d\boldsymbol{x}\ \phi(\boldsymbol{x})\delta(\boldsymbol{x} - \boldsymbol{x}_0), \tag{A.2.8}$$

with $\boldsymbol{x} \equiv (x_1, x_2, ..., x_n)$[3] and

$$\delta(\boldsymbol{x} - \boldsymbol{x}_0) \equiv \delta(x_1 - x_{10})\delta(x_2 - x_{20})...\delta(x_n - x_{n0}). \tag{A.2.9}$$

The n-dimensional test function $\phi(\boldsymbol{x})$ may be represented as the product of n one-dimensional C_0^∞ test functions, or it may be a function that is a C_0^∞ function of all of its n variables.

---

[3]In this section, the symbol n refers only to the nth dimension of space; it is not being used as an index counter as it was in the previous sections.

Analogous to the one-dimensional case, each of the delta functions may be, in turn, dependent on a function of $\boldsymbol{x}$, that is, $\delta(g(\boldsymbol{x}))$. Furthermore, it is possible for each of these functions to be zero on domains that intersect in such a way as to make all of the functions zero at one or more points. That is to say, a single delta function with vector function as its argument can be equivalent to the product of a collection of delta functions with scalar functions as their arguments,

$$\delta(\boldsymbol{g}(\boldsymbol{x})) \equiv \delta(g_1(\boldsymbol{x}))\delta(g_2(\boldsymbol{x}))...\delta(g_n(\boldsymbol{x})),$$

where $\boldsymbol{g}(\boldsymbol{x}_a) = \boldsymbol{0}$, at one or more points $\boldsymbol{x}_a$, and the Jacobian

$$\left.\frac{\partial(\boldsymbol{g}(\boldsymbol{x}))}{\partial(\boldsymbol{x})}\right|_{\boldsymbol{x}=\boldsymbol{x}_a} \equiv \frac{\partial(\boldsymbol{g}(\boldsymbol{x}_a))}{\partial(\boldsymbol{x})} \neq 0.$$

As in the one-dimensional case, we can think of writing an integral that states the sifting property by making a change of variables from $\boldsymbol{x}$ to $\boldsymbol{u} = \boldsymbol{g}(\boldsymbol{x})$, introducing this Jacobian in the denominator of the integrand in the new integral. Without carrying out the details this yields the higher-dimensional the sifting property,

$$\int_D d^n x\, \phi(\boldsymbol{x})\delta(\boldsymbol{g}(\boldsymbol{x})) = \sum_a \frac{\phi(\boldsymbol{x}_a)}{\left|\frac{\partial(\boldsymbol{g}(\boldsymbol{x}_a))}{\partial(\boldsymbol{x})}\right|}. \tag{A.2.10}$$

The equality above suggests that

$$\delta(\boldsymbol{g}(\boldsymbol{x})) = \sum_a \frac{\delta(\boldsymbol{x}-\boldsymbol{x}_a)}{\left|\frac{\partial(\boldsymbol{g}(\boldsymbol{x}_a))}{\partial(\boldsymbol{x})}\right|}, \tag{A.2.11}$$

where the equality here is in the sense that each quantity has the equivalent action under integration with a test function.

The Singular Function

The *singular function*, $\gamma(\boldsymbol{x})$, of a surface is a distribution with the property

$$\int_D dV\, \gamma(\boldsymbol{x}) f(\boldsymbol{x}) = \int_S dS\, f(\boldsymbol{x}), \tag{A.2.12}$$

meaning that the support of $\gamma(\boldsymbol{x})$ is on the surface S only.[4] The singular function may therefore be thought of as a delta function of a single

[4]The plot of the singular function of the surface constitutes mathematical imaging of the surface. In many places in this text a bandlimited form of the singular function of reflector surfaces appears as a natural result of seismic inversion formulas. Bandlimited distributions are discussed below. Clearly, it is the bandlimited singular function that is plotted.

argument, which is the normal distance η from the prescribed surface. Alternatively, if the surface is represented by the equation, $g(\boldsymbol{x}) = 0$, then the singular function can then be defined as

$$\gamma(\boldsymbol{x}) = \delta\left(g(\boldsymbol{x})\right)|\nabla g(\boldsymbol{x})|. \tag{A.2.13}$$

To see why this is so, consider using this definition on the left side in (A.2.12) and then setting $dV = dSdg/|\nabla g(\boldsymbol{x})|$, with dS, being the differential surface area on the level surface(s) described by the condition $g(\boldsymbol{x}) =$ constant. The integration with respect to g then yields exactly the right side of (A.2.12). Alternatively, the singular function can be viewed as a delta function of normal distance from the surface of interest, expressed symbolically as $\delta(\eta)$. A change of variables to two parameters on the surface, s^1 and s^2, and one parameter orthogonal to the surface, say σ, can then be introduced. For example, this approach can be tied to the one above by thinking of this third variable as being given by $\sigma = g(\boldsymbol{x})$. Then $\boldsymbol{x} \equiv \boldsymbol{x}(s^1, s^2, \sigma)$ with the coordinates $(s^1, s^2, 0)$ parameterizing the surface S. Note that the Jacobian of transformation between these coordinate systems takes the form

$$\begin{aligned}
\frac{\partial(x_1, x_2, x_3)}{\partial(s^1, s^2, \sigma)} &= \frac{\partial(x_1, x_2, x_3)}{\partial s^1} \times \frac{\partial(x_1, x_2, x_3)}{\partial s^2} \cdot \frac{\partial(x_1, x_2, x_3)}{\partial \sigma} \\
&= \pm \left| \frac{\partial(x_1, x_2, x_3)}{\partial s^1} \times \frac{\partial(x_1, x_2, x_3)}{\partial s^2} \right| \left| \frac{\partial(x_1, x_2, x_3)}{\partial \sigma} \right| . \\
&= \pm \left| \frac{\partial(x_1, x_2, x_3)}{\partial s^1} \times \frac{\partial(x_1, x_2, x_3)}{\partial s^2} \right| \frac{\partial \eta}{\partial \sigma}
\end{aligned}$$

Here, the ambiguity of sign is of no consequence as only the absolute value of this determinant appears in the transformation

$$dV = dx_1 dx_2 dx_3 = \left| \frac{\partial(x_1, x_2, x_3)}{\partial(s^1, s^2, \sigma)} \right| ds^1 ds^2 d\sigma,$$

to be used below. The directions of increasing σ and η are chosen agree for simplicity, without loss of generality. These results can now be used on the left side of (A.2.12) as follows.

$$\begin{aligned}
&\int_D dV f(\boldsymbol{x}) \gamma(\boldsymbol{x}) \\
&\quad = \int_{D'} ds^1 ds^2 d\sigma \left| \frac{\partial(x_1, x_2, x_3)}{\partial(s^1, s^2, \sigma)} \right| f\left(\boldsymbol{x}(s^1, s^2, \sigma)\right) \delta(\eta(s^1, s^2, \sigma)) \\
&= \int_{D'} ds^1 ds^2 d\sigma \left| \frac{\partial(x_1, x_2, x_3)}{\partial s^1} \times \frac{\partial(x_1, x_2, x_3)}{\partial s^2} \right| \frac{\partial \eta}{\partial \sigma} f\left(\boldsymbol{x}(s^1, s^2, \sigma)\right) \delta(\eta)
\end{aligned}$$

$$= \int_{D'} ds^1 ds^2 d\eta \left| \frac{\partial(x_1, x_2, x_3)}{\partial s^1} \times \frac{\partial(x_1, x_2, x_3)}{\partial s^2} \right| f\left(\boldsymbol{x}(s^1, s^2, \sigma(\eta))\right) \delta(\eta)$$

$$= \int_{S'} ds^1 ds^2 \left| \frac{\partial(x_1, x_2, x_3)}{\partial s^1} \times \frac{\partial(x_1, x_2, x_3)}{\partial s^2} \right| f\left(\boldsymbol{x}(s^1, s^2, \sigma)\right)\Big|_{\sigma=0} \tag{A.2.14}$$

$$\equiv \int_S dS f(\boldsymbol{x}).$$

In these equations, D' and S' are the images of D and S in the s^1, s^2, σ-domain. In the third line, we have replaced the product $d\sigma(d\eta/d\sigma)$ by $d\eta$. Alternatively, returning to the relationship $\sigma = g(\boldsymbol{x})$, then $d\sigma(d\eta/d\sigma) = dg/|\nabla g(\boldsymbol{x})|$, from which it follows that

$$d\sigma \frac{d\eta}{d\sigma} \gamma(\boldsymbol{x}) = \frac{dg}{|\nabla g(\boldsymbol{x})|} |\nabla g(\boldsymbol{x})| \delta(g) = \delta(g) dg,$$

leading to the same conclusion.

The reader is encouraged to try this definition for the special cases of the singular function of a plane or the singular function of the surface of a sphere of radius R, represented in spherical coordinates by $\delta(r - R)$.

Because we also consider curves in 2D or 2.5D in our studies, we must also consider the analog, the singular function of a curve in 2D. Of course, we define the singular function in complete analogy with (A.2.12). That is, we define the distribution $\gamma(x_1, x_2)$ by its action,

$$\int_S dS\, \gamma(\boldsymbol{x}) f(\boldsymbol{x}) = \int_C ds\, f(\boldsymbol{x}), \tag{A.2.15}$$

where s is arclength along the curve. In 2D, there are complete analogies with the discussion above; we will not present them here.

A.3 Fourier Transforms of Distributions

Many of the results in this text involve Fourier transforms or Fourier transform–like integrals. It is necessary, therefore, to be able to discuss Fourier transforms of distributions and test functions.

The forward and inverse Fourier transforms are defined by the relations

$$\tilde{f}(\omega) = \int_{-\infty}^{\infty} dt\, f(t) e^{i\omega t},$$

$$f(t) = \frac{1}{2\pi} \int_{-\infty}^{\infty} d\omega\, \tilde{f}(\omega) e^{-i\omega t}. \tag{A.3.1}$$

We want to make sense of the same expressions for the situation when $f(t)$ or $\tilde{f}(\omega)$ is a distribution.

Because distributions cannot be defined without also defining test functions the analysis of the problem must begin with an expression of the form of equation (A.2.3). Beginning in the frequency domain, with $\tilde{f}(\omega)$ defined as the Fourier transform of the distribution $f(t)$ and $\tilde{\phi}(\omega)$ defined as a C_0^∞ test function of ω, we may write

$$\begin{aligned}\frac{1}{2\pi}\int_{-\infty}^{\infty} d\omega\ \tilde{f}(\omega)\tilde{\phi}(\omega) &= \frac{1}{2\pi}\int_{-\infty}^{\infty} d\omega \int_{-\infty}^{\infty} dt\ f(t)e^{i\omega t}\tilde{\phi}(\omega) \\ &= \int_{-\infty}^{\infty} dt\ f(t)\left[\frac{1}{2\pi}\int_{-\infty}^{\infty} e^{i\omega t}\tilde{\phi}(\omega)\ d\omega\right] \\ &= \int_{-\infty}^{\infty} dt\ f(t)\phi(-t).\end{aligned}$$

See Titchmarsh [1948].

This means that we are trying to define the Fourier transform of the distribution $f(t)$ by the formal expression

$$\frac{1}{2\pi}\int_{-\infty}^{\infty} d\omega\ \tilde{f}(\omega)\tilde{\phi}(\omega) = \int_{-\infty}^{\infty} dt\ f(t)\phi(-t). \tag{A.3.2}$$

It would be desirable that $\tilde{\phi}(\omega)$, $\bar{\tilde{\phi}}(\omega)$, and $\phi(t)$ all be C_0^∞ functions in order to make the definition above be consistent with the original definition of distributions. However, it is easy to show that it is impossible for the Fourier transform of a C_0^∞ function to also be a C_0^∞ function. To see why this is true, consider a C_0^∞ test function, $\phi(t)$. The Fourier transform of this function is defined as an integral on some closed interval $a \le t \le b$, containing the support of $\phi(t)$. That is to say,

$$\tilde{\phi}(\omega) = \int_a^b \phi(t)e^{i\omega t}\ dt. \tag{A.3.3}$$

However, $\tilde{\phi}(\omega)$ can be shown to be analytic everywhere in the complex ω plane; its derivative, in fact, is the same type of integral with integrand $it\ \phi(t)$ in place of $\phi(t)$. Such functions are called *entire*. It is a straightforward result in complex function theory that an entire function that is constant on an interval is identically constant. Thus, $\tilde{\phi}(\omega)$ cannot vanish on any interval without being identically zero in the entire ω-plane. However, $\tilde{\phi}(\omega) = 0$ implies that $\phi(t) = 0$. Therefore $\tilde{\phi}(\omega)$ cannot have compact support.

The only way out of this dilemma is to choose a new class of test functions. The condition of only choosing test functions that are C_0^∞ is too restrictive for permitting a self-consistent definition of Fourier transforms of distributions.

A.4 Rapidly Decreasing Functions

There are other infinitely differentiable functions that, while they do not have compact support, *do* decay rapidly enough so as to vanish at infinity and provide us with a useful class of test functions that will permit us to define the distributions that we need, as well as their Fourier transforms.

Such a class of rapidly decaying test functions may be defined by first representing the function by its Fourier transform

$$\tilde{\phi}(\omega) = \int_{-\infty}^{\infty} \phi(t) e^{i\omega t}\, dt. \tag{A.4.1}$$

It is possible to construct a formal result that will imply the necessary decay conditions in t and ω to define this new class of test functions.

Differentiating both sides of (A.4.1) with respect to ω, m times, yields the result

$$\tilde{\phi}^{(m)}(\omega) = \int_{-\infty}^{\infty} (it)^m \phi(t) e^{i\omega t}\, dt. \tag{A.4.2}$$

Integrating the right-hand side of (A.4.2) by parts $(n+1)$ times yields

$$\tilde{\phi}^{(m)}(\omega) = \left(\frac{-1}{i\omega}\right)^{n+1} \int_{-\infty}^{\infty} \frac{d^{n+1}}{dt^{n+1}} \left[(it)^m \phi(t)\right] e^{i\omega t}\, dt. \tag{A.4.3}$$

Here, all of the integrated terms from the repetitive integrations by parts have been assumed to vanish, implying that $t^m \phi(t)$ and all of its derivatives vanish at infinity. Rewriting equation (A.4.3) so that the left-hand side is expressed as a product of $(-i\omega)^n$ and $\tilde{\phi}^{(m)}(\omega)$ produces

$$(-i\omega)^n \tilde{\phi}^{(m)}(\omega) = \frac{-1}{i\omega} \int_{-\infty}^{\infty} \frac{d^{n+1}}{dt^{n+1}} \left[(it)^m \phi(t)\right] e^{i\omega t}\, dt. \tag{A.4.4}$$

Equation (A.4.4) may be used to define the new set of test functions. If the functions $\phi(t)$ decay as $|t| \to \infty$ according to the rule

$$\lim_{|t|\to\infty} \left| t^m \phi^{(n)}(t) \right| = 0 \qquad m = (1, 2, 3, \ldots) \quad \text{and} \quad n = (1, 2, 3, \ldots), \tag{A.4.5}$$

then the integral in equation (A.4.4) converges. Taking the limit as $|\omega| \to \infty$ implies that

$$\lim_{|\omega|\to\infty} \left| \omega^n \tilde{\phi}^{(m)}(\omega) \right| = 0, \qquad m = (1, 2, 3, \ldots) \quad \text{and} \quad n = (1, 2, 3, \ldots). \tag{A.4.6}$$

Equations (A.4.5) and (A.4.6) state the decay conditions for the set of "rapidly decreasing" test functions. Note that a function that is rapidly decreasing in the direct domain is automatically rapidly decreasing in the transform domain, and vice versa. This property is called "continuity under the Fourier transform" and the set of rapidly decreasing functions is

often called the "Schwartz space," and is designated by the symbol $\mathcal{S}$. Because functions with compact support also vanish at infinity, the set of C_0^∞ functions is a subset of $\mathcal{S}$, when equivalence is judged by differentiability and decay. However, as seen above, the Fourier transform of a C_0^∞ function is *not* a C_0^∞ function, even though it *is* a rapidly decreasing function. In this case, it is the compact support that is lost. However, the decay of the transformed function is still "rapid" in the sense defined above, so the cascade of forward and inverse transforms of a C_0^∞ functions is still defined, in that the rapid decay at infinity guarantee that the respective integrals converge.

An example of a rapidly decreasing function is $\exp\{-t^2/2\}$, with Fourier transform $\exp\{-\omega^2/2\}$ within a constant scale factor. In this particular case, $\tilde{\phi}(\omega)$ is an entire function with the right decay properties *on the real ω-axis*, which is the only location of concern to us, here. More generally, equations (A.4.5) and (A.4.6) tell us that any C^∞ function that decays faster than any arbitrary algebraic power at infinity will be in the class of rapidly decreasing functions.

A.5 Temperate Distributions

By choosing test functions from the set of "rapidly decreasing" C^∞ functions, we constrain the permissible class of functions that can be used as delta sequence functions. Because we can define distributions only through integration with test functions, existence of integrals of the type

$$\int_{-\infty}^{\infty} f(t)\phi(t)\, dt \tag{A.5.1}$$

will define the properties of $f(t)$.

Noting that $\phi(t)$ vanishes at infinity, it follows that any absolutely integrable function $f(t)$ will make this integral converge. Also, $f(t)$ may be any function of polynomial growth, such that $|f(t)| \leq k|t|^n$ as $|t| \to \infty$, where k is some constant. On the other hand, $f(t)$ may *not* be a function of exponential growth. Because all of these conditions imply slow growth, distributions associated with rapidly decreasing test functions must be slow growing (as $t \to \infty$)—hence the name "temperate." It follows that all distributions with bounded (but not necessarily compact) support are temperate distributions, because they fit the criterion of "slow growth" stated above.

All of the usual properties of the Fourier transform may, therefore, be extended to temperate distributions.

A.6 The Support of Distributions

There is a remaining problem, however. It is desirable to define the Fourier transform pair

$$\tilde{f}(\omega) = \int_{-\infty}^{\infty} f(t)e^{i\omega t}\, dt,$$

$$f(t) = \frac{1}{2\pi}\int_{-\infty}^{\infty} \tilde{f}(\omega)e^{-i\omega t}\, d\omega,$$

with $f(t)$ or $\tilde{f}(\omega)$ being a distributional quantity. While the exponential quantity in each of these integrals *does* have the property of being infinitely differentiable, these functions do not have the property of being members of the set of rapidly decreasing test functions discussed above.

This problem is solved by considering the *support* of distributional quantities. The support of a function is that part of that function's domain where it is nonzero. In contrast, the support of a distribution is determined by considering the intersection of all sets for which the integral of the distribution with an appropriate test function is nonzero.

In general we would like to determine what conditions are necessary for the integral

$$I = \int_{-\infty}^{\infty} f(t)\phi(t)\, dt \tag{A.6.1}$$

to converge when $\phi(t)$ is infinitely differentiable, but not rapidly decreasing in the sense discussed above. If the support of $f(t)$ is contained within some interval $a \leq x \leq b$, then we may rewrite the integral above as

$$I = \int_{-\infty}^{\infty} f(t)\phi(t)\, dt = \int_{a}^{b} f(t)\phi(t)\, dt. \tag{A.6.2}$$

However, the support of $f(t)$ may be represented equally well by a C_0^∞ function $\nu(t)$ that has a value of 1 in the region where $f(t) \neq 0$, but vanishes C_0^∞ smoothly away from from this region. The integral I may then be rewritten as

$$I = \int_{-\infty}^{\infty} f(t)\nu(t)\phi(t)\, dt = \int_{-\infty}^{\infty} f(t)\psi(t)\, dt, \tag{A.6.3}$$

where the function $\psi(t) \equiv \nu(t)\phi(t)$ is a C_0^∞ function identically equal to $\phi(t)$ on the support of $f(t)$ but decaying away to zero C_0^∞ smoothly outside of that support. The function $\nu(t)$ is an example of a *neutralizer* function.

For the delta function $\delta(t)$, we know that the support is the origin itself. Applying a neutralizing function $\nu_\varepsilon(t)$, defined such that $\nu_\varepsilon(t) = 0$ for $|t| \geq \varepsilon$, and that $\nu_\varepsilon(t) = 1$ for $|t| < \varepsilon$, we now are free to write the "obvious" statement

$$\int_{-\infty}^{\infty} \nu_\varepsilon(t)\delta(t)e^{i\omega t}\,dt = 1, \tag{A.6.4}$$

for ε chosen arbitrarily small. From this result, it is equally correct to set

$$\delta(t) \equiv \frac{1}{2\pi}\int_{-\infty}^{\infty} 1e^{-i\omega t}\,d\omega, \tag{A.6.5}$$

and be assured that $\delta(t)$ means the same thing here as in the earlier discussions. In fact, replacing the 1 in this last equation by any sequence of neutralizers with progressively larger support approaching the entire real line provides a delta sequence. Each element of such a sequence is a *bandlimited* delta function, of the type discussed below.

These observations lead to the relations between the derivatives of the delta function and their Fourier transforms, as follows:

$$\delta^{(m)}(t) \equiv \frac{1}{2\pi}\int_{-\infty}^{\infty} (-i\omega)^m e^{-i\omega t}\,d\omega \tag{A.6.6}$$

and

$$\int_{-\infty}^{\infty} \delta^{(m)}(t)e^{i\omega t}\,dt = (i\omega)^m. \tag{A.6.7}$$

The first of these relations may be verified by formally differentiating both sides of (A.6.5) m times with respect to t. The second relation may be verified through m integrations by parts. Again, we can be assured that $\delta^{(m)}(t)$ has the same meaning as in the original definition.

A.7 Step Functions

Equation (A.6.5) gives us a meaning for the Fourier transform that is identically equal to a constant. An equally important and comparable function that arises in practice is one that is a constant for $\omega > 0$ and the negative of that constant for $\omega < 0$. This is an odd function, which implies that its inverse Fourier transform will be odd—certainly not an ordinary function, but an odd distribution. In order to make that distribution *real* back in the time domain, the constant in the frequency domain should be chosen to be *imaginary*. Thus, we are led to consider in the frequency domain, the function

$$\tilde{p}(\omega) = i\,\mathrm{sgn}\,(\omega) = e^{i\,\mathrm{sgn}\,(\omega)\pi/2} = \begin{cases} i, & \omega > 0, \\ 0, & \omega = 0, \\ -i & \omega < 0. \end{cases} \tag{A.7.1}$$

Here, the value at $\omega = 0$ is not important. However, the choice made here arises naturally in two ways. First, Fourier transforms of piecewise continuous absolutely integrable *functions* take on the average value at

their jumps. Second, numerical Fourier transforms of functions that are discontinuous at the origin will return an average, as well. If, however, the limits of integration are not symmetric, then the value at the discontinuity will also be a weighted average reflecting the asymmetry.

The objective, now, is to determine $p(t)$. Given the development of Fourier transforms of distributions above, it is necessary that the rules relating multiplication in one domain to differentiation in the transform domain still must hold. Thus, differentiation of (A.7.1) in a distributional sense leads to the conclusion that

$$it\,p(t) \leftrightarrow p'(\omega) = 2i\delta(\omega), \tag{A.7.2}$$

from which it follows from the inverse transform of the right side that

$$t\,p(t) = \frac{1}{\pi}. \tag{A.7.3}$$

Here, a factor of i has been dropped from both sides of the equation.

A particular solution to this equation is obtained by dividing both sides by t. However, a little more care is necessary here, since this is a distributional equation. If $p(t)$ satisfies (A.7.3), so does $p(t) + C\delta(t)$, for any constant C, because the distribution $t\delta(t) = 0$. However, evenness and oddness come into play here. Because $\tilde{p}(\omega)$ is odd, the same must be true for $p(t)$. Because $\delta(t)$ is even, it follows that the only choice for C is zero and

$$p(t) = \frac{1}{\pi t}. \tag{A.7.4}$$

So, why the big fuss over what is apparently a nonissue? Consider the function $2iH(\omega)$, which is neither even nor odd. The derivation of the inverse transform would start the same way, with the derivative of this function again being $2i\delta(\omega)$. The inverse transform of this function, however, clearly cannot also be $p(t)$. In fact, by setting

$$2iH(\omega) = \tilde{p}(\omega) + i,$$

it follows immediately that the inverse transform of this function is equal to $p(t) + i\delta(t)$; that is, $C = i$ for this function.

We still need to interpret the *distribution*, $p(t)$. The issue is how this distribution "acts" on test functions. The key to the interpretation is (A.3.2). Let us define the integral on the left as the symmetric limit as $A \to \infty$ of integrals over intervals $(-A, A)$ and use that limit to truncate $\tilde{p}(\omega)$. Each truncation leads to an inverse transform, $p_A(t)$, that is no longer singular at the origin, but remains smooth in the neighborhood of the origin, as well as having odd symmetry. It takes some work to show that the integrals on the right side of (A.3.2) then have the same limit as the integral

$$\lim_{\epsilon \to 0} \int_{-\infty}^{-\epsilon} + \int_{\epsilon}^{\infty} dt\, p(t)\phi(-t),$$

where we have simply truncated away the neighborhood of the origin, but then taken a symmetric limit as the endpoints converge on the origin. This is called the (Cauchy) *principal-value* integral and is standardly denoted by a dashed integral sign (−):

$$\fint_{-\infty}^{\infty} dt\, p(t)\phi(-t).$$

Correspondingly, the notation

$$p(t) = PV\frac{1}{\pi t}$$

is also used.

Of in the course of our derivations throughout the text, the functions,

$$\operatorname{sgn}(t) = \begin{cases} 1, & t > 0, \\ 0, & t = 0, \\ -1, & t < 0, \end{cases} \qquad \text{and} \qquad H(t) = \begin{cases} 1, & t > 0, \\ \frac{1}{2}, & t = 0, \\ 0, & t < 0, \end{cases}$$

also arise. From the results obtained in the discussion above, it is straightforward to conclude that

$$\widetilde{\operatorname{sgn}}(\omega) = \frac{2i}{\omega} \qquad \text{and} \qquad \tilde{H}(\omega) = \frac{i}{\omega} + \frac{\delta(\omega)}{2}. \tag{A.7.5}$$

Here, the tilde $\widetilde{\ }$ over the function symbol, rather than over the entire expression, indicates that this is the inverse transform of the function—sgn or H—evaluated at the argument ω.

A.7.1 Hilbert Transforms

This last function is closely related to the *Hilbert transform*, defined by

$$\mathcal{H}[f(t)] = \frac{1}{\pi}\fint_{-\infty}^{\infty} \frac{f(t')}{t'-t}dt'. \tag{A.7.6}$$

This result can be recast in terms of convolution as

$$\mathcal{H}[f(t)] = f(t) * \left[-\frac{1}{\pi t}\right], \tag{A.7.7}$$

with the convolution to be interpreted in the principal-value sense. By writing the Hilbert transform as a convolution, we now know how to rewrite it in terms of Fourier transforms of the function, $f(t)$, and the transform of the kernel, $-1/\pi t$. From (A.7.4),

$$-\frac{1}{\pi t} = -p(t)$$

and therefore, using (A.7.1), we conclude that

$$\int_{-\infty}^{\infty} \frac{-1}{\pi t} e^{i\omega t} dt = -i \operatorname{sgn}(\omega) = e^{-i \operatorname{sgn}(\omega)\pi/2} = \begin{cases} -i, & \omega > 0, \\ 0, & \omega = 0, \\ i & \omega < 0. \end{cases} \tag{A.7.8}$$

We use the fact that the Fourier transform of a convolution is the product of the transforms to rewrite (A.7.7) in the Fourier domain as

$$\tilde{\mathcal{H}}[\tilde{f}(\omega)] = -i \operatorname{sgn}(\omega) \tilde{f}(\omega). \tag{A.7.9}$$

That is, we may calculate the Hilbert transform of a function by taking its Fourier transform, multiplying by $-i \operatorname{sgn}(\omega)$ and taking the inverse Fourier transform.

Hilbert Transforms and Causality

Suppose that $f(t)$ is a causal function; that is, $f(t) \equiv 0$ for $t < 0$. Then, from (A.7.6),

$$\mathcal{H}[f(t)] = \frac{1}{\pi} \int_0^{\infty} \frac{f(t')}{t' - t} dt'. \tag{A.7.10}$$

In particular, for $t < 0$, the Hilbert kernel is nonsingular and

$$\mathcal{H}[f(t)] = \frac{1}{\pi} \int_0^{\infty} \frac{f(t')}{t' - t} dt', \quad t < 0.$$

That is, the Hilbert transform is an ordinary integral, in this case. However, *it is not necessarily equal to zero*, which means that the Hilbert transform of a causal function need not, itself, also be causal.

A.8 Bandlimited Distributions

A final result of this discussion is the concept of the "bandlimited distribution." Many places in this text we refer to "bandlimited step functions," "bandlimited delta functions," and "bandlimited singular functions" that occur as the output of the seismic inversion formulas we derive.

Using the Fourier transform results discussed above, it is possible to write

$$\delta_B(t) \equiv \frac{1}{2\pi} \int_{-\infty}^{\infty} \tilde{\phi}(\omega) e^{-i\omega t} \, d\omega. \tag{A.8.1}$$

If $\tilde{\phi}(\omega)$ is bounded, locally integrable, and has bounded support, then this integral will converge, meaning that $\tilde{\phi}(\omega)$ may be considered to be a distribution that has a Fourier transform. For this transform to be considered a bandlimited delta function, it would further be necessary that $\tilde{\phi}(\omega)$ be nearly equal to 1 over a significant part of its support. We prefer not to be more precise than that, but suggest only that impulsive sources produce signals that we view as bandlimited delta functions.

The function $\tilde{\phi}(\omega)$ may also be interpreted as being a "filter" (similar to the $F(\omega)$ used throughout the text) that has all of the properties of a distribution, or we may view the inverse transform of $\tilde{\phi}(\omega)$ as a member of a delta sequence. Note that, for the output to be purely real in the time-domain, **Re** $\{\tilde{\phi}(\omega)\}$ must be an even function, and **Im** $\{\tilde{\phi}(\omega)\}$ must be odd. In either case, the idea of a "bandlimited delta function" is entirely compatible with the concepts of distributions discussed above.

It is also possible to use the definition of the Fourier transform of the step function given in (A.7.5) to define the "bandlimited step function" as

$$H_B(t) \equiv \frac{1}{2\pi} \int_{-\infty}^{\infty} \left(\frac{i}{\omega} + \frac{\delta(\omega)}{2} \right) \tilde{\phi}(\omega) e^{-i\omega t} \, d\omega. \tag{A.8.2}$$

Here, the second term contributes only if the support of $\tilde{\phi}(\omega)$ contains the origin. If this is the case, then the constant displacement from the zero line of the step function is preserved and is represented by this second term. Note that most measured data (such as seismic data) does not contain information at zero frequency. Consequently, we cannot recover the magnitude of a step from such a bandlimited step. It is this observation that motivated our introduction of a derivative operator in our inversions to produce bandlimited delta functions in order to recover the discontinuities—the reflectors—in the Earth.

Again, we must require that **Re** $\{\tilde{\phi}(\omega)\}$ be an even function, and **Im** $\{\tilde{\phi}(\omega)\}$ be odd, so that the output of the Fourier transform will be purely real.

We remark that the elements of the sequence of box functions do not fit this description of bandlimited delta functions. For the function

$$S_n(t) = \begin{cases} \dfrac{n}{2}, & |t| < \dfrac{1}{n} \\ 0, & |t| > \dfrac{1}{n}, \end{cases}$$

the Fourier transform is

$$\hat{S}_n(\omega) = \begin{cases} \dfrac{n}{\omega} \sin\left(\dfrac{\omega}{n}\right), & \omega \neq 0, \\ 1, & \omega = 0. \end{cases}$$

This function is real and even for ω real, but it is not bandlimited; it is not zero beyond some finite value of $|\omega|$. However, it is "near" 1 for some neighborhood of $\omega = 0$ that increases with n; the main lobe of this sinc-like function is the interval $(-n\pi, n\pi)$. Thus, we could introduce a neutralizer in the frequency domain, whose support also increases with n, say, larger than the interval $(-n\pi, n\pi)$, and thereby create a bandlimited version of the box sequence in the time domain, behaving somewhat more smoothly than the box sequence itself, but still being a delta sequence.

As a second example, let us interchange the roles of the box and the sinc-like function:

$$S_n(t) = \begin{cases} \dfrac{\sin n\pi t}{\pi t}, & t \neq 0, \\ \dfrac{n}{\pi}, & t = 0. \end{cases}$$

Now, the Fourier transform is given by

$$\hat{S}_n(\omega) = \begin{cases} 1, & |\omega| < n \\ 0 & |\omega| > n. \end{cases}$$

Now the Fourier transform has bounded support for each n, and is an even function of n. In practice, we would usually "taper" this function to zero with something simple, such as a quarter cycle of a sine-function. This would reduce the size of the side lobes in the time domain, leading to a bandlimited delta function for which more of the energy lies in the main lobe than is the case for each S_n defined here.

Finally, we present an example that is better suited for application to causal functions (or to functions of the radial variable in polar coordinates). Let

$$S_n(t) = \begin{cases} 0, & t < 0 \\ n^2 t e^{-nt}, & t > 0. \end{cases}$$

This function peaks at $t = 1/n$, with peak value n/e. Its Fourier transform is

$$\hat{S}_n(\omega) = \frac{n^2}{(n - i\omega)^2} = n^2 \left[\frac{n^2 - \omega^2}{(n^2 + \omega^2)^2} + \frac{2i\omega n}{(n^2 + \omega^2)^2} \right].$$

For this function, $\mathbf{Re}\ \hat{S}_n(\omega)$ is even, while the imaginary part is odd. Again, for ω real, $\hat{S}_n(\omega)$ is "near" 1 in some symmetric region around the origin, but $S_n(t)$ is not bandlimited. However, one can show that

$$\lim_{n\to\infty} \int_0^\infty S_n(t) f(t) dt = \lim_{t\to 0+} f(t).$$

The last expression here denotes the limit through positive values of t only. For causal functions of an appropriate class, this is the "right" type of delta sequence to use in order to obtain a meaningful definition of $\delta(t)$.

Again, we could create a bandlimited delta sequence from this one, by introducing a neutralizer function that is equal to 1 on an appropriate interval around the origin, that interval necessarily increasing with n. For example, we could choose that interval to be the one in which $\hat{S}_n(\omega) > 1/2$.

In summary, we can see here how that there are useful delta sequences that are not bandlimited, but which are "close" to others that are. Clearly, physical experiments must lead to bandlimited impulsive sources. On the other hand, in mathematical modeling, it is easier to work with sequences that have relatively simple analytical expressions in the time domain, such as the first and third examples here. For many applications, it is rea-

sonable to work with the simpler analytical examples and then introduce bandlimiting only at the very end of the analysis.

Appendix B
The Fourier Transform of Causal Functions

In several places in this text, integrals are interpreted as being either forward or inverse "causal" Fourier transforms. In this appendix, we will define and discuss this concept. Any forward transform that has semi-infinite integration limits may be interpreted as being a causal or anticausal transform. However, care must be taken in defining the inverse causal Fourier transform. Fundamental to this definition is a stipulation of choosing an integration contour that passes above all singularities in the complex-ω domain. Here, we clarify what we mean by the term "causal Fourier transform" and we show how this choice of integration contour comes about.

B.1 Introduction

Idealized physical models are often described as being of infinite spatial extent in one or more dimensions. Correspondingly, any wavefields that propagate in such models will have a domain of definition that is of similarly infinite extent as well. Because wavefields may be represented as Fourier integrals, the infinite limits of such integrals reflect the infinite spatial extent of the domain of the problem. An example in one spatial dimension is the forward transform

$$F(k) = \int_{-\infty}^{\infty} f(x) e^{-ikx} dx \tag{B.1.1}$$

and corresponding inverse transform

$$f(x) = \frac{1}{2\pi} \int_{-\infty}^{\infty} F(k) e^{ikx} dk. \tag{B.1.2}$$

Physical signals, however, have the property of always being "turned on" at some finite time that can be set equal to zero. Thus, the time-dependence of functions describing physical models will always be of *semi*-infinite extent. This is the property of *causality*, and all such functions that are zero before time zero are called *causal functions*. Correspondingly, the semi-infinite domain in time of causal functions will be represented as semi-infinite limits of integration in Fourier representations of these functions, as for the forward transform

$$F(\omega) = \int_{0}^{\infty} f(t) e^{i\omega t} dt, \tag{B.1.3}$$

with corresponding inverse transform

$$f(t) = \frac{1}{2\pi} \int_{-\infty}^{\infty} F(\omega) e^{-i\omega t} d\omega. \tag{B.1.4}$$

There are two differences in character, one aesthetic, the other substantive, between equations (B.1.1) and (B.1.3).

The aesthetic difference is that the sign of the exponent has changed. This means that the phase of the forward transform (B.1.1) will be of opposite sign to that in (B.1.3). Then, when inverting the Fourier transform of a function of k and ω, we have the general form

$$f(x,t) = \frac{1}{(2\pi)^2} \int_{-\infty}^{\infty} dk \int_{-\infty}^{\infty} d\omega F(k,\omega)\, e^{i\{kx-\omega t\}}.$$

We view the right side here as a superposition over frequency ω and wavenumber k of contributions of the form $F(k,\omega)\ \exp[i\{kx - \omega t\}]$. Each such contribution represents a complex wave—a composition of sines and cosines—that propagates along the line with coordinate x as time progresses. The way we see this propagation is through the motion of the crests of the sines and cosines, or, for that matter, the way any point of fixed phase propagates with time. That is, we examine the movement of points where $kx - \omega t =$ constant. The speed with which such a point propagates is called the "phase speed" of the wave, and is given by $v_{phase} = \omega/k$. Had we not reversed the signs in these two transforms, then the phase speed would have been $-\omega/k$, which is somewhat less aesthetically pleasing, because we like to think of *forward* propagation as being represented by a *positive* quotient of like-signed variables. It often happens that, if we carry out the k-integration here, we find that not all ω–k combinations propagate, but only a subset, for which $\omega = \omega(k)$. Such a relationship, along with its generalizations to higher dimensional problems, is called a "dispersion relation."

The more substantive difference between the definitions is that the lower limit is $-\infty$ in the forward spatial transform (B.1.1), whereas the lower limit

of the forward temporal transform (B.1.3) is 0. Note that, in the former, if k becomes complex, the exponent has a real part, $\mathbf{Im}\ \{k\}x$, where we are considering x as always being real-valued. If $\mathbf{Im}\ \{k\} < 0$ and $x \to -\infty$, or if $\mathbf{Im}\ \{k\} > 0$ and $x \to +\infty$, then the resulting factor of $\exp(\mathbf{Im}\ \{k\}x)$ in the integrand will *grow* exponentially beyond all bounds, meaning that the integral will not converge in these respective cases. Conversely, if $\mathbf{Im}\ \{k\} > 0$ and $x \to -\infty$, or if $\mathbf{Im}\ \{k\} < 0$ and $x \to +\infty$, then the resulting factor of $\exp(\mathbf{Im}\ \{k\}x) = \exp(-|\mathbf{Im}\ \{k\}x|)$ will *decay* faster than any algebraic power of x.

Conversely, in (B.1.3), with ω considered as a complex variable and t restricted to be positive only, the corresponding quantity $|\exp\{\mathbf{Re}\ (i\omega t)\}| = \exp\{-\mathbf{Im}\ \{\omega\}t\}$ will *decay* exponentially for $\mathbf{Im}\ \{\omega\} > 0$ and $t \to \infty$. Furthermore, increasing $\mathbf{Im}\ \{\omega\}$ increases the rate of exponential decay of the integrand and improves the rate of convergence of the integral. Indeed, even if $f(t)$ were to grow as a linear exponential—say, $\exp\{at\}$—we need only take $\mathbf{Im}\ \{\omega\} > a$ to have an exponentially decaying integrand in this definition of the Fourier transform. Note that if t is allowed to approach both $\pm\infty$, as we did with x in the previous example, this trick will not work.

So, in light of this discussion, the class of causal functions that have a classical[1] Fourier transform can be expanded to include functions that are locally integrable[2] with possible exponential growth, $f(t) = O(\exp\{at\})$, as long as the imaginary part of ω is restricted to be "large enough." That is, we define

$$F(\omega) = \int_0^\infty f(t)e^{i\omega t}dt, \qquad \mathbf{Im}\ \{\omega\} > a. \tag{B.1.5}$$

Now, not only does the given integral converge in this restricted domain, but so do all of the integrals of the form

$$F^{(n)}(\omega) = \int_0^\infty (it)^n f(t)e^{i\omega t}dt, \quad \mathbf{Im}\ \{\omega\} > a, \quad n = 1, 2, \ldots .$$

These integrals represent the derivatives of $F(\omega)$. These are functions that decay faster than any power of t. (Such "rapidly-decreasing" functions are discussed in Appendix A.) Thus, where this Fourier transform exists—in some upper half ω-plane defined by $\mathbf{Im}\ \{\omega\} > a$—$F(\omega)$ is an *analytic function* of the complex variable ω, with the further property that $|F(\omega)| \to 0$, as do all of its derivatives, as $|\omega| \to \infty$, as long as $\mathbf{Im}\ \{\omega\} > a$. This fact

---

[1] We mean to make a distinction between "classical" versus "distributional" Fourier transforms. Distributional Fourier transforms are discussed in Appendix A.

[2] "Locally integrable" means that the integral of $f(t)$ over any finite interval exists, even as an improper integral.

allows us to bring the whole machinery of analytic function theory to bear on the analysis of the causal temporal transforms.

To have a clearer view of how all of this works, we will explicitly write ω as complex variable

$$\omega = \mu + i\nu, \tag{B.1.6}$$

with real part μ and imaginary part ν. Equation (B.1.5) becomes

$$F(\mu + i\nu) = \int_0^\infty f(t)e^{i\mu t - \nu t}dt, \quad \nu > a,$$

or (B.1.7)

$$F_\nu(\mu) = \int_0^\infty \left[f(t)e^{-\nu t}\right] e^{i\mu t}dt, \quad \nu > a.$$

In the second form, ν plays the role of a parameter in the Fourier transform of the function

$$g_\nu(t) = \begin{cases} 0, & t < 0, \\ f(t)e^{-\nu t}, & t > 0, \end{cases}$$

to a function of the transform variable μ. Now, however, this is a standard Fourier transform of an integrable function, $g(t)$, on the time interval, $(-\infty, \infty)$. The inversion, then, is immediate:

$$g_\nu(t) = \frac{1}{2\pi}\int_{-\infty}^\infty F_\nu(\mu)e^{-i\mu t}d\mu, \qquad \nu > a,$$

or, rewriting the result in terms of $f(t)$,

$$\frac{1}{2\pi}\int_{-\infty}^\infty F(\mu + i\nu)e^{-i(\mu+i\nu)t}d\mu = \begin{cases} 0, & t < 0, \\ & \\ f(t), & t > 0, \end{cases}, \qquad \nu > a.$$

Note that transferring the real exponential back to the left side has no effect on the integration in μ, because ν and t are constants of this integration.

To complete the story, this result must be reinterpreted as a *contour integral* in ω. The contour in the complex ω-plane is a straight line along which $\mu = \mathbf{Re}\ \{\omega\}$ varies from $-\infty$ to ∞, while $\nu = \mathbf{Im}\ \{\omega\}$ is large enough that the contour of integration *is located in the domain of analyticity of the function*, $F(\omega)$. More succinctly, the contour is required to pass *above all singularities* of $F(\omega)$ in the complex $\omega-$plane. Thus,

$$\frac{1}{2\pi}\int_\Gamma F(\omega)e^{-i\omega t}d\omega = \begin{cases} 0, & t < 0, \\ f(t), & t > 0, \end{cases} \tag{B.1.8}$$

with Γ being any contour that passes above all singularities of $F(\omega)$, along which **Re** ω ranges from $-\infty$ to ∞. If there are no singularities down to and on the real ω-axis, then the contour can be replaced by the real axis. If $F(\omega)$ has no singularities above the real axis, but one or more *on* the real axis, then the contour of integration must pass *above* those singularities that lie on the real axis [Titchmarsh, 1948].

It is straightforward now to show by contour integration methods that the representation in (B.1.8) is zero for $t < 0$. This result uses *Jordan's lemma*, which states that

$$\lim_{R\to\infty} \int_C \left|e^{ia\omega}\right| |d\omega| \leq \frac{\pi}{a}.$$

Here, $|d\omega| = Rd\phi$ is the differential arclength on C.

For $a < 0$, Jordan's lemma is true for a semicircle in the lower half plane, with a replaced by $|a|$ on the right side of the above equation. (Of course, the same bound holds for any segment of the semicircle in question as well.)

Now, consider, again the representation, (B.1.8), with t negative (and hence $-t$, in the exponent, positive). Replace the contour Γ by Γ_R, the segment of Γ on which **Re** $\{\omega\}$ ranges from $-R$ to R. Note that in the limit, as $R \to \infty$, this contour approaches the original contour Γ. Close the finite contour of integration with a semicircle, C, in the upper half plane. See Figure B.1. The integrand is analytic on the closed contour. Furthermore, on the one hand, the integral around this closed path is equal to zero, by Cauchy's theorem. On the other hand,

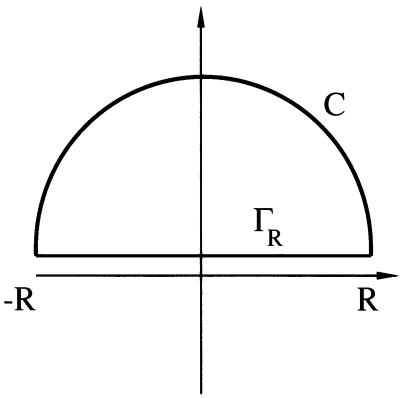

FIGURE B.1. The portion of the contour labeled Γ_R passes above any poles in the integrand. The contour labeled C, yields a vanishing contribution as $|R| \to \infty$, by Jordan's lemma. The result of integration around the full contour is zero, by Cauchy's theorem, because no poles are enclosed.

$$\begin{aligned}\left|\frac{1}{2\pi}\int_C F(\omega)e^{-i\omega t}d\omega\right| &\leq \frac{1}{2\pi}\int_C |F(\omega)|\,|e^{-i\omega t}|\,|d\omega| \\ &\leq \frac{1}{2\pi}\max_{\omega \text{ on } C}(|F(\omega)|)\int_C |e^{-i\omega t}|\,|d\omega| \\ &\leq \frac{1}{2|t|}\max_{\omega \text{ on } C}(|F(\omega)|) \\ &\to 0, \text{ as } R \to \infty.\end{aligned}$$

Here, in going from the second to the third line, we used Jordan's lemma; in going from the third line to the fourth line, we used the fact that $|F(\omega)| \to 0$ as $|\omega| \to \infty$ in the domain of analyticity. Thus, if the integral on the semicircle approaches zero in this limit and the integral around the entire path is identically zero, the integral on Γ must be zero as well. Hence, the structure of this Fourier representation assures the causality of the inverse transform, always. On the other hand, for $t > 0$, the contour could only be closed in the lower half plane, if at all. However, in general, $F(\omega)$ will not be analytic there and we could not use the same trick to conclude that $f(t)$ was zero for $t > 0$.

The reader familiar with Laplace transforms should hear echoes of that theory in this discussion. With $i\omega = -s$, this is the Laplace transform. The right half plane of analyticity of that theory is the upper half plane of analyticity of the present theory. Similarly, the "Bromwich contour," to the right of all singularities of the transformed function, used for inversion in that theory, is a contour in the upper half plane, above all singularities, in this theory.

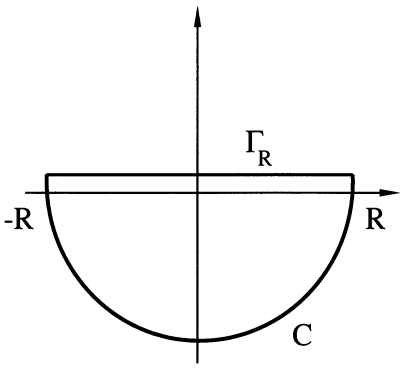

FIGURE B.2. The portion of the contour labeled Γ_R passes above the poles at $\pm ck$ in the integrand, as in the previous example. However, the contour labeled C is chosen to close in the lower half plane of ω. The contribution due to C vanishes by Jordan's lemma, but the integral around the full contour yields a nonzero result by the residue theorem.

B.2 Example: the 1D Free-Space Green's Function

We now carry out an example to show how the machinery of complex contour integration facilitates the inversion of a Fourier wavefield representation. Fourier inversion will be carried out on the one-dimensional free-space Green's function for the wave equation, which is a solution of the problem

$$\frac{d^2g(x,t)}{dx^2} - \frac{1}{c^2}\frac{d^2g(x,t)}{dt^2} = -\delta(x)\delta(t), \quad g(x,0) = \left.\frac{\partial g(x,t)}{\partial t}\right|_{t=0} = 0. \quad \text{(B.2.1)}$$

This Green's function is causal in time, and its Fourier transform is given by

$$G(k,\omega) = \int_0^\infty dt \int_{-\infty}^\infty dx\; g(x,t)e^{i\{\omega t - kx\}}. \quad \text{(B.2.2)}$$

This Fourier transform is to be applied to the differential equation above. One subtle point is that the endpoint of integration, $t = 0$, is right at the support of the temporal delta function. For causal functions, such delta functions are to be defined as delta sequences, all of whose support resides in $t \geq 0$. In this case, the "full strength" of the delta function acts on the integral in the Fourier transform. (The last example of the previous appendix provided a delta sequence that would lead to just such a delta function). Alternatively, define $g(x,t)$ for t on $(-\infty,\infty)$ to be identically zero for $t \leq 0$. Then, the Fourier transform of g with respect to t is still the causal transform, but we do not have to worry about this subtlety for defining a full-strength delta function at the initial time. In either case, transforming the differential equation and solving for $G(k,\omega)$ leads to the result

$$G(k,\omega) = -\frac{c^2}{\omega^2 - c^2k^2}. \quad \text{(B.2.3)}$$

Note that in the complex ω-plane, the right side has two poles at $\omega = \pm ck$, but no other singularities. Thus, if we were to carry out the Fourier transform in ω first, the contour of integration would be required *to pass above the real ω-axis*. See Figure B.1. That is,

$$g(x,t) = -\frac{c^2}{4\pi^2}\int_{-\infty}^\infty dk \int_\Gamma d\omega \frac{e^{i\{kx-\omega t\}}}{\omega^2 - c^2k^2}. \quad \text{(B.2.4)}$$

One can readily check for this specific example that the representation on the right is zero for $t < 0$, by following precisely the procedure outlined above for the general case. Thus, the solution, $g(x,t)$ is, indeed, a causal function.

Now, for $t > 0$, again consider Γ_R, the segment of Γ for which **Re** $\{\omega\}$ ranges from $-R$ to R. Close the contour of integration on a semicircle in the lower half plane. See Figure B.2. For the specific integrand, one can

verify that the integral on this semicircle will approach zero in the limit as $R \to \infty$, again by using Jordan's lemma and estimating the integral as above. However, for every R the integral can be calculated in terms of the residues at the poles $\omega = \pm ck$. The result is

$$g(x,t) = -\frac{ic}{4\pi} \int_{-\infty}^{\infty} dk\, e^{ikx} \frac{e^{ickt} - e^{-ickt}}{k}. \tag{B.2.5}$$

This integral is, again, standardly calculated by complex contour integration methods.

The careful reader may recognize each of the parts of this integral as being related to the inverse Fourier transform of the signum function, discussed in Appendix A. However, the calculation of this integral is left to the reader.

We simply state the result:

$$g(x,t) = \frac{c}{2} H(ct - |x|), \tag{B.2.6}$$

with $H(x) = 1$ for $x > 0$ and $H(x) = 0$ for $x < 0$. The real point of the discussion is that a causal solution was produced by carefully defining the inverse Fourier transform with respect to ω.

Alternatively, the k-integration could be carried out first. In this case, the poles at $k = \pm\omega$ are not on the real axis. If we think of the k-integral as producing a function of complex ω, then the value of this function on the real ω-axis can be determined by analytic continuation. For this purpose, the k integral is interpreted as a contour integral in the complex k-domain, with that contour being the real axis in k. The pole at ω/c lies above the contour, while the pole at $-\omega/c$ lies below the contour. Deform the contour below the pole at ω/c on a small semicircle below the real k-axis and deform the contour above the pole at $-\omega/c$ on a small semicircle above the real k-axis. Now, let $\mathbf{Im}\ \{\omega\}$ approach zero. The integration in k makes sense in this limit and the result defines a contour integral in k with $\mathbf{Im}\ \{\omega\} = 0$. The contour in k can be described as a path on which $\mathbf{Re}\ \{k\}$ varies from $-\infty$ to ∞, passing *above* the singularity at $-\omega/c$ and passing *below* the singularity at ω/c.

Often, in the literature, this choice of contour is justified by "adding a little dissipation" to give a real frequency variable ω a positive imaginary part. It can be seen from this discussion that such an artifice is not necessary, nor should it be: the original problem is well-posed and the integral transform technique does not require artificial dissipation to go forward.

Now, for $x > 0$ the contour integral in k can be closed with a large semicircle in the upper half plane, while for $x < 0$ the contour can be closed with a semicircle in the lower half plane. In the former case, the integral can be computed in terms of a residue at $k = \omega/c$, while in the latter case, the integral can be computed in terms of a residue at $k = -\omega/c$. After some manipulation, this leads to the result

$$g(x,t) = \frac{ic}{4\pi} \int_{\Gamma} d\omega \frac{e^{i\omega[|x|/c-t]}}{\omega}. \tag{B.2.7}$$

Now, for $|x|/c - t > 0$, we obtain zero for this integral, by the same line of reasoning as above, while for $|x|/c - t < 0$, we obtain the result by evaluating the residue at $\omega = 0$. Thus, we obtain the result (B.2.6), again.

For additional information about analysis of functions of a complex variable, see Butkov [1968], Duffy [1994], Levinson and Redheffer [1970], Morse and Feshbach [1953], or equivalent texts.

Appendix C
Dimensional Versus Dimensionless Variables

Throughout this text we relate quantities such as frequency, wavenumber, and wavespeed to each other within the spatial and temporal domains of the problems being considered. Many of the derivations we present rely on asymptotic methods that depend on the identification of a "large parameter." Because *dimensional* variables (variables with dimensions such as length and time) may contain arbitrary scaling factors, we must remove all dependence on these arbitrary factors before relative sizes of quantities may be compared.

There are two issues related to dimensional scaling. First, all dimensional quantities are expressed in terms of units of measurement that must balance in any formula. Second, there may be "natural" scaling factors that are imposed by the physics of the problem being considered. These natural scaling factors result if the parameters in an equation have a preferred range of values. Both of these issues of dimensional scaling must be dealt with in formulas that describe physical problems. However, the notations that we employ throughout this text do not appear to distinguish between "dimensional" and "dimensionless" variables. Furthermore, we freely use data examples that are described in terms of the standard units of m, s, Hz, m/s, and so forth, with formulas created using asymptotic methods—implying that the formulas are dimensionally independent.

This appendix has been included for two purposes. First, we wish to reassure the reader that proper care has been taken in dealing with dimensional versus dimensionless representations. Second, we want provide the reader with general examples of how to deal with the issue of dimensionality.

C.1 The Wave Equation

The fundamental governing equation for all problems in this text is some form of the *wave equation*, with the 1D version being

$$\left(\frac{\partial^2}{\partial x^2} - \frac{1}{c^2(x)}\frac{\partial^2}{\partial t^2}\right) U(x,t) = -\delta(x)\delta(t). \tag{C.1.1}$$

Here, x, $c(x)$, t, and $U(x,t)$ are dimensional variables. To convert to dimensionless variables, X, T, and W, we make the substitutions $x \to LX$, $t \to \overline{T}T$, $c(x) \to c_0 C(X)$, and $U(x,t) \to \overline{U}W(X,T)$. The quantities L, $\overline{T}$, and c_0 are dimensional scale factors that define the units that express length, time, and wavespeed in the respective relationships between the dimensionless and dimensional variables. The parameter $\overline{U}$ represents the scale factor relating the dimensional representation of the field U to the dimensionless field W.

The product of delta functions of dimensional arguments carry dimensions of their own. To see why, note that $-\delta(x)\delta(t) = -\delta(LX)\delta(\overline{T}T) = -\delta(X)\delta(T)/L\overline{T}$. By convention, we interpret the function symbol, δ, as having no inherent dimensions of its own, so that $\delta(X)\delta(T)$ also carries no dimensions. Consequently, we must conclude that the delta function of a dimensional argument must carry a dimension that is the inverse dimension of that argument; that is, the dimension of $\delta(x)$ must be inverse length—1/m, 1/ft, 1/km, etc.—while the dimension of $\delta(t)$ must be inverse time—1/s, $1/\mu$ sec, etc. Thus, depending on the dimensions assigned to $\overline{U}$, the dimensions of the two sides of the equation might not match, which is unacceptable. We will deal with that in two different ways in the next two subsections.

C.1.1 Mathematical Dimensional Analysis

Using the transformations to dimensionless variables in the wave equation yields

$$\left(\frac{1}{L^2}\frac{\partial^2}{\partial X^2} - \frac{1}{c_0^2}\frac{1}{C^2(X)}\frac{1}{\overline{T}^2}\frac{\partial^2}{\partial T^2}\right) \overline{U}W(X,T) = -\frac{1}{L\overline{T}}\delta(T)\delta(X). \tag{C.1.2}$$

For the purpose of this appendix, let $[L]$ mean the *dimensions of* L, and so forth. Analysis of the units of the scaling factors in (C.1.2), above, yields

$$[L] = \text{Length}, \qquad [\overline{T}] = \text{Time}, \qquad \text{and} \qquad [c_0] = \frac{\text{Length}}{\text{Time}}.$$

Often, the only need we have for dimensional analysis is to confirm consistency in the equations that arise in our modeling and inversion. For this purpose, we need not prescribe the dimensions to the unknown, u, or equivalently, to $\overline{U}$ that arise from the underlying physical problem that the

equation models. Instead, can use a *default dimension* dictated by requiring a balance between the two sides of the equation, with the dimensions of the right side being just $1/[L][\overline{T}]$. Let us proceed with this intent, then, to find the default dimensions of u, or equivalently, those of $[\overline{U}]$. Applying the brackets, [], to the wave operator yields

$$\left[\left(\frac{1}{L^2}\frac{\partial^2}{\partial X^2} - \frac{L^2}{c_0^2}\frac{1}{C^2(X)}\frac{1}{\overline{T}^2}\frac{\partial^2}{\partial T^2}\right)\right] = \frac{1}{\text{Length}^2}.$$

Thus, the dimensionless representation of the wave equation may be written as

$$\frac{\overline{U}}{L^2}\left\{\left(\frac{\partial^2}{\partial X^2} - \frac{L^2}{c_0^2}\frac{1}{C^2(X)}\frac{1}{\overline{T}^2}\frac{\partial^2}{\partial T^2}\right)W(X,T)\right\} = -\frac{1}{L\overline{T}}\left\{\delta(T)\delta(X)\right\}. \tag{C.1.3}$$

Here the parts in braces, { }, are dimensionless quantities. To make the units on the two sides match, we conclude that the default dimensions of $\overline{U}$ are

$$[\overline{U}] = \frac{\text{Length}}{\text{Time}}, \tag{C.1.4}$$

which are the units of particle velocity.

The reader is encouraged to perform a similar analysis with the two- and three-dimensional wave equations, with $\boldsymbol{x} \equiv L\boldsymbol{X} = (LX_1, LX_2)$ in 2D and $\boldsymbol{x} \equiv L\boldsymbol{X} = (LX_1, LX_2, LX_3)$ in 3D. The delta function sources then become

$$-\delta(x_1)\delta(x_2)\delta(t) = -\delta(T)\delta(X_1)\delta(X_2)/[L]^2[\overline{T}]$$

in 2D, and

$$-\delta(x_1)\delta(x_2)\delta(x_3)\delta(t) = -\delta(T)\delta(X_1)\delta(X_2)\delta(X_3)/[L]^2[\overline{T}]$$

in 3D. The reader will see that the default dimensions of the factor of $\overline{U}$ are $1/[\overline{T}] = 1/\text{Time}$ in two dimensions and $1/[L][\overline{T}] = 1/\text{Length} \cdot \text{Time}$ in three dimensions, neither of which seem particularly physical.

We note that in each of these cases, the units of the scale factors cancel, meaning that changing the equation into dimensionless form could have been accomplished by simply substituting the dimensionless variable symbols in place of the dimensional ones. In spite of this good fortune, a potential benefit of doing dimensional analysis is in checking results. The units of terms that are added or subtracted must be the same, and the units on both sides of an equality must balance, meaning that dimensional analysis can easily reveal an incorrect equation if the units fail to balance. Unfortunately, this is not a foolproof test, as it is possible to have incorrect equations whose units also balance.

C.1.2 Physical Dimensional Analysis

One point that we must stress is that the analysis above is a *mathematical* scaling analysis intended to check consistency between the two sides of a given equation. Such an analysis cannot account for the dimensions that are attached to quantities as a result of derivations based on physical considerations. The wave equation, (C.1.1), arises from a description of the dynamics of some physical phenomenon. As such, the function $U(x,t)$ can be expected to have dimensions of its own that depend on the physical model that is the basis of the derivation of the equation. Even in the simple case of 1D wave propagation on a vibrating string, "vibration" can mean *displacement*, *velocity*, or *acceleration*, or indeed, vibration can be a *dimensionless* quantity, depending on how we formulate the problem.

How, then, do we resolve the inconsistency of this observation with the conclusion presented in the dimensional analysis of equation (C.1.4)? The answer lies in our interpretation of the source mechanism on the right side of (C.1.1). In that equation, we have described the right side totally in terms of the "natural" dimensions of the delta functions. Yet, in the formulation of the physical problem, we may represent the source (or forcing function) as a force-density, a force, or a displacement. In each case, $[\,\overline{U}\,]$ will be different.

[Stakgold, 1979] One common derivation of 1D wave propagation on a string begins by formulating the problem with the $\partial^2/\partial x^2$ term having a coefficient that is a tension, which is a force, and with the $\partial^2/\partial t^2$ term being multiplied by a density. If the forcing function of the equation is a quantity with units of force per unit length (a force-density), we then have

$$\left(\mathcal{T}\frac{\partial^2}{\partial x^2} - \rho\frac{\partial^2}{\partial t^2}\right) U(x,t) = -\mathcal{F}. \tag{C.1.5}$$

Here,

$$[\mathcal{T}] = \text{Force} = \text{Mass} \cdot \frac{\text{Length}}{\text{Time}^2},$$

$$[\rho] = \frac{\text{Mass}}{\text{Length}},$$

$$[\mathcal{F}] = \frac{\text{Force}}{\text{Length}} = \frac{\text{Mass}}{\text{Time}^2}.$$

Applying the brackets [ ] to the wave operator in (C.1.5) yields

$$\left[\left(\mathcal{T}\frac{\partial^2}{\partial x^2} - \rho\frac{\partial^2}{\partial t^2}\right)\right] = \frac{\text{Mass}}{\text{Length} \cdot \text{Time}^2}$$

Therefore, for the two sides of (C.1.5) to have the same dimensions, $[U] \equiv [\,\overline{U}\,] = \text{L}$; that is, U is a displacement. For U to be particle velocity, as in equation (C.1.1), we would choose the source to be a force per length-time

and to obtain $[U]$ = Acceleration, we would choose the source to be a force per length-time squared.

C.2 The Helmholtz Equation

It should be no surprise that the units cancel in the problem stated above, because the dimensional scaling factors relating wavespeed to space and time have been designed by common agreement to be mutually compatible. If our interest is in applying asymptotic analysis to a formula, however, then we must identify a large (or small) parameter. The formula is then expanded in an asymptotic series in the parameter. The asymptotic expansion is then truncated to a desired order of accuracy measured in terms of the large (small) parameter. An example of this process is the *stationary phase formula.* This formula results from saving the first term of the asymptotic expansion of a general Fourier-like integral.

Many of the results in this text depend on the validity of the high-frequency or, more generally, the *large-wavenumber* assumption. To understand what "high-frequency" means, we will need to transform the wave equation into its frequency domain form—the Helmholtz equation. To do this, we apply the temporal Fourier transform to both sides of the wave operator. The temporal Fourier transform

$$\tilde{f}(\omega) = \int_0^\infty f(t) e^{i\omega t}\, dt$$

may be written in a dimensionless form by the substitutions $t \to \overline{T}T$ and $\omega \to \omega_0 \Omega = \Omega/\overline{T}$ as

$$\tilde{F}(\Omega) = \int_0^\infty F(T) e^{i\omega_0 \Omega \overline{T} T}\, \overline{T} dT.$$

Thus, the temporal Fourier transform introduces a factor of $\overline{T}$. In fact, from either of these equations, the dimensions of the function and its temporal transform must differ by a scale of time:

$$\left[\tilde{f}(\omega)\right] = \text{Time} \cdot [f(t)]; \quad \left[\tilde{F}\right] = \text{time} \cdot [F(T)].$$

This is consistent with the Helmholtz equation

$$\left(\frac{\partial^2}{\partial x^2} + \frac{\omega^2}{c^2(x)}\right) u(x,\omega) = -\delta(x), \tag{C.2.1}$$

which, when written in dimensionless variables, is

$$\frac{\overline{u}}{L^2}\left\{\left(\frac{\partial^2}{\partial X^2} + \frac{\omega_0^2 L^2}{c_0^2}\frac{\Omega^2}{C^2(X)}\right) w(X,\Omega)\right\} = \frac{1}{L}\left\{-\delta(X)\right\}. \tag{C.2.2}$$

Here, the substitutions $x \to LX$, $\omega \to \omega_0 \Omega$, and $u(x,\omega) \to \overline{u} w(X,\Omega)$ have been made. Again, the terms in braces { }, are dimensionless quantities.

From the standpoint of balancing units, we see that the Fourier transform makes $\overline{u} = L$, meaning that the units of the Helmholtz equation do, indeed, balance. In fact, in either form, the overall scale factor of the Helmholtz equation differs from the temporal form, (C.1.2), by a factor having the scale of time, resulting from applying the temporal Fourier transform. If we cancel the net factor of $1/L$ that appears on both sides of the dimensionless Helmholtz equation (taking the default scale, $[\overline{u}] \equiv L$), we are left with the dimensionless Helmholtz equation

$$\left(\frac{\partial^2}{\partial X^2} + \lambda^2 \frac{\Omega^2}{C^2(X)}\right) w(X, \Omega) = -\delta(X), \tag{C.2.3}$$

where

$$\lambda \equiv \frac{\omega_0 L}{c_0}.$$

We may now interpret ω_0, L, and c_0 as values of length, frequency, and wavespeed that characterize the specific problems we are interested in solving. The quantity ω_0/c_0 represents the wavenumber of the "characteristic" waves that propagate, while L represents the "characteristic length scale" of the medium in which the waves are propagating. The characteristic wavelength is $\Lambda \equiv 2\pi c_0/\omega_0$ meaning that the ratio of the characterizing length scale L to the characteristic wave length Λ is related to the parameter λ through the expression

$$\lambda = \frac{2\pi L}{\Lambda}.$$

We want to choose the dimensional scales in such a manner that λ reflects the relative size between w and its second derivative term on the left side of (C.2.3). For this to be the case, the combination of length, time and wavespeed scales must be taken in such a manner that $\Omega^2/C^2(X)$, the squared ratio of dimensionless frequency to dimensionless wavespeed, should be an "order one" quantity. That is, it should neither be particularly large or particularly small compared to unity. Then, λ will characterize the relative scale between the two terms on the left side of (C.2.3) as we wanted. The solution of this equation can then be characterized as "high-frequency" if the parameter λ is *large* compared to unity. In practice, we have found that in wave propagation problems, $\lambda \geq \pi$ is large enough. That condition translates to

$$\begin{aligned} \pi &\leq \frac{2\pi L}{\Lambda}, \\ 1 &\leq \frac{2L}{\Lambda}, \\ \frac{\Lambda}{2} &\leq L, \end{aligned}$$

meaning that values of L must be larger than $\Lambda/2$ for the high-frequency condition to be true.

This example deals with one-way propagation. In the inverse scattering problem, the wave propagation is two-way, meaning that the characteristic wavenumber is given by $c_0/2\omega_0$. Making this replacement in the definition of λ,

$$\lambda \equiv \frac{2\omega_0 L}{c_0},$$

and again choosing $\lambda \geq \pi$, yields a condition for high frequency (or large wavenumber) that is the same as the Rayleigh criterion for resolution for single-frequency waves, $L \geq \Lambda/4$, (discussed more fully in Section 3.4).

The typical wavelength Λ is determined by both the wavespeed and the bandwidth of the source or initial data of the underlying problem. The origin of the length scale L is a little more obscure. There are many possibilities, depending on the problem under consideration. For example, L could be a typical distance of propagation from an isolated source to the first scattering surface in the earth. A second choice might be the radius of curvature of a reflector. Another candidate might be a length scale associated with the variations of the propagation speed in the medium, determined as a typical value of

$$\frac{c(x)}{\left|\dfrac{dc(x)}{dx}\right|} \qquad \text{or} \qquad \sqrt{\frac{c(x)}{\left|\dfrac{d^2c(x)}{dx^2}\right|}}.$$

In the first case, L characterizes the slope of the wavespeed; in the second case, L characterizes the curvature of the wavespeed (somewhat crudely).

How, then do we choose L? The answer is that the problem "chooses" the length scale for us. Intuitively, we know that "high frequencies are better," in modeling and inversion problems. In the former, high-frequency wave propagation tends to look more like the propagation of plane waves in homogeneous media. In the latter, high frequencies are synonymous with better resolution of reflector images. We also know, however, there are natural constraints on the range of available frequencies dictated by the underlying physical experiment and medium configuration. For the seismic imaging problems, the experience derived from the long history of data acquisition has given the exploration geophysics community certain expectations of the ranges of frequencies that are reasonable to expect, as well as the range of depths in the earth that it is reasonable to expect to be able to probe with those frequencies. Seismic sources and detectors have been designed to operate within these parameters, with survey cost being the primary constraining factor beyond this.

All other parameters we have discussed here are beyond the control of the explorationist, being properties of the medium. Yet an analysis based on the limiting ranges of parameters such as the slope and curvature of the

wavespeed profile may be critical in interpreting the successes and, perhaps more importantly, the failures of imaging techniques that occur even when everything was done "right" by the experimentalist.

Again, the reader is encouraged to try the computations for the higher-dimensional forms of the Helmholtz equation, which correspond to those we have done here for the 1D problem. The results will be similar.

The reader should not confuse the characterization of high-frequency with the constraints introduced in Section 3.6.1 for the validity of a *specific* high frequency asymptotic method. We note that the parameter we have called λ here was only a factor in the ultimate dimensionless parameter that we bounded below by π in that discussion. When that particular method fails, there are other, more sophisticated asymptotic approximations available. They, too, are high-frequency methods, required when the conditions for validity of the simple stationary phase formula are not satisfied.

The point is that the high-frequency constraints that we have described here mark a point of departure for introducing approximate—high frequency—methods for the solution of our forward modeling or inverse problems.

C.3 Inversion Formulas

In several locations in the text, important results are obtained by applying the method of stationary phase to Fourier transform–like integrals. These integrals may be inversion formulas, or may be the cascade of inversion formulas with forward modeling formulas—such as may result when we test an inversion formula with Kirchhoff data.

To use the method of stationary phase, a large parameter must be identified in the formula being considered. This means that the equation in question must be rewritten in dimensionless form.

In Section 3.6.1 we list several equations: (3.4.13), (3.4.19), (3.4.20), (3.5.3) (3.5.4), and (3.5.5), as examples of integrals that may be analyzed via the method of stationary phase. We will recast equation (3.4.13) in dimensionless form here as a demonstration, and leave the problem of recasting the other equations listed as exercises for the reader.

Equation (3.4.13) is rewritten here as

$$\beta(\boldsymbol{x}) = \frac{4c^2}{\pi^2} \int_{\Sigma} d^2\xi \int_{D_k} d^3k \frac{k_3}{\omega} e^{2i[k_1(x_1-\xi_1)+k_2(x_2-\xi_2)-k_3x_3]} \cdot \int_0^{\infty} dt\, tU_S(\boldsymbol{\xi}, t)e^{i\omega t}.$$

Several slight notational changes have been made here from the original form of equation (3.4.13) that appears in Section 3.6. In the original usage, the symbol c_0 was used to denote the (constant) background wavespeed.

The symbol ω_0 denoted frequency as defined in equation (3.3.14). We have replaced these with the symbols c and ω, respectively, because those subscripts are not relevant to the current discussion, but we have another use for those subscripts, below. Also, the expression $\boldsymbol{\kappa} \cdot (\boldsymbol{\rho} - \boldsymbol{\xi})$ that appears in the exponent of equation (3.4.13) has been rewritten in the expanded form as $k_1(x_1 - \xi_1) + k_2(x_2 - \xi_2)$. The symbol Ω denoting the k-aperture (the domain of wavenumber integration) has been replaced with the symbol D_k. Otherwise, the notation is unchanged from the usage in the text.

To convert this equation into dimensionless form, we make the following substitutions,

$$
\begin{aligned}
&(x_1, x_2, x_3) \to (LX_1, LX_2, LX_3), && (\xi_1, \xi_2, \xi_3) \to (LX_{01}, LX_{02}, LX_{03}),\\
&\omega \to \omega_0 \Omega, && t \to \overline{T} T,\\
&U_S(\boldsymbol{x}, t) \to \overline{U} W_S(\boldsymbol{X}, T), && \beta(\boldsymbol{x}) \to \overline{B} B(\boldsymbol{X}),\\
&(k_1, k_2, k_3) \to (\overline{K} K_1, \overline{K} K_2, \overline{K} K_3). &&
\end{aligned}
$$

Equation (3.4.13) becomes

$$
\overline{B} B(\boldsymbol{X}) = \frac{4c^2}{\pi^2} \int_\Sigma L^2 d^2 \boldsymbol{X}_0 \int_{D_k} \overline{K}^3 d^3 K \frac{\overline{K} K_3}{\omega_0 \Omega} e^{2i\Phi} \cdot \int_0^\infty \overline{T} dT\, \overline{T} T\, \bar{U} W_S(\boldsymbol{X}, T) e^{i\omega_0 \Omega \overline{T} T}, \qquad \text{(C.3.1)}
$$

where $\Phi \equiv \{\overline{K} K_1 (LX_1 - LX_{01}) + \overline{K} K_2 (Lx_2 - LX_{02}) - \overline{K} K_3 L X_3\}$. Simplifying yields

$$
\overline{B} B(\boldsymbol{X}) = \left(\frac{c^2 L^2 \overline{K}^4 \overline{T}^2 \overline{U}}{\omega_0} \right) \frac{4}{\pi^2} \int_\Sigma d^2 \boldsymbol{X}_0 \int_{D_k} d^3 K \frac{K_3}{\Omega} e^{2i\overline{K} L \Psi} \cdot \int_0^\infty dT\, T\, W_S(\boldsymbol{X}, T) e^{i\omega_0 \overline{T} \Omega T}, \qquad \text{(C.3.2)}
$$

where $\Psi \equiv \{K_1(X_1 - X_{01}) + K_2(x_2 - X_{02}) - K_3 X_3\}$. Checking that the units balance requires that we recognize the following relationships:

$$
[L] \to \text{Length}, \qquad [\overline{T}] \to \text{Time}, \qquad [\omega_0] \to \frac{1}{\text{Time}}, \qquad [\overline{K}] \to \frac{1}{\text{Length}},
$$

$$
[c] \to \frac{\text{Length}}{\text{Time}}, \qquad [\overline{U}] \to \frac{1}{\text{Length} \cdot \text{Time}}.
$$

The last of these results arises from the 3D version of (C.1.2), for which the dimensions of $\partial^2 U / \partial x_j^2$ must balance the dimensions of the 3D point source

$$
-\delta(t)\delta(\boldsymbol{x}) \equiv -\frac{1}{\overline{T} L^3} \delta(T)\delta(X_1)\delta(X_2)\delta(X_3).
$$

The result is that the right-hand side of equation (C.3.2) has the dimension of $1/L$, meaning that $\overline{B}$ also has the dimension of $1/L$. This is exactly

what we should expect for a reflectivity function, which is a reflection coefficient (a dimensionless quantity, even when expressed in dimensional variables) multiplied by a bandlimited singular function, a one-dimensional delta function with dimension $1/L$.

We must identify a large parameter in equation (C.3.2) as a prelude to asymptotic evaluation by the method of stationary phase. If we intend to apply the method of stationary phase to the T integral, then the large parameter is $\omega_0\overline{T}$. If, however, we intend (as in Section 3.6.1) to apply stationary phase to the $\boldsymbol{K}$ and/or the $\boldsymbol{X}_0$ integral, then the large parameter is $2\overline{K}L$, which is analogous to the factor of $2\pi L/\Lambda$ seen in the discussion in the previous section.

Note from the derivation of this inversion formula, however, that the choices $\omega_0\overline{T}$ and $2\overline{K}L$ are not independent in the applications in the text. The frequency and wavenumber in the original variables are tied by the *dispersion relation* (3.3.14),

$$\omega = c\sqrt{k_1^2 + k_2^2 + k_3^2}$$

or

$$\frac{\omega_0}{c\overline{K}}\Omega = \operatorname{sgn}(K_3)\sqrt{K_1^2 + K_2^2 + K_3^2}.$$

We want the dimensionless frequency Ω and the dimensionless wavenumber K to be of comparable size. Thus, the dimensionless frequency and wavenumber are tied to one another through the dimensionless scale $\omega_0/c\overline{K}$, which must characterize the ratio of the dimensional variables ω, c, and k in the original problem.

There is a further aspect of scaling that we must address in the method of stationary phase. Consider the case of a dimensionless amplitude, $f(X)$, and a dimensionless phase, $\omega T\Phi(X)$, with Φ dimensionless. Recall that the first term in the asymptotic expansion is proportional to

$$f(X)\frac{1}{\sqrt{\left|\omega T\dfrac{d^2\Phi}{dX^2}\right|}}.$$

While we have not derived the correction terms in the text, suffice it to say that they are made up of higher derivatives of f and Φ. In particular, one of the correction terms at next order has the form

$$\frac{C_1}{\sqrt{\left|\omega T\dfrac{d^2\Phi}{dX^2}\right|}}, \qquad C_1 \approx \frac{d^2f(X)}{dX^2}\frac{1}{\left|\omega T\dfrac{d^2\Phi}{dX^2}\right|}.$$

Here, we have neglected unimportant constants for this discussion.

Suppose that L_1 is the length scale of Φ and L_2 is the length scale of f. Then, if $x = L_1X$,

$$C_1 \approx L_1^2 \frac{d^2 f(x)}{dx^2} \frac{1}{\left| L_1^2 \omega T \frac{d^2 \Phi}{dx^2} \right|} = \frac{L_1^2}{L_2^2} \left[L_2^2 \frac{d^2 f(x)}{dx^2} \right] \frac{1}{\left| L_1^2 \omega T \frac{d^2 \Phi}{dx^2} \right|}.$$

Here, in the last line, we have written the second derivative of f with the scale L_2^2. By the assumption that L_2 is the proper length scale of this function, that product is comparable in size to f itself, which appears in the leading-order term of the asymptotic expansion. We have done this at the cost of an extra multiplier, L_1^2/L_2^2.

Suppose, then, that we were to use our asymptotic criterion with $L = L_1$:

$$\left| L_1^2 \omega T \frac{d^2 \Phi}{dx^2} \right| \geq \pi.$$

If $L_1^2/L_2^2 \leq 1$, then the amplitude of this term would be comparable to the amplitude of the first term, except for the bounding factor, $1/\pi$, resulting from our assumption. On the other hand, if $L_1^2/L_2^2 > 1$, then the growth of the amplitude factor might lead to this term not having sufficient decay compared to the first term. Of course, subsequent terms would have even larger powers of this offending ratio.

How do we get out of this dilemma? Let us consider setting $x = L_2 X$. Then,

$$C_1 \approx L_2^2 \frac{d^2 f(x)}{dx^2} \frac{1}{\left| L_2^2 \omega T \frac{d^2 \Phi}{dx^2} \right|}.$$

With this choice, the second derivative of f has the "right" scale to make it comparable to f itself. To insure that our asymptotic expansion yield a result of sufficient numerical accuracy, we simply require that

$$\left| L_2^2 \omega T \frac{d^2 \Phi}{dx^2} \right| \geq \pi.$$

That is, when there are two or more natural length scales in a particular application of the method of stationary phase, we should always choose the smaller (smallest!) length scale when setting our criterion. This insures the asymptotic expansion will yield a formula that will have sufficient numerical accuracy. Note that the additional factors on the right side, beyond ωT, have to do with utility of the stationary phase formula. If ωT were not large, the method of stationary phase might still be valid, say, in the far field, where the magnitude of L might compensate for the magnitudes of the other quantities here, so that this inequality is satisfied. That is, there is some interchange of physical characterizations possible, such as far field as an alternative to high frequency. In this case, we would think of the characterization "many wavelengths" as arising from range considerations as opposed to frequency considerations.

Finally, we would caution the reader that not all length scales of the stationary phase analysis are apparent in the integral. Some arise from the actual calculations of the elements of the stationary phase formula, most specifically, from the second derivative, in one dimension, or the Hessian determinant of the matrix of second derivatives, in higher dimensions. In particular, in the example of Section 4.4.2, we saw that the Hessian was a function of the radii of curvature of the surface over which the integration was carried out. Thus, these are additional length scales that must satisfy our asymptotic criterion. More subtly, the radii of curvature of the isochrons of the phase arise in some applications as well. Therefore, it is necessary to search for the smallest length scale in the final asymptotic formula and not in the integrand itself.

Appendix D
An Example of Ill-Posedness

In the text, we have discussed the concept of *ill-posedness* of inverse problems. As defined by the French mathematician Jacques Hadamard [1865–1963] a problem is said to be *well-posed* when a solution exists, is unique, and depends continuously on the initial data. On the other hand, a problem is said to be *ill-posed* if it fails to satisfy at least one of these criteria. (See Hadamard [1923]. Remember also that we use the word "data" in the mathematicians' sense of "known values," rather than the geophysicists' sense of "field measurements.") Historically, many mathematicians have viewed this distinction of problems as equating "well-posed" with "solvable," and "ill-posed" with "intractable."

While it is certain that problems having no solution are, indeed, intractable, the same cannot be said of problems with nonunique solutions, or those having solutions that depend discontinuously on the data. We often deal with problems having a family of solutions, meaning that there is no single unique solution. We choose between the possible solutions by constraining the "acceptable output" through comparison with auxiliary data or through a statistical treatment. In seismic applications, the background wavespeed profile is a necessary piece of information for imaging the subsurface, but it is also the unknown quantity that we are attempting to find. We constrain the acceptable range of possible wavespeed profiles with borehole measurements or, at least, with the "stacking velocities" obtained from seismic velocity analysis, or some other estimate of reasonable wavespeeds.

For problems with solutions that do not depend continuously on the initial data, we associate a more familiar term with ill-posedness. This is

instability. In the remainder of this appendix, we discuss one example of a problem resembling our seismic inverse problem, by considering it from the standpoint of *ill-posedness as instability.*

D.1 Ill-posedness in Inversion

In several places in the text, we characterize our solution process for the inverse-scattering imaging problem as the reverse propagation of data from positions on the recording surface, back into the interior of the domain of interest. The intent is that the final position of the most singular part of the downward-propagated data has its peak values on the reflectors in the subsurface. We have shown in Section 3.8 that, at least for the constant-background zero-offset case, there is a close relationship between inversion represented as back-propagation, and a solution of the wave equation with data prescribed on the recording surface, which for this example is $z = x_3 = 0$. We saw in Section 3.8 that this was asymptotically true to two orders in ω. Here, we start with the wave equation with data prescribed on the surface $x_3 = 0$. Our objective is to expose the inherent instability in the solution of this problem.

To begin, let us suppose that $U(\boldsymbol{x}, t)$ is a solution of the wave equation

$$\frac{\partial^2 U}{dx_1^2} + \frac{\partial^2 U}{dx_2^2} + \frac{\partial^2 U}{dx_3^2} - \frac{1}{c^2}\frac{\partial^2 U}{\partial t^2} = 0, \tag{D.1.1}$$

for $x_3 > 0$ (positive downward), with the observed data for U being its value at $x_3 = 0$, say $U(x_1, x_2, 0, t)$, and zero initial conditions,

$$U = \frac{\partial U}{\partial t} = 0, \qquad t = 0.$$

We begin by introducing the cascade of the forward transverse spatial Fourier transform and the forward temporal Fourier transform of U, given by

$$u(k_1, k_2, x_3, \omega) = \int_0^\infty dt \int_{-\infty}^\infty \int_{-\infty}^\infty dx_1 dx_2 \; U(\boldsymbol{x}, t) e^{i\{-k_1 x_1 - k_2 x_2 + \omega t\}}.$$

Then u is a solution of the following Helmholtz-like equation:

$$\frac{\partial^2 u}{dx_3^2} + \left[\frac{\omega^2}{c^2} - k_1^2 - k_2^2\right] u = 0, \tag{D.1.2}$$

with the Fourier transform of the data on the surface given by

$$\begin{aligned} u(k_1, k_2, 0, \omega) &= \int dk_1 \; dk_2 \; d\omega \; U(x_1, x_2, 0, t) e^{i\{-k_1 x_1 - k_2 x_2 + \omega t\}} \\ &\equiv A(k_1, k_2, \omega). \end{aligned} \tag{D.1.3}$$

Equation (D.1.2) is a second-order ODE in the variable x_3. If we consider the data represented in the Fourier-transformed form of equation (D.1.3), as subjecting this equation to a single boundary condition, we recognize that (D.1.3) has nonunique solutions, which is the first evidence of ill-posedness. These solutions consist of the family of all linear combinations of the two solutions,

$$u_{\pm}(k_1, k_2, x_3, \omega) = A(k_1, k_2, \omega) e^{\pm i k_3 x_3}. \tag{D.1.4}$$

The problem reveals itself when we define the k_3 via the expressions

$$\begin{aligned} k_3 &= \sqrt{\omega^2/c^2 - k_1^2 - k_2^2}, \qquad \omega^2/c^2 > k_1^2 + k_2^2, \\ k_3 &= i\sqrt{k_1^2 + k_2^2 - \omega^2/c^2}, \qquad \omega^2/c^2 < k_1^2 + k_2^2, \end{aligned} \tag{D.1.5}$$

with the square roots on the right side understood to be positive. When the inequality in the first line of (D.1.5) is satisfied, the solutions in (D.1.4) are both oscillatory and bounded for all choices of the spatial variables. When the inequality in the second line of this equation is satisfied, then one solution, with the negative sign, grows exponentially with increasing x_3, while the other, with positive sign, decays exponentially with increasing x_3. At the boundary between these two regions, k_3 vanishes, and the solutions are bounded, but are not oscillatory in x_3.

With the value of u at $x_3 = 0$, only, we do not have enough information to choose between the two solutions represented by the $\pm$ choice in (D.1.4). At best we know only that we can take any linear combination with coefficients that sum to unity. This should elicit concern in light of our observation that one of the two solutions grows exponentially, which is to say, is unstable, when $\omega^2/c^2 < k_1^2 + k_2^2$.

We would be happy if we had only the solution that decays (the stable solution). Can we be sure that this is the case? In fact, on physical grounds, the answer is, emphatically, No! Recall that we are assuming that we have observed a wave that has propagated up to us, *through decreasing values of* x_3; (recall that the values of x_3 increase downward in our problem). It is reasonable to expect that this solution was attenuating—exponentially decaying—in the direction of propagation, based on the principle of conservation of energy. If we were to reproduce this wave from the surface data, then, of necessity, that solution would have to *grow* exponentially in the reverse direction—which is the direction we propose to back-propagate the data. Thus, the inversion process we describe clearly has an identifiable instability associated with the choice of exponent sign. It would seem that we cannot avoid this bad choice.

Suppose that the data we observe did not contain any energy in this problematic part of the spectrum; then we would not see the instability. Unfortunately, in any practical numerical solution, this part of the spectrum would come back to haunt us anyway through *numerical noise*. To see why, consider a specific choice of A in (D.1.3),

$$A(k_1, k_2, \omega) = \frac{\epsilon}{1 + k_1^2 + k_2^2}, \tag{D.1.6}$$

and consider this solution for small values of ϵ. The value of u at the surface in (D.1.3) can be made as small as we like, simply by taking this number small enough. Furthermore, the same is true of its first derivative with respect to x_3 at $x_3 = 0$ (which is the missing piece of data required to make the solution to the wave equation unique). As noted earlier, for fixed ω and $k_1^2 + k_2^2$ large enough, the solution (D.1.4) is characterized by exponential—as opposed to oscillatory—behavior in x_3. In particular, for the lower sign in the second half of (D.1.5), the solution grows exponentially as x_3 increases. This exponential behavior causes the solution to grow beyond all bounds with increasing x_3, no matter how small the amplitude of the original data at $x_3 = 0$, which is to say, no matter how small we take ϵ.

So, how does noise enter the problem? Assume that we have a discrete process for propagating the data back into the Earth. Then there will be characteristic sampling intervals in space and time, say Δx_1, Δx_2, Δt. Associated with these sampling intervals will be maximum wave numbers and a maximum frequency of the observed data, the Nyquist wavenumbers and frequency, $k_{1max} = \pi/\Delta x_1$, $k_{2max} = \pi/\Delta x_2$, and $\omega_{max} = \pi/\Delta t$. Inevitably, numerical noise will infiltrate the computation of the solution of this problem at all wavenumbers and frequencies up to their maxima. Thus, if some part of the spectrum of the noise in the data satisfies the lower inequality in (D.1.5), then this noise will be treated as "small-valued signal," which will grow exponentially with increasing depth; that is, this noise in the undesirable part of the spectrum will produce a large inaccuracy in the computed solution at depth.

In summary, we have a problem in which the solution exists, and which we could make the solution unique by prescribing $\partial u/\partial x_3$ at $x_3 = 0$,[1] but the solution *does not depend continuously on the data*; small data amplitude can produce a large contribution—arbitrarily large—at sufficient depth, because of the exponential growth with increasing x_3. As discussed in the introduction to this appendix, such problems are *ill-posed* in the sense of Hadamard, meaning that our inverse problem is ill-posed.

Stable solutions to such problems can only be obtained by finding a way to assure that these exponentially growing contributions do not infiltrate our solution process. We do this by avoiding the "bad part" of the spectrum in our integral processing. In doing so, we must acknowledge that some information may also be lost, if the "true" solution contained data in this part of the spectrum. This *regularized* solution, therefore, is the best solution we can hope for in this situation. Fortunately, as can be seen in text, our regularized solutions provide us a great deal of useful information about

[1] The choice $\partial u/\partial x_3 = -ik_3 u(x_1, x_2, 0, t, k_1, k_2, \omega)$ at $x_3 = 0$, will produce only exponentially growing solutions at depth.

the subsurface. The key here is that our inversion is a Fourier synthesis. That synthesis requires only real values of the wavevector, which is exactly what our regularized solution provides. Of course, this rationalization fails, if we consider a modified wave equation that accounts for attenuation; in filtering out the imaginary values of k_3, we lose all hope of inverting for attenuation effects.

We have still not addressed the question of uniqueness in the range of real values of the wave-vector. The solution that we have chosen assumes that all of the scattered field is *upward propagating*; that is, it arrives at the receivers from below. In this case, in the Fourier domain, the normal derivative is related to the observed data themselves by multiplication by $-i\,\mathrm{sgn}\,(\omega)k_3$, with k_3 defined by (D.1.5). In fact, in ocean environments, multiple reflections arrive at the receivers from above. For our inversion formalism, those arrivals produce "ghost images." The elimination of multiples, both these ocean surface multiples and internal multiples, is beyond the scope of this book.

The example presented here is a minor variation on one that is standardly used in partial differential equations courses to show that *Cauchy problems* (which is to say, "initial value" problems) for elliptic equations—and certain Cauchy problems for hyperbolic equations—can be ill-posed. A Cauchy problem for a second-order partial differential equation is one in which the unknown, u, and its normal derivative $\partial u/\partial n$ are prescribed on some surface (or hypersurface in higher dimensions, such as in our four-dimensional problem—three space, one time). The wave equation is a hyperbolic partial differential equation. If the hypersurface where Cauchy data are given is $t = 0$, then the problem for the wave equation is well-posed and the solutions depend continuously on the data. If, on the other hand, the hypersurface is $x_3 = 0$, then, as we have demonstrated with the example in this appendix, the Cauchy problem is ill-posed. An interested reader can read more about these ideas in texts on the theory of partial differential equations, such as John [1982] or Garabedian [1964].

Appendix E

An Elementary Introduction to Ray Theory and the Kirchhoff Approximation

In Chapters 5 and 6, we make use of certain ray-theoretic results to approximate Green's functions and to simplify computations involving Beylkin determinants. This is different from the usual geophysical role of ray theory as a computational method for generating synthetic seismic data.

Though we cannot do justice to the broader issues of ray theory in this appendix, we can draw a rough sketch of the mathematical justification of the subject. Indeed, the mathematical basis of ray theory is often poorly treated in geophysical literature, as authors focus on practical issues of computation or concentrate on more theoretical issues related to the subject, assuming that the more elementary aspects are already known to the reader. Hence, many ray-theoretic technical papers begin with the set of first-order ordinary differential equations, known as the *ray equations*, without ever telling the reader the origin of these formulas. (We refer the reader to the text of Kravtsov and Orlov [1990] for a comprehensive overview of ray theory.)

Such treatments may be leave readers puzzled regarding the validity of the general ideas of ray theory. This confusion is often exhibited in the attitude that the ray representation is either an obvious consequence of geometry, and is therefore somehow "exact," or the reverse, that ray techniques are based on *ad hoc* arguments, and are therefore to be mistrusted. Another prevalent attitude is that all of the technical issues of ray theory have been solved long ago, and that raytracing has no new research problems to offer. While the latter issue is far from true, addressing it is beyond the scope of this appendix; we hope to shed some light on the first two issues.

E.1 The Eikonal and Transport Equations

For our purposes, *ray theory is that collection of mathematical results obtained by solving the eikonal and transport equations.* To use ray-theoretic representations, therefore, implies that we are primarily interested in modeling waves only in the high-frequency regime—the regime where the eikonal and transport equations are valid. From Chapter 3, we have seen that the eikonal and transport equations may be obtained by substituting the WKBJ trial solution (also known as the Debye series),

$$u(\boldsymbol{x},\omega) \sim \omega^{\beta} e^{i\omega\tau(\boldsymbol{x})} \sum_{j=0}^{\infty} \frac{A_j(\boldsymbol{x})}{(i\omega)^j}, \tag{E.1.1}$$

into the homogeneous (zero forcing function) form of the Helmholtz equation,

$$\mathcal{L}u = \left[\nabla^2 + \frac{\omega^2}{c^2(\boldsymbol{x})}\right] u(\boldsymbol{x},\omega) = 0.$$

In equation (E.1.1), $\tau(\boldsymbol{x})$ is traveltime and the A_j's are the frequency-independent parameters representing wave amplitude that we must solve for in order to construct the asymptotic solution.

The motivations for choosing this form of solution are many. In 1D, where the Laplacian is replaced by a single second derivative, the Helmholtz equation is an ordinary differential equation. It can be shown rigorously that linearly independent solutions of the 1D Helmholtz equation can be written in the asymptotic form prescribed by the 1D form of (E.1.1) as $|\omega| \to \infty$.[1] Second, there are many cases where the known exact solutions to the higher-dimensional form of the Helmholtz equation have the asymptotic form of (E.1.1).

Third, on physical grounds, (E.1.1) also makes a sense from our experience with simple wave propagation. The inverse Fourier transform,

$$\omega^{\beta} e^{i\omega\tau(\boldsymbol{x})} \to F(t - \tau(\boldsymbol{x})),$$

represents a progressing wave in which the function $F(t)$—the inverse transform of ω^{β}—propagates in the direction of increasing $\tau(\boldsymbol{x})$. Division by increasing powers of $i\omega$ represents successive integrations in the time domain that may be interpreted as progressively smoother counterparts of F [Lewis, 1965]. Thus, the inverse transform of the first term in (E.1.1) represents the sharpest part or "most singular part" of the solution—something we might associate with high frequency—while the later terms

[1] In complex function theory, the "point at infinity" in ω is an *essential singularity* of the solution as a function of ω. Further, the type of essential singularity is one for which the structure of the solution is of the form (E.1.1) when there is only one independent variable.

represent progressively smoother—lower-frequency—contributions to the solution. Thus, this structure represents the general notion of what we mean by "high-frequency" approximation.

Further, the factor of ω^β may be necessary to balance powers of ω that may occur in source or other initial data of a specific problem for which the inhomogeneous form of the Helmholtz equation is used. (Actually, in some applications, multipliers involving $\text{sgn}(\omega)$ appear as well.) Finally, we could have as a multiplier any function $\tilde{F}(\omega)$, leading to the inverse transform, $F(t-\tau(\boldsymbol{x}))$. Of course, we are most interested in such functions for which the bandwidth—the range in ω where $\tilde{F}(\omega)$ is substantially different from zero—qualifies as *high-frequency* for the length scales and time scales of the underlying problem. Still, the subsequent terms of the asymptotic series lead to progressively higher iterated integrals of $F(t-\tau(\boldsymbol{x}))$, meaning progressively smoother terms in the propagating wavefield being represented.

Given these motivations, we will apply the technique. The first step is to substitute this trial solution with unknown coefficients into the Helmholtz equation to derive differential equations for the traveltime and the coefficients in the representation (E.1.1).[2]

Here, from all that we have stated, we do not expect the final solution to yield a *convergent* series. Rather, we expect the form of the result to be an *asymptotic* series, with only the first one or two terms actually being relevant.[3]

To continue with the derivation, we substitute the trial series solution into the Helmholtz equation to obtain the following series:

---

[2]We want to be clear that we are *not* talking about the classical *method of Frobenius*, which may be familiar to the reader from his or her experience with the theory of ordinary differential equations (ODEs). In the method of Frobenius, the trial solution consists of series of positive powers of the dependent variable of the ODE being solved. The result of such a solution is a convergent series solution to the ODE. That method works when the differential equation has a so-called *singularity of the first kind*. For ODEs, solutions similar to (E.1.1), but as series in the independent variable, can also occur. Such solutions arise, however, when the differential equation has a singularity of the second kind. Both for the ODEs and for the problem here, the method does not, in general, yield a convergent series; it yields asymptotic series.

[3]Students often learn that only convergent series are "good," whereas divergent series are "bad." Furthermore, there is a prevalent idea that *more* terms will give a *better* representation of a function via a series expansion. For asymptotic series, both of these ideas are generally incorrect. Asymptotic series are often better representations than exact series results because there is no guarantee that a convergent representation will converge rapidly. By design, asymptotic representations are forced to have initial terms that start out closer to the values of the function they represent. For a discussion of this and other aspects of asymptotic series, see Erdélyi [1956], Bleistein and Handelsman [1986], Bleistein [1984]; for a numerical example, see Stockwell [1995a].

$$\mathcal{L}u = \omega^\beta e^{i\omega\tau} \sum_{j=0}^{\infty} \frac{1}{(i\omega)^j} \left[\omega^2 \left\{ \frac{1}{c^2} - (\nabla\tau)^2 \right\} A_j \right. \tag{E.1.2}$$
$$\left. + i\omega \left\{ 2\nabla\tau \cdot \nabla A_j + A_j \nabla^2 \tau \right\} + \nabla^2 A_j \right].$$

In general, the terms of different powers of ω cannot be assumed to cancel each other. This means that the coefficients of the series must vanish independently. Thus, we will equate the coefficient of each power of ω separately equal to zero, starting with the highest power, which is $\beta + 2$. This power arises only in the first series in (E.1.2) and only for $j = 0$; setting its coefficient equal to zero yields the "eikonal" equation

$$(\nabla\tau(\boldsymbol{x}))^2 - \frac{1}{c^2(\boldsymbol{x})} = 0.$$

Note that we have not made the alternative choice, $A_0 = 0$; we assume that the series in (E.1.1) starts with a first nonzero term. Note also that, with this choice, the entire first series in (E.1.2) is zero and we can focus our attention on the remaining two series. For the middle series, the highest nonvanishing power of ω is $\beta + 1$, which arises, again, from the term for which $j = 0$. Note that the third series starts with a smaller power of ω, which here is β. Setting the coefficient of this now-highest power of ω equal to zero yields the (first) "transport" equation

$$2\nabla\tau(\boldsymbol{x}) \cdot \nabla A_0(\boldsymbol{x}) + A_0 \nabla^2 \tau(\boldsymbol{x}) = 0.$$

It is the solution of these two equations that will be discussed in the majority of this appendix. After solving these two equations, we can construct the solutions to all other A_j, recursively. We will briefly discuss those higher-order transport equations at the end of the appendix.

E.2 Solving the Eikonal Equation by the Method of Characteristics

To attempt a direct solution of the eikonal equation for $\tau(\boldsymbol{x})$ is not feasible in more than one dimension because, in general, the equation is nonlinear in this variable and its derivatives; indeed, for variable wavespeed $c(\boldsymbol{x})$ the eikonal equation is nonlinear in the derivatives. We derive here a somewhat indirect technique called the "method of characteristics" to find its solution.

In general, we are interested in solving an equation of the form, $F(x, y, z, u, u_x, u_y, u_z) = 0$. Here, the x, y, and z are the spatial variables, and u, u_x, u_y, and u_z are the solution and its respective partial derivatives with respect to x, y, and z. The u corresponds to the τ in the eikonal equation, and the u_x, u_y, u_z correspond to the components of the gradient of τ. We can look at the statement

$$F(x, y, z, u, u_x, u_y, u_z) = 0$$

as describing a function in a seven-dimensional space. We can also look at this as being a function that defines a family of level surfaces in x, y, z–space, one surface for each given constant value of u. The gradient of u describes vectors pointing normal to these level surfaces. For the eikonal equation, the level surfaces are the surfaces of equal traveltime (wavefronts), with the gradient of u (the ray direction) pointing normal to the traveltime surfaces. Here, we will derive a system of ordinary differential equations that tells us how to move from one level surface of u to another. The solutions for the spatial coordinates will describe curves in the physical space. In general, those curves are called *characteristics*; hence the name, "method of characteristics."[4] The solutions for the components of the gradient will tell us how that vector changes along each of the curves, while the solution for u itself tells us how the unknown u changes along the characteristics. We will find that it is most convenient to describe the characteristics in terms of an auxiliary set of variables—two to label each characteristic curve and a third that will act as a "running variable"—such as arclength or time—along each characteristic.

Using a slightly more compact notation, we can write the spatial variables as $x = x_1$, $y = x_2$, and $z = x_3$, respectively, and the components of the gradient of u as

$$u_x = p_1, \quad u_y = p_2, \quad u_z = p_3,$$

respectively. To emphasize that we view these quantities as new variables, we write the general expression for F as

$$F(x_1, x_2, x_3, u, p_1, p_2, p_3) = F(\boldsymbol{x}, u, \boldsymbol{p}) = 0. \tag{E.2.1}$$

We certainly do not have, in hand, a technique for solving general nonlinear partial differential equations of this stated form. Accordingly, our first objective will be to rewrite (E.2.1) in a form that we *know* we can solve—a system of *linear*, first-order ordinary differential equations. The equation $F = 0$ can be thought of as describing a surface (really a hypersurface) embedded in a seven-dimensional space.

Our first step to reveal the structure of the system of the seven linear ODEs will be to see what happens when we move a small distance along the hypersurface described by $F = 0$. That is to say, we will move from a point $\boldsymbol{x}$ to another point, $\boldsymbol{x} + \delta\boldsymbol{x}$. Of course, when we do this, both u and $\boldsymbol{p}$ change as well, but it is still true that

---

[4] A common source of confusion in terminology may result here. The curves in the full seven-dimensional space, which together compose the surface $F = 0$, are often also called "characteristics," but are more properly called *bicharacteristics*. The term *Lagrangian manifold* is often used for the surface $F = 0$ for the class of problems that includes all raytracing applications.

$$F(\boldsymbol{x}+\delta\boldsymbol{x}, u+\delta u, \boldsymbol{p}+\delta\boldsymbol{p}) = 0$$

because we have not left the solution surface, even though we have perturbed the coordinates. Because $F = 0$ at the unperturbed point, we have, to linear order in the perturbations, that

$$\begin{aligned} F(\boldsymbol{x}+\delta\boldsymbol{x}, u+\delta u, \boldsymbol{p}+\delta\boldsymbol{p}) - F(\boldsymbol{x}, u+\delta u, \boldsymbol{p}) \\ = \sum_{i=1}^{3} \frac{\partial F}{\partial x_i}\delta x_i + \frac{\partial F}{\partial u}\delta u + \sum_{j=1}^{3} \frac{\partial F}{\partial p_j}\delta p_j = 0. \end{aligned} \tag{E.2.2}$$

In the last expression, the partial derivatives of F are evaluated at the unperturbed point, $(\boldsymbol{x}, u, \boldsymbol{p})$.

Ultimately, u, and therefore, $\boldsymbol{p}$ depends on $\boldsymbol{x}$. Hence, we can write the perturbations of these quantities in terms of the perturbation in $\boldsymbol{x}$, through

$$\delta u = \sum_{i=1}^{3} \frac{\partial u}{\partial x_i}\delta x_i = \sum_{i=1}^{3} p_i \delta x_i$$

and

$$\delta p_j = \sum_{i=1}^{3} \frac{\partial p_j}{\partial x_i}\delta x_i = \sum_{i=1}^{3} \frac{\partial^2 u}{\partial x_i \partial x_j}\delta x_i = \sum_{i=1}^{3} \frac{\partial p_i}{\partial x_j}\delta x_i, \qquad j = 1, 2, 3.$$

In the second line above, we have used the definition of p_j as a derivative of u; in the third line, we have effectively interchanged the orders of differentiation with respect to x_i and x_j in order to write a result in terms of p_i.

We now substitute these results into (E.2.2) to obtain the result

$$\sum_{i=1}^{3} \left[F_{x_i} + F_u p_i + \sum_{j=1}^{3} F_{p_j} p_{i_{x_j}} \right] \delta x_i = 0. \tag{E.2.3}$$

In this equation, we have adopted the subscript notation for partial derivatives,

$$F_{x_i} = \frac{\partial F}{\partial x_i}.$$

We remark here that the δx_i's (E.2.3) are actually independent. For any choice of these variables, the sum over i has to produce zero for u and $\boldsymbol{p}$ to be the elements of a solution to (E.2.1). In particular, we could take $\delta\boldsymbol{x} = (dx_1, 0, 0)$ or $= (0, dx_2, 0)$ or $= (0, 0, dx_3)$, and the equation would be satisfied. Because the multipliers of these three differentials are all independent of the differentials, the equation is satisfied only if the multipliers are each separately equal to zero. That is, we must have

$$F_{x_i} + F_u p_i + \sum_{j=1}^{3} F_{p_j} p_{i_{x_j}} = 0, \qquad i = 1, 2, 3,$$

which we rewrite as

$$\sum_{j=1}^{3} F_{p_j} p_{i_{x_j}} = -\left[F_{x_i} + F_u p_i\right], \qquad i = 1, 2, 3. \tag{E.2.4}$$

The left side of all three of these equations is of the identical form, $\nabla_{\boldsymbol{p}} F \cdot \nabla_{\boldsymbol{x}} p_i$. The reader may recognize this as the structure of a *directional derivative*, with differentiation taken in a direction in $\boldsymbol{x}$, identified with the vector, $\nabla_{\boldsymbol{p}} F$. While these equations are nonlinear in $\boldsymbol{p}$, they are *linear* in these first derivatives. Such equations are called *quasi-linear* and have a standard method of solution, which the reader may find in textbooks on partial differential equations, such as Garabedian, [1964], John, [1982], or Bleistein [1984]. This is the method that we discuss here.

Let us introduce a differential vector $d\boldsymbol{x}/d\sigma$ and then define the direction of this vector by setting

$$\frac{d\boldsymbol{x}}{d\sigma} = \lambda \nabla_{\boldsymbol{p}} F. \tag{E.2.5}$$

Here, the scale factor λ characterizes the relative lengths of the vector $d\boldsymbol{x}/d\sigma$ and the vector $\nabla_{\boldsymbol{p}} F$. It also provides us a mechanism for choosing $d\sigma$ as some appropriate multiple between σ and the differential arclength $ds = \sqrt{dx_1^2 + dx_2^2 + dx_3^2}$. We use this equation in (E.2.4) to rewrite that equation as

$$\nabla_{\boldsymbol{p}} F \cdot \nabla_{\boldsymbol{x}} \boldsymbol{p} = \frac{1}{\lambda} \frac{d\boldsymbol{x}}{d\sigma} \cdot \nabla_{\boldsymbol{x}} \boldsymbol{p} = \frac{1}{\lambda} \frac{d\boldsymbol{p}}{d\sigma}.$$

Finally, (E.2.4) becomes

$$\frac{d\boldsymbol{p}}{d\sigma} = -\lambda \left[\nabla_{\boldsymbol{x}} F + F_u \boldsymbol{p}\right]. \tag{E.2.6}$$

Equations (E.2.5) and (E.2.6) are actually six equations. The first three define a direction in space, and a rate of change of $\boldsymbol{x}$ in that direction (modulo the choice of λ) and the last three equations tell us about the rate of change of $\boldsymbol{p}$ in that direction. Thus, we can think of the physical space as being filled with a field of tangent vectors, which in turn describe curves as streamlines of those tangent vectors. Those curves are the characteristic curves or characteristics of this method, the method of characteristics. Then, at each point on a characteristic curve, the vector $\boldsymbol{p}$ defines a normal direction to a level surface of u. If we attach a differential tangential plate to each of these normals, then we essentially construct the level surfaces of u from these tangent plates. However, the function F might depend on u as well, and we do not yet know how to determine these values at each point on the characteristic; thus, we cannot totally define the characteristic curves and the differential tangent plates until we know we have a means of determining u itself on those characteristics.

To complete the story, then, we need an equation for the rate of change of u along the characteristics. We obtain this equation as follows. We set

$$\frac{du}{d\sigma} = \sum_{j=1}^{3} \frac{\partial u}{\partial x_j}\frac{dx_j}{d\sigma} = \lambda \sum_{j=1}^{3} p_j F_{p_j} = \boldsymbol{p} \cdot \lambda \nabla_{\boldsymbol{p}} F. \tag{E.2.7}$$

The first equality here is simply a chain rule description of the derivative in the characteristic direction; the second equality uses the definitions of the partial derivatives and (E.2.5); the third merely expresses the result in vector form to parallel the discussion above.

It is useful now to write out all of the ordinary differential equations we have derived, explicitly. They are

$$\begin{aligned}
\frac{dx_1}{d\sigma} &= \lambda F_{p_1}, & \frac{dp_1}{d\sigma} &= -\lambda(F_{x_1} + p_1 F_u),\\
\frac{dx_2}{d\sigma} &= \lambda F_{p_2}, & \frac{dp_2}{d\sigma} &= -\lambda(F_{x_2} + p_2 F_u),\\
\frac{dx_3}{d\sigma} &= \lambda F_{p_3}, & \frac{dp_3}{d\sigma} &= -\lambda(F_{x_3} + p_3 F_u),
\end{aligned}$$

$$\frac{du}{d\sigma} = \lambda \sum_{j=1}^{3} p_j F_{p_j}. \tag{E.2.8}$$

We can think of σ, in calculus terms, as a dummy variable of integration. In physical terms, σ is a running parameter along the characteristic curve, which, in our application of describing ray theory for the Helmholtz equation, will be a ray. The appropriate problem for this system of equations is an initial value problem, in which all of the variables are defined for some value of σ. We may consider integrating this coupled system of equations to find the values of $(x_1, x_2, x_3, u, p_1, p_2, p_3)$ in terms of σ, modulo those initial values. As it is not our purpose here to develop the general theory of the method of characteristics, we will postpone the determination of those initial values to the discussion of the specialization to the eikonal equation.

E.2.1 Characteristic Equations for the Eikonal Equation

Returning to the eikonal equation

$$(\nabla\tau(\boldsymbol{x}))^2 - \frac{1}{c^2(\boldsymbol{x})} = 0,$$

we can identify τ with u, and the components of $\nabla\tau$ with p_i. Note, however, that τ does not explicitly appear in this equation, meaning that all derivatives with respect to $u = \tau$, represented by the F_u in the characteristic equations (E.2.8) above, will be zero. Thus, the special case of applying the method of characteristics to the eikonal equation is considerably simpler than the general problem. We can define the magnitude of the $\boldsymbol{p}$ vector as $p \equiv |\boldsymbol{p}| = |\nabla\tau| = 1/c$, and then rewrite the eikonal equation as

$$F(x_1, x_2, x_3, p_1, p_2, p_3) = p_1^2 + p_2^2 + p_3^2 - 1/c^2(\boldsymbol{x}) = 0. \tag{E.2.9}$$

We note, again, that there is no explicit dependence on τ itself in this equation. The characteristic equations become

$$\begin{aligned}
\frac{dx_1}{d\sigma} &= 2\lambda p_1, & \frac{dp_1}{d\sigma} &= \lambda \frac{\partial}{\partial x_1}\left(\frac{1}{c^2(x_1,x_2,x_3)}\right),\\
\frac{dx_2}{d\sigma} &= 2\lambda p_2, & \frac{dp_2}{d\sigma} &= \lambda \frac{\partial}{\partial x_2}\left(\frac{1}{c^2(x_1,x_2,x_3)}\right),\\
\frac{dx_3}{d\sigma} &= 2\lambda p_3, & \frac{dp_3}{d\sigma} &= \lambda \frac{\partial}{\partial x_2}\left(\frac{1}{c^2(x_1,x_2,x_3)}\right),\\
& & \frac{d\tau}{d\sigma} &= \lambda \sum_{j=1}^{3} 2p_j^2 = \frac{2\lambda}{c^2(x_1,x_2,x_3)}.
\end{aligned} \tag{E.2.10}$$

These are the general form of the *ray equations*. These are seven equations in eight unknowns, if we include λ as an unknown, each given as a function of the parameter σ. Thus, we have to either find another equation or eliminate one of the unknowns, to make the number of equations and unknowns equal, permitting the system to be solved. However, as noted above, λ plays a special role, allowing us a normalization between the Cartesian variables of the original problem and the running parameter σ. Thus, λ is at our disposal; we will discuss various options in the following sections.

Unless we make λ a function of τ, the first six equations are independent of τ and form a closed system of equations for the six variables of $\boldsymbol{x}$ and $\boldsymbol{p}$. Thus, for the eikonal equation, we can solve for the rays without ever determining the traveltime along the rays. For example, we could find all the rays normal to a reflector, essentially depicting the specular travel paths for zero-offset seismic surveys. We leave as an exercise for the reader to try this with the example of Figure 1.1, where the rays are straight lines. The region corresponding to the "bow tie" in the time plot will be seen to correspond to a region in the ray plot where more than one ray arrives at each point of the upper surface. Further, the cusps of the bow tie will be seen to correspond to points where an *envelope* of the rays cuts the upper surface.

As we will see below, studies of ray plots also help us to predict amplitude variations on a qualitative basis.

E.2.2 Choosing $\lambda = \frac{1}{2}$: σ as the Running Parameter

A more compact form of the characteristic equations can be written using vector notation and assuming that $\lambda = 1/2$. This choice is motivated by a desire to eliminate the factor of 2 appearing in several of the equations in (E.2.10). The result is

$$\frac{d\boldsymbol{x}}{d\sigma} = \boldsymbol{p}, \qquad \frac{d\boldsymbol{p}}{d\sigma} = \frac{1}{2}\nabla\left(\frac{1}{c^2(\boldsymbol{x})}\right) = -\frac{\nabla c(\boldsymbol{x})}{c^3(\boldsymbol{x})}, \qquad \frac{d\tau}{d\sigma} = \frac{1}{c^2(\boldsymbol{x})}. \tag{E.2.11}$$

This is the form of the ray equations as they appear in Chapters 5 and 6.

We can use our dimensional analysis of Appendix C to analyze the dimensions of σ in this case. We leave it as an exercise for the reader to check that with this choice, $\lambda = 1/2$, σ is a parameter with the units of Length^2/Time.

This was the scaling of choice in Chapter 6. Although we are getting ahead of the story about amplitude determination, we point out here that for 2.5D in-plane wave propagation, this choice of σ arose naturally as a parameter that describes out-of-plane behavior.

E.2.3 Choosing $\lambda = c^2/2$: τ, Traveltime, as the Running Parameter

For the choice $\lambda = c^2(\boldsymbol{x})/2$, the characteristic equations (E.2.10) take the form

$$\frac{d\boldsymbol{x}}{d\sigma} = c^2(\boldsymbol{x})\boldsymbol{p}, \qquad \frac{d\boldsymbol{p}}{d\sigma} = \frac{c^2(\boldsymbol{x})}{2}\nabla\left(\frac{1}{c^2(\boldsymbol{x})}\right) = -\frac{\nabla c(\boldsymbol{x})}{c(\boldsymbol{x})}, \qquad \frac{d\tau}{d\sigma} = 1.$$

The last equation here implies that $\sigma = \tau$ to within an additive constant. We may represent the ray equations in terms of traveltime as

$$\frac{d\boldsymbol{x}}{d\tau} = c^2(\boldsymbol{x})\boldsymbol{p} = c(\boldsymbol{x})\hat{\boldsymbol{p}}, \qquad \frac{d\boldsymbol{p}}{d\tau} = -\frac{\nabla c(\boldsymbol{x})}{c(\boldsymbol{x})}. \tag{E.2.12}$$

Here, we have introduced the unit vector, $c(\boldsymbol{x})\boldsymbol{p} = \hat{\boldsymbol{p}}$, in the first equation.

This choice of λ may be better suited for numerical computations; at the very least, τ is immediately known on each ray, as it is the running parameter, or independent variable, along the ray.

E.2.4 Choosing $\lambda = c(\boldsymbol{x})/2$: s, Arclength, as the Running Parameter

In differential geometry, arclength s is often referred to as the "natural" parameter of geometrical systems [Kreyszig, 1991]. To trace rays with arclength as the running parameter, we choose $\lambda = c(\boldsymbol{x})/2$, yielding the form

$$\frac{d\boldsymbol{x}}{d\sigma} = c(\boldsymbol{x})\boldsymbol{p}, \qquad \frac{d\boldsymbol{p}}{d\sigma} = \frac{c(\boldsymbol{x})}{2}\nabla\left(\frac{1}{c^2(\boldsymbol{x})}\right) = -\frac{\nabla c(\boldsymbol{x})}{c^2(\boldsymbol{x})}, \qquad \frac{d\tau}{d\sigma} = \frac{1}{c(\boldsymbol{x})},$$

permitting us to replace σ with s to write the ray equations with arclength as the running parameter; that is,

$$\frac{d\boldsymbol{x}}{ds} = c(\boldsymbol{x})\boldsymbol{p} = \hat{\boldsymbol{p}}, \qquad \frac{d\boldsymbol{p}}{ds} = -\frac{\nabla c(\boldsymbol{x})}{c^2(\boldsymbol{x})}, \qquad \frac{d\tau}{ds} = \frac{1}{c(\boldsymbol{x})}. \tag{E.2.13}$$

In this case, of course, the right side in the first vector equation is, indeed, just this unit vector, because

$$\frac{d\boldsymbol{x}}{ds} \cdot \frac{d\boldsymbol{x}}{ds} = 1.$$

A nice qualitative insight into the way rays turn is readily derivable from this form of the ray equations in arclength variables. Recall that the *curvature* vector of a curve is given by

$$\boldsymbol{\kappa} = \frac{d^2\boldsymbol{x}}{ds^2}.$$

Here, we can calculate that derivative from the first form of the equation for $d\boldsymbol{x}/ds$, as follows.

$$\begin{aligned}\boldsymbol{\kappa} = \frac{dc(\boldsymbol{x})}{ds}\boldsymbol{p} + c(\boldsymbol{x})\frac{d\boldsymbol{p}}{ds} &= \nabla c(\boldsymbol{x}) \cdot \frac{d\boldsymbol{x}}{ds}\boldsymbol{p} - c(\boldsymbol{x})\frac{\nabla c(\boldsymbol{x})}{c^2(\boldsymbol{x})} \\ &= -\frac{1}{c(\boldsymbol{x})}\left\{\nabla c(\boldsymbol{x}) - \left[\nabla c(\boldsymbol{x}) \cdot \frac{d\boldsymbol{x}}{ds}\right]\frac{d\boldsymbol{x}}{ds}\right\}.\end{aligned}$$

Here, we have used the ray equations themselves to move between $\boldsymbol{p}$ and $d\boldsymbol{x}/ds$. The term in braces, { } is the part of the gradient of the wavespeed that is perpendicular to the ray, because the second term in the bracket removes the tangential part of the gradient. Recall that the curvature points to the center of a circle that makes at least second-order contact (higher than tangential contact) with the curve itself; the length of the curvature vector is the reciprocal of the radius of that circle. Here, we see that the curvature vector points in the opposite direction of the gradient of the wavespeed, which is to say, it points in the direction of decreasing wavespeed. Rays follow the circle of curvature; that is, they bend in the direction of the curvature vector. Hence, we conclude that rays tend to bend in the direction of decreasing wavespeed and away from the direction of increasing wavespeed.

We can think of refraction as an extreme case of this result, wherein the magnitude of the gradient has become infinite. Consider replacing that sharp discontinuity by a rapid but smooth transition zone. Then, when moving from a higher-velocity zone to a lower-velocity zone, rays will tend to bend towards the normal—away from the gradient of the velocity—while the opposite will be the case when rays move from a lower-velocity zone to a higher-velocity zone. That is, rays tend to focus when moving from higher velocity to lower velocity and defocus when moving from lower velocity to higher velocity.

For water waves, in shallow water, the wavespeed is proportional to the squareroot of the depth of the water. Hence, rays bend in the shallower-water direction. Consequently, even waves that start out obliquely to a beach in deep water, tend to line up so that their wavefronts, the waves that ultimately break, are more nearly parallel to the beach.

In summary, now, for each of the choices of λ above we have reduced the eikonal equation to a system of first-order ordinary differential equations that may then be integrated by a variety of methods, depending on the

given problem and the desired degree of accuracy. For the discussions that follow, we will assume the form of the ray equations that result by taking $\lambda = 1/2$, as in (E.2.11).

E.3 Ray Amplitude Theory

The solution of the eikonal equation yields information about only the traveltime behavior of the wavefield. The transport equation,

$$2\nabla\tau(\boldsymbol{x}) \cdot \nabla A(\boldsymbol{x}) + A\nabla^2\tau(\boldsymbol{x}) = 0, \tag{E.3.1}$$

(here we have written A_0 as A) must be solved, if amplitudes are desired. We can simplify the transport equation by multiplying by an additional factor of A. The result can be recognized as an exact divergence via

$$2A\nabla\tau(\boldsymbol{x}) \cdot \nabla A(\boldsymbol{x}) + A^2\nabla^2\tau(\boldsymbol{x}) = \nabla \cdot (A^2\nabla\tau(\boldsymbol{x})) = 0. \tag{E.3.2}$$

Invoking the divergence theorem, we can write that, for any volume D bounded by the surface ∂D,

$$\int_D \nabla \cdot (A^2\nabla\tau(\boldsymbol{x}))dV = \int_{\partial D} A^2\nabla\tau(\boldsymbol{x}) \cdot \hat{\boldsymbol{n}}\, dS = 0.$$

Here, $\hat{\boldsymbol{n}}$ is an outward-pointing unit normal to the boundary ∂D. If we choose the volume D to be a tube composed of rays on the sides, with end caps consisting of surfaces of constant σ, we may then write

$$\begin{aligned}\int_{\partial D} A^2\nabla\tau(\boldsymbol{x}) \cdot \hat{\boldsymbol{n}}\, dS = \int_{\text{Sides}} & A^2\nabla\tau \cdot \hat{\boldsymbol{n}}\, dS \\ & + \int_{\Sigma(\sigma_2)} A^2\nabla\tau(\boldsymbol{x}) \cdot \hat{\boldsymbol{\sigma}}_2\, dS_2 \\ & - \int_{\Sigma(\sigma_1)} A^2\nabla\tau(\boldsymbol{x}) \cdot \hat{\boldsymbol{\sigma}}_1\, dS_1 = 0.\end{aligned} \tag{E.3.3}$$

In this equation, we have defined the $\hat{\boldsymbol{\sigma}}_1$-direction to point *interior* to D on the $\Sigma(\sigma_1)$ end cap and have similarly defined the $\hat{\boldsymbol{\sigma}}_2$-direction to point *exterior* to D on the $\Sigma(\sigma_2)$ end cap. With this choice, both unit vectors make acute angles with the rays in the tube for small enough ray tube cross-section. Because the divergence theorem that we use here requires an outward-pointing normal direction, we have adjusted the last expression to account for this by introducing a minus sign.

Now, the integral over the sides of the ray tube vanishes; the sides are parallel to the $\nabla\tau = \boldsymbol{p}$ direction, which is the direction tangent to the raypaths that make up the sides. Hence, $\hat{\boldsymbol{n}}$ is orthogonal to $\boldsymbol{p}$ on the sides and the integrand over that part of the ray tube is equal to zero. This leaves only the integrals over the end caps to be considered

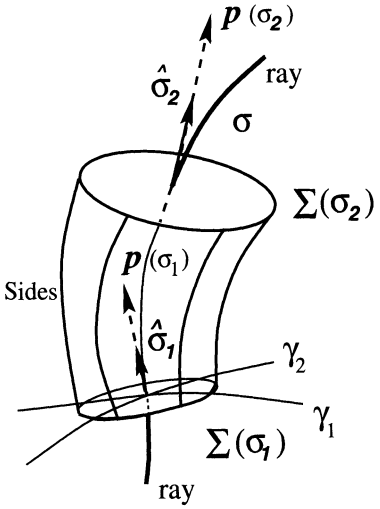

FIGURE E.1. Schematic of a ray tube. The sides of the tube are made of rays, while the end caps are surfaces of constant σ. The end caps, designated $\Sigma(\sigma_1)$ and $\Sigma(\sigma_2)$, have unit normal vectors $\hat{\boldsymbol{\sigma}}_1$ and $\hat{\boldsymbol{\sigma}}_2$, respectively. The coordinates γ_1 and γ_2, which parameterize the end caps, serve to label each ray, being constants on each ray. The coordinate σ is a running parameter along each ray. Note that the vectors $\boldsymbol{p}(\sigma_1)$ and $\boldsymbol{p}(\sigma_2)$ also point perpendicular to the respective surfaces of constant σ.

$$\int_{\Sigma(\sigma_2)} A^2 \boldsymbol{p} \cdot \hat{\boldsymbol{\sigma}}_2 \, dS_2 - \int_{\Sigma(\sigma_1)} A^2 \boldsymbol{p} \cdot \hat{\boldsymbol{\sigma}}_1 \, dS_1 = 0, \tag{E.3.4}$$

where we have rewritten $\nabla\tau$ as $\boldsymbol{p}$.

Let us now introduce coordinates γ_1, γ_2, to parameterize the surface $\Sigma(\sigma_1)$, as in Figure E.1. Because each ray passes through a point of this surface, the rays may be distinguished by these parameters as well; that is, the rays are described by

$$\boldsymbol{x} = \boldsymbol{x}(\sigma, \gamma_1, \gamma_2),$$

with the rays at $\sigma = \sigma_1$ being on the surface $\Sigma(\sigma_1)$. In fact, given the range of values (γ_1, γ_2)—call it $\Gamma(\gamma_1, \gamma_2)$—on $\Sigma(\sigma_1)$, the same set of values fills out the domain D as σ varies from σ_1 to σ_2. Therefore, we can use the same parameters, γ_1, γ_2 in the range $\Gamma(\gamma_1, \gamma_2)$ to describe the surface $\Sigma(\sigma_2)$ if only we evaluate $\boldsymbol{x} = \boldsymbol{x}(\sigma_2, \gamma_1, \gamma_2)$.

Explicitly rewriting (E.3.4) in terms of the new coordinate system $(\sigma, \gamma_1, \gamma_2)$ yields

$$\int_{\Gamma(\gamma_1,\gamma_2)} A^2 \boldsymbol{p} \cdot \hat{\boldsymbol{\sigma}}_2 \left| \frac{\partial \boldsymbol{x}}{\partial \gamma_1} \times \frac{\partial \boldsymbol{x}}{\partial \gamma_2} \right|_{\Sigma(\sigma_2)} d\gamma_1 d\gamma_2$$
$$- \int_{\Gamma(\gamma_1,\gamma_2)} A^2 \boldsymbol{p} \cdot \hat{\boldsymbol{\sigma}}_1 \left| \frac{\partial \boldsymbol{x}}{\partial \gamma_1} \times \frac{\partial \boldsymbol{x}}{\partial \gamma_2} \right|_{\Sigma(\sigma_1)} d\gamma_1 d\gamma_2 = 0.$$

The vector cross products here are normal to the integration surfaces. Furthermore, $d\boldsymbol{x}/d\sigma = \boldsymbol{p}$ also points in the normal direction, $\hat{\boldsymbol{\sigma}}_1$ or $\hat{\boldsymbol{\sigma}}_2$, as the case may be. Thus, the vector cross product and the scalar dot product in this last result can be combined to yield

$$\int_{\Gamma(\gamma_1,\gamma_2)} A^2(\sigma_2) \left| \frac{\partial \boldsymbol{x}}{\partial \sigma} \cdot \frac{\partial \boldsymbol{x}}{\partial \gamma_1} \times \frac{\partial \boldsymbol{x}}{\partial \gamma_2} \right| (\sigma_2) d\gamma_1 d\gamma_2 \tag{E.3.5}$$
$$- \int_{\Gamma(\gamma_1,\gamma_2)} A^2(\sigma_1) \left| \frac{\partial \boldsymbol{x}}{\partial \sigma} \cdot \frac{\partial \boldsymbol{x}}{\partial \gamma_1} \times \frac{\partial \boldsymbol{x}}{\partial \gamma_2} \right| (\sigma_1) d\gamma_1 d\gamma_2 = 0.$$

The triple scalar product that appears in each of these integrals is the (3D, in this case) *ray Jacobian*,

$$J_{3D}(\sigma) = \left[\frac{\partial \boldsymbol{x}}{\partial \sigma} \cdot \frac{\partial \boldsymbol{x}}{\partial \gamma_1} \times \frac{\partial \boldsymbol{x}}{\partial \gamma_2} \right] (\sigma). \tag{E.3.6}$$

Because the cross section $\Gamma(\gamma_1, \gamma_2)$ is arbitrary, and can be taken as a differential cross section in (γ_1, γ_2), we conclude that the integrands must be equal, pointwise. Therefore, we equate the integrands in (E.3.5) and write the general expression for the square of the amplitude $A^2(\sigma)$ as

$$A^2(\sigma) = A^2(\sigma_0) \frac{J_{3D}(\sigma_0)}{J_{3D}(\sigma)}. \tag{E.3.7}$$

Here, we have rewritten σ_1 as σ_0 to represent an initial value of the running parameter σ along the ray. The general value of this parameter is represented by replacing σ_2 with σ, itself.

The derivation in two dimensions is similar:

$$A^2(\sigma) = A^2(\sigma_0) \frac{J_{2D}(\sigma_0)}{J_{2D}(\sigma)}, \tag{E.3.8}$$

with the exception being that we now have the 2D ray Jacobian

$$J_{2D}(\sigma) = \left| \frac{\partial \boldsymbol{x}}{\partial \sigma} \times \frac{\partial \boldsymbol{x}}{\partial \gamma_1} \right|.$$

Therefore, we will write

$$A^2(\sigma) = A^2(\sigma_0) \frac{J(\sigma_0)}{J(\sigma)}, \tag{E.3.9}$$

where the ray Jacobian is either J_{2D} or J_{3D}, depending on whether the problem is in two or three dimensions.

E.3.1 The ODE Form of the Transport Equation

It is possible to convert the transport equation (E.3.1) into an ODE with respect to σ. This is most easily done for A^2, rather than for A itself. A first form of this ODE may be obtained by rewriting the first term of the transport equation, using the equality

$$\frac{\partial \boldsymbol{x}}{\partial \sigma} = \boldsymbol{p} = \nabla \tau$$

from the first ray equation. By using this result in (E.3.1), we find that

$$2A\frac{\partial \boldsymbol{x}}{\partial \sigma} \cdot \nabla A = -A^2(\sigma)\nabla^2 \tau,$$

which simplifies to

$$\frac{dA^2(\sigma)}{d\sigma} = -A^2(\sigma)\nabla^2 \tau. \tag{E.3.10}$$

There is another way of constructing the derivative of A^2, however. We may differentiate (E.3.9) to obtain

$$\frac{dA^2}{d\sigma} = A^2(\sigma_0)J(\sigma_0)\frac{d}{d\sigma}\left[\frac{1}{J(\sigma)}\right].$$

This expression may be rewritten as

$$\frac{dA^2}{d\sigma} = J(\sigma)A^2(\sigma)\frac{d}{d\sigma}\left[\frac{1}{J(\sigma)}\right] = -\frac{1}{J(\sigma)}A^2(\sigma)\frac{d}{d\sigma}\left[J(\sigma)\right],$$

where we have used equation (E.3.9) to replace the $A^2(\sigma_0)J(\sigma_0)$ on the right-hand side above. Recognizing the logarithmic derivative of J in the rightmost expression here allows us to rewrite the transport equation as

$$\frac{dA^2}{d\sigma} = -A^2(\sigma)\frac{d}{d\sigma}\ln\left[J(\sigma)\right]. \tag{E.3.11}$$

A comparison of equations (E.3.10) and (E.3.11) suggests the identity

$$\frac{d}{d\sigma}\ln\left[J(\sigma)\right] = \nabla^2 \tau. \tag{E.3.12}$$

To verify that this is true, we can either work in generalized coordinates on the right side to confirm that it equals the left side, or directly differentiate the determinant on the left side to confirm that it is equal to the right side. We choose to do the latter. Because differentiation of determinants is a relatively lesser-known subject, we provide a derivation here, specifically for the 3D case. In the next two sections, we will apply the derived determinant-differentiation result to the left side of (E.3.12).

E.3.2 Differentiation of a Determinant

Consider a 3×3 determinant M, with elements, $\mu_{ij}(\sigma)$, that are all functions of some independent variable, σ, as indicated. For the purposes of this derivation, it is easiest to start from the general formula for the determinant as a sum of all appropriately chosen products of three elements. That formula is

$$M = \sum_{i,j,k=1}^{3} \mu_{1i}\mu_{2j}\mu_{3k}\epsilon_{ijk}. \tag{E.3.13}$$

In this equation, we have introduced the symbol ϵ_{ijk}, defined as follows:

$$\epsilon_{ijk} = \begin{cases} +1, & ijk = 123,\ 312,\ 231, \\ -1, & ijk = 132,\ 213,\ 321, \\ 0, & \text{otherwise.} \end{cases}$$

That is, ϵ_{ijk} is equal to $+1$ when ijk is a cycle permutation of the numbers $1, 2, 3$, is equal to -1 when ijk is an anticyclic permutation of 123, and is equal to 0 when two or more of the indices are the same.

The reason this formula for the determinant is a good place to start is that we know how to differentiate a product. By the product rule, a function consisting of three factors will yield three terms, with only one factor being differentiated in each term. That is,

$$\frac{dM}{d\sigma} = \sum_{i,j,k=1}^{3} \frac{d\mu_{1i}}{d\sigma}\mu_{2j}\mu_{3k}\epsilon_{ijk} + \sum_{i,j,k=1}^{3} \frac{d\mu_{2j}}{d\sigma}\mu_{3k}\mu_{1i}\epsilon_{ijk} \tag{E.3.14}$$

$$+ \sum_{i,j,k=1}^{3} \frac{d\mu_{3k}}{d\sigma}\mu_{1i}\mu_{2j}\epsilon_{ijk}.$$

This result is a sum of three determinants (n determinants, if we were considering the $n \times n$ case). In each determinant, a column of the matrix $[\mu_{ij}]$ has been modified—it has been replaced by its derivative.

Typically, the derivative formula is left in this form; however, we will need a slightly different version of this result that requires us to continue the analysis. Returning to the definition of M in (E.3.13), we observe that we can separate out any one of the sums to rewrite that result as

$$M = \sum_{i=1}^{3} \mu_{1i}\,\mathrm{cof}\,(\mu_{1i}) = \sum_{j=1}^{3} \mu_{2j}\,\mathrm{cof}\,(\mu_{2j}) = \sum_{k=1}^{3} \mu_{3k}\,\mathrm{cof}\,(\mu_{3k}), \tag{E.3.15}$$

where

$$\mathrm{cof}\,(\mu_{1i}) = \sum_{j,k=1}^{3} \mu_{2j}\mu_{3k}\epsilon_{ijk}, \qquad \mathrm{cof}\,(\mu_{2j}) = \sum_{i,k=1}^{3} \mu_{1i}\mu_{3k}\epsilon_{ijk},$$

$$\mathrm{cof}\,(\mu_{3k}) = \sum_{i,j=1}^{3} \mu_{1i}\mu_{2j}\epsilon_{ijk}.$$

We prefer to rewrite this result with all of the indices cyclically rotated, so that the index on the left is always i. That is,

$$\mathrm{cof}\,(\mu_{1i}) = \sum_{j,k=1}^{3} \mu_{2j}\mu_{3k}\epsilon_{ijk}, \qquad \mathrm{cof}\,(\mu_{2i}) = \sum_{k,j=1}^{3} \mu_{1k}\mu_{3j}\epsilon_{ijk},$$

$$\operatorname{cof}(\mu_{3i}) = \sum_{j,k=1}^{3} \mu_{1j}\mu_{2k}\epsilon_{ijk}. \tag{E.3.16}$$

We use this result in (E.3.15) to obtain

$$\frac{dM}{d\sigma} = \sum_{i,q=1}^{3} \frac{d\mu_{qi}}{d\sigma} \operatorname{cof}(\mu_{qi}). \tag{E.3.17}$$

Now suppose that in the first line of (E.3.15) we were to replace μ_{1i} by μ_{2i} or μ_{3i}. In each case, we would be calculating the determinant of a different matrix, in fact, a matrix in which the first row was the same as the second row, or the first row was the same as the third row. We know that such matrices have determinant zero; that is,

$$\sum_{i=1}^{3} \mu_{pi} \operatorname{cof}(\mu_{1i}) = M\delta_{p1} = \begin{cases} 1, & p = 1, \\ 0, & p \neq 1. \end{cases}$$

Similarly, by using the other definitions of the determinant in (E.3.15), we can conclude that

$$\sum_{i=1}^{3} \mu_{pi} \operatorname{cof}(\mu_{qi}) = M\delta_{pq}, \quad p, q = 1, 2, 3.$$

This is exactly the calculation to determine the elements of the product of two matrices, except for the fact that the summation here would seem to be performed on the column index in both factors. There is an easy way to fix that; we need only introduce the transpose of the matrix of elements of the right factor. To complete this small derivation, then, we set

$$\nu_{iq} = \operatorname{cof}(\mu_{qi})/M, \quad i, p, q = 1, 2, 3, \tag{E.3.18}$$

and observe that

$$\sum_{i=1}^{3} \mu_{pi}\nu_{iq} = \delta_{pq}, \quad p, q = 1, 2, 3. \tag{E.3.19}$$

In words: the cofactors that appear in the formula (E.3.15) are the elements of the transpose of the inverse of the matrix with elements μ_{ij} multiplied by the original determinant M.

By using (E.3.18) in (E.3.17), we can rewrite the derivative in terms of the elements of the inverse matrix, as follows.

$$\frac{1}{M}\frac{dM}{d\sigma} = \sum_{i,q=1}^{3} \frac{d\mu_{qi}}{d\sigma}\nu_{iq}. \tag{E.3.20}$$

Now, we have the tools we need to verify (E.3.12).

E.3.3 Verification of (E.3.12)

Let us now return to the definition of J_{3D} in (E.3.6). We will take $J_{3D} = M$ of the discussion above. In order to use an index notation as in the previous section, let us set

$$\sigma = \gamma_3, \quad \mu_{qi} = \frac{\partial x_q}{\partial \gamma_i}.$$

We note that

$$\sum_{i=1}^{3} \frac{\partial x_q}{\partial \gamma_i} \frac{\partial \gamma_i}{\partial x_r} = \frac{\partial x_q}{\partial x_r} = \delta_{qr}, \quad q, r = 1, 2, 3.$$

Here, the first equality is just a consequence of the chain rule and the second equality arises from the independence of the three Cartesian variables. The significance of this result is that it allows us to identify the elements of the inverse matrix, $[\nu_{iq}]$ that we need, in order to use (E.3.20). In fact,

$$\nu_{iq} = \frac{\partial \gamma_i}{\partial x_q}.$$

Let us now substitute the results of this discussion into (E.3.20). The result is

$$\frac{1}{J_{3D}} \frac{dJ_{3D}}{d\sigma} = \sum_{i,q=1}^{3} \left[\frac{\partial}{\partial \gamma_3} \frac{\partial x_q}{\partial \gamma_i} \right] \frac{\partial \gamma_i}{\partial x_q}.$$

Now, interchange the order of differentiation with respect to the independent variables, γ_i and γ_3, in the first factor on the right to obtain

$$\frac{1}{J_{3D}} \frac{dJ_{3D}}{d\sigma} = \sum_{i,q=1}^{3} \left[\frac{\partial}{\partial \gamma_i} \frac{\partial x_q}{\partial \gamma_3} \right] \frac{\partial \gamma_i}{\partial x_q}.$$

Next, recall that $\gamma_3 = \sigma$ and use the ray equations, again

$$\frac{\partial x_q}{\partial \gamma_3} = \frac{dx_q}{d\sigma} = p_q = \frac{\partial \tau}{\partial x_q}.$$

Substitute this result in the previous equation to obtain

$$\frac{1}{J_{3D}} \frac{dJ_{3D}}{d\sigma} = \sum_{i,q=1}^{3} \left[\frac{\partial}{\partial \gamma_i} \frac{\partial \tau}{\partial x_q} \right] \frac{\partial \gamma_i}{\partial x_q}.$$

We can see here that the summation over i is just a chain rule differentiation with respect to x_q. Therefore,

$$\frac{1}{J_{3D}} \frac{dJ_{3D}}{d\sigma} = \sum_{q=1}^{3} \frac{\partial}{\partial x_q} \frac{\partial \tau}{\partial x_q} = \nabla^2 \tau, \tag{E.3.21}$$

which is what we wanted to prove.

E.3.4 Higher-Order Transport Equations

To correctly formulate ray amplitude theory, we need to say something about transport equations that result from considering the coefficients of the higher-order terms of equation (E.1.2). Recall, the amplitudes $A(\sigma)$ that we solved for above are the 0-th order amplitudes. Whether in 3D or in 2D, we may write the following recursion formula for the higher-order amplitudes A_j as

$$2\nabla\tau \cdot \nabla A_j + A_j \nabla^2 \tau = -\nabla^2 A_{j-1}, \tag{E.3.22}$$

where $j > 0$. Using (E.3.12), multiplying by a factor of $\sqrt{J(\sigma)}$, and applying the first ray equation, we have

$$\sqrt{J(\sigma)}\frac{dA_j}{d\sigma} + \frac{A_j}{2}\sqrt{J(\sigma)}\ln[J(\sigma)] = -\frac{\sqrt{J(\sigma)}}{2}\nabla^2 A_{j-1},$$

which may be rewritten as

$$\frac{d\left(\sqrt{J(\sigma)}A_j\right)}{d\sigma} = -\frac{\sqrt{J(\sigma)}}{2}\nabla^2 A_{j-1}(\sigma).$$

This expression may be integrated, to provide the recursion formula for the amplitude factors A_j

$$A(\sigma) = A_j(\sigma_0)\sqrt{\frac{J(\sigma_0)}{J(\sigma)}} - \frac{1}{2J(\sigma)}\int_{\sigma_0}^{\sigma}\sqrt{J(\sigma')}\nabla^2 A_{j-1}(\sigma')d\sigma'.$$

We could use the values of $A_0 = A(\sigma)$, derived previously, in the recursion relation to solve for amplitudes of higher order. More terms do not necessarily guarantee that an asymptotic series will give a better representation, however. For most applications, the leading-order amplitude A_0 is sufficient.

E.4 Determining Initial Data for the Ray Equations

We pointed out earlier that we need initial data for the ray equations, (E.2.11), in order to be able to completely solve for the traveltime. Similarly, the solution of the transport equation, (E.3.7), has a constant of integration, given by $A^2(\sigma_0)J_{3D}(\sigma_0)$. Here, we show how these constants are determined for various problems of interest. We start with the 3D and 2D Green's functions, which are of direct interest. In particular, note that for this problem, the rays all emanate from the source point, meaning that the cross-sectional area of the ray tube becomes zero in this limit. We should expect, then, that J_{3D} and J_{2D} will be zero at this point, and the solution formulas (E.3.7) and (E.3.8) become singular as well. Thus, for

this problem of greatest interest, finding the appropriate "initial data" is somewhat delicate.

We will also show how one determines initial data for reflected and transmitted waves from initial data for incident waves. This is a much more straightforward problem.

E.4.1 Initial Data for the 3D Green's Function

Let us suppose that we have a point source $\delta(\boldsymbol{x} - \boldsymbol{x}_0)$ for the Helmholtz equation. We need to generate the initial data for the ray equations, (E.2.11). It is reasonable for this problem to assume that the rays all emanate from the source point and start with traveltime equal to zero. That is, we set

$$\boldsymbol{x} = \boldsymbol{x}_0, \qquad \tau = 0, \qquad \text{for } \sigma = 0.$$

We also need initial values for $\boldsymbol{p}$. Again, we use our insight to define such data. We expect that no direction of propagation from the point source will be distinguished from any other. We note from (E.2.11) that the directions of the rays—in particular, the *initial* directions of the rays—are given by $\boldsymbol{p}$. We propose, then, to allow these initial vectors to range over all angular directions. Furthermore, these vectors must have length $p(\boldsymbol{x}_0) = |\boldsymbol{p}(\boldsymbol{x}_0)| = 1/c(\boldsymbol{x}_0)$, where the latter result comes from the eikonal equation itself. Thus the initial data also includes the initial values of the quantities

$$\boldsymbol{p}(\boldsymbol{x}_0) = p(\boldsymbol{x}_0)\hat{\boldsymbol{p}}, \quad \text{where} \quad \hat{\boldsymbol{p}} = (\sin\phi\cos\theta, \sin\phi\sin\theta, \cos\phi).$$

Here, $0 \leq \theta < 2\pi$ and $0 \leq \phi \leq \pi$. As they vary over these ranges, the initial ray directions cover the entire unit sphere of possible directions. Each fixed pair, (θ, ϕ), determines a unique ray through its starting value. Thus, θ and ϕ are a particular choice for the coordinates γ_1 and γ_2 of our derivation. We remark that these are not the only choices. For example, we could have taken two of the components of $\boldsymbol{p}(\boldsymbol{x}_0)$ for these parameters and then determined the initial value of the third component from the eikonal equation, again. We will continue the discussion here with this specific choice, however. What remains is to determine the constant in the solution for the amplitude, A. We argue that this initial value should depend only on the medium in the neighborhood of the source point, $\boldsymbol{x}_0$. Thus, even for heterogeneous media, the constant we seek should be the same as for the problem in which we take $c(\boldsymbol{x}) = c(\boldsymbol{x}_0)$. To complete the derivation of the ray amplitude theory, then, we will determine the constant of the solution by determining its value for homogeneous media. To do so, we will need to draw on the fact that for a constant-wavespeed medium the Green's function is known to be

$$g(\boldsymbol{x}, \boldsymbol{x}_0, \omega) = \frac{1}{4\pi|\boldsymbol{x} - \boldsymbol{x}_0|} e^{i\omega|\boldsymbol{x}-\boldsymbol{x}_0|},$$

meaning that $A(\boldsymbol{x}) = 1/4\pi|\boldsymbol{x} - \boldsymbol{x}_0|$ in a constant wavespeed (homogeneous) medium and that it should behave the same in the limit at the source point, even in a heterogeneous medium.

For the constant wavespeed medium, we note from (E.2.11) that $\boldsymbol{p}$ is a constant vector, $\boldsymbol{p} = p(\boldsymbol{x}_0)\,\hat{\boldsymbol{p}}$. From the first ray equation, we may solve for the distance from the source as a function of σ to yield

$$\boldsymbol{x} - \boldsymbol{x}_0 = \int_0^\sigma p(\boldsymbol{x}_0)\,\hat{\boldsymbol{p}}\,d\sigma' = \hat{\boldsymbol{p}}\,p(\boldsymbol{x}_0)\sigma,$$

which means that

$$|\boldsymbol{x} - \boldsymbol{x}_0| = p(\boldsymbol{x}_0)\sigma.$$

If we use this result for $|\boldsymbol{x} - \boldsymbol{x}_0|$ in the equation, $A(\boldsymbol{x}) = 1/4\pi|\boldsymbol{x} - \boldsymbol{x}_0|$, we conclude that the correct expression for $A(\sigma)$ is

$$A(\sigma) = \frac{1}{4\pi p(\boldsymbol{x}_0)\,\sigma}. \tag{E.4.1}$$

We have, here, a solution of the constant-wavespeed problem in terms of σ. It exhibits the appropriate singular behavior at $\sigma = 0$. This solution, however, was not our final objective. We want to use it to determine a value of $A^2(\sigma_0)J_{3D}(\sigma_0)$ in (E.3.9). We want a solution for all $\sigma > 0$, because of our desire to use the same constant of the solution for point-source problems in heterogeneous media. This suggests that we should take $\sigma_0 = 0$. However, the singular behavior of the solution at that point precludes a simple evaluation. This is what makes the determination of initial data for the point-source problem "delicate."

In light of this observation, let us modify our objective to seek a solution to (E.3.9) of the form

$$A(\sigma) = \frac{K}{\sqrt{J_{3D}(\sigma)}}, \quad \sigma > 0,$$

with K being a constant (with respect to σ) to be determined. Comparing this equation with (E.3.9), we see that

$$K = \lim_{\sigma_0 \to 0} A^2(\sigma_0)J_{3D}(\sigma_0).$$

To find this limit, we will compute J_{3D} and combine it with the explicit form of the solution, (E.4.1) and then take the limit.

We will determine J from the above explicit solution of the ray equations in homogeneous media, which we write out in detail as

$$\begin{aligned} x_1 - x_{10} &= p(\boldsymbol{x}_0)\sigma \sin\phi\cos\theta, \\ x_2 - x_{20} &= p(\boldsymbol{x}_0)\sigma \sin\phi\sin\theta, \\ x_3 - x_{30} &= p(\boldsymbol{x}_0)\sigma \cos\phi. \end{aligned}$$

Now, calculating J_{3D} with respect to these variables is fairly straightforward. The result is

$$J_{3D}(\sigma_0) \equiv \frac{\partial(\boldsymbol{x}(\sigma_0))}{\partial(\sigma,\theta,\phi)} = p^3(\boldsymbol{x}_0)\sigma_0^2 \sin\phi.$$

We may use this expression for $J_{3D}(\sigma_0)$ and (E.4.1) for $A(\sigma_0)$ to rewrite equation (E.3.9) as

$$\begin{aligned} A^2(\sigma)J_{3D}(\sigma) &= A^2(\sigma_0)J_{3D}(\sigma_0) \\ &= \left[\frac{1}{4\pi p(\boldsymbol{x}_0)\sigma_0}\right]^2 p^3(\boldsymbol{x}_0)\sigma_0^2 \sin\phi = \frac{p(\boldsymbol{x}_0)\sin\phi}{4\pi}. \end{aligned}$$

We see here that for constant wavespeed, the product A^2J is actually independent of the choice of σ_0. This permits us to take the limit we need and write the solution of the transport equation for $A(\sigma)$, in terms of the Jacobian J, as

$$A(\sigma) = \left[\frac{1}{4\pi p(\boldsymbol{x}_0)}\right] p^3(\boldsymbol{x}_0)\sigma^2 \sin\phi = \frac{1}{4\pi}\sqrt{\frac{p(\boldsymbol{x}_0)\sin\phi}{J_{3D}(\sigma)}}, \tag{E.4.2}$$

where, again,

$$J_{3D}(\sigma) = \frac{\partial(\boldsymbol{x}(\sigma))}{\partial(\sigma,\theta,\phi)}.$$

We propose to use this last form of solution even for problems with a heterogeneous wavespeed profile. If we carry out power series expansions near $\sigma = 0$ we can confirm that we have the "right" constant of integration for those problems as well.

Thus, if we had the solution of the inhomogeneous problem for the rays, traveltime and amplitude, we would write the leading-order, or WKBJ (ray-theoretic) Green's function in 3D as

$$\begin{aligned} g(\boldsymbol{x},\boldsymbol{x}_0,\omega) &\sim A(\boldsymbol{x},\boldsymbol{x}_0)e^{i\omega\tau(\boldsymbol{x}_0,\boldsymbol{x})} \qquad \text{(E.4.3)} \\ &= \frac{1}{4\pi}\sqrt{\frac{p(\boldsymbol{x}_0)\sin\phi}{J_{3D}(\sigma)}} \exp\left(i\omega\int_0^\sigma 1/c^2(\boldsymbol{x}(\sigma'))d\sigma'\right). \end{aligned}$$

Again, we point out that another choice of the parameters, γ_1, γ_2, would lead to a different constant of integration in the amplitude, corresponding to a different Jacobian as well. In particular, it should be noted that this solution has some numerical pathology near $\phi = 0$ or $\phi = \pi$. The numerator of the amplitude is nearly zero there. The same must be true for J_{3D} for this choice of ray parameter, so that the quotient remains finite and nonzero in this region. This is much like the behavior of the surface area element on the unit sphere, $\sin\phi\, d\phi\, d\theta$; it is a pathology of the choice of parameters and not of the underlying problem. Clearly, this is not a good choice for numerical calculations. See the exercise below for an alternative choice of ray parameters that does not have this pathology.

Exercises

E.1 For downward-propagating waves, an alternative choice of the parameters γ_1, γ_2 would be the initial values of p_1 and p_2, say, $p_{10} = p_1(\boldsymbol{x}_0)$ and $p_{20} = p_2(\boldsymbol{x}_0)$. Then, the initial value of p_3 would be the positive square root

$$p_{30} = \sqrt{1/c^2(\boldsymbol{x}_0) - p_{10}^2 - p_{20}^2}.$$

a. Show that for this choice and constant wavespeed,

$$J_{3D} = \frac{\sigma^2}{c^2 p_3}, \quad A(\boldsymbol{x}) = \frac{K}{\sigma c\sqrt{p_3}},$$

with K, a constant to be determined, different from the choice of K above, for the parameters, ϕ and θ.

b. Use this result and the known amplitude for the constant-wavespeed Green's function amplitude to conclude that even for variable wavespeed,

$$A(\boldsymbol{x}) = \frac{1}{4\pi c(\boldsymbol{x}_0)\sqrt{J_{3D}\, p_3(\boldsymbol{x}_0)}}.$$

Note that we have exchanged a pathology at $\phi = 0$ in the example in the text with a pathology at $p_3(\boldsymbol{x}_0) = 0$ in the current solution. As above, the product, $J_{3D}\, p_3(\boldsymbol{x}_0)$ remains finite in this limit, but there are problems with numerical calculations. In the application to seismic inverse problems, we are less interested in horizontally propagating initial rays than we are with rays that propagate in the vertical near $\phi = 0$. So this would be a better choice of ray-labeling parameters than the polar angles for our applications.

E.4.2 Initial Data for the 2D Green's Function

We will describe here the determination of initial values for the 2D ray theoretic solution for the Green's function. As above, we expect that the rays are initiated at the source point, $\boldsymbol{x} = \boldsymbol{x}_0$ at $\sigma = 0$. We take the initial value of the traveltime to be zero, such that $\tau = 0$ when $\sigma = 0$.

Next, we need initial values for $\boldsymbol{p}$. As in 3D, we use the fact that these initial values determine the initial directions of the rays. Thus, in order to allow for rays in all directions, we take those initial values to be $\boldsymbol{p}(\boldsymbol{x}_0) = p(\boldsymbol{x}_0)(\sin\theta, \cos\theta)$, with $0 \leq \theta < 2\pi$.

As above, we will determine an appropriate constant for the amplitude solution, because the Jacobian is zero at the initial point. To find this constant, we again consider the constant-wavespeed solution and argue that the constant value we derive for this solution will be correct for the variable-wavespeed solution as well.

Given the Green's function for constant-wavespeed media in 2D,

$$g(\boldsymbol{x},\omega) = \frac{i\,\mathrm{sgn}\,(\omega)}{4} H_0^{(1)}\left(\frac{\omega\,|\boldsymbol{x}-\boldsymbol{x}_0|}{c(\boldsymbol{x}_0)}\right), \tag{E.4.4}$$

we will compare this amplitude with the ray-theoretic 2D amplitude in order to determine the constant in that solution.[5] In this particular case, we may consider replacing the Hankel function with its large-argument asymptotic form. The Green's function can be rewritten for large argument as

$$g(\boldsymbol{x},\omega) \sim \frac{1}{2}\sqrt{\frac{c(\boldsymbol{x}_0)}{2\pi|\omega|\,|\boldsymbol{x}-\boldsymbol{x}_0|}}\, e^{i\omega|\boldsymbol{x}-\boldsymbol{x}_0|/c(\boldsymbol{x}_0)+i\,\mathrm{sgn}\,(\omega)\pi/4}, \tag{E.4.5}$$

where we have used the asymptotic form of the Hankel function,

$$H_0^{(1)}(z) \sim \sqrt{\frac{2}{\pi z}}\, e^{iz-i\pi/4}, \qquad -\pi < \arg(z) < 2\pi,$$

$$\sim \sqrt{\frac{2}{\pi|z|}}\, e^{iz-i\,\mathrm{sgn}\,(z)\pi/4}, \qquad z \text{ real}.$$

As before, the first ray equation yields the result for the $|\boldsymbol{x}-\boldsymbol{x}_0| = p(\boldsymbol{x}_0)\sigma_0$. Recognizing that $p = 1/c$, we may rewrite equation (E.4.5) as

$$g(\boldsymbol{x}(\sigma_0),\omega) \sim \frac{1}{2\sqrt{2\pi\,|\omega|p^2(\boldsymbol{x}_0)\sigma}}\, e^{\omega i p(\boldsymbol{x}_0)\,\sigma + i\,\mathrm{sgn}\,(\omega)\pi/4}.$$

The factor of $(1/\sqrt{|\omega|})\exp\{i\,\mathrm{sgn}\,(\omega)\pi/4\}$ that appears here should be viewed as a generalization of the factor ω^β in equation (E.1.1), so we conclude that the amplitude, given by $A(\boldsymbol{x}(\sigma_0))$, is

$$A(\boldsymbol{x}(\sigma_0)) = \frac{1}{2\sqrt{2\pi\, p^2(\boldsymbol{x}_0)\sigma}}. \tag{E.4.6}$$

For constant wavespeed, $\boldsymbol{p}$ = constant on the rays. Thus, this vector is given by its initial value and

$$x_1 = p(\boldsymbol{x}_0)\sigma\cos\theta, \qquad x_2 = p(\boldsymbol{x}_0)\sigma\sin\theta. \tag{E.4.7}$$

Now we can compute the ray Jacobian,

$$J_{2D}(\sigma) = \frac{\partial(\boldsymbol{x}(\sigma))}{\partial(\sigma,\theta)} = p^2(\boldsymbol{x}_0)\sigma, \tag{E.4.8}$$

and conclude that

---

[5] This result is usually stated only for ω positive. For causal functions, such as our Green's functions, we need results for both positive and negative ω as analytic continuations from the upper half ω-plane. The stated result is that continuation.

$$A(\sigma) = \frac{K}{\sqrt{J_{2D}(\sigma)}}.$$

We compare this result with (E.4.6) and conclude that

$$K = \frac{1}{2\sqrt{2\pi}} \qquad \text{and} \qquad A(\sigma) = \frac{1}{2\sqrt{2\pi J_{2D}}}$$

for heterogeneous media as well. We may, therefore, write the leading order, or WKBJ, (ray-theoretic) Green's function in 2D as

$$\begin{aligned} g(\boldsymbol{x}, \boldsymbol{x}_0, \omega) &\sim A(\boldsymbol{x}, \boldsymbol{x}_0) e^{i\omega\tau(\boldsymbol{x}_0, \boldsymbol{x})} \qquad \text{(E.4.9)} \\ &= \frac{1}{2\sqrt{2|\omega|\pi J_{2D}(\sigma)}} \exp\left(i\omega \int_{\sigma_0}^{\sigma} 1/c^2(\boldsymbol{x}(\sigma'))d\sigma' + i \operatorname{sgn}(\omega)\pi/4 \right), \end{aligned}$$

where, again, we have written the traveltime $\tau(\boldsymbol{x}_0, \boldsymbol{x})$ by integrating the third ray equation, $d\tau/d\sigma = 1/c^2$.

E.4.3 Initial Data for Reflected and Transmitted Rays

The discussions of the previous sections have shown how the ray equations can be solved for continuous-wavespeed media. The presence of the gradient of wavespeed in the ray equations suggests that the wavespeed profile must be a function that is at least once-differentiable. We know, however, that an important part of wave propagation deals with reflections from interfaces—places where there are jumps in wavespeed.

Because we have shown how to compute the amplitudes A_j in equation (E.1.1), we may now assume that this equation represents the general form of the wavefield throughout any continuous medium. Indeed, because ray theory is the solution of a system of linear ODEs, we know that we can continue such a solution across a discontinuity in wavespeed by representing the discontinuity as the usual boundary conditions of continuity of the field, and continuity of the normal derivative of the field applied at a boundary (a reflecting surface). Thus (E.1.1) can be said to represent the general form of the wavefield in a medium with jumps in wavespeed, provided that the total wavespeed profile is piecewise continuous, with any discontinuities being confined to specific boundaries.

Given an incident field u_{I} of the form

$$u_{\mathrm{I}}(\boldsymbol{x}, \omega) \sim \omega^{\beta} e^{i\omega\tau_{\mathrm{I}}(\boldsymbol{x})} \sum_{j=0}^{\infty} \frac{A_j^{\mathrm{I}}(\boldsymbol{x})}{(i\omega)^j}, \qquad \text{(E.4.10)}$$

we can assume that reflected and transmitted fields, u_{R} and u_{T}, respectively, are generated at such a boundary. Thus, we assume that the total field is $u = u_{\mathrm{I}} + u_{\mathrm{R}}$ on one side of the boundary, and is $u = u_{\mathrm{T}}$ on the other. Because we will assume that u_{I} is known, the application of continuity conditions on the boundary between regions with different wavespeeds will permit us to solve for the initial data for the reflected field, u_{R}, and

the transmitted field u_{T} in terms of the elements of the incident wavefield evaluated on the boundary. By the term "initial data" we mean the values of the reflected and transmitted fields on the boundary.

Application of *continuity of the field* says that $u_{\mathrm{I}} + u_{\mathrm{R}} = u_{\mathrm{T}}$ on the boundary. Hence,

$$\omega^{\beta_{\mathrm{I}}} e^{i\omega\tau_{\mathrm{I}}(\boldsymbol{x})} \sum_{j=0}^{\infty} \frac{A_j^{\mathrm{I}}(\boldsymbol{x})}{(i\omega)^j} + \omega^{\beta_{\mathrm{R}}} e^{i\omega\tau_{\mathrm{R}}(\boldsymbol{x})} \sum_{j=0}^{\infty} \frac{A_j^{\mathrm{R}}(\boldsymbol{x})}{(i\omega)^j} = +\omega^{\beta_{\mathrm{T}}} e^{i\omega\tau_{\mathrm{T}}(\boldsymbol{x})} \sum_{j=0}^{\infty} \frac{A_j^{\mathrm{T}}(\boldsymbol{x})}{(i\omega)^j}. \quad \text{(E.4.11)}$$

In this equation, we have taken u_{R} and u_{T} to have series of the same form as u_{I} in (E.4.10), but with I replaced by R and T, respectively. An immediate consequence of this relationship is that

$$\beta_{\mathrm{I}} = \beta_{\mathrm{R}} = \beta_{\mathrm{T}} \quad \text{(E.4.12)}$$

because, in general, terms of a different order in ω cannot be equal. We must also have

$$\tau_{\mathrm{I}} = \tau_{\mathrm{R}} = \tau_{\mathrm{T}} \quad \text{(E.4.13)}$$

on the boundary before we can even hope to match terms of like power in ω that appear in (E.4.11). Note that this determines the initial values of the transmitted traveltime for the reflected and transmitted wavefields.

If the boundary surface is parameterized by the coordinates (σ_1, σ_2) such that $\boldsymbol{x} = \boldsymbol{x}(\sigma_1, \sigma_2)$, then direct differentiation with respect to these coordinates leads to the conclusion that like-derivatives of τ_{I}, τ_{R}, and τ_{T}, with respect to these coordinates, must also be equal

$$\frac{\partial \boldsymbol{x}}{\partial \sigma_j} \cdot \nabla \tau_{\mathrm{I}} = \frac{\partial \boldsymbol{x}}{\partial \sigma_j} \cdot \nabla \tau_{\mathrm{R}} = \frac{\partial \boldsymbol{x}}{\partial \sigma_j} \cdot \nabla \tau_{\mathrm{T}}, \quad j = 1, 2. \quad \text{(E.4.14)}$$

This equation determines two components of the vectors $\boldsymbol{p}_{\mathrm{R}}$ and $\boldsymbol{p}_{\mathrm{T}}$ on the boundary, specifically, the projections of these vectors along two linearly independent directions on the boundary surface.

Next, we need to determine the normal components of $\boldsymbol{p}_{\mathrm{R}}$ and $\boldsymbol{p}_{\mathrm{T}}$. We define a normal coordinate $\hat{\boldsymbol{n}}$ to the boundary, and a directional derivative (the normal derivative) in that direction as

$$\hat{\boldsymbol{n}}(\hat{\boldsymbol{n}} \cdot \nabla) = \hat{\boldsymbol{n}} \frac{\partial}{\partial n}$$

and the tangential or in-plane gradient on the interface as

$$\nabla_\sigma = \nabla - \hat{\boldsymbol{n}} \frac{\partial}{\partial n}.$$

Then the equality above becomes

$$\nabla_\sigma \tau_{\mathrm{I}} = \nabla_\sigma \tau_{\mathrm{R}} = \nabla_\sigma \tau_{\mathrm{T}} \quad \text{(E.4.15)}$$

and the gradient of traveltime becomes

$$\boldsymbol{p} = \hat{\boldsymbol{n}}\frac{\partial \tau}{\partial n} + \nabla_\sigma \tau.$$

We will use the notation p_- and p_+ to denote the magnitude of traveltime on the incident and transmitted sides of the boundary. The wavespeeds on the incident and transmitted sides are c_- and c_+, respectively; that is, $p_\pm = 1/c_\pm$. Thus, we can write the normal derivatives of traveltime as

$$\begin{aligned}
\frac{\partial \tau_{\mathrm{I}}}{\partial n} &= \operatorname{sgn}\left[\frac{\partial \tau_{\mathrm{I}}}{\partial n}\right]\sqrt{p_-^2 - (\nabla_\sigma \tau_{\mathrm{I}})^2}, \\
\frac{\partial \tau_{\mathrm{R}}}{\partial n} &= \operatorname{sgn}\left[\frac{\partial \tau_{\mathrm{R}}}{\partial n}\right]\sqrt{p_-^2 - (\nabla_\sigma \tau_{\mathrm{R}})^2}, \\
\frac{\partial \tau_{\mathrm{R}}}{\partial n} &= \operatorname{sgn}\left[\frac{\partial \tau_{\mathrm{T}}}{\partial n}\right]\sqrt{p_+^2 - (\nabla_\sigma \tau_{\mathrm{T}})^2}.
\end{aligned} \tag{E.4.16}$$

Several simplifications are possible. Because $\nabla\tau_{\mathrm{I}}$ and $\nabla\tau_{\mathrm{R}}$ must both satisfy the same eikonal equation, $|\nabla\tau_{\mathrm{I}}| = |\nabla\tau_{\mathrm{R}}|$. However, from (E.4.15), the in-surface components of the gradients are equal, so that the magnitudes of the normal derivatives of incident and reflected traveltimes must also be equal. For the incident waves to be traveling toward the boundary and the reflected waves to be traveling away from the boundary, however, the sign of the normal derivatives of the incident traveltime must be opposite that of the normal derivative of the reflected traveltime,

$$\frac{\partial \tau_{\mathrm{I}}}{\partial n} = -\frac{\partial \tau_{\mathrm{R}}}{\partial n} = -\operatorname{sgn}\left[\frac{\partial \tau_{\mathrm{I}}}{\partial n}\right]\sqrt{p_-^2 - (\nabla_\sigma \tau_{\mathrm{I}})^2}. \tag{E.4.17}$$

This determines the normal component of $\boldsymbol{p}_{\mathrm{R}}$ in terms of the data for the incident field.

Now, let us turn to the normal component of $\boldsymbol{p}_{\mathrm{T}}$. We note that the sign of this component must be the same as that of the normal component of $\boldsymbol{p}$ for the incident wave. In this manner, where the incident wave is directed toward the boundary on one side, the transmitted wave travels away from the boundary on the other side. We may write,

$$\frac{\partial \tau_{\mathrm{T}}}{\partial n} = \operatorname{sgn}\left[\frac{\partial \tau_{\mathrm{I}}}{\partial n}\right]\sqrt{p_+^2 - (\nabla_\sigma \tau_{\mathrm{T}})^2} = \operatorname{sgn}\left[\frac{\partial \tau_{\mathrm{I}}}{\partial n}\right]\sqrt{p_+^2 - p_-^2 + \left(\frac{\partial \tau_{\mathrm{I}}}{\partial n}\right)^2}.$$

The square roots are assumed to be real, that is, we assume that the reflection is precritical. The method can be extended to postcritical reflection, but that is beyond the scope of this appendix. We refer the reader to the references for further development.

With this last result, we have completed the determination of the initial data for the rays and the traveltime of the reflected and transmitted wavefields. What remains is to determine the data for the amplitudes of these wavefields. To do so, we need to introduce a second boundary condition.

For the purposes of this exposition, we will apply a fairly standard condition, *continuity of the normal derivatives* of the total wavefield through the boundary. Thus, the normal derivatives on the two sides should agree.

Taking the normal derivative of both sides of equation (E.4.11), canceling the factor of ω^β, and setting $\tau_\mathrm{I} = \tau_\mathrm{R} = \tau_\mathrm{T}$, yields

$$\sum_{j=0}^{\infty}\left\{\frac{1}{(i\omega)^{j-1}}\left[\frac{\partial\tau_\mathrm{I}}{\partial n}A_j^\mathrm{I}(\boldsymbol{x})+\frac{\partial\tau_\mathrm{R}}{\partial n}A_j^\mathrm{R}(\boldsymbol{x})-\frac{\partial\tau_\mathrm{T}}{\partial n}A_j^\mathrm{T}(\boldsymbol{x})\right]\right.$$

$$\left.+\frac{1}{(i\omega)^j}\left[\frac{\partial A_j^\mathrm{I}}{\partial n}+\frac{\partial A_j^\mathrm{R}}{\partial n}-\frac{\partial A_j^\mathrm{T}}{\partial n}\right]\right\}=0 \quad \text{(E.4.18)}$$

Equating terms of like powers in $i\omega$, it is possible to rewrite equations (E.4.11) and (E.4.18) as the recursion formulas

$$\frac{\partial\tau_\mathrm{I}}{\partial n}A_j^\mathrm{I}(\boldsymbol{x})+\frac{\partial\tau_\mathrm{R}}{\partial n}A_j^\mathrm{R}(\boldsymbol{x})=\frac{\partial\tau_\mathrm{T}}{\partial n}A_j^\mathrm{T}(\boldsymbol{x})+\frac{\partial}{\partial n}\left[A_{j-1}^\mathrm{T}(\boldsymbol{x})-A_{j-1}^\mathrm{I}+A_{j-1}^\mathrm{R}\right]$$

$$A_j^\mathrm{I}+A_j^\mathrm{R}=A_j^\mathrm{T}. \quad \text{(E.4.19)}$$

Taking $A_{-1}=0$, as was done in previous sections, and considering only the 0-order term, yields the relations

$$A_0^\mathrm{I}+A_0^\mathrm{R}=A_0^\mathrm{T}, \qquad \frac{\partial\tau_\mathrm{I}}{\partial n}A_0^\mathrm{I}(\boldsymbol{x})+\frac{\partial\tau_\mathrm{R}}{\partial n}A_0^\mathrm{R}(\boldsymbol{x})=\frac{\partial\tau_\mathrm{T}}{\partial n}A_0^\mathrm{T}(\boldsymbol{x}). \quad \text{(E.4.20)}$$

These are two equations for the initial data for A_0^R and A_0^T. We choose to write the solution to these equations in terms of the reflection coefficient R and the transmission coefficient T defined by

$$A_0^\mathrm{R}=RA_0^\mathrm{I} \qquad A_0^\mathrm{T}=TA_0^\mathrm{I}. \quad \text{(E.4.21)}$$

The solution is made somewhat simpler by using the fact that

$$\frac{\partial\tau_\mathrm{R}}{\partial n}=-\frac{\partial\tau_\mathrm{I}}{\partial n}.$$

Then, equation (E.4.20) becomes

$$1+R=T, \qquad \frac{\partial\tau_\mathrm{I}}{\partial n}-\frac{\partial\tau_\mathrm{I}}{\partial n}R=\frac{\partial\tau_\mathrm{T}}{\partial n}T. \quad \text{(E.4.22)}$$

By solving these equations, we find that the reflection coefficient is given by

$$R=\frac{\dfrac{\partial\tau_\mathrm{I}}{\partial n}-\dfrac{\partial\tau_\mathrm{T}}{\partial n}}{\dfrac{\partial\tau_\mathrm{I}}{\partial n}+\dfrac{\partial\tau_\mathrm{T}}{\partial n}}=\frac{\dfrac{\partial\tau_\mathrm{I}}{\partial n}-\operatorname{sgn}\left[\dfrac{\partial\tau_\mathrm{I}}{\partial n}\right]\sqrt{p_+^2-p_-^2+\left(\dfrac{\partial\tau_\mathrm{I}}{\partial n}\right)^2}}{\dfrac{\partial\tau_\mathrm{I}}{\partial n}+\operatorname{sgn}\left[\dfrac{\partial\tau_\mathrm{I}}{\partial n}\right]\sqrt{p_+^2-p_-^2+\left(\dfrac{\partial\tau_\mathrm{I}}{\partial n}\right)^2}} \quad \text{(E.4.23)}$$

and the transmission coefficient is given by

$$T = \frac{2\frac{\partial \tau_{\mathrm{I}}}{\partial n}}{\frac{\partial \tau_{\mathrm{I}}}{\partial n} + \frac{\partial \tau_{\mathrm{T}}}{\partial n}} = \frac{2\frac{\partial \tau_{\mathrm{I}}}{\partial n}}{\frac{\partial \tau_{\mathrm{I}}}{\partial n} + \operatorname{sgn}\left[\frac{\partial \tau_{\mathrm{I}}}{\partial n}\right]\sqrt{p_+^2 - p_-^2 + \left(\frac{\partial \tau_{\mathrm{I}}}{\partial n}\right)^2}}. \tag{E.4.24}$$

These are the WKBJ forms of the reflection and transmission coefficients that appear in several places in the text. In the present context, they provide the initial data for the leading-order amplitudes of the reflected and transmitted wavefields. The conclusion is that, to leading order, the ray-theoretic reflection coefficients are the same as those derived for plane waves incident on planar interfaces in piecewise-constant media, except that the wave vector is a local (pointwise) quantity along the interface.

If we introduce θ_{I} as the acute angle that the incident and reflected rays make with the normal direction to the surface, then we can set

$$\frac{\partial \tau_{\mathrm{I}}}{\partial n} = \operatorname{sgn}\left[\frac{\partial \tau_{\mathrm{I}}}{\partial n}\right] p_- \cos\theta_{\mathrm{I}},$$

and rewrite the above equations as

$$R = \frac{p_- \cos\theta_{\mathrm{I}} - \sqrt{p_+^2 - p_-^2 \sin^2\theta_{\mathrm{I}}}}{p_- \cos\theta_{\mathrm{I}} + \sqrt{p_+^2 - p_-^2 \sin^2\theta_{\mathrm{I}}}}, \tag{E.4.25}$$

and

$$T = \frac{2p_- \cos\theta_{\mathrm{I}}}{p_- \cos\theta_{\mathrm{I}} + \sqrt{p_+^2 - p_-^2 \sin^2\theta_{\mathrm{I}}}}. \tag{E.4.26}$$

By using (E.4.18), recursively, we could determine the initial data for higher-order amplitudes of the wavefield. As noted above, in practice, these higher-order corrections are rarely either justified or computed.

E.5 2.5 D Ray Theory

In Chapter 6, we made use of the 2.5D ray theory of Bleistein [1986]. The objective of 2.5D ray theory (and 2.5D inversion) is to create a mathematical theory that allows us to process a single line of seismic data, but nonetheless characterize the wave propagation as being 3D. With the thought experiments that we introduced in Chapters 1 and 6, we showed that, under reasonable assumptions about the seismic survey, we needed 3D wave propagation results only in a vertical plane below the survey line. In particular, when the survey line is described by $x_2 = 0$, and it is assumed that the wavespeed is independent of x_2, we then found that we need to know only about the 3D wavefield in the vertical plane, $x_2 = 0$.

Of course, for these specialized solutions and the consequent inversion results to be of practical value, the x_1-direction should be the direction of

dominant dip in the actual Earth model. There is some discussion of this issue in the text.

Our objective, then, is to develop a special case of three-dimensional ray-theoretic wave propagation in which the wavespeed depends only on two variables, x_1 and x_3, and further specialize to evaluating this wavefield only in the vertical plane in which $x_2 = 0$. Thus, our wavefield will contain 3D geometrical spreading loss. However, as we shall see below, analysis of the 3D wavefield elements reduce to calculations in-plane only; that is, in 2D.

E.5.1 2.5D Ray Equations

We may write the ray equations for the 2.5D problem by assuming that the wavespeed varies only as $c = c(x_1, x_3)$. Then, (E.2.11) becomes

$$\begin{aligned}
\frac{dx_1}{d\sigma} &= p_1, & \frac{dp_1}{d\sigma} &= \frac{1}{2}\frac{\partial}{\partial x_1}\left[\frac{1}{c^2(x_1,x_3)}\right], \\
\frac{dx_2}{d\sigma} &= p_2, & \frac{dp_2}{d\sigma} &= \frac{1}{2}\frac{\partial}{\partial x_2}\left[\frac{1}{c^2(x_1,x_3)}\right] = 0, \\
\frac{dx_3}{d\sigma} &= p_3, & \frac{dp_3}{d\sigma} &= \frac{1}{2}\frac{\partial}{\partial x_3}\left[\frac{1}{c^2(x_1,x_3)}\right], \\
& & \frac{d\tau}{d\sigma} &= \frac{1}{c^2(x_1,x_3)}.
\end{aligned} \tag{E.5.1}$$

We may solve for p_2 and x_2 directly, to yield

$$p_2 = p_{20}, \qquad x_2 = x_{20} + p_{20}\sigma, \tag{E.5.2}$$

where $p_{20} = p_2(\boldsymbol{x}(0))$. Vertical propagation is described by those rays for which $x_2 = 0$, which can occur only if we set $p_{20} = 0$. To obtain our 2.5D wavefield from our 3D ray theory, we will repeatedly return to this specialization.

Having solved for x_2, we can now reexamine (E.5.1) in light of this solution:

$$\begin{aligned}
\frac{dx_1}{d\sigma} &= p_1, & \frac{dp_1}{d\sigma} &= \frac{1}{2}\frac{\partial}{\partial x_1}\left[\frac{1}{c^2(x_1,x_3)}\right], \\
\frac{dx_3}{d\sigma} &= p_3, & \frac{dp_3}{d\sigma} &= \frac{1}{2}\frac{\partial}{\partial x_3}\left[\frac{1}{c^2(x_1,x_3)}\right], \\
& & \frac{d\tau}{d\sigma} &= \frac{1}{c^2(x_1,x_3)}.
\end{aligned}$$

Thus, the system of ray equations in 2.5D is the same as the system we would encounter in a 2D medium with coordinates (x_1, x_3), with the eikonal equation being the same as that for a 2D problem, $p_1^2 + p_2^2 = 1/c^2(x_1, x_3)$. Of course, for the in-plane propagation, we still have one parameter free to label the rays; that will be determined as in any other 2D problem.

E.5.2 2.5D Amplitudes

Because the 2.5D problem involves the full 3D wave operator, it must be that the amplitudes (in a high-frequency sense) are governed by some form of $J_{3D}(\sigma)$.

Since $p_2 = p_{20}$ is constant on the rays, we will take that to be one of the ray parameters, say γ_2, and note that x_2 is a function of this ray parameter only. The other ray parameter, γ_1, along with p_{20}, will arise only in the solution for x_1 and x_3 along the rays. Therefore, let us examine the second column of J_{3D}, which involves only derivatives of x_2 with respect to the ray parameters. We find that

$$\frac{dx_2}{d\sigma} = p_{20}, \quad \frac{dx_2}{d\gamma_1} = 0, \quad \frac{dx_2}{d\gamma_2} = \sigma.$$

We evaluate J_{3D} at $p_2 = 0$, in order to determine the special Jacobian that we define as $J_{2.5D}$. We find that

$$J_{2.5D}(\sigma) = \det \begin{vmatrix} \frac{\partial x_1}{\partial \sigma} & p_2 & \frac{\partial x_3}{\partial \sigma} \\ \frac{\partial x_1}{\partial \gamma_1} & \frac{\partial x_2}{\partial \gamma_1} & \frac{\partial x_3}{\partial \gamma_1} \\ \frac{\partial x_1}{\partial p_2} & \sigma & \frac{\partial x_3}{\partial p_2} \end{vmatrix} = \det \begin{vmatrix} \frac{\partial x_1}{\partial \sigma} & 0 & \frac{\partial x_3}{\partial \sigma} \\ \frac{\partial x_1}{\partial \gamma_1} & 0 & \frac{\partial x_3}{\partial \gamma_1} \\ \frac{\partial x_1}{\partial p_2} & \sigma & \frac{\partial x_3}{\partial p_2} \end{vmatrix}_{p_2=0}$$

$$J_{2.5D}(\sigma) = \sigma J_{2D}(\sigma). \tag{E.5.3}$$

The zeros here are a consequence of the specific evaluation at $p_{20} = 0$ and the fact that x_2 is independent of γ_1 as can be seen from (E.5.2); that is, x_2 is a function of σ and p_{20} only.

E.5.3 The 2.5D Transport Equation

Given the 2.5D ray Jacobian and eikonal equations, it is possible compute 3D amplitudes in a wavespeed profile that varies in only two dimensions if we restrict our evaluation to the vertical plane, $x_2 = 0$. However, to complete the analogy between 2D or 3D, and 2.5D, we will derive a 2.5D transport equation [Stockwell, 1995b]. That is, we want to derive an in-plane ($x_2 = 0$) propagating equation for the 3D amplitude, under the assumption that the wavespeed is independent of x_2.

We begin with (E.3.12) and evaluate that equation in-plane as follows.

$$2\nabla_{2D}\tau(\boldsymbol{x}) \cdot \nabla_{2D} A(\boldsymbol{x}) + A(\boldsymbol{x}) \left[\nabla^2_{2D}\tau(\boldsymbol{x}) + \frac{\partial^2 \tau(\boldsymbol{x})}{\partial x_2^2} \right] = 0, \qquad x_2 = 0. \tag{E.5.4}$$

Here, we have already simplified the first term with the observation that the second component of $\nabla\tau = p_2$ is equal to zero when we evaluate this equation in-plane. We have also separated the Laplacian into two terms. In

the first term, we can evaluate both A and τ at $x_2 = 0$. In the second term, we must determine the second derivative with respect to x_2 before setting x_2 equal to zero. We can do this indirectly, by using the ray equation for x_2, (E.5.2). It is important to realize here that the ray parameters $p_2 = p_{20}$ and σ can be viewed as functions of x_2, determined by solving the parametric equations for the rays for these variables (and γ_1). Thus, we differentiate this equation implicitly with respect to x_2 to obtain

$$1 = \frac{\partial p_2}{\partial x_2}\sigma + p_2\frac{\partial \sigma}{\partial x_2} = \frac{\partial^2 \tau}{\partial x_2}\sigma + p_2\frac{\partial \sigma}{\partial x_2}.$$

Now, we can solve this equation for the second derivative we seek:

$$\frac{\partial^2 \tau}{\partial x_2^2} = \frac{1}{\sigma}\left[1 - p_2\frac{\partial \sigma}{\partial x_2}\right].$$

We do not know the derivative of σ with respect to x_2. Thus, in general, we cannot use this equation to solve for the τ-derivative we seek. However, in-plane, we know that $p_2 = 0$. Further, by examining power series solutions near $p_2 = 0$, one can verify that the σ-derivative is finite there. In fact, σ has a minimum on the in-plane ray, when compared to nearby values for nonzero x_2 and $\partial\sigma/\partial x_2 = 0$.

Thus, we conclude that the full 3D Laplacian of τ is given by the following decomposition in the $x_2 = 0$-plane

$$\nabla^2\tau(x_1, x_2, x_3)\big|_{x_2=0} = \frac{1}{\sigma} + \nabla_{2D}^2\tau(x_1, 0, x_3),$$

We now use (E.3.12) to rewrite this result in terms of Jacobians:

$$\frac{d}{d\sigma}\left[\ln J_{3D}(\sigma)\right]\Big|_{x_2=0} = \frac{1}{\sigma} + \frac{d}{d\sigma}\left[\ln J_{2D}(\sigma)\right].$$

This result can be used to rewrite (E.5.4) as

$$2\nabla_{2D}\tau(\boldsymbol{x}) \cdot \nabla_{2D}A(\boldsymbol{x}) + A(\boldsymbol{x})\nabla_{2D}^2\tau(\boldsymbol{x}) + \frac{A(\boldsymbol{x})}{\sigma} = 0, \tag{E.5.5}$$

where $\boldsymbol{x} = (x_1, 0, x_3)$. We see that this equation is the 2D transport equation plus an extra term containing the out-of-plane component of geometrical spreading.

To continue the analogy between 2.5D ray amplitude theory and the corresponding theory in two and three dimensions, we may also write (E.5.5) in the form of an exact divergence as,

$$\nabla_{2D} \cdot \left(\sigma A^2(\boldsymbol{x}\nabla_{2D}\tau(\boldsymbol{x})\right) = 0, \quad \boldsymbol{x} = (x_1, 0, x_3). \tag{E.5.6}$$

This result may be verified by directly applying the 2D divergence in (E.5.6) to yield

$$2\sigma A\nabla_{2D}\tau(\boldsymbol{x}) \cdot \nabla_{2D}A(\boldsymbol{x}) + \sigma A^2(\boldsymbol{x})\nabla_{2D}^2\tau(\boldsymbol{x}) + A^2(\boldsymbol{x})\nabla_{2D}\sigma \cdot \nabla_{2D}\tau = 0, \tag{E.5.7}$$

where $\boldsymbol{x} = (x_1, 0, x_3)$. Recognizing that $\nabla\sigma = c(\boldsymbol{x})\hat{\boldsymbol{p}}$ and $\nabla\tau = \hat{\boldsymbol{p}}/c(\boldsymbol{x})$, yields $\nabla_{2D}\sigma \cdot \nabla_{2D}\tau = 1$, in-plane. Then, dividing each term of (E.5.7) by $\sigma A(\boldsymbol{x})$ gets us back to (E.5.5). Comparing the divergence form of the 2.5D transport equation with the corresponding equation for 3D in (E.3.2) shows that $\sqrt{\sigma}A_{2D} = \text{constant} \cdot A_{2.5D}$, in agreement with the result determined from Jacobians above. Here, the constant is the ratio of the 2D to 3D amplitudes.

In addition, we may write the 2.5D result corresponding to equation (E.4.3) by substituting σJ_{2D} for J_{3D} to yield

$$g_{2.5D}(\boldsymbol{x}, \boldsymbol{x}_0, \omega) \sim A(\boldsymbol{x}, \boldsymbol{x}_0) e^{i\omega\tau(\boldsymbol{x}_0, \boldsymbol{x})} \tag{E.5.8}$$

$$= \frac{1}{4\pi}\sqrt{\frac{p(\boldsymbol{x}_0)\,\sin\phi}{\sigma J_{2D}(\sigma)}}\exp\left(i\omega\int_{\sigma_0}^{\sigma} 1/c^2(\boldsymbol{x}(\sigma'))d\sigma'\right).$$

Finally, it must be mentioned that because 2.5D ray-theoretic results are just a special case of the corresponding results in 3D, we have the same theory of reflected and transmitted waves, as discussed in Section E.4.3, except that p_2 is always zero.

E.6 Raytracing in Variable-Density Media

All of the ray-theoretic results derived in this appendix may be extended to variable-density media. The governing equation for wave propagation in such a medium is the homogeneous form of the variable-density Helmholtz equation,

$$\mathcal{L}u(\boldsymbol{x}, \omega) = \rho(\boldsymbol{x})\nabla \cdot \left[\frac{1}{\rho(\boldsymbol{x})}\nabla u(\boldsymbol{x}, \omega)\right] + \frac{\omega^2}{c^2(\boldsymbol{x})}u(\boldsymbol{x}, \omega) = 0. \tag{E.6.1}$$

Here $\rho(\boldsymbol{x})$ is the density of the medium.

As in the constant-density problem, we substitute a series trial solution,

$$u(\boldsymbol{x}, \omega) \sim \omega^{\beta} e^{i\omega\tau(\boldsymbol{x})} \sum_{j=0}^{\infty} \frac{B_j(\boldsymbol{x})}{(i\omega)^j}, \tag{E.6.2}$$

into (E.6.1) to yield the series

$$\mathcal{L}u = \omega^{\beta} e^{i\omega\tau} \sum_{j=0}^{\infty} \frac{1}{(i\omega)^j}\left[\omega^2\left\{\frac{1}{c^2} - (\nabla\tau)^2\right\}B_j\right. \tag{E.6.3}$$

$$\left. + i\omega\left\{2\nabla\tau \cdot \nabla B_j + \rho\nabla(1/\rho) \cdot \nabla\tau B_j + B_j\nabla^2\tau\right\} + \nabla^2 B_j\right].$$

As above, we set the coefficients of each power of ω equal to zero. Setting the coefficient of the term of order $\omega^{\beta+2}$ equal to zero leads to the same eikonal equation as was obtained for constant-density wave propagation.

Thus, variable density does not affect wavespeed. That is, kinematically, variable-density media are the same as constant-density media.

E.6.1 Ray Amplitude Theory in Variable-Density Media

Setting the coefficient of the term of order $\omega^{\beta+1}$ equal to zero leads to the (first) transport equation,

$$2\nabla\tau \cdot \nabla B + \rho\nabla(1/\rho) \cdot \nabla\tau B + B\nabla^2\tau = 0, \tag{E.6.4}$$

where we have dropped the subscript, writing B_0 simply as B. Here can see that variable density *does* effect amplitudes. To see how, we multiply equation (E.6.4) through by a factor of B/ρ, yielding

$$\frac{2B}{\rho}\nabla\tau \cdot \nabla B + B^2\nabla\left(\frac{1}{\rho}\right) \cdot \nabla\tau + \frac{B^2}{\rho}\nabla^2\tau = 0. \tag{E.6.5}$$

The left side of this equation is an exact divergence, leading to the equation

$$\nabla \cdot \left(\frac{B^2}{\rho}\nabla\tau\right) = 0. \tag{E.6.6}$$

By comparing equations (E.3.2) and (E.6.6) we see that $B/\sqrt{\rho}$ satisfies the same differential equation as A; thus the amplitudes of the variable-density problem differ from the amplitudes of the constant-density problem only by a factor that is proportional to $\sqrt{\rho(\boldsymbol{x})}$, such that

$$B(\boldsymbol{x}, \boldsymbol{x}_0) = \text{constant} \cdot \sqrt{\rho(\boldsymbol{x})}A(\boldsymbol{x}, \boldsymbol{x}_0). \tag{E.6.7}$$

To find the constant multiplier on the right-hand side, we consider the source region to be both constant wavespeed and constant density. In this case, $B = A$. This is true only if the constant $= 1/\sqrt{\rho(\boldsymbol{x}_0)}$, where $\rho(\boldsymbol{x}_0)$ is the density at the source point. Thus,

$$B(\boldsymbol{x}, \boldsymbol{x}_0) = \sqrt{\frac{\rho(\boldsymbol{x})}{\rho(\boldsymbol{x}_0)}}A(\boldsymbol{x}, \boldsymbol{x}_0). \tag{E.6.8}$$

This means that we may write the variable-density result corresponding to equation (E.4.3) as

$$\begin{aligned} g^{vd}(\boldsymbol{x}, \boldsymbol{x}_0, \omega) &\sim B(\boldsymbol{x}, \boldsymbol{x}_0)e^{i\omega\tau(\boldsymbol{x}_0, \boldsymbol{x})} \\ &= \frac{1}{4\pi}\sqrt{\frac{\rho(\boldsymbol{x})p(\boldsymbol{x}_0)\ \sin\phi}{\rho(\boldsymbol{x}_0)J_{3D}(\sigma)}}\exp\left(i\omega\int_{\sigma_0}^{\sigma} 1/c^2(\boldsymbol{x}(\sigma'))d\sigma'\right). \end{aligned} \tag{E.6.9}$$

Also, we may write the 2.5D, variable-density, ray-theoretic Green's function by making a similar modification to equation (E.5.8),

$$\begin{aligned} g^{vd}_{2.5D}(\boldsymbol{x}, \boldsymbol{x}_0, \omega) &\sim B(\boldsymbol{x}, \boldsymbol{x}_0)e^{i\omega\tau(\boldsymbol{x}_0, \boldsymbol{x})} \\ &= \frac{1}{4\pi}\sqrt{\frac{\rho(\boldsymbol{x})p(\boldsymbol{x}_0)\ \sin\phi}{\rho(\boldsymbol{x}_0)\sigma J_{2D}(\sigma)}}\exp\left(i\omega\int_{\sigma_0}^{\sigma} 1/c^2(\boldsymbol{x}(\sigma'))d\sigma'\right). \end{aligned} \tag{E.6.10}$$

In Section 5.6, we point out that the Green's function and its adjoint are related by

$$g^\star(\boldsymbol{x}, \boldsymbol{x}_0, \omega) = g(\boldsymbol{x}_0, \boldsymbol{x}, \omega).$$

We can see from the analysis here that the only asymmetry in the WKBJ Green's function is in the amplitude $B(\boldsymbol{x}, \boldsymbol{x}_0)$ in (E.6.8). Thus, we can immediately write down the relationship between the amplitude, $B^\star(\boldsymbol{x}, \boldsymbol{x}_0)$, of the adjoint Green's function and the amplitude, $A(\boldsymbol{x}, \boldsymbol{x}_0)$, which is to say,

$$B^\star(\boldsymbol{x}(\boldsymbol{x}_0) = \sqrt{\frac{\rho(\boldsymbol{x}_0)}{\rho(\boldsymbol{x})}} A(\boldsymbol{x}, \boldsymbol{x}_0).$$

Thus, by just using the ratio $\sqrt{\rho(\boldsymbol{x}_0)/\rho(\boldsymbol{x})}$ in place of $\sqrt{\rho(\boldsymbol{x})/\rho(\boldsymbol{x}_0)}$ in (E.6.9) and (E.6.10), we obtain the leading-order WKBJ adjoint Green's functions for the variable density wave equation.

E.6.2 Reflected and Transmitted Rays in Variable-Density Media

We may complete the discussion of ray-theoretic results by formulating reflection and transmission coefficients in variable-density media, as we did in Section E.4.3. That is, we again want to determine initial data for the amplitude of the reflected and transmitted waves in terms of the amplitude and traveltime of the incident wave. As a first interface condition we again require that the total wavefield be continuous. Thus, the analysis for the initial values of the traveltime and ray directions of the reflected and transmitted wavefields are the same as for the constant-density case.

The variable-density case differs from the constant-density case in the choice of second boundary condition: consistent with the differential equation (E.6.1) we require that $1/\rho$ times the normal derivative be continuous. If we again use subscripts, $-$ on the incident wave side and $+$ on the transmitted wave side of the boundary, then equation (E.4.18) is replaced by

$$\sum_{j=0}^{\infty} \left\{ \frac{1}{(i\omega)^{j-1}} \left[\frac{1}{\rho_-} \frac{\partial \tau_{\mathrm{I}}}{\partial n} B_j^{\mathrm{I}}(\boldsymbol{x}) + \frac{1}{\rho_-} \frac{\partial \tau_{\mathrm{R}}}{\partial n} B_j^{\mathrm{R}}(\boldsymbol{x}) - \frac{1}{\rho_+} \frac{\partial \tau_{\mathrm{T}}}{\partial n} B_j^{\mathrm{T}}(\boldsymbol{x}) \right] \right.$$
$$\left. + \frac{1}{(i\omega)^j} \left[\frac{1}{\rho_-} \frac{\partial B_j^{\mathrm{I}}}{\partial n} + \frac{1}{\rho_-} \frac{\partial B_j^{\mathrm{R}}}{\partial n} - \frac{1}{\rho_+} \frac{\partial B_j^{\mathrm{T}}}{\partial n} \right] \right\} = 0.$$

The equations corresponding to (E.4.20) and (E.4.21) now become

$$\frac{1}{\rho_-} \frac{\partial \tau_{\mathrm{I}}}{\partial n} B_0^{\mathrm{I}}(\boldsymbol{x}) + \frac{1}{\rho_-} \frac{\partial \tau_{\mathrm{R}}}{\partial n} B_0^{\mathrm{R}}(\boldsymbol{x}) = \frac{1}{\rho_+} \frac{\partial \tau_{\mathrm{T}}}{\partial n} B_0^{\mathrm{T}}(\boldsymbol{x}),$$
$$B_0^{\mathrm{I}} + B_0^{\mathrm{R}} = B_0^{\mathrm{T}}. \tag{E.6.11}$$

It is apparent that the solutions of these equations are exactly like our constant-density results, provided we make the following replacements

$$\frac{\partial \tau_{\mathrm{I}}}{\partial n} \to \frac{1}{\rho_-}\frac{\partial \tau_{\mathrm{I}}}{\partial n}, \quad \frac{\partial \tau_{\mathrm{R}}}{\partial n} \to \frac{1}{\rho_-}\frac{\partial \tau_{\mathrm{R}}}{\partial n}, \quad \frac{\partial \tau_{\mathrm{T}}}{\partial n} \to \frac{1}{\rho_+}\frac{\partial \tau_{\mathrm{T}}}{\partial n}.$$

Thus, we set

$$B_0^{\mathrm{R}} = RB_0^{\mathrm{I}}, \quad \text{and} \quad B_0^{\mathrm{T}} = TB_0^{\mathrm{I}}. \tag{E.6.12}$$

We can solve for the variable-density reflection coefficient R as

$$R = \frac{\frac{1}{\rho_-}\frac{\partial \tau_{\mathrm{I}}}{\partial n} - \frac{1}{\rho_+}\frac{\partial \tau_{\mathrm{T}}}{\partial n}}{\frac{1}{\rho_-}\frac{\partial \tau_{\mathrm{I}}}{\partial n} + \frac{1}{\rho_+}\frac{\partial \tau_{\mathrm{T}}}{\partial n}} = \frac{\frac{1}{\rho_-}\frac{\partial \tau_{\mathrm{I}}}{\partial n} - \frac{1}{\rho_+}\operatorname{sgn}\left[\frac{\partial \tau_{\mathrm{I}}}{\partial n}\right]\sqrt{p_+^2 - p_-^2 + \left(\frac{\partial \tau_{\mathrm{I}}}{\partial n}\right)^2}}{\frac{1}{\rho_-}\frac{\partial \tau_{\mathrm{I}}}{\partial n} + \frac{1}{\rho_+}\operatorname{sgn}\left[\frac{\partial \tau_{\mathrm{I}}}{\partial n}\right]\sqrt{p_+^2 - p_-^2 + \left(\frac{\partial \tau_{\mathrm{I}}}{\partial n}\right)^2}}, \tag{E.6.13}$$

and the transmission coefficient T as

$$T = \frac{\frac{2}{\rho_+}\frac{\partial \tau_{\mathrm{I}}}{\partial n}}{\frac{1}{\rho_-}\frac{\partial \tau_{\mathrm{I}}}{\partial n} + \frac{1}{\rho_+}\frac{\partial \tau_{\mathrm{T}}}{\partial n}} = \frac{\frac{2}{\rho_+}\frac{\partial \tau_{\mathrm{I}}}{\partial n}}{\frac{1}{\rho_-}\frac{\partial \tau_{\mathrm{I}}}{\partial n} + \frac{1}{\rho_+}\operatorname{sgn}\left[\frac{\partial \tau_{\mathrm{I}}}{\partial n}\right]\sqrt{p_+^2 - p_-^2 + \left(\frac{\partial \tau_{\mathrm{I}}}{\partial n}\right)^2}}. \tag{E.6.14}$$

These are the WKBJ forms of the reflection and transmission coefficients in the variable-density case. As in previous cases, the WKBJ results reduce to plane-wave reflection and transmission coefficients for constant wavespeed and density, and a plane interface.

Again, as we did in the constant density case, we introduce θ_{I} as the acute angle that the incident and reflected rays make with the normal direction to the surface. Then, the variable-density reflection coefficients become

$$R = \frac{\frac{p_-}{\rho_-}\cos\theta_{\mathrm{I}} - \frac{1}{\rho_+}\sqrt{p_+^2 - p_-^2\sin^2\theta_{\mathrm{I}}}}{\frac{p_-}{\rho_-}\cos\theta_{\mathrm{I}} + \frac{1}{\rho_+}\sqrt{p_+^2 - p_-^2\sin^2\theta_{\mathrm{I}}}} \tag{E.6.15}$$

and

$$T = \frac{2\frac{p_-}{\rho_-}\cos\theta_{\mathrm{I}}}{\frac{p_-}{\rho_-}\cos\theta_{\mathrm{I}} + \frac{1}{\rho_+}\sqrt{p_+^2 - p_-^2\sin^2\theta_{\mathrm{I}}}}. \tag{E.6.16}$$

E.7 Dynamic Raytracing

The term "dynamic raytracing" refers to a method of generating ray amplitudes by solving additional ordinary differential equations along the rays

to obtain the elements of the ray Jacobian, (E.3.6). (The most extensive discussion of dynamic raytracing, along with citations for original sources, can be found in Červený [2000].) Because we already have an equation for the elements of the first vector in that equation, dynamic ray tracing amounts to deriving differential equations for the vectors $\partial \boldsymbol{x}/\partial\gamma_1$ and $\partial \boldsymbol{x}/\partial\gamma_2$. These differential equations are derivable from the ray equations that we already have. Specifically, we start from the first six equations in (E.2.13) that are formulated in arclength coordinates. We prefer, for this discussion, to rewrite those equations as

$$\frac{d\boldsymbol{x}}{ds} = c(\boldsymbol{x})\boldsymbol{p} \qquad \frac{d\boldsymbol{p}}{ds} = \nabla\left[\frac{1}{c(\boldsymbol{x})}\right]. \tag{E.7.1}$$

For the moment, there is no need to distinguish between γ_1 and γ_2, so we will consider a *generic* variable, γ, that labels the rays, with arclength s as the running parameter along each ray. Further, let us define the γ-derivatives by using the new symbols $\boldsymbol{Q}$ and $\boldsymbol{P}$,

$$\frac{\partial \boldsymbol{x}}{\partial\gamma} = \boldsymbol{Q}, \qquad \frac{\partial \boldsymbol{p}}{\partial\gamma} = \boldsymbol{P}, \tag{E.7.2}$$

to simplify the notation.

We begin the derivation of the new equations by differentiating both equations in (E.7.1) with respect to γ, noting that the order of differentiation in γ and s can be interchanged, as these are independent variables on the family of rays. The result of this differentiation is a system of ordinary differential equations for the propagation of $\boldsymbol{Q}$ and $\boldsymbol{P}$ along the rays. Those equations are

$$\frac{d\boldsymbol{Q}}{ds} = c(\boldsymbol{x})\boldsymbol{P} + \boldsymbol{p}\nabla v \cdot \boldsymbol{Q}, \qquad \frac{d\boldsymbol{P}}{ds} = \boldsymbol{Q} \cdot \nabla\left[\nabla\left[\frac{1}{c(\boldsymbol{x})}\right]\right]. \tag{E.7.3}$$

These equations can be simplified by using the fact that the derivative of $\boldsymbol{Q}$ is orthogonal to the ray. This can be seen by differentiating the following dot product of a unit vector with itself:

$$\frac{d\boldsymbol{x}}{ds} \cdot \frac{d\boldsymbol{x}}{ds} = 1.$$

Differentiation of the right-hand side yields 0, so we have from the differentiation of the left-hand side,

$$0 = \frac{\partial}{\partial\gamma}\left[\frac{d\boldsymbol{x}}{ds} \cdot \frac{d\boldsymbol{x}}{ds}\right] = 2\frac{d\boldsymbol{Q}}{ds} \cdot \frac{d\boldsymbol{x}}{ds}.$$

We take the dot product of the first vector differential equation in (E.7.3) with $d\boldsymbol{x}/ds$ to obtain

$$0 = c(\boldsymbol{x})\boldsymbol{P} \cdot \frac{d\boldsymbol{x}}{ds} + \left(\frac{d\boldsymbol{x}}{ds} \cdot \boldsymbol{p}\right)(\nabla v \cdot \boldsymbol{Q})$$

$$= c(\boldsymbol{x})\boldsymbol{P} \cdot \frac{d\boldsymbol{x}}{ds} + \frac{1}{c(\boldsymbol{x})} \nabla v \cdot \boldsymbol{Q}. \tag{E.7.4}$$

This equation allows us to solve for $\nabla v \cdot \boldsymbol{Q}$ in terms of $\boldsymbol{P}$ and substitute the result back into (E.7.3), yielding

$$\frac{d\boldsymbol{Q}}{ds} = c(\boldsymbol{x})\boldsymbol{P} - c(\boldsymbol{x})\boldsymbol{P} \cdot \frac{d\boldsymbol{x}}{ds} \frac{d\boldsymbol{x}}{ds}. \tag{E.7.5}$$

The role of the second term, here, is now more apparent. We know that $d\boldsymbol{Q}/ds$ is orthogonal to the ray. However, that need not be true for $c(\boldsymbol{x})\boldsymbol{P}$. The second term subtracts out the component of $c(\boldsymbol{x})\boldsymbol{P}$ along the ray, to make the right side orthogonal to the ray, as well.

We propose, now to write our system of equations in matrix form for the vectors written vertically—we will not bother with a superscript T to denote the transpose. Using (E.7.5) for the differential equation for $\boldsymbol{Q}$ and (E.7.3) for the differential equation for $\boldsymbol{P}$, we find that

$$\frac{d\boldsymbol{Q}}{ds} = c(\boldsymbol{x})\,[I - D]\,\boldsymbol{P}, \qquad \frac{d\boldsymbol{P}}{ds} = W\boldsymbol{Q}. \tag{E.7.6}$$

In these equations,

$$W_{ij} = \frac{\partial^2 (1/c(\boldsymbol{x}))}{\partial x_i \partial x_j} = -\frac{1}{c^2(\boldsymbol{x})} \frac{\partial^2 c(\boldsymbol{x})}{\partial x_i \partial x_j} + \frac{2}{c^3(\boldsymbol{x})} \frac{\partial c(\boldsymbol{x})}{\partial x_i} \frac{\partial c(\boldsymbol{x})}{\partial x_j},$$

$$D_{ij} = \frac{dx_i}{ds} \frac{dx_j}{ds} = c^2(\boldsymbol{x}) p_i p_j, \qquad i,j = 1,2,3. \tag{E.7.7}$$

Now, we only need to use this same system of equations, with $\gamma = \gamma_1$ or $\gamma = \gamma_2$, to determine the propagation of the vectors of the second and third rows of the ray Jacobian along the rays. They will only be distinguished by their initial conditions. When solving, then, we would use these equations with $\boldsymbol{P}$ and $\boldsymbol{Q}$ distinguished, say, by a superscript, as follows:

$$\frac{\partial \boldsymbol{x}}{\partial \gamma_i} = \boldsymbol{Q}^{(i)}, \qquad \frac{\partial \boldsymbol{p}}{\partial \gamma_i} = \boldsymbol{P}^{(i)}, \qquad i = 1,2. \tag{E.7.8}$$

Červený [2000] presents the equations (E.7.7) in different coordinate systems and with respect to different ray parameters. One distinguished system is called *ray-centered coordinates*, which he denotes by $\boldsymbol{q} = (q_1, q_2, q_3)$. The coordinate, q_3 is a running parameter along the ray, such as our σ, s, or τ. The coordinates (q_1, q_2), are coordinates in a right-handed orthogonal system centered on a specific ray, denoted by Ω. This system of coordinates confines $\boldsymbol{P}$ and $\boldsymbol{Q}$ to the plane orthogonal to the ray direction, so that it is necessary to solve for only two components of $\boldsymbol{Q}$ and two components of $\boldsymbol{P}$; thus, ray centered coordinates lead to a system of four equations, while the result here is a system of six equations. However, the point of this discussion is not necessarily the determination of an optimum system of equations for computation, but only a demonstration of the

possibility of determining the amplitude from a system of equations that describes the propagation of $\boldsymbol{Q}^{(1)}$ and $\boldsymbol{Q}^{(2)}$ along the rays.

On the other hand, equations (E.7.6) and (E.7.7) tells us something about the types of wavespeed model we need in order to obtain a well-posed[6] solution for the amplitude. For linear systems of ordinary differential equations, such as this one for the combined variables $\boldsymbol{P}$ and $\boldsymbol{Q}$, the criterion reduces to boundedness of the elements of the matrix of coefficients on the right side of the equation. Because those coefficients depend on derivatives of the propagation speed, their boundedness implies a requirement of boundedness on those derivatives. In this example, then, it is necessary for the second derivatives of the wave speed, which appear in W, to be bounded in order that the solution be well-posed. Indeed for numerical computation, we need this boundedness of the second derivatives, as well.

If there are to be interfaces in our model, across which the propagation speed is discontinuous, then we need to do something other than integrating the differential equations across those interfaces in order to obtain the solution. In fact, we imposed interface conditions and solved for reflection and transmission coefficients to get through the interfaces, beyond which the solution for rays and amplitude can be continued by solving the system of differential equations, again.

This constraint on second derivatives further suggests that the interfaces have to be reasonably well behaved also. It is necessary that second derivatives can be calculated in arbitrary directions on either side of the interface, right up to the interface. In some sense, then, the interface itself has to be sufficiently smooth, say, with a differentiable normal, implying differentiable tangent vectors along the interface. This is important in numerical modeling.

Further, wavespeeds that are continuous, but have a discontinuous derivative, are not smooth enough for well-posed amplitude calculations. This is a popular type of model for raytracing in which the wavespeed model is described on a tetrahedral grid (triangular grid in 2D) in which the grid is small enough that a constant gradient wavespeed in each grid element is sufficient to describe a complex model. The discontinuity of the first derivative of the wavespeed across grid boundaries implies an unbounded second derivative and ill-posedness for amplitude calculations.

E.7.1 A Simple Example, Raytracing in Constant-Wavespeed Media

We will show, here, a simple calculation of $\boldsymbol{P}$ and $\boldsymbol{Q}$ for the example of Section E.4.1. We take the ray parameters of that example to be

---

[6]Recall, from Appendix D that a solution is well-posed if it exists, is unique, and depends continuously on the initial data.

$$\theta = \gamma_1, \quad \phi = \gamma_2.$$

The initial data for the problem are

$$\boldsymbol{x} = \boldsymbol{x}_0, \quad \boldsymbol{p} = p_0 \hat{\boldsymbol{r}}_0(\boldsymbol{\gamma}), \quad s = 0. \tag{E.7.9}$$

In this equation,

$$p_0 = 1/c_0, \quad \hat{\boldsymbol{r}}_0(\boldsymbol{\gamma}) = (\cos\gamma_1 \sin\gamma_2, \sin\gamma_1, \sin\gamma_2, \cos\gamma_2).$$

For constant wave speed, $\boldsymbol{p}$ is constant on the rays, given by its initial value above. The solution of the ray equations for $\boldsymbol{x}$, in arclength variables, (E.2.13), is

$$\boldsymbol{x} = \boldsymbol{x}_0 + s\hat{\boldsymbol{r}}_0(\boldsymbol{\gamma}). \tag{E.7.10}$$

Then, by direct differentiation, we find that

$$\boldsymbol{Q}^{(1)} = s\sin\gamma_2 \hat{\boldsymbol{\gamma}}_1, \qquad \boldsymbol{Q}^{(2)} = s\hat{\boldsymbol{\gamma}}_2, \tag{E.7.11}$$

with the two unit vectors here given by

$$\hat{\boldsymbol{\gamma}}_1 = (-\sin\gamma_1, \cos\gamma_1, 0), \qquad \hat{\boldsymbol{\gamma}}_2 = (\cos\gamma_1 \cos\gamma_2, \sin\gamma_1 \cos\gamma_2, -\sin\gamma_2). \tag{E.7.12}$$

It is now an easy matter to take the triple scalar product and find that

$$J = \frac{d\boldsymbol{x}}{ds} \cdot \boldsymbol{Q}^{(1)} \times \boldsymbol{Q}^{(2)} = s^2 \sin\gamma_2. \tag{E.7.13}$$

Now, we want to determine $\boldsymbol{Q}^{(1)}$ and $\boldsymbol{Q}^{(2)}$ from the differential equations (E.7.6). First, we need the initial values for these variables. Those are obtained by differentiating the initial values for $\boldsymbol{x}$ and $\boldsymbol{p}$ with respect to γ_1 and γ_2 in equation (E.7.9). Thus, we find that

$$\boldsymbol{Q}^{(1)} = \boldsymbol{Q}^{(2)} = \boldsymbol{0}, \quad \boldsymbol{P}^{(1)} = p_0 \hat{\boldsymbol{\gamma}}_1 \sin\gamma_2, \quad \boldsymbol{P}^{(2)} = p_0 \hat{\boldsymbol{\gamma}}_2. \tag{E.7.14}$$

For constant wave speed, W, (E.7.7), is a zero matrix and then, from (E.7.6), $\boldsymbol{P}^{(1)}$ and $\boldsymbol{P}^{(2)}$ are constant on the rays, given by their initial values, (E.7.14). Note that these initial values are both orthogonal to $d\boldsymbol{x}/ds$, so that the equations for $\boldsymbol{Q}^{(1)}$ and $\boldsymbol{Q}^{(2)}$ in (E.7.6) reduce to

$$\frac{d\boldsymbol{Q}^{(1)}}{ds} = \hat{\boldsymbol{\gamma}}_1 \sin\gamma_2, \qquad \frac{d\boldsymbol{Q}^{(2)}}{ds} = \hat{\boldsymbol{\gamma}}_2. \tag{E.7.15}$$

The solution of these two equations is just the result, (E.7.11), obtained by direct differentiation.

E.7.2 Dynamic Raytracing in σ

We can also derive dynamic equations in the ray parameter σ, for which the ray equations are given by (E.2.11). We need only differentiate that system of equations with respect to γ to conclude that

$$\frac{d\boldsymbol{Q}}{d\sigma} = \boldsymbol{P}, \qquad \frac{d\boldsymbol{P}}{d\sigma} = W^{(\sigma)}\boldsymbol{Q}. \tag{E.7.16}$$

Here,

$$W_{ij}^{(\sigma)} = \frac{1}{2}\frac{\partial^2\left(1/c^2(\boldsymbol{x})\right)}{\partial x_i \partial x_j}, \qquad i,j = 1,2,3.$$

E.7.3 Dynamic Raytracing in τ

We can derive differential equations for $\boldsymbol{P}$ and $\boldsymbol{Q}$ in terms of τ by starting from (E.2.12). The derivation is similar to the derivation of the equations in s. The result is

$$\frac{d\boldsymbol{Q}}{d\tau} = c^2(\boldsymbol{x})\left[I - D^{(\tau)}\right]\boldsymbol{P}, \qquad \frac{d\boldsymbol{P}}{d\tau} = W^{(\tau)}\boldsymbol{Q}. \tag{E.7.17}$$

Here,

$$W_{ij}^{(\tau)} = \frac{1}{c^2(\boldsymbol{x})}\frac{\partial c}{\partial x_i}\frac{\partial c}{\partial x_j} - \frac{1}{c(\boldsymbol{x})}\frac{\partial^2 c}{\partial x_i \partial x_j},$$

$$D_{ij}^{(\tau)} = -2\frac{1}{c^2(\boldsymbol{x})}\frac{dx_i}{d\tau}\frac{dx_j}{d\tau} = -2c^2(\boldsymbol{x})p_i p_j, \qquad i,j = 1,2,3.$$

E.7.4 Two Dimensions

Whether we are doing 2D modeling or 2.5D modeling, the ray Jacobian that is needed is J_{2D}, belonging to a two-dimensional in-plane ray-family. In this case, γ is a scalar. In fact, there is nothing new to do here to find $\partial\boldsymbol{x}/\partial\gamma$. It is only necessary to reinterpret the derivation above, in 2D. Thus, the vectors $\boldsymbol{x}$, $\boldsymbol{p}$, $\boldsymbol{Q}$ and $\boldsymbol{P}$, in the above equations, should be reinterpreted as two-dimensional vectors, and the matrices, D, W, etc., should now be interpreted as 2×2 matrices. With this done, (E.7.6) provides the equations for $\boldsymbol{Q}$ and $\boldsymbol{P}$ in s, (E.7.16) provides the equations in σ, and (E.7.17) provides the equations in τ.

E.7.5 Conclusions

In summary, we have derived a system of equations that describes the propagation of the second and third rows of the matrix whose determinant is the Jacobian, J, needed in the solution for the amplitude along the rays. In this manner, the computation of the amplitude is incorporated into an enhanced system of ray equations. The differential equations are given for s, σ, or τ, the running variable along the ray. The example demonstrates the use of this system of equations to determine those Jacobian elements.

We have not described the system of equations in ray-centered coordinates. We cannot do justice to this approach in this appendix, and strongly refer the reader interested in implementation to Červený [2000].

E.8 The Kirchhoff Approximation

Green's theorem allows us to represent a wavefield on either side of a surface of infinite extent in terms of the wavefield and its normal derivative on the surface. Here, we distinguish between "representation" and "solution." By a Kirchhoff solution, we mean an integral over the surface in which the values of the wavefield are replaced by known quantities, so the representation is transformed into an integral formula that describes the wavefield away from the surface.

The Kirchhoff approximation is a means by which we can transform the Kirchhoff integral representation into an approximate solution for the wavefield "scattered" upward or downward from an infinite interface. The method can be extended in a straightforward manner to reflectors of finite extent. (That extension will be mentioned in context, below). It can also be extended to vector wavefields: elastic—both isotropic and anisotropic—and electromagnetic.

The essence of the approximation is the replacement of the unknown values of the upward and downward propagating wavefields and their normal derivatives by corresponding elements of the (assumed known) incident wavefield at the interface. Of course, we are going to use the results we developed about reflection and transmission in the earlier sections of this appendix to identify those values.

The integrand of the Kirchhoff-approximate solution will have the familiar form, $F(\omega)A\exp\{i\omega\tau\}$. When the method of stationary phase is applied to the integral, the stationary point for the upward-scattered field is the specular reflection point for the given source and receiver points; for the downward-scattered field, the stationary point is the point that couples the incident and reflect wavefields through Snell's law. When the stationary point is simple—that is, when the matrix of second derivatives is nonsingular—we would expect that the result of stationary phase will agree with the reflected or transmitted wavefield derived from ray theory. In simple examples, this can be verified, but a general proof of this agreement is not available, although it is generally accepted that the results agree. When the leading-order expansion arises from a higher order stationary point, the Kirchhoff approximation will still provide a reflected or transmitted wavefield, while the ray theory that we have developed will not. The reason is that in this case the wavefield is being evaluated right on a caustic surface where our simple ray theory breaks down because the Jacobian of the amplitude function is zero.

With appropriate modifications of the amplitude in the Kirchhoff approximation, it can further account for caustics in the wavefields of the point-source ray families from the source and receiver. Further, for finite reflectors, in regions dominated by diffractions, the Kirchhoff approximation will get the traveltime values and the amplitude decay right, but will only provide an approximate diffraction coefficient. However, in transition

regions between reflection and diffraction, the approximate diffraction is sufficiently accurate for the Kirchhoff-approximate solution to provide a usable approximation of the transitional field. Thus, for numerical modeling of the upward-scattering field, it can prove to be superior to ray methods.

Because of these features of the Kirchhoff-approximate wavefield, we hesitate to call the upward-scattered field the "reflected field," but have chosen, above, to call it the (upward) scattered field. Below, then, we will use the notation u_S for this wavefield.

The amplitude and phase of the Kirchhoff approximation are functions of the observation point, as well as functions of the integration variables. Some applications will require differentiation of this wavefield. Caution is in order when carrying out those differentiations. We need to think of the amplitude as the first term of an asymptotic expansion of the type

$$\left[A + \frac{A_1}{i\omega} + \cdots\right] e^{i\omega\tau}.$$

Here, $(\cdots)$ stands for lower-order terms in $i\omega$. Now, let D represent any sort of spatial derivative operator and calculate derivatives of this two-term expression.

$$D\left[A + \frac{A_1}{i\omega} + \cdots\right] e^{i\omega\tau} = \left[i\omega\left(A(D\tau) + DA + A_1(D\tau)\right) + \cdots\right] e^{i\omega\tau}$$

$$D^2\left[A + \frac{A_1}{i\omega} + \cdots\right] e^{i\omega\tau}$$

$$= \left[(i\omega)^2 A(D^2\tau) + i\omega\{2(DA)(D\tau) + A(D^2\tau) + A_1(D^2\tau)\} + \cdots\right] e^{i\omega\tau}.$$

At each order of differentiation, we can see that the second order expression on the right side involves both A and A_1. Thus if, in the integrand of the Kirchhoff-approximation of the wavefield, we use only the amplitude, A, and do not include the first correction term, A_1, we can only retain the first-term approximation of the derivatives of the amplitude; the second-order term arising from differentiation of A and τ only, is incorrect.

There is one exception to this rule. Suppose that $D = \nabla$, for which $D^2 = \nabla^2$ and $(DA)(D\tau) = \nabla A \cdot \nabla\tau$. Suppose further that the phase satisfied an eikonal equation,

$$(\nabla\tau)^2 = \frac{1}{c^2}.$$

Now consider the combination,

$$\left[\nabla^2 + \frac{\omega^2}{c^2}\right]\left[A + \frac{A_1}{i\omega} + \cdots\right] e^{i\omega\tau} = \left[i\omega[2(\nabla A)(\nabla\tau) + A(\nabla^2\tau)] + \cdots\right] e^{i\omega\tau},$$

just as in our development of ray theory. Now the two-term expansion has led to a leading-order expression solely in terms of τ and A; that is, not involving the next order amplitude, A_1. Hence, for this exceptional case,

a two-order expansion in $i\omega$ is valid. This idea is exploited in Section 3.8, where the phase satisfies the eikonal equation with wavespeed, $c/2$.

E.8.1 Problem Formulation

Let us consider a problem in which a point source is set off above an infinite interface, denoted by S, across which the propagation speed $c(\boldsymbol{x})$ and/or the density $\rho(\boldsymbol{x})$, changes. As earlier in this appendix, we will use a subscripts $-$ and $+$ on variables above and below S, respectively. Thus, the total wavefield is governed by equation (E.6.1) with subscripts $-$ above the interface, and by the same equation with subscripts $+$ on the coefficients below the interface. When necessary to distinguish the differential operator below the interface, we will use a subscript $+$ on the operator, as well.

The total field is assumed to satisfy the Sommerfeld radiation conditions, which are

$$\lim_{r\to\infty} ru = \text{bounded}, \quad \lim_{r\to\infty} r\left[\frac{\partial u}{\partial r} - \frac{i\omega}{c}u\right] = 0. \tag{E.8.1}$$

Furthermore, the total field satisfies the equations,

$$\begin{aligned}
\mathcal{L}_- u(\boldsymbol{x}, \boldsymbol{x}_s\omega) &= \rho_-(\boldsymbol{x})\nabla\cdot\left[\frac{1}{\rho_-(\boldsymbol{x})}\nabla u(\boldsymbol{x}, \boldsymbol{x}_s\omega)\right] + \frac{\omega^2}{c^2(\boldsymbol{x})}u(\boldsymbol{x}, \omega) \\
&= -F(\omega)\delta(\boldsymbol{x} - \boldsymbol{x}_s), \qquad \text{above } S, \\
\mathcal{L}_+ u(\boldsymbol{x}, \boldsymbol{x}_s\omega) &= \rho_+(\boldsymbol{x})\nabla\cdot\left[\frac{1}{\rho_+(\boldsymbol{x})}\nabla u(\boldsymbol{x}, \boldsymbol{x}_s\omega)\right] + \frac{\omega^2}{c_+^2(\boldsymbol{x})}u(\boldsymbol{x}, \boldsymbol{x}_s\omega) \\
&= 0, \qquad \text{below } S.
\end{aligned} \tag{E.8.2}$$

We write the total solution as follows:

$$u = \begin{cases} u_I + u_S, & \text{above } S, \\ u_T, & \text{below } S. \end{cases} \tag{E.8.3}$$

We think of u_I as "the incident wave," u_S as the "scattered wave" above the reflector, and u_T as the "transmitted wave" below the reflector. We further require that

$$\begin{aligned}
\mathcal{L}_- u_I(\boldsymbol{x}, \boldsymbol{x}_s, \omega) = -F(\omega)\delta(\boldsymbol{x} - \boldsymbol{x}_s), \quad \mathcal{L}_- u_S(\boldsymbol{x}, \boldsymbol{x}_s, \omega) = 0, \quad \text{above } S, \\
\mathcal{L}_+ u_T(\boldsymbol{x}, \boldsymbol{x}_s, \omega) = 0, \quad \text{below } S.
\end{aligned} \tag{E.8.4}$$

Actually, for u_I, we propose to consider an extended wavefield below S in which the wavespeed and density have been continued in a smooth manner from their values above S. Further, we want that smooth extension not to admit turned rays. Then, for any extension of the medium parameters, the ray theoretical solution for u_I will remain unchanged. We think of u_I, then, as a "free-space" incident wave.

Moreover, if we denote by $g(\boldsymbol{x}, \boldsymbol{x}_s, \omega)$ the equivalent free-space Green's function, that is, the function that satisfies the extended form of (E.8.4) with $F(\omega) = 1$, then

$$u_I(\boldsymbol{x}, \boldsymbol{x}_s, \omega) = F(\omega)\, g(\boldsymbol{x}, \boldsymbol{x}_s, \omega). \tag{E.8.5}$$

As in Section E.6.2, we couple these wavefields above and below the reflector by requiring that the total wavefield be continuous and that the normal derivative multiplied by the density also be continuous across the reflector.

Below, we will develop a Kirchhoff-approximate solution for the scattered wavefield, u_S, above the reflector.

E.8.2 Green's Theorem and the Wavefield Representation

We begin the discussion with equation (3.1.10). However, we have no need of the subscript zero, here. Thus, we rewrite that equation here as

$$\int_D \{g^\star \mathcal{L} u - u \mathcal{L}^\star g^\star\}\, dV = \int_{\partial D} \left\{ g^\star \frac{\partial u}{\partial n} - u \frac{\partial g^\star}{\partial n} \right\} dS. \tag{E.8.6}$$

In this equation, the normal direction in the differentiations is the *outward*-pointing normal to the boundary, ∂D. The function $g^\star$ is the adjoint Green's function that satisfies (5.6.2), that is,

$$\mathcal{L}^\star g^\star(\boldsymbol{x}, \boldsymbol{x}_g, \omega) = -\delta(\boldsymbol{x} - \boldsymbol{x}_g). \tag{E.8.7}$$

As with u_I, this will be a *free-space* Green's function, satisfying (5.6.2) everywhere with the medium parameters extended smoothly as described above.

We introduce a sphere of large radius, $\mathcal{R}$ (that will eventually approach infinity). See Figure E.2. This sphere will cut S in such a manner that the domains above and below S, say D_a and D_b, respectively, are roughly hemispherical. We denote by $S_{\mathcal{R}}$ the part of S inside of D and by S_a and

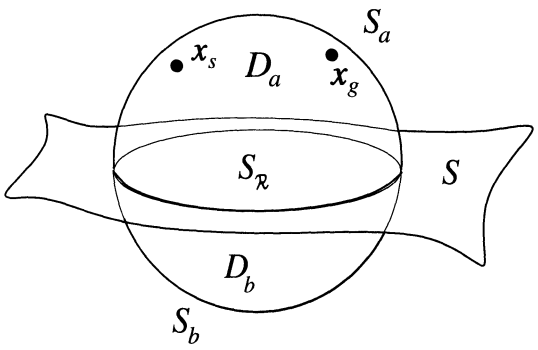

FIGURE E.2. Diagram describing the domains used in the derivation of the Kirchhoff approximation.

S_b the parts of the spherical surface, ∂D, that lie above and below S, respectively.

In (E.8.6), we take D to be D_a. In this domain, by using the differential equations (E.8.2) and (E.8.7) on the left side of (E.8.6), we may write the integral equation

$$\begin{aligned}\int_{D_a} \{g^\star \mathcal{L}u - u\mathcal{L}^\star g^\star\}\, dV &= u(\boldsymbol{x}_g, \boldsymbol{x}_s, \omega) - F(\omega) g^\star(\boldsymbol{x}_s, \boldsymbol{x}_g, \omega) \\ &= u_I(\boldsymbol{x}_g, \boldsymbol{x}_s\omega) + u_S(\boldsymbol{x}_g, \boldsymbol{x}_s\omega) - F(\omega) g^\star(\boldsymbol{x}_s, \boldsymbol{x}_g, \omega) \\ &= \int_{S_\mathcal{R}+S_a} \left\{ g^\star \frac{\partial(u_I + u_S)}{\partial n} - (u_I + u_S)\frac{\partial g^\star}{\partial n} \right\} dS.\end{aligned} \tag{E.8.8}$$

The Green's identity, (E.8.6), can also be applied to the functions, $g^\star$ and u_I themselves, yielding

$$\begin{aligned}\int_{D_a} \{g^\star \mathcal{L}u_I - u_I\mathcal{L}^\star g^\star\}\, dV &= u_I(\boldsymbol{x}_g, \boldsymbol{x}_s\omega) - F(\omega) g^\star(\boldsymbol{x}_s, \boldsymbol{x}_g, \omega) \\ &= \int_{S_\mathcal{R}+S_a} \left\{ g^\star \frac{\partial u_I}{\partial n} - u_I \frac{\partial g^\star}{\partial n} \right\} dS.\end{aligned} \tag{E.8.9}$$

We use this identity in the last two lines of the previous equation to arrive at the result

$$u_S(\boldsymbol{x}_g, \boldsymbol{x}_s\omega) = \int_{S_\mathcal{R}+S_a} \left\{ g^\star \frac{\partial u_S}{\partial n} - u_S \frac{\partial g^\star}{\partial n} \right\} dS. \tag{E.8.10}$$

The next step is to examine the consequences in this identity of the limit as $\mathcal{R}$ approaches infinity. First, note that $S_\mathcal{R}$ approaches S in that limit and we need only concern ourselves with the convergence of the integral over that surface of infinite extent; this will be discussed below.

Now consider the integral over S_a. We can set

$$dS = \mathcal{R}^2 d\Omega,$$

where $d\Omega$ represents the differential solid angle on the surface of the sphere (or, equivalently, on the surface of the unit sphere with the same center). For increasing radius, the normal to $S_\mathcal{R}$ approaches the unit vector in the Cartesian radial direction, no matter the finite difference between the center of $S_\mathcal{R}$ and the origin of the coordinate system. Thus,

$$\left\{ g^\star \frac{\partial u_S}{\partial n} - u_S \frac{\partial g^\star}{\partial n} \right\} dS = \left\{ g^\star \left[\frac{\partial u_S}{\partial \mathcal{R}} - \frac{i\omega}{c} u_S \right] - u_S \left[\frac{\partial g^\star}{\partial \mathcal{R}} - \frac{i\omega}{c} g^\star \right] \right\} \mathcal{R}^2 d\Omega.$$

On the right side, the normal direction has been identified as the direction of increasing $\mathcal{R}$. Further, the expression $i\omega u_S g^\star/c$ has been subtracted and added in order to create the linear combination of function and derivative appearing in the second Sommerfeld condition in equation (E.8.1).

Now, in each expression on the right, we combine terms to yield two factors of the form $\mathcal{R}u_S$ and $\mathcal{R}g^\star$ and two factors of the form $\mathcal{R}$ times one of the square-bracketed expressions. According to the Sommerfeld radiation conditions, the former pair of factors remains bounded as $\mathcal{R} \to \infty$ while the latter pair approaches zero in that limit. Thus, in the integral over S_a on the right side of (E.8.10), written as an integral in Ω, the integrand approaches zero with increasing $\mathcal{R}$ while the domain of integration remains bounded in Ω (by 4π). Hence, in the limit, $\mathcal{R} \to \infty$, the integral over S_a in (E.8.10) is zero. Thus, we can write

$$u_S(\boldsymbol{x}_g, \boldsymbol{x}_s\omega) = \int_S \left\{ g^\star \frac{\partial u_S}{\partial n} - u_S \frac{\partial g^\star}{\partial n} \right\} dS.$$

Finally, we will make one more change in this equation. Recall that in Green's identity, the normal direction is pointed *outward* from the domain of integration. That, in turn, implies that the normal to S here is pointed *downward*. Our preference is to have a representation in terms of an *upward* directed normal. Thus, we write

$$u_S(\boldsymbol{x}_g, \boldsymbol{x}_s\omega) = \int_S \left\{ u_S \frac{\partial g^\star}{\partial n} - g^\star \frac{\partial u_S}{\partial n} \right\} dS, \tag{E.8.11}$$

where now it is to be understood that $\hat{\boldsymbol{n}}$ is an *upward*-pointing normal to the surface S. This, then, is our representation of the upward-scattered field above a surface in terms of the values of the wavefield and its normal derivative on the surface.

It should be noted that S need not necessarily be a reflecting surface with discontinuous medium parameters on the two sides. The derivation, up to this point, makes no use of that part of the formulation of the previous section; that will become important only in the next section, when we discuss the Kirchhoff approximation. On the other hand, if S were a reflector, it need not be of infinite extent. One would need only to extend a finite reflector in some manner to infinity, allowing the possibility that the medium parameters were discontinuous only across a part of S.

Remark E.1. In the derivation, no use was made of the relationship between u_I and the Green's function, g. From this relationship, one can verify that

$$u_I(\boldsymbol{x}_g, \boldsymbol{x}_s, \omega) - F(\omega) g^\star(\boldsymbol{x}_s, \boldsymbol{x}_g, \omega) = F(\omega) \left[g(\boldsymbol{x}_g, \boldsymbol{x}_s, \omega) - g^\star(\boldsymbol{x}_s, \boldsymbol{x}_g, \omega) \right].$$

By using Green's theorem over the entire sphere, $D_a + D_b$, in the extended "$-$" domain, one can show that the Green's function difference in this equation is zero; that is, the free-space[7] Green's functions of the differential equation and its adjoint differ only in the order of the spatial variables—the interchange between apparent source and observation point in their

[7] Equally true for the complete exact Green's functions of the original problem.

arguments:

$$g(\boldsymbol{x}_g, \boldsymbol{x}_s, \omega) = g^\star(\boldsymbol{x}_s, \boldsymbol{x}_g, \omega). \tag{E.8.12}$$

Then, the surface integral in (E.8.9) must also be zero. Again, this is easy to verify. Simply surround the surface, $S_{\mathcal{R}}+S_a$, by an even larger sphere whose radius will eventually move off to infinity while this surface remains fixed. Now, apply Green's theorem to the volume between these two surfaces. On the one hand, the volume integral is zero because there are no sources between the two surfaces. On the other hand, the Sommerfeld radiation conditions assure that the integral over the larger surface approaches zero as the radius of the surface approaches infinity. Thus, the integral over $S_{\mathcal{R}} + S_a$ must also be zero.

Finally, we remark that, in the limit, as $\mathcal{R} \to \infty$, the integral over each of the surfaces, $S_{\mathcal{R}}$ and S_a must approach zero, separately. The Sommerfeld radiation conditions assure that the integral over $S_{\mathcal{R}}$ approaches zero with increasing radius just as did the integral over this surface with wavefield, u_S. Now, with the Green's function difference equal to zero, the only remaining term in the second equality in (E.8.9) is the integral over S_a. Hence it must be zero as well.

This last can be verified independently, as follows. Consider the integral over the domain bounded by $S_{\mathcal{R}}$ and S_b. This, again, is equal to a corresponding volume integral by Green's theorem. However, there are no sources inside the interior volume bounded by these two surfaces. So, that volume integral is zero. On the other hand, the integral over S_b will approach zero with increasing radius, again as a consequence of the Sommerfeld radiation conditions. Hence, the integral over $S_{\mathcal{R}}$ must approach zero in this limit as well.

The reader may wonder why the surface integral in (E.8.11) cannot be shown to be zero by the same sort of argument that was applied to the integral with u_I in place of u_S. There is a fundamental difference between these two functions at the surface S. Both u_I and $g^\star$ are *downward-propagating* functions at S and their continuations in the extended domain both satisfy the Sommerfeld conditions, (E.8.1). We can think of these two functions as *outgoing* functions. On the other hand, u_S is upward propagating at S. Hence, it is *incoming*; its continuation in the extended medium for which $\mathcal{L}_-$ remains the governing equation, would *not* satisfy the same Sommerfeld radiation condition at infinity in the lower domain. In fact, we would have to change the sign in the Sommerfeld condition, essentially replacing $-i$ by $+i$. So, now suppose that we tried to "close" $S_{\mathcal{R}}$ with the approximate hemisphere S_b, and use the same trick of adding and subtracting a term in the integrand. Then,

$$\int_{S_b} \left\{ g^\star \frac{\partial u_S}{\partial n} - u_S \frac{\partial g^\star}{\partial n} \right\} dS$$
$$= \int_{S_b} \left\{ g^\star \left[\frac{\partial u_S}{\partial \mathcal{R}} - \frac{i\omega}{c} u_S \right] - u_S \left[\frac{\partial g^\star}{\partial \mathcal{R}} - \frac{i\omega}{c} g^\star \right] \right\} \mathcal{R}^2 d\Omega.$$

The Sommerfeld conditions assure us that the second integral on the right will approach zero as before; $g^\star$ satisfies the Sommerfeld conditions, (E.8.11), in all directions. However, the opposite sign in the Sommerfeld condition for u_S in the lower domain allows us only to conclude that

$$\int_{S_b} \left\{ g^\star \frac{\partial u_S}{\partial n} - u_S \frac{\partial g^\star}{\partial n} \right\} dS \approx -2 \int_{S_b} \frac{i\omega}{c} g^\star u_S \mathcal{R}^2 d\Omega.$$

While the first Sommerfeld condition assures that this integral is bounded, it is certainly not guaranteed to approach zero as $S_{\mathcal{R}} \to \infty$.

One point remains to be cleared up in our derivation: the convergence of the surface integral in (E.8.11). Actually, there is nothing to prove, here. The equality between this surface integral and $u_S(\boldsymbol{x}_g, \boldsymbol{x}_s, \omega)$ assures us that the integral converges. This follows because u_S is a solution of a well-posed problem and is itself bounded as a consequence of the first Sommerfeld condition.

E.8.3 The Kirchhoff Approximation

We now have all the tools in place to write down a Kirchhoff approximation for the upward-scattered field from a reflecting surface. In fact, for the purpose of analysis of our inversion formulas for reflectivity, what we really care about is making an approximation that gets the reflected wave right. Anything more should be considered a bonus!

We assume that some known wave u_I is incident at the surface, S. In fact, we think of u_I as being exactly the function $u_I(\boldsymbol{x}, \boldsymbol{x}_s, \omega)$ of the previous section. As a minimum, we cannot hope to get the reflected wave right in the upper medium if we do not get it "right" on the surface S itself. In earlier sections, we developed initial data on a reflecting surface by imposing appropriate interface conditions and then simultaneously solving for the initial values of the phase and leading-order amplitude of the reflected and transmitted waves. Whether dealing with the constant-density case, equations (E.4.21) and (E.4.23), or the variable-density case, equations (E.6.12) and (E.6.13), one relationship between the leading-order incident and upward-scattered wave is

$$u_R = R\, u_I, \quad \text{on } S.$$

To leading order, we also saw in those discussions, that calculating the normal derivative simply amounted to

(i) multiplying by $i\omega$ times the normal derivative of the travel time and
(ii) noting that the normal derivative of the reflected wave is just the negative of normal derivative of the incident wave.

That is, *to leading order* in $i\omega$,

$$\frac{\partial u_R}{\partial n} = -R\frac{\partial u_I}{\partial n}, \quad \text{on } S.$$

We now propose to identify our upward-scattered wave with this reflected wave on S and take as the Kirchhoff approximation the two conditions,

$$u_S = R\, u_I, \qquad \frac{\partial u_S}{\partial n} = -R\frac{\partial u_I}{\partial n}, \quad \text{on } S. \tag{E.8.13}$$

While we have written a normal derivative of the total wavefield here, we must remember to retain only the leading-order term in $i\omega$ in applying these approximations. Furthermore, in the ray theory, this approximation is coupled to an initial reflected ray direction that satisfies Snell's law. Here, we take the angle in the reflection coefficient as the angle that the incident wave makes with the normal to the reflector at each point. Thus, a different direction of reflection is picked out at each point on the reflector. Not all of these directions correspond to reflected rays that arrive at $\boldsymbol{x}_g$. However, as we have seen in examples throughout the text (Section 3.7.2, Exercise 20, Section 5.4.1 and Section 7.4.1), the method of stationary phase will pick out the reflection points on the surface.[8] For any other type of wave, we should not expect a correct amplitude and can only hope (and check!) that the traveltime is right.

We now use this approximation in (E.8.11) to transform that wavefield representation into the the Kirchhoff-approximate solution for the upward scattered wave. The result is

$$u_S(\boldsymbol{x}_g, \boldsymbol{x}_s\omega) = \int_S R\left\{u_I\frac{\partial g^\star}{\partial n} + g^\star\frac{\partial u_I}{\partial n}\right\} dS = \int_S R\frac{\partial(u_I g^\star)}{\partial n} dS. \tag{E.8.14}$$

This, then, is the Kirchhoff approximation to the upward-scattered wave. Historically, modeling formulas of the form of (3.7.1) were created to describe the phenomenon of the diffraction of light through a perforated screen (a solid plane with a hole in it). (The term "diffraction" refers to ray bending that cannot be accounted for by either

---

[8] It is a harder task to prove, in general, that the leading-order asymptotic expansion gives the same amplitude as the ray-theoretic reflected field at $\boldsymbol{x}_g$. In fact, the literature contains only approximate proofs, depending on ray-centered coordinate systems. The problem is that the Hessian matrix for the stationary phase analysis, involves mixed second derivatives of the the total traveltime. The ray Jacobian for the reflected wave contains only second derivatives of the reflected traveltime, which, of course, is linked to the incident traveltime through the boundary conditions. The connections are by no means trivial and we are not aware of a complete proof of the equivalence. We cite some of the literature on the approximate proof: Bortfeld [1989], Goldin [1986], Hubral et al, [1992].

reflection or refraction.) Equation (E.8.14) most closely resembles the classical "Rayleigh-Sommerfeld" diffraction formula—the classical "Kirchhoff" diffraction formula of optics has a slightly different form. However, the name "Kirchhoff" is applied here because the "Kirchhoff approximation" is made as part of the derivation. See Goodman [1996], Born and Wolf [1980], or Bleistein [1984].

We need also to address the possibility that the rays from a particular source point do not illuminate the entire surface. In that case, we would set $R = 0$ in the "shadow regions" on S, effectively reducing the domain of integration. Similarly, if the reflector had edges and did not extend to infinity, we would still treat S as infinite, but having reflection coefficient zero where the actual reflector did not exist, again effectively limiting the domain of integration to the reflector.

To proceed further, suppose we denote the ray theoretic amplitude of the point-source free-space Green's function by $A(\boldsymbol{x}, \boldsymbol{x}_s)$. This is just the amplitude discussed in Section E.3. Then according to (E.6.8), for the variable-density case, we should set

$$B(\boldsymbol{x}, \boldsymbol{x}_s) = \sqrt{\frac{\rho(\boldsymbol{x})}{\rho(\boldsymbol{x}_s)}} A(\boldsymbol{x}, \boldsymbol{x}_s). \tag{E.8.15}$$

Then, by using (E.8.12), we can also express the leading-order amplitude for $g^\star$ as

$$B^\star(\boldsymbol{x}, \boldsymbol{x}_g) = \sqrt{\frac{\rho(\boldsymbol{x}_g)}{\rho(\boldsymbol{x})}} A(\boldsymbol{x}_g, \boldsymbol{x}). \tag{E.8.16}$$

In this last equation, the interchange in arguments in A, as compared to the previous equation, is not important, because of the symmetry of the amplitude A in its arguments. However, the interchange of arguments in the quotient of densities is *extremely* important.

We use these last two results in (E.8.14) and extract the leading-order expression in ω to find that

$$\begin{aligned} u_S(\boldsymbol{x}_g, \boldsymbol{x}_s \omega) = i\omega \int_S R \sqrt{\frac{\rho(\boldsymbol{x}_g)}{\rho(\boldsymbol{x}_s)}} A(\boldsymbol{x}_g, \boldsymbol{x}) A(\boldsymbol{x}, \boldsymbol{x}_s) \\ \cdot (\hat{\boldsymbol{n}} \cdot \nabla [\tau(\boldsymbol{x}_g, \boldsymbol{x}) + \tau(\boldsymbol{x}, \boldsymbol{x}_s)]) \\ \cdot e^{i\omega\{\tau(\boldsymbol{x}_g, \boldsymbol{x}) + \tau(\boldsymbol{x}, \boldsymbol{x}_s)\}} dS. \end{aligned} \tag{E.8.17}$$

In this formula, R is given by (E.6.13) for variable-density media. We set the ratio of densities equal to unity and R is given (E.4.23) for constant density media. Of course, we will regularly use this result with $\boldsymbol{x}$ as the first argument in the amplitudes and traveltime.

E.8.4 2.5D

It is not difficult to specialize (E.8.17) to 2.5D. We need only make the same assumptions about the wavespeed and density that were made in the formulation of 2.5D ray theory, which is to say that these functions are independent of the out-of-plane variable, x_2. In addition, we must take the out-of-plane source and receiver coordinates to be the same, $x_{s2} = x_{g2} = x_{20}$, as well. For this case we also have the result (E.5.2) for the second component of the rays

$$\begin{aligned} p_{s2} &= p_{s20}, \qquad x_2 = x_{20} + p_{s20}\sigma_s, \\ p_{g2} &= p_{g20}, \qquad x_2 = x_{20} + p_{g20}\sigma_g. \end{aligned} \tag{E.8.18}$$

Furthermore, we define the surface S by a curve in (x_1, x_3) for any value of x_2; that is, we set

$$dS = dx_2 ds,$$

with s being arclength along the defining curve, C.

We now proceed with stationary phase analysis in x_2 on the phase function

$$\phi(x_2) = \tau(\boldsymbol{x}_g, \boldsymbol{x}) + \tau(\boldsymbol{x}, \boldsymbol{x}_s), \tag{E.8.19}$$

with first derivative

$$\frac{d\phi(x_2)}{dx_2} = p_{s2} + p_{g2}. \tag{E.8.20}$$

From the ray equations, (E.8.18), we can see that p_{s2} and p_{g2} must have the same sign for any choice of x_2 on S. Therefore, the only way that the first derivative can be equal to zero is if the separate terms on the left side of this last equation are separately equal to zero. However, returning to (E.8.18), we can see that this means that, for stationarity, $x_2 = x_{20}$; that is, x_2 is the common second coordinate at the source and receiver.

Now, we may consider the second derivative of the phase,

$$\frac{d^2\phi(x_2)}{dx_2^2} = \frac{\partial p_{s2}}{dx_2} + \frac{\partial p_{g2}}{dx_2}. \tag{E.8.21}$$

By differentiating the ray equations implicitly, we find that

$$1 = \frac{\partial p_{s2}}{dx_2}\sigma_s + p_{s2}\frac{\partial \sigma_s}{dx_2} = \frac{\partial p_{g2}}{dx_2}\sigma_g + p_{g2}\frac{\partial \sigma_g}{dx_2}.$$

At the stationary point, the second term in each of the last two expressions is equal to zero, so we conclude that

$$\frac{\partial p_{s2}}{dx_2} = \frac{1}{\sigma_s}, \qquad \frac{\partial p_{g2}}{dx_2} = \frac{1}{\sigma_g},$$

and

$$\frac{d^2\phi(x_2)}{dx_2^2} = \frac{1}{\sigma_s} + \frac{1}{\sigma_g}, \qquad \text{sgn}\left(\frac{d^2\phi(x_2)}{dx_2^2}\right) = 1, \tag{E.8.22}$$

at the stationary point.

Finally, we apply the stationary phase formula to transform (E.8.17) into the equivalent 2.5D result,

$$\begin{aligned} u_S(\boldsymbol{x}_g, \boldsymbol{x}_s\omega) = \sqrt{|\omega|}e^{3i\pi\,\text{sgn}\,(\omega)/4} \\ \cdot \int_C R\sqrt{\frac{\rho(\boldsymbol{x}_g)}{\rho(\boldsymbol{x}_s)}}A(\boldsymbol{x}_g, \boldsymbol{x})A(\boldsymbol{x}, \boldsymbol{x}_s)\sqrt{\frac{\sigma_s\sigma_g}{\sigma_s + \sigma_g}} \\ \cdot (\hat{\boldsymbol{n}} \cdot \nabla\left[\tau(\boldsymbol{x}_g, \boldsymbol{x}) + \tau(\boldsymbol{x}, \boldsymbol{x}_s)\right])\, e^{i\omega\{\tau(\boldsymbol{x}_g, \boldsymbol{x}) + \tau(\boldsymbol{x}, \boldsymbol{x}_s)\}} ds. \end{aligned} \tag{E.8.23}$$

Here, all dependence on the out-of-plane variable is gone and all vectors are two-dimensional, with components in the in-plane directions, $(1, 3)$, only.

E.8.5 Summary

Through the application of Green's theorem, we have constructed high-frequency representations of the scattered field u_S. We obtained an integral over the reflecting surface for 3D, and, respectively, an integral over the defining curve on the surface for 2.5D. These integrals are written in terms of the reflection coefficient R, rather than in terms of the perturbation in wavespeed $\alpha(\boldsymbol{x})$ that we saw in the Born-approximate integral equations that we used in the first part of the text. Because we wish to construct inversion formulas that are integrals in survey coordinates, which permit us to solve for reflectivity, these Kirchhoff representations of u_S provide a better starting point for constructing our inversion formulas than our original Born-approximate integral equations. Yet, in reality, the results obtained by starting from either the Born approximation or the Kirchhoff approximation to derive an inversion formula are much the same. In either case, we arrive at high-frequency asymptotic representations of reflectivity as our inversion results.

References

Abramowitz, I., 1965. *Handbook of mathematical functions.* Dover, New York.

Armstrong, J., 1978. An analysis of the aperture-limited Fourier inversion of characteristic functions. Ph.D. thesis, University of Denver, ONR Research Report number MS-R-7812.

Aki, K., and P., Richards, 1980. *Quantitative seismology: theory and methods vols. 1 and 2.* Freeman, New York.

Artley, C., 1994. Dip moveout processing for depth-variable velocity. *Geophysics* **59** no. 4, 610–622.

Backus, M. M., 1959. Water reverberations—their nature, elimination. *Geophysics* **24**, 233–261.

Berkhout, A. J., and D. J. Verschuur, 1997. Estimation of multiple scattering by iterative inversion, part I,: theoretical considerations. *Geophysics* **62**, No. 3, 1568–1595.

Berkhout, A. J., 1999. Multiple removal based on the feedback model: *The Leading Edge* **18**, no. 1, 127–131.

Ben-Menahem , A. and S. J. Singh, 1981. *Seismic waves and sources.* Springer-Verlag, New York.

Berryhill, J. R., 1979. Wave-equation datuming. *Geophysics* **44**, 1329–1344.

Berryhill, J. R., 1984. Wave-equation datuming before stack (short note). *Geophysics* **49**, 2064–2066.

Bevc, D., 1995. Imagining under rugged topography and complex velocity structure. Ph. D. thesis. Stanford University, Stanford, CA.

Bevc, D., 1999. Flooding the topography: wave equation datuming of land data with rugged acquisition topography, *Geophysics* **62**, to appear.

Beylkin, G., 1985. Imaging of discontinuities in the inverse scattering problem by the inversion of a causal Radon transform. *J. Math. Phys.* **26**, 99–108.

Beylkin, D., and N. Oristaglio, 1985. Spatial resolution of migration algorithms, in, *Acoustic Imaging 14*. A. J., Berkhout, J. Ridder, and L. A. van der Waals, Plenum, New York, 155–167.

Biondi, N., 1994. Transformation of 3-D pre-stack data by azimuthal moveout 64th Ann. Int. Mtg. SEG, *Expanded abstracts*, 1541–1544.

Black, J. L., K. L. Schleicher, and L. Zhang, 1993. True amplitude imaging and dip moveout. *Geophysics* **58**, 47–66.

Bleistein, N., 1984. *Mathematical Methods for Wave Phenomena*. Academic Press Inc. (Harcourt Brace Jovanovich Publishers), New York.

Bleistein, N., 1986a. Kirchhoff inversion for reflector imaging and sound speed and density variations. in *Deconvolution and Inversion* Proceedings of EAEG/SEG Workshop on Deconvolution and Inversion, Rome, Italy, tech. editor M. Worthington. 305–320. Blackwell Scientific Publications, Oxford.

Bleistein, N., 1986b. Two-and-one-half dimensional in-plane wave propagation. *Geophysical Prospecting* **34**, 686–703.

Bleistein, N., 1987a. On the imaging of reflectors in the earth. *Geophysics* **52**, 931-942.

Bleistein, N., 1987b. Kirchhoff inversion for reflector imaging and soundspeed and density variations, in *Proceedings of the First Joint EAEG/SEG Workshop on Deconvolution and Inversion.* Rome, Italy, 1986. Blackwell Scientific Publications, Oxford.

Bleistein, N., 1988. Analysis of post stacking of common-shot inversions for parameter estimation. Center for Wave Phenomena Res. Rep. CWP-071R, Colorado School of Mines, Golden, CO.

Bleistein, N., 1989. Large-wavenumber aperture-limited Fourier inversion and inverse scattering. *Wave Motion* **11**, 113–136.

Bleistein, N., 1999. Hagedoorn told us how to do Kirchhoff migration and inversion. *The Leading Edge* **18**, 918–927.

Bleistein, N., J. K. Cohen, and F. G., Hagin, 1985. Computational and asymptotic aspects of velocity inversion. *Geophysics* **50**, 1253–1265.

Bleistein, N., J. K. Cohen, and F. Hagin, 1987. Two-and-one-half dimensional Born inversion with an arbitrary reference. *Geophysics* **52**, 26–36.

Bleistein, N., J. K. Cohen, and H. Jaramillo, 1999. True-amplitude transformation to zero-offset of data from curved reflectors. *Geophysics* **64**, no. 1, 112–129.

Bleistein, N., S. H. Gray, 1985. An extension of the Born inversion method to a depth dependent reference profile. *Geophysical Prospecting* **33**, 999–1022.

Bleistein, N., R. A. Handelsman, 1986. *Asymptotic expansions of integrals.* Dover Publications Inc., New York.

Bleistein, N., and H. Jaramillo, 2000. A platform for data mapping in scalar models of data acquisition. *Geophysical Prospecting* **48**, no. 1, 135–161.

Bojarski, N. N., 1967. Three dimensional electromagnetic short pulse inverse scattering. Spec. Proj. Lab. Rept., Syracuse Univ. Res. Corp., Syracuse, New York.

Bojarski, N. N., 1968. Electromagnetic inverse scattering theory. Spec. Proj. Lab. Rept., Syracuse Univ. Res. Corp., Syracuse, New York.

Bojarski, N. N., 1982. A survey of physical optics inverse scattering identity. *IEEE Trans. Antenna and Prop.* **40**, 989–989.

Born, E., 1980. *Principles of Optics.* Pergammon Press, New York.

Bortfeld, R., 1989. Geometrical ray theory: rays and traveltimes in seismic systems (second-order approximation of traveltimes). *Geophysics* **54**, 342–349.

Bremmer, H., 1950. The W. K. B. Approximation as the First Term of a Geometrical-Optics Series, in *The theory of electromagnetic waves.* Kline, M., editor 1951. Dover Publications Inc. New York.

Butkov, E., 1968. *Mathematical Physics.* Addison-Wesley Publishing Company, Reading Massachussetts.

Byun, B. editor, 1990. *Velocity analysis of multichannel seismic data,* Society of Exploration Geophysicists, Tulsa.

Červený, V., 1995. Seismic wavefields in three-dimensional isotropic and anisotropic structures. Lecture Notes, University of Trondheim, Norway.

Červený, V., 2000. *Seismic Ray Theory.* Cambridge University Press, Cambridge.

Červený, V., I. A. Molotkov, and I. Psencik, 1977. *Ray methods in seismology.* Univerzita Karlova, Prague.

Claerbout, J. F., 1970. Course grid calculations of waves in inhomogeneous media with application to delineation of complicated seismic structure. *Geophysics* **35**, 407–418.

Claerbout, J. F., 1976. *Fundamentals of geophysical data Processing.* McGraw-Hill, New York.

Claerbout, J. F., 1985. *Imaging the Earth's Interior.* Blackwell Scientific Publications, Oxford.

Claerbout, J. F., and A. G. Johnson, 1971. Extrapolation of time-dependent wave forms along their path of propagation. *Geophysical Journal of the Royal Astronomical Society* **26**, 285–293.

Claerbout, J. F., 1972. Downward continuation of moveout corrected seismograms. *Geophysics* **37**, 741–768.

Coddington, E. A., and N. Levinson, 1984. *Theory of ordinary differential equations.* Krieger Publishing Malabar. FL 1984 reprint of the original 1955 McGraw-Hill edition.

Cohen, J. K., and N. Bleistein, 1979a. Velocity inversion procedure for acoustic waves. *Geophysics* **44**, 1077–1087.

Cohen, N., 1979b. The singular function of a surface and physical optics scattering. *Wave Motion* **1**, 153–161.

Cohen, J. K. and N. Bleistein, 1983. The influence of out-of-plane surface properties on unmigrated time sections. *Geophysics* **48**, 125–132.

Cohen, J. K. and N. Bleistein, 1986. Multidimensional seismic inversion: Asymptotic methods for seismic modeling and inversion, CWP-#043: Presented as a short course at the Norwegian Institute of Technology, Trondheim, Norway.

Cohen, J. K. and F. G. Hagin, 1985. Velocity inversion using a stratified reference. *Geophysics* **50**, 1683–1700.

Cohen, J. K., F. G. Hagin, and N. Bleistein, 1986. Three-dimensional Born inversion with an arbitrary reference. *Geophysics* **51**, 1552–1558.

Colton, R., 1983. *Integral equation methods in scattering theory.* John Wiley & Sons, New York.

Courant, R., 1964. *Methods of Mathematical Physics Vol. 2, Partial Differential Equations.* Wiley, New York.

de Hoop, M. V., 1998. Asymptotic inversion: multipathing and caustics. Sixty-eighth International Meeting of the Society of Exploration Geophysicists, *Expanded abstracts*, SEG, Tulsa, 1534–1537.

de Hoop, M. V., and N. Bleistein, 1997. Generalised Radon transform inversions for reflectivity in anisotropic elastic media. *Inverse Problems* **13**, 669–690.

de Hoop, M. V. and S. Brandesberg-Dahl, 2000. Maslov asymptotic extension of generalized Radon transform inversions in anisotropic elastic media: A least-squares approach. *Inverse Problems* in press.

de Hoop, M. V., C. Spencer, and R. Burridge, 1999. The resolving power of seismic amplitude data: An anisotropic inversion/migration approach. *Geophysics* **64**, no. 3, 852–873.

Devaney, A. J., and M. L. Oristaglio, 1984. Geophysical diffraction tomography: Presented at the 54th Ann. Internat. Mtg. Soc. Explor. Geophys., 330–333.

Dobrin, M. B., 1976. *Introduction to geophysical prospecting*, McGraw-Hill, New York.

Dong, W., 1990. CXZCS: A 2.5D common shot inversion program in a $c(x, z)$ medium. Edited by Z. Liu, CWP Program documentation number U13R.

Dong, W., and Bleistein, N., 1990. 2.5D Kirchhoff inversion theory applied to VSP and crosshole data. Center for Wave Phenomena Research Report number CWP-101, Colorado School of Mines, Golden, CO.

Dong, W., M. J. Emanuel, P. Bording, and N. Bleistein, 1991. A computer implementation of 2.5D common-shot inversion. *Geophysics* **56**, no. 9, 1384–1394.

Docherty, P., 1987. Ray theoretical modeling, migration and inversion in two-and-one-half-dimensional layered acoustic media. Center for Wave Phenomena Research Report number CWP-051, Colorado School of Mines, Golden, CO.

Docherty, P., 1988. CXZ: Fortran program for laterally varying velocity inversion: CWP Program documentation number U09. Ph. D. thesis, Colorado School of Mines, Golden, CO.

Docherty, P., 1991. Documentation for the 2.5-D common shot program CSHOT: CWP Program documentation number U08R. Center for Wave Phenomena, Colorado School of Mines, Golden CO.

Dragoset, B., and A. Weglein, 1999. An introduction: The new world of multiple attenuation. *The Leading Edge* **18**, no. 1, 38.

Duffy, D. G., 1994. *Transform Methods for Solving Partial Differential Equations.* CRC Press, Boca Raton.

Erdélyi, A., 1954. *Asymptotic Expansions of Integrals.* Dover Publications Inc., New York.

Filpo, M., 1999. Deep water multiple suppression in the near-offset range. *The Leading Edge* **18**, no. 1, 81–84.

Fomel, S., 1995a. Amplitude preserving offset continuation in theory, Part 1: the offset continuation equation. Stanford Exploration Project preprint, SEP-84, 179–196, Stanford University, Stanford, CA.

Fomel, S., 1995b. Amplitude preserving offset continuation in theory, Part 2: solving the equation. Stanford Exploration Project preprint, SEP-89, Stanford University, Stanford, CA.

Fomel, S., 1997. Velocity continuation and the anatomy of pre-stack residual migration. 67th Annual International Meeting of the Society of Exploration Geophysicists, *Expanded abstracts, Vol II.* Tulsa, 1762–1765.

Fomel, S., H. Jaramillo, 1996. True amplitude DMO, offset continuation and AVA/AVO for curved reflectors: 66th Annual International Meeting of the Society of Exploration Geophysicists, *Expanded abstracts, vol II*, Tulsa, 1731–1734.

French, W. S., 1975. Computer migration of oblique seismic reflection profiles, *Geophysics* **40**, 961–980.

Friedlander, F. G., 1982. *Introduction to the theory of distributions.* Cambridge University Press, Cambridge.

Garabedian, P. R., 1964. *Partial differential equations.* Wiley, New York.

Gardner, G. H. F., 1985. *Migration of seismic data.* Geophysical reprint series, no. 4, Society of Exploration Geophysics.

Gardner, G. H. F., and D. Forel, 1988. Amplitude preservation equations for DMO: 58th Annual International Meeting of the Society of Exploration Geophysicists, *Expanded abstracts*, 1106–1108, Session: S17.2.

Gardner, G. H. F., and D. Forel, 1995. Amplitude preservation equations for dip moveout. *Geophysics* **55**, 485–487.

Gazdag, J. and P. Sguazzero, 1984. Migration of seismic data by phase-shift plus interpolation. *Geophysics* **49**, no. 2, 124–131.

Geoltrain, S., 1989. Asymptotic solutions to direct and inverse scattering in anisotropic elastic media. Ph.D. thesis, CWP Res. Rep. CWP-082, Colorado School of Mines, Golden, CO.

Geoltrain, S., and E. Chovet, 1991. Automatic association of kinematic information to prestack images: the International Meeting and Exposition of the Society of Exploration Geophysicists, *Expanded abstracts*, SEG, Tulsa, 890–892.

Goldin, S., 1986. *Seismic traveltime inversion.* SEG Monograph, Tulsa.

Goodman, J. W., 1996. *Introduction to Fourier Optics.* McGraw-Hill, New York.

Gray, S. H., 1986. Efficient traveltime calculations for Kirchhoff migration. *Geophysics* **51**, 1685–1688.

Gray, S. H., 1988. Computational inverse scattering in multidimensions. *Inverse Problems* **4** 87–101.

Gray, S. H., 1992. Frequency-selective design of the Kirchhoff migration operator. Geophys. Prosp., **40**, 565–572.

Gray, S. H., 1997. True-amplitude seismic migration: a comparison of three approaches. *Geophysics* **62**, 929–936.

Gray, S. H., 1998. Speed and accuracy of seismic migration methods. Proceedings of the Mathematical Geophysics Summer School on Seismic Imaging, Stanford University, Stanford, CA, August 3-21, to appear. Available on the web at http:sep//www.stanford.edu/etc/sam_gray/.

Gray, S. H. and W. P. May, 1994. Kirchhoff migration using eikonal equation traveltimes. *Geophysics* **59**, No. 5, 810–817.

Gray, S. H. and K. J. Marfurt, 1995. Migration from topography: improving the near-surface image. *Can. J. Expl. Geophys* **31**, 18-24.

Hadamard, J., 1923. *Lectures on the Cauchy problem in linear partial differential equations.* Yale University Press, New Haven, CT.

Hagedoorn, J. G., 1954. A process of seismic reflection interpretation. *Geophysical Prospecting* **2**, 85-127.

Hale, I. D., C. Artley, 1993. Squeezing dip moveout for depth-variable velocity. *Geophysics* **58**, no. 2, 257-264.

Hale, I. D., 1984. Dip-moveout by Fourier transform. *Geophysics* **49**, no. 6, 741-757.

Hale, I. D., editor, 1995. *DMO Processing*, Society of Exploration Geophysicists, Tulsa.

Hanitzsch, C., 1995. Amplitude preserving prestack Kirchhoff depth migration/inversion in laterally inhomogeneous media: PhD dissertation, University of Karlsruhe.

Hanitzsch, C., 1997. Comparison of weights in prestack amplitude-preserving Kirchhoff depth migration. *Geophysics* **62**, no. 6, 1812–1816.

Hörmander, L., 1983. *The analysis of linear partial differential operators, Vol. I*, Springer-Verlag, New York.

Hubral, P., Schleicher, M., 1992. Three-dimensional paraxial ray properties, Part I: Basic relations. *J. Seismic Exploration*, **1**, 265–279.

Hubral, P., M. Tygel, and J. Schleicher, 1995. Geometrical-spreading decomposition of elementary seismic waves. 57th Mtg. Eur. Assoc. Expl. Geophys., *Extended abstracts.* Session:D014.

Hsu, C., 1992. CXZCO: A 2.5D common offset inversion program in a $c(x, z)$ medium. Edited by Z. Liu. CWP Program documentation number U15. Center for Wave Phenomena, Colorado School of Mines, Golden, CO.

Jaramillo, H., 1998. Seismic data mapping. Ph.D. thesis. Center for Wave Phenomena Research Report number CWP-284, Colorado School of Mines, Golden, CO.

Jaramillo, H. and N. Bleistein, 1998. Seismic data mapping. *Expanded abstracts*, Society of Exploration Geophysicists International Meeting, September, 1998, to appear.

Jaramillo, H. and N. Bleistein, 1999. The link of Kirchhoff migration and demigration to Kirchhoff and Born modeling. *Geophysics* **64**, 1793–1805.

John, F., 1982. *Partial differential equations.* Springer-Verlag, New York.

Karcher, C. L., 1973. *The reflection seismograph, its invention and use in the discovery of oil and gas fields.* American Institute of Physics, College Park, MD.

Kravtsov, Yu. A., and Yu. I. Orlov, 1990. *Geometrical optics of inhomogeneous media.* Springer-Verlag, New York.

Kreyszig, E., 1991. *Differential geometry.* Dover, New York.

Levinson, N. , R. M. Redheffer, 1970. *Complex variables.* Holden-Day Inc., Oakland, CA.

Lewis, R. M., 1965. Asymptotic theory of wave-propagation. *Arch. Rat. Mech. and Anal.* **20**, no. 3, 191–250.

Liner, C. L., 1990. General theory and comparative anatomy of dip moveout. *Geophysics* **55**, 595–607.

Liner, C. L., 1991, Born theory of wave-equation dip moveout. *Geophysics* **56**, 182–189.

Ludwig, D. L., 1966. Uniform asymptotic expansions at a caustic. *Comm. Pure and Appl. Math.* **XIX**, 215–250.

Mager, N., 1978. An examination of the limited aperture problem of physical optics inverse scattering. *IEEE Trans. Antennas Propagat.* **18**, 194.

Melrose, R. B., 1995. *Geometric Scattering Theory.* Cambridge University Press.

Miller, N., and Beylkin, G., 1987. A new slant on the seismic imaging: Migration and integral geometry. *Geophysics* **52**, 943–964.

Mora, P. R., 1987. Nonlinear two-dimensional elastic inversion of multi-offset seismic data. *Geophysics* **52**, no. 9, 1211–1228.

Morse, M. M. and H. Feshbach, 1953. *Methods of modern physics (vol.I & II)*. McGraw-Hill, New York.

Musgrave, A. W., 1961. Wave-front charts and three dimensional migrations. *Geophysics* **26**, 738–753.

Najmi, A., 1996. Closed form solutions for the geometrical spreading in inhomogeneous media. *Geophysics* **61**, no. 3, 1189–1197.

Nussenzveig, H. M., 1968. *Causality and dispersion relations.* Academic Press Inc., New York.

Oliveira, M., and E. Filpo, 1997. On the application of true-amplitude DMO. *Journal of Seismic Exploration* **6**, 279–290.

Petersen, Bent, E., 1983. *Introduction to the Fourier transform and pseudo-differential operators.* Pittman, Boston.

Jacewitz, C. A. and S. H. Gray, 1994. Subsalt imaging via target-oriented 3-D prestack depth migration. *The Leading Edge* **13**, no. 3, 163-170.

Rayleigh, Lord (Strutt, J. W.) 1879. Contribution. *Philosophical Magazine (5)*, **8**, 261.

Robinson, E. A. and O. M. Osman, editors, 1996. *Deconvolution 2*, Geophysical reprint series no. 17, Society of Exploration Geophysicists, Tulsa.

Sabatier, P. C., editor 1987. *Tomography and Inverse Problems.* Adam Hilger, IOP Publishing Ltd., Philadelphia.

Saint Raymond, X., 1994. *An elementary introduction to the theory of pseudo-differential operators.* CRC Press, Boca Raton, Florida.

Schwartz, L., 1954. *Théorie des Distributions Vols. 1 and 2*, Hermann, Paris.

Schneider, W. A., 1978. Integral formulation for migration in two and three dimensions. *Geophysics* **43**, 49–76.

Sen, F., and J. B. Stoffa, 1998. An unified Treatment to free surface multiple elimination methods. *J. Seismic Explor.* **7**, 129–143.

Sheaffer, S., and N. Bleistein, 1998. 2.5D downward continuation using data mapping theory. Center for Wave Phenomena Research Report CWP-270, Colorado School of Mines, Golden, CO.

Slotnick, M. M., 1959. *Lessons in seismic computing*, Society of Exploration Geophysicists, Tulsa.

Sneddon, I. N., 1972. *The use of integral transforms.* McGraw-Hill, New York.

Sommerfeld, A. 1964. *Optics, lectures on theoretical physics vol. 4.* Academic Press, New York.

Spiegel, M., 1953. *Complex variables.* Schaum's Outline Series, McGraw-Hill, New York.

Stakgold, I. 1979, *Green's functions and boundary value problems.* John Wiley and Sons, New York.

Stockwell, Jr. J. W., 1995a. Convergent versus asymptotic representations. *The Mathematica Journal* Classroom Notes, **5**, No. 4, 54–56.

Stockwell, Jr. J. W., 1995b. 2.5-D wave equations and high frequency asymptotics. *Geophysics* **60**, 556–562.

Stockwell, Jr., J. W., 1997. Free software in education: A case study of CWP/SU: Seismic Unx. *The Leading Edge*, July 1997 issue, 1054–1049.

Stockwell, Jr., J. W., 1999. The CWP/SU: Seismic Unx package. *Computers and Geosciences* **25**, 415–419.

Stolt, R. M. 1978, Migration by Fourier transform. *Geophysics* **43**, 23–49.

Sullivan, J. K., 1987. Pre-stack Kirchhoff inversion of common offset data. *Geophysics* **52**, 745–754.

Sumner, B., 1988. Asymptotic solutions to forward and inverse problems in isotropic elastic media. Ph.D. thesis, Center for Wave Phenomena Res. Rep. CWP-075, Colorado School of Mines, Golden, CO.

Symes, W., 1990. Velocity inversion: A case study in infinite- dimensional optimization. *Math. Programming* **48**, 71–102.

Tarantola, A. 1987. *Inverse problem theory*, Elsevier Science Publishing, Amsterdam, New York.

Taylor, M. E., 1981. *Pseudodifferential operators.* Princeton University Press.

Telford, W. M. et al. 1976. *Applied geophysics.* Cambridge University Press.

Titchmarsh, E. C., 1948. *Introduction to the theory of Fourier integrals.* Clarendon, Oxford.

Treves, F., 1967, "Topological vector Spaces, distributions, and kernels," Academic Press, New York.

Treves, F., 1980, "Introduction to pseudodifferential and Fourier integral operators, vols. I and II," Plenum Press, New York.

Tygel, E., and A. Oliveira, 1997. True-amplitude MZO in laterally varying media: experiments on synthetic data. Presented at the 5th Intern. Congr. of the Braz. Geoph. Soc., Sao Paulo, Brazil. *Expanded abstracts*, 151–154.

Tygel, M., P. Hubral, and J. Schleicher, 1994. A unified approach to seismic reflection imaging. 56th Mtg. Eur. Assoc. Expl. Geoph., *Extended abstracts*, Session:H029.

Tygel, P., and J. Schleicher, 1995. Seismic imaging operators derived from chained stacking integrals. Internat. Mtg. Soc. Opt. Eng., San Diego, USA. Mathematical Methods in Geophysical Imaging III: Proceedings, vol. 2571, 138–149.

Tygel, P., and J. Schleicher, 1996. 2.5D true-amplitude Kirchhoff migration to zero offset (MZO). *Extended abstracts*, paper X051, EAGE 58th Conference and Technical Exhibition, Amsterdam, The Netherlands.

Tygel, J. and P. Hubral, 1995a. Dualities between reflectors and reflection time surfaces. *Journal of Seismic Exploration*, **4**, 123-150.

Tygel, J. and P. Hubral, 1995b. True-amplitude migration to zero-offset (MZO) by diffraction stack. preprint, Insitituto de Matemática Es-

tatística e Ciência da Computação, Universidade Estadual de Campinas, Brazil.

Tygel, J. and P. Hubral, 1996a. Amplitude-preserving MZO in laterally inhomogeneous media. *Mathematical methods in geophysical imaging IV*, vol. 2822, pp. 17–28. Proceedings of the International SPIE Congress, August, 04 to 09, Denver, USA.

Tygel, J. and P. Hubral, 1996b. 2.5D Kirchhoff MZO in laterally inhomogeneous media. 66th Annual International Meeting of the Society of Exploration Geophysics (SEG), *Expanded abstracts*, 483–486.

Tygel, M., J. Schleicher, and L. T. Santos, 1998. 2.5-D true-amplitude Kirchhoff migration to zero-offset in laterally inhomogeneous media. *Geophysics* **63**, no. 2, 557–573.

Verschuur, D.J., A. J. Berkhout, and C. P. A. Wapenaar, 1992. Adaptive surface-related multiple elimination. *Geophysics* **57**, 116–1177.

Watson, G. N., 1980. *A Treatise on the Theory of Bessel Functions.* University Press, Cambridge.

Webster, G. M. editor, 1978. *Deconvolution, Vol. I and II*, Geophysical reprint series No. 1, Society of Exploration Geophysicists, Tulsa.

Weglein, A. B., 1999. Multiple attenuation: an overview of recent advances and the road ahead. *The Leading Edge* **18**, No. 1, 40–45.

Weglein, A. B., F. A. Gasparotto, P. M. Carvalho, and R. Stolt, 1997. An inverse-scattering series method for attenuating multiples in seismic reflection data. *Geophysics* **62**, No. 6, 1975–1989.

Weglein, A. B., and K. H. Matson, 1998. Inverse scattering internal multiple attenuation: an analytic example and subevent interpretation, in *Mathematical Methods in Geophysical Imaging V.* Siamak Hassanzadeh, editor, Proceedings of SPIE, Vol. 3453, 108–117.

White, J. E., 1983. *Underground Sound.* Elsevier, New York.

Xu, M., 1996a. Amplitude calculation for 3-D common offset $v(z)$ inversion. Center for Wave Phenomena Res. Rep. CWP-213, Colorado School of Mines, Golden, CO.

Xu, M., 1996b. 3-D common offset inversion in depth dependent media and its parallel implementation. Center for Wave Phenomena Res. Rep. CWP-228, M.Sc. thesis, Colorado School of Mines, Colorado School of Mines, Golden, CO.

Ziolkowski, R. W., and G. A. Deschamps, 1980. The Maslov method and the asymptotic Fourier transform: Caustic analysis. Electromagnetic Laboratory Scientific Rep. No. 80-9. University of Illinois, Urbana-Champaign.

Ziolkowski, R. W., and G. A. Deschamps, 1984. Asymptotic evaluation of high frequency fields near a caustic: an introduction to Maslov's method. *Radio Science* **19**, 1001–1025.

Author Index

Subject Index

Interdisciplinary Applied Mathematics

1. *Gutzwiller:* Chaos in Classical and Quantum Mechanics
2. *Wiggins:* Chaotic Transport in Dynamical Systems
3. *Joseph/Renardy:* Fundamentals of Two-Fluid Dynamics: Part I: Mathematical Theory and Applications
4. *Joseph/Renardy:* Fundamentals of Two-Fluid Dynamics: Part II: Lubricated Transport, Drops and Miscible Liquids
5. *Seydel:* Practical Bifurcation and Stability Analysis: From Equilibrium to Chaos
6. *Hornung:* Homogenization and Porous Media
7. *Simo/Hughes:* Computational Inelasticity
8. *Keener/Sneyd:* Mathematical Physiology
9. *Han/Reddy:* Plasticity: Mathematical Theory and Numerical Analysis
10. *Sastry:* Nonlinear Systems: Analysis, Stability, and Control
11. *McCarthy:* Geometric Design of Linkages
12. *Winfree:* The Geometry of Biological Time
13. *Bleistein/Cohen/Stockwell:* Mathematics of Multidimensional Seismic Imaging, Migration, and Inversion